TRANSACTIONS
OF THE ASME
Series E

Journal of APPLIED MECHANICS

September 1961

DYNAMICS • VIBRATIONS • ELASTICITY • LUBRICATION AND WEAR
RHEOLOGY • FRACTURES • STRUCTURES • HYDRAULICS • AERODYNAMICS
INTERNAL FLOW • MECHANICAL PROPERTIES OF METALS • THERMODYNAMICS
TURBULENCE • HEAT TRANSFER • COMPUTING DEVICES AND METHODS
BOUNDARY LAYERS • AEROELASTICITY • EXPERIMENTAL STRESS ANALYSIS

Published Quarterly by
THE AMERICAN SOCIETY OF MECHANICAL ENGINEERS

TRANSACTIONS
OF THE ASME
Series E

EDITORIAL DEPARTMENT

Editor, J. J. JAKLITSCH, JR.
Consulting Editor, LEO SLOGGETT
Art Editor, HENRY BALFOUR
Production, MILDA K. WILBUS

APPLIED MECHANICS DIVISION

Chairman, A. M. WAHL
Secretary, E. REISSNER
Technical Editor, D. C. DRUCKER
Technical Editor, J. KESTIN

OFFICERS OF THE ASME

President, W. H. BYRNE
Secretary, C. B. SCHIER, II
Treasurer, E. J. KATES
Assistant Treasurer, H. J. BAUER

PUBLICATIONS COMMITTEE

Chairman, HENDLEY H. BLACKBURN
MARTIN GOLAND
VITO L. SALERNO
F. J. HEINZE
R. E. DERBY

Junior Representatives
J. W. FOLLANSBEE
STEWART H. ROSS

REGIONAL ADVISORY BOARD

Region I, H. M. ROGERS, JR.
Region II, ROBERT E. ABBOTT
Region III, A. F. BOCHENEK
Region IV, FRANCIS C. SMITH
Region V, WM. J. TITZEL
Region VI, C. R. EARLE
Region VII, RALPH L. SCORAH
Region VIII, G. CORRY McDONALD
Region IX, M. S. UMBENHAUER
Region X, CARL J. ECKHARDT

Published quarterly by The American Society of Mechanical Engineers. Publication office at 20th and Northampton Streets, Easton, Pa. The editorial department is at ASME headquarters, United Engineering Center, 345 East 47th Street, New York 17, N. Y. Cable address, "Mechaneer," New York. Price $3.00 a copy, $10.00 annually. To members, $2.50 a copy, $8.00 annually. Add 50 cents for postage to all countries outside the United States and Canada. Changes of address must be received at Society headquarters seven weeks before they are to be effective on the mailing list. Please send old as well as new address. By-Laws: The Society shall not be responsible for statements or opinions advanced in papers or . . . printed in its publications (B13, Par. 4). . . . Second-Class mail privileges authorized at Easton, Penna. . . . This publication is authorized to be mailed at the special rates of postage prescribed by Section 132.122 . . . © Copyright, 1961, by The American Society of Mechanical Engineers. Reprints from this publication may be made on condition that full credit be given the TRANSACTIONS of the ASME, Series E—Journal of Applied Mechanics, and the author, and that date of publication be stated.

TRANSACTIONS OF THE ASME
is indexed by the Engineering Index, Inc.

Journal of
APPLIED MECHANICS
VOLUME 28 • SERIES E • NUMBER 3
September 1961

CONTENTS

TECHNICAL PAPERS

321 **John Moyes Lessells 1888—1961**

323 **Investigation of Flat-Plate Hypersonic, Turbulent Boundary Layers With Heat Transfer** (60—WA-205)
Eva M. Winkler

330 **On the Parametric Excitation of Pendulum-Type Vibration Absorber** (61—APMW-4)
Eugene Sevin

335 **Mixing of Compressible Fluids** (61—APMW-3)
E. D. Kennedy

339 **The Laminar Boundary Layer on a Hot Cylinder Fixed in a Fluctuating Stream** (60—WA-203)
R. J. Gribben

347 **Diffraction of a Pressure Wave by a Cylindrical Cavity in an Elastic Medium** (61—APM-26)
M. L. Baron and A. T. Matthews

355 **Whirling of Unsymmetrical Rotors** (61—APM-10)
P. J. Brosens and S. H. Crandall

363 **Torsion of Sandwich Plates of Trapezoidal Cross Section** (61—APM-22)
Shun Cheng

367 **Natural Frequencies of Vibration of Fixed-Fixed Sandwich Beams** (61—APMW-2)
M. E. Raville, En-Shiuh Ueng, and Ming-Min Lei

372 **Combined Stresses in an Orthotropic Plate Having a Finite Crack** (61—APM-19)
D. D. Ang and M. L. Williams

379 **The Effect of a Rigid Elliptic Inclusion on the Bending of a Thick Elastic Plate** (61—APM-13)
Fu Chow

383 **An Addition to the Theory of Whirling** (61—APMW-1)
T. R. Kane

387 **Bending of a Cantilver Plate Supported From an Elastic Half Space** (61—APM-11)
N. C. Small

395 **The Elastic, Plastic Bending of a Simply Supported Plate** (61—APM-18)
G. Eason

402 **Bending and Stretching of Certain Types of Heterogeneous Aeolotropic Elastic Plates** (61—APM-21)
E. Reissner and Y. Stavsky

409 **Bowing of Cryogenic Pipelines** (61—APMW-7)
W. G. Flieder, J. C. Loria, and W. J. Smith

417 **Dynamic Membrane Stresses in a Circular Elastic Shell** (61—APMW-10)
R. G. Payton

421 **An Extension of Duhamel's Analogy to Plasticity** (61—APM-9)
S. A. Murch

427 **Bending of a Thin Cylindrical Shell Subjected to a Line Load Around a Circumference** (61—APM-15)
H. R. Meck

434 **The Stresses in an Elastoplastic Bar Subjected to a Sudden Change of Surface Temperature** (61—APM-16)
E. W. Parkes

439 **Plastic Stress-Strain Relationships—Further Experiments on the Effect of Loading History** (61—APM-24)
J. Parker and J. Kettlewell

447 **On the Dynamic Behavior of a Frank-Read Source** (60—WA-204)
J. D. Campbell, J. A. Simmons, and J. E. Dorn

(Continued on inside back cover)

John Moyes Lessells 1888-1961

JOHN MOYES LESSELLS was born on February 5, 1888, in Dunfermline, a town situated some fourteen miles northwest of Edinburgh, Scotland. He carried the lowland Scot's burr in his language and the Celtic red hair throughout his life. He died of a heart attack on May 17, 1961, in Boston, Mass. One of the most prominent members of The American Society of Mechanical Engineers, his death is mourned by a host of friends, in the Society and out of it, who will miss his cheerful laughter and helping hand.

John Lessells became a mechanical engineer in typical British fashion. At the end of his elementary schooling in 1904 he became an apprentice in Dunfermline, his apprenticeship lasting for six years. During these six years he was a student at the Lauder Technical School in Dunfermline. At the end of this period he went to the Heriot-Watt College in Edinburgh from 1911 to 1912. Here he received a Lauder (Carnegie) Scholarship in 1912 and proceeded into the University of Glasgow from which he was graduated with a BS in Engineering in 1915. A mature man of twenty-seven, with eleven years of industrial experience and continual technical education, he entered the war effort by becoming an Inspector of Aircraft Materials for the British War Office. This service he carried out at the Whitworth Company, Ltd., in Newcastle-on-Tyne, and the Rolls-Royce Company, Ltd., in Derby. He later served as a special engineer for the Rolls-Royce Company at Derby until 1919.

During World War I he married Gladys Jackson on April 5, 1917. The couple had no children. The marriage was a happy one, as all who enjoyed merry hospitality in their home can attest. Mrs. Lessells will sorely miss his cheerful companionship in the years to come.

It was during the war years that Lessells started on his lifelong interest in the strength and endurance properties of metals. His personal contributions to mechanics were all in this field.

The "bottom dropped out" in Britain after World War I, so John and wife came to the United States in 1920 and became naturalized citizens of this country in 1930. He was employed by the Westinghouse Electric and Manufacturing Company in East Pittsburgh, Pa., starting his career in the office of George M. Eaton, Chief Mechanical Engineer. The meeting of these two men held far-reaching consequences for the development of applied mechanics in this country. Mr. Eaton felt that a deeper study of material properties was needed than it was getting in the Company's "busting laboratories." Through his influence, a division for mechanics was started in 1920 as part of the Westinghouse Research Laboratory, and John Lessells was installed, in that year, as its first manager. Started in 1920 with a single tensile testing machine and very few employees, this department exploded rapidly into one of the great world centers for the study of materials and vibration problems. In its forty-one years of existence this division has had only two managers. R. E. Peterson succeeded him as manager in 1931.

In 1922 Stephen P. Timoshenko became a member of the Mechanics Division in the Westinghouse Research Laboratory, where he remained for five years before going to The University of Michigan. The magnitude of the impulse that Ti-

John Moyes Lessells

moshenko gave to theoretical mechanics in the United States cannot be overestimated. The combination of Lessells and Timoshenko was highly important in this development.

In 1925 the Westinghouse Technical Night School Press issued a volume entitled "Applied Mechanics" by Timoshenko and Lessells. This was the first of the long series of brilliant works on mechanics published in English by Timoshenko. Lessells wrote the second part of this book in which his favorite subject of metal properties was treated. "Applied Mechanics" started an epoch in mechanics in this country and has long since become a collector's item. The book was promptly translated into German by I. Malken and was published by Springer in Berlin in 1928. George Eaton, Stephen Timoshenko, and John Lessells were prominent among the founders of the Applied Mechanics Division of the ASME in 1927.

John Lessells was made Manager of Engineering of the Steam Turbine Division of the Westinghouse Company at South Philadelphia in 1931. He held this position during the difficult depression years until 1935. In 1935 he became an independent consulting engineer. In the same year the Publications Committee of the ASME authorized the issue of the JOURNAL OF APPLIED MECHANICS as a separate quarterly publication in the Society's *Transactions*. John Lessells was made Technical Editor of the JOURNAL and continued in that capacity from 1935 until 1956. He made a brilliant success of the twenty-one years of continuous and exacting contact with the sensitive writers of the technical papers which appeared in the JOURNAL. This was a labor of love with no monetary compensation. Under his editorship the JOURNAL achieved worldwide renown. Since retiring from active editing, he carried the title of Honorary Technical Editor of the JOURNAL OF APPLIED MECHANICS.

John Lessells joined the ASME in 1923. In 1952 he was made a Fellow in the Society. In the same year he also became an honorary member of the ASME with the citation "..for outstanding contributions to the development of applied mechanics within The American Society of Mechanical Engineers..and for his initiative and vision during the early days of the Division of Applied Mechanics, for his steadfastness of purpose in supporting it throughout the years, and for his long years of service in maintaining the high standards of the JOURNAL OF APPLIED MECHANICS."

One of the founders of the Applied Mechanics Division, he served a term as its Chairman. He was a member of the Professional Divisions Committee for four years and served as its Chairman for one year.

John Lessells was also a member of the Society of Automotive Engineers, the American Society for Testing Materials, The Institution of Mechanical Engineers (London) which gave him its Bernard Hall Prize in 1926, the Iron and Steel Institute (London), and the Franklin Institute which gave him its Levy Medal in 1941. He was also a Fellow of the Academy of Arts and Sciences.

He was an Associate Professor of Mechanical Engineering at the Massachusetts Institute of Technology from 1936 until 1953. While he was teaching at the Institute he formed the consulting engineering firm known as Lessells and Associates, Inc., in 1946. Just prior to his death he had resigned from the Presidency of the Company and had become Chairman of the Board.

In 1938 he edited the "Stephen Timoshenko 60th Anniversary Volume" which was published by The Macmillan Company.

In 1953 he edited a group of papers selected from the JOURNAL OF APPLIED MECHANICS entitled "Design Data and Methods; Applied Mechanics" which was published by the Applied Mechanics Division of the ASME.

His well-known treatise on "Strength and Resistance of Metals" appeared in 1954. In this he summed up his lifelong experience in his chosen field. He also was the author of many technical papers on the testing of the properties of metals.

What a varied career! Engineer, company executive, author, editor, educator, and exceedingly valuable member of technical societies! Varied, but unified around a single objective—the application of mechanics to actual problems.

John Lessells was a gentle man, well-read—in many fields outside of engineering—and an ardent golfer. He held memberships in country clubs in Pittsburgh, in Swarthmore, and, at the time of his death, was a member of the Braeburn Country Club near Boston.

John had too strong a sense of humor to be a good "organization man." Often at the end of some interminable and chaotic meeting, so typical in organizations in the wake of technical troubles, he bemoaned the fact that he lacked the ability of a Rabelais to record the satire and humor of the situation. His "vignettes of life" drawn from his own experience were wildly hilarious, and John enjoyed his own stories so thoroughly that his auditors experienced a double joy in hearing them.

In the renaissance of mechanics which has occurred in the past forty years in this country, John Lessells played the role of a powerful catalytic agent. Everywhere he went he surrounded himself with enthusiastic, creative young talent. To those who worked for him he was known as the boss who provided "negative damping."

The Society meetings will miss his booming laughter, his twinkling blue eyes, and his sage advice. His personal friends will remember his unfailing good nature and his generosity as two of his outstanding characteristics. When they meet, they will remember him with affection and will repeat his favorite toast: "Here's tae us; wha's like us."

—*Prof. J. Ormondroyd.*

Investigation of Flat-Plate Hypersonic, Turbulent Boundary Layers With Heat Transfer[1]

EVA M. WINKLER
Chief,
High-Temperature Aerodynamics Group,
Aerophysics Division,
U. S. Naval Ordnance Laboratory,
Silver Spring, Md.

Naturally turbulent boundary layers on a cooled flat plate have been investigated at several distances from the leading edge of the plate at a Mach number of 5.2 for three rates of steady-state heat transfer to the surface. Measurements of Pitot and static pressures and of total and wall temperatures made it possible to compute velocity profiles, static-temperature profiles, and boundary-layer parameters without resorting to assumptions. The data demonstrate that the Reynolds analogy between skin friction and heat transfer is valid for all conditions of the present experiments. With increasing rate of heat transfer to the surface, the skin-friction coefficient was found to decrease, a phenomenon opposite to that predicted by theories and empirical relations. On the basis of the present data and other published results of compressible and incompressible turbulent boundary-layer skin friction, a simple relation was devised which describes closely the variation of the skin-friction coefficient with Mach number, heat-transfer rate, and momentum-thickness Reynolds number.

THE present study was stimulated by both practical and academic reasons. The designer of supersonic and hypersonic vehicles wants to know with increasing accuracy the value of skin friction and its variation with Mach number, Reynolds number, and heat-transfer rate. The academic interest aims, of course, toward a general understanding of the mechanisms in turbulent boundary layers which could, in turn, lead to an adequate theoretical analysis of the problem. So far, none of the theoretical treatments is sufficiently adequate to give confidence in theoretical predictions beyond the range where experimental data are available.

The purposes of the investigation were:

(*a*) To extend the range of heat-transfer conditions for which experimental turbulent boundary-layer data are available.

(*b*) To check the relationship between turbulent boundary-layer skin-friction and heat-transfer coefficients; i.e., the Reynolds analogy.

(*c*) To supply sufficiently detailed data of the boundary-layer characteristics for comparison with theories.

[1] This investigation was jointly sponsored by the U. S. Bureau of Naval Weapons and the U. S. Air Force. A more detailed account of the work has been published as NOL NAVORD Report 6631 under the co-authorship of Moon H. Chr, who participated in the experimental program and in part of the data analysis.

Contributed by the Applied Mechanics Division and presented at the Winter Annual Meeting, New York, N. Y., November 27–December 2, 1960, of THE AMERICAN SOCIETY OF MECHANICAL ENGINEERS.

Discussion of this paper should be addressed to the Editorial Department, ASME, United Engineering Center, 345 East 47th Street, New York 17, N. Y., and will be accepted until October 10, 1961. Discussion received after the closing date will be returned.

Manuscript received by ASME Applied Mechanics Division, July 19, 1960. Paper No. 60—WA-205.

Nomenclature

c_f = local skin-friction coefficient based on free-stream conditions, $2\tau_w/\rho_\infty u_\infty^2$
c_{f_i} = incompressible local skin-friction coefficient for zero heat transfer based on free-stream conditions
c_p = specific heat at constant pressure
H = boundary-layer shape parameter, δ^*/θ
k = thermal conductivity
M = Mach number
n^{-1} = velocity-profile exponent
p = static pressure
p_0 = supply air pressure
p_0' = pitot pressure
Re = Reynolds number based on free-stream conditions
St = Stanton number based on free-stream conditions, $k(dT/dy)/(T_r - T_w)c_p\rho_\infty u_\infty$
T = local static temperature
T' = reference temperature, defined in Appendix
T_c = coolant temperature
T_0 = stagnation temperature
u = velocity
u' = fluctuating velocity component parallel to wall
x = leading-edge distance
y = distance perpendicular to wall
δ = total boundary-layer thickness
δ^* = boundary-layer displacement thickness
θ = boundary-layer momentum thickness
ν = kinematic viscosity
ρ = density
τ = shear stress

Subscripts

e = equilibrium value for zero heat transfer
L = edge of laminar sublayer
T = temperature profile
u = velocity profile
w = values based on wall conditions
x = leading-edge distance
θ = values based on boundary-layer momentum thickness
∞ = values based on free-stream conditions outside boundary layer

Experimental Equipment and Techniques

The experiments were performed in the NOL Hypersonic Tunnel No. 4 on an internally instrumented and cooled, impermeable-wall flat plate at a free-stream Mach number of 5.2. The instrumentation provided for the measurement of wall pressures and wall heat-transfer rates at several stations from the leading edge of the plate. The wall heat-transfer rates and the plate surface temperatures at the boundary-layer survey stations were obtained from temperature measurements in the plate wall. At each station five thermocouples were installed at various distances from the surface of the plate following a previously adopted technique [1].[2,3]

The plate was attached to the tunnel side walls with the tunnel center line lying along the testing surface. The arrangement is shown in Fig. 1. The boundary layer was surveyed with Pitot and total-temperature probes. Both types of probes had nearly rectangular entrance openings of half-heights between 0.010 and 0.013 cm. The design of the total-temperature probes followed, in principle, that of reference [2]. The probes were mounted in a microtraverse mechanism which has a positioning accuracy of ±0.0013 cm. The point of wall contact of the probes needed to evaluate absolute wall distances was established with a vacuum-tube ohmmeter. Pressures above 35 mm Hg were read with an absolute mercury manometer which has a reading accuracy of ±0.1 mm Hg. For pressures below 35 mm Hg a silicon-oil manometer [3] was used; its reading accuracy is ±0.001 mm Hg. The total temperatures were recorded on Brown recorders of appropriate range to give an accuracy of the individual reading of ±0.5 deg C.

[2] With this technique, the thermocouples were embedded in separate plugs which were ground to fit appropriate holes in the plate wall. Because of practical reasons, the holes were not cut through but terminated 0.16 cm below the plate surface.

[3] Numbers in brackets designate References at end of paper.

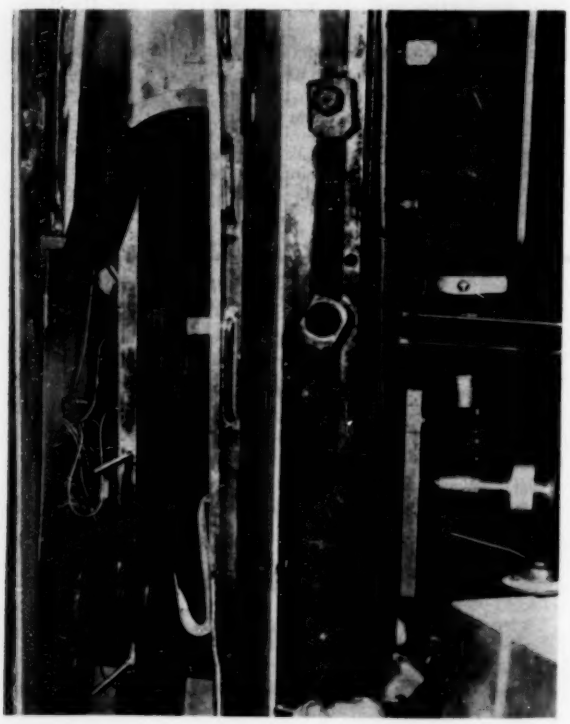

Fig. 1 Test arrangement in hypersonic tunnel

For the heat-transfer data, two kinds of temperature measurements were made. At each station readings of the five absolute temperatures were alternated with those of the differences between them. The temperatures were measured with a Leeds & Northrup K-2-type potentiometer as a function of time to insure that the data refer to truly steady-state conditions. The reading accuracy of these data is ±0.01 deg C.

For each of the conditions of the test program, the wall static pressures and the wall temperatures were recorded for all instrumented stations. These measurements showed that the static pressure along the plate was constant within 1.3 per cent, and that the plate surface was practically isothermal for leading-edge distances of $x > 14$ cm. For $x < 14$ cm, the surface temperature deviated from the isothermal value by amounts dependent on the test conditions; for the highest heat-transfer conditions of the present tests ($p_0 \simeq 7$ atm, $T_0 \simeq 490$ K, and $T_w/T_0 \simeq 0.56$) the deviation was about 10 per cent.

Data-Reduction Procedure

The data reduction followed the conventional procedure leading to the following quantities: M, u, T, δ^*, θ, τ_w, n, T_s, and St_∞. The Mach-number distribution was evaluated from the measured Pitot and static pressures, assuming the latter constant across the boundary layer, and making use of the compressible flow tables of [4]. Then the measured temperature data were reduced to stagnation and static temperatures by reference to the probe-calibration curve and the computed Mach-number profile.[4]

The displacement thickness δ^* and the momentum thickness θ were obtained by graphical integration of the mass-flow and momentum-flux deficiencies within the boundary layer. The shear stress τ_w was evaluated from the slope $(du/dy)_w$ of the velocity profile at the wall. The equilibrium wall temperature for zero heat transfer T_s was computed using $Pr^{1/3}$ as the value of the recovery factor.

The flat-plate wall temperature gradients were evaluated from the recorded temperature data after steady-state conditions had been reached. Since the temperature showed a linear variation with distance from the surface, it was possible to extrapolate to the surface to determine T_w. Accounting for the positioning accuracy of the center of the thermocouple junctions in the plate, and the repeatability of the temperature readings, the wall temperature gradients could be determined within ±3 per cent. From the gradient and the known conductivity of the plate material[5] the wall heat transfer and, eventually, the Stanton number St_∞ were computed. Colburn's version of Reynolds' analogy ($c_f = 2\,St_\infty Pr^{2/3}$) was used to compute the skin-friction coefficient from the Stanton number.

Results

Boundary-Layer Profiles. Naturally turbulent boundary layers were investigated on a smooth flat plate at a Mach number of 5.2 and for three different conditions of heat transfer to the plate, namely, $T_w/T_0 \simeq 0.85$, 0.76, and 0.60. The tests were conducted at free-stream conditions for which transition was observed to occur about 17 cm from the leading edge of the plate where $Re_x \sim 2.2 \times 10^6$. The boundary layers were then surveyed and the wall heat transfer was measured at four stations downstream of the transition region; i.e., at $x = 21.6$ cm, 29.25 cm, 36.85 cm, and 44.5 cm. The rate of heat transfer to the plate was controlled by the supply-air temperature and by the temperature of

[4] In some cases, the wall distances at which temperature measurements were made in the boundary layer are not the same as those where pressure data were obtained. Then the temperature data were interpolated for the positions at which the pressure measurements were obtained.

[5] Measured by the National Bureau of Standards using a sample from the plate stock [5].

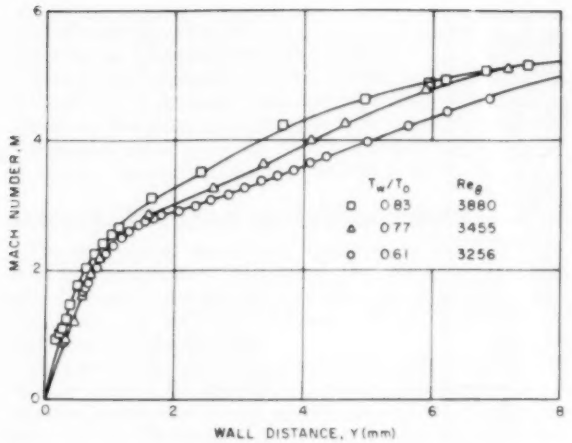

Fig. 2 Mach-number variation across boundary layer, $M_\infty = 5.2$

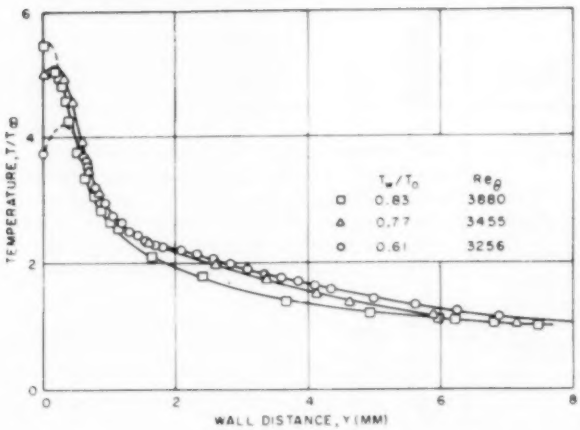

Fig. 3 Temperature variation across boundary layer, $M_\infty = 5.2$

the coolant circulated through the plate. Table 1 gives a summary of the test conditions and evaluated boundary-layer parameters. The data in this table are separated into three groups, each corresponding to a different mean value of T_w/T_0. Some sample graphical presentations of the boundary-layer profiles are shown in Figs. 2, 3, and 4, which give the Mach-number profiles and the temperature and velocity distributions in terms of the nondimensional quantities T/T_∞ and u/u_∞ versus y.

In general, all the profiles show the same characteristics; namely, a laminar sublayer followed by a buffer layer and a fully turbulent outer layer. Close examination of the experimental points nearest to the wall, Figs. 2 and 4, shows that they deviate from the distribution expected in a laminar layer. This may result from wall-probe interference or the effects of the turbulent velocity fluctuations u' on the Pitot pressure readings. Because of the fluctuating component u', the measured Pitot pressure is always somewhat greater than the effective total pressure by the amount $\frac{1}{2}\rho\overline{u'^2}$. Close to the wall the corrections for the latter, using the data of references [6 and 7], can amount to as much as 11 or 12 per cent.

Skin-Friction, Heat-Transfer Coefficients, and Reynolds' Analogy. The variation of the skin-friction coefficients with momentum-thickness Reynolds number is shown in Fig. 5 [31]. The figure shows the skin-friction values computed from the velocity-profile slopes and from the measurements of wall heat transfer, using

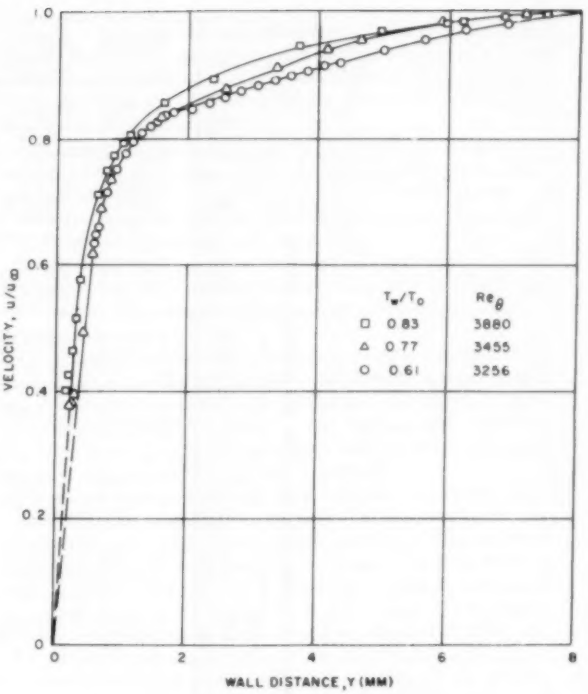

Fig. 4 Velocity variation across boundary layer, $M_\infty = 5.2$

Colburn's version of Reynolds' analogy. The two sets of data agree in most cases within ±4 per cent. Because of this close agreement and the fact that the discrepancies between the heat-transfer and velocity-profile data do not appear to be of a systematic nature but rather representative of experimental errors, it is concluded that Colburn's version of Reynolds' analogy is valid for the present test conditions. A determination of c_f from the increase in momentum-flux deficiency could not be made because the conditions for tests performed at different leading-edge distances were not kept sufficiently constant, Table 1. As a consequence, the increase of θ with x, as given in Table 1, cannot be considered representative of the variation of c_f along the plate for constant ambient conditions and a constant wall heat-transfer rate.

As shown by the three sets of data, the skin-friction coefficient decreases with increasing momentum-thickness Reynolds number; for a given value of Re_θ, c_f decreases with increasing rate of heat transfer to the plate (the highest heat-transfer rate corresponds to the lowest T_w/T_0 ratio).

Discussion of Data

In general, the present data of the skin-friction coefficient, its variation with momentum-thickness Reynolds number and with heat-transfer rate to the wall support previously reported results [1] which were evaluated from surveys of the turbulent boundary layers at the wall of a wedge nozzle. However, the shapes of some of the profiles obtained during the present investigation deviate from that believed to be characteristic for fully turbulent boundary layers. Also, in the u^+, y^+-representation, the profiles in question do not show the upward trend with increasing Reynolds number Re_θ, and heat-transfer parameter $(T_s - T_w)/T_s$ that is exhibited by the other profiles. It is surmised that these profiles are not fully turbulent but only highly transitional. The speculation is supported by the comparatively low values of Re_θ

Table 1 Summary of experimental data and comparison with skin-friction coefficients computed from theoretical and empirical relations

									EXPERIMENT			THEORY										
x	M_∞	P_o	δ	δ^*	θ	n	$Re_x \times 10^{-6}$	R_{e_θ}	$C_f \times 10^4$	$C_f \times 10^4$	$\frac{C_f}{C_{f_1}}$	$C_f \times 10^4$	$C_f \times 10^4$	$C_f \times 10^4$	$C_f \times 10^4$	$C_f \times 10^4$	$St_\infty \times 10^4$	$\frac{T_e - T_w}{T_e}$	$\frac{U_\delta}{U_\infty}$	$\left(\frac{\delta_1}{\delta}\right)_\delta$	$\left(\frac{\delta_1}{\delta}\right)_1$	$u_\delta^+ = y_\delta^+$
in.		Atm	in.	in.	in.				*	**	***	(1)	(2)	(3)	(4)	(5)						
216	5.21	7.11	4.5	1.66	0.166	9.9	2.72	2,099	14.65	14.87	0.408	13.93	16.32	12.70	10.20	12.50	9.37	0.126	0.793	0.0904	0.202	12.90
216	5.14	7.08	4.8	1.57	0.189	10.0	3.36	2,936	13.89	—	0.413	—	—	—	—	—	—	0.044	0.780	0.0775	0.144	12.60
292.5	5.20	7.21	6.4	2.46	0.228	9.3	4.07	3,173	14.32	13.48	0.434	12.69	14.62	11.53	9.33	11.30	8.58	0.084	0.750	0.0585	0.102	12.10
368.5	5.26	7.31	6.6	2.86	0.284	8.2	5.04	3,880	13.46	13.43	0.423	12.06	13.32	10.95	9.08	10.71	8.47	0.062	0.705	0.0589	0.108	11.65
445	5.29	7.09	8.0	4.00	0.322	7.0	5.94	4,300	13.08	12.76	0.419	11.62	12.52	10.53	8.81	10.29	8.04	0.078	0.655	0.0482	0.0875	10.88
216	4.98	5.42	5.2	1.96	0.179	9.7	2.29	1,900	13.35	13.48	0.365	15.17	17.86	14.01	11.31	13.77	8.53	0.183	0.778	0.0875	0.154	14.20
216	5.18	7.01	4.6	1.55	0.149	11.2	2.56	1,782	16.06	—	0.433	14.51	17.24	13.39	10.79	13.15	—	0.189	0.800	0.0794	0.146	13.00
292.5	5.20	7.05	7.3	2.51	0.227	9.9	3.61	2,960	12.48	11.65	0.373	13.55	14.92	12.25	10.10	11.98	7.35	0.179	0.760	0.0575	0.090	13.90
368.5	5.24	6.99	7.4	3.22	0.280	8.0	4.55	3,455	11.51	11.70	0.354	12.64	14.02	11.56	9.62	11.32	7.38	0.156	0.703	0.0612	0.122	13.20
445	5.24	6.55	7.7	3.88	0.330	6.7	5.11	3,790	—	10.63	0.332	12.14	12.98	11.18	9.37	10.92	6.71	0.163	0—	—	—	—
216	5.17	6.77	2.6	1.22	0.114	6.9	2.01	1,055	14.70	15.47	0.352	15.90	21.60	15.02	12.18	14.74	9.68	0.331	0.757	0.152	0.189	14.20
292.5	5.16	6.71	4.8	2.05	0.188	9.5	2.57	1,652	13.23	13.35	0.352	15.35	19.04	14.58	12.03	14.22	8.35	0.360	0.765	0.0928	0.150	15.50
292.5	5.10	6.84	5.3	1.93	0.186	10.3	2.73	1,735	13.35	—	0.359	—	—	—	—	—	—	0.370	0.780	0.0775	0.114	15.90
368.5	5.11	7.20	7.0	2.84	0.281	9.8	3.27	2,488	12.36	12.79	0.356	14.84	17.74	14.19	11.95	13.80	7.99	0.384	0.760	0.0631	0.114	16.30
368.5	5.20	7.51	6.7	2.78	0.256	9.1	3.57	2,482	12.03	—	0.348	—	—	—	—	—	—	0.357	0.750	0.0666	0.114	15.80
445	5.12	7.00	8.8	3.74	0.343	8.7	4.22	3,256	10.54	10.75	0.320	13.94	16.42	13.14	11.16	12.78	6.72	0.340	0.710	0.0558	0.108	15.90

Note: Unless specified otherwise, all fluid properties involved in the Reynolds numbers and skin friction coefficients are evaluated at the edge of the boundary layer.

* obtained from the velocity profile slope at the wall

** obtained from heat transfer measurements in flat plate

*** C_{f_1} obtained from Karman-Schoenherr equation for zero heat transfer

(1) Van Driest, ref. (15)

(2) Persh ref. (8)

(3) Colburn } ref. (16)

(4) Nikuradse }

(5) Schultz-Grunow }

(≤ 2000) and the values of δ, δ^*, and θ as compared to those obtained for the surveys for which $Re_\theta > 2000$.

As far as n is concerned, when $Re_\theta > 2000$, the boundary layers indicate that n decreases with increasing Re_θ. This trend is opposite to that deduced in [8] on the basis of predominantly incompressible data. However, the compressible data, references [1, 9–14], do not support a unique relationship between n and Re_θ.

Comparison With Theory and Empirical Relations

The experimental skin-friction data were compared with the theoretical predictions of Van Driest [15], Persh [8], and with some frequently used empirical relations [16] proposed by Colburn, Nikuradse, and Schultz-Grunow. The pertinent relations used are given in the Appendix.

To compute the skin-friction coefficients according to [15], use was made of the charts of [17] with a certain amount of graphical interpolation for the specific values of M_∞, T_w/T_0, and Re_x encountered in the experimental data. It has been estimated that the errors introduced by this procedure are not greater than $\pm$ 1.5 per cent. In computing the skin-friction coefficients by the method of reference [8], the experimental values of M_∞, Re_θ, $(T_w - T_e)/T_e$, and n were used.

In applying the empirical relations of Colburn, Nikuradse, and Schultz-Grunow, the property values were evaluated at a reference temperature T' according to Rubesin and Johnson [18] (see Appendix).

The comparison of the various computed skin-friction values and the experimental data is given in Table 1 and Fig. 5.

In general, none of the theoretical or empirical relations was found capable of predicting the skin-friction coefficients with equal accuracy for the entire range of the test conditions. Rather, each of the methods appears to agree best in a different limited range of T_w/T_0. For small heat-transfer rates ($T_w/T_0 \sim 0.85$) Persh's relation gives very good agreement in the higher range of Reynolds numbers ($Re_\theta > 3000$). The agreement becomes less favorable as T_w/T_0 decreases. At $T_w/T_0 \sim 0.6$ the predicted values are too large by as much as 54 per cent.

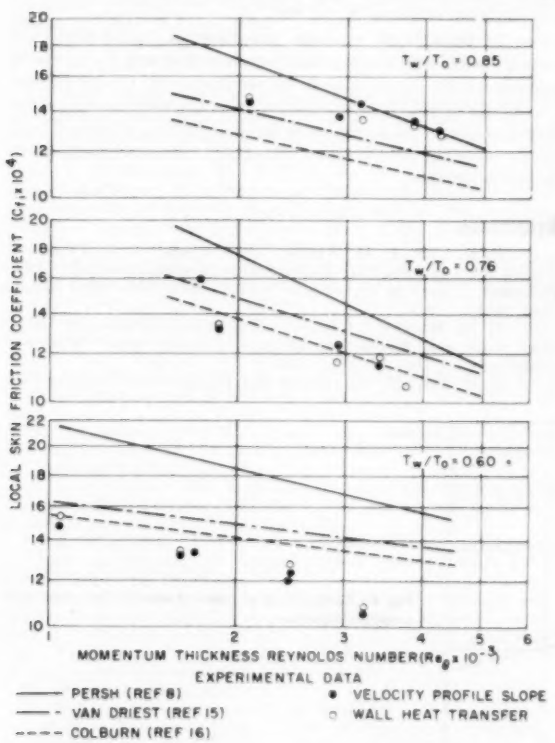

Fig. 5 Variation of skin-friction coefficient with momentum-thickness Reynolds number

Van Driest's relation underestimates the skin friction at low heat-transfer rates but gives fairly close agreement (within 11 per cent) at moderate heat-transfer rates; i.e., $T_w/T_0 \sim 0.76$. It overestimates the skin friction for higher rates of heat transfer ($T_w/T_0 \sim 0.6$) by as much as 34 per cent.

The same is true, more or less, for the empirical relations. Among them the combination of the Schultz-Grunow scheme and the reference temperature appears to give the best fit to the experimental data obtained for $T_w/T_0 \sim 0.6$.

Each of the theoretical and empirical relations considered here predicts that the skin-friction coefficient increases with increasing rate of heat transfer to the wall for a given value of the momentum-thickness Reynolds number. The experimental data support the opposite trend; i.e., for a given value of Re_θ, c_f decreases with increasing rate of heat transfer to the wall.

The discrepancy between the empirical and theoretical skin-friction relations and the experimental results is actually not surprising in view of the assumptions made in applying the foregoing relations. With the empirical relations the T'-method is used which was developed for laminar flow. Sommer and Short [19] adjust one numerical constant in the original T'-relation to fit their zero heat-transfer data at a Mach number of 3.82. By doing so, they obtain excellent agreement for all zero heat-transfer data for $M > 2.82$ (but depart from a good fit for $M < 2.5$). This procedure, however, improves only slightly the agreement between predicted and measured c_f for other than zero heat transfer. In general, the predicted values are too high. This, of course, raises the question of the compatibility of the T'-equation in the present form to account for the effect of heat transfer and Mach number.

For the theoretical predictions, the situation is more difficult to analyze. This is because of the various assumptions or approximations introduced into the boundary-layer equations. It is believed that the presently available experimental data will be of some assistance in evaluating the correctness of some of these assumptions. Such an analysis is currently being performed at NOL and may stimulate revisions leading to a better comparison between data and prediction over the entire range where experimental data exist. However, without a basic understanding of the momentum and energy-transfer mechanisms in a turbulent boundary layer, such a revised formulation may again be subject to lack of confidence when applied to conditions where no experimental check points are available.

New Empirical Skin-Friction Relations

The present skin-friction data were also compared with other experimental results [1, 9, 10, 20–27]. These references comprise all available published data for which Re_θ and T_e/T_w could be evaluated directly from measurements. The comparison covers data for the following ranges of conditions:

$$\left.\begin{aligned} 2.43 &\leq M \leq 9 \\ 0.60 &\leq T_e/T_w \leq 2.0 \\ 880 &\leq Re_\theta \leq 14{,}000 \end{aligned}\right\} \text{compressible data}$$

$$\left.\begin{aligned} 400 &\leq Re_\theta \leq 9000 \\ T_e/T_w &= 1 \end{aligned}\right\} \text{incompressible data}$$

Using the incompressible data of references [24–27], the following relation between skin-friction coefficient and momentum-thick-

ness Reynolds number was evaluated using the method of least squares:

$$c_{f_i} = 0.0246 \mathrm{Re}_\theta^{-0.251} \quad (1)$$

Fig. 6 shows this relation in comparison to the data; the maximum deviation is ±5 per cent. The compressible data [1, 9, 10, 20–23] indicate definite trends of the c_f-variation with Mach number and heat-transfer rate which suggested that the compressible skin-friction coefficient for any heat-transfer condition should reduce to an incompressible zero heat-transfer equivalent by multiplying the compressible value by $(T_0/T_\infty)^{1/2}(T_e/T_w)^{1/4}$. The results of such a reduction are shown in Fig. 7 together with the empirical relation evaluated from incompressible data. Equation (1) represents the reduced compressible data within ±12 per cent.[6]

[6] Since the completion of the present analysis, additional compressible skin-friction data became available [32]. In the reduced form, they are represented by equation (1) within 12 per cent.

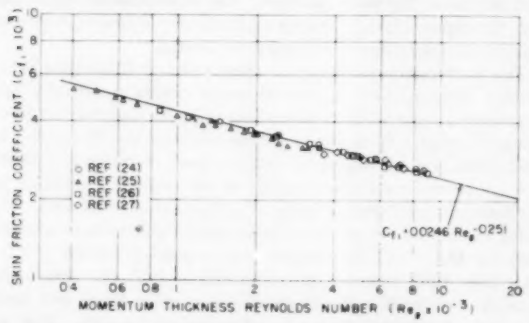

Fig. 6 Variation of incompressible skin-friction coefficient with momentum-thickness Reynolds number

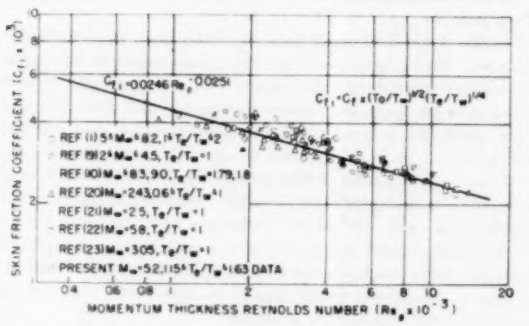
SKIN FRICTION COEFFICIENT (C_f, x 10^{-3})
C_{f_i}=.0246 $Re_\theta^{-.025}$
C_{f_i}=C_f x $(T_0/T_\infty)^{1/2}(T_e/T_w)^{1/4}$
REF (1) $5^1 M_\infty$=8.2, T_0/T_∞=2
REF (9) $2^4 M_\infty$=4.5, T_0/T_∞=1
REF (10) M_∞=8.3, 9.0, T_0/T_∞=1.79, 1.8
REF (20) M_∞=2.43, 3.06 T_0/T_∞=1
REF (21) M_∞=2.5, T_0/T_∞=1
REF (22) M_∞=5.8, T_0/T_∞=1
REF (23) M_∞=3.05, T_0/T_∞=1
PRESENT M_∞=5.2, $11^5 T_0/T_\infty$=1.63 DATA
MOMENTUM THICKNESS REYNOLDS NUMBER (Re_θ x 10^{-3})

Fig. 7 Variation of reduced skin-friction coefficient with momentum-thickness Reynolds number

The reduced compressible data were also compared with three other frequently used incompressible skin-friction relations; namely, those of Karman-Schoenherr [28], Colburn [29], and Coles [30], as shown in Fig. 8. Within the range of the experimental incompressible data, the foregoing three relations agree with equation (1) within about ±10 per cent. In comparison with these empirical formulations and the theoretical relations discussed previously, the advantage of the present method, i.e., equation (1) in combination with the reduction factor $(T_0/T_\infty)^{1/2}(T_e/T_w)^{1/4}$, is its simplicity and accuracy in the calculation of skin-friction coefficients for engineering purposes.

Summary

Detailed investigations of the turbulent boundary-layer velocity and temperature profiles have been made on a flat plate at a Mach number of 5.2 and for three rates of surface heat transfer. Simultaneously with the boundary-layer surveys, wall heat-transfer measurements were made.

The present experimental results confirm data previously obtained on the wall of a wedge nozzle [1]. The data support the applicability of Reynolds' analogy for turbulent boundary layers in hypersonic flow. Values of skin-friction coefficients calculated from the heat-transfer measurements by using Colburn's version of Reynolds' analogy agree (for most cases, within 4 per cent) with the skin-friction values deduced from the velocity-profile slope.

The decrease in the value of the skin-friction coefficient with increasing momentum-thickness Reynolds number is consistent with the predictions and data reported in other publications.

The experimental data show that for a fixed value of the momentum-thickness Reynolds number the skin-friction coefficient decreases with increasing rate of heat transfer to the flat plate. This behavior is opposite to that predicted by theories and empirical relations [8, 15, 16].

On the basis of all available experimental compressible and incompressible skin-friction data for which Re_θ and T_e/T_w can be evaluated from measurements (references [1, 9, 10, 20–27] and the present results), a new simple relation has been devised which describes closely the variation of the skin-friction coefficient with Mach number, heat-transfer rate, and momentum-thickness Reynolds number.

References

1 R. K. Lobb, E. M. Winkler, and J. Persh, "NOL Hypersonic Tunnel No. 4 Results, VII: Experimental Investigation of Turbulent Boundary Layers in Hypersonic Flow," NOL NAVORD Report 3880, March, 1955.

2 E. M. Winkler, "Stagnation Temperature Probes for Use at High Supersonic Speeds and Elevated Temperatures," NOL NAVORD Report 3834, October, 1954.

3 J. M. Kendall, "Equipment and Techniques for Making Pres-

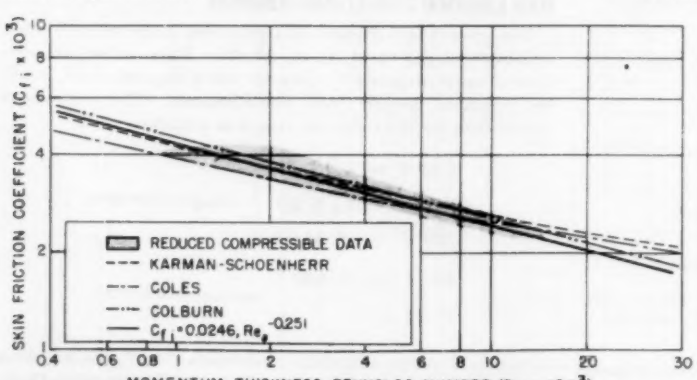

Fig. 8 Comparison of reduced skin-friction data with empirical relation

sure Measurements in Supersonic Wind Tunnels at Mach Numbers Up to 5," NOL NAVORD Report 2580, August, 1952.

4 Ames Research Staff, "Equations, Tables, and Charts for Compressible Flow," NACA Report 1135, 1953.

5 L. E. Richards and H. E. Robinson, "Thermal Conductivity of a Specimen of Stainless Steel Type 302," NBS Report 4132, June, 1955.

6 J. Laufer, "Investigation of Turbulent Flow in a Two-Dimensional Channel," NACA Report 1053, 1951.

7 J. Laufer, "The Structure of Turbulence in Fully Developed Pipe Flow," NACA TN 2954, 1954.

8 J. Persh, "A Theoretical Investigation of Turbulent Boundary Layer Flow With Heat Transfer at Supersonic and Hypersonic Speeds," NOL NAVORD Report 3854, May, 1955.

9 D. Coles, "Measurements in the Boundary Layer on a Smooth Flat Plate In Supersonic Flow, III. Measurements in a Flat-Plate Boundary Layer at the Jet Propulsion Laboratory," JPL-CIT Report No. 20-71, June, 1953.

10 F. K. Hill, "Boundary Layer Measurements in Hypersonic Flow," *Journal of the Aeronautical Sciences*, vol. 23, 1956, p. 35.

11 R. M. O'Donnell, "Experimental Investigation at a Mach Number of 2.41 of Average Skin-Friction Coefficients and Velocity Profiles for Laminar and Turbulent Boundary Layers and an Assessment of Probe Effects," NACA TN 3122, January, 1954.

12 W. D. Bradfield, D. G. DeCoursin, and C. B. Blumer, "Characteristics of Laminar and Turbulent Boundary Layer at Supersonic Velocity," University of Minnesota Research Report No. 83, July, 1952.

13 I. D. V. Faro, "Boundary Layer Measurements in Hypersonic Flow," paper presented at the Third U. S. Navy Symposium on Aeroballistics, Laurel, Md., October, 1954.

14 R. E. Wilson, "Turbulent Boundary Layer Characteristics at Supersonic Speeds—Theory and Experiment," *Journal of the Aeronautical Sciences*, vol. 17, 1950, p. 585.

15 E. R. Van Driest, "The Turbulent Boundary Layer With Variable Prandtl Number," North American Aviation, Inc., Report No. AL-1914, April, 1954.

16 H. Schlichting, "Boundary Layer Theory," McGraw-Hill Book Company, Inc., New York, N. Y., 1955, pp. 440–441.

17 D. B. Lee and M. A. Faget, "Charts Adapted From Van Driest's Turbulent Flat-Plate Theory for Determining Values of Turbulent Aerodynamic Friction and Heat-Transfer Coefficients," NACA TN 3811, October, 1956.

18 M. W. Rubesin and H. A. Johnson, "A Critical Review of Skin-Friction and Heat-Transfer Solutions of a Flat Plate," TRANS. ASME, vol. 71, 1949, p. 383.

19 S. C. Sommer and B. J. Short, "Free-Flight Measurements of Turbulent Boundary Layer Skin Friction in the Presence of Severe Aerodynamic Heating at Mach Numbers From 2.8 to 7.0," NACA TN 3391, March, 1955.

20 R. J. Monaghan and J. R. Cooke, "The Measurement of Heat-Transfer and Skin-Friction at Supersonic Speeds, Part III: Measurements of Over-All Heat-Transfer and of the Associated Boundary Layers on a Flat Plate at M = 2.43," RAE Technical Note Aerodynamics 2125, March, 1954.

21 M. W. Rubesin, R. C. Maydew, and S. A. Varga, "An Analytical and Experimental Investigation of the Turbulent Boundary Layer on a Flat Plate at Supersonic Speeds," NACA TN 2305, 1951.

22 R. H. Korkegi, "Transition Studies and Skin-Friction Measurements on an Insulated Flat Plate at a Hypersonic Mach Number," GALCIT Memorandum No. 17, 1954.

23 P. F. Brinich and N. S. Diaconis, "Boundary Layer Development and Skin Friction at Mach Number of 3.05," NACA TN 2742, 1952.

24 L. Landweber and T. T. Siao, "Comparison of Two Analyses of Boundary-Layer Data on a Flat Plate," *Journal of Ship Research*, vol. 1, March, 1958, pp. 21–33.

25 F. R. Hama, "The Turbulent Boundary Layer Along a Flat Plate, I and II," *Report of the Institute of Science and Technology*, Tokyo, Japan, vol. 1, 1947, pp. 13 and 49.

26 K. Wieghardt, "Ueber die Wandschubspannung in Turbulenten Reibungsschichten bei Veraenderlichem Aussendruck," ZWB, KWI. U & M 6603, December, 1943.

27 P. S. Klebanoff and Z. W. Diehl, "Some Features of Artificially-Thickened Fully-Developed Turbulent Boundary Layers With Zero Pressure Gradient," NACA TN 2475, October, 1951.

28 T. von Karman, "Turbulence and Skin Friction," *Journal of the Aeronautical Sciences*, vol. 1, 1934, pp. 1–20.

29 Reference [16], p. 433.

30 D. Coles, "Measurements in the Boundary Layer on a Smooth Flat Plate in Supersonic Flow, I. The Problem of the Turbulent Boundary Layer," JPL-CIT Report 20-60, June, 1953.

31 E. M. Winkler and M. H. Cha, "Experimental Investigations of the Effect of Heat Transfer on Hypersonic Turbulent Boundary-Layer Skin Friction," *Journal Aero/Space Sciences*, vol. 26, 1959, p. 123.

32 F. K. Hill, "Turbulent Boundary Layer Measurements at Mach Numbers From 8 to 10," *Physics of Fluids*, vol. 2, 1959, p. 668.

APPENDIX

Theoretical and Empirical Skin-Friction Relations Used for Comparison With the Experimental Results

Reference [8]:

$$c_f = 2(20n)^{\frac{1-n}{1+n}} \left(\frac{\theta}{\mathrm{Re}_\theta \delta}\right)^{\frac{2}{1+n}} \left(\frac{T_\infty}{T_L}\right)^{\frac{n-2\omega-1}{1+n}} \tag{2}$$

with

$$\frac{T_L}{T_\infty} = 1 + 0.179\mathbf{M}_\infty^2 \left[1 - \left(\frac{u_L}{u_\infty}\right)^2\right] + \frac{T_w - T_r}{T_\infty}\left(1 - \frac{u_L}{u_\infty}\right) \tag{3}$$

and

$$\frac{u_L}{u_\infty} = \left(\frac{20n\theta}{\mathrm{Re}_\theta \delta}\right)^{\frac{1}{n+1}} \left\{1 + 0.179\mathbf{M}_\infty^2 \left[1 - \left(\frac{u_L}{u_\infty}\right)^2\right] + \frac{T_w - T_r}{T_\infty}\left(1 - \frac{u_L}{u_\infty}\right)\right\}^{\frac{\omega+1}{n+1}} \tag{4}$$

where $\omega = 0.76$.

Reference [15]:

$$0.41 + \log_{10} \mathrm{Re}_x c_f - \omega \log_{10} \frac{T_w}{T_\infty} = \frac{0.242}{A\left(c_f \times \frac{T_w}{T_\infty}\right)^{1/2}} \left\{\sin^{-1} \frac{A - \frac{B}{2A}}{\left[\left(\frac{B}{2A}\right)^2 + 1\right]^{1/2}} + \sin^{-1} \frac{\frac{B}{2A}}{\left[\left(\frac{B}{2A}\right)^2 + 1\right]^{1/2}}\right\} \tag{5}$$

where

$$A^2 = 0.2\mathbf{M}_\infty^2/(T_w/T_\infty)$$
$$B = [(1 + 0.2\mathbf{M}_\infty^2)/(T_w/T_\infty)] - 1$$
$$\omega = 0.76$$

Reference [16]:

Colburn

$$c_f' = 0.0592\ \mathrm{Re}_x'^{-1/5} \tag{6}$$

Schultz-Grunow

$$c_f' = 0.370\ (\log_{10} \mathrm{Re}_x')^{-2.584} \tag{7}$$

Nikuradse

$$c_f' = 0.02296\ \mathrm{Re}_x'^{-0.139} \tag{8}$$

where the prime denotes evaluation at the reference temperature, T'. The relationship between the primed quantities and c_f, Re_x, and T is

$$c_f' = (T'/T_\infty)c_f \tag{9}$$

$$\mathrm{Re}_x' = \frac{\mathrm{Re}_x}{(T'/T_\infty)^{2.6}(T_\infty + 110.33)/(T' + 110.33)} \tag{10}$$

$$T'/T_\infty = 1 + 0.035\mathbf{M}_\infty^2 + 0.45[(T_w/T_\infty) - 1] \tag{11}$$

EUGENE SEVIN
Assistant Director of Mechanics Research, Armour Research Foundation, Chicago, Ill.
Mem. ASME

On the Parametric Excitation of Pendulum-Type Vibration Absorber

The free motion of an undamped pendulum-type vibration absorber is studied on the basis of approximate nonlinear equations of motion. It is shown that this type of mechanical system exhibits the phenomenon of autoparametric excitation; a type of "instability" which cannot be accounted for on the basis of the linearized system. Complete energy transfer between modes is shown to occur when the beam frequency is twice the simple pendulum frequency. On the basis of a numerical solution, approximately 150 cycles of the beam oscillation take place during a single cycle of energy interchange.

ISOLATION absorbers of the type illustrated in Fig. 1, consisting of a platform suspended on hangers, appear to be gaining increased application. A desired low-frequency response of the platform to an excitation of the base support is achieved through pendulum action of the hangers. The platform may be viewed either as accommodating a single piece of equipment, or as an entire floor system supporting numerous pieces of equipment.

For platforms of sufficient rigidity, the small amplitude motion of the system is characterized by that of the linear oscillator. However, the influence of platform flexibility appears not to have been considered in detail. As will be shown, the behavior of the system in this case is essentially different.

Equations of Motion

The pendulum-type vibration absorber in Fig. 1 is studied on the basis of an idealized system consisting of a flexible beam simply supported at either end by hangers as shown in Fig. 2. No damping is provided and only free vibrations will be considered.

With reference to Fig. 2 the deflected shape of the beam is approximated by

$$y(x, t) = \sum_{n=1}^{N} a_n(t) \sin \frac{n\pi x}{L} \tag{1}$$

which satisfies the conditions of simple support. The kinetic energy, T, and potential energy, V, of the system have the values

$$T = \int_0^L \frac{m}{2} v^2 dx = \frac{m}{2} \int_0^L (l^2\dot{\theta}^2 - 2l\dot{\theta}\dot{y} \sin\theta + \dot{y}^2) dx$$

or, upon substitution of equation (1)

$$T = \tfrac{1}{2} mLl^2\dot{\theta}^2 + \frac{mL}{\pi} l\dot{\theta}\left[\sum_{n=1}^{N} \frac{\dot{a}_n}{n}\right] + \frac{mL}{4} \sum_{n=1}^{N} \dot{a}_n^2$$

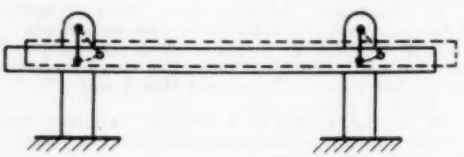

Fig. 1 Pendulum-type vibration absorber

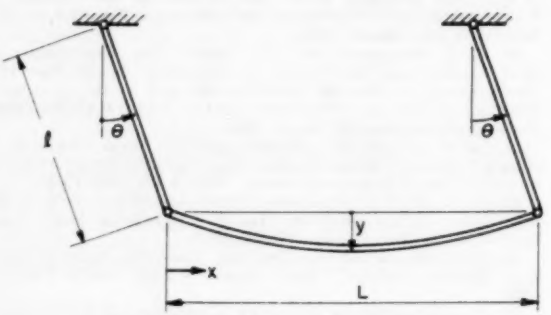

Fig. 2 Idealized beam-pendulum system

Presented at the West Coast Conference of the Applied Mechanics Division, Seattle, Wash., August 28–30, 1961, of THE AMERICAN SOCIETY OF MECHANICAL ENGINEERS.
Discussion of this paper should be addressed to the Editorial Department, ASME, United Engineering Center, 345 East 47th Street, New York 17, N. Y., and will be accepted until October 10, 1961. Discussion received after the closing date will be returned. Manuscript received by ASME Applied Mechanics Division, June 17, 1960. Paper No. 61—APMW-4.

Nomenclature

L = length of beam
EI = modulus of beam
m = mass per unit length of beam
x = co-ordinate measured along length of beam
l = length of pendulum hanger
θ = angular displacement of pendulum hanger
θ_0 = amplitude of θ
a = displacement of beam relative to pendulum supports
A = amplitude of a
g = gravitational constant
$\omega_b = \frac{\pi^2}{L^2}\left(\frac{EI}{m}\right)^{1/2}$ = first mode circular frequency of beam on fixed supports
$\omega_p = (g/l)^{1/2}$ = circular frequency of simple pendulum
$\beta = \omega_p/\omega_b$ = pendulum-beam frequency ratio
$\tau = \frac{L^2}{\pi^2}\left(\frac{m}{EI}\right)^{1/2}$ = time parameter
u = vertical displacement of beam relative to fixed reference
u_0 = vertical displacement of rigid beam relative to fixed reference
t = time

Overbars pertain to nondimensional quantities; primes and dots represent differentiation with respect to x (or l) and t, respectively.

and,

$$V = \frac{EI}{2}\int_0^L (y'')^2 dx + \int_0^L mgl(1 - \cos\theta)dx$$

or

$$V = \frac{\pi^4 EI}{4L^3}\sum_{n=1}^{N} n^4 a_n^2 + mgLl(1 - \cos\theta)$$

Applying Lagrange's equations, the equations of motion are found to be

$$\ddot{\theta} + \frac{\sin\theta}{\pi l}\sum_{n=1}^{N}\frac{\ddot{a}_n}{n} + \frac{g}{l}\sin\theta = 0$$

$$\ddot{a}_n - \frac{2l}{n\pi}(\ddot{\theta}\sin\theta + \dot{\theta}^2\cos\theta) + \frac{n^4\pi^4 EI}{mL^4}a_n = 0 \tag{2}$$

Equations (2) are now simplified by considering only the first term in the expression for beam deflection ($N = 1$), and by restricting attention to sufficiently small angular displacements such that $\sin\theta \approx \theta$, $\cos\theta \approx 1$. In nondimensional form, the equations of motion become,

$$\bar{a}'' + \bar{a} - \bar{\theta}\bar{\theta}'' - (\bar{\theta}')^2 = 0$$
$$\bar{\theta}'' + \beta^2\bar{\theta} - \bar{\theta}\bar{a}'' = 0 \tag{3}$$

where the nondimensional variables are defined by

$$\bar{\theta} = (\sqrt{2}/\pi)\theta$$
$$\bar{a} = \frac{a}{\pi l} \tag{4}$$
$$\bar{l} = t/\tau$$

and

$$\tau = \frac{L^2}{\pi^2}\left(\frac{m}{EI}\right)^{1/2}$$
$$\beta^2 = \frac{g\tau^2}{l} \tag{5}$$

and where the primes denote differentiation with respect to $\bar{l}$. The quantity β is the ratio of the pendulum frequency for a rigid beam, ω_p, to the first-mode frequency of the beam on rigid simple supports, ω_b, i.e.,

$$\beta = \frac{\omega_p}{\omega_b} \tag{6}$$

where

$$\omega_p = \left(\frac{g}{l}\right)^{1/2}$$
$$\omega_b = \frac{\pi^2}{L^2}\left(\frac{EI}{m}\right)^{1/2}$$

The approximate theory of free oscillations of the beam-pendulum system is seen to be governed by equations (3), representing a pair of nonlinear ordinary differential equations. These reduce to the equations of small oscillations of a simple pendulum for $\bar{a} = 0$, and to the first normal-mode equation of a simply-supported beam for $\bar{\theta} = 0$. It can also be shown that equations (3) are the exact equations of motion for a mass suspended from a linear spring and constrained to move vertically, while the spring executes a small amplitude pendulum motion in the plane. A related problem wherein the motion of the mass is in the direction of the spring is discussed by Minorsky.[1] While a complete analytical solution to equations (3) is not possible, the general behavior of the solution can be described.

Ordinary Periodic Solutions

We consider first the motion which results if the pendulum is given an initial displacement and the beam starts from rest. The term $\ddot{\theta}\bar{a}''$ in the second of equations (3) represents the coupling effect of the beam on the motion of the pendulum and is negligible provided

$$\beta^2 \gg \frac{\max}{l}(\bar{a}'')$$

Assuming this to be the case for the moment, the equation becomes,

$$\bar{\theta}'' + \beta^2\bar{\theta} = 0 \tag{7}$$

with

$$\bar{\theta}(0) = \bar{\theta}_0;\ \bar{\theta}'(0) = 0$$

Equation (7) has the solution

$$\bar{\theta}(\bar{t}) = \bar{\theta}_0\cos\beta\bar{t} \tag{8}$$

Using this result, the first of equations (3) yields

$$\bar{a}'' + \bar{a} = (\bar{\theta}\bar{\theta}')' = -\beta^2\bar{\theta}_0^2\cos 2\beta\bar{t} \tag{9}$$

with

$$\bar{a}(0) = \bar{a}'(0) = 0$$

The solution of equation (9) is found to be,

$$\bar{a}(\bar{t}) = C(\cos 2\beta\bar{t} - \cos\bar{t}) \tag{10}$$

where

$$C = \frac{\beta^2\bar{\theta}_0^2}{4\beta^2 - 1};\quad \beta^2 \neq \tfrac{1}{4}$$

Equation (10) describes a periodic motion of amplitude less than or equal to $2C$, and a period which is the greater of 2π or π/β. It now may be shown that our original assumption

$$\beta^2 \gg \frac{\max}{l}(\bar{a}'')$$

implies

$$\bar{\theta}_0^2\left(\frac{4\beta^2 + 1}{4\beta^2 - 1}\right) \ll 1 \tag{11}$$

For small amplitude oscillations $\bar{\theta}_0 \ll 1$, so that equation (11) is primarily a condition excluding β from the neighborhood of $\beta = 1/2$. A second approximation to the motion of the pendulum is obtained by substituting $\bar{a}''$, as obtained from equation (10), into equation (7). There results a Hills' equation of the form

$$\bar{\theta}'' + [\beta^2 + C\phi(\bar{t})]\bar{\theta} = 0 \tag{12}$$

where

$$\phi(\bar{t}) = 4\beta^2\cos 2\beta\bar{t} - \cos\bar{t}$$

and C is as defined in equation (10).

The stability of solutions to equation (12), is not treated herein, but it is known that the solutions may be either stable or un-

[1] N. Minorsky, "Introduction to Non-Linear Mechanics," J. W. Edwards Company, Inc., Ann Arbor, Mich., 1947.

stable[3] depending on the values of β and C.[3] It is shown in the next section that the motion definitely is unstable for $\beta = 1/2$, and we infer that this will be the case also for β differing only slightly from $\beta = 1/2$. However, it remains to divide completely the (β, C) plane into its stable and unstable regions.

To the extent that the beam is considered rigid ($\beta = 0$), its amplitude relative to a fixed reference u_0 equals the vertical displacement of the supports; i.e.,

$$u_0 = l(1 - \cos \bar{\theta}_0) = \frac{l\bar{\theta}_0^2}{2} = \frac{l\pi^2\bar{\theta}_0^2}{4}$$

The amplitude of the flexible beam, then, is

$$u = u_0 \pm \max a = u_0 \pm \pi l(\max \bar{a})$$

The amplitude ratio is

$$\frac{u}{u_0} = 1 + \frac{4\beta^2 A_m}{|4\beta^2 - 1|} \tag{13}$$

where

$$A_m = \frac{\max}{l} |\cos 2\beta l - \cos l|$$

Equation (13) is valid only for

$$|\beta - \tfrac{1}{2}| > \epsilon(\bar{\theta}_0)$$

in accordance with equation (11).

The amplitude ratio, equation (13), is plotted as a function of β in Fig. 3. It is seen that the frequency of the beam must be less than 1.4 or greater than 2.5 times the pendulum frequency (i.e., $0.4 > \beta > 0.7$) in order for the amplitude of the beam to be less than 20 per cent of the vertical displacement of the supports.

[3] Stability here refers to the ordinary periodic solutions. The system, being conservative, remains stable in the usual sense for all values of the parameters.

[3] J. J. Stoker, "Nonlinear Vibrations," Interscience Publishers, Inc., New York, N. Y., 1950.

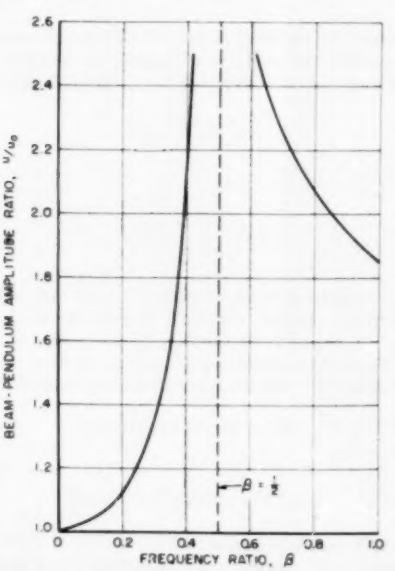

Fig. 3 Amplitude of "stable" beam motion

An "Unstable" Solution

For $\beta = 1/2$, equation (9) has the secular solution

$$\bar{a} = -\frac{\bar{\theta}_0^2}{8} l \sin l \tag{14}$$

According to this result the beam motion is an oscillation with ever-increasing amplitude; i.e., an unstable solution. Equation (14), of course, is valid only until such time as the initial linearization involving $\bar{a}''$ in equations (3) becomes unacceptable. As the beam motion grows, the motion of the pendulum must attenuate, since we are dealing with a conservative system. What, then, is the long-time motion?

Inspection of equations (3) shows that a possible motion is the beam in a steady-state oscillation with the pendulum at rest.[4] Thus there exists the possibility that either the energy is transferred wholly (or partially) from one mode to another in a cyclical fashion, or that the pendulum motion ceases. One is led, then, to consider the effect of a perturbation of the pendulum motion from a state of rest on the periodic oscillations of the beam. Before doing so, it may be noted that if complete energy transfer from the pendulum mode[5] to the beam mode occurs, the maximum amplitude of the beam will be

$$\max \bar{a} = \bar{\theta}_0$$

There is a simple physical explanation[2] for the unstable solution when $\beta = 1/2$ as given by equation (14). The $\bar{\theta}$-motion can be likened to that of a variable-length pendulum due to the coupling effect of the beam. Where the coupling is negligible, the pendulum should execute harmonic motion; viz., equation (8). This motion, in turn, gives rise to a centrifugal force of frequency, 2β; twice that of the primary pendulum motion. Since this force effectively acts to drive the beam, a condition of resonance will occur when the beam and forcing frequencies are equal, or when $2\beta = 1$.

Stability of the Beam Mode

Consider a possible solution of equation (3) corresponding to oscillation of the beam with the pendulum at rest; i.e.,

$$\left.\begin{aligned} \bar{a} &= A \cos l \\ \bar{\theta} &= 0 \end{aligned}\right\} \quad t < 0 \tag{15}$$

Now, perturb the motion slightly,

$$\left.\begin{aligned} \bar{a} &= A \cos l + \epsilon\, \alpha(t) \\ \bar{\theta} &= \epsilon\, \mu(t) \end{aligned}\right\} \quad t \geq 0; \quad \epsilon \ll 1 \tag{16}$$

There results upon substitution of equation (16) into equations (3) and retaining only linear terms in the perturbation parameter ϵ,

$$\alpha'' + \alpha = 0 \tag{17}$$

and

$$\mu'' + (\beta^2 + A \cos l)\mu = 0 \tag{18}$$

Equation (17) shows that the periodic motion of the beam continues, but with an amplitude and phase shift; i.e.,

$$\bar{a} = A_1 \cos (l + \psi) \tag{19}$$

[4] As has been seen, the converse is not possible.

[5] The term "mode" is used only in a descriptive sense. The pendulum mode refers to a simple periodic motion for $\bar{\theta}$ as previously described; the beam mode refers to a similar motion for $\bar{a}$

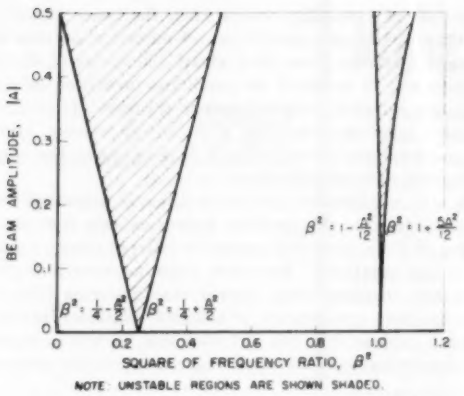

Fig. 4 Approximate stability diagram for equation (18)

The pendulum, however, is seen to satisfy a Mathieu equation, equation (18), which implies that the stability of the perturbed motion depends on the relative values of the parameters β and A. Therefore, for certain (β, A) the pendulum motion must remain of the order of the perturbation, while for other values the tendency will be for the pendulum motion to increase at the expense of the beam oscillation. Approximate equations for the characteristic curves of the Mathieu equation valid for small A and $0 \leqslant \beta^2 \leqslant 1$ are given by Stoker.[3] These are shown in the stability diagram in Fig. 4; the shaded regions correspond to values of (β, A) for which solutions to equation (18) are unstable.

Of particular interest in Fig. 4 is the fact that the solution is unstable for $\beta = 1/2$ and any $A \neq 0$.[4] This same value of β earlier was seen to lead to unstable solutions for the pendulum motion when the beam starts from rest. Thus, as the pendulum motion dies out, this condition too is unstable and the pendulum motion will subsequently grow. This results in an amplitude (and possibly frequency) modulated motion of both the beam and pendulum of presently unknown frequency and minimum-to-maximum amplitude ratio.

Numerical Results

Equations (3) were solved by numerical integration (Runge-Kutta-Gill method) for several values of β in the neighborhood of $1/2$, and two sets of initial conditions. For $\beta = 1/2$ the initial conditions were taken to be

$$\bar{\theta}_0 = 0.0354$$

$$\bar{\theta}'(0) = \bar{a}(0) = \bar{a}'(0) = 0$$

The resulting solution for $\bar{a}(t)$ and $\bar{\theta}(t)$ is shown in Fig. 5 for $0 \leqslant \bar{t} \leqslant 1000$. The energy of the system was observed to remain constant to three significant figures throughout the motion, indicating the use of a sufficiently fine integration interval ($\Delta\bar{t} = 1/8$).

With reference to Fig. 5, the period of both the beam and pendulum oscillation remains constant (2π and 4π, respectively) throughout one complete cycle of energy transfer. The period of the latter phenomenon, $\bar{T}_\theta^* = \bar{T}_a^* = 293\pi$, encompasses about 146 cycles of the beam oscillation or 73 cycles of the pendulum oscillation. For practical purposes the energy transfer between the two modes is complete. The initial motions of the beam are in accordance with equation (14), and max $\bar{a}$ agrees with $\bar{\theta}_0/2$ to within four significant figures, lending considerable confidence to the numerical results.

Fig. 6 shows the envelope of the pendulum motion for three values of β in the vicinity of $1/2$. The initial conditions for all solutions were

$$\bar{a}(0) = 0.02$$

$$\bar{\theta}(0) = 0.002$$

$$\bar{a}'(0) = \bar{\theta}'(0) = 0$$

These correspond to perturbing the pendulum in the presence of a steady beam oscillation, as discussed in the preceding section. According to the stability diagram, Fig. 4, solutions I(β = 0.485) and III (β = 0.513) are stable, whereas solution II(β = 0.500) is unstable. As is evident from Fig. 6, the character of the two stable solutions is quite different, although in both cases the pendulum motion remains small. This behavior is in accordance with solutions of the Mathieu equation, equation (18), where the (β, A) lie between different characteristic curves of the

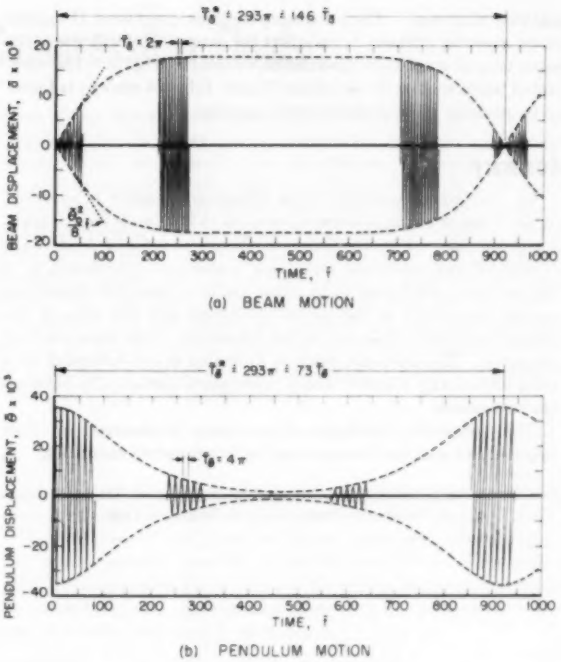

Fig. 5 Numerical solution for $\beta = 1/2$

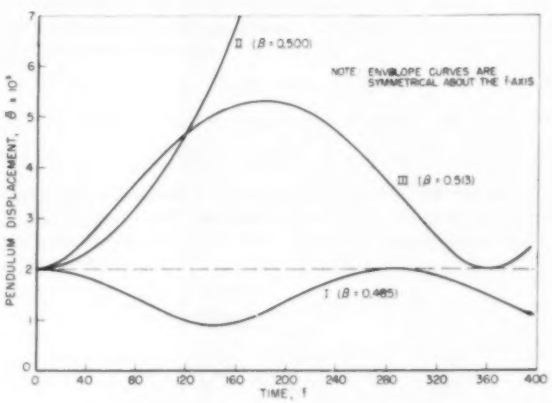

Fig. 6 Stable and unstable pendulum motions

[4] The solutions to equation (18) are known to be unstable for $\beta^2 = n^2/4$ ($n = 1, 2, \ldots$) and $A \neq 0$.

stability diagram.[7] The pendulum motions in solution II appear to be growing without bound, but for later times will show the same type of amplitude modulation evident in Fig. 5. The associated beam motion for solutions II and III (not shown) is found to be periodic in accordance with equation (19).

Summary

An undamped pendulum-type vibration absorber is analyzed on the basis of a simple beam suspended at both ends from a gravity pendulum. The approximate theory developed leads to a system of two nonlinear equations whose free vibrations, in a certain sense, are found to be either stable or unstable depending on the magnitude of the initial conditions and the ratio of the simple pendulum frequency to the frequency of the beam on fixed supports. The unstable mode of vibration is characterized by a complete energy transfer which takes place periodically between the two modes.

This essentially nonlinear phenomenon is observed in other applications and has been termed autoparametric excitation. A critical case of instability occurs when the beam frequency is twice that of the simple pendulum. A numerical solution of the nonlinear equations shows that about 150 cycles of the beam oscillation and 75 cycles of the pendulum oscillation take place during one complete cycle of energy transfer. It remains to establish a fuller understanding of the energy transfer, including such considerations as the influence of damping or the response of the system to forced vibrations.

It is to be emphasized that the condition of parametric excitation encountered in this problem derives entirely from the nonlinearity of the system and cannot be inferred from a linearized form of the equations. Moreover, these nonlinearities are due to dynamic coupling terms (rather than restoring forces) and thus arise from consideration of a flexible platform (beam). It is further evident that this situation can be met in numerous other mechanical systems employing pendulum-like elements.

Acknowledgment

The material reported herein was based in part on work performed by the author at the Armour Research Foundation for the Air Force Ballistic Missiles Division under Contract AF04-(647)-391.

[7] N. W. McLachlan, "Theory and Application of Mathieu Functions," Oxford University Press, Oxford, England, 1947.

Mixing of Compressible Fluids[1]

E. D. KENNEDY
Senior Scientist,
General Applied Sciences Laboratories, Inc.,
Westbury, L. I., N. Y.

The problem of the mixing of two streams of the same compressible fluid in a constant-area duct is solved by applying certain dimensionless parameters first used by Kiselev. The extension to dissimilar fluids or to more than two streams is straightforward. Although the analysis is unrestricted, detailed results are given only for the case where one stream is sonic or supersonic and the other sonic or subsonic at the origin of mixing. For this case, the second law of thermodynamics indicates that, of the two solutions of the conservation equations, the subsonic one is always permitted while some of the supersonic solutions are thermodynamically impossible. Upon examination of experimental data, it is further concluded that of the admissible supersonic solutions, only one may be expected to occur. The establishment of this supersonic solution with its relatively high stagnation pressure leads to the conclusion that when the initial temperatures are sufficiently different, there exist thermodynamically possible solutions with a stagnation pressure higher than that of either of the two initial streams.

Analyses of the mixing problem may be divided into two types—one concerned with details of the mixing process and where the problem is one of solving the Navier-Stokes equations and the other which disregards the mixing process per se and settles for the solution given by the integrated forms of the conservation equations. In this respect, the problem is analogous to shock-wave theory where the Rankine-Hugoniot equations result from the integrated conservation equations, while details of the shock structure must come from a more elaborate analysis.

In the second group, with which this paper is concerned, the usual assumption of one-dimensional flow at the beginning and end of mixing allows one to solve for the state and velocity of the mixed flow. (For the justification and limitations of the one-dimensional approach, the reader is referred to Crocco's extensive article [2].[2]) A different approach is that of Fabri and Siestrunck [3] who consider the separate flows near the origin of mixing with the one-dimensional approximation. As is well known, the result of such an analysis is a double-valued solution for the state and velocity of the mixed flow—one solution corresponding to a supersonic and the other to a subsonic velocity. In a number of typical publications [4–7], the supersonic solution is recognized as a mathematical possibility but there is an apparent reluctance (and even a refusal) to admit its physical existence.

The purposes of this paper are to repeat the analysis by applying parameters first used by Kiselev [8] which reduce the equations to simple forms and to show by means of thermodynamic considerations and experimental data that the supersonic solution is possible and does, in fact, occur.

Analysis

The equations of conservation of mass, momentum, and energy for one-dimensional, steady, parallel flow of the assumed perfect gas are (neglecting leakage, friction, and heat transfer at the wall of the constant area duct)

$$m_1 + m_2 = m_3 \tag{1}$$

$$P_1A_1 + P_2A_2 - P_3A_3 = m_3v_3 - m_1v_1 - m_2v_2 \tag{2}$$

$$m_1C_pT_{01} + m_2C_pT_{02} = m_3C_pT_{03} \tag{3}$$

Using the definitions $\mu = m_2/m_1$, $f = A_1/A_3$, $\mathbf{M}^* = v/a^*$, $\tau^2 = T_{02}/T_{01}$, $\nu = P_2/P_1$, the geometric condition $A_1 + A_2 = A_3$, and the equation of state $P = \rho RT$, the following results are easily obtained:

$$K_3 = \frac{P_{03}}{P_{01}} = \frac{\theta(\mathbf{M}_1^*)}{\theta(\mathbf{M}_3^*)} f[(1+\mu)(1+\mu\tau^2)]^{1/2} \tag{4}$$

$$[(1+\mu)(1+\mu\tau^2)]^{1/2}\left(\mathbf{M}_3^* + \frac{1}{\mathbf{M}_3^*}\right) = \mathbf{M}_1^* + \frac{1}{\mathbf{M}_1^*} + \mu\tau\left(\mathbf{M}_2^* + \frac{1}{\mathbf{M}_2^*}\right) \tag{5}$$

$$\frac{T_{03}}{T_{01}} = \frac{1+\mu\tau^2}{1+\mu} \tag{6}$$

[1] The results given here include and extend work done in 1954 and presented as a Master's Thesis in the Department of Aeronautical Engineering at the University of Minnesota [1].

[2] Numbers in brackets designate References at end of paper

Presented at the West Coast Conference of the Applied Mechanics Division, Seattle, Wash., August 28–30, 1961, of The American Society of Mechanical Engineers.

Discussion of this paper should be addressed to the Editorial Department, ASME, United Engineering Center, 345 East 47th Street, New York 17, N. Y., and will be accepted until October 10, 1961. Discussion received after the closing date will be returned. Manuscript received by ASME Applied Mechanics Division, April 25, 1960. Paper No. 61—APMW-3.

Nomenclature

a^* = speed of sound at $\mathbf{M}^* = 1$
A = area
C_p = specific heat at constant pressure
f = area ratio A_1/A_3
K = stagnation pressure divided by P_{01}
m = mass flow
$\mathbf{M}$ = Mach number
$\mathbf{M}^*$ = dimensionless velocity; related to $\mathbf{M}$ by relationship

$$\mathbf{M}^{*2} = \frac{\frac{\gamma+1}{2}\mathbf{M}^2}{1 + \frac{\gamma-1}{2}\mathbf{M}^2}$$

P = pressure
R = gas constant
T = temperature
v = velocity
γ = ratio of specific heats
μ = m_2/m_1, mass-flow ratio
ν = P_2/P_1, initial-pressure ratio
ρ = density
τ^2 = T_{02}/T_{01}, ratio of initial stagnation temperatures

(Continued on next page)

This is the complete solution for the mixed flow, given more or less in this form by Kiselev.

In the numerical calculations, the procedure has been to assign values of M_1^* μ, f, and τ and then run through a range of values of M_2^*. For each M_2^*, equation (5) furnishes two values of M_3^* from which the stagnation pressure ratio, K_3, may be calculated using tabulated values of $\theta(M_3^*)$. Equation (5) is quite convenient for numerical calculation since, in addition to its symmetry, neither the area ratio, f, the initial pressure ratio, ν, nor the specific-heat ratio, γ, appears. However, when $\mu = 0$, the right-hand side cannot be evaluated (since $M_2^* = 0$ also). In this case, μ can be eliminated in favor of ν and f by means of the identity

$$\mu = \frac{\nu}{\tau}\frac{1-f}{f}\frac{M_2^*}{1-\frac{\gamma-1}{\gamma+1}M_2^{*2}}\frac{1-\frac{\gamma-1}{\gamma+1}M_1^{*2}}{M_1^*} \tag{7}$$

to yield, for $M_2^* = 0$

$$M_3^* + \frac{1}{M_3^*} = M_1^* + \frac{1}{M_1^*} + \frac{1-f}{f}\nu\frac{1-\frac{\gamma-1}{\gamma+1}M_1^{*2}}{M_1^*} \tag{8}$$

Equation (8) has been derived by Hermann [9] in connection with the free-jet wind tunnel.

It follows from either equation (5) or (8) that the two roots satisfy $M_{3\alpha}^* M_{3\beta}^* = 1$ (where $M_{3\alpha}^* \geq 1$ and $M_{3\beta}^* \leq 1$) which is recognized as the relationship between velocities before and behind a normal shock.

Introducing the function $\vartheta(M^*)$, first used by Hermann [10], defined by $\vartheta(M^*) = \theta(M^*)/K_{NS}(M^*)$ and having the property $\vartheta(M^*) = \theta(1/M^*)$, we establish that

$$K_{3\beta}/K_{3\alpha} = \theta(M_{3\alpha})/\theta(M_{3\beta}) = \theta(M_{3\alpha})/\vartheta(M_{3\alpha}) = K_{NS}(M_{3\alpha}^*) \tag{9}$$

It follows that the state and velocity of the subsonic β solution correspond exactly to conditions downstream of a normal shock at the supersonic (α) solution. However, it will be shown that the subsonic solution is not reached in this way in general.

It is perhaps appropriate at this point to call attention to a certain formal similarity between equation (5) and the corresponding equation for the case of constant pressure mixing where we have

$$[(1+\mu)(1+\mu\tau^2)]^{1/2} M_3^* = M_1^* + \mu\tau M_2^* \tag{10}$$

which is identical with equation (5) if the quantity M^* replaces the group $M^* + 1/M^*$. However, if the pressure is prescribed, there is no double solution.

Physical Limitations of the Solution

There are two minor limitations which must be noted: (a) Solutions with

$$M_3^* > \left(\frac{\gamma+1}{\gamma-1}\right)^{1/2}$$

are discarded since

$$M \to \infty \text{ as } M^* \to \left(\frac{\gamma+1}{\gamma-1}\right)^{1/2}$$

and (b) for fixed M_1^*, μ and τ, there is a range of values of M_2^* which gives $M_2^* + 1/M_3^* < 2$ and hence imaginary M_3^*. This range will always include $M_2^* = 1$ and will be bounded by values of M_2^* which are reciprocals. The establishment of these bounds has been the subject of an extended discussion in [7].

The principal limitation, however, is that resulting from the second law of thermodynamics. Since the stagnation temperature of the mixed flow is fixed by equation (6), the second law can be used to define an upper limit of the stagnation pressure of the mixed stream. Using the perfect-gas expression for entropy, we have

$$K_{3L} = \frac{P_{03}}{P_{01}} \leq \left[\left(\frac{T_{03}}{T_{01}}\right)\left(\frac{T_{01}}{T_{02}}\right)^{\frac{\mu}{1+\mu}}\right]^{\frac{\gamma}{\gamma-1}}\left[\frac{P_{02}}{P_{01}}\right]^{\frac{\mu}{1+\mu}} \tag{11}$$

or, in terms of the chosen parameters,

$$K_{3L} \leq \left[\left(\frac{1+\mu\tau^2}{1+\mu}\right)\left(\frac{1}{\tau^2}\right)^{\frac{\mu}{1+\mu}}\right]^{\frac{\gamma}{\gamma-1}}\left[\frac{\mu\tau f}{1-f}\frac{\theta(M_1^*)}{\theta(M_2^*)}\right]^{\frac{\mu}{1+\mu}} \tag{12}$$

It should be noted that, if $T_{02} \ll T_{01}$, the right side of equation (12) will become large and hence there are thermodynamically valid solutions with the stagnation pressure of the mixed stream greater than that of either of the two initial streams.

Graphical Results and Comparison With Experiment

Since most data appearing in the literature are for the case where one stream is sonic or supersonic and the other sonic or subsonic, this case has been chosen for detailed discussion. The experimental data are from [3] and [11] and require some preliminary discussion.

In both cases, one of the streams was drawn from the atmosphere by the action of the other and the mixed stream discharged to the atmosphere either directly or with a simple divergent diffuser attached to the constant-area duct. The experimental procedure in both [3] and [11] was to fix the pressure of the high-speed stream and then to vary the pressure and velocity (and hence the mass flow) of the other stream by means of an adjustable valve. Further details of the experimental procedure (which was the same in both [3] and [11]) are available in [3]. Since neither [3] nor [11] reports any measurements of mixed-flow parameters, these must be inferred from the data as follows:

In the case with a diffuser at the end of the mixing tube, if the subsonic solution is established, its stagnation pressure is (neglecting diffusion losses) the back pressure or atmospheric pressure.

Nomenclature

$\theta(M^*) = \frac{A^*}{A} = \left(\frac{\gamma+1}{2}\right)^{\frac{1}{\gamma-1}} M^*\left(1-\frac{\gamma-1}{\gamma+1}M^{*2}\right)^{\frac{1}{\gamma-1}}$

$K_{NS}(M^*)$ = normal shock stagnation pressure ratio

$K_{3\beta}' = K_{3\beta}\left(1-\frac{\gamma-1}{\gamma+1}M_{3\beta}^{*2}\right)^{\frac{\gamma}{\gamma-1}}$

$\vartheta(M^*) = \left(\frac{\gamma+1}{2}\right)^{\frac{1}{\gamma-1}}\frac{1}{M^*}\cdot\left(1-\frac{\gamma-1}{\gamma+1}\frac{1}{M^{*2}}\right)^{\frac{1}{\gamma-1}}$

Subscripts

- 0 = stagnation
- 1, 2 = initial streams
- 3 = mixed flow conditions
- L = conditions at the limit of ν
- NS = normal shock
- b = conditions downstream of mixing tube
- α = supersonic solution
- β = subsonic solution

If there is no diffuser, the static pressure of the mixed subsonic stream is that of the atmosphere and so in this case the experimental ratios, P_b/P_{01}, should lie below the $K_{3\beta}$-curve by a factor

$$\left(1 - \frac{\gamma - 1}{\gamma + 1} M_{3\beta}^{*2}\right)^{\frac{\gamma}{\gamma - 1}}$$

If the supersonic solution is established, the conditions at the origin of mixing must be independent of P_b.

The data from [11] are compared with the analysis in Figs. 1 and 2 for $\tau^2 = 1.0$ and 0.5, respectively. The various total-pressure ratios ($K_{3\alpha}$, $K_{3\beta}$, $K_{3\beta}'$, K_{3L}, and P_b/P_{01}) are plotted against the pressure ratio, ν, which, while not being a directly measured quantity, may be derived easily from the data. The upper limit of ν depends only upon M_1^* and is that value where a normal shock stands in the high-speed stream. It is realized that flow separation may occur before this limit is reached; however, for our purposes this value of ν, designated ν_{NS}, will be used as a convenient upper limit. The lowest value of ν corresponds to the point where the α and β-solutions merge; i.e., $M_3^* = 1$. The supersonic branch of the solution rises quite rapidly from this point, while the subsonic branch is very nearly linear and rises much more slowly. The $K_{3\beta}'$ curve, lying below that of $K_{3\beta}$ by the factor

$$\left[1 - \frac{(\gamma - 1)}{(\gamma + 1)} M_{3\beta}^{*2}\right]^{\frac{\gamma}{\gamma - 1}}$$

deserves no special comment. The subsonic branch always lies below the second law limit, i.e., the equality sign in equation (12), and so is thermodynamically possible for all ν. The supersonic branch, rising from the point where $M_3^* = 1$, intersects the limit curve and so is possible only in a restricted range. We denote the value of ν at the intersection by ν_L. In the range of $\nu > \nu_L$, i.e., where only the subsonic solution is possible, the data agree well with the analysis for both values of τ^2. However, in the vicinity of ν_L (where the supersonic solution first becomes valid) the experimental data indicate that ν reaches a limit and becomes independent of the pressure ratio P_b/P_{01}. The existence of this limit is explained by considering the effect of a gradual lowering of the downstream pressure, P_b, while holding μ, τ^2, M_1^* and P_{01} fixed. (As noted previously, the experimental data were obtained with P_b, τ^2, M_1^*, and P_{01} fixed and μ varying. However, the point about to be made becomes much clearer if we replot the data as in this paper; i.e., μ considered fixed and P_b varying. In order to run an actual experiment in this manner would require, in the case of the subsonic solution, that the back pressure and the valve position be varied together so that the mass-flow ratio would remain constant. In the case of the supersonic solution, the mass-flow ratio would remain fixed if the valve position were fixed—no matter what the back pressure.)

Suppose the initial point is at ν_{NS}—the extreme right of either Fig. 1 or 2. As the back pressure is lowered, ν decreases (and M_2^* increases) for fixed μ while only the subsonic solution is possible. As the back pressure is lowered further, a value of ν is reached at which the supersonic solution is possible. If the supersonic solution occurs at this point, any further lowering of the back pressure can have no effect upon ν and hence the remainder of the thermodynamically valid solutions at lower values of ν become unattainable. The low back pressure will simply cause the supersonic mixed flow to expand to a higher velocity outside the mixing tube.

The fact that the experimental data reach a limit where the back pressure plays no role in determining the initial conditions establishes the existence of the supersonic solution since ν must decrease with decrease in back pressure if the subsonic solution is established. In every case it may be noted that the experimental limit of ν is slightly lower than the value at the $K_{3L} - K_{3\alpha}$ intersection. However, recalling that the K_{3L} curve corresponds to zero entropy change (i.e., no mixing losses), this result is not too surprising. Consideration of the losses would lower the limit curve and bring the analysis and data into closer agreement. It is now obvious that, in general, the subsonic solution is not reached by a normal shock from the supersonic solution since over most of the admissible range of ν, the supersonic solution is impossible.

The effect of different temperatures may be seen by comparing Figs. 1 and 2. The subsonic branch and the value of ν_L change only slightly, and, as expected, the K_{3L} curve for $\tau^2 = 0.5$ is significantly higher than the equal temperature case.

The second set of experimental data [3] is for $f = 0.43$, $\tau^2 = 1$, $M_1^* = 1.778$. These data are compared with the analysis for $\mu = 0$, 0.35, and 0.49 in Fig. 3. The left-hand limit corresponds to $M_2^* = 1$ rather than $M_3^* = 1$ as before since for $M_1^* > 1$ and $\tau^2 = 1$, it is impossible to reach $M_3^* = 1$. The data show the same trends as those previously discussed and the same general remarks apply.

We end the discussion of the experimental data with a few remarks. The behavior exhibited by the data from [3] and [11] is typical of many such data and has been noted by other writers. However, the significance seems to have been missed and Lee [6], having discovered the experimental limit of ν, concluded that it was proof of the nonexistence of the supersonic solution—just the opposite of the conclusion in this paper. The analysis for the subsonic branch agrees well with the data while the value of ν where

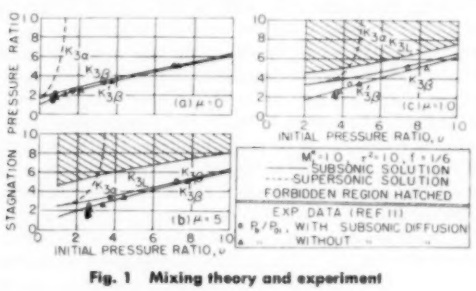

Fig. 1 Mixing theory and experiment

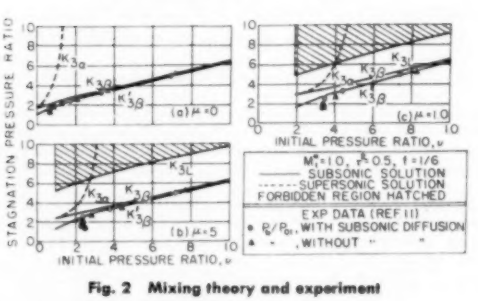

Fig. 2 Mixing theory and experiment

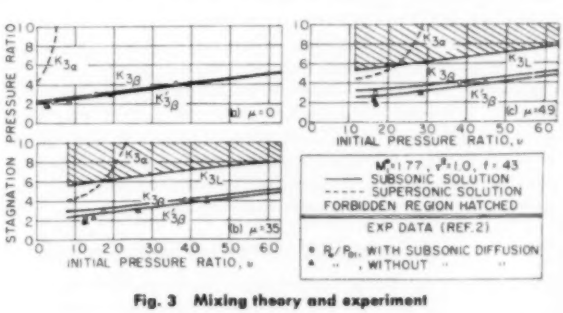

Fig. 3 Mixing theory and experiment

$K_{3s} = K_{3L}$ at least serves as a first approximation to the experimental value of ν_L. The fact that only a single supersonic solution occurs is quite important.

Conclusions

The supersonic solution, hitherto regarded with some skepticism, has been shown to play an important part in understanding the mixing process. The second law and experimental data were essential in establishing its existence. With this information, it seems advisable to re-evaluate such devices as the ram rocket and the jet compressor since performance estimates have invariably been based upon the subsonic solution.

Acknowledgment

The calculations reported herein were performed on the IBM 704 at Convair, San Diego, while the author was employed there. The assistance of Convair and Dr. Marvin Stern is gratefully acknowledged.

References

1 E. D. Kennedy, "The Ejector Flow Process," Master of Science Thesis, University of Minnesota, Minneapolis, Minn., 1955.

2 L. Crocco, "Fundamentals of Gas Dynamics (Section B)," Princeton University Press, Princeton, N. J., 1958.

3 J. Fabri and R. Siestrunck, "Supersonic Air Ejectors," *Advances in Applied Mechanics*, vol. 5, Academic Press, Inc., New York, N. Y., 1958.

4 H. R. Hunczak and M. D. Rousso, "Starting and Operating Limits of Two Supersonic Wind Tunnels Utilizing Auxiliary Air Injection Downstream of the Test Section," NACA TN 3262, September 1954.

5 Harry Bernstein, "Effects of Parallel-Jet Mixing on Downstream Mach Number and Stagnation Pressure With Application to Engine Testing in Supersonic Tunnels," NACA TN 2918, March, 1953.

6 J. D. Lee, "The Induction of Flow by an Injector Nozzle," Proceedings of The Fourth Midwestern Conference on Fluid Mechanics, Purdue University, September, 1955.

7 H. J. Hoge, "On the Theory of Mixing of Fluid Streams," Quartermaster Research and Engineering Center, Pioneering Research Division, Technical Report PR-2, February, 1959.

8 B. Kiselev, "Calculation of One-Dimensional Gas Flows," USAF Technical Report No. F-TS-1209-1A, January, 1959 (translated from the Russian by Brown University).

9 Rudolf Hermann, "Diffuser Efficiency of Free-Jet Supersonic Wind Tunnels at Variable Test Chamber Pressure," *Journal of the Aeronautical Sciences*, vol. 19, 1952, pp. 375–384

10 Rudolf Hermann, "Supersonic Diffuser Problems for Inlet Ducts and Wind Tunnels in One-Dimensional Analysis," *Proceedings of The Second Midwestern Conference on Fluid Mechanics*, Ohio State University, March, 1952.

11 R. V. DeLeo and R. D. Wood, "Report on Progress on the Investigation of the Use of Hot Gas Ejectors for Boundary Layer Control," Contract No. AF 33(616)2178, University of Minnesota, Department of Aeronautical Engineering, July, 1954.

The Laminar Boundary Layer on a Hot Cylinder Fixed in a Fluctuating Stream

R. J. GRIBBEN[1]

Department of Mathematics,
Massachusetts Institute of Technology,
Cambridge, Mass.

The equations for nonsteady, two-dimensional low-speed compressible flow in the laminar boundary layer are solved approximately by use of the Pohlhausen technique with the assumption of quartic profiles for the velocity and temperature. The external flow considered is of the form of a steady basic velocity with a superimposed small amplitude oscillation such as may arise, for example, when a sound wave is present in a uniform incident stream. The analysis is then applicable to the case of a hot cylinder fixed in such a stream. Terms of the order of the incident stream Mach number are neglected in the expressions for external flow quantities (whereas the low-speed boundary-layer equations involve errors of the order of only the square of this Mach number). Two special cases are worked out—the flow over a flat plate for which there is fair agreement with available exact calculations, and the flow over a circular cylinder.

1 Introduction

In this paper two-dimensional oscillatory flow past a fixed body with a steady mean component of velocity is considered, and solutions of the boundary-layer equations for low-speed, compressible flow are found by using Pohlhausen's approximate method of integration.

For incompressible flow, Lighthill (1954)[2] has applied the method to the case of a main stream which oscillates in magnitude. He obtained solutions, in the form of expressions for the skin friction and heat transfer, for oscillating flow around both a flat plate and a circular cylinder for small values of the frequency parameter. For large values of this parameter he solved the equations by a different approximate technique and was able to join up the two solutions to give a satisfactory solution for the whole frequency range. Also Lin (1957) for an arbitrary main stream has obtained solutions which are valid for finite amplitudes and very high frequencies of oscillation.

In the theory of compressible flows, Moore (1951) has considered the case of a heat-insulated plate moving with a varying velocity in a uniform atmosphere. He solved the equations in series and determined the skin friction. Ostrach (1955), using the same method of analysis, obtained the heat transfer when the plate was at a specified temperature instead of being heat insulated. These exact solutions of the equations of motion have been supplemented by those of Illingworth (1958). With viscous dissipation neglected he treated the case of a stream containing a sound wave flowing past a flat plate. (Only for incompressible flow is the mathematical problem of a body oscillating about a fixed, mean position in a steady stream the same as that of the stream oscillating about a steady mean velocity past a fixed body.) Illingworth's work includes an exact treatment of the present problem for the flat plate.

As in Lighthill's work, which was, however, restricted to small temperature differences, we consider a fixed obstacle in a low-speed flow for small values of the frequency parameter, but here we allow for compressibility effects arising from a high wall temperature. Since the main stream is slow we may neglect dissipation in the boundary layer.

In Section 2 the general theory is developed starting from the boundary-layer equations for low-speed compressible flow. While this implies that terms of the order of the square of the free-stream Mach number, $\mathbf{M}_\infty$, are small compared with those of the order of the maximum temperature difference in the flow, $(T_w - T_\infty)/T_\infty$ where T_w and T_∞ are the wall and free-stream temperatures, we subsequently simplify the work further by neglecting terms of $0(\mathbf{M}_\infty)$. The Karman-Pohlhausen method of integration across the boundary layer is then employed to solve the equations with quartic profiles assumed for the velocity and temperature.

The first example, considered in Section 3, is the simple case of fluctuating flow over a flat plate for which some exact solutions are known. The skin friction and heat transfer are each obtained as a series in the frequency parameter. When $T_w/T_\infty = 1$ there is good agreement with the series for the skin friction obtained (without approximation) by Moore at low frequencies but the results for the heat transfer when compared with those obtained by Ostrach, are somewhat less satisfactory. For T_w/T_∞ different from 1, the results are compared with those of Illingworth when the present approximate treatment is seen to yield results that are still fairly satisfactory.

We then apply the method to a further relatively simple special case, which concerns the flow over a circular cylinder. We have in mind the physical phenomenon of the Rijke tube discussed by Rayleigh (1894) in which sound waves are produced when a stream flows down a pipe containing a cross section of red-hot wire mesh at one place along its length. Therefore we consider the unsteadiness of the main stream to be due specifically to the presence of a sound wave in the incident stream. The expression used for the main stream takes account of the scattering of the sound by the cylinder assuming that the radius R of the cylinder is small compared with the wave length of the sound. In Section 4 the skin friction and heat transfer are obtained as series in ascending or descending powers of $ikR/\mathbf{M}_\infty$, where k is the wave number, according as this parameter is small or large. It is necessary now, however, to perform a separate calculation for each value of T_w/T_∞ to obtain the numerical coefficients in the series.

2 The Pohlhausen Method for Unsteady Flow

The laminar boundary-layer equations for unsteady, plane, compressible flow are,

---

[1] Now at Department of Mathematics, The University, Southampton, England.

[2] References at end of paper are designated by author and year.

Contributed by the Applied Mechanics Division and presented at the Winter Annual Meeting, New York, N. Y., November 27–December 2, 1960, of The American Society of Mechanical Engineers.

Discussion of this paper should be addressed to the Editorial Department, ASME, United Engineering Center, 345 East 47th Street, New York 17, N. Y., and will be accepted until October 10, 1961. Discussion received after the closing date will be returned. Manuscript received by ASME Applied Mechanics Division, August 3, 1960. Paper No. 60—WA-203.

$$\frac{\partial \rho}{\partial t} + \frac{\partial}{\partial x}(\rho u) + \frac{\partial}{\partial y}(\rho v) = 0, \tag{1}$$

$$\frac{\partial}{\partial t}(\rho u) + \frac{\partial}{\partial x}(\rho u^2) + \frac{\partial}{\partial y}(\rho uv) = \rho_e\left(\frac{\partial u_e}{\partial t} + u_e\frac{\partial u_e}{\partial x}\right) + \frac{\partial}{\partial y}\left(\mu\frac{\partial u}{\partial y}\right), \tag{2}$$

$$\rho\left(\frac{\partial I}{\partial t} + u\frac{\partial I}{\partial x} + v\frac{\partial I}{\partial y}\right) - \left(\frac{\partial p_e}{\partial t} + u\frac{\partial p_e}{\partial x}\right) = \frac{1}{\sigma}\frac{\partial}{\partial y}\left(\mu\frac{\partial I}{\partial y}\right) + \mu\left(\frac{\partial u}{\partial y}\right)^2 \tag{3}$$

Here t is the time, x and y are curvilinear co-ordinates measured along and perpendicular to the wall, respectively, u and v are the corresponding velocity components, p is the pressure, ρ the density, μ the viscosity, I the enthalpy, and σ the Prandtl number assumed to be constant. The suffix e refers to values in the main stream. In writing down the energy equation (3) it has been assumed that the specific heats are constant. In addition, we shall assume that (i) the main stream is homentropic so that $\rho_e dI_e = dp_e$, and (ii) the gas is perfect so that we may write $\rho/\rho_e = I_e/I$ to express the fact that the pressure is constant across the boundary layer.

We suppose that the main stream is slow so that compressibility effects present in the boundary layer are entirely due to a large temperature difference between the wall and the stream. In such a case it is well known that the dissipation term in (3) may be neglected and we may write the energy equation in the form,

$$\frac{\partial}{\partial t}\left(\frac{\rho T}{T_e}\right) + \frac{\partial}{\partial x}\left(\frac{\rho u T}{T_e}\right) + \frac{\partial}{\partial y}\left(\frac{\rho v T}{T_e}\right) = \frac{1}{\sigma}\frac{\partial}{\partial y}\left[\mu\frac{\partial}{\partial y}\left(\frac{T}{T_e}\right)\right] \tag{4}$$

Equation (4) implies that $\mathbf{M}_\infty^2 \ll (T_w - T_\infty)/T_\infty$ and we notice that the terms involving the pressure gradient have not been neglected but are absorbed in the new dependent variable T/T_e.

We intend to study the unsteadiness associated with a main stream consisting of an oscillating perturbation superimposed upon a steady streaming motion, such as may arise when a sound wave is present in a steady stream. This flow, when a circular cylinder is placed in the stream, is considered in Section 4 and the appropriate main stream is obtained in the Appendix. In our other special case in Section 3, we consider the flow over a flat plate but here we choose $kx = 0$, thus obtaining solutions that are valid for values of x which are small compared with the wave length of the sound. In either case it may be shown by consideration of the acoustic equations that

$$T_e = T_\infty[1 + 0(\mathbf{M}_\infty)]$$

From now on we shall assume that terms of $0(\mathbf{M}_\infty)$ may be neglected and hence

$$T_e = \text{const} = T_\infty,$$

and therefore

$$\rho_e = \text{const} = \rho_\infty$$

Equations (1), (2), and (4) are now integrated across the boundary layer in the standard, Pohlhausen manner and use is made of the integrated form of (1) to eliminate the normal velocity component.

By introducing the co-ordinate

$$Y = \frac{1}{\rho_w}\int_0^y \rho\, dy$$

some simple analysis shows that the integrated momentum and energy equations may be written in the form,

$$\frac{\partial}{\partial t}\left[u_e\int_0^\Delta (1-f)dY\right] + \frac{\partial}{\partial x}\left[u_e^2\int_0^\Delta f(1-f)dY\right] + u_e\frac{\partial u_e}{\partial x}\int_0^\Delta (1-f)dY + \left(\frac{\partial u_e}{\partial t} + u_e\frac{\partial u_e}{\partial x}\right)\int_0^{\chi\Delta} g\,dY = \nu_w u_e(\partial f/\partial Y)_{Y=0}, \tag{5}$$

and

$$\frac{\partial}{\partial t}\left[\int_0^{\chi\Delta} g dY\right] + \frac{\partial}{\partial x}\left[u_e\int_0^{\chi\Delta} fg\, dY\right] = -\frac{\nu_w}{\sigma}\left(\frac{\partial g}{\partial Y}\right)_{Y=0}, \tag{6}$$

where ν_w is the (constant) kinematic viscosity at the wall and Δ and $\chi\Delta$ are the thicknesses of the velocity and temperature boundary layers in terms of Y. In (5) and (6), f and g are the velocity and temperature-distribution functions in the boundary layer defined by

$$u/u_e = f(x, Y, t); \quad \frac{T - T_e}{T_e} = \frac{T}{T_\infty} - 1 = g(x, Y, t)$$

Finally, we have assumed a viscosity-temperature law of the type used by Chapman and Rubesin (1949). This is

$$\mu = (\mu_w/T_w)T,$$

where μ_w is to be calculated from T_w by the more accurate Sutherland law. It follows that $\mu\rho = \mu_w\rho_w$.

In order to solve equations (5) and (6) we shall suppose the functions f and g are quartic functions $F(\eta)$, $G(\eta)$ of the variable $\eta = Y/\Delta$. Thus as in incompressible boundary-layer theory,

$$F(\eta) = \eta(2 - 2\eta^2 + \eta^3) + \eta(1 - \eta^2)\lambda/6, \tag{7}$$

which satisfies

$$F(0) = 0, \quad F''(0) = -\lambda; \quad F(1) = 1, \quad F'(1) = F''(1) = 0,$$

and the dashes denote differentiation with respect to η. Since, from (2), we require that

$$\frac{\partial u_e}{\partial t} + u_e\frac{\partial u_e}{\partial x} = -\frac{1}{\rho_e}\left[\frac{\partial}{\partial y}\left(\mu\frac{\partial u}{\partial y}\right)\right]_{y=0} = -\nu_w u_e\left[\frac{\rho}{\rho_e}\frac{d^3 f}{dY^3}\right]_{Y=0},$$

it follows that

$$\lambda = \frac{\Delta^2}{\nu_w}\left(\frac{1}{u_e}\frac{\partial u_e}{\partial t} + \frac{\partial u_e}{\partial x}\right)\frac{T_w}{T_\infty} \tag{8}$$

Also,

$$G(\eta) = \left(\frac{T_w - T_\infty}{T_\infty}\right)(1 + \eta/\chi)(1 - \eta/\chi)^3, \tag{9}$$

which satisfies

$$G(0) = \left(\frac{T_w - T_\infty}{T_\infty}\right), \quad G''(0) = 0; \quad G(\chi) = G'(\chi) = G''(\chi) = 0$$

We shall assume that T_w is independent of t whence it follows from (4) that

$$\left[\frac{\partial}{\partial y}\left(\mu\frac{\partial T}{\partial y}\right)\right]_{y=0} = 0,$$

which implies that $G''(0) = 0$.

Thus with the expressions (7) and (9) we have satisfied the boundary conditions $u = 0$, $T = T_w$ and the differential equations at the wall and we have insured, as far as is possible with quartic expressions, that the velocity and temperature pass over to their main stream values smoothly at the outer edge of the boundary layer.

We next observe that, for the present case,

$$\int_0^1 (1 - F)d\eta = P_1(\lambda) = {}^3/_{10} - {}^1/_{120}\cdot\lambda,$$

$$\int_0^1 F(1 - F)d\eta = P_2(\lambda) = {}^{37}/_{315} - {}^1/_{945}\cdot\lambda - {}^1/_{9072}\cdot\lambda^2, \quad (10)$$

$$\int_0^\chi G d\eta = \left(\frac{T_w}{T_\infty} - 1\right) Q_1(\chi), \text{ where } Q_1(\chi) = 3\chi/10$$

If $\chi \leq 1$, the integral

$$\int_0^\chi FG\, d\eta$$

may be found by direct substitution of F and G. If $\chi > 1$, however, it must be written in the form

$$\int_0^1 FG\, d\eta + \int_1^\chi G\, d\eta$$

since for $1 \leq \eta \leq \chi$, $F = 1$. In either case the result may be written as

$$\int_0^\chi FG\, d\eta = (T_w/T_\infty - 1)[Q_2(\chi) + \lambda Q_3(\chi)],$$

where

$$Q_2(\chi) = \begin{cases} \chi^2({}^2/_{15} - {}^3/_{140}\cdot\chi^2 + {}^1/_{180}\cdot\chi^3), & (\chi \leq 1) \\ {}^3/_{10}(\chi - 1) + {}^2/_{15}\, 1/\chi \\ \quad - {}^3/_{140}\, 1/\chi^3 + {}^1/_{180}\, 1/\chi^4 & (\chi \geq 1) \end{cases} \quad (11)$$

$$Q_3(\chi) = \begin{cases} \chi^2({}^1/_{90} - {}^1/_{84}\cdot\chi + {}^3/_{560}\cdot\chi^2 - {}^1/_{1080}\cdot\chi^3), & (\chi \leq 1) \\ {}^1/_{120} - {}^1/_{180}\, 1/\chi + {}^1/_{840}\, 1/\chi^3 \\ \quad - {}^1/_{1024}\cdot 1/\chi^4, & (\chi \geq 1) \end{cases}$$

The substitution of these integrals into equations (5) and (6), (when these are written with η as independent variable) leads to the following two simultaneous, first-order, partial differential equations for λ, Δ, and χ,

$$\frac{\partial}{\partial t}\left[u_e \Delta P_1(\lambda)\right] + \frac{\partial}{\partial x}\left[u_e{}^2 \Delta P_2(\lambda)\right] + u_e \frac{\partial u_e}{\partial x}\Delta P_1(\lambda) + \left(\frac{\partial u_e}{\partial t} + u_e \frac{\partial u_e}{\partial x}\right)\left(\frac{T_w}{T_\infty} - 1\right)\Delta Q_1(\chi) = \frac{\nu_w}{\Delta} u_e\left(2 + \frac{\lambda}{6}\right), \quad (12)$$

$$\frac{\partial}{\partial t}\left[\Delta Q_1(\chi)\right] + \frac{\partial}{\partial x}\left\{u_e \Delta[Q_2(\chi) + \lambda Q_3(\chi)]\right\} = \frac{\nu_w}{\sigma}\frac{2}{\Delta\chi} \quad (13)$$

In the present problem with a slow flow, as we have seen, compressibility effects do not extend to the main stream. We may therefore consider unsteadiness of the stream of the type discussed by Lighthill in his work on incompressible boundary layers and we write,

$$u_e(x, t) = V_0(x) + \epsilon V_1(x) e^{-i\omega t} \quad (14)$$

where ϵ is a small constant, and ω is the frequency of oscillation. For a stream fluctuating in magnitude only we should have $V_0(x) = V_1(x)$.

Now that we have chosen the form (14) for $u_e(x, t)$ we may assume that the remaining quantities associated with the boundary layer can be expressed in a similar manner, each consisting of a steady part depending on x and a superimposed oscillating part whose amplitude depends on x only. Thus if H is any boundary-layer quantity (such as λ, χ, or Δ), we may write

$$H = H_0(x) + \epsilon H_1(x) e^{-i\omega t} \quad (15)$$

This enables us to separate the steady and nonsteady components of the flow (denoted by the suffixes 0 and 1). Hence after eliminating Δ by relation (8), we obtain, from (12) and (13), two pairs of ordinary differential equations for the unknowns λ_0, χ_0, and λ_1, χ_1, respectively. In fact, we have

$$\left[\frac{1}{2}P_2(\lambda_0) + \lambda_0 P_2'(\lambda_0)\right] d\lambda_0/dx = \frac{1}{2}\lambda_0 P_2(\lambda_0)\, \frac{d^2V_0}{dx^2}\Big/\frac{dV_0}{dx} + \left[\left(2 + \frac{1}{6}\lambda_0\right)\frac{T_w}{T_\infty} - \lambda_0 P_1(\lambda_0) - 2\lambda_0 P_2(\lambda_0) - \lambda_0 Q_1(\chi_0)\left(\frac{T_w}{T_\infty} - 1\right)\right]\frac{dV_0}{dx}\Big/ V_0, \quad (16)$$

$$\frac{1}{2}\chi_0[Q_2(\chi_0) + 3\lambda_0 Q_3(\chi_0)]\frac{d\lambda_0}{dx} + \lambda_0\chi_0[Q_3'(\chi_0) + \lambda_0 Q_3'(\chi_0)]\frac{d\chi_0}{dx} = \frac{1}{2}\lambda_0\chi_0[Q_2(\chi_0) + \lambda_0 Q_3(\chi_0)]\frac{d^2V_0}{dx^2}\Big/\frac{dV_0}{dx} + \left[\frac{2}{\sigma}\frac{T_w}{T_\infty} - \lambda_0\chi_0 Q_2(\chi_0) - \lambda_0{}^2\chi_0 Q_3(\chi_0)\right]\frac{dV_0}{dx}\Big/ V_0, \quad (17)$$

for λ_0 and χ_0, together with

$$\begin{aligned} &\left[\frac{1}{2}P_2(\lambda_0) + \lambda_0 P_2'(\lambda_0)\right]\frac{d\lambda_1}{dx} \\ &= \Big\{ - \left[\frac{3}{2}P_2'(\lambda_0) + \lambda_0 P_2''(\lambda_0)\right]\frac{d\lambda_0}{dx} \\ &\quad + \frac{1}{2}[P_2(\lambda_0) + \lambda_0 P_2'(\lambda_0)]\frac{d^2V_0}{dx^2}\Big/\frac{dV_0}{dx} \\ &\quad + \left[\frac{1}{6}\frac{T_w}{T_\infty} - P_1(\lambda_0) - 2P_2(\lambda_0) - \lambda_0 P_1'(\lambda_0) - 2\lambda_0 P_2'(\lambda_0)\right. \\ &\quad \left. - Q_1(\chi_0)\left(\frac{T_w}{T_\infty} - 1\right)\right]\frac{dV_0}{dx}\Big/ V_0 + \left[\frac{1}{2}P_1(\lambda_0) + \lambda_0 P_1'(\lambda_0)\right]\frac{i\omega}{V_0}\Big\}\lambda_1 \\ &\quad - \left[\lambda_0 Q_1'(\chi_0)\left(\frac{T_w}{T_\infty} - 1\right)\frac{dV_0}{dx}\Big/ V_0\right]\cdot\chi_1 \\ &\quad - \frac{1}{2}\lambda_0 P_1(\lambda_0)\left(-\frac{i\omega V_1}{V_0} + \frac{dV_1}{dx}\right)\frac{i\omega/V_0}{dx}\frac{dV_0}{dx} \\ &\quad + \frac{1}{2}\lambda_0 P_2(\lambda_0) i\omega V_1 \frac{d^2V_0}{dx^2}\Big/ V_0\left(\frac{dV_0}{dx}\right)^2 \\ &\quad - \left[\left(\frac{dV_1}{dx}\Big/\frac{dV_0}{dx} - \frac{V_1}{V_0}\right)\frac{\lambda_0 P_2(\lambda_0)}{2}\right. \\ &\quad + \frac{V_1}{V_0}\frac{T_w}{T_\infty}\left(2 + \frac{\lambda_0}{6}\right) - \lambda_0 P_1(\lambda_0)\frac{V_1}{V_0} \\ &\quad \left. - \lambda_0 Q_1(\chi_0)\frac{V_1}{V_0}\left(\frac{T_w}{T_\infty} - 1\right)\right]\frac{i\omega}{V_0} - \left[2\lambda_0 P_2(\lambda_0) + \lambda_0 P_1(\lambda_0)\right. \\ &\quad \left. + \left(\frac{T_w}{T_\infty} - 1\right)\lambda_0 Q_1(\chi_0) - \frac{T_w}{T_\infty}\left(2 + \frac{\lambda_0}{6}\right)\right] \\ &\quad \times \left(\frac{dV_1}{dx}\Big/\frac{dV_0}{dx} - \frac{V_1}{V_0}\right)\frac{dV_0}{dx}\Big/ V_0 \\ &\quad - \frac{1}{2}\lambda_0 P_2(\lambda_0)\left[\frac{d^2V_0}{dx^2}\Big/\frac{dV_0}{dx} - \frac{d^2V_1}{dx^2}\Big/\frac{dV_1}{dx}\right]\frac{dV_1}{dx}\Big/\frac{dV_0}{dx}, \end{aligned} \quad (18)$$

$$\begin{aligned} &\frac{\chi_0}{2}\,[Q_2(\chi_0) + 3\lambda_0 Q_3(\chi_0)]\frac{d\lambda_1}{dx} + \lambda_0\chi_0[Q_2'(\chi_0) + \lambda_0 Q_3'(\chi_0)]\frac{d\chi_1}{dx} \\ &= \Big\{ - \frac{3}{2}\chi_0 Q_3(\chi_0)\frac{d\lambda_0}{dx} \\ &\quad - \chi_0[Q_3'(\chi_0) + 2\lambda_0 Q_3'(\chi_0)]\frac{d\chi_0}{dx} \\ &\quad + \chi_0\left[\frac{1}{2}Q_2(\chi_0) + \lambda_0 Q_3(\chi_0)\right]\frac{d^2V_0}{dx^2}\Big/\frac{dV_0}{dx} \end{aligned}$$

$$- \chi_0[Q_2(\chi_0) + 2\lambda_0 Q_3(\chi_0)] \frac{dV_0}{dx}\Big/ V_0 + \frac{1}{2}\chi_0 Q_1(\chi_0) \frac{i\omega}{V_0}\Big\} \lambda_1$$

$$+\Big\{-\frac{1}{2}[Q_2(\chi_0) + \chi_0 Q_2'(\chi_0) + 3\lambda_0 Q_3(\chi_0) + 3\lambda_0\chi_0 Q_3'(\chi_0)]\frac{d\lambda_0}{dx}$$

$$- [Q_2'(\chi_0) + \chi_0 Q_2''(\chi_0) + \lambda_0 Q_3'(\chi_0) + \lambda_0\chi_0 Q_3''(\chi_0)]\lambda_0 \frac{d\chi_0}{dx}$$

$$+ \lambda_0[Q_2(\chi_0) + \chi_0 Q_2'(\chi_0) + \lambda_0 Q_3(\chi_0) + \lambda_0\chi_0 Q_3'(\chi_0)]$$

$$\times \left(\frac{1}{2}\frac{d^2V_0}{dx^2}\Big/\frac{dV_0}{dx} - \frac{dV_0}{dx}\Big/ V_0\right) + \lambda_0\chi_0 Q_1'(\chi_0)\frac{i\omega}{V_0}\Big\}\chi_1$$

$$+ \frac{1}{2}\lambda_0\chi_0 Q_1(\chi_0)\left(\frac{i\omega V_1}{V_0} - \frac{dV_1}{dx}\right)\frac{i\omega}{V_0 dV_0/dx}$$

$$+ \frac{1}{2}\lambda_0\chi_0[Q_2(\chi_0) + \lambda_0 Q_3(\chi_0)]\left(V_1\frac{d^2V_0}{dx^2}\Big/\frac{dV_0}{dx}\right.$$

$$\left. + V_1\frac{dV_0}{dx}\Big/ V_0 - \frac{dV_1}{dx}\right)\frac{i\omega}{V_0 dV_0/dx}$$

$$+ \left[\frac{2}{\sigma}\frac{T_w}{T_\infty} - \lambda_0\chi_0 Q_3(\chi_0) - \lambda_0^2\chi_0 Q_3(\chi_0)\right]$$

$$\times \left(\frac{dV_1}{dx}\Big/\frac{dV_0}{dx} - \frac{V_1}{V_0}\right)\frac{dV_0}{dx}\Big/ V_0 - \frac{1}{2}\lambda_0\chi_0[Q_2(\chi_0) + \lambda_0 Q_3(\chi_0)]$$

$$\times \left(\frac{d^2V_0}{dx^2}\Big/\frac{dV_0}{dx} - \frac{d^2V_1}{dx^2}\Big/\frac{dV_1}{dx}\right)\frac{dV_1}{dx}\Big/\frac{dV_0}{dx} - \frac{2}{\sigma}\frac{T_w}{T_\infty}\frac{i\omega V_1}{V_0^2}, \quad (19)$$

for λ_1 and χ_1. The dashes affixed to the P_i and Q_i denote differentiation with respect to λ and χ, respectively,

The solution of the second pair of equations for λ_1 and χ_1, although in general involving laborious computation, is in principle perfectly straightforward once λ_0 and χ_0 have been determined from (16) and (17). The latter equations arise from the terms independent of ϵ and the values of λ_0 and χ_0 are appropriate to a steady boundary-layer flow with main stream $V_0(x)$.

The important physical quantities in the flow are the skin friction τ_w and the heat transfer at the wall q_w, which we shall also write in the form (15). Now τ_w is defined as $\mu_w(\partial u/\partial y)_{y=0}$ and hence

$$\tau_w = \frac{\mu_w u_r}{\Delta}(2 + \lambda/6)$$

Then, on substituting for the various quantities involved and equating powers of ϵ in the usual way we obtain, for the steady part of the skin friction,

$$\tau_{w0} = \frac{\mu_w V_0}{\Delta_0}(2 + \lambda_0/6), \quad (20)$$

and, for the unsteady part,

$$\tau_{w1} = \left[\frac{V_1}{V_0} - \frac{\Delta_1}{\Delta_0} + \frac{\lambda_1}{6(2 + \lambda_0/6)}\right]\tau_{w0} \quad (21)$$

Similarly, for the heat transfer from the surface to the air $q_w = -k_w(\partial T/\partial y)_{y=0}$, we obtain

$$q_{w0} = 2\mu_w C_p(T_w - T_\infty)/\sigma\chi_0\Delta_0, \quad (22)$$

and

$$q_{w1} = -(\chi_1/\chi_0 + \Delta_1/\Delta_0)q_{w0} \quad (23)$$

In the foregoing expressions Δ_0 and Δ_1 may be expressed in terms of λ_0 and λ_1 from the relation (8).

We shall consider two relatively easy special cases, the boundary layer on a flat plate for which $V_0(x) = V_1(x) = \text{const}$ and the boundary layer near the forward stagnation point of a blunt-nosed cylinder for which $V_0(x)$ and $V_1(x)$ are each proportional to x. Since various exact solutions have been obtained for the first of these cases (by Moore, Ostrach, and Illingworth), the results for the flat plate will serve as a test of the accuracy of the present method. We may then apply the method to the second case with a sound wave in the incident stream. The main stream here, taking into account the scattering of the sound and, for simplicity assuming the cylinder to be circular, is obtained in the Appendix as an expression which is valid for low frequency.

3 The Flat Plate

In this section the flow in the boundary layer over a flat plate is considered. We shall write here $V_0(x) = V_1(x) = \text{const} = V$, say, and it follows from (8) that

$$\lambda_0 = 0, \quad \lambda_1 = -i\omega\Delta_0^2/\nu_w \cdot T_w/T_\infty \quad (24)$$

It is convenient in this case to refer directly back to equations (12) and (13) which give, from terms independent of ϵ,

$$P_2(0)\frac{d\Delta_0}{dx} = 2\nu_w/\Delta_0 V,$$

$$d/dx[\Delta_0 Q_2(\chi_0)] = 2\nu_w/\sigma\Delta_0\chi_0 V$$

Hence,

$$\Delta_0 = 2[\nu_w x/VP_2(0)]^{1/2}, \quad (25)$$

and χ_0, a constant, is the positive root of the equation

$$\chi Q_2(\chi) = P_2(0)/\sigma \quad (26)$$

The terms containing the factor $\epsilon e^{-i\omega t}$ in (12) and (13) then yield the following equations for Δ_1/Δ_0, a new dependent variable, and χ_1:

$$\frac{d}{dx}\left(\frac{\Delta_1}{\Delta_0}\right) + \left[\frac{1}{x} - \frac{i\omega}{V}\frac{P_1(0)}{P_2(0)}\right]\frac{\Delta_1}{\Delta_0} = -\frac{1}{2x}$$

$$+\Big\{\frac{T_w}{T_\infty}\left[\frac{6P_2'(0)}{P_2(0)} - \frac{1}{6}\right] + P_1(0) + Q_1(\chi_0)\left(\frac{T_w}{T_\infty} - 1\right)\Big\}\frac{i\omega}{VP_2(0)}$$

$$- \left(\frac{i\omega}{V}\right)^2\frac{T_w}{T_\infty}\frac{4P_1'(0)}{[P_2(0)]^2}\cdot x, \quad (27)$$

$$Q_2'(\chi_0)\frac{d\chi_1}{dx} + Q_2(\chi_0)\frac{d}{dx}\left(\frac{\Delta_1}{\Delta_0}\right)$$

$$+\Big\{\frac{1}{2}\left[Q_2'(\chi_0) + \frac{Q_2'(\chi_0)}{\chi_0}\right]\frac{1}{x} - \frac{i\omega}{V}Q_1'(\chi_0)\Big\}\chi_1$$

$$+\left[\frac{Q_2(\chi_0)}{x} - \frac{i\omega}{V}Q_1(\chi_0)\right]\frac{\Delta_1}{\Delta_0} = -\frac{Q_2(\chi_0)}{x} + 6\frac{i\omega}{V}\frac{T_w}{T_\infty}\frac{Q_2(\chi_0)}{P_2(0)} \quad (28)$$

We shall in fact be concerned only with the solution of these equations for small values of ω. [Actually, by writing equation (27) with Δ_1 as dependent variable and Δ_0 as the new independent variable, a solution for Δ_1 in closed form is readily obtained for general ω.] First we note that equation (27) for Δ_1/Δ_0 does not contain χ_1 and so may be solved independently of (28). We look for a series solution in ascending powers of the nondimensional frequency parameter $i\omega x/V$, of the form,

$$\Delta_1/\Delta_0 = b_0 + b_1\frac{i\omega x}{V} + \ldots\ldots \quad (29)$$

After substituting this expression into the differential equation and equating like powers of x, b_0, and b_1 are found to be given by,

$$b_0 = -1/2,$$

$$b_1 = \frac{1}{2P_2(0)}\Big\{\frac{P_1(0)}{2} + \frac{T_w}{T_\infty}\left[\frac{6P_2'(0)}{P_2(0)} - \frac{1}{6}\right]$$

$$+ Q_1(\chi_0)\left(\frac{T_w}{T_\infty} - 1\right)\Big\}$$

Equation (28) is an equation for χ_1 now that Δ_1 is known. We assume χ_1 is expressible in ascending powers of $i\omega x/V$ in the form,

$$\chi_1 = c_0 + c_1 \frac{i\omega x}{V} + \ldots,$$

when equation (28) yields,

$$c_0 = 0,$$

$$c_1 = \frac{\left[-Q_1(\chi_0) + 12\,\frac{Q_2(\chi_0)}{P_2(0)}\,\frac{T_w}{T_\infty}\right] - 4Q_2(\chi_0)b_1}{3Q_2'(\chi_0) + Q_2(\chi_0)/\chi_0}$$

The physical quantities of interest are the skin friction and the heat transfer and the foregoing solutions for Δ_1 and χ_1 enable us to calculate the first two terms of the series for these quantities. The numerical computations involved have been carried out for the quartic profiles given in Section 2. Here the P_i, Q_i are those defined by (10) and (11) and therefore (25) gives

$$\Delta_0 = 5.836(\nu_w x/V)^{1/2}$$

Now equation (26) is a relation between the Prandtl number σ and χ_0. It is easily verified that $\sigma = 1$, $\chi_0 = 1$ satisfies this equation and we shall evaluate the results for this case as the computations are comparatively easy to carry out. Also, with $\chi_0 = 1.130$, (26) yields σ equal to 0.714, a value more appropriate for air, which is adopted for a second computation.

From (20), the steady part of the skin friction is,

$$\tau_{w0} = 2\mu_w V/\Delta_0 = 0.343(\mu_w \rho_w V^3/x)^{1/2}$$

For flow along a plate, the unsteady part of the skin friction is given by,

$$\tau_{w1}/\tau_{w0} = 1 - \frac{\Delta_1}{\Delta_0} + \frac{\lambda_1}{12} = {}^1/_2 - \left[b_1 + \frac{1}{3P_2(0)} \cdot \frac{T_w}{T_\infty}\right]\frac{i\omega x}{V} + \ldots,$$

from (21) together with (24) and (29). The results are,

$$\tau_{w1}/\tau_{w0} = 1.5 + (0.639 - 3.175\ T_w/T_\infty)\,\frac{i\omega x}{V} + \ldots, \text{ for } \sigma = 1,$$

$$\tau_{w1}/\tau_{w0} = 1.5 + (0.805 - 3.341\ T_w/T_\infty)\,\frac{i\omega x}{V} + \ldots, \quad \text{for } \sigma = 0.714 \quad (30)$$

Similarly, the two parts of the heat transfer are obtained from (22) and (23) and, for $\sigma = 0.714$, we must use the values of $Q_2(\chi_0)$ and $Q_3(\chi_0)$ appropriate to $\chi_0 > 1$. The steady term is

$$q_{w0} = 0.343C_p(T_w - T_\infty)(\mu_w \rho_w V/x)^{1/2} \quad \text{for} \quad \sigma = 1,$$

$$q_{w0} = 0.425C_p(T_w - T_\infty)(\mu_w \rho_w V/x)^{1/2} \quad \text{for} \quad \sigma = 0.714,$$

and the unsteady term, after substituting for Δ_1/Δ_0 and χ_1, is given by

$$q_{w1}/q_{w0} = {}^1/_2 - (b_1 + c_1/\chi_0)\,\frac{i\omega x}{V} + \ldots,$$

which yields

$$q_{w1}/q_{w0} = 0.5 + (0.639 - 0.624\ T_w/T_\infty)\,\frac{i\omega x}{V} + \ldots, \text{ for } \sigma = 1,$$

$$q_{w1}/q_{w0} = 0.5 + (0.661 - 0.636\ T_w/T_\infty)\,\frac{i\omega x}{V} + \ldots, \text{ for } \sigma = 0.714 \quad (31)$$

We may compare these expressions with known exact results. When $T_w/T_\infty = 1$, Moore's (1951) results for the skin friction on a heat-insulated flat plate moving in a compressible fluid are applicable to our problem. He calculates,

$$\tau_{w1}/\tau_{w0} = 1.5 - 2.555\ i\omega x/V - 1.414(i\omega x/V)^2 + \ldots$$

Ostrach (1955) also calculates the heat transfer for the same problem when the wall temperature is constant. When $T_w/T_\infty = 1$ and dissipation is neglected his expression for the heat transfer reduces to,

$$q_{w1}/q_{w0} = 0.5 + 0.069\,\frac{i\omega x}{V} - 0.423\left(\frac{i\omega x}{V}\right)^2 + \ldots, \text{ for } \sigma = 0.72$$

Our results, when $T_w/T_\infty = 1$ and $\sigma = 0.714$, become

$$\tau_{w1}/\tau_{w0} = 1.5 - 2.536\ i\omega x/V + \ldots,$$

$$q_{w1}/q_{w0} = 0.5 + 0.025\ i\omega x/V + \ldots$$

One notices from the foregoing expressions that the Pohlhausen method with quartic profiles for the velocity and temperature distributions predicts rather well the coefficient of $i\omega x/V$ given by Moore for the skin friction. Somewhat less satisfactory agreement is obtained for the corresponding heat-transfer term when compared with Ostrach's results. For values of T_w/T_∞ different from unity, Moore's and Ostrach's results on the one hand and ours on the other are not comparable since they consider the plate to be moving in the compressible fluid, whereas we suppose the plate to be fixed. However, Illingworth (1958) has obtained an exact solution to our problem and for $T_w/T_\infty = 2$, for example, he obtains

$$\left.\begin{aligned}\tau_{w1}/\tau_{w0} &= 1.5 - 6.217\ i\omega x/V + \ldots,\\ q_{w1}/q_{w0} &= 0.5 - 0.770\ i\omega x/V + \ldots\end{aligned}\right\} \quad \text{for} \quad \sigma = 0.72$$

For this case, the expressions (30) and (31) yield,

$$\tau_{w1}/\tau_{w0} = 1.5 - 5.877\ i\omega x/V + \ldots,$$

$$q_{w1}/q_{w0} = 0.5 - 0.611\ i\omega x/V + \ldots$$

Thus for the case of a zero external pressure gradient the method appears to predict fairly satisfactorily the second terms in the series for the skin friction and the heat transfer obtained by exact solutions of the equations of motion.

4 The Circular Cylinder

Having found in the preceding section that the Pohlhausen method gives reasonably good results at least for the skin friction in unsteady flow over a flat plate, we consider now its application to the case of a circular cylinder fixed in a slow stream which, although basically steady with velocity U_∞, contains a sound wave. The presence of the wave introduces the unsteadiness into the problem. Such a model is suggested by the Rijke tube phenomenon. The expression for the main stream for this problem is obtained in the Appendix and may be written in the form

$$u_e(x, t) = V(x)(1 + \epsilon e^{-i\omega t}), \quad (32)$$

where $\epsilon = ik(1 + ikR)E$. Here, k is the wave number, R the radius of the cylinder, and $V(x) = 2U_\infty x/R = cx$, say. The quantity $U_\infty E$ is the amplitude of the fluctuation in the velocity potential of the incident wave (Appendix). Expression (32) is valid for the external flow near the forward stagnation point of the cylinder (so that x is considered to be small) when the frequency is small. Also, since terms of $0(\mathbf{M}_\infty)$ have been neglected in obtaining (32) we may apply the theory of Section 2. It follows from (8), with

$$V_0(x) = V_1(x) = V(x) = cx,$$

that now $$\lambda_0 = \frac{c}{\nu_w} \cdot \frac{T_w}{T_\infty} \Delta_0^2,$$

and $$\lambda_1 = \frac{c}{\nu_w} \cdot \frac{T_w}{T_\infty}\left[\left(1 - \frac{i\omega}{c}\right)\Delta_0^2 + 2\Delta_0\Delta_1\right] \quad (33)$$

It is well known that for steady flow near a stagnation point Δ_0 is constant and so λ_0 is constant. The momentum equation (16) reduces to,

$$(2 + \lambda_0/6)\frac{T_w}{T_\infty} = \lambda_0\left[P_1(\lambda_0) + 2P_2(\lambda_0) + Q_1(\chi_0) \times \left(\frac{T_w}{T_\infty} - 1\right)\right] \quad (34)$$

Here, all terms are independent of x, except possibly $Q_1(\chi_0)$ from which it follows that χ_0 itself is a constant. Hence equation (17) for χ_0 reduces to

$$\lambda_0\chi_0[Q_2(\chi_0) + \lambda_0 Q_2(\chi_0)] = 2\,T_w/\sigma T_\infty \quad (35)$$

Now (34) and (35) are two simultaneous, algebraic equations for λ_0 and χ_0 involving the two parameters σ and T_w/T_∞. We take $\sigma = 0.714$ as before but now λ_0 and χ_0 cannot easily be expressed in terms of T_w/T_∞, and the calculation must be repeated for each value of T_w/T_∞. In practice it is found more convenient to start with a given χ_0 and then solve (34) and (35) for λ_0 and T_w/T_∞. This procedure leads to sets of values such as are given in Table 1, from which λ_0 and χ_0 for a selected value of T_w/T_∞ may be determined by inverse interpolation.

Table 1 Sets of values of χ_0, λ_0, and T_w/T_∞ for $\sigma = 0.714$

χ_0	λ_0	T_w/T_∞
1.4	6.784	0.817
1.5	7.052	1.013
1.6	6.912	1.162
1.7	6.638	1.288
1.8	6.323	1.403
1.9	6.001	1.509
2.0	5.688	1.611
2.1	5.391	1.709
2.2	5.113	1.803
2.3	4.854	1.895
2.4	4.614	1.986
2.5	4.391	2.074

We now turn to the equations for the nonsteady parts of λ and χ and define new dependent variables by

$$\lambda_1 = (i\omega/c)\Lambda_1, \quad \chi_1 = (i\omega/c)\Psi_1$$

Equations (18) and (19) become for the present case,

$$D_0 x\frac{d\Lambda_1}{dx} + \left(D_1\frac{i\omega}{c} + D_2\right)\Lambda_1 + D_3\Psi_1 + D_4\frac{i\omega}{c} + D_5 = 0, \quad (36)$$

$$E_0 x\frac{d\Lambda_1}{dx} + E_1 x\frac{d\Psi_1}{dx} + \left(E_2\frac{i\omega}{c} + E_3\right)\Lambda_1 + \left(E_4\frac{i\omega}{c} + E_5\right)\Psi_1 + E_6\frac{i\omega}{c} + E_7 = 0, \quad (37)$$

where the D_i and E_i are determinable constants (for each particular value of σ and T_w/T_∞) and are given explicitly in the Appendix.

Solutions of these equations satisfying the physical requirement of a finite boundary-layer thickness at the front of the cylinder are the constants,

$$\Lambda_1 = \frac{-D_4E_4(i\omega/c)^2 + (D_3E_6 - D_2E_4 - D_4E_5)i\omega/c + D_3E_7 - D_2E_5}{D_1E_4(i\omega/c)^2 + (D_1E_5 + D_2E_4 - D_3E_2)i\omega/c + D_2E_5 - D_3E_3} \quad (38)$$

$$\Psi_1 = \frac{(D_1E_7 - D_1E_6)(i\omega/c)^2 + (D_3E_7 + D_4E_3 - D_2E_6 - D_1E_7)i\omega/c + D_1E_3 - D_2E_7}{D_1E_4(i\omega/c)^2 + (D_1E_5 + D_2E_4 - D_3E_2)i\omega/c + D_2E_5 - D_3E_3} \quad (39)$$

Our first choice of T_w/T_∞ is unity when the equations reduce to those for the incompressible case. This is of special interest because the momentum equation (2) becomes independent of the energy equation (4). A consequence of this is that the equation for λ_0 may be written down immediately from (34) and reduces to,

$$5\lambda_0^3 + 237\lambda_0^2 - 8352\lambda_0 + 45{,}360 = 0$$

The required solution is $\lambda_0 = 7.052$ [see Schlichting (1955), chapter 12]. Since $D_3 = 0$ for this case equation (36) for Λ_1 may be solved independently of (37). Numerical computation yields

$$\lambda_1 = \frac{i\omega}{c}\,\frac{(-2.325 + 0.851\,i\omega/c)}{(0.188 - 0.062\,i\omega/c)}$$

Our original assumptions, that $\mathbf{M}_\infty$, $kR \ll 1$, imply that $i\omega/c = ikR/2\mathbf{M}_\infty$ is the ratio of two small quantities. Thus we consider two cases. We shall consider $i\omega/c$ to be very small or large implying that the values of kR are much smaller or larger than those of the Mach number in this problem, although of course both parameters are small compared with unity. We may therefore expand the expression for λ_1 in powers of $i\omega/c$ and inverse powers of $i\omega/c$, respectively, for these two cases.

For the steady component of skin friction we obtain,

$$\tau_{w0} = 3.382(\mu_w\rho_w)^{1/2}(U_\infty/R)^{3/2}x,$$

while the nonsteady component, after substitution for λ_1 (and hence Δ_1) for the two cases mentioned previously, becomes from (21),

$$\tau_{w1}/\tau_{w0} = \begin{cases} 1.5 - 0.272\,i\omega/c - 0.008(i\omega/c)^2 + \ldots, & \dfrac{i\omega}{c}\ \text{small}, \\ -0.247\,i\omega/c + 1.578 + 0.236(i\omega/c)^{-1} + \ldots, & \dfrac{i\omega}{c}\ \text{large} \end{cases}$$

Equation (35) becomes a quintic equation for χ_0 now that λ_0 is known and has the solution $\chi_0 = 1.492$, while equation (37) for Ψ_1 remains unchanged except that $T_w/T_\infty = 1$ in the definition of the E_i. The solution for χ_1 is given by

$$\chi_1 = \frac{i\omega}{c}\,\frac{(0.392 - 1.979\,i\omega/c)}{(4.633 - 3.157\,i\omega/c)}$$

The steady part of the heat transfer is

$$q_{w0} = 1.000\,C_p(T_w - T_\infty)(\mu_w\rho_wU_\infty/R)^{1/2},$$

and the unsteady part is, from (23),

$$q_{w1}/q_{w0} = \begin{cases} -0.5 - 0.320\,i\omega/c - 0.215(i\omega/c)^2 + \ldots, & i\omega/c\ \text{small}, \\ +0.055\,i\omega/c + 0.266 + 0.127(i\omega/c)^{-1} + \ldots, & i\omega/c\ \text{large} \end{cases}$$

Here, in the incompressible case, the expressions for the skin friction and heat transfer for small frequency agree with those found by Lighthill (who calculated only the first two terms in the series) to the order of accuracy of his results. This agreement, however, only provides a check on the computations and not on the method since Lighthill himself used the Pohlhausen technique.

Finally, equations (36) and (37) are solved for values of the D_i and E_i corresponding to $T_w/T_\infty = 2.003$. This ratio insures that the flow is compressible and is appropriate for the red-hot wires in the Rijke tube. With $\sigma = 0.714$ we have $\lambda_0 = 4.568$ and $\chi_0 = 2.420$ for this case. Expressions (38) and (39) for Λ_1 and Ψ_1 now become,

$$\Lambda_1 = \begin{cases} 1.671 + 2.399\, i\omega/c + \ldots, & i\omega/c \text{ small}, \\ -6.439 - 32.23(i\omega/c)^{-1} - 140.4(i\omega/c)^{-2} + \ldots, & i\omega/c \text{ large}, \end{cases}$$

and

$$\Psi_1 = \begin{cases} -2.166 - 0.884\, i\omega/c + \ldots, & i\omega/c \text{ small}, \\ 0.496 + 9.736(i\omega/c)^{-1} + 40.59(i\omega/c)^{-2} + \ldots, & i\omega/c \text{ large} \end{cases}$$

The steady and nonsteady parts of the skin friction and heat transfer are,

$$\tau_{w0} = 5.172(\mu_w\rho_w)^{1/2}(U_\infty/R)^{3/2}x,$$
$$q_{w0} = -1.084\, C_p(T_w - T_\infty)(\mu_w\rho_w U_\infty/R)^{1/2},$$

$$\tau_{w1}/\tau_{w0} = \begin{cases} 1.5 - 0.582\, i\omega/c - 0.118(i\omega/c)^2 + \ldots, & i\omega/c \text{ small}, \\ -0.184\, i\omega/c + 3.082 + 6.896(i\omega/c)^{-1} + \ldots, & i\omega/c \text{ large}, \end{cases}$$

and

$$q_{w1}/q_{w0} = \begin{cases} 0.5 + 0.212\, i\omega/c + 0.103(i\omega/c)^2 + \ldots, & i\omega/c \text{ small}, \\ 0.004 - 1.399(i\omega/c)^{-1} + \ldots, & i\omega/c \text{ large} \end{cases}$$

It would be interesting to compare the foregoing expressions with exact results but the author does not know of any exact treatment of the present problem for a hot cylinder.

Acknowledgment

This work was completed as part of a PhD thesis in the Mathematics Department of the University of Manchester. The author is indebted to Mr. C. R. Illingworth for suggesting the problem and for his subsequent help in its solution. Acknowledgment also is made with thanks for the award of a D.S.I.R. maintenance grant during this period.

References

D. R. Chapman and M. W. Rubesin (1949), "Temperature and Velocity Profiles in Compressible Laminar Boundary Layer With Arbitrary Distribution of Surface Temperature," *Journal of the Aeronautical Sciences*, vol. 16, 1949, pp. 547–565.

C. R. Illingworth (1958), "The Effects of a Sound Wave on the Compressible Boundary Layer on a Flat Plate," *Journal of Fluid Mechanics*, vol. 3, 1958, pp. 471–493.

M. J. Lighthill (1954), "The Response of Laminar Skin Friction and Heat Transfer to Fluctuations in the Stream Velocity," *Proceedings of The Royal Society*, series A, vol. 224, 1954, pp. 1–23.

C. C. Lin (1957), "Motion in the Boundary Layer With a Rapidly Oscillating External Flow," IXe Congrès International de Mécaniqué Applique, Actes. Tome IV, Brussels, 1957, pp. 155–167.

F. K. Moore (1951) "Unsteady Laminar Boundary-Layer Flow," NACA TN 2471, 1951.

Simon Ostrach (1955), "Compressible Laminar Boundary Layer and Heat Transfer for Unsteady Motions of a Flat Plate," NACA TN 3569, 1955.

Lord Rayleigh (1894), "Theory of Sound," second edition, The Macmillan Company, London, England, 1894.

H. Schlichting (1955), "Boundary Layer Theory," McGraw-Hill Book Company, Inc., New York, N. Y.

APPENDIX

Here we derive the potential flow when a uniform stream carrying a sound wave impinges on a fixed circular cylinder. The equations which govern such a (nonsteady) flow may be written in their vector forms as

$$\partial\Phi/\partial t + {}^1/_2(\nabla\Phi)^2 + C^2/(\gamma - 1) = \text{const}, \tag{40}$$

and

$$\partial\rho/\partial t + \nabla\cdot(\rho\nabla\Phi) = 0, \tag{41}$$

where Φ is the complete velocity potential and C is the sound speed. We shall consider the unsteadiness as a linear perturbation to the basic steady flow and we may therefore write,

$$\Phi = U_\infty[r\cos\theta + \phi + Ee^{-i\omega t}(e^{ikr\cos\theta/1+\mathbf{M}_\infty} + \psi)] \tag{42}$$

and

$$\rho = \rho_\infty\left[1 + \bar{\rho} + \frac{ik\mathbf{M}_\infty}{1+\mathbf{M}_\infty}Ee^{-i\omega t}(e^{ikr\cos\theta/1+\mathbf{M}_\infty} + \xi)\right], \tag{43}$$

where r and θ are the plane polar co-ordinates with the origin at the center of the cylinder and the line $\theta = 0$ in the downstream direction. The first two terms in each of these expressions represent the steady flow past the cylinder wherein the disturbances $U_\infty\phi$ and $\rho_\infty\bar{\rho}$ caused by the cylinder are assumed to be given in general by the Janzen-Rayleigh expansions,

$$\phi = \phi_0 + \mathbf{M}_\infty^2\phi_1 + \ldots, \quad \bar{\rho} = \mathbf{M}_\infty^2\bar{\rho}_1 + \ldots$$

Since we are neglecting terms of $0(\mathbf{M}_\infty^2)$, in these expressions we need retain only $\phi_0 = (R^2/r)\cos\theta$. The incident sound wave is represented by the third terms in (42) and (43) and our problem is to determine the scattered field which is represented by the terms containing the unknowns, ψ and ξ. The relevant boundary conditions for (40) and (41) are

$$\partial\Phi/\partial r = 0, \quad r = R; \quad \Phi \to U_\infty r\cos\theta, \ \rho \to \rho_\infty \text{ as } r \to \infty$$

By replacing ϕ by ϕ_0 in (42) and $\bar{\rho}$ by 0 in (43) and substituting these expressions into the flow equations, the steady terms drop out and the terms in E yield two simultaneous, partial differential equations for ψ and ξ. We now set $\mathbf{M}_\infty = 0$, consistent with the assumptions made in the boundary-layer problem, and to this accuracy $\psi = \xi$.

In general, one might suppose that ψ and ξ are expressible as power series in $\mathbf{M}_\infty$ (of which we are here calculating the first term); viz.,

$$\psi = \psi_0 + \psi_1\mathbf{M}_\infty + \psi_2\mathbf{M}_\infty^2 + \ldots,$$
$$\xi = \xi_0 + \xi_1\mathbf{M}_\infty + \xi_2\mathbf{M}_\infty^2 + \ldots$$

As a further calculation which is of special interest apart from our present problem an attempt has been made to determine the coefficients ψ_1 and ξ_1. The function ψ_1 was found to satisfy an inhomogeneous wave equation which, however, had no solution satisfying the boundary condition at infinity, that ψ_1 should vanish there.

Returning to the case $\mathbf{M}_\infty = 0$, it may easily be shown that ψ satisfies the two-dimensional wave equation in the (r, θ)-plane. Hence the expression for ψ which satisfies the condition of zero normal velocity on the cylinder and represents an outgoing wave is,

$$\psi = -\frac{J_0'(kR)}{H_0'(kR)}H_0(kr) - 2\sum_{n=1}^{\infty} i^n\frac{J_n'(kR)}{H_n'(kR)}H_n(kr)\cos n\theta,$$

where the J_n and H_n are Bessel and Haenkel functions of the first kind and dashes denote differentiation with respect to kr.

The fluid velocity tangential to the surface of the cylinder is given by $(-1/r\ \partial\Phi/\partial\theta)_{r=R}$ which yields, on the assumption that kR is small,

$$u_e(x, t) = V(x)[1 + ik(1 + ikR)Ee^{-i\omega t}] \quad (44)$$

This expression represents the flow near the stagnation point since we have replaced $\sin\theta$ and $\sin 2\theta$ by x/R and $2x/R$. In addition, $V(x) = 2U_\infty x/R$ and terms of $0(kR)^3$ are neglected. The boundary-layer problem associated with the main stream (44) was the one treated in Section 4.

Constants D_i and E_i

$$D_0 = {}^1/_2 P_2(\lambda_0) + \lambda_0 P_2'(\lambda_0),$$
$$D_1 = -{}^1/_2 P_1(\lambda_0) - \lambda_0 P_1'(\lambda_0),$$
$$D_2 = 2/\lambda_0 \cdot T_w/T_\infty + \lambda_0 P_1'(\lambda_0) + 2\lambda_0 P_2'(\lambda_0),$$
$$D_3 = \lambda_0 Q_1'(\chi_0)(T_w/T_\infty - 1),$$
$$D_4 = -{}^1/_2\, \lambda_0 P_1(\lambda_0),$$
$$D_5 = \lambda_0[{}^1/_2 P_1(\lambda_0) + 2P_2(\lambda_0)],$$
$$E_0 = {}^1/_2\chi_0[Q_2(\chi_0) + 3\lambda_0 Q_2(\chi_0)],$$
$$E_1 = \lambda_0\chi_0[Q_2'(\chi_0) + \lambda_0 Q_2'(\chi_0)],$$
$$E_2 = -\chi_0 Q_1(\chi_0)/2,$$
$$E_3 = \chi_0[Q_2(\chi_0) + 2\lambda_0 Q_2(\chi_0)],$$
$$E_4 = -\lambda_0\chi_0 Q_1'(\chi_0),$$
$$E_5 = \lambda_0[Q_2(\chi_0) + \lambda_0 Q_2(\chi_0)] + \lambda_0\chi_0[Q_2'(\chi_0) + \lambda_0 Q_2'(\chi_0)],$$
$$E_6 = -{}^1/_2\lambda_0\chi_0 Q_1(\chi_0),$$
$$E_7 = {}^1/_2\lambda_0\chi_0 Q_1(\chi_0) + 2/\sigma \cdot T_w/T_\infty$$

Diffraction of a Pressure Wave by a Cylindrical Cavity in an Elastic Medium[1]

M. L. BARON[2]
Associate,
Paul Weidlinger,
Consulting Engineer,
New York, N. Y.
Mem. ASME

A. T. MATTHEWS
Engineer,
Paul Weidlinger,
Consulting Engineer,
New York, N. Y.

An infinitely long cylindrical cavity in an infinite elastic homogeneous and isotropic medium is enveloped by a plane shock wave whose front is parallel to the axis of the cavity. An integral transform technique is used to determine the stress field produced in the medium by the diffraction of the incoming shock wave by the cavity. Expressions for the radial stress σ_{rr}, the hoop stress $\sigma_{\theta\theta}$, and the shear stress $\sigma_{r\theta}$ are derived as inversion integrals, and numerical results are presented for the time-history of the hoop stress $\sigma_{\theta\theta}$ at the boundary of the cavity. The amplifications of the hoop-stress concentration factors due to the dynamic loading are noted. The problem is considered for pressure waves with a step distribution in time. These results may be used as influence coefficients to determine, by means of Duhamel integrals, the stress field produced by waves with time-varying pressures.

An infinitely long cylindrical cavity in an infinite elastic homogeneous and isotropic medium is acted on by a plane shock wave whose front is parallel to the axis of the cavity. The shock wave propagates through the medium with a constant velocity c_p and envelopes the cavity, Fig. 1. The direct stress components $\sigma u(t)$ and $\epsilon\sigma u(t)$ which are, respectively, parallel and perpendicular to the direction of wave propagation, are carried by the shock wave.

An integral transform technique is used to determine the stress field produced in the medium by the diffraction of the incoming shock wave by the cavity. Expressions for the radial stress σ_{rr}, the hoop stress $\sigma_{\theta\theta}$, and the shear stress $\sigma_{r\theta}$ are derived and numerical results are presented for the hoop stress $\sigma_{\theta\theta}$ at the boundary of the cavity. Although the problem is considered for pressure waves with a step distribution in time, the results obtained for this case may be used as influence coefficients to determine, by means of Duhamel integrals, the stress field produced by waves with time-varying pressures.

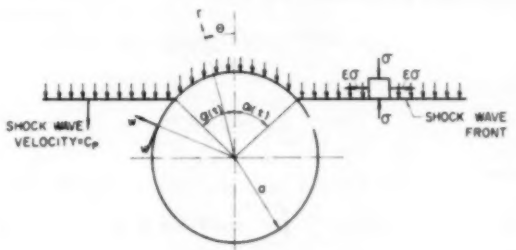

Fig. 1 Geometry of problem

The procedure consists essentially of evaluating the time-dependent coefficients of a Fourier series on the stresses in question. A discussion of the effects of the truncation of this series on the accuracy and applicability of the numerical results is presented in the last section.

1 General Procedure

Consider an infinite elastic medium which does not contain a cavity. The stresses σ_{rr}, $\sigma_{r\theta}$, and $\sigma_{\theta\theta}$ produced by the incoming

[1] This paper is a result of investigations sponsored by The RAND Corporation under contract with Paul Weidlinger, Consulting Engineer. These investigations were presented in part in RAND publication P-2109, October, 1960.

[2] Also, Adjunct Associate Professor of Civil Engineering, Columbia University, New York, N. Y.

Presented at the Summer Conference of the Applied Mechanics Division, Chicago, Ill., June 14–16, 1961, of THE AMERICAN SOCIETY OF MECHANICAL ENGINEERS.

Discussion of this paper should be addressed to the Editorial Department, ASME, United Engineering Center, 345 East 47th Street, New York 17, N. Y., and will be accepted until October 10, 1961. Discussion received after the closing date will be returned. Manuscript received by ASME Applied Mechanics Division, July 28, 1960. Paper No. 61—APM-26.

Nomenclature

θ, r = polar co-ordinates, Fig. 1

$\mathbf{u}(r, \theta, t)$ = displacement vector of a point in the medium

$w(r, \theta, t)$, $v(r, \theta, t)$ = radial and tangential displacements of a point in medium (note that a positive displacement w is outward)

a = radius of cylindrical cavity

$a_n(t)$, $b_n(t)$ = Fourier series coefficients for expansion of stresses σ_{rr} and $\sigma_{r\theta}$

c_p, c_s = propagation velocity of dilatational and shear waves, respectively, in medium

$f(r, \theta, t)$, $f(r, \theta, \Omega)$ = function of r, θ, t and corresponding transformed function with respect to time

$H_n^{(1)}, H_n^{(2)}$ = Hankel functions of first and second kind of order n

$I(\xi, r)$, $L(\xi, r)$, $M(\xi, r)$ = functions appearing in transformed stresses

$I_n(y), K_n(y)$ = modified Bessel functions of first and second kind, respectively, of order n

$\mathbf{k}_r, \mathbf{k}_\theta$ = unit vectors in r and θ-directions, respectively

k = coefficient

t = time

(Continued on next page)

shock wave at points lying on a circle of radius a, Fig. 2, are given by the expressions

$$\sigma_{rr} = -\sigma[\cos^2\theta - \epsilon \sin^2\theta] \tag{1}$$

$$\sigma_{r\theta} = \sigma\left[\frac{1+\epsilon}{2}\right]\sin 2\theta \tag{2}$$

$$\sigma_{\theta\theta} = -\sigma[\sin^2\theta - \epsilon\cos^2\theta] \tag{3}$$

The superposition of the tractions

$$\sigma_{rr} = \sigma[\cos^2\theta - \epsilon \sin^2\theta] \tag{4}$$

$$\sigma_{r\theta} = -\sigma\left[\frac{1+\epsilon}{2}\right]\sin 2\theta \tag{5}$$

which are equal and opposite to those given by equations (1) and (2) on the surface $r = a$, produces a traction-free surface which can be considered to be the boundary of a cavity of radius a in the medium. The total stress field produced by the incoming pressure wave is obtained by superimposing the free field stresses, equations (1)–(3), and the stresses produced by the application of the surface tractions σ_{rr} and $\sigma_{r\theta}$, equations (4)–(5), to the boundary of the cavity.

The boundary tractions σ_{rr} and $\sigma_{r\theta}$, equations (4)–(5), are expanded into a Fourier series, Fig. 2(*b*):

$$\sigma_{rr} = \frac{a_0(t)}{2} + \sum_{n=1}^{\infty} a_n(t)\cos n\theta \tag{6}$$

$$\sigma_{r\theta} = \sum_{n=1}^{\infty} b_n(t)\sin n\theta \tag{7}$$

where

$$a_n(t) = \frac{2}{\pi}\int_0^{\alpha(t)} \sigma_{rr}(\theta)\cos n\theta\, d\theta \tag{8}$$

$$b_n(t) = \frac{2}{\pi}\int_0^{\alpha(t)} \sigma_{r\theta}(\theta)\sin n\theta\, d\theta \tag{9}$$

For times which are less than one full envelopment, i.e., $t \leq 2a/c_p$, the angle $\alpha(t)$ is given by the expression

$$\alpha(t) = \cos^{-1}\left(1 - \frac{c_p t}{a}\right) \tag{10}$$

For $t > 2a/c_p$, i.e., times greater than one full envelopment time, the angle $\alpha(t) = \pi$. Substituting equations (4) and (5) into equations (8) and (9), the expansion coefficients become:

During envelopment $t \leq 2a/c_p$:

$$\frac{a_0(t)}{2} = \frac{\sigma}{\pi}\left[\frac{\alpha(1-\epsilon)}{2} + \left(\frac{1+\epsilon}{4}\right)\sin 2\alpha\right] \tag{11}$$

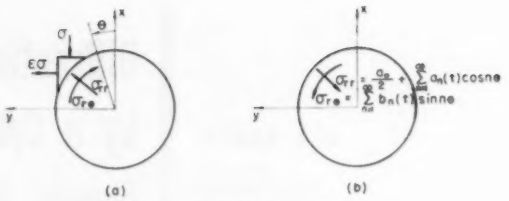

Fig. 2 Boundary tractions

$$a_n(t) = \frac{2\sigma}{\pi(n+2)}\left[\sin n\alpha(\cos^2\alpha - \epsilon\sin^2\alpha) + \left(\frac{1-\epsilon}{2-n}\right)\sin(2-n)\alpha + \left(\frac{1-\epsilon}{n}\right)\sin n\alpha\right] \tag{12}$$

$$b_n(t) = -\frac{\sigma}{2\pi}(1+\epsilon)\left[\frac{\sin(2-n)\alpha}{2-n} - \frac{\sin(2+n)\alpha}{2+n}\right] \tag{13}$$

After envelopment $t > 2a/c_p$:

$$\frac{a_0(t)}{2} = \sigma\left(\frac{1+\epsilon}{2}\right) \tag{14}$$

$$a_n(t) = b_n(t) = 0 \quad n \neq 0 \text{ and } 2 \tag{15}$$

$$a_2(t) = -b_2(t) = \sigma\left(\frac{1+\epsilon}{2}\right) \tag{16}$$

For a wave with a plane wave front, the relation

$$\sigma_{yy} = \frac{\nu}{1-\nu}\sigma_{zz} \tag{17}$$

is easily derived; consequently, the parameter ϵ becomes for the present problem

$$\epsilon = -\frac{\nu}{1-\nu} \tag{18}$$

It should be noted that only the series terms for which $n = 0$ and 2 have nonzero coefficients after envelopment; therefore, only these modes will contribute to the long-time (static) solution for the stress field in the medium.

The plane-strain problem for the stress field around a cavity of radius a which has the surface tractions $\sigma_{rr\,a}$ and $\sigma_{r\theta\,a}$ applied to the boundary $r = a$, is now considered. The surface tractions $\sigma_{rr\,a}$ and $\sigma_{r\theta\,a}$ are given by

$$\left.\begin{aligned}\sigma_{rr\,a} &= a_n(t)\cos n\theta\\ \sigma_{r\theta\,a} &= b_n(t)\sin n\theta\end{aligned}\right\} \tag{19}$$

$$2\sigma_{rr\,a} = a_0(t);\ \sigma_{r\theta\,a} = 0 \tag{20}$$

Nomenclature

$P(t)$ = variable pressure-time history of incoming pressure wave, see Section 6
$u(t)$ = unit step function
$\alpha(t)$ = angle of envelopment
n = number of circumferential waves, integer
ϵ = ratio of stress components in incoming wave, Fig. 1
λ = Lamé constant
μ = shear modulus of medium
ν = Poisson ratio
$\xi = \Omega a/c$
ρ = mass density of medium
σ_{rr}, $\sigma_{\theta\theta}$, $\sigma_{r\theta}$ = radial, hoop and shear stresses, respectively, at a point in medium
σ = stress intensity of incoming wave
$\phi(r, \theta, t)$, $\psi(r, \theta, t)$ = potential functions of reflected and radiated waves in medium
Ω = transform variable

Additional symbols are defined as they occur in the text. Subscripts and dots used with displacement and potential functions indicate differentiation; e.g., $u_{rr} = \dfrac{\partial^2 u}{\partial r^2}$, $\ddot{u} = \dfrac{\partial^2 u}{\partial t^2}$, and so on.

To make the problem more tractable, the tractions $\sigma_{rr\,n}$ and $\sigma_{r\theta\,n}$ are first applied to the cavity boundary as step functions in time:

$$\sigma_{rr\,n} = \sigma u(t) \cos n\theta \tag{21}$$

$$\sigma_{r\theta\,n} = k\sigma u(t) \sin n\theta \tag{22}$$

$$\sigma_{rr\,0} = \sigma u(t) \tag{23}$$

The stress field components produced by the pressure inputs of equations (21)–(23) are evaluated in Section 2 and are used as influence coefficients in Duhamel integrals for the determination of the corresponding components produced by the true boundary tractions of equations (19) and (20). For convenience, the auxiliary problem is solved for the following three sets of applied boundary tractions:

$$\left.\begin{aligned} \sigma_{rr\,n} &= u(t) \cos n\theta \\ \sigma_{r\theta\,n} &= 0 \end{aligned}\right\} \tag{24}$$

$$\left.\begin{aligned} \sigma_{rr\,n} &= 0 \\ \sigma_{r\theta\,n} &= u(t) \sin n\,\theta \end{aligned}\right\} \tag{25}$$

$$\sigma_{rr\,0} = u(t), \quad \sigma_{r\theta\,0} = 0 \tag{26}$$

As an illustration of this procedure, consider the hoop stress $\sigma_{\theta\theta}$ at the cavity boundary. Let the quantities $\sigma_{\theta\theta\,n}{}^{*}$, $\sigma_{\theta\theta\,n}{}^{**}$, and $\sigma_{\theta\theta\,0}{}^{*}$ be the time-dependent portions of the hoop stress $\sigma_{\theta\theta}$ at $r = a$ produced by the applied tractions given by equations (24)–(26), respectively. The corresponding stress components due to the boundary tractions of equations (19), (20) are given by the Duhamel integrals:

$$\bar{\sigma}_{\theta\theta\,n} = \int_0^t [\dot{a}_n(\tau)\sigma_{\theta\theta\,n}{}^{*}(t-\tau)]d\tau \tag{27}$$

$$\bar{\bar{\sigma}}_{\theta\theta\,n} = \int_0^t [\dot{b}_n(\tau)\sigma_{\theta\theta\,n}{}^{**}(t-\tau)]d\tau \tag{28}$$

$$\bar{\sigma}_{\theta\theta\,0} = \int_0^t \tfrac{1}{2}\,[\dot{a}_0(\tau)\sigma_{\theta\theta\,0}{}^{*}(t-\tau)]d\tau \tag{29}$$

The total hoop stress $\sigma_{\theta\theta}$ produced at the boundary of the cavity by the incoming shock wave is given by the superposition of the free field stress, equation (3), and the stresses from equations (27)–(29):

$$\sigma_{\theta\theta}(t) = -\sigma[\sin^2\theta - \epsilon\cos^2\theta] + \sigma_{\theta\theta\,0}(t) + \sum_{n=1}^{\infty} [\bar{\sigma}_{\theta\theta\,n}(t) + \bar{\bar{\sigma}}_{\theta\theta\,n}(t)] \cos n\theta \tag{30}$$

The method of superposition can also be used in a similar manner to evaluate the stress field, σ_{rr}, $\sigma_{\theta\theta}$, $\sigma_{r\theta}$ at points in the medium beyond the boundary of the cavity; i.e., $r > a$.

2 Auxiliary Problems

Stress field produced by boundary tractions $\sigma_{rr\,n} = u(t) \cos n\theta$ and $\sigma_{r\theta\,n} = ku(t) \sin n\theta$, Fig. 3. The equations of motion for the linearly elastic medium are given by

$$\mu\nabla^2\mathbf{u} + (\lambda + \mu)\nabla\nabla\cdot\mathbf{u} = \rho\ddot{\mathbf{u}} \tag{31}$$

where for the plane-strain problem, the displacement $\mathbf{u}$ contains two components

$$\mathbf{u} = u(r, \theta, t)\mathbf{k}_r + v(r, \theta, t)\mathbf{k}_\theta \tag{32}$$

Defining two potential functions, $\phi(r, \theta, t)$ and $\psi(r, \theta, t)$ such that

$$u(r, \theta, t) = \phi_r + \frac{1}{r}\,\psi_\theta \tag{33}$$

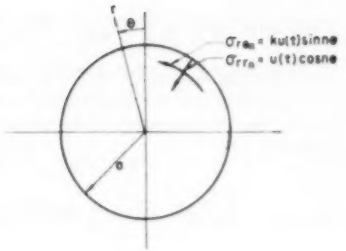

Fig. 3 Auxiliary problem

$$v(r, \theta, t) = \frac{1}{r}\,\phi_\theta - \psi_r \tag{34}$$

and substituting equations (33) and (34) into equation (31), the functions ϕ and ψ satisfy the following wave equations:

$$c_p{}^2\nabla^2\phi = \ddot{\phi} \tag{35}$$

$$c_s{}^2\nabla^2\psi = \ddot{\psi} \tag{36}$$

where

$$c_p = \left(\frac{\lambda + 2\mu}{\rho}\right)^{1/2}; \quad c_s = (\mu/\rho)^{1/2} \tag{37}$$

are the velocities of propagation of dilatational and shear waves, respectively, in the infinite elastic medium.

A transform with respect to time is applied:

$$\bar{f}(r, \theta, \Omega) = \frac{1}{2\pi}\int_0^\infty f(r, \theta, t)e^{-i\Omega t}\,dt \tag{38}$$

$$f(r, \theta, t) = \int_{-\infty - i\gamma}^{\infty - i\gamma} f(r, \theta, \Omega)e^{i\Omega t}\,d\Omega \tag{39}$$

Writing the transformed potentials $\bar{\phi}$ and $\bar{\psi}$ as

$$\bar{\phi}(r, \theta, \Omega) = \bar{\bar{\phi}}(r, \Omega)\cos n\theta \tag{40}$$

$$\bar{\psi}(r, \theta, \Omega) = \bar{\bar{\psi}}(r, \Omega)\sin n\theta \tag{41}$$

the transformed wave equations become

$$\bar{\bar{\phi}}_{rr} + \frac{1}{r}\,\bar{\bar{\phi}}_r + \left(\frac{\Omega^2}{c_p{}^2} - \frac{n^2}{r^2}\right)\bar{\bar{\phi}} = 0 \tag{42a}$$

$$\bar{\bar{\psi}}_{rr} + \frac{1}{r}\,\bar{\bar{\psi}}_r + \left(\frac{\Omega^2}{c_s{}^2} - \frac{n^2}{r^2}\right)\bar{\bar{\psi}} = 0 \tag{42b}$$

and the solutions for divergent waves are given by the expressions

$$\bar{\phi}_n(r, \theta, \Omega) = A_n H_n{}^{(2)}\left(\frac{\Omega r}{c_p}\right)\cos n\theta \tag{43}$$

$$\bar{\psi}_n(r, \theta, \Omega) = B_n H_n{}^{(2)}\left(\frac{\Omega r}{c_s}\right)\sin n\theta \tag{44}$$

The coefficients A_n and B_n are obtained from the boundary conditions at the cavity boundary $r = a$:

$$\sigma_{rr}]_{r=a} = \sigma u(t)\cos n\theta \tag{45}$$

$$\sigma_{r\theta}]_{r=a} = k\,\sigma\,u(t)\sin n\theta \tag{46}$$

The stress $\sigma_{\theta\theta}$,[3] σ_{rr}, and $\sigma_{r\theta}$ are first expressed in terms of the potential functions ϕ and ψ

$$\sigma_{rr} = \lambda\nabla^2\phi + 2\mu\left[\phi_{rr} - \frac{1}{r^2}\,\psi_\theta + \frac{1}{r}\,\psi_{r\theta}\right] \tag{47}$$

$$\sigma_{r\theta} = \mu\left[\frac{2}{r}\,\phi_{r\theta} - \frac{2}{r^2}\,\phi_\theta + \frac{1}{r}\,\psi_r - \psi_{rr} + \frac{1}{r^2}\,\psi_{\theta\theta}\right] \tag{48}$$

[3] The stress $\sigma_{\theta\theta}$ is obtained in terms of the potential functions ϕ and ψ for later computations; it does not appear in the boundary conditions at $r = a$.

$$\sigma_{\theta\theta} = \lambda\nabla^2\phi + 2\mu\left[\frac{1}{r^2}\phi_{\theta\theta} - \frac{1}{r}\psi_r + \frac{1}{r}\phi_r + \frac{1}{r^2}\psi_\theta\right] \quad (49)$$

Transforming equations (47), (48) and substituting equations (43) and (44) into the transformed equations, the constants A_n and B_n may be computed. The transformed potential functions become[4]

$$\bar{\phi}_n = \frac{\sigma a^2(B + kE)}{2\pi i\Omega\mu[FB + DE]} H_n^{(2)}\left(\frac{\Omega r}{c_p}\right)\cos n\theta \quad (50)$$

$$\bar{\psi}_n = \frac{\sigma a^2(-D + kF)}{2\pi i\Omega\mu[FB + DE]} H_n^{(2)}\left(\frac{\Omega r}{c_s}\right)\sin n\theta \quad (51)$$

where

$$F = [2n(n+1) - 3\xi^2]H_n^{(2)}(\xi) - 2\xi H_{n-1}^{(2)}(\xi) \quad (52)$$

$$B = \left[-2n(n+1) + \frac{c_p^2}{c_s^2}\xi^2\right] H_n^{(2)}\left(\frac{c_p}{c_s}\xi\right) + 2\frac{c_p}{c_s}\xi H_{n-1}^{(2)}\left(\frac{c_p}{c_s}\xi\right) \quad (53)$$

$$D = 2n(n+1)H_n^{(2)}(\xi) - 2n\xi H_{n-1}^{(2)}(\xi) \quad (54)$$

$$E = 2n(n+1)H_n^{(2)}\left(\frac{c_p}{c_s}\xi\right) - 2n\frac{c_p}{c_s}\xi H_{n-1}^{(2)}\left(\frac{c_p}{c_s}\xi\right) \quad (55)$$

and

$$\xi = \frac{\Omega a}{c_p} \quad (56)$$

The transformed stresses $\bar{\sigma}_{rr\,n}$, $\bar{\sigma}_{\theta\theta\,n}$, and $\bar{\sigma}_{r\theta\,n}$ are obtained by substituting equations (50) and (51) into the transformed equations (47)–(49):

$$\bar{\sigma}_{rr\,n}(r, \theta, \Omega) = \frac{\sigma}{2\pi i\Omega}\frac{L(\xi, r)\cos n\theta}{(FB + DE)} \quad (57)$$

$$\bar{\sigma}_{\theta\theta\,n}(r, \theta, \Omega) = \frac{\sigma}{2\pi i\Omega}\frac{I(\xi, r)\cos n\theta}{(FB + DE)} \quad (58)$$

$$\bar{\sigma}_{r\theta\,n}(r, \theta, \Omega) = \frac{\sigma}{2\pi i\Omega}\frac{M(\xi, r)\sin n\theta}{(FB + DE)} \quad (59)$$

where

$$L(\xi, r) = \left\{\begin{array}{l}[B + kE]\left[-2\xi\frac{a}{r}H_{n-1}^{(2)}\left(\frac{\xi r}{a}\right) + \left\{(2n^2 + 2n)\frac{a^2}{r^2} - 3\xi^2\right\}H_n^{(2)}\left(\frac{\xi r}{a}\right)\right] \\ -[D - kF]\left[2n\xi\frac{c_p}{c_s}\frac{a}{r}H_{n-1}^{(2)}\left(\frac{c_p\xi r}{c_s a}\right) - (2n^2 + 2n)\frac{a^2}{r^2}H_n^{(2)}\left(\frac{c_p\xi r}{c_s a}\right)\right]\end{array}\right\} \quad (60)$$

$$I(\xi, r) = \left\{\begin{array}{l}[B + kE]\left[2\xi\frac{a}{r}H_{n-1}^{(2)}\left(\frac{\xi r}{a}\right) - \left\{(2n^2 + 2n)\frac{a^2}{r^2} + \xi^2\right\}H_n^{(2)}\left(\frac{\xi r}{a}\right)\right] \\ + [kF - D]\left[2n(n+1)\frac{a^2}{r^2}H_n^{(2)}\left(\frac{c_p\xi r}{c_s a}\right) - \frac{2c_p na}{c_s r}\xi H_{n-1}^{(2)}\left(\frac{c_p\xi r}{c_s a}\right)\right]\end{array}\right\} \quad (61)$$

$$M(\xi, r) = \left\{\begin{array}{l}[B + kE]\left[-2n\xi\frac{a}{r}H_{n-1}^{(2)}\left(\xi\frac{r}{a}\right) + (2n^2 + 2n)\frac{a^2}{r^2}H_n^{(2)}\left(\frac{\xi r}{a}\right)\right] \\ + [kF - D]\left[2\frac{c_p}{c_s}\xi\frac{a}{r}H_{n-1}^{(2)}\left(\frac{c_p\xi r}{c_s a}\right) - \left\{(2n^2 + 2n)\frac{a^2}{r^2} - 3\xi^2\right\}H_n^{(2)}\left(\frac{\xi r c_p}{c_s a}\right)\right]\end{array}\right\} \quad (62)$$

The stress components $\sigma_{\theta\theta\,n}$, $\sigma_{rr\,n}$, and $\sigma_{r\theta\,n}$ may be evaluated from the inversion integral, equation (39); i.e.,

$$\frac{\sigma_{\theta\theta\,n}(r, \theta, t)}{\cos n\theta} = \frac{\sigma}{2\pi i}\int_{-\infty-i\gamma}^{\infty-i\gamma}\frac{I(r, \xi)e^{i\xi\frac{c_p t}{a}}}{\xi[FB + DE]}\,d\xi \quad (63)$$

Similar inversion integrals for

$$\frac{\sigma_{rr\,n}}{\cos n\theta} \text{ and } \frac{\sigma_{r\theta\,n}}{\sin n\theta}$$

may be obtained by substituting $L(r, \xi)$ and $M(r, \xi)$, respectively, for $I(r, \xi)$ in equation (63).

The integral of equation (63) will be evaluated in Section 3 to obtain the hoop stress $\sigma_{\theta\theta\,n}$ at the boundary of the cavity, $r = a$.

3 Inversion of Equation (63) for the Hoop Stress $\sigma_{\theta\theta\,n}$ at Cavity Boundary, $r = a$

The stress $\sigma_{\theta\theta\,n}$ at $r = a$ is evaluated by inverting the integral

$$\frac{\sigma_{\theta\theta\,n}(a, \theta, t)}{\sigma\cos n\theta} = \frac{1}{2\pi i}\int_{-\infty-i\gamma}^{\infty-i\gamma}\frac{I_n(a, \xi)e^{i\xi\frac{c_p t}{a}}}{\xi[FB + DE]}\,d\xi \quad (64)$$

where

$$I_n(a, \xi) = \left\{\begin{array}{l}[B + kE][2\xi H_{n-1}^{(2)}(\xi) - \{(2n^2 + 2n) + \xi^2\}H_n^{(2)}(\xi)] \\ + [kF - D]\left[2n(n+1)H_n^{(2)}\left(\frac{c_p}{c_s}\xi\right) - \frac{2c_p n\xi}{c_s}H_{n-1}^{(2)}\left(\frac{c_p}{c_s}\xi\right)\right]\end{array}\right\} \quad (65)$$

All computations were made using a value of Poisson's ratio $\nu = 1/4$; this corresponds physically to a granitic rock medium. For $\nu = 1/4$, the relation

$$c_p = \sqrt{3}\,c_s \quad (66)$$

exists between the dilatational and shear-wave velocities and this will be introduced into equation (65) in the following transform inversion.

[4] The following results are given for the specific case of $\lambda = \mu$, i.e., for a value of Poisson's ratio $\nu = 1/4$.

The singularities of the integrand of equation (64) are a branch point at the origin, $\xi = 0$, a simple pole at the origin, and further simple poles ξ_j defined by the roots of the equation $FB + DE = 0$:

$$\left\{\begin{array}{l} 4\sqrt{3}\,\xi^2(n^2-1)H_{n-1}^{(2)}(\xi)H_{n-1}^{(2)}(\sqrt{3}\,\xi) + 3\xi^2[4n(n+1) - 3\xi^2]H_n^{(2)}(\xi)\,H_n^{(2)}(\sqrt{3}\,\xi) \\ +[-6\xi^2 + 4n\xi(1-n^2)]H_{n-1}^{(2)}(\xi)H_n^{(2)}(\sqrt{3}\,\xi) + [-6\sqrt{3}\,\xi^2 + 4\sqrt{3}\,\xi n(1-n^2)]H_n^{(2)}(\xi)\,H_{n-1}^{(2)}(\sqrt{3}\,\xi) \end{array}\right\} = 0 \quad (67)$$

Consider the contour $ABCDEF$ shown in Fig. 4 where the arcs AB and EF are of infinite radius and the lines BC and DE are branch cuts. By the residue theorem and Jordan's lemma, the integral of equation (64) may be evaluated as

$$\int_A^F \frac{1}{2\pi i}\,\frac{I_n(a,\xi)e^{i\xi\frac{c_p t}{a}}}{\xi[FB+DE]}\,d\xi = \int_{BCDE} \frac{1}{2\pi i}\,\frac{I_n(a,\xi)e^{i\xi\frac{c_p t}{a}}}{\xi[FB+DE]}\,d\xi + 2\pi i\sum_j R_j \quad (68)$$

where $\sum_j R_j$ is the sum of the residues of the poles defined by equation (67) of the pertinent branch of the integrand.

The contribution to the stress ($\sigma_{\theta\theta\,n}/\sigma\cos n\theta$) of the integration over the path CD comes from the simple pole at the origin, $\xi = 0$, and is equal to -1. This value represents the asymptotic value of the stress ($\sigma_{\theta\theta\,n}/\sigma\cos n\theta$) for very long times.

The contribution of the integration over the branch cuts BC and DE leads to a branch integral which must be evaluated numerically. Letting

$$\xi_{DE} = ye^{\frac{i\pi}{2}}\,;\quad \xi_{BC} = ye^{-\frac{i3\pi}{2}} \quad (69)$$

and using the recurrence relations

$$\begin{aligned} H_n^{(2)}(\xi e^{-2\pi i}) &= e^{2n\pi i}H_n^{(2)}(\xi) - 4e^{n\pi i}\cos n\pi J_n(\xi) \\ H_n^{(2)}(\xi) &= 2J_n(\xi) - H_n^{(1)}(\xi) \\ H_n^{(2)}(\xi e^{-2\pi i}) &= -2J_n(\xi) - H_n^{(1)}(\xi) \end{aligned} \quad (70)$$

the branch integral becomes

$$I = (-1)^n\int_0^\infty \frac{(N_1 - kN_2)}{y^2 D_n}\,e^{-\frac{c_p t}{a}y}\,dy \quad (71)$$

where

$$N_1 = 8y\left\{\begin{array}{l} +2n^2(n+1)[3y^2 + 2(n^2-1)][\pi^2 I_n^2(y) + K_n^2(y)] \\ +12(n^2-1)y^2[\pi^2 I_{n-1}^2(\sqrt{3}y) + K_{n-1}^2(\sqrt{3}y)] \\ -[9y^4 - 6n(n+1)(n-2)y^2 - 4n^2(n+1)(n^2-1)][\pi^2 I_n^2(\sqrt{3}y) + K_n^2(\sqrt{3}y)] \\ -2n^2y[3y^2 + 2(n^2-1)][\pi^2 I_n(y)I_{n-1}(y) - K_n(y)K_{n-1}(y)] \\ -2\sqrt{3}y[3(n^2-2)y^2 + 2n(n^2-1)(n+2)][\pi^2 I_n(\sqrt{3}y)I_{n-1}(\sqrt{3}y) - K_n(\sqrt{3}y)K_{n-1}(\sqrt{3}y)] \end{array}\right\} \quad (72)$$

$$N_2 = 8ny\left\{\begin{array}{l} +[9y^4 + 6(n+1)(2n-1)y^2 + 4n(n+1)(n^2-1)][\pi^2 I_n^2(y) + K_n^2(y)] \\ +12(n^2-1)y^2[\pi^2 I_{n-1}^2(\sqrt{3}y) + K_{n-1}^2(\sqrt{3}y)] \\ -2(n+1)[3y^2 - 2n(n^2-1)][\pi^2 I_n^2(\sqrt{3}y) + K_n^2(\sqrt{3}y)] \\ -2y[3y^2 + 2(n^2-1)][\pi^2 I_n(y)I_{n-1}(y) - K_n(y)K_{n-1}(y)] \\ +2\sqrt{3}y[3y^2 - 2(2n+1)(n^2-1)][\pi^2 I_n(\sqrt{3}y)I_{n-1}(\sqrt{3}y) - K_n(\sqrt{3}y)K_{n-1}(\sqrt{3}y)] \end{array}\right\} \quad (73)$$

$$D_n = \left\{\begin{array}{l} 9y^2[3y^2 + 4n(n+1)]^2[\pi^2 I_n^2(y) + K_n^2(y)][\pi^2 I_n^2(\sqrt{3}y) + K_n^2(\sqrt{3}y)] \\ +48y^2(n^2-1)^2[\pi^2 I_{n-1}^2(y) + K_{n-1}^2(y)][\pi^2 I_{n-1}^2(\sqrt{3}y) + K_{n-1}^2(\sqrt{3}y)] \\ +12[3y^2 - 2n(n^2-1)]^2[\pi^2 I_n^2(y) + K_n^2(y)][\pi^2 I_{n-1}^2(\sqrt{3}y) + K_{n-1}^2(\sqrt{3}y)] \\ +4[3y^2 - 2n(n^2-1)]^2[\pi^2 I_{n-1}^2(y) + K_{n-1}^2(y)][\pi^2 I_n^2(\sqrt{3}y) + K_n^2(\sqrt{3}y)] \\ +8\sqrt{3}[-9(n^2-2)y^4 - 12n(n^2-1)(n+2)y^2 + 4n^2(n^2-1)^2][\pi^2 I_n(y)I_{n-1}(y) \\ \qquad - K_n(y)K_{n-1}(y)][\pi^2 I_n(\sqrt{3}y)I_{n-1}(\sqrt{3}y) - K_n(\sqrt{3}y)K_{n-1}(\sqrt{3}y)] \\ +12\sqrt{3}y[-9y^4 + 6n(n-3)(n+1)y^2 + 8n^2(n+1)(n^2-1)][\pi^2 I_n^2(y) + K_n^2(y)][\pi^2 I_n(\sqrt{3}y)I_{n-1}(\sqrt{3}y) \\ \qquad - K_n(\sqrt{3}y)K_{n-1}(\sqrt{3}y)] \\ +12y[-9y^4 + 6n(n-3)(n+1)y^2 + 8n^2(n+1)(n^2-1)][\pi^2 I_n(y)I_{n-1}(y) - K_n(y)K_{n-1}(y)][\pi^2 I_n^2(\sqrt{3}y) \\ \qquad + K_n^2(\sqrt{3}y)] \\ +48y(n^2-1)[3y^2 - 2n(n^2-1)][\pi^2 I_n(y)I_{n-1}(y) - K_n(y)K_{n-1}(y)][\pi^2 I_{n-1}^2(\sqrt{3}y) + K_{n-1}^2(\sqrt{3}y)] \\ +16\sqrt{3}y(n^2-1)[3y^2 - 2n(n^2-1)][\pi^2 I_{n-1}^2(y) + K_{n-1}^2(y)][\pi^2 I_n(\sqrt{3}y)I_{n-1}(\sqrt{3}y) \\ \qquad - K_n(\sqrt{3}y)K_{n-1}(\sqrt{3}y)] \\ +8\pi^2[9n^2y^2 + 12n^2(n^2-1) + \frac{4n^2}{y^2}(n^2-1)^2] \end{array}\right\} \quad (74)$$

Equation (71) may be evaluated numerically for values of the time parameter $c_p t/a$.

The contributions from the poles ξ_j which are roots of equation (67) may be evaluated by the residue theorem:

$$R = 2\pi i \sum_j R_j$$

where

$$2\pi i R_j = \frac{\left\{\begin{array}{l}[4\sqrt{3}\,\xi_j(1-n^2)][H_{n-1}^{(2)}(\xi_j)H_{n-1}^{(2)}(\sqrt{3}\,\xi_j)] \\ [-3\xi_j^3 - 4\xi_j n(n+1) - k8\xi_j n(n+1)][H_n^{(2)}(\xi_j)H_n^{(2)}(\sqrt{3}\,\xi_j)] \\ [+6\xi_j^2 + 4n(n^2-1)][H_{n-1}^{(2)}(\xi_j)H_n^{(2)}(\sqrt{3}\,\xi_j)] \\ [-2\sqrt{3}\,\xi_j^3 + 4\sqrt{3}\,n(n^2-1) + k8\sqrt{3}\,\xi_j^2 n] \\ [H_n^{(2)}(\xi_j)H_{n-1}^{(2)}(\sqrt{3}\,\xi_j)]\end{array}\right\} e^{i\xi_j\left(\frac{c_p t}{a}\right)}}{\left\{\begin{array}{l}[-12\sqrt{3}\,\xi_j^2]\,[H_{n-1}^{(2)}(\xi_j)H_{n-1}^{(2)}(\sqrt{3}\,\xi_j)] \\ [+6\xi_j^3(3n-2) + 8\xi_j n(1-n^2)][H_n^{(2)}(\xi_j)H_n^{(2)}(\sqrt{3}\,\xi_j)] \\ [+3\xi^2(4n - 3\xi_j^2)][H_{n-1}^{(2)}(\xi_j)H_n^{(2)}(\sqrt{3}\,\xi_j)] \\ [+8\sqrt{3}\,\xi_j^2(n^2-1) + 3\sqrt{3}\,\xi_j^2(4n - 3\xi_j^2)] \\ [H_n^{(2)}(\xi_j)H_{n-1}^{(2)}(\sqrt{3}\,\xi_j)]\end{array}\right\}} \quad (75)$$

The hoop stress $\sigma_{\theta\theta\,n}$ then becomes

$$\frac{\sigma_{\theta\theta_n}}{\sigma} = [-1 + R + I]\cos n\theta \quad (76)$$

4 Stress Field Produced by the Boundary Tractions $\sigma_{rr0} = u(t)$ and $\sigma_{r\theta 0} = 0$

The displacement $\mathbf{u}$ for the case $n = 0$ has a radial component only:

$$\mathbf{u} = w(r, t)\mathbf{k}_r \quad (77)$$

The coefficient $w(r, t)$ is expressed in terms of a single potential function $\phi(r, t)$:

$$w(r, t) = \phi_r(r, t) \quad (78)$$

which satisfies the relation

$$c_p^2\nabla^2\phi = \ddot{\phi} \quad (79)$$

Proceeding as in the section "Auxiliary Problems," the hoop stress $\sigma_{\theta\theta 0}$ and the radial stress σ_{rr0} can be obtained from an inversion of the following integrals:

$$\frac{\sigma_{\theta\theta\,0}(r, t)}{\sigma} = \int_{-\infty-i\gamma}^{\infty-i\gamma} \frac{1}{2\pi i}\left[\frac{2\frac{a}{r}H_1^{(2)}\left(\frac{\xi r}{a}\right) + \xi H_0^{(2)}\left(\frac{\xi r}{a}\right)}{\xi[3\xi H_0^{(2)}(\xi) - 2H_1^{(2)}(\xi)]}\right] e^{i\xi\frac{c_p t}{a}}\,d\xi \quad (80)$$

$$\frac{\sigma_{rr\,0}(r, t)}{\sigma} = \int_{-\infty-i\gamma}^{\infty-i\gamma} \frac{1}{2\pi i}\left[\frac{3\xi H_0^{(2)}\left(\frac{\xi r}{a}\right) - \frac{2a}{r}H_1^{(2)}\left(\frac{\xi r}{a}\right)}{\xi[3\xi H_0^{(2)}(\xi) - 2H_1^{(2)}(\xi)]}\right] e^{i\xi\frac{c_p t}{a}}\,d\xi \quad (81)$$

The hoop stress $\sigma_{\theta\theta}$ at the cavity boundary is evaluated by integrating equation (80) with $r = a$ over the contour $ABCDEF$, Fig. 4. Proceeding as in Section 3, $\sigma_{\theta\theta\,0}$ is computed from the relation

$$\frac{\sigma_{\theta\theta_n}}{\sigma}(a, t) = [-1 + R + I] \quad (82)$$

where the branch integral I and the sum of the residues R are given as follows:

$$I = \int_0^\infty \frac{-8e^{\frac{-yc_p t}{a}}\,dy}{y\{[3yK_0(y) + 2K_1(y)]^2 + \pi^2[3yI_0(y) - 2I_1(y)]^2\}} \quad (83)$$

$$R = \sum_j \left[\frac{2H_1^{(2)}(\xi_j) + \xi_j H_0^{(2)}(\xi_j)}{4\xi_j H_0^{(2)}(\xi_j) - 3\xi_j^2 H_1^{(2)}(\xi_j)}\right] e^{i\xi_j\frac{c_p t}{a}} \quad (84)$$

The summation over j in equation (84) is carried out for all values of ξ_j which lie in the first and second quadrants and are roots of the equation

$$3\xi H_0^{(2)}(\xi) - 2H_1^{(2)}(\xi) = 0 \quad (85)$$

5 Computational Procedure

The hoop stress components $\sigma_{\theta\theta\,n}$ which are produced by the boundary traction inputs of equations (24)–(26), respectively, are first evaluated, using the analytical expressions developed in Section 3 for $n \neq 0$ and Section 4 for $n = 0$. Computations were made for $\sigma_{\theta\theta\,n}$, $n = 0$, 1, and 2.[5]

For each value of n, the number of complex poles lying within the contour $ABCDEF$ was established, using the procedure given by Watson.[6] These poles, which are the complex roots of equation (67), were located by a numerical search procedure on an electronic computer and are given in Table 1.

[5] A discussion of the truncation of the series for the hoop stress, equation (30), after the term $n = 2$ is presented in the following section of this paper.

[6] G. N. Watson, "A Treatise on the Theory of Bessel Functions," Cambridge University Press, Cambridge, England, 1952, p. 511.

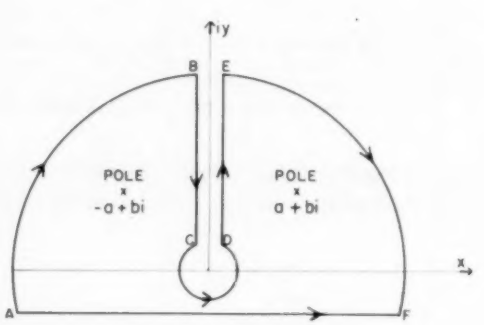

Fig. 4 Integration contour

Table 1 Poles for evaluation of $\sigma_{\theta\theta}$ [2]

$n = 0$	$\xi_{1,2} = \pm 0.4464 + 0.4410\,i$
$n = 1$	$\xi_{1,2} = \pm 1.0929 + 0.7652\,i$
$n = 2$	$\xi_{1,2} = \pm 1.9076 + 0.8978\,i$
	$\xi_{3,4} = \pm 0.2862 + 0.2786\,i$

It is of interest to note that the delay time in the rise of the peak hoop stress $\sigma_{\theta\theta}$ is due primarily to the time-decay coefficient which comes from the residues corresponding to the $\xi_{3,4}$ poles in the mode $n = 2$; namely, $e^{-0.278\,ct/a}$.

Although there is in each case a significant contribution from the branch integral at early times, the decay times from the residues of the poles essentially control the rise of the hoop-stress curves.

Upon the evaluation of the residues, equation (75), and the branch integrals, equation (71), the hoop stresses due to the applied unit step-boundary tractions are computed from equations (76) and (82). These quantities are used as influence coefficients in Duhamel integrals, equations (27)–(29), to evaluate the corresponding hoop stresses $\tilde{\sigma}_{\theta\theta\,n}$ and $\hat{\sigma}_{\theta\theta\,n}$ which are produced by boundary tractions with the time variations $a_n(t)$ and $b_n(t)$, respectively. The total hoop stress is then evaluated from equation (30).

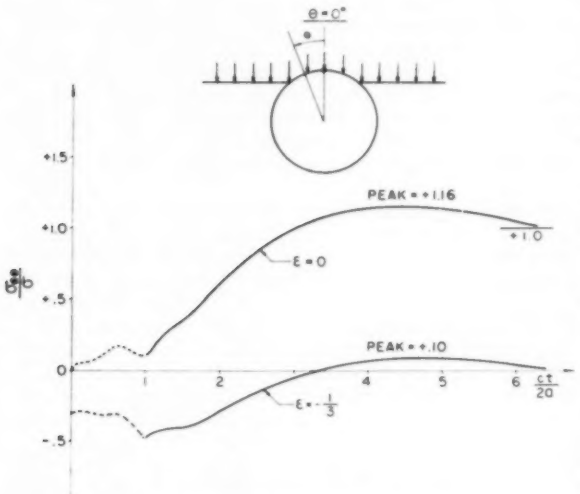

Fig. 5 Hoop stress, $\sigma_{\theta\theta}/\sigma$ at cavity boundary, $r = a$, $\theta = 0°$

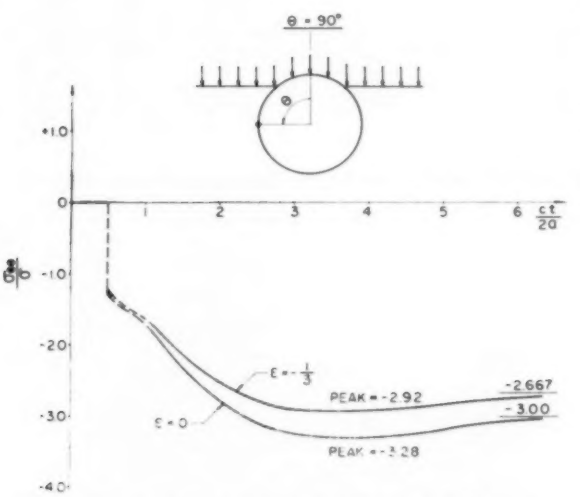

Fig. 6 Hoop stress, $\sigma_{\theta\theta}/\sigma$ at cavity boundary, $r = a$, $\theta = 90°$

6 Numerical Results and Conclusions

Numerical results are presented for the hoop stress at $r = a$, which is produced by an incoming plane shock wave with a step pressure distribution in time. It was found that the maximum values of the stress are not materially affected by the early time stress contributions which come from the coefficients $\tilde{\sigma}_{\theta\theta\,n}$ and $\hat{\sigma}_{\theta\theta\,n}$, n larger than 2 and, consequently, the series in equation (30) is terminated after the $n = 2$ term for computational purposes.

At this point, some comments on the accuracy of the numerical results are in order. The terms for $n > 2$ which are neglected in the numerical computations would contribute substantially to the early time values of the hoop stress. Consequently, the numerical results which are given by the present analysis will be inaccurate at early times (up to about one full transit time, $t = 2a/c$). However, for later times, $t > 2a/c$, the contributions from the $n > 2$ components become quite small and may be neglected. The numerical results obtained from the present analysis are valid in this range. It is also of interest to note that only the contributions from the $n = 0$ and $n = 2$ components combine with the free field stress in equation (30) to give the asymptotic long-time value of $\sigma_{\theta\theta}$.

A short-time asymptotic solution for the maximum value of the hoop stress at very early times ($t < a/c$) is given by Gilbert.[7] This analysis, which is valid for limited values of the angle $|\theta| < 60°$, is discussed and compared with the present analysis by Baron, et al.[8] It is concluded that the maximum values of the hoop stress $\sigma_{\theta\theta}$ do not occur at the very early times at which the present theory is inaccurate, but rather at later times ($t > 2a/c$) for which the present theory gives valid results.

Figs. 5 and 6 show the hoop stress $\sigma_{\theta\theta}$ at the cavity boundary for the locations $\theta = 0°$ and $\theta = 90°$, respectively. The curve for $\epsilon = 0$ is shown purely for comparison purposes; at large values of the time, the stress must approach the well-known static solution for a cylindrical hole in a uniaxial pressure field. It is seen that the stress concentration is amplified by the dynamic loading in the ratio of 3.28 to 3 at $\theta = 90°$ and 1.16 to 1.00 at $\theta = 0°$. The more realistic plane-wave case, with $\epsilon = -1/3$, shows an amplification in the stress concentration in the ratio of 2.92 to 2.667 at $\theta = 90°$ and 0.10 to 0.00 at $\theta = 0°$.

The hoop stress $\sigma_{\theta\theta}$ produced by the step shock wave may be used as an influence function to determine the hoop stress pro-

[7] J. F. Gilbert, "Elastic Wave Interaction With a Cylindrical Cavity," E. H. Plesset Associates, Inc., Air Force Ballistic Missiles Division, December 1, 1959.

[8] M. L. Baron, H. H. Bleich, and P. Weidlinger, "Theoretical Studies on Ground Shock Phenomena," The MITRE Corporation Report No. SR-19, October, 1960, pp. 102–104.

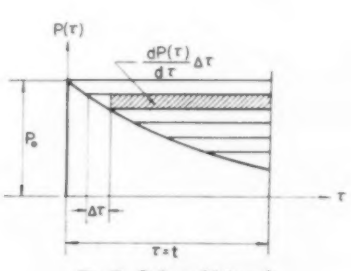

Fig. 7 Duhamel integral

duced by a wave with a varying pressure-time history. Denoting the hoop stress produced by the step wave as $\sigma_{\theta\theta_s}$, the stress due to a wave with the pressure-time histroy $P(t)$ [9] is easily computed from the Duhamel integral, equation (86), by numerical integration, Fig. 7:

$$\sigma_{\theta\theta} = P_0\sigma_{\theta\theta_s} + \int_0^t \frac{dP(\tau)}{d\tau}\,\sigma_{\theta\theta_s}(t-\tau)d\tau \qquad (86)$$

Applications of this technique for waves with time decaying pressures are given elsewhere.[6]

[9] The pressure-time history $P(t)$ should be such that no significant high-frequency components with time constants of less than $^1/_8$ of a transit time are present.

P. J. BROSENS
Assistant Professor of Mechanical Engineering, Massachusetts Institute of Technology, Cambridge, Mass.

S. H. CRANDALL
Professor of Mechanical Engineering, Massachusetts Institute of Technology, Cambridge, Mass.
Mem. ASME

Whirling of Unsymmetrical Rotors[1]

A study of the motion of elastically supported rotors having unequal diametral moments of inertia is presented. It is found that some rotors are dynamically unstable above a certain speed and that some of these may return to a stable condition at a sufficiently high speed depending on the particular magnitudes of the gyroscopic coupling and the inertia inequality. The effect on rotor stability due to nonrotating inequality in the supporting stiffnesses is studied. For small stiffness inequality this effect is only of second order; as the stiffness inequality is increased, new unstable speed regions may appear. Test results on an unsymmetrical rotor verify the theoretical predictions.

THE vibrations of elastically supported rotors are described by Den Hartog [1][2] for the case of symmetrical rotors overhung on an elastic shaft, and by Biezeno and Grammel [2] for the cases where the supporting rotating *or* nonrotating stiffnesses are unsymmetrical. The case where the supporting stiffnesses are a *combination* of rotating and nonrotating unsymmetrical stiffnesses was studied by Smith [3], and by Foote, Poritsky, and Slade [4]. There is a brief discussion of the stability of rotors with unsymmetric inertias in [3] when the angular motion of the rotor is uncoupled from the motion of its centroid.

This paper presents a study of the motion of overhung rotors rotating at constant speed, having unequal diametral moments of inertia, and supported pivotally with unequal stiffnesses about mutually perpendicular stationary axes. Gyroscopic coupling is included throughout.

The mathematics encountered is analogous to that of Foote, Poritsky, and Slade [4] while the results are somewhat similar to those obtained by Coleman and Feingold [5] in an interesting analysis of the plane motion of hinged two-bladed helicopter rotors with nonisotropic pylon elasticity.

[1] This paper is based on a thesis presented to the Department of Mechanical Engineering of the Massachusetts Institute of Technology in partial fulfillment of the requirements of the Degree of Doctor of Science.

[2] Numbers in brackets designate References at end of paper.

Presented at the Summer Conference of the Applied Mechanics Division, Chicago, Ill., June 14–16, 1961, of THE AMERICAN SOCIETY OF MECHANICAL ENGINEERS.

Discussion of this paper should be addressed to the Editorial Department, ASME, United Engineering Center, 345 East 47th Street, New York 17, N. Y., and will be accepted until October 10, 1961. Discussion received after the closing date will be returned. Manuscript received by ASME Applied Mechanics Division, May 2, 1960. Paper No. 61—APM-10.

Description of Model and Derivation of Equations of Motion

The general geometry of the system is shown in Fig. 1. A rigid rotor of any dimensions is supported by a rigid shaft pivotally mounted at O. The axes xyz are fixed in space with origin at O. The axes $\xi\eta\zeta$ are fixed in the rotor system and also originate at O. The axes x_1 and y_1 are the projections of the xy-axes on the $\xi\eta$-plane.

It will be assumed throughout that the stiffness characteristics at the pivot point O are such that the displacements ϕ_x and ϕ_y are opposed by moments $K_x\phi_x$ and $K_y\phi_y$ at O.

Notice that the assumed configuration also applies to the case of

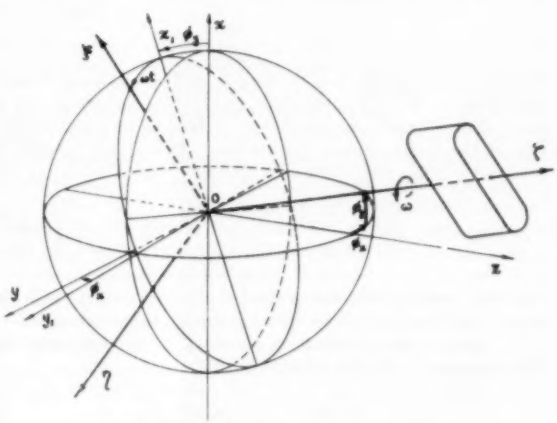

Fig. 1 Pictorial view of co-ordinate system

Nomenclature

A_n = coefficient in the expansion of $\bar{u}$

a_n = main diagonal coefficient in $\Delta(\lambda)$

B_n = coefficient in the expansion of $\bar{u}$

b_n = main diagonal coefficient in $\Delta(\lambda)$

c_n = off-diagonal coefficient in $\Delta(\lambda)$

d_n = off-diagonal coefficient in $\Delta(\lambda)$

e_n = off-diagonal coefficient in $\Delta(\lambda)$

H_α = component of angular momentum in α-direction

I = inertia inequality factor $= (I_x - I_y)/(I_x + I_y)$

I_α = moment of inertia about α-axis

$I_{\alpha\beta}$ = product of inertia about $\alpha\beta$-axes

J = gyroscopic coupling factor $= I_\xi/\frac{1}{2}(I_\xi + I_\eta)$

K = stiffness inequality factor $= (K_x - K_y)/(K_x + K_y)$

K_α = stiffness coefficient acting on ϕ_α-co-ordinate

$l_{\alpha\beta}$ = direction cosine = co $(\widehat{\alpha 0 \beta})$

n = harmonic exponent in the expansions of $\bar{u}$ and $\bar{\bar{u}}$

S = dimensionless speed = ω/ω_0

t = time

$U(\tau)$, $\bar{U}(\tau)$ = factors of $e^{i\lambda\tau}$ in the particular solutions for u and $\bar{u}$

u = complex displacement = $\phi_x + i\phi_y$

(Continued on next page)

an unsymmetrical rotor with its center of gravity at the center of a uniform flexible shaft symmetrically supported in the x and y-planes, since the angular motions (which are the subject of this paper) of the rotor in this condition are uncoupled from the translational motions and hence the assumption of pivotal support is satisfied.

The angular momentum of the system is given by

$$[H] = [I][\omega] \tag{1}$$

where $[H]$ is a column matrix formed by the three components of $\mathbf{H}$ in the particular co-ordinate system (1, 2, 3) used, $[I]$ is the instantaneous inertia matrix:

$$\begin{bmatrix} I_1 & -I_{12} & -I_{13} \\ -I_{21} & I_2 & -I_{2_3} \\ -I_{31} & -I_{32} & I_3 \end{bmatrix} \tag{2}$$

and $[\omega]$ is a column matrix of the same nature as $[H]$. The expression (1) is valid for a stationary as well as a moving co-ordinate system. We will apply equation (1) using the xyz-system of axes. The inertia in the xyz-system is obtained by a transformation of the inertia in the $\xi\eta\zeta$-system. This transformation is achieved by first transforming to the $x_1y_1\zeta$-axes (which are obtained by a simple rotation of the $\xi\eta\zeta$ triad about ζ through the angle $-\omega t$), and then from the $x_1y_1\zeta$-axes to the xyz-reference.

For the transformation from the $x_1y_1\zeta$ to the xyz-frame the following matrix transformation is used:

$$[I]_{xyz} = [l]^T[I]_{x_1y_1\zeta}[l] \tag{3}$$

where $[l]$ is the matrix of direction cosines specifying the position of the xyz-co-ordinates with respect to the $x_1y_1\zeta$-frame:

$$[l] = \begin{bmatrix} l_{x_1x} & l_{x_1y} & l_{x_1z} \\ l_{y_1x} & l_{y_1y} & l_{y_1z} \\ l_{\zeta x} & l_{\zeta y} & l_{\zeta z} \end{bmatrix} \cong \begin{bmatrix} 1 & 0 & -\phi_y \\ 0 & 1 & \phi_x \\ \phi_y & -\phi_x & 1 \end{bmatrix} \tag{4}$$

and $[l]^T$ is the transpose of $[l]$.

Expanding equation (1) and assuming ϕ_x and ϕ_y are small so that their powers and products with their time derivatives may be omitted, the following expression is obtained for the x and y-components of the angular momentum of the rotor:

$$\begin{bmatrix} H_x \\ H_y \end{bmatrix} = \omega \begin{bmatrix} I_{x_1} & -I_{x_1y_1} & [-I_{x_1\zeta} + \phi_y(I_\zeta - I_{x_1}) - \phi_x I_{x_1y_1}] \\ -I_{x_1y_1} & I_{y_1} & [-I_{y_1\zeta} - \phi_x(I_\zeta - I_{y_1}) + \phi_y I_{x_1y_1}] \end{bmatrix} \begin{bmatrix} (\dot\phi_x + \phi_y) \\ (\dot\phi_y - \phi_x) \\ 1 \end{bmatrix} \tag{5}$$

where dotted quantities stand for their differentiation with respect to the angle τ, equal to ωt.

Differentiating equation (5), the expression obtained for the x and y-components of the rate of change of the angular momentum is in the case of no unbalance ($I_{\xi\eta} = I_{\eta\zeta} = I_{\zeta\xi} = 0$)[Ref. 6]:

$$\begin{bmatrix} \frac{dH_x}{dt} \\ \frac{dH_y}{dt} \end{bmatrix} = \omega^2 \begin{bmatrix} \left[\frac{I_\xi + I_\eta}{2} + \frac{I_\xi - I_\eta}{2}\cos 2\tau\right] & \left[\frac{I_\xi - I_\eta}{2}\sin 2\tau\right] \\ \left[\frac{I_\xi - I_\eta}{2}\sin 2\tau\right] & \left[\frac{I_\xi + I_\eta}{2} - \frac{I_\xi - I_\eta}{2}\cos 2\tau\right] \end{bmatrix} \begin{bmatrix} \ddot\phi_x \\ \ddot\phi_y \end{bmatrix}$$
$$+ \omega^2 \begin{bmatrix} 0 & I_\zeta \\ -I_\zeta & 0 \end{bmatrix} \begin{bmatrix} \phi_x \\ \phi_y \end{bmatrix} + \omega^2 \begin{bmatrix} -(I_\xi - I_\eta)\sin 2\tau & (I_\xi - I_\eta)\cos 2\tau \\ (I_\xi - I_\eta)\cos 2\tau & (I_\xi - I_\eta)\sin 2\tau \end{bmatrix} \begin{bmatrix} \dot\phi_x \\ \dot\phi_y \end{bmatrix} \tag{6}$$

Applying then the principle of angular momentum the equation of motion for the case of no unbalance is

$$\begin{bmatrix} (1 + I\cos 2\tau) & I\sin 2\tau \\ I\sin 2\tau & (1 - I\cos 2\tau) \end{bmatrix} \begin{bmatrix} \ddot\phi_x \\ \ddot\phi_y \end{bmatrix} + \begin{bmatrix} 0 & J \\ -J & 0 \end{bmatrix} \begin{bmatrix} \dot\phi_x \\ \dot\phi_y \end{bmatrix}$$
$$+ \begin{bmatrix} -2I\sin 2\tau & 2I\cos 2\tau \\ 2I\cos 2\tau & 2I\sin 2\tau \end{bmatrix} \begin{bmatrix} \dot\phi_x \\ \dot\phi_y \end{bmatrix} + \mu \begin{bmatrix} (1 + K) & 0 \\ 0 & (1 - K) \end{bmatrix} \begin{bmatrix} \phi_x \\ \phi_y \end{bmatrix} = 0 \tag{7}$$

where I is the inertia inequality factor,

$$I = \frac{I_\xi - I_\eta}{I_\xi + I_\eta}, \tag{8}$$

J is the gyroscopic coupling factor,

$$J = \frac{I_\zeta}{\frac{1}{2}(I_\xi + I_\eta)}, \tag{9}$$

Nomenclature

$\bar u$ = complex displacement = $\phi_x - i\phi_y$

v = complex displacement = $\phi_\xi + i\phi_\eta$

$\bar v$ = complex displacement = $\phi_\xi - i\phi_\eta$

xyz = stationary orthogonal co-ordinates with origin at 0

$x_1y_1\zeta$ = set of orthogonal co-ordinates obtained by projecting x and y on the $\xi\eta$-plane

$\xi\eta\zeta$ = orthogonal co-ordinates rotating with rotor, origin at 0

$\Delta(\lambda)$ = determinant of coefficients of A_n and B_n in recurrence formulas for A_n and B_n

λ = exponential exponent in solution for ϕ_ξ and ϕ_η and in expansions of $\bar u$ and $\ddot{\bar u}$

μ = speed parameter = ω_0^2/ω^2

τ = angular co-ordinate = ωt

ϕ_α = angular displacement in α-direction

$\dot\phi_\alpha$ = rate of change of ϕ_α with $\tau = \dfrac{d\phi_\alpha}{d\tau} = \dfrac{1}{\omega}\dfrac{d\phi_\alpha}{dt}$

ω = angular velocity of rotor

ω_n = angular frequency of motion component as seen from stationary co-ordinates

ω_0 = characteristic natural frequency = $\left(\dfrac{K_x + K_y}{I_\xi + I_\eta}\right)^{1/2}$

μ is a speed parameter,

$$\mu = \frac{\omega_0^2}{\omega^2}, \tag{10}$$

ω_0 is the characteristic natural frequency,

$$\omega_0^2 = \frac{K_x + K_y}{I_\xi + I_\eta}, \tag{11}$$

and K is the stiffness inequality factor,

$$K = \frac{K_x - K_y}{K_x + K_y} \tag{12}$$

Because of the various periodic coefficients appearing in them, equations (7) are not well suited to study the stability of their solutions. Since all the factors involved in equations (7) except the spring inequality K rotate with the rotor, there is an advantage in expressing these in terms of the rotating co-ordinates ϕ_ξ and ϕ_η. We make this transformation in three steps because we shall have future need for one of the intermediate formulations. Let u and $\bar{u}$ be conjugate complex variables defined by

$$\begin{aligned} u &= \phi_x + i\phi_y \\ \bar{u} &= \phi_x - i\phi_y \end{aligned} \tag{13}$$

Then if the second of equations (7) is multiplied by i and added to and subtracted from the first we obtain the following intermediate formulation:

$$\begin{aligned} I\ddot{u}e^{2i\tau} + \bar{u} + 2iI\dot{u}e^{2i\tau} - iJ\dot{u} + \mu(u + K\bar{u}) &= 0 \\ I\ddot{u}e^{-2i\tau} + \ddot{\bar{u}} - 2iI\dot{u}e^{-2i\tau} + iJ\dot{\bar{u}} + \mu(\bar{u} + Ku) &= 0 \end{aligned} \tag{14}$$

Now changing to the co-ordinates v and $\bar{v}$ which are related to u and $\bar{u}$ as follows:

$$\begin{aligned} u &= ve^{i\tau} \\ \bar{u} &= \bar{v}e^{-i\tau} \end{aligned} \tag{15}$$

equations (14) become

$$\begin{aligned} I\ddot{v} + I\bar{v} + \bar{v} + i\dot{v}(2 - J) \\ - v(1 - J - \mu) + \mu K\bar{v}e^{-2i\tau} &= 0 \\ I\ddot{\bar{v}} + Iv + \ddot{v} - i\dot{\bar{v}}(2 - J) \\ - \bar{v}(1 - J - \mu) + \mu Kve^{2i\tau} &= 0 \end{aligned} \tag{16}$$

Finally, it is easily verified that the rotating co-ordinates ϕ_ξ and ϕ_η are given by

$$\begin{aligned} \tfrac{1}{2}(v + \bar{v}) &= \phi_\xi \\ \tfrac{1}{2}(v - \bar{v}) &= i\phi_\eta \end{aligned} \tag{17}$$

so that mutual addition and subtraction of equations (16) leads to

$$\begin{aligned} -\ddot{\phi}_\xi(1 + I) + \dot{\phi}_\eta(2 - J) + \phi_\xi[(1 - J - \mu) - I] \\ - \mu K(\phi_\xi \cos 2\tau - \phi_\eta \sin 2\tau) &= 0 \\ -\ddot{\phi}_\eta(1 - I) - \dot{\phi}_\xi(2 - J) + \phi_\eta[(1 - J - \mu) + I] \\ + \mu K(\phi_\xi \sin 2\tau + \phi_\eta \cos 2\tau) &= 0 \end{aligned} \tag{18}$$

which are the equations of motion in rotating co-ordinates.

In the case of unbalanced rotors it is found that the right-hand members of equations (18) become constants proportional to the amount of unbalance [6].

Solution for the Case of Equal Stiffnesses

When the stiffness inequality vanishes ($K = 0$), equations (18) reduce to linear simultaneous ordinary differential equations with constant coefficients. Their solutions are of the form

$$\begin{aligned} \phi_\xi &= \phi_{0\xi}e^{i\lambda\tau} \\ \phi_\eta &= \phi_{0\eta}e^{i\lambda\tau} \end{aligned} \tag{19}$$

where the values of λ, $\pm\lambda_1$, and $\pm\lambda_2$, are given by the roots of the characteristic equation

$$\begin{aligned} [\lambda^2(1 - I) + (1 - J - \mu) + I][\lambda^2(1 + I) \\ + (1 - J - \mu) - I] - \lambda^2(2 - J)^2 = 0 \end{aligned} \tag{20}$$

The general solution to (18) consists of a linear combination of four terms of the form of (19) with the four roots $\pm\lambda_1$ and $\pm\lambda_2$. Only if both λ_1 and λ_2 are real can the motion be stable. This in turn requires that both λ_1^2 and λ_2^2 be real and positive.

The expressions for the roots of equation (20) indicate upon inspection that instability is reached as the roots of smaller magnitude, $\pm\lambda_1$ approach each other at the origin and recede along the imaginary axis. It may be shown [6] that the necessary and sufficient condition for stable motion is

$$|(1 - J - \mu)| > I \tag{21}$$

The borderline conditions for (21) are (a): $(1 - J - \mu) = -I$ and (b): $(1 - J - \mu) = I$. Now, $\mu = \omega_0^2/\omega^2$ so that with increasing ω the motion is stable until the condition (a) is reached. The motion remains unstable until (b) is obtained and then it becomes stable again. The restriction that μ remain positive means, however, that, depending on the inertia distribution of the rotor, it may not be possible to achieve either or both of (a) and (b). For values of I and J satisfying $(1 - J + I) \leqslant 0$ the condition (21) is satisfied for all positive μ and thus the motion is stable at all speeds, while for values of I and J satisfying $|(1 - J)| < I$ the motion will become unstable at a sufficiently large speed and remain so as the speed is further increased to infinity. If the values of I and J satisfy $(1 - J - I) \geqslant 0$, the motion becomes unstable at a sufficiently large speed but will return to a stable condition upon a sufficient further increase in speed. The results of this analysis lead to the stability boundaries shown in Fig. 2 which are in agreement with the qualitative predictions of Smith [3]. The areas for which $2I > J$ are not shown because they represent forbidden combinations of I and J as may easily be seen if it is considered that all possible inertia distributions for a rotor with $I_{\xi\eta} = I_{\eta\zeta} = I_{\zeta\xi} = 0$ may be achieved by a proper choice of the axial dimensions and overhang of an overhung ellipsoid. If $\bar{L}$ is the overhang and a_ξ, a_η, a_ζ are the semiaxes of the ellipsoid in the ξ, η, ζ-directions, it is found that

$$J - 2I = \frac{4a_\zeta^2}{(a_\xi^2 + a_\eta^2 + 2a_\zeta^2) + 10\bar{L}^2} \tag{22}$$

and hence J must be larger than or equal to $2I$ for any real rotor.

When the motions (19) are stable, they represent ellipses traced out at frequencies $\lambda\omega$ with respect to the rotating co-ordinate system $\xi\eta\zeta$. In order to describe these in terms of the nonrotating reference x, y, z, it is convenient to visualize each elliptical motion as the superposition of two circularly polarized motions one rotating in the same sense as the ellipse with amplitude $(a + b)/2$ and the other rotating in the opposite direction with amplitude $(a - b)/2$ where the semimajor and semiminor axes of the ellipse are a and b, respectively. In a nonrotating co-ordinate system, these circularly polarized motions remain circularly polarized but now have frequencies $\omega_n = \omega \pm \lambda\omega$. These resultant frequencies are shown in Fig. 3 for a system with $I = 0.234$ and $J = 0.543$. The curves are labeled A-A and B-B to indicate that a component on one branch of the A-curve, say, is invariably accompanied by a component on the other A-branch. In the region of instability the B-curves defining the angular

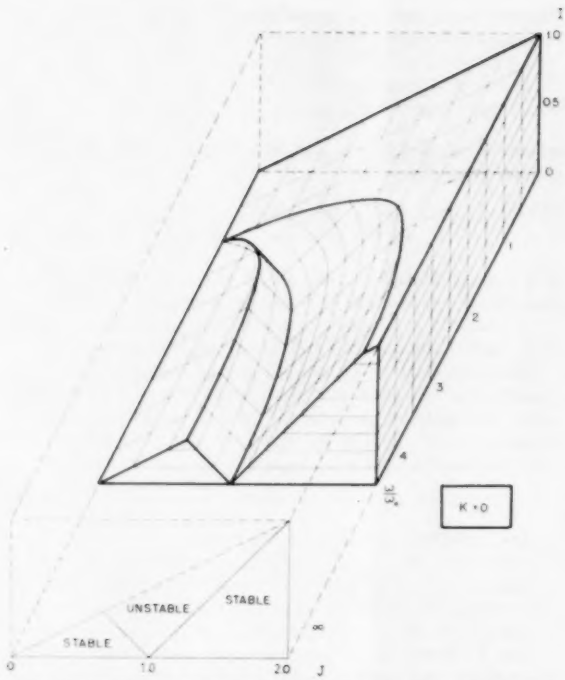

Fig. 2 Stable and unstable speed regions in case of equal supporting stiffnesses

velocity of one of the ellipses are absent because the roots of smaller magnitude, $\pm\lambda_1$, have become imaginary, thereby ceasing to define an elliptic motion.

An interesting phenomenon is associated with the point P in Fig. 3. There, ω is approximately one half of ω_0 and there is a motion component *which does not rotate*. It could be expected that this motion could be excited by a nonrotating excitation such as gravity acting on a rotor overhung on a horizontal shaft. A rotor with $I = 0.234$, $J = 0.543$, and $K = 0.22$ was tested for this effect. It was found that a slight resonance would appear only when the action of gravity was oriented in the more compliant direction. The motion was small and no attempt was made to measure it. It did appear, however, at the predicted speed and could be recognized with no difficulty by contrast with the smoother rotation at other speeds in the general vicinity of this resonance. A similar situation is found in the secondary critical speeds of horizontal shafts with different principal bending stiffnesses resulting from an unsymmetrical cross section ("flat" shafts) [1, 2, 3, 4]. The motion may again be described in stationary co-ordinates in terms of circularly polarized-motion components one of which will be stationary when the shaft rotates at the secondary critical speed. Analogous critical speeds for two-bladed helicopter rotors were predicted in the analysis of Coleman and Feingold [5].

Stability Analysis for the Case of Stationary Stiffness Inequality

Equations (18) are linear differential equations with periodic coefficients for which no solutions in closed form are known. W. R. Foote, J. Poritsky, and J. J. Slade, Jr. [4] and Coleman and

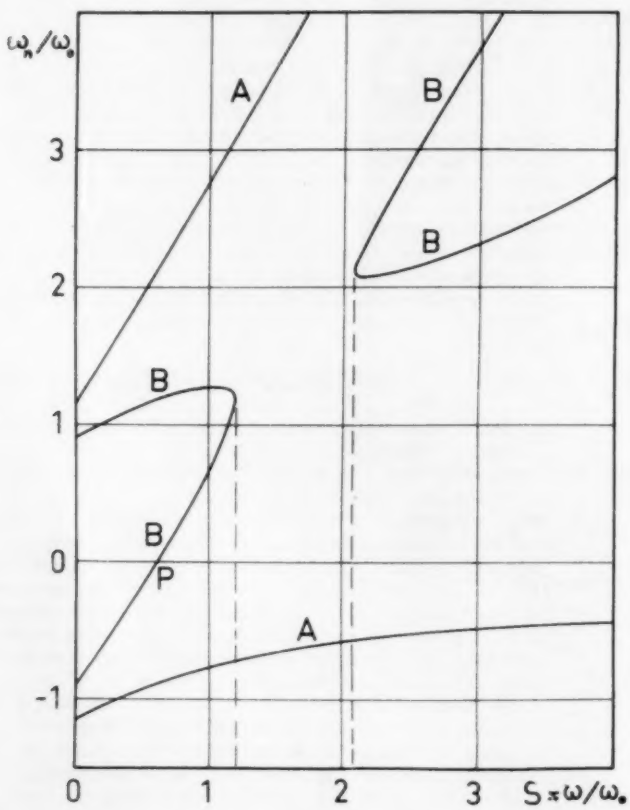

Fig. 3 Analysis of motion in terms of circularly polarized motions

Feingold [5] have encountered equations similar to these. Foote, Poritsky, and Slade developed a method to determine the stability of the solution to equations of the type of (18) which is used here. The reader interested in the details of this method is referred to the paper of Coleman and Feingold where a full discussion is presented.

The stability analysis in the case of stationary unequal stiffnesses actually takes its simplest form when considering the intermediate formulation (14) rather than equations (18). It is known that equations of this type will admit solutions of the form

$$u = U(\tau)e^{i\lambda\tau}$$
$$\ddot{u} = \ddot{U}(\tau)e^{i\lambda\tau} \tag{23}$$

where $U(\tau)$ and $\ddot{U}(\tau)$ are periodic functions of the same period as the periodic coefficients in the differential equations and therefore may be represented in the form:

$$U(\tau) = \sum_{\pm 1,\ \pm 3,\ \ldots} U_n e^{in\tau}$$
$$\ddot{U}(\tau) = \sum_{\pm 1,\ \pm 3,\ \ldots} \ddot{U}_n e^{in\tau} \tag{24}$$

Actually, for reasons of mathematical convenience, the second derivatives are taken to have the form (23)

$$\ddot{u} = \sum_{\pm 1,\ \pm 3,\ \ldots} A_n e^{i(\lambda+n)\tau}$$
$$\ddot{u} = \sum_{\pm 1,\ \pm 3,\ \ldots} B_n e^{i(\lambda+n)\tau} \tag{25}$$

For a fourth-order system there will be four independent values of the characteristic root λ. Thus, in general, u and $\ddot{u}$ will be expressed by a linear combination of four series such as in (25). It is clear that if any of these terms has a λ-value with negative imaginary part, a positive exponential power will result, hence instability.

Substitution of the forms (25) into equations (14) yields

$$\sum_{\pm 1,\ \pm 3,\ \ldots} \left[\left\{ \frac{-\mu K}{(\lambda+n)^2} A_n + \left[1 + \frac{J}{\lambda+n} - \frac{\mu}{(\lambda+n)^2} \right] B_n \right\} e^{in\tau} - \left[\frac{2I}{\lambda+n} - I \right] A_n e^{i(n-2)\tau} \right] = 0$$
$$\sum_{\pm 1,\ \pm 3,\ \ldots} \left[\left[\frac{2I}{\lambda+n} + I \right] B_n e^{i(n+2)\tau} + \left\{ \left[1 - \frac{J}{\lambda+n} - \frac{\mu}{(\lambda+n)^2} \right] A_n - \frac{\mu K}{(\lambda+n)^2} B_n \right\} e^{in\tau} \right] = 0 \tag{26}$$

Equating to zero the net coefficients of each exponential, the following recurrence relationships are obtained between the A_n and B_n:

$$-\frac{\mu K}{(\lambda+n)^2} A_n + \left[1 + \frac{J}{(\lambda+n)} - \frac{\mu}{(\lambda+n)^2} \right] B_n + \left[\frac{(\lambda+n)I}{\lambda+n+2} \right] A_{n+2} = 0$$
$$\frac{(\lambda+n)I}{\lambda+n-2} B_{n-2} + \left[1 - \frac{J}{(\lambda+n)} - \frac{\mu}{(\lambda+n)^2} \right] A_n - \frac{\mu K}{(\lambda+n)^2} B_n = 0 \tag{27}$$

Equations (27) constitute an infinite set of algebraic equations in the infinite number of unknowns A_n and B_n. In order that this set be satisfied by nonzero values of the A_n and B_n, the infinite determinant $\Delta(\lambda)$ of the coefficients of the A_n and B_n must be zero. This determinant may be written as

$$\Delta(\lambda) = \begin{vmatrix} \cdots\cdots & & & & & & \\ d_{-2} & b_{-1} & c_{-1} & & & & \\ & c_{-1} & a_{-1} & d_{-1} & & & \\ & & e_1 & a_1 & c_1 & & \\ & & & c_1 & b_1 & d_2 & \\ & & & & e_2 & a_2 & c_2 \\ & & & & & \cdots\cdots & \end{vmatrix} \tag{28}$$

where terms other than those on the three diagonals are zero. In equation (28) the following nomenclature has been used, for positive values of n:

$$a_n(\lambda) = 1 - \frac{J}{(2n-1+\lambda)} - \frac{\mu}{(2n-1+\lambda)^2}$$
$$b_n(\lambda) = 1 + \frac{J}{(2n-1+\lambda)} - \frac{\mu}{(2n-1+\lambda)^2} \tag{29}$$
$$c_n(\lambda) = \frac{-\mu K}{(2n-1+\lambda)^2}$$
$$d_n(\lambda) = \frac{2n-3+\lambda}{2n-1+\lambda} I$$
$$e_n(\lambda) = \frac{2n-1+\lambda}{2n-3+\lambda} I$$

For negative values of n it is found that $a_{-n}(\lambda) = a_n(-\lambda)$ and similarly for the other coefficients. It is therefore possible to compute all the coefficients with a negative subscript by replacing λ by $-\lambda$ in equations (29).

In order to find the roots of $\Delta(\lambda)$ it is convenient to introduce the finite determinant $\Delta_n(\lambda)$ defined by the square array of $4n$ columns and rows centered on the origin of $\Delta(\lambda)$, this origin being at the intersection of the dashed lines in equation (28). It can be shown that

$$\Delta_n(\lambda) = D_n(\lambda)D_n(-\lambda) - N_n(\lambda)N_n(-\lambda) \tag{30}$$

where $D_n(\lambda)$ is the determinant of the terms on the right and below the origin of $\Delta_n(\lambda)$, $D_n(-\lambda)$ is the value of $D_n(\lambda)$ when λ is replaced by $-\lambda$, $N_n(\lambda)$ is the determinant obtained by replacing the first column of $D_n(\lambda)$ by $-e_1, 0, 0, 0, \ldots$ and $N_n(-\lambda)$ is the value of $N_n(\lambda)$ when λ is replaced by $-\lambda$. These determinants may be calculated from the recurrence formulas,

$$D_n(\lambda) = b_n C_n(\lambda) - c_n^2 D_{n-1}(\lambda)$$
$$C_n(\lambda) = a_n D_{n-1}(\lambda) - I^2 C_{n-1}(\lambda) \tag{31}$$

and

$$N_n(\lambda) = b_n M_n(\lambda) - c_n^2 N_{n-1}(\lambda)$$
$$M_n(\lambda) = a_n N_{n-1}(\lambda) - I^2 M_{n-1}(\lambda)$$

where $C_n(\lambda)$ and $M_n(\lambda)$ are determinants of order $2n-1$ obtained from $D_n(\lambda)$ and $N_n(\lambda)$, respectively, by dropping their last row and column. The initial values of all these are

$$C_1(\lambda) = a_1$$
$$M_1(\lambda) = -e_1$$
$$D_1(\lambda) = a_1 b_1 - c_1^2 \tag{32}$$
$$N_1(\lambda) = -e_1 b_1$$

As n approaches infinity, the recurrence relations (31) become

$$\begin{aligned} D_n(\lambda) &= C_n(\lambda) \\ C_n(\lambda) &= D_{n-1}(\lambda) - I^2 C_{n-1}(\lambda) \\ N_n(\lambda) &= M_n(\lambda) \\ M_n(\lambda) &= N_{n-1}(\lambda) - I^2 M_{n-1}(\lambda) \end{aligned} \tag{33}$$

hence for large n,

$$\begin{aligned} D_n(\lambda) &= D_{n-j}(1 - I^2)^j \\ N_n(\lambda) &= N_{n-j}(1 - I^2)^j \end{aligned} \tag{34}$$

and therefore, for large n, the function

$$F_n(\lambda) = \frac{\Delta_n(\lambda)}{(1 - I^2)^{2n}}$$

must approach a finite limit $F(\lambda)$. This function $F(\lambda)$ can be shown to have fourth-order poles at $\lambda = \pm 1, \pm 3, \ldots \pm (1 + 2s)$ where s is any integer. It has roots $\lambda_1 \pm 2s$ and $\lambda_2 \pm 2s$. Therefore the function

$$G(\lambda) = \frac{F(\lambda) \cos^4\left(\frac{\pi\lambda}{2}\right)}{\left[\sin^2\frac{\pi\lambda}{2} - \sin^2\frac{\pi\lambda_1}{2}\right]\left[\sin^2\frac{\pi\lambda}{2} - \sin^2\frac{\pi\lambda_2}{2}\right]} \tag{35}$$

is analytic everywhere in the complex plane and, from Liouville's theorem, it must be a constant. Letting λ approach infinity along the imaginary axis it is found that

$$G(\lambda) = \frac{1}{1 - I^2} \tag{36}$$

hence,

$$\left[\sin^2\frac{\pi\lambda}{2} - \sin^2\frac{\pi\lambda_1}{2}\right]\left[\sin^2\frac{\pi\lambda}{2} - \sin^2\frac{\pi\lambda_2}{2}\right] = (1 - I^2)F(\lambda) \cos^4\left(\frac{\pi\lambda}{2}\right) \tag{37}$$

If two arbitrary values of λ are successively substituted in equation (37), two simultaneous equations in λ_1 and λ_2 are obtained which may be solved for λ_1 and λ_2. It is convenient to use the values $\lambda = 0$ and $\lambda = 1.0$ for this purpose. The equations obtained are

$$K(0) \equiv \sin^2\frac{\pi\lambda_1}{2} \sin^2\frac{\pi\lambda_2}{2} = (1 - I^2)F(0) \tag{38}$$

and

$$K(1) \equiv \cos^2\frac{\pi\lambda_1}{2} \cos^2\frac{\pi\lambda_2}{2} = \lim_{\lambda \to 1.0} \left\{(1 - I^2)F(\lambda) \cos^4\left(\frac{\pi\lambda}{2}\right)\right\} \tag{39}$$

Given $K(0)$ and $K(1)$, the values of λ_1 and λ_2 are obtained from

$$\begin{aligned} [K(1)]^{1/2} + [K(0)]^{1/2} &= \cos\left[\frac{\pi}{2}(\lambda_1 - \lambda_2)\right] \\ [K(1)]^{1/2} - [K(0)]^{1/2} &= \cos\left[\frac{\pi}{2}(\lambda_1 + \lambda_2)\right] \end{aligned} \tag{40}$$

and it is then evident that for stability it is necessary to have

$$\begin{aligned} 0 \leqslant K(0) \leqslant 1 \\ 0 \leqslant K(1) \leqslant 1 \\ [K(1)]^{1/2} + [K(0)]^{1/2} \leqslant 1 \end{aligned} \tag{41}$$

To compute $K(0)$ and $K(1)$, equations (38) and (39) may be used but they are found to converge much too slowly with n. Convergence factors may be derived taking second-order approximations for the recurrence relations (31) at large n. The derivation of convergence factors in this manner is explained in detail in the paper of Coleman and Feingold [5]. The expressions obtained are

$$K(0) = \lim_{n \to \infty}\left[\frac{K_n(0) \cos^2\frac{\pi\beta^{1/2}}{2}}{\prod_{j=1}^{n}\left(1 - \frac{\beta}{(2j-1)^2}\right)^2}\right] \tag{42}$$

$$K(1) = \lim_{n \to \infty}\left[\frac{K_n(1) \sin^2\frac{\pi\beta^{1/2}}{2}}{\left(1 - \frac{\beta}{4n^2}\right)\frac{\pi^2\beta}{4}\prod_{j=1}^{n-1}\left(1 - \frac{\beta}{4j^2}\right)^2}\right] \tag{43}$$

where

$$\beta = \frac{2\mu + J^2 - 2I^2 J}{1 - I^2} \tag{44}$$

The improvement in convergence obtained by this method is considerable, particularly at small values of μ. For instance, for $\mu = 1.0$, $J = 0.543$, $I = 0.234$, and $K = 0.22$, the successive approximations to $K(0)$ computed with and without the use of a convergence factor are given in Table 1.

Table 1

n	$K(0)$ (without convergence factor)	$K(0)$ (with convergence factor)
1	0.04717	0.01414
2	0.02136	0.01178
3	0.01665	0.01120
4	0.01489	0.01107
5	0.01402	0.01107
6	0.01345	0.01106

This numerical procedure was developed to investigate the changes in the stability regions in Fig. 2 when K is finite. Calculations were made only for a rotor with $J = 0.543$, $I = 0.234$ with the result that the unstable speed region in Fig. 2 is not greatly affected by the stiffness inequality. In the process, however, it was found that the stiffness inequality gave rise to two new regions of instability. The manner in which these new instabilities are obtained is illustrated in Fig. 4 where the values of $K(0)$ and $K(1)$ are plotted as a function of speed for the case $K = 0.707$. At zero speed the value of $K(1)$ is infinite and that of $K(0)$ is zero. As the speed is increased, the value of $K(1)$ decreases and that of $K(0)$ increases until it reaches a maximum and then decreases too. At a sufficiently large speed, $S = 0.53$, $K(0)$ becomes negative, and the motion is unstable. It remains so until $S = 0.57$ when $K(0)$ becomes positive again. At $S = 0.68$, $K(1)$ vanishes. Then, at $S = 0.92$, the motion becomes again unstable as the third condition (41) is violated. This instability ceases at $S = 1.02$. At $S = 1.35$ instability is attained as $K(0)$ becomes negative for the second time,then, from $S = 2.25$ to infinity, the motion remains stable.

Of the three instabilities obtained, the one from $S = 1.35$ to $S = 2.25$ is the strongest since then, $K(0)$ becomes relatively large

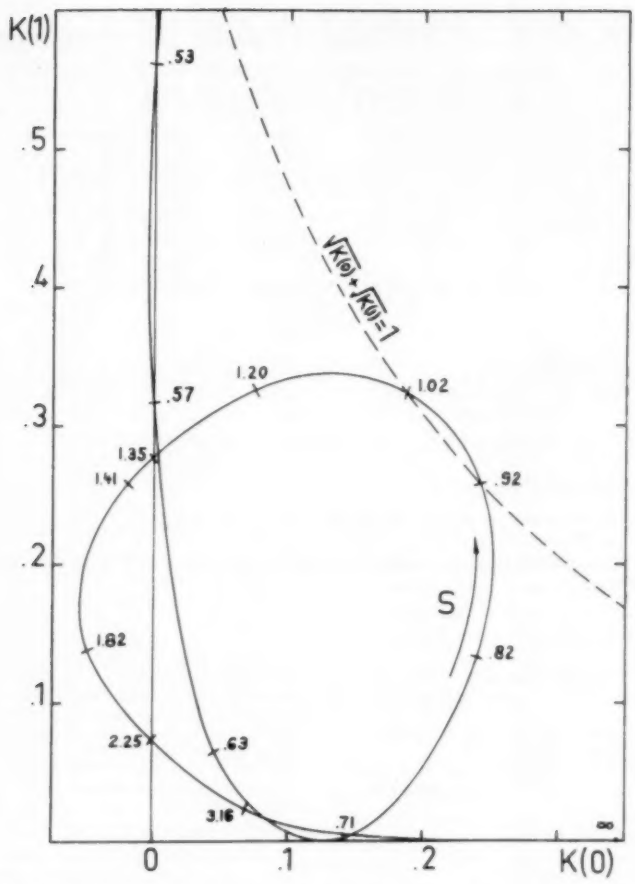

Fig. 4 Values of $K(0)$ and $K(1)$ as a function of speed for case $J = 0.543$, $I = 0.234$, and $K = 0.707$

and negative which means that λ will have an imaginary part of considerable magnitude. This instability is that which is obtained, when $K = 0$, within the speed range given by equation (21). For $J = 0.543$ and $I = 0.234$ this range is $S = 1.20$ to $S = 2.12$. It may be noted in equation (32) that the stiffness inequality K will always appear as K^2 in the expansion for $\Delta(\lambda)$. Therefore for small K, the effect of K on this strongest rotor instability may be expected to be of the second order. This conclusion is supported by detailed numerical analysis of the stability conditions with small K.

The instability from $S = 0.92$ to $S = 1.02$ is quite peculiar in that it is known to be absent when $K = 0$ and appears to be absent also when $K = 1.0$ because the expansion for $K(1)$ gives a finite coefficient times $(1 - K^2)$ and hence, when $K = 1.0$, $K(1)$ is zero and an intersection with the limit $[K(0)]^{1/2} + [K(1)]^{1/2} = 1.0$ is no longer possible.

Experimental verifications were attempted with the setup illustrated in Fig. 5 which consisted of a 9.6-lb rotor with $J = 0.543$ and $I = 0.234$. The stiffness inequality K was given the successive values 0.27, 0.60, and 0.91. In every case, three regions of instability were observed. The low-speed instability never resulted in runaway amplitudes while the other two instabilities always did. The calculated and observed frequency regions are shown in Fig. 6. The agreement with theory is excellent for the large region of instability. For the other regions, some discrepancies seem to exist. It is felt, however, that the experimental apparatus used may very well have been responsible for these. In any event, in the present investigation little more has been done than to discover and verify the existence of the additional instabilities. A thorough study of these should be presented in a subsequent paper.

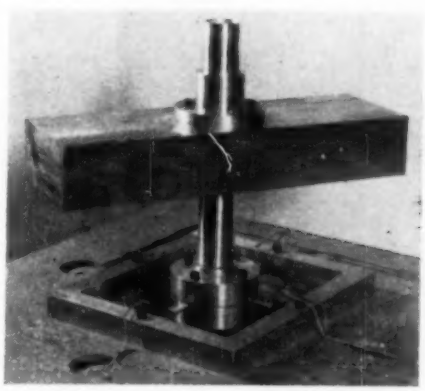

Fig. 5 Tested unsymmetrical rotor

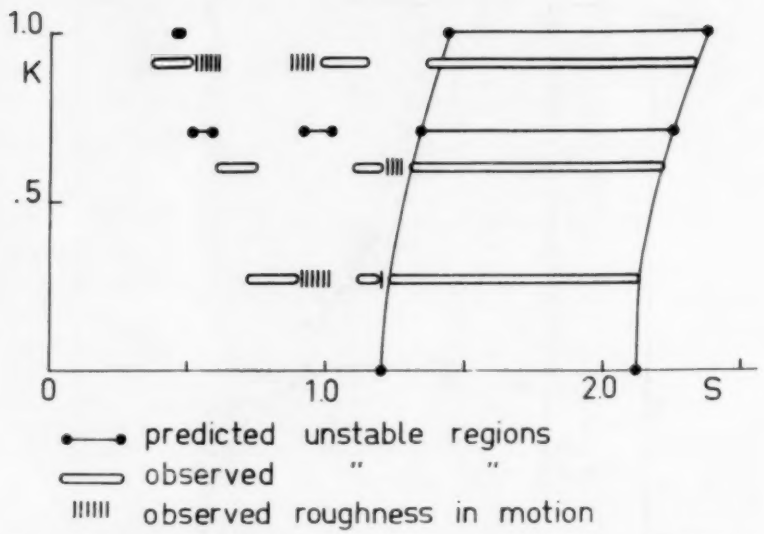

Fig. 6 Calculated and observed unstable speed regions as a function of K for case $J = 0.543$ and $I = 0.234$

References

1 J. P. Den Hartog, "Mechanical Vibrations," McGraw-Hill Book Company, Inc., New York, N. Y., fourth edition, 1956, pp. 258-265.

2 C. B. Biezeno and R. Grammel, "Engineering Dynamics," vol. 3, Blackie and Son Limited, London, England, 1954.

3 D. M. Smith, "The Motion of a Rotor Carried by a Flexible Shaft in Flexible Bearings," *Proceedings of The Royal Society*, Series A, vol. 142, 1933, pp. 92-118.

4 W. R. Foote, H. Poritsky, and J. J. Slade, Jr., "Critical Speeds of a Rotor With Unequal Shaft Flexibilities, Mounted in Bearings of Unequal Flexibilities, I," JOURNAL OF APPLIED MECHANICS, vol. 10, TRANS. ASME, vol. 65, 1943, pp. A-77-A-84.

5 R. P. Coleman and A. M. Feingold, "Theory of Self-Excited Mechanical Oscillations of Helicopter Rotors With Hinged Blades," NACA Report 1351, 1958, chapters 2 and 3.

6 P. J. Brosens, "Whirling of Unsymmetrical Rotors," ScD thesis, Massachusetts Institute of Technology, Cambridge, Mass., May, 1959.

SHUN CHENG
Department of Mechanics,
University of Wisconsin,
Madison, Wis.

Torsion of Sandwich Plates of Trapezoidal Cross Section

A system of suitable stress-strain relations as well as equations of equilibrium are derived and solved for the torsion of sandwich plates of trapezoidal cross section. The facings are treated as isotropic solid membranes of equal thickness while the core is of such a nature that its stiffnesses associated with plane-stress components are negligibly small.

INVESTIGATIONS of torsion of rectangular sandwich plates have been carried out by P. Seide [1],[1] H. G. McComb [2], and the present author [3]. The solution for a slender isosceles triangular cross section with a constant-thickness-shell wall around the sides may be found in reference [2]. In 1958 F. Essenburg and P. M. Naghdi provided the solution for torsion of a homogeneous isotropic solid plate of trapezoidal cross section [4]. The present paper is devoted to the study of torsion of sandwich plates of trapezoidal cross section. Such sandwich panels are employed in certain airframe components such as stabilizing fins and control surfaces. The facings are taken to be isotropic solid membranes of equal thickness. The core is considered as an orthotropic honeycomb structure.

A system of suitable stress-strain relations as well as equations of equilibrium are derived and solved for the torsional stiffness of trapezoidal sandwich plates. There will be no difficulty so far as the derivation of the equations of equilibrium are concerned. The problem consists of the formulation of stress-strain relations of such constructions. This is accomplished here by means of the variational theorem of complementary energy which states that the true state of stress is distinguished from all other statically correct states of stress by the condition that the complementary energy be a minimum [5, 6]. The complementary energy is defined as the difference between the strain energy and the work which the surface stresses do over that portion of the surface where the displacements are prescribed. When the equilibrium equations are known in terms of stresses, the stress displacement or stress-strain relations may be derived from the principle of complementary energy. Without resource to this approach these derivations may require much lengthier calculations. Such is the case of the present problem.

[1] Numbers in brackets designate References at end of paper.

Presented at the Summer Conference of the Applied Mechanics Division, Chicago, Ill., June 14–16, 1961, of THE AMERICAN SOCIETY OF MECHANICAL ENGINEERS.

Written discussion on this paper should be addressed to the Editorial Department, ASME, United Engineering Center, 345 East 47th Street, New York 17, N. Y., and will be accepted until October 10, 1961. Discussion received after the closing date will be returned. Manuscript received by ASME Applied Mechanics Division, November 3, 1959. Paper No. 61—APM-22.

Analysis

The core is tapered so that its cross section taken perpendicular to the x-axis is a trapezoid. Its cross section taken perpendicular to the y-axis is rectangular as shown in Fig. 1. The external torque T is applied in the yz-plane.

Let the xy-plane be the middle plane of the core and the x_1y_1-plane be the plane of the facing plate with the z_1-axis along the normal to this plane. The equation of the x_1y_1-plane is given by

$$z = h + y \tan \alpha \tag{1}$$

For points in this plane

$$x_1 = x, \quad y_1 = \frac{y}{\cos \alpha}, \quad z_1 = 0 \tag{2}$$

Since $x_1 = x$, only x will be used hereafter.

The assumptions made in the present paper have been used in

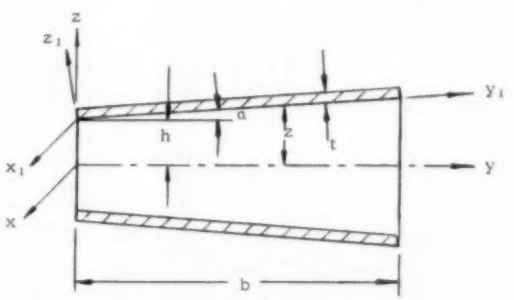

Fig. 1 Cross section of plate

Nomenclature

x, y, z = rectangular co-ordinates for core (Fig. 1)
x_1, y_1, z_1 = rectangular co-ordinates for facings (Fig. 1)
b = width of sandwich
h = half thickness of smaller side of core (Fig. 1)
t = thickness of facings
α = slope of facing (Fig. 1)
U = strain energy
E, ν = Young's modulus of elasticity and Poisson's ratio of facings
$G = \frac{E}{2(1+\nu)}$, shear modulus of facings
G_{xz}, G_{yz} = shear moduli of core
$\sigma_x, \sigma_{y1}, \tau$ = stresses in facings
τ_{xz}, τ_{yz} = stresses in core
V_1, V_2, V_3 = generalized boundary displacements, Lagrangian multipliers
u = Lagrangian multiplier
C_1, C_2 = constants
I_0, K_0, I_1, K_1 = modified Bessel functions of first and second kind of order zero and one
$r = \frac{4G_{xz}}{G \cdot t \cdot \cos \alpha \cdot \tan^2 \alpha}$
T = applied torque
θ = angle of twist
l = length of sandwich

many previous analyses [5, 7, 8] and are known to represent usual sandwich constructions having honeycomb cores. These assumptions are as follows:

(*a*) The core stiffnesses associated with plane-stress components in the xy-plane are negligibly small, as previously stated. Thus, of the six components of the stress tensor, the three present in the xy-plane are assumed to be absent in the present analysis.

(*b*) The facings are treated as isotropic solid membranes of equal thickness. Hence the shearing stresses in facings normal to their planes may be neglected and the stresses in facings parallel to their planes may be assumed to be distributed uniformly over the thickness of the facings.

(*c*) Normal strains in the core in the direction perpendicular to the xy-plane of the sandwich plate are disregarded.

(*d*) Guided by the Saint Venant theory of torsion, we assume all stresses independent of the longitudinal axis x.

Results based on the assumption of membrane facings are somewhat limited in applicability, but they should be sufficiently accurate for the majority of sandwich panels. If the facings are not sufficiently thin to be considered membranes, they should be treated as thin plates with transverse shears and bending stiffnesses. It is felt that the core assumptions (*a*) fairly accurately represent the cores presently in use, especially those of the honeycomb type. The third assumption may be justified for the present study since, even if normal strains in the core in the direction perpendicular to the xy-plane of the sandwich plate exist, these normal strains do not affect the distortion of the central plane of the plate and therefore have no effect on the computed torsional rigidity of the sandwich plate. The earlier investigations of sandwich plates [7] have proved this assumption to be satisfactory in sandwich analysis.

After these assumptions, the stresses left to be considered are the normal stress σ_{y_1}, the shearing stress τ in the plane of the facings (x_1y_1-plane), and the transverse shearing stresses τ_{xz} and τ_{yz} of the core. Hence the strain energy of the sandwich plate can be written as

$$U = \iint_f \left(\frac{t}{E}\sigma_{y_1}^2 + \frac{t}{G}\tau^2\right) dx\, dy_1 + \frac{1}{2}\iiint_c \left(\frac{\tau_{xz}^2}{G_{xz}} + \frac{\tau_{yz}^2}{G_{yz}}\right) dx\, dy\, dz \quad (3)$$

where the subscript f refers to the facings and c to the core.

Since all stresses are assumed independent of x, we can integrate equation (3) with respect to x

$$U = l\int_f \left(\frac{t}{E}\sigma_{y_1}^2 + \frac{t}{G}\tau^2\right) dy_1 + \frac{l}{2}\iint_c \left(\frac{\tau_{xz}^2}{G_{xz}} + \frac{\tau_{yz}^2}{G_{yz}}\right) dy\, dz \quad (4)$$

As the stress σ_x, σ_y, and τ_{xy} have been assumed to be zero in the core material, the differential equations of equilibrium in x and y-directions of the core become

$$\frac{\partial \tau_{xz}}{\partial z} = 0, \quad \frac{\partial \tau_{yz}}{\partial z} = 0 \quad (5)$$

From equation (5) it is seen that the transverse shear stresses τ_{xz} and τ_{yz} do not vary across the thickness of the core. Thus equation (4), with (2) and (5), becomes

$$U = l\int_0^b \left[\frac{t}{\cos\alpha}\left(\frac{\sigma_{y_1}^2}{E} + \frac{\tau^2}{G}\right) + z\left(\frac{\tau_{xz}^2}{G_{xz}} + \frac{\tau_{yz}^2}{G_{yz}}\right)\right] dy \quad (6)$$

From the summation of moments and forces acting on a differential element $dx\, dy$ of the sandwich plate as shown in Fig. 2 and the assumption that all stresses are independent of the x-axis, the following equations of equilibrium are obtained:

$$t\left(\frac{2z}{\cos\alpha} + t\right)\frac{\partial \tau}{\partial y_1} - 2z\tau_{xz} = 0 \quad (7)$$

$$t\left(2z + \frac{t}{\cos\alpha}\right)\frac{\partial \sigma_{y_1}}{\partial y_1} - 2z\tau_{yz} = 0 \quad (8)$$

$$\tau_{yz}\tan\alpha + z\frac{\partial \tau_{yz}}{\partial y} + t\tan\alpha\frac{\partial \sigma_{y_1}}{\partial y_1} = 0 \quad (9)$$

By applying equation (2) and the assumptions (*a*) and (*d*), we may write

$$\frac{\partial \tau}{\partial y_1} = \frac{d\tau}{dy}\cos\alpha, \quad \frac{\partial \sigma_{y_1}}{\partial y_1} = \frac{d\sigma_{y_1}}{dy}\cos\alpha$$

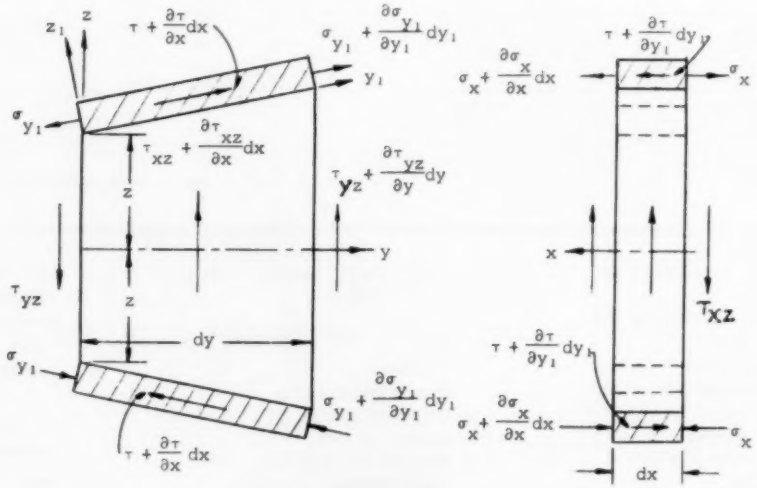

Fig. 2 Differential element

Hence, equations (7), (8), and (9), with equation (5) reduce to

$$t(2z + t\cos\alpha)\frac{d\tau}{dy} - 2z\tau_{xz} = 0 \tag{10}$$

$$t(2z\cos\alpha + t)\frac{d\sigma_{y_1}}{dy} - 2z\tau_{yz} = 0 \tag{11}$$

$$\tau_{yz}\tan\alpha + z\frac{d\tau_{yz}}{dy} + t\sin\alpha\frac{d\sigma_{y_1}}{dy} = 0 \tag{12}$$

where all the stresses τ, τ_{xz}, σ_{y_1}, and τ_{yz} are functions of y only. Solving the differential equations (11) and (12) for τ_{yz} and σ_{y_1} and using the boundary conditions that both stresses are zero when $y = 0$ and $y = b$, we can show that

$$\tau_{yz} = \sigma_{y_1} = 0 \tag{13}$$

The problem is now reduced to finding the stresses τ and τ_{xz}. Equation (10) is one of the equations needed for the solution of these two unknowns. To obtain further equations, use is made of the stress-strain relations. These relations will be obtained in this analysis, as previously explained, through the use of the variational theorem of complementary energy in conjunction with Lagrangian multipliers, the Euler equations of which are equivalent to the required stress-strain relations. Because of equation (13), the strain energy of the sandwich plate, equation (6), becomes

$$U = l\int_0^b \left(\frac{t\tau^2}{G\cos\alpha} + \frac{z\tau_{xz}^2}{G_{xz}}\right)dy \tag{14}$$

The stresses τ and τ_{xz} distributed over the ends of the sandwich plate represent a couple the magnitude of which is equal to the applied torque T. Taking the moments with respect to the x-axis and applying equations (1) and (2), we find

$$T = 2t\left(h + \frac{t}{2\cos\alpha}\right)\int_0^b \tau dy - 2\int_0^b yz\tau_{xz}dy \tag{15}$$

With equations (14) and (15), the complementary energy may be expressed as

$$l\int_0^b \left(\frac{t\tau^2}{G\cos\alpha} + \frac{z\tau_{xz}^2}{G_{xz}}\right)dy - \theta\left[2t\left(h + \frac{t}{2\cos\alpha}\right)\int_0^b \tau dy - 2\int_0^b yz\tau_{xz}dy\right] \tag{16}$$

Since the sum of the last two terms ($= \theta T$) represents the work of the boundary stresses, it follows that θ is the angle of twist of the sandwich plate.

The boundary conditions of the present problem are:

(i) $$\tau = 0 \quad \text{at} \quad y = 0 \tag{17}$$

(ii) $$\tau = 0 \quad \text{at} \quad y = b \tag{18}$$

(iii) The summation of forces in the vertical direction is equal to zero

$$2\int_0^b (z\tau_{xz} + t\tau\tan\alpha)dy = 0 \tag{19}$$

To make the complementary energy (16) a minimum subject to the equation of equilibrium (10) and boundary conditions (17), (18), and (19), these equations are multiplied, according to the rules of the calculus of variations, by Lagrangian multipliers $u(y)$, V_1, V_2, and V_3, respectively, and added to the integrand of the complementary energy (16). The variation of the resulting expression is then made to vanish:

$$\delta\left\{\int_0^b \left[l\left(\frac{t\tau^2}{G\cos\alpha} + \frac{z\tau_{xz}^2}{G_{xz}}\right) + u\left(\sqrt{2tz + t^2\cos\alpha}\,\frac{d\tau}{dy} - 2z\tau_{xz}\right)\right]dy - \theta\left[2t\left(h + \frac{t}{2\cos\alpha}\right)\int_0^b \tau dy - 2\int_0^b yz\tau_{xz}dy\right] + V_1\tau(0) + V_2\tau(b) + 2V_3\int_0^b (z\tau_{xz} + t\tau\tan\alpha)dy\right\} = 0 \tag{20}$$

where V_1, V_2, and V_3 are constants representing the generalized boundary displacements of the problem; u is a function of y to be determined later. After carrying out the variations with respect to the stresses τ and τ_{xz}, eliminating the variation of derivative

$$\left(\delta\frac{d\tau}{dy}\right)$$

by integration by parts and regrouping the terms, the variation equations (Euler equations) which render the complementary energy a minimum take the following forms:

$$u - V_3 = \frac{l\tau_{xz}}{G_{xz}} + \theta y \tag{21}$$

$$\left(z + \frac{t\cos\alpha}{2}\right)\frac{du}{dy} + (u - V_3)\tan\alpha - \frac{l\tau}{G\cos\alpha} + \theta\left(h + \frac{t}{2\cos\alpha}\right) = 0 \tag{22}$$

In addition to the two Euler equations, we obtain for the boundary

$$V_2 = -2t\left(h + b\tan\alpha + \frac{t\cos\alpha}{2}\right)u(b) \tag{23}$$

$$V_1 = 2t\left(h + \frac{t\cos\alpha}{2}\right)u(0) \tag{24}$$

Substituting the expression $u - V_3$ from equation (21) into equation (22), we obtain

$$\left(z + \frac{t\cos\alpha}{2}\right)\left(\frac{1}{G_{xz}}\frac{d\tau_{xz}}{dy} + \frac{\theta}{l}\right) + \left(\frac{\tau_{xz}}{G_{xz}} + \frac{\theta}{l}\right)\tan\alpha - \frac{\tau}{G\cos\alpha} + \frac{\theta}{l}\left(h + \frac{t}{2\cos\alpha}\right) = 0 \tag{25}$$

The differentiation of equation (10) with respect to y and substitution the result $(d\tau_{xz}/dy)$ into equation (25) yields

$$\frac{d^2\tau}{dy^2} + \frac{(2z\tan\alpha - t\sin\alpha)}{z(2z + t\cos\alpha)}\frac{d\tau}{dy} - \frac{4G_{xz}z\tau}{tG\cos\alpha(2z + t\cos\alpha)^2} = \frac{-2G_{xz}\theta z\left(4z + t\cos\alpha + \dfrac{t}{\cos\alpha}\right)}{tl(2z + t\cos\alpha)^2} \tag{26}$$

This equation, with equation (2), can be written as

$$z\frac{d^2\tau}{dz^2} + \frac{\left(1 - \dfrac{t}{2z}\cos\alpha\right)}{\left(1 + \dfrac{t}{2z}\cos\alpha\right)}\frac{d\tau}{dz}$$

$$- \frac{G_{xz}\tau}{tG \cos \alpha \tan^2 \alpha \left(1 + \frac{t}{2z} \cos \alpha\right)^2}$$

$$= \frac{-2\theta G_{xz} z \left(1 + \frac{t}{4z} \cos \alpha + \frac{t}{4z \cos \alpha}\right)}{lt \tan^2 \alpha \left(1 + \frac{t}{2z} \cos \alpha\right)^2}$$

Since facings are treated as membranes, $t/2h$ is relatively small as compared with 1; with this consideration, the foregoing equation may be reduced to

$$z \frac{d^2\tau}{dz^2} + \frac{d\tau}{dz} - \frac{G_{xz}\tau}{tG \cos \alpha \tan^2 \alpha} = \frac{-2\theta G_{xz} z}{lt \tan^2 \alpha} \tag{27}$$

By using a transformation $z = z_1^2$, the differential equation (27) can be transformed to the Bessel's differential equation [9]. Its complete solution for τ with two arbitrary constants of integration C_1 and C_2 is

$$\tau = 2 \frac{\theta}{l} G \cos \alpha \left[\frac{4}{r} + z + C_1 I_0(rz)^{1/2} + C_2 K_0(rz)^{1/2}\right] \tag{26}$$

where I_0 and K_0 are modified Bessel functions of first and second kind of order zero. The two arbitrary constants C_1 and C_2 determined from the boundary conditions that $\tau = 0$ at $y = 0$ and $y = b$ are

$$C_1 = \frac{\begin{vmatrix} \left(h + \frac{4}{r}\right) & K_0(rh)^{1/2} \\ \left(h + b \tan \alpha + \frac{4}{r}\right) & K_0\{[r(h + b \tan \alpha)]^{1/2}\} \end{vmatrix}}{\begin{vmatrix} I_0(rh)^{1/2} & K_0(rh)^{1/2} \\ I_0\{[r(h + b \tan \alpha)]^{1/2}\} & K_0\{[r(h + b \tan \alpha)]^{1/2}\} \end{vmatrix}}$$

$$C_2 = \frac{\begin{vmatrix} I_0(rh)^{1/2} & \left(h + \frac{4}{r}\right) \\ I_0\{[r(h + b \tan \alpha)]^{1/2}\} & \left(h + b \tan \alpha + \frac{4}{r}\right) \end{vmatrix}}{\begin{vmatrix} I_0(rh)^{1/2} & K_0(rh)^{1/2} \\ I_0\{[r(h + b \tan \alpha)]^{1/2}\} & K_0\{[r(h + b \tan \alpha)]^{1/2}\} \end{vmatrix}} \tag{27}$$

Substituting the value of τ_{xz} from equation (10) into equation (15) and integrating by parts yields

$$T = 4t \int_0^b \tau z dy + t^2 \frac{(1 + \cos^2 \alpha)}{\cos \alpha} \int_0^b \tau dy \tag{28}$$

Finally, substituting the expression for τ from equation (26) into equation (28) and carrying out the integration, we obtain the torsional stiffness as follows:

$$\frac{T}{\frac{\theta}{l}} = \left(2tG \frac{\cos \alpha}{\tan \alpha}\right) \left\{\frac{4z^3}{3} + \frac{8z^2}{r} + \frac{t(1 + \cos^2 \alpha)}{\cos \alpha} \left(\frac{z^2}{2} + \frac{4z}{r}\right)\right.$$

$$+ 2\sqrt{rz} \left[\frac{4(rz + 4) \cos \alpha + tr(1 + \cos^2 \alpha)}{r^2 \cos \alpha}\right]$$

$$[C_1 I_1(rz)^{1/2} - c_2 K_1(rz)^{1/2}]$$

$$\left. - \frac{16z}{r} [C_1 I_0(rz)^{1/2} + C_2 K_0(rz)^{1/2}]\right\}_h^{h + b \tan \alpha} \tag{29}$$

where I_0, K_0, I_1, and K_1 are modified Bessel functions of first and second kind of order zero and one; $(h + b \tan \alpha)$ and h are the upper and lower limits for the variable z.

Remarks

It is felt that the torsional stiffness presented in this paper is sufficiently accurate for the majority of sandwich panels in use such as stabilizing fins and control surfaces of airplanes. For such panels, the slope of the facings (α) is usually less than 30 deg and the constructions are of such a nature that renders the basic assumptions applicable. The range of applicability of the solution could be somewhat increased if thin-plate theory rather than membrane theory were used in regard to the facings. By setting $\alpha = 0$, equation (26) is reduced to the same differential equation for the shearing stress τ in the facings as given in a previous paper which has been recently submitted by the present author for publication [10]. In that paper the author found from numerical computations that the results of the present method for a rectangular sandwich plate is essentially the same as the infinite-series solution given in reference [3].

Acknowledgment

The author wishes to express his gratitude to Prof. Gerald Pickett of the Engineering Mechanics Department, University of Wisconsin, for his encouragement and critical comments of this investigation.

References

1 P. Seide, "On the Torsion of Rectangular Sandwich Plates," JOURNAL OF APPLIED MECHANICS, vol. 23, TRANS. ASME, vol. 78, 1956, pp. 191–194.

2 H. G. McComb, Jr., "Torsional Stiffness of Thin-Walled Shells Having Reinforcing Cores and Rectangular, Triangular, or Diamond Cross Sections," NACA TN 3749, 1956.

3 S. Cheng, "Torsion of Rectangular Sandwich Plates," Forest Products Laboratory, Madison Wis., Report No. 1871, 1959.

4 F. Essenburg and P. M. Naghdi, "On Elastic Plates of Variable Thickness," *Proceedings of the Third U. S. National Congress of Applied Mechanics*, 1958, pp. 313–319.

5 E. Reissner, "On Bending of Elastic Plates," *Quarterly of Applied Mathematics*, vol. 5, 1947, pp. 55–68.

6 C. T. Wang, "Applied Elasticity," McGraw-Hill Book Company, Inc., New York, N. Y., 1953.

7 E. Reissner, "Finite Deflections of Sandwich Plates," *Journal of the Aeronautical Sciences*, vol. 15, 1948, pp. 435–440.

8 M. E. Raville, "Analysis of Long Cylinders of Sandwich Construction Under Uniform External Lateral Pressure," Forest Products Laboratory, Report No. 1844, 1954.

9 N. W. McLachlan, "Bessel Functions for Engineers," Oxford University Press, London, England, 1955.

10 S. Cheng, "A Formula for the Torsional Stiffness of Rectangular Sandwich Plates," JOURNAL OF APPLIED MECHANICS, vol. 28, TRANS. ASME, vol. 83, Series E, June, 1961, pp. 307–310.

M. E. RAVILLE
Professor and Head,
Department of Applied Mechanics,
Kansas State University,
Manhattan, Kan.

EN-SHIUH UENG
MING-MIN LEI
Graduate Research Assistants,
Department of Applied Mechanics,
Kansas State University

Natural Frequencies of Vibration of Fixed-Fixed Sandwich Beams[1]

In this paper, the problem of the determination of the natural frequencies of vibration of fixed-fixed sandwich beams is analyzed by an energy approach in which the Lagrangian multiplier method is utilized to satisfy the boundary conditions of the problem. The solution is in the form of a rapidly converging infinite series. Experimental results are given for 21 sandwich beams having different dimensions and physical constants. Corresponding theoretical results, obtained by means of a digital computer, are in close agreement with the experimental results.

The natural frequencies of vibration of a fixed-fixed sandwich beam are determined by an energy approach in which the Lagrangian multiplier method is utilized to satisfy the boundary conditions. The same method can be applied to the analysis of vibration problems of sandwich beams with other combinations of end conditions and can be extended to the analysis of sandwich plates. The analysis is carried out according to the following assumptions:

1 The facings of the sandwich are homogeneous, isotropic, and elastic thin plates of equal or unequal thickness.

2 The core consists of an elastic, orthotropic continuum whose load-carrying capacity in the plane of the sandwich is negligible.

3 The modulus of elasticity of the core in the direction perpendicular to the facings is infinite.

4 Perfect continuity exists at the interfaces. The dimensions of the beam and the co-ordinate system used in the analysis are illustrated in Fig. 1.

Mathematical Analysis

Core Equilibrium Equations. A differential element of the deformed core is shown in Fig. 2. Summation of forces in the x and z-directions, respectively, yields the two equilibrium equations

$$\frac{\partial \tau_{xz}}{\partial z} = 0 \tag{1}$$

and

$$\frac{\partial \sigma_z}{\partial z} + \frac{\partial \tau_{xz}}{\partial x} = \delta \frac{\partial^2 w_c}{\partial t^2} \tag{2}$$

where δ is the mass density per unit volume of the core. Consistent with the assumption that the core modulus E_c is infinite, τ_{xz} and w_c can be expressed as follows:

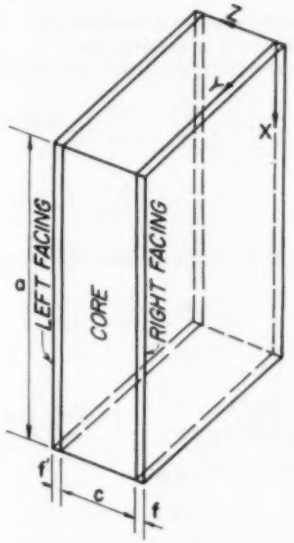

Fig. 1 Sandwich strip

[1] The results presented in this paper were obtained in the course of research conducted under National Science Foundation Grant NSF-G-9699.

Presented at the West Coast Conference of the Applied Mechanics Division, Seattle, Wash., August 28–30, 1961, of THE AMERICAN SOCIETY OF MECHANICAL ENGINEERS.

Discussion of this paper should be addressed to the Editorial Department, ASME, United Engineering Center, 345 East 47th Street, New York 17, N. Y., and will be accepted until October 10, 1961. Discussion received after the closing date will be returned. Manuscript received by ASME Applied Mechanics Division, September 6, 1960. Paper No. 61—APMW-2.

Nomenclature

x, y, z = rectangular co-ordinates
t = time co-ordinate, sec
a = length of sandwich beam, in.
c = thickness of core, in.
f, f' = thickness of right and left facings, respectively, in.
E = modulus of elasticity of facings, psi
ν = Poisson's ratio of facings
E_c = modulus of elasticity of core, psi
G_{xz} = modulus of rigidity of core in xz-plane, psi
u_c, w_c = displacement of core in x and z-directions, respectively, in.
w = displacement in z-direction of any point in sandwich, in.
$\epsilon_{zc}, \gamma_{xzc}$ = normal and shear strains, respectively, in core
$\epsilon_{xM}, \epsilon_{xM'}$ = membrane strains in right and left facings, respectively

(Continued on next page)

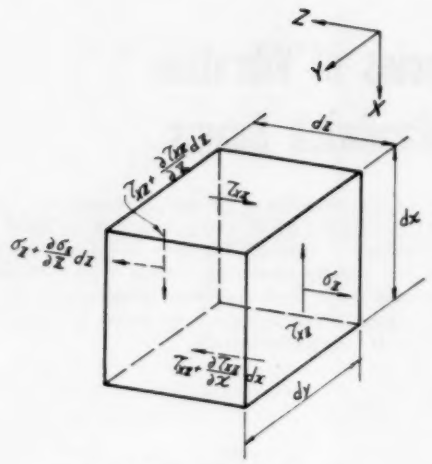

Fig. 2 Differential element of core

$$\tau_{xz} = \sum_{m=1,2,3}^{\infty} A_m \sin \frac{m\pi x}{a} \sin \omega t \tag{3}$$

and

$$w_c = \left[\frac{C_0}{2} + \sum_{m=1,2,3}^{\infty} C_m \cos \frac{m\pi x}{a} \right] \sin \omega t \tag{4}$$

where equation (4) satisfies the boundary conditions on the slope at the two ends but not on the deflection.

Substitution of equations (3) and (4) into equation (2) gives

$$\sigma_z = \left\{ \left[-\frac{\delta}{2} \omega^2 C_0 - \sum_{m=1,2,3}^{\infty} \left(\frac{m\pi}{a} A_m + \delta \omega^2 C_m \right) \right] z + \sum_{m=0,1,2}^{\infty} B_m \right\} \cos \frac{m\pi x}{a} \sin \omega t \tag{5}$$

Substitution of equations (3) and (4) into the equation

$$\tau_{xz} = G_{xz} \left(\frac{\partial u_c}{\partial z} + \frac{\partial w_c}{\partial x} \right) \tag{6}$$

gives

$$u_c = \sum_{m=1,2,3}^{\infty} \left[\left(\frac{A_m}{G_{xz}} + \frac{m\pi}{a} C_m \right) z + F_m \right] \sin \frac{m\pi x}{a} \sin \omega t \tag{7}$$

The boundary conditions are

$$w(0, t) = 0 \tag{8}$$

$$w(a, t) = 0 \tag{8a}$$

$$\frac{\partial w}{\partial x}(0, t) = 0 \tag{9}$$

$$\frac{\partial w}{\partial x}(a, t) = 0 \tag{9a}$$

Equation (4) satisfies equations (9) and (9a) but does not satisfy equations (8) and (8a); therefore the constraint conditions are

$$\frac{C_0}{2} + \sum_{m=1,2,3}^{\infty} C_m = 0 \tag{10}$$

and

$$\frac{C_0}{2} + \sum_{m=1,2,3}^{\infty} (-1)^m C_m = 0 \tag{11}$$

For $m = 0, 2, 4, 6, \ldots$ or $m = 1, 3, 5, \ldots$, equation (11) is equivalent to equation (10). Therefore only one constraint condition needs to be considered, say equation (10), if the even and odd terms are treated separately.

Strain Energy in the Core. Equations (4) and (7) permit the core strains to be expressed as

$$\epsilon_{zc} = \frac{\partial w_c}{\partial z} = 0 \tag{12}$$

and

$$\gamma_{xzc} = \frac{\partial u_c}{\partial z} + \frac{\partial w_c}{\partial x} = \sum_{m=1}^{\infty} \frac{A_m}{G_{xz}} \sin \frac{m\pi x}{a} \sin \omega t \tag{13}$$

The elastic strain energy of the core can then be expressed as

$$V_c = \frac{1}{2} \int_0^a \int_0^c G_{xz} \gamma_{xzc}^2 \, dx \, dz \tag{14}$$

Substitution of equation (13) into equation (14) and integration gives

$$V_c = \frac{ac}{4G_{xz}} \sum_{m=1}^{\infty} A_m^2 \sin^2 \omega t \tag{15}$$

Elastic Strain Energy in Facings Associated With Membrane Strains in Facings. The membrane strain in the right facing, ϵ_{zM}, can be expressed in terms of the core displacements as

$$\epsilon_{zM} = \left(\frac{\partial u_c}{\partial x} + \frac{f}{2} \frac{\partial^2 w_c}{\partial x^2} \right)_{z=0} \tag{16}$$

Substitutions of equations (4) and (7) into equation (16) give

$$\epsilon_{zM} = \sum_{m=1}^{\infty} \left[\frac{-f}{2} \frac{m^2 \pi^2}{a^2} C_m + \frac{m\pi}{a} F_m \right] \cos \frac{m\pi x}{a} \sin \omega t \tag{17}$$

Nomenclature

$\epsilon_{zB}, \epsilon_{zB}'$ = bending strains in right and left facings, respectively

σ_z, τ_{xz} = normal and shear stresses in core, respectively, psi

V_c = elastic energy per unit width of core, lb

V_{MF}, V_{MF}' = elastic energy per unit width associated with membrane strains in right and left facings, respectively, lb

V = total elastic energy per unit width of panel, lb

T = kinetic energy per unit width of panel, lb

δ = mass density of core per unit volume, lb sec^2/in^4

ρ = mass density of composite beam per unit length and width, lb sec^2/in^3

ω = natural frequency of vibration of beam, radian/sec

m = positive integer

A_m, B_m, C_m, F_m = configuration parameters

λ = Lagrangian multiplier

The elastic strain energy, V_{MF}, associated with the membrane strain in the right facing can then be expressed as

$$V_{MF} = \frac{Eaf}{4(1-\nu^2)} \sum_{m=1}^{\infty} \left[\frac{-f}{2} \frac{m^2\pi^2}{a^2} C_m + \frac{m\pi}{a} F_m \right]^2 \sin^2 \omega t \quad (18)$$

In like manner, the strain energy, V'_{MF}, associated with the membrane strain in the left facing can be expressed as

$$V'_{MF} = \frac{Eaf'}{4(1-\nu^2)} \sum_{m=1}^{\infty} \left[\frac{A_m}{G_{xz}} \frac{m\pi c}{a} + \frac{m^2\pi^2}{a^2} \left(c + \frac{f'}{2} \right) C_m + \frac{m\pi}{a} F_m \right]^2 \sin^2 \omega t \quad (19)$$

Elastic Strain Energy of Facings Associated With Bending of Facings About Their Own Middle Surfaces. The bending strain, ϵ_{xB}, in the right facing can be expressed in terms of the core displacement as

$$\epsilon_{xB} = \left(z + \frac{f}{2} \right) \left(\frac{\partial^2 w_c}{\partial x^2} \right)_{z=0} \quad (20)$$

Substitution of equation (4) into equation (20) yields

$$\epsilon_{xB} = -\left(z + \frac{f}{2} \right) \sum_{m=1}^{\infty} \frac{m^2\pi^2}{a^2} C_m \cos \frac{m\pi x}{a} \sin \omega t \quad (21)$$

The elastic strain energy, V_{BF}, associated with the strain caused by bending of the right facing about its middle surface can be written as

$$V_{BF} = \frac{Eaf^3}{48(1-\nu^2)} \sum_{m=1}^{\infty} \frac{m^4\pi^4}{a^4} C_m^2 \sin^2 \omega t \quad (22)$$

In like manner, the elastic strain energy, V'_{BF}, associated with the strain caused by bending of the left facing about its middle surface can be expressed as

$$V'_{BF} = \frac{Ea(f')^3}{48(1-\nu^2)} \sum_{m=1}^{\infty} \frac{m^4\pi^4}{a^4} C_m^2 \sin^2 \omega t \quad (23)$$

Total Elastic Strain Energy. Summing equations (15), (18), (19), (22), and (23) gives the total elastic strain energy

$$V = \sum_{m=1}^{\infty} \left\{ \frac{ac}{4G_{xz}} A_m^2 + \frac{Eaf}{4(1-\nu^2)} \left(\frac{-f}{2} \frac{m^2\pi^2}{a^2} C_m + \frac{m\pi}{a} F_m \right)^2 + \frac{Eaf'}{4(1-\nu^2)} \left[\frac{A_m}{G_{xz}} \frac{m\pi c}{a} + \frac{m^2\pi^2}{a^2} \left(c + \frac{f'}{2} \right) C_m + \frac{m\pi}{a} F_m \right]^2 + \frac{Ea[f^3 + (f')^3]}{48(1-\nu^2)} \frac{m^4\pi^4}{a^4} C_m^2 \right\} \sin^2 \omega t \quad (24)$$

Kinetic Energy of Vibrating Beam. An expression for the kinetic energy, T, of the vibrating beam with infinite E_c can be written as

$$T = \frac{1}{2} \rho \int_0^a \left(\frac{\partial w}{\partial t} \right)^2 dx \quad (25)$$

where w refers to the displacement of any element of the entire sandwich beam whose location is defined by the co-ordinate x; i.e., $w = w_c$.

The relation expressed in equation (4) permits equation (25) to be written as

$$T = \frac{\rho\omega^2 a}{4} \left[\frac{C_0^2}{2} + \sum_{m=1}^{\infty} C_m^2 \right] \cos^2 \omega t \quad (26)$$

Frequency Equations. The vibrating system is assumed to be conservative so that the expressions

$$\mathcal{O} = \left[V_{max} - T_{max} + \lambda \left(\frac{C_0}{2} + \sum_{m=2,4,6}^{\infty} C_m \right) \right] \quad (27)$$

and

$$\mathcal{O} = \left[V_{max} - T_{max} + \lambda \sum_{m=1,3,5}^{\infty} C_m \right] \quad (28)$$

must be made stationary. This requirement leads to the following set of equations:

$$C_0 = \frac{2\lambda}{\rho a \omega^2} \quad (29)$$

$$\frac{ac}{2G_{xz}} A_m + \frac{m\pi c}{a} \frac{Eaf'}{2G_{xz}(1-\nu^2)} \left[\frac{m\pi c}{a} \frac{A_m}{G_{xz}} + \frac{m^2\pi^2}{a^2} \left(c + \frac{f'}{2} \right) C_m + \frac{m\pi}{a} F_m \right] = 0 \quad (30)$$

$$-\frac{m^2\pi^2}{a^2} \frac{Eaf^2}{4(1-\nu^2)} \left(\frac{m\pi}{a} F_m - \frac{f}{2} \frac{m^2\pi^2}{a^2} C_m \right) + \frac{m^2\pi^2}{a^2} \left(c + \frac{f'}{2} \right) \frac{Eaf'}{2(1-\nu^2)} \left[\frac{m\pi c}{a} \frac{A_m}{G_{xz}} + \frac{m^2\pi^2}{a^2} \left(c + \frac{f'}{2} \right) C_m + \frac{m\pi}{a} F_m \right] + \frac{m^4\pi^4}{a^4} \frac{Ea[f^3 + (f')^3]}{24(1-\nu^2)} C_m - \frac{\rho\omega^2 a}{2} C_m = -\lambda \quad (31)$$

$$\frac{m\pi}{a} \frac{Eaf}{2(1-\nu^2)} \left(\frac{m\pi}{a} F_m - \frac{f}{2} \frac{m^2\pi^2}{a^2} C_m \right) + \frac{m\pi}{a} \frac{Eaf'}{2(1-\nu^2)} \left[\frac{m\pi c}{a} \frac{A_m}{G_{xz}} + \frac{m^2\pi^2}{a^2} \left(c + \frac{f'}{2} \right) C_m + \frac{m\pi}{a} F_m \right] = 0 \quad (32)$$

Simultaneous solution of equations (30), (31), and (32) gives

$$C_m = \frac{-2\lambda}{\rho a \left[\frac{m^4\pi^4 E}{a^4(1-\nu^2)\rho} \left(\frac{I_T}{1 + m^2 S} + I_F \right) - \omega^2 \right]} \quad (33)$$

where $m \geq 1$, and

$$I_T = \frac{ff'}{f+f'} \left(c + \frac{f+f'}{2} \right)^2,$$

$$I_F = \frac{f^3 + (f')^3}{12},$$

and

$$S = \frac{\pi^2 cff'}{a^2(f+f')} \frac{E}{G_{xz}(1-\nu^2)}$$

Substitutions of equations (29) and (33) into equation (10) give the following frequency equations:

$$\sum_{m=1,3,5}^{\infty} \frac{1}{\left[\frac{m^4\pi^4 E}{a^4(1-\nu^2)\rho} \left(\frac{I_T}{1 + m^2 S} + I_F \right) - \omega^2 \right]} = 0 \quad (34)$$

and

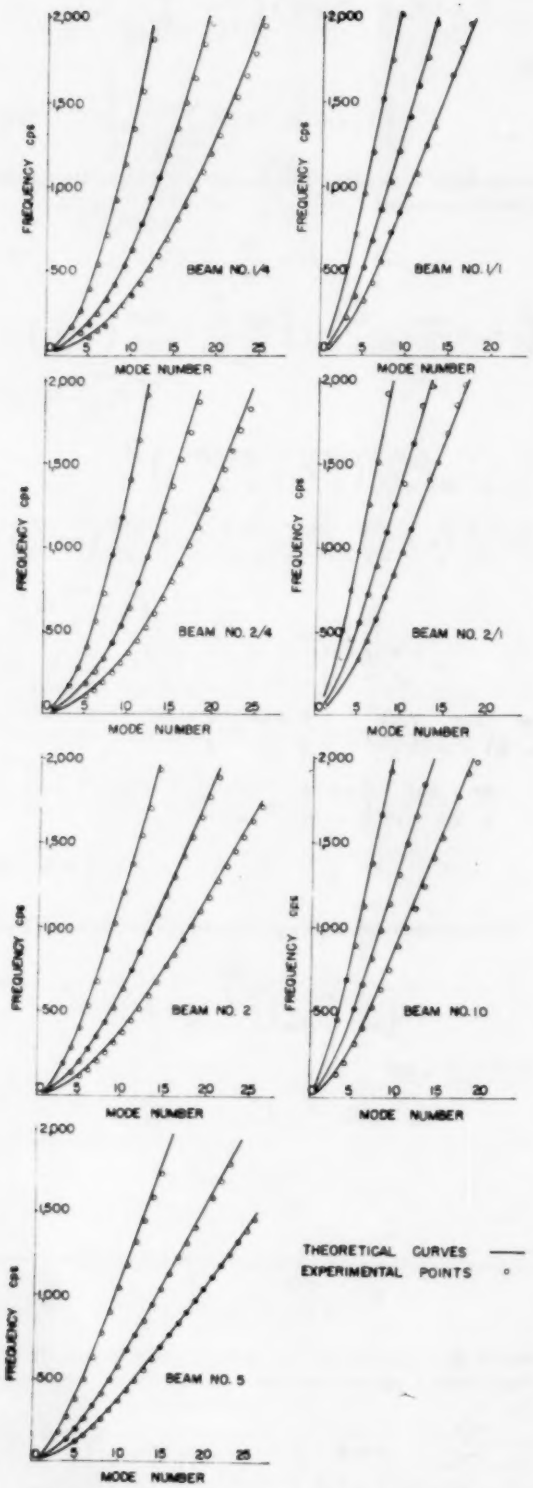

Fig. 3 Comparison of theoretical and experimental results

$$\frac{-1}{2\omega^2} + \sum_{m=2,4,6}^{\infty} \frac{1}{\left[\dfrac{m^4\pi^4 E}{a^4(1-\nu^2)\rho}\left(\dfrac{I_T}{1+m^2S}+I_F\right)-\omega^2\right]} = 0 \tag{35}$$

Equation (34) gives the frequencies for the even modes whereas equation (35) gives the frequencies for the odd modes, since the odd terms in equation (4) represent the antisymmetrical curves and the even terms in equation (4) represent the symmetrical curves. For example, if only two terms are considered in equation (35), an approximate value for the frequency of the first mode of vibration is obtained. If three terms are considered, a better approximation for the first mode and an approximate value for the third mode are obtained. Since the series involved in equations (34) and (35) are rapidly convergent, good accuracy can be obtained with a number of terms only slightly greater than the number of frequency values desired. It is estimated that if three terms in equation (35) are used, the value obtained for the fundamental frequency will be accurate to within one and one half per cent. This estimation was obtained from a comparison with values based on twenty-six terms of equation (35).

If the parameter S in equations (34) and (35) is set equal to zero, i.e., the effect of shear in the core is neglected, these equations then represent the solution to the problem of the free transverse vibrations of a homogeneous fixed-ended beam in which the effect of transverse shear and rotatory inertia is neglected.

Theoretical and Experimental Results

Natural frequencies of vibration were determined experimentally for seven sandwich beams having different combinations of thickness and physical properties of the core material. Three different lengths of each of the seven sandwich beams were tested to obtain some idea as to the effectiveness of the method of determining end fixity. The span lengths used were 8, 6, and 4 ft. The pertinent dimensions and physical constants are shown in Table 1.

Theoretical results based on equations (34) and (35) for the twenty-one beams described in Table 1 were determined with the use of a digital computer. In each case, the number of terms used in the series was twice as great as the number of values of the frequency that were recorded. It was felt that this was more than adequate to insure the required accuracy. Curves based on the numerical results are shown in Fig. 3.

Analysis of the results show that the agreement between theory and experiment is very good; most of the values agree to within 5 per cent. The fact that the experimental values are consistently lower than the theoretical values is accounted for primarily by the fact that ideal fixed ends can never be exactly achieved experimentally, and lack of complete fixity results in lower frequencies. Also, the theoretical values may be slightly high since only a finite number of terms is considered in computing these values; in this solution the answers approach the theoretically exact answers from the high side as more and more terms are taken. The experimental points on the curves indicate the modes for which the experimental values were determined. In most cases the percentage error between experimental and theoretical values is greatest at the lower modes. The experimental determination of the frequencies corresponding to the first four to five modes of vibration was found to be extremely difficult if not impossible with the equipment available. This is attributed to the fact that the vibration exciter was not capable of generating a forcing function of the proper magnitude and frequency. No attempt was made to modify the equipment to enable the more accurate measurement of the modes having frequencies lower than 100 cps since the effect of the shear in the core is negligible

Table 1 Description of test specimens

Beam No.	Material: Facings	Material: Core	a, in.	c, in.	$f(=f')$, in.	ν	E, 10^6 psi	G_{xz}, 10^3 psi	ρ, 10^{-5} lb sec^2/in^3
2	Al	Paper	96 72 48	0.250	0.016	0.33	10.0	10.0	1.0837
5	Al	Paper	96 72 48	0.250	0.016	0.33	10.0	5.7	1.02081
10	Al	Paper	96 72 48	1.000	0.016	0.33	10.0	7.5	1.5384
1/4	Al	Al	96 72 48	0.250	0.016	0.33	10.6	58.0	1.59233
1/1	Al	Al	96 72 48	1.000	0.016	0.33	10.6	8.0	1.4018
2/4	Al	Al	96 72 48	0.250	0.016	0.33	10.6	58.0	1.51685
2/1	Al	Al	96 72 48	1.000	0.016	0.33	10.6	8.0	1.38745

in this region. It is evident that the well-established homogeneous beam solution is applicable here.

Conclusions

On the basis of the theoretical and experimental results shown in this paper, it is concluded that the theoretical analysis is sufficiently rigorous to predict quite accurately the frequencies of vibration of fixed-ended sandwich beams. For the range of frequencies considered, the assumptions that E_c is infinite and that the effect of rotatory inertia is negligible appear to be justified. Undoubtedly, as higher frequencies are considered, a more accurate analysis would ultimately be found necessary.

It is reasonable to expect that analogous solutions involving sandwich plates having various combinations of fixed and simply supported boundaries can be obtained using the procedure outlined in this paper.

Bibliography

1 M. E. Raville and W. R. Kimel, "On Small Deflection for Sandwich Construction," Kansas State College Bulletin, Manhattan, Kan., Special Report No. 2, January, 1959.

2 W. R. Kimel, M. E. Raville, P. G. Kirmser, and M. P. Patel, "Natural Frequencies of Vibration of Simply Supported Sandwich Beams," *Proceedings of The Midwestern Conference on Solid and Fluid Mechanics*, Austin, Tex., September 9–11, 1959.

3 M. E. Raville and E. S. Ueng, "The Lagrangian Multiplier Method in Eigenvalue Problems," Kansas State University Bulletin, Manhattan, Kan., Special Report No. 5, 1960.

4 B. Budiansky and P. C. Hu, "The Lagrangian Multiplier Method of Finding Upper and Lower Limits to Critical Stresses of Clamped Plates," NACA Report No. 848, 1946.

5 G. A. Thurston, "Bending and Buckling of Clamped Sandwich Plates," *Journal of the Aeronautical Sciences*, vol. 24, 1957, pp. 407–412.

6 M. P. Patel, "Natural Frequencies of Vibration of Sandwich Panels," Master's thesis presented to the Department of Applied Mechanics, Kansas State University, 1959.

7 E. Reissner, "Buckling of Plates With Intermediate Rigid Supports," *Journal of the Aeronautical Sciences*, vol. 12, 1945, p. 375.

Combined Stresses in an Orthotropic Plate Having a Finite Crack[1]

D. D. ANG
Lecturer, University of Saigon, Saigon, Viet-Nam.
Formerly, California Institute of Technology, Pasadena, Calif.

M. L. WILLIAMS
Professor of Aeronautics, Guggenheim Aeronautical Laboratory, California Institute of Technology, Pasadena, Calif.

Using a formulation in integral equations, a solution for the combined extension-classical bending stress and displacement solution is presented for the case of an infinite orthotropic flat plate containing a finite crack. While the solution can be expressed in closed form for the entire field, primary emphasis is placed upon the stresses near the crack point. Qualitatively, no major difference in behavior due to orthotropy was found although certain quantitative features are noted, mainly as a function of the characteristic rigidity ratio $(E_x/E_y)^{1/2}$. The inverse square-root character of the isotropic stress bending and extension is not changed by orthotropy, although amplitudes and distribution are affected. Account is taken of recent important work by Knowles and Wang dealing with Reissner bending of the plate which shows that the extensional and surface bending stresses are identical in singular character and circumferential distribution. A bending-extension interaction curve for fracture initiation is derived and shown to be linear when based upon the more exact bending theory.

Introduction

One of the classes of problems which has continually attracted the attention of investigators in the field of solid mechanics, and more particularly in the analysis of fracture, is that related to the stress and displacement distribution around stationary finite and infinite cracks in assumed continuous media [1–7].[2] Notwithstanding such interest, there are few solutions available in relatively simple closed form. One of the purposes of this paper, therefore, is to report a rather straightforward method of solution employing integral equations which, inasmuch as little additional complication is introduced by considering orthotropy, contains the isotropic medium situation as a special case. Furthermore, as the orthotropic field equations for stretching and bending of a thin plate are essentially the same within the usual plane stress and Kirchhoff assumptions, both loadings will be discussed. Another objective is to provide some fundamental information relating to stress distributions under biaxial stressing and combined loadings.

Extensional Analysis

Beginning with the usual plane stress assumptions, $\sigma_{zz} = \tau_{xz} = \tau_{yz} = 0$, write the stress-strain relations as

$$\epsilon_x = \frac{1}{E_x}\sigma_x - \frac{\nu_x}{E_x}\sigma_y \tag{1}$$

$$\epsilon_y = -\frac{\nu_y}{E_y}\sigma_x + \frac{1}{E_y}\sigma_y \tag{2}$$

$$\gamma_{xy} = \frac{1}{G_{xy}}\tau_{xy} \tag{3}$$

where because of the symmetry of the stress-strain matrix,

$$\nu_x/E_x = \nu_y/E_y \tag{4}$$

As the equations of equilibrium are independent of the mechanical properties, a stress function $\chi(x, y)$ can be chosen in the usual fashion as

$$\sigma_x = \chi_{yy};\ \sigma_y = \chi_{xx};\ \tau_{xy} = -\chi_{xy} \tag{5}$$

along with the compatibility relation

$$\frac{\partial^2\epsilon_y}{\partial x^2} + \frac{\partial^2\epsilon_x}{\partial y^2} = \frac{\partial^2\gamma_{xy}}{\partial x\partial y} \tag{6}$$

to yield upon combining (1)–(6)

$$\chi_{xxxx} + 2A\chi_{xxyy} + B\chi_{yyyy} = 0 \tag{7}$$

where the orthotropic plate constants

$$A \equiv \frac{E_y}{2G_{xy}} - \nu_y;\quad B \equiv \frac{E_y}{E_x} = \frac{\nu_y}{\nu_x} \tag{8}$$

have been defined.

Let now the field equation (7) be factored as

$$\left(\frac{\partial^2}{\partial x^2} + \frac{1}{K_1^2}\frac{\partial^2}{\partial y^2}\right)\left(\frac{\partial^2}{\partial x^2} + \frac{1}{K_2^2}\frac{\partial^2}{\partial y^2}\right)\chi = 0 \tag{9}$$

where

$$K_1^2 \equiv [A + (A^2 - B)^{1/2}]/B;\ K_2^2 = [A - (A^2 - B)^{1/2}]/B \tag{10}$$

Thus a solution is

$$\chi(x, y) = \chi_1(x, y) + \chi_2(x, y) \tag{11}$$

where

$$\left(\frac{\partial^2}{\partial x^2} + \frac{1}{K_i^2}\frac{\partial^2}{\partial y^2}\right)\chi_i(x, y) = 0;\quad i = 1, 2 \tag{12}$$

Consider now a geometry such that there exists a finite crack along the x-axis ($y = 0$), between $-b \leqslant x \leqslant b$, and where the mechanical properties E_x, E_y, and so on, are alined with respect

---

[1] This research was supported in whole or in part by the United States Air Force under Contract No. AF33(616)-5740, monitored by the Aeronautical Research Laboratory, Wright Air Development Division.

[2] Numbers in brackets designate References at end of paper.

Presented at the Summer Conference of the Applied Mechanics Division, Chicago, Ill., June 14–16, 1961, of The American Society of Mechanical Engineers.

Discussion of this paper should be addressed to the Editorial Department, ASME, United Engineering Center, 345 East 47th Street, New York 17, N. Y., and will be accepted until October 10, 1961. Discussion received after the closing date will be returned. Manuscript received by ASME Applied Mechanics Division, April 19, 1960. Paper No. 61—APM-19.

to the (x, y)-co-ordinate system. Require that the normal and shear stresses at infinity be constant; viz.,

$$\sigma_x = \bar{\sigma}_x, \quad \tau_{xy} = \bar{\tau}_{xy} \quad \text{at} \quad |x| \to \infty$$

and

$$\sigma_y = \bar{\sigma}_y, \quad \tau_{xy} = \bar{\tau}_{xy} \text{ at } |y| \to \infty$$

Let the desired stress system be composed of two parts, one the uniform stress field and the other a perturbation field, $\sigma_{ij}^{(c)}$, due to the crack which dies out at infinity. Inasmuch as the boundary conditions along the free edges of the crack $|x| < b$ require $\sigma_y = \tau_{xy} = 0$, it is possible to formulate the problem as one of finding solutions for the perturbation solution satisfying the field equations (12), and boundary conditions

$$\sigma_y^{(c)}(x, 0) = -\bar{\sigma}_y \quad |x| < b \tag{13}$$

$$\tau_{xy}^{(c)}(x, 0) = -\bar{\tau}_{xy} \quad |x| < b \tag{14}$$

$$\tau_{ij}^{(c)}(x, y) \to 0 \quad \text{as} \quad |x^2 + y^2|^{1/2} \to \infty \tag{15}$$

In the sequel, the superscript will be suppressed since no confusion is likely to occur.

The required solution will now be constructed in two parts, one for $y > 0$ and the other for $y < 0$; subsequently, they will be matched to insure continuity of the solution and its derivatives for $|x| \geq b$, $y = 0$.

Symmetrical Solution. First, the symmetrical part of the solution will be constructed, namely, that part for which the stress function is even in x and y. In this fashion, that part of the perturbation solution satisfying (13) and (15) will be found, for which $\tau_{xy}^{(c)}(x, 0) = 0$ for $|x| < b$.

Let such a solution be represented as

$$\chi(x, y) = \sum_{i=1}^{2} \int_0^\infty G_i(t) \cos tx \, e^{-K_i t|y|} dt \tag{16}$$

where $G_i(t)$ is the unknown function to be determined. Continuity conditions require that at $y = 0$, $|x| \geq b$, $\partial\chi^+/\partial y^n - \partial\chi^-/\partial y^n = 0$, $n = 0, 1, 2, 3$ where the $(+)$ and $(-)$ superscripts refer to the limits obtained by approaching the x-axis from above and from below, respectively. The condition will be automatically met for $n = 0, 2$, but for $n = 1$ and $n = 3$, respectively, find in carrying through the calculations in detail for $n = 1$

$$\frac{\partial\chi(x, y^+)}{\partial y} = \sum_{i=1}^{2} \int_0^\infty (-K_i t) G_i(t) \cos tx \, e^{-K_i t y} dt \tag{17}$$

$$\frac{\partial\chi(x, y^-)}{\partial y} = \sum_{i=1}^{2} \int_0^\infty (K_i t) G_i(t) \cos tx \, e^{K_i t y} dt \tag{18}$$

so that

$$\frac{\partial\chi^+}{\partial y} - \frac{\partial\chi^-}{\partial y} = \sum_{i=1}^{2} \int_0^\infty [-2K_i t G_i(t)] \cos tx \, dt = 0; \quad |x| \geq b \tag{19}$$

or

$$\int_0^\infty t[K_1 G_1(t) + K_2 G_2(t)] \cos tx \, dt = 0; \quad |x| \geq b \tag{20}$$

In a similar fashion, it is found for $n = 3$ that

$$\int_0^\infty t^3[K_1^3 G_1(t) + K_2^3 G_2(t)] \cos tx \, dt = 0; \quad |x| \geq b \tag{21}$$

Turning now to a consideration of the boundary conditions, for $|x| < b$, there results

$$\frac{\partial^2\chi(x, 0)}{\partial x^2} = \int_0^\infty -t^2[G_1(t) + G_2(t)] \cos tx \, dt = -\bar{\sigma}_y; \quad |x| < b \tag{22}$$

$$-\frac{\partial^2\chi(x, 0)}{\partial x \partial y} = \int_0^\infty t^2[K_1 G_1(t) + K_2 G_2(t)] \sin tx \, dt = 0; \quad |x| < b \tag{23}$$

The solution depends now upon finding $G_i(t)$ such that (20–23) are satisfied.

Suppose therefore that

$$K_1 G_1(t) = -K_2 G_2(t) \tag{24}$$

so that (20) and (23) are satisfied identically. With this substitution in (21) and (22) find

$$K_1(K_1^2 - K_2^2) \int_0^\infty t^3 G_1(t) \cos tx \, dt = 0; \quad |x| \geq b \tag{25}$$

$$[1 - (K_1/K_2)] \int_0^\infty t^2 G_1(t) \cos tx \, dt = \bar{\sigma}_y \quad |x| < b \tag{26}$$

In order to simplify the integral equations, it is noted that (25) may be replaced by the integrated condition

$$-K_1(K_1^3 - K_2^3) \int_0^\infty t G_1(t) \cos tx \, dt = 0; \quad |x| \geq b \tag{25a}$$

because the constants of integration represent rigid-body motions at most. Thus the dual integral equations become, upon introducing the notation $G(t) \equiv tG_1(t)$

$$\int_0^\infty G(t) \cos tx \, dt = 0; \quad |x| \geq b \tag{27}$$

$$\int_0^\infty tG(t) \cos tx \, dt = \frac{\bar{\sigma}_y}{1 - (K_1/K_2)}; \quad |x| < b \tag{28}$$

These equations, which incidentally occur also in Yoffe's work [8], can be solved most conveniently and directly using the Sonine integrals [9]. Thus

$$G(t) = \frac{b\bar{\sigma}_y}{1 - \dfrac{K_1}{K_2}} \cdot \frac{J_1(bt)}{t} \tag{29}$$

or

$$G_1(t) = \frac{b\bar{\sigma}_y}{1 - \dfrac{K_1}{K_2}} \cdot \frac{J_1(bt)}{t^2} \tag{30}$$

$$G_2(t) = \frac{b\bar{\sigma}_y}{1 - \dfrac{K_2}{K_1}} \cdot \frac{J_1(bt)}{t^2} \tag{31}$$

Therefore the symmetrical perturbation stress function $\chi^{(c)}(x, y)$ is determined as

$$\chi^{(c)}(x, y^+) = \frac{b\bar{\sigma}_y}{K_2 - K_1} \int_0^\infty \frac{J_1(bt)}{t^2} [K_2 e^{-K_1 t y} - K_1 e^{-K_2 t y}] \cos tx \, dt; \quad y > 0 \tag{32}$$

$$\chi^{(c)}(x, y^-) = \frac{b\bar{\sigma}_y}{K_2 - K_1} \int_0^\infty \frac{J_1(bt)}{t^2} [K_2 e^{K_1 t y} - K_1 e^{K_2 t y}] \cos tx \, dt; \quad y < 0 \tag{33}$$

leading to the same solution given by Sawin [4].

It remains to investigate the solution for the isotropic situation $K_1 = K_2 = 1$. This can be achieved by a limiting process

$$\chi^{(a)}(x, y^+) = \lim_{K_i \to 1} b\bar{\sigma}_y \int_0^\infty \frac{J_1(bt)e^{-K_1 t y}}{t^2} \left[\frac{1 - \frac{K_1}{K_2} e^{-K_2 t y[1-(K_1/K_2)]}}{1 - \frac{K_1}{K_2}} \right] \cos tx \, dt \quad (34)$$

$$= b\bar{\sigma}_y \int_0^\infty (1 + ty)t^{-2} J_1(bt) e^{-ty} \cos tx \, dt$$

One incidental matter should also be noted: the integral is not convergent at the lower limit $t = 0$. It is therefore necessary to interpret it symbolically as the integral with respect to y (say) of a convergent integral. The displacements which are derivatives of χ give no difficulty.

Antisymmetrical Solution. In a similar manner, the companion antisymmetrical solution can be constructed where $\chi(x, y)$ is odd in both x and y. Let

$$\chi(x, y)^s = \mp \sum_{i=1}^{2} \int_0^\infty G_i(t) \sin tx \, e^{-K_i t|y|} dt \quad (35)$$

where the $(\pm)$ signs refer to the upper and lower half planes, respectively. Here the continuity conditions along $|x| \geq b$, $y = 0$ are automatically satisfied for the first and third derivatives in y, with the zero and second derivatives leading, respectively, to the requirements that

$$\int_0^\infty [G_1(t) + G_2(t)] \sin tx \, dt = 0; \quad |x| \geq b \quad (36)$$

$$\int_0^\infty t^2[K_1^2 G_1(t) + K_2^2 G_2(t)] \sin tx \, dt = 0; \quad |x| \geq b \quad (37)$$

The antisymmetrical conditions along the crack, namely, $\sigma_y(x, 0) = 0$, $\tau_{xy}(x, 0) = -\bar{\tau}_{xy}$ lead to

$$\frac{\partial^2 \chi(x, 0)}{\partial x^2} = -\int_0^\infty t^2[G_1(t) + G_2(t)] \sin tx \, dt = 0; \quad |x| < b \quad (38)$$

$$-\frac{\partial^2 \chi(x, 0)}{\partial x \partial y} = -\int_0^\infty t^2[K_1 G_1(t) + K_2 G_2(t)] \cos tx \, dt = -\bar{\tau}_{xy}; \quad |x| < b \quad (39)$$

Taking

$$G_1(t) = -G_2(t) \quad (40)$$

which satisfies (36) and (38), and inserting this relation in (37) and (39) gives

$$(K_1^2 - K_2^2) \int_0^\infty t^2 G_1(t) \sin tx \, dt = 0; \quad |x| \geq b \quad (41)$$

$$(K_1 - K_2) \int_0^\infty t^2 G_1(t) \cos tx \, dt = \bar{\tau}_{xy} \quad |x| < b \quad (42)$$

But integrating (41) with respect to x and setting the rigid-body displacements equal to zero, and again using $G(t) \equiv tG_1(t)$ gives the integral equations

$$\int_0^\infty G(t) \cos tx \, dt = 0; \quad |x| \geq b \quad (43)$$

$$\int_0^\infty tG(t) \cos tx \, dt = \frac{\bar{\tau}_{xy}}{K_1 - K_2}; \quad |x| < b \quad (44)$$

whose solution as in (29) is

$$G(t) = tG_1(t) = -tG_2(t) = \frac{b\bar{\tau}_{xy}}{K_1 - K_2} \cdot \frac{J_1(bt)}{t} \quad (45)$$

The antisymmetric stress function is then

$$\chi^{(s)}(x, y^+) = \mp \frac{b\bar{\tau}_{xy}}{K_1 - K_2} \int_0^\infty \frac{J_1(bt)}{t^2} [e^{-K_1 t|y|} - e^{-K_2 t|y|}] \sin tx \, dt \quad (46)$$

where it easily checked that for the isotropic media

$$\chi^{(s)}(x, y^+) = \mp b\bar{\tau}_{xy} \int_0^\infty (1 - ty)t^{-2} J_1(bt) e^{-t|y|} \sin tx \, dt \quad (47)$$

Combined Extensional Stress Field. Combining the symmetric and antisymmetric perturbation functions with the appropriate function for a uniform stress field at infinity, one has

$$\chi(x, y) = \chi^{(a)}(x, y) + \chi^{(s)}(x, y) + \bar{\sigma}_x y^2/2 + \bar{\sigma}_y x^2/2 - \bar{\tau}_{xy} xy \quad (48)$$

It develops that the stresses depend essentially upon integrals of the type [10].

$$J' \equiv \int_0^\infty J_1(bt) e^{-(Ky - ix)t} dt = b \left\{ \sqrt{(Ky - ix)^2 + b^2} \left[Ky - ix + \sqrt{(Ky - ix)^2 + b^2} \right] \right\}^{-1} \quad (49)$$

Particular values of interest are for $x = 0$, $y > 0$ where

$$J'(0, y^+) = b \left\{ \sqrt{b^2 + K^2 y^2} \left[Ky + \sqrt{b^2 + K^2 y^2} \right] \right\}^{-1} \quad (50)$$

For $y = 0$, $x \geq b$

$$J'[(x - b)^+, 0] = -b \left\{ \sqrt{x^2 - b^2} \left[x + \sqrt{x^2 - b^2} \right] \right\}^{-1} \quad (51)$$

and for $y = 0$, $x < b$

$$J'[(x - b)^-, 0] = \frac{1}{b} + i \frac{x/b}{\sqrt{b^2 - x^2}} \quad (52)$$

Summarizing these stresses, one has

$$\sigma_x(0, y^+) = \frac{\bar{\sigma}_y b^2 K_1 K_2}{K_2 - K_1} \left\{ \frac{K_1}{\sqrt{b^2 + K_1^2 y^2} \left[K_1 y + \sqrt{b^2 + K_1^2 y^2} \right]} - \frac{K_2}{\sqrt{b^2 + K_2^2 y^2} \left[K_2 y + \sqrt{b^2 + K_2^2 y^2} \right]} \right\} + \bar{\sigma}_x \quad (53)$$

$$\sigma_y(0, y^+) = \frac{\bar{\sigma}_y b^2}{K_1 - K_2} \left\{ \frac{K_2}{\sqrt{b^2 + K_1^2 y^2} \left[K_1 y + \sqrt{b^2 + K_1^2 y^2} \right]} - \frac{K_1}{\sqrt{b^2 + K_2^2 y^2} \left[K_2 y + \sqrt{b^2 + K_2^2 y^2} \right]} \right\} + \bar{\sigma}_y \quad (54)$$

$$\tau_{xy}(0, y^+) = \frac{\bar{\tau}_{xy} b^2}{K_2 - K_1} \left\{ \frac{K_1}{\sqrt{b^2 + K_1^2 y^2} \left[K_1 y + \sqrt{b^2 + K_1^2 y^2} \right]} - \frac{K_2}{\sqrt{b^2 + K_2^2 y^2} \left[K_2 y + \sqrt{b^2 + K_2^2 y^2} \right]} \right\} + \bar{\tau}_{xy} \quad (55)$$

$$\sigma_x(x^+, 0) = \bar{\sigma}_x - \bar{\sigma}_y(K_1 K_2) - (K_1 + K_2) \bar{\tau}_{xy} x (b^2 - x^2)^{-1/2}; \quad x < b \quad (56)$$

$$= \bar{\sigma}_x + K_1 K_2 \bar{\sigma}_y b^2 \left\{ \sqrt{x^2 - b^2} \left[x + \sqrt{x^2 - b^2} \right] \right\}^{-1}; \quad x \geq b \quad (56a)$$

$$\sigma_y(x^+, 0) = \bar{\sigma}_y \left[1 + \frac{b^2}{\sqrt{x^2 - b^2} \left[x + \sqrt{x^2 - b^2} \right]} \right]; \quad x > b \quad (57)$$

$$\tau_{xy}(x^+, 0) = \bar{\tau}_{xy}\left[1 + \frac{b^2}{\sqrt{x^2 - b^2}\,[x + \sqrt{x^2 - b^2}]}\right]; \quad x > b \tag{58}$$

The displacements, on the other hand, are found to depend upon the integral [10]

$$J \equiv \int_0^\infty \frac{J_1(bt)}{t} e^{-(Ky - ix)t}\, dt = \frac{b}{Ky - ix + \sqrt{(Ky - ix)^2 + b^2}} \tag{59}$$

Upon integrating the stresses, one finds

$$u(x, y) = \frac{1}{E_x}\left\{\frac{-b\bar{\tau}_{xy}}{K_2 - K_1}\int_0^\infty [K_1{}^2 e^{-K_1 ty} - K_2{}^2 e^{-K_2 ty} + \nu_x(e^{-K_1 ty} - e^{-K_2 ty})]t^{-1}J_1(bt)\cos tx\, dt + \frac{b\bar{\sigma}_y}{K_2 - K_1}\int_0^\infty [K_1K_2(K_1e^{-K_1 ty} - K_2e^{-K_2 ty}) + \nu_x(K_2e^{-K_1 ty} - K_1e^{-K_2 ty})]t^{-1}J_1(bt)\sin tx\, dt + (\bar{\sigma}_x - \nu_x\bar{\sigma}_y)x\right\} + \frac{\bar{\tau}_{xy}}{2G_{xy}}\, y \tag{60}$$

$$v(x, y) = \frac{1}{E_y}\left\{\frac{b\bar{\tau}_{xy}}{K_2 - K_1}\int_0^\infty [K_1{}^{-1}e^{-K_1 ty} - K_2{}^{-1}e^{-K_2 ty} + \nu_y(K_1e^{-K_1 ty} - K_2e^{-K_2 ty})]t^{-1}J_1(bt)\sin tx\, dt + \frac{b\bar{\sigma}_y}{K_2 - K_1}\int_0^\infty [(K_2/K_1)e^{-K_1 ty} - (K_1/K_2)e^{-K_2 ty} + \nu_yK_1K_2(e^{-K_1 ty} - e^{-K_2 ty})]t^{-1}J_1(bt)\cos tx\, dt + (\bar{\sigma}_y - \nu_y\bar{\sigma}_x)y\right\} + \frac{\bar{\tau}_{xy}}{2G_{xy}}\, x \tag{61}$$

Along the line of the crack, the appropriate integrals may be evaluated from (59) to find

$$u(x^+, 0) = \frac{1}{E_x}\left[\bar{\tau}_{xy}(K_1 + K_2)\sqrt{b^2 - x^2} + \bar{\sigma}_y(\nu_x - K_1K_2)x + (\bar{\sigma}_x - \nu_x\bar{\sigma}_y)x\right]; \quad x \leqslant b \tag{62}$$

$$= \frac{1}{E_x}\left[\frac{\bar{\sigma}_y(\nu_x - K_1K_2)b^2}{x + \sqrt{x^2 - b^2}} + (\bar{\sigma}_x - \nu_x\bar{\sigma}_y)x\right]; \quad x \geqslant b$$

$$v(x^+, 0) = \frac{1}{E_y}\left[(K_1{}^{-1}K_2{}^{-1} - \nu_y)\bar{\tau}_{xy}x + (K_1 + K_2)\bar{\sigma}_y\sqrt{b^2 - x^2}\right] + \frac{\bar{\tau}_{xy}x}{2G_{xy}}; \quad x \leqslant b \tag{63}$$

$$= \frac{1}{E_y}\left[\frac{1 - \nu_yK_1K_2}{K_1K_2}\frac{\bar{\tau}_{xy}b^2}{x + \sqrt{x^2 - b^2}}\right] + \frac{\bar{\tau}_{xy}x}{2G_{xy}}; \quad x \geqslant b$$

Bending Analysis

In the same manner as for the plate in extension, one may formulate the classical orthotropic-plate theory in terms of the governing differential equation

$$\frac{\partial^4 w}{\partial x^4} + 2\frac{H}{D_x}\frac{\partial^4 w}{\partial x^2\partial y^2} + \frac{D_y}{D_x}\frac{\partial^4 w}{\partial y^4} = \frac{q}{D_x} \tag{64}$$

where in analogy with (7), write

$$A \equiv \frac{H}{D_x} \equiv \frac{D_1 + 2D_{xy}}{D_x} = \frac{E'' + 2G_{xy}}{E_x{}'} = \frac{\nu_xE_y + 2(1 - \nu_x\nu_y)G_{xy}}{E_x} \tag{65}$$

$$B \equiv \frac{D_y}{D_x} = \frac{E_y{}'}{E_x{}'} = \left(\frac{E_x}{E_y}\right)^- \tag{66}$$

Here, following standard notation, the stress-strain law (1) has been used and

$$E_x{}' \equiv \frac{E_x}{1 - \nu_x\nu_y}; \quad E_y{}' \equiv \frac{E_y}{1 - \nu_x\nu_y}; \quad E'' \equiv \frac{\nu_yE_x}{1 - \nu_x\nu_y} = \frac{\nu_xE_y}{1 - \nu_x\nu_y} \tag{67}$$

$$D_x \equiv E_x{}'h^3/12; \quad D_y = E_y{}'h^3/12; \quad D_1 \equiv E''h^3/12; \quad D_{xy} = G_{xy}h^3/12 \tag{68}$$

The field equation can be factored as in (9), where one simply reads w instead of χ, and solutions such as (11) are now to be considered.

Assuming the same geometry as before, there are several boundary conditions which can be imposed at infinity. In analogy with the extension case, take specifically, however, the situation where the deflection (i.e., χ) is to be a quadratic function of the co-ordinates:

$$w_\infty = \frac{D_1\bar{M}_y - D_y\bar{M}_x}{D_xD_y - D_1{}^2}\cdot\frac{x^2}{2} + \frac{D_1\bar{M}_x - D_x\bar{M}_y}{D_xD_y - D_1{}^2}\cdot\frac{y^2}{2} + \frac{\bar{M}_{xy}}{D_{xy}}\cdot\frac{xy}{2} \tag{69}$$

such that $M_x = \bar{M}_x$, $M_y = \bar{M}_y$, $M_{xy} = \bar{M}_{xy}$ at infinity. Along the crack, the usual Kirchhoff boundary conditions

$$V_y = Q_y + \partial M_{yx}/\partial x = -D_y\partial^3 w/\partial y^3 - (D_1 + 4D_{xy})\partial^3 w/\partial x^2\partial y \tag{70}$$

$$M_y = -D_y\partial^2 w/\partial y^2 - D_1\partial^2 w/\partial x^2 \tag{71}$$

will be assumed to apply. For completeness, the remaining moments and shears will be written down

$$V_x = Q_x - \partial M_{xy}/\partial y = -D_x\partial^3 w/\partial x^3 - (D_1 + 4D_{xy})\partial^3 w/\partial x\partial y^2 \tag{72}$$

$$M_x = -D_x\partial^2 w/\partial x^2 - D_1\partial^2 w/\partial y^2 \tag{73}$$

$$M_{xy} = -M_{yx} = 2D_{xy}\,\partial^2 w/\partial x\partial y \tag{74}$$

One now proceeds to determine a deflection perturbation function $w^{(c)}(x, y)$ such that

$$M_y{}^{(c)}(x, 0) = -\bar{M}_y; \quad |x| < b \tag{75}$$

$$V_y{}^{(c)}(x, 0) = -\bar{V}_y; \quad |x| < b \tag{76}$$

$$w^{(c)}(x, y) \to 0; \quad |x^2 + y^2|^{1/2} \to \infty \tag{77}$$

with rigid-body deflections excepted.

Symmetrical Solution. Upon defining the deflection as in (16) continuity for $|x| \geqslant b$ requires (20) and (21) be satisfied, whereas (75) and (76) lead, respectively, to

$$\int_0^\infty \{D_y[K_1{}^2G_1 + K_2{}^2G_2] - (H - 2D_{xy})[G_1 + G_2]\}\, t^2\cos tx\, dt = \bar{M}_y \tag{78}$$

$$\int_0^\infty \{D_y[K_1^2G_1 + K_2^2G_2] - (H + 2D_{xy})[K_1G_1 + K_2G_2]\} t^3 \cos tx\, dt = 0 \quad (79)$$

As a linear combination of the derivative with respect to x of (20) plus (21) is still zero, which incidentally is the same as requiring for this symmetrical loading that the shear $V_y = 0$ for all x along the crack, satisfy (79) by requiring

$$G_2(t) = \frac{-D_yK_1^2 + (H + 2D_{xy})}{D_yK_2^2 - (H + 2D_{xy})} \frac{K_1}{K_2} G_1(t) \equiv -\lambda \frac{K_1}{K_2} G_1(t) \quad (80)$$

whereupon substitution into (20) gives

$$(1 - \lambda)K_1 \int_0^\infty tG_1(t) \cos tx\, dt = 0; \quad |x| \geq b \quad (81)$$

and into (78) gives

$$\left\{[D_yK_1^2 - (H - 2D_{xy})] - \lambda \frac{K_1}{K_2}[D_yK_2^2 - (H - 2D_{xy})]\right\} \int_0^\infty t^2G_1(t) \cos tx\, dt = \bar{M}_y \quad |x| < b \quad (82)$$

or using the notation

$$\lambda' \equiv \frac{D_yK_1^2 - (H - 2D_{xy})}{D_yK_2^2 - (H - 2D_{xy})} \quad (83)$$

the two integral equations become

$$\int_0^\infty tG_1(t) \cos tx\, dt = 0 \quad |x| \geq b \quad (84)$$

$$\int_0^\infty t^2G_1(t) \cos tx\, dt = \frac{\bar{M}_y}{D_yK_2^2 - (H - 2D_{xy})} \cdot \frac{1}{\lambda' - \lambda\left(\frac{K_1}{K_2}\right)} \quad |x| < b \quad (85)$$

with the solution

$$G_1(t) = \frac{b\bar{M}_y}{D_yK_2^2 - (H - 2D_{xy})} \cdot \frac{1}{\lambda' - \lambda(K_1/K_2)} \cdot \frac{J_1(bt)}{t^2} \quad (86)$$

The complete symmetrical solution is therefore

$$w(x, y) = w_\infty(x, y) + \frac{b\bar{M}_y}{[D_yK_2^2 - (H - 2D_{xy})][\lambda' - \lambda(K_1/K_2)]} \int_0^\infty \left[e^{-K_1t|y|} - \lambda \frac{K_1}{K_2} e^{-K_2t|y|}\right] t^2J_1(bt) \cos tx\, dt \quad (87)$$

As previously, the integral (87) is understood as the formal integral with respect to y of a convergent integral. The limit situation for isotropy gives as $K_i \to 1$

$$w(x, y) = \frac{b\bar{M}_y}{D(1 - \nu)} \int_0^\infty (1 + ty)e^{-ty}t^{-2}J_1(bt) \cos tx\, dt - \frac{\bar{M}_x - \nu\bar{M}_y}{D(1 - \nu^2)} \frac{x^2}{2} - \frac{\bar{M}_y - \nu\bar{M}_x}{D(1 - \nu^2)} \frac{y^2}{2} + \frac{\bar{M}_{xy}}{D(1 - \nu)} xy \quad (88)$$

Antisymmetrical Solution. For this part of the solution, one requires a perturbation solution which vanishes at infinity, and gives zero moment $\bar{M}_y$ and a constant shear $\bar{V}_y$ along the crack to wash out the contribution from the quadratic deflection function $w_\infty(x, y)$. However, it is found that this latter function produces no shear at the crack in the Kirchhoff sense and hence there is no perturbation function needed. From the physical standpoint, it would be necessary to treat the problem by the higher order theory where three independent boundary conditions are prescribed along the crack, instead of combining the direct shear and the rate of change of the twisting moment. A higher order asymmetry such as $w_\infty \sim xy^3$ can be treated. However, the present purpose is to inquire into quadratic terms only of the stress and deflection functions at infinity.

The Bending Stress Field. The stress field is found by calculating the moments, $\sigma_x = 6M_x/h^2$, and so on from (87) and (49). Along the y axis for example, there results using (71), (73), and (74)

$$M_x(0, y^+) = \bar{M}_x - \frac{\bar{M}_yb^2}{[D_yK_2^2 - (H - 2D_{xy})][\lambda' - \lambda(K_1/K_2)]} \left\{\frac{D_1K_1^2 - D_x}{\sqrt{b^2 + K_1^2y^2}\,[K_1y + \sqrt{b^2 + K_1^2y^2}]} - \frac{\lambda D_1K_1K_2 - \lambda D_x(K_1/K_2)}{\sqrt{b^2 + K_2^2y^2}\,[K_2y + \sqrt{K_2^2y^2 + b^2}]}\right\} \quad (89)$$

$$M_y(0, y^+) = \bar{M}_y - \frac{\bar{M}_yb^2}{[D_yK_2^2 - (H - 2D_{xy})][\lambda' - \lambda(K_1/K_2)]} \left\{\frac{D_yK_1^2 - D_1}{\sqrt{b^2 + K_1^2y^2}\,[K_1y + \sqrt{b^2 + K_1^2y^2}]} - \frac{\lambda D_yK_1K_2 - \lambda D_1(K_1/K_2)}{\sqrt{b^2 + K_2^2y^2}\,[K_2y + \sqrt{b^2 + K_2^2y^2}]}\right\} \quad (90)$$

$$M_{xy}(0, y^+) = \bar{M}_{xy} \quad (91)$$

On the other hand, a similar calculation gives along the crack, $(x > 0)$

$$M_x(x, 0) = \bar{M}_x + \bar{M}_y \frac{(K_1^2 - \lambda K_1K_2)D_1 - [1 - \lambda(K_1/K_2)]D_x}{[D_yK_2^2 - (H - 2D_{xy})][\lambda' - \lambda(K_1/K_2)]} \begin{cases} 1; & x < b \\ \left\{\sqrt{\left(\frac{x}{b}\right)^2 - 1}\left[\frac{x}{b} + \sqrt{\left(\frac{x}{b}\right)^2 - 1}\right]\right\}^{-1}; & x > b \end{cases} \quad (92)$$

$$M_y(x, 0) = \bar{M}_y + \bar{M}_y \frac{(K_1^2 - \lambda K_1K_2)D_y - [1 - \lambda(K_1/K_2)]D_1}{[D_yK_2^2 - (H - 2D_{xy})][\lambda' - \lambda(K_1/K_2)]} \begin{cases} 1; & x < b \\ \left\{\sqrt{\left(\frac{x}{b}\right)^2 - 1}\left[\frac{x}{b} + \sqrt{\left(\frac{x}{b}\right)^2 - 1}\right]\right\}^{-1}; & x > b \end{cases} \quad (93)$$

$$M_{xy}(x, 0) = \bar{M}_{xy} - \frac{(1 - \lambda)K_1\bar{M}_y}{[D_yK_2^2 - (H - 2D_{xy})][\lambda' - \lambda(K_1/K_2)]} \begin{cases} \left(\frac{x}{b}\right)\left[1 - \left(\frac{x}{b}\right)^2\right]^{-1/2}; & x < b \\ 0; & x > b \end{cases} \quad (94)$$

Combined Field (Symmetrical)

As indicated earlier, it is interesting to examine the combined stress field in the small deformation region where bending and extension are assumed to be noninteracting. Inasmuch as the formulas have been derived in some generality previously, only the stresses along the prolongation of the crack will be considered. Thus, with some algebraic simplification one can write, for symmetrical loadings,

$$\sigma_x(0, x) = \bar{\sigma}_{x_e} + \bar{\sigma}_{x_b} + [K_1K_2\bar{\sigma}_{y_e} + \gamma_1\bar{\sigma}_{y_b}] \frac{b^2}{\sqrt{x^2 - b^2}\,[x + \sqrt{x^2 - b^2}]} \quad (95)$$

$$\sigma_y(0, x) = \bar{\sigma}_{y_e} + \bar{\sigma}_{y_b} + [\bar{\sigma}_{y_e} + \gamma_2\bar{\sigma}_{y_b}] \frac{b^2}{\sqrt{x^2 - b^2}\,[x + \sqrt{x^2 - b^2}]} \quad (96)$$

where

$$\gamma_1 = \frac{(K_1^2 - \lambda K_1K_2)D_1 - [1 - \lambda(K_1/K_2)]D_x}{[D_yK_2^2 - (H - 2D_{xy})][\lambda' - \lambda(K_1/K_2)]}$$

$$\gamma_2 = \frac{(K_1^2 - \lambda K_1K_2)D_y - [1 - \lambda(K_1/K_2)]D_1}{[D_yK_2^2 - (H - 2D_{xy})][\lambda' - \lambda(K_1/K_2)]} \quad (97)$$

$$K_1^2K_2^2 = 1/B = E_x/E_y$$

are orthotropic parameters.

For the particular case of $K_i = 1$, $\gamma_1 = -(1 - \nu)/(3 + \nu)$, $\gamma_2 = 1$, $D_x = D_y = D$, $D_1 = \nu D$, $H - 2D_{xy} = \nu D$, and

$$\sigma_x(x, 0)|_{\text{iso}} = [\bar{\sigma}_{x_e} + \bar{\sigma}_{x_b}] + \left[\bar{\sigma}_{y_e} - \frac{1 - \nu}{3 + \nu}\bar{\sigma}_{y_b}\right] \frac{b^2}{\sqrt{x^2 - b^2}\,[x + \sqrt{x^2 - b^2}]} \quad (98)$$

$$\sigma_y(x, 0)|_{\text{iso}} = [\bar{\sigma}_{y_e} + \bar{\sigma}_{y_b}] + [\bar{\sigma}_{y_e} + \bar{\sigma}_{y_b}] \frac{b^2}{\sqrt{x^2 - b^2}\,[x + \sqrt{x^2 - b^2}]} \quad (99)$$

Near the crack point the first constant term may be neglected and one finds upon defining $x = b + \epsilon$

$$\sigma_x(0, \epsilon)|_{\text{iso}} = \left[\bar{\sigma}_{y_e} - \frac{1 - \nu}{3 + \nu}\bar{\sigma}_{y_b}\right] \frac{1}{\sqrt{2\epsilon/b}} + \dots \quad (100)$$

$$\sigma_y(0, \epsilon)|_{\text{iso}} = [\bar{\sigma}_{y_e} + \bar{\sigma}_{y_b}] \frac{1}{\sqrt{2\epsilon/b}} + \dots \quad (101)$$

It may be recalled that the earlier work [5, 11] dealing with stress singularities revealed only the order of stress variation, namely, $\epsilon^{-1/2}$, without determining the constant of proportionality. The present results, however, include this constant. For example, in the symmetrical isotropic extensional problem, comparison of any of equations (56–58) near the crack point with corresponding formulas in reference [6] gives

$$a_1 = -\bar{\sigma}_{y_e}\sqrt{b/2}$$

The present results can therefore be used in some generality, including the orthotropic situation, while detailed information of the isotropic elastic stresses near the crack point may be obtained from the previous work.

An important distinction between the extensional and bending behavior is indicated in (100) and (101). It may be observed that at the crack point the extensional contributions of the principal stresses σ_x and σ_y are identical, whereas the respective bending stresses are of opposite sign and in approximately a 1:5 ratio depending upon Poisson's ratio. Recently, however, Knowles and Wang [12] have established a most important point by replacing the classical linear theory of isotropic plate bending and approximate Kirchhoff boundary conditions by the Reissner theory of plate bending. It is thus possible to account for the unloaded edge of the crack through use of three separate boundary conditions. They have found that the multiplicative factors $-(1 - \nu)/(3 + \nu)$ and $+1$ are both changed to $+(1 + \nu)/(3 + \nu)$ such that the normal bending stress components are also identical. (Parenthetically, it is interesting to observe that the average stress $\sigma_x + \sigma_y$ at the crack point is the same for both theories, Fig. 1.)

Furthermore, the circumferential stress variation is the same as that obtained for the extensional stresses. Therefore, while the classical bending theory is valid a "boundary-layer's distance" from the edge, i.e., $\exp(-\sqrt{10}y/h) \ll 1$ where h is the plate thickness, it is necessary to include the higher order theory near the crack point. Along the free edges of the crack, they show further that the classical estimate for M_x and M_y is satisfactory, but there is a boundary-layer modification to M_{xy}, Q_x, and Q_y.

While it is not the purpose of the present paper to examine fracture criteria, assume a distortion-energy theory of failure and consider the implication of the differences in bending stress calculation for an isotropic plate subjected to combined extension and bending. Along the crack axis the octahedral stress becomes, using classical bending theory

$$\tau_{\text{oct}}(\epsilon, 0) = \frac{\sqrt{2}}{3}\frac{\bar{\sigma}_{y_e}}{(2\epsilon/b)^{1/2}}\left[1 + \frac{2(1 + \nu)}{3 + \nu}\frac{\bar{\sigma}_{y_b}}{\bar{\sigma}_{y_e}} + \frac{13 + 2\nu + \nu^2}{(3 + \nu)^2}\left(\frac{\bar{\sigma}_{y_b}}{\bar{\sigma}_{y_e}}\right)^2\right]^{1/2} \quad (102)$$

whereas using Knowles and Wang's results

$$\tau_{\text{oct}}(\epsilon, 0) = \frac{\sqrt{2}}{3}\frac{\bar{\sigma}_{y_e}}{(2\epsilon/b)^{1/2}}\left[1 + \frac{1 + \nu}{3 + \nu}\frac{\bar{\sigma}_{y_b}}{\bar{\sigma}_{y_e}}\right] \quad (103)$$

In the form of bending-extension interaction curves, assuming this criterion significant, these become, respectively,

$$\left[\frac{\bar{\sigma}_{y_e}}{3(\epsilon/b)^{1/2}\tau_{\text{oct}}}\right]^2 + \frac{2(1 + \nu)}{3 + \nu}\left[\frac{\bar{\sigma}_{y_e}}{3(\epsilon/b)^{1/2}\tau_{\text{oct}}} \cdot \frac{\bar{\sigma}_{y_b}}{3(\epsilon/b)^{1/2}\tau_{\text{oct}}}\right] + \frac{13 + 2\nu + \nu^2}{(3 + \nu)^2}\left[\frac{\bar{\sigma}_{y_b}}{3(\epsilon/b)^{1/2}\tau_{\text{oct}}}\right]^2 = 1 \quad (104)$$

and

$$\left[\frac{\bar{\sigma}_{y_e}}{3(\epsilon/b)^{1/2}\tau_{\text{oct}}}\right] + \frac{(1 + \nu)}{(3 + \nu)}\left[\frac{\bar{\sigma}_{y_b}}{3(\epsilon/b)^{1/2}\tau_{\text{oct}}}\right] = 1 \quad (105)$$

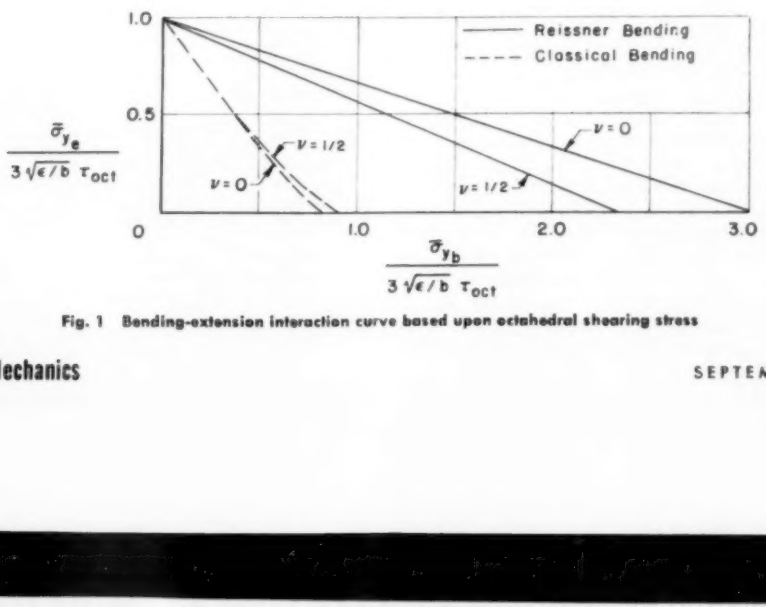

Fig. 1 Bending-extension interaction curve based upon octahedral shearing stress

Further, if it proves valid to consider the radius at failure independent of load proportion, which must at this time remain open to question because the stress distribution through the sheet thickness is characteristically different in bending and extension, then one may graph these latter two curves. Observe that while the predicted magnitude of critical bending stress alone is three times higher, in both cases the interaction curve is essentially a straight line, lending some theoretical basis to a possible design postulate. It would therefore be interesting to examine this question experimentally by evaluating bending and extension fracture separately and then simultaneously to see if such a linear interaction curve can be verified.[2]

Returning to the effect of orthotropy, particularly for extensional loading only, (96) shows that variation in the material properties affects only the stress parallel to the crack. In particular

$$\sigma_x - \sigma_{x_0} + (E_x/E_y)^{1/2}\vartheta_{y_0}(2\epsilon/b)^{-1/2}$$

implies of course that this stress component is decreased as the relative stiffness is decreased parallel to the crack. Such a situation would tend to upset the isotropic equality of the normal stresses and suggest a larger yield region. This effect of the $(E_x/E_y)^{1/2}$ ratio also extends to the σ_x stress along the cracked portions; e.g., (56). The extension stress ϑ_{y_0} induces a compressive stress $(E_x/E_y)^{1/2}\vartheta_{y_0}$ along the crack edge, such that for symmetrical loading

$$\sigma_x(x^+, 0) = \vartheta_x - (E_x/E_y)^{1/2}\vartheta_y \tag{106}$$

This is the stress component which gives trouble in crack experiments because when (for $\sigma_x = 0$) σ_y exceeds approximately the clamped plate Euler load,

$$4\pi^2 D/(2b)^2 h \sim E(h/b)^2,$$

the specimen will buckle laterally at the crack and lead to additional tearing loads not included in the analysis. The orthotropic sensitivity is indicated by the characteristic square-root rigidity ratio; where it may be noted that a ϑ_x may be applied to eliminate this effect without changing the elastic stress distributions near the crack point. It may also be shown that there is a minimum strain energy of distortion at $E_x/E_y = 1/2$, at which ratio the energy is 15 per cent lower than in the isotropic material.

Finally, in common with the isotropic extensional case the deformed orthotropic crack surface is also elliptical for a symmetrical loading; e.g., (62) and (63) for $x \leq b$

$$\frac{(u/b)^2}{\left[\dfrac{\vartheta_x}{E_x} - \dfrac{K_1K_2\vartheta_y}{E_x}\right]^2} + \frac{(v/b)^2}{\left[\dfrac{(K_1 + K_2)\vartheta_y}{E_y}\right]^2} = 1 \tag{107}$$

The radius of curvature at the crack point may be calculated from the major and minor axes of the deformed ellipse as

$$[(K_1 + K_2)\vartheta_y/E_y]^2/\{1 + [\vartheta_x - K_1K_2\vartheta_y]/E_x\}$$

Generally speaking, the effect of orthotropy, in so far as it affects fracture initiation, does not change the stress fields qualitatively. The quantitative effect seems to be mainly confined to the parameter $(E_x/E_y)^{1/2}$.

In conclusion, it should be emphasized that the solution presented is an elastic one, requiring therefore careful judgment in applying the results in practical situations where plastic enclaves actually occur at the crack point prior to crack propagation [13]. Nevertheless, elastic analyses provides a useful guide in the absence of solutions to the more complicated elastic-plastic problem.

[2] If the bending effect exceeds the extensional, the bottom edges of the plate may touch, invalidating the theory. The maximum rotation of the faces of the crack at the plate surface is

$$[\partial w(0, 0)/\partial y](h/2) = -M_0 hb/[D(1 - \nu)(3 + \nu)].$$

whereas the extensional displacement is $V(0, 0) = 2b\vartheta_{y_0}/E$. Thus there will be no touching if

$$\vartheta_{y_0} > [(1 + \nu)/(3 + \nu)]\vartheta_{y_0}$$

References

1 C. E. Inglis, "Stresses in a Plate Due to the Presence of Cracks and Sharp Corners," *Transactions of The Institution of Naval Architects*, London, England, vol. 60, 1913, p. 219.

2 A. A. Griffith, "The Phenomena of Rupture and Flow in Solids," *Philosophical Transactions of The Royal Society of London*, England, vol. 221, 1921, pp. 163–198.

3 H. M. Westergaard, "Bearing Pressures and Cracks," JOURNAL OF APPLIED MECHANICS, vol. 6, TRANS. ASME, vol. 61, 1939, p. A-49.

4 G. N. Sawin, "Spannungserhohung am Rande von Lochern," *VEB Verlag Technik*, Berlin, Germany, 1956, pp. 167–175 and 355–364.

5 M. L. Williams, "On the Stress Distribution at the Base of a Stationary Crack," JOURNAL OF APPLIED MECHANICS, vol. 24, TRANS. ASME, vol. 79, 1957, pp. 109–114.

6 G. R. Irwin, "Analysis of Stresses and Strain Near the End of a Crack Transversing a Plate," JOURNAL OF APPLIED MECHANICS, vol. 24, TRANS. ASME, vol. 79, 1957, pp. 361–364.

7 W. Olszak, "Cracks in Structural Elements Considered as a Problem of the Theory of Elasticity and Plasticity," *Archiwum Inzynierii Ladowej* (Poland), vol. 4, February, 1958.

8 E. H. Yoffe, "The Moving Griffith Crack," *Philosophical Magazine*, vol. 42, part 2, 1951, pp. 379–750.

9 G. N. Watson, "Bessel Functions," Cambridge University Press, Cambridge, England, 1944, p. 405.

10 A. Erdélyi, "Table of Integral Transforms," McGraw-Hill Book Company, Inc., New York, N. Y., vol. 1, 1954, p. 184.

11 M. L. Williams, "The Bending Stress Distribution at the Base of a Stationary Crack," JOURNAL OF APPLIED MECHANICS, vol. 28, TRANS. ASME, vol. 83, Series E, 1961, pp. 78–82.

12 J. K. Knowles and N. M. Wang, "On the Bending of an Elastic Plate Containing a Crack," GALCIT SM 60-11, July, 1960, submitted for publication in the *Journal of Mathematics and Physics*.

13 L. D. Stimpson and D. M. Eaton, "The Extent of Elasto-Plastic Yielding at the Crack Point of an Externally Notched Plane Stress Tensile Specimen," Report ARL-24, ARL, Wright Patterson AFB, January, 1961.

The Effect of a Rigid Elliptic Inclusion on the Bending of a Thick Elastic Plate[2]

FU CHOW[1]
Graduate Student,
Polytechnic Institute of
Brooklyn, Brooklyn, N. Y.

The effect of a rigid elliptic inclusion on both plain bending and pure twist of a thick elastic plate is investigated on the basis of Reissner's plate theory [1, 2].[3] Comparison is made for the limiting cases of vanishing focal distanceof the elliptic inclusion (a rigid circular inclusion), and vanishing thickness (Poisson-Kirchhoff plate theory), with the solutions of C. Pai [3], R. A. Hirsch [4], and M. Goland [5]. The stress-concentration factors are lower than those predicted by the classical plate theory.

THE purpose of the paper is to investigate the effect of a rigid elliptic inclusion on both plain bending and pure twist of a thick elastic plate including the effect of transverse-shear deformation.

Problems on the effect of circular holes and inclusions on the bending of plates have been analyzed on the basis of the Poisson-Kirchhoff theory by J. N. Goodier [6] and M. Goland [5]. As is well known, the Poisson-Kirchhoff theory does not include the effect of transverse-shear deformation.

The theory developed by E. Reissner [1, 2] includes the effect of transverse-shear deformation on the bending of elastic plate and is to be used in this investigation. E. Reissner [1], C. Pai [3], and R. Hirsch [4] have solved the cases of circular holes and inclusions and P. M. Naghdi [7] has solved the case of an elliptic hole using this theory.

In this paper Reissner's theory is further made use of in solving the problem of a rigid elliptic inclusion on the transverse flexure of a thick plate. Limiting cases of the present results are checked with previous results wherever possible.

Transverse load is neglected throughout the paper.

In discussing problems of stress concentration, due to elliptic holes or inclusions, it is convenient to use elliptic cylindrical coordinates. The transformation to this system has been carried out by Naghdi [7].

Solution for Plain Bending and Pure Twist

The boundary conditions for the problem are, when Reissner plate theory is used

$$\xi \to \infty: \quad M_\xi = \frac{M_0}{2}(1 + \Gamma \cos 2\eta)$$

$$H_{\xi\eta} = -\frac{\Gamma}{2} M_0 \sin 2\eta \tag{1}$$

$$V_\xi = 0$$

where $\Gamma = \pm 1$, depending on whether M_0 is applied about the y or x-axis. Around the rigid inclusion the boundary conditions are

$$w = \beta_\xi = \beta_\eta = 0 \tag{2}$$

Take as in reference [7]

$$Dw = \bar{E}_0 + \bar{F}_0\xi + \frac{c^2}{8} A_0(\cosh 2\xi + \cos 2\eta) + (\bar{E}_2 e^{-2\xi} + \bar{F}_2 e^{2\xi}) \cos 2\eta - \frac{c^2}{16} A_2(e^{-2\xi} + \cos 2\eta) \tag{3}$$

and

$$\chi = C^{(2)}(q) \frac{Gek_2(\xi, -q)}{Gek_2(\xi_0, -q)} se_2(\eta, -q) + A_2 e^{-2\xi} \sin 2\eta \tag{4}$$

Since $w = \beta_\eta = 0$ at $\xi = \xi_0$, the coefficient of $\cos 2\eta$ in equation (3), and equation (2) yield, respectively,

$$-\frac{c^2}{8} A_2 + 2(\bar{E}_2 e^{-2\xi_0} + \bar{F}_2 e^{2\xi_0}) + \frac{c^2}{4} A_0 = 0 \tag{5}$$

$$C^{(2)}(q) \frac{Gek_2'(\xi_0, -q)}{Gek_2(\xi_0, -q)} se_2(\eta, -q) = \left\{ 2A_2 e^{-2\xi_0} + \frac{5(1-\nu)}{h^2} \left[-\frac{c^2}{8} A_2 + \frac{c^2}{4} A_0 + 2(\bar{E}_2 e^{-2\xi_0} + \bar{F}_2 e^{2\xi_0}) \right] \right\} \sin 2\eta \tag{6}$$

Substituting equation (5) in equation (6), we get

$$C^{(2)}(q) \frac{Gek_2'(\xi_0, -q)}{Gek_2(\xi_0, -q)} se_2(\eta, -q) = 2A_2 e^{-2\xi_0} \sin 2\eta \tag{7}$$

Substituting equation (7) in equation (4), the stress function is obtained

$$\chi = \left[2e^{-2\xi_0} \frac{Gek_2(\xi, -q)}{Gek_2'(\xi_0, -q)} + e^{-2\xi} \right] A_2 \sin 2\eta \tag{8}$$

which is no longer the same as Naghdi's result of χ for the hole problem.

After some lengthy calculations, we obtain expressions for the stress couples and shear resultants involving the unknown constants A_0, A_2, $\bar{E}_2$, $\bar{F}_0$, and $\bar{F}_2$. Substituting these together with w and χ in the boundary conditions equations (1) and (2), the constants and the stress couples and shear resultants may be determined completely. Of the highest interest are the values of the stress couples M_ξ and M_η and shear resultants V_ξ and V_η at the bond of the inclusion. Denoting by α and β the ratios h/a

---

[1] Now Stress Analysis Engineer, Equipment Division, Foster Wheeler Corporation, New York, N. Y.

[2] This paper represents part of a thesis submitted to Polytechnic Institute of Brooklyn in partial fulfillment of the requirements for the degree of MS in Mechanical Engineering, June, 1960.

[3] References in brackets designate References at end of paper.

Presented at the Summer Conference of the Applied Mechanics Division, Chicago, Ill., June 14–16, of THE AMERICAN SOCIETY OF MECHANICAL ENGINEERS.

Discussion of this paper should be addressed to the Editorial Department, ASME, United Engineering Center, 345 East 47th Street, New York 17, N. Y., and will be accepted until October 10, 1961. Discussion received after the closing date will be returned. Manuscript received by ASME Applied Mechanics Division, March 28, 1960. Paper No. 61—APM-13.

and b/a (a and b being the semimajor and semiminor axes of the boundary $\xi = \xi_0$), respectively, they are

$$\frac{M_\xi(\xi_0)_B}{M_0} = \frac{1}{Q}\left\{\Gamma(1+\nu)\frac{Gek_2'}{Gek_2}\left[-(1-\beta^2)(3+2\beta+3\beta^2)\right.\right.$$
$$+ 4(1+\beta)^2(1-\beta+\beta^2)\cos 2\eta - (1+\beta)^2(1-\beta^2)\cos 4\eta$$
$$+\left[4(1-\nu)\beta(1+\beta^2)\frac{Gek_2'}{Gek_2}\right.$$
$$\left.+\frac{16\alpha^2}{5(1+\beta)^2}\left(2+\frac{Gek_2'}{Gek_2}\right)(3+2\beta^2+3\beta^4)\right]$$
$$-4(1-\beta^2)\cos 2\eta\left[\beta(1-\nu)\frac{Gek_2'}{Gek_2}\right.$$
$$\left.+\frac{16\alpha^2}{5(1+\beta)^2}(1+\beta^2)\left(2+\frac{Gek_2'}{Gek_2}\right)\right]$$
$$\left.-\frac{16\alpha^2}{5}(1-\beta)^2\cos 4\eta\left[2+\frac{Gek_2'}{Gek_2}\right]\right\} \quad (9)$$

$$\frac{M_\eta(\xi_0)_B}{M_0} = \nu\frac{M_\xi(\xi_0)_B}{M_0} \quad (10)$$

$$\frac{V_\xi(\xi_0)_B}{M_0/a} = -\frac{2\sqrt{2}\left(2+\frac{Gek_2'}{Gek_2}\right)\cos 2\eta\left[\Gamma+\frac{1-\nu}{1+\nu}\frac{1-\beta}{1+\beta}\right]}{[(1+\beta^2)-(1-\beta^2)\cos 2\eta]^{1/2}\left[\frac{1-\nu}{2}\frac{Gek_2'}{Gek_2}+\frac{8\alpha^2}{5(1+\beta)^2}\left(2+\frac{Gek_2'}{Gek_2}\right)\right]} \quad (11)$$

$$\frac{V_\eta(\xi_0)_B}{M_0/a} = 0 \quad (12)$$

where Gek_2'/Gek_2 stands for $Gek_2'(\xi, -q)/Gek_2(\xi_0, -q)$ and

$$Q = 2(1-\nu^2)[(1+\beta^2)-(1-\beta^2)\cos 2\eta]^2$$
$$\times\left[\frac{Gek_2'}{Gek_2}+\frac{16\alpha^2}{5(1-\nu)(1+\beta)^2}\left(2+\frac{Gek_2'}{Gek_2}\right)\right]$$

The expression of $M_\xi(\xi_0)_B/M_0$ has its greatest value at $\eta = 0°$, when $\Gamma = 1$. Hence

$$k_B = \frac{M_\xi(\xi_0, 0°)_B}{M_0}$$
$$= \beta^2[2+(1+\nu)\beta]\frac{Gek_2'}{Gek_2}$$
$$+\frac{4\alpha^2}{5(1+\beta)^2}[-1+2\beta^2+3\beta^4]\left(2+\frac{Gek_2'}{Gek_2}\right)$$
$$\overline{(1-\nu^2)\beta^4\left[\frac{Gek_2'}{Gek_2}+\frac{16\alpha^2}{5(1-\nu)(1+\beta)^2}\left(2+\frac{Gek_2'}{Gek_2}\right)\right]} \quad (13)$$

The expression of $V_\xi(\xi_0)_B/(M_0/a)$ has its greatest value at $\eta = \pi/2$, when $\Gamma = 1$. Thus

$$\frac{V_\xi\left(\xi_0, \frac{\pi}{2}\right)_B}{M_0/a} = \frac{\left(2+\frac{Gek_2'}{Gek_2}\right)\left[1+\frac{1-\nu}{1+\nu}\frac{1-\beta}{1+\beta}\right]}{\frac{1-\nu}{4}\frac{Gek_2'}{Gek_2}+\frac{4\alpha^2}{5(1+\beta)^2}\left(2+\frac{Gek_2'}{Gek_2}\right)} \quad (14)$$

With the results for the case of plain bending available, the stress-concentration factor k_T for the case of an infinite plate with a rigid elliptic inclusion subjected to a pure twisting couple M_0 at infinity may be deduced on the basis of the fact that the stresses and displacements in the latter case are obtainable by suitable superposition of plain positive bending about the y-axis and plain negative bending about the x-axis. It follows that

$$\frac{M_\xi(\xi_0)_T}{M_0} = \left[\frac{M_\xi(\xi_0)_B}{M_0}\right]_{\Gamma=1} - \left[\frac{M_\xi(\xi_0)_B}{M_0}\right]_{\Gamma=-1} \quad (15)$$

Since this expression has its greatest value at $\eta = 0°$, therefore

$$k_T = \frac{M_\xi(\xi_0, 0°)_T}{M_0}$$
$$= \frac{2(1+\beta)\frac{Gek_2'}{Gek_2}}{(1-\nu)\beta\left[\frac{Gek_2'}{Gek_2}+\frac{16\alpha^2}{5(1-\nu)(1+\beta)^2}\left(2+\frac{Gek_2'}{Gek_2}\right)\right]} \quad (16)$$

We have also

$$\frac{M_\eta(\xi_0, 0°)_T}{M_0} = \nu\frac{M_\xi(\xi_0, 0°)_T}{M_0} \quad (17)$$

Similarly, the expression

$$\frac{V_\xi(\xi_0)_T}{M_0/a} = \left[\frac{V_\xi(\xi_0)_B}{M_0/a}\right]_{\Gamma=1} - \left[\frac{V_\xi(\xi_0)_B}{M_0/a}\right]_{\Gamma=-1} \quad (18)$$

has its greatest value at $\eta = \pi/2$; thus

$$\frac{V_\xi\left(\xi_0, \frac{\pi}{2}\right)_T}{M_0/a} = \frac{2\left(2+\frac{Gek_2'}{Gek_2}\right)}{\frac{1-\nu}{4}\frac{Gek_2'}{Gek_2}+\frac{4\alpha^2}{5(1+\beta)^2}\left(2+\frac{Gek_2'}{Gek_2}\right)} \quad (19)$$

We further have

$$\frac{V_\eta(\xi_0)_T}{M_0/a} = 0 \quad (20)$$

Reduction to Limiting Cases

The limiting cases of the foregoing solution are obtained by (a) vanishing the focal distance, and (b) vanishing the plate thickness. The solutions for these limiting cases should agree with the solution of a rigid circular inclusion in a thick plate, and the solution of a rigid elliptic inclusion in a thin plate, respectively.

Case (a). When a confocal ellipse of semi-major axis r tends to a circle with this radius [8], $\xi \to \infty$, and $c \to 0$, at $\eta = 0°$, such that $(c/2)e^\xi \to r$. Then

$$\pi Gek_2'(\xi, -q) \to s_2' k_1 r K_2'\left(\frac{\sqrt{10}\,r}{h}\right), \quad \text{where} \quad k_1 r = \sqrt{q}\,e^\xi$$

$$\pi Gek_2(\xi, -q) \to s_2' K_2\left(\frac{\sqrt{10}\,r}{h}\right)$$

We note that as $\beta \to 1$

$$\frac{Gek_2'(\xi_0, -q)}{Gek_2(\xi_0, -q)} \to u\frac{K_2'(u)}{K_2(u)}$$

where

$$u = \frac{\sqrt{10}\,a}{h}, \quad q = \frac{5c^2}{2h^2}, \quad c^2 = a^2 - b^2$$

and K_2 = modified Bessel function of the second kind. Thus equations (13), (16), (14), and (19) for $\beta = 1$ agree with the results given in reference [3].

Case (*b*). Vanishing the plate thickness; i.e., $\alpha = h/a \to 0$. Equations (13) and (16) for $\alpha = 0$ reduce to the results given in reference [5]. In particular, as $\alpha = 0, \beta = 3/4, \nu = 1/3$, equations (13) and (16) agree with equations (18) and (26) of reference [5].

Numerical Examples

Figs. 1 and 2 show the plottings of the stress-concentration factors and shear-stress resultants for both plain bending and pure twist. In both cases, $\beta = b/a$ is taken as $3/4$ and Poisson's ratio is assumed to be $1/3$. The stress-concentration factors found in Fig. 1 are lower than those predicted by the classical plate theory. In fact, the classical theory is too much on the safe side for $a/h < 1$. Table 1 shows the percentage difference of the stress-concentration factor for various values a/h at $\eta = 0°$.

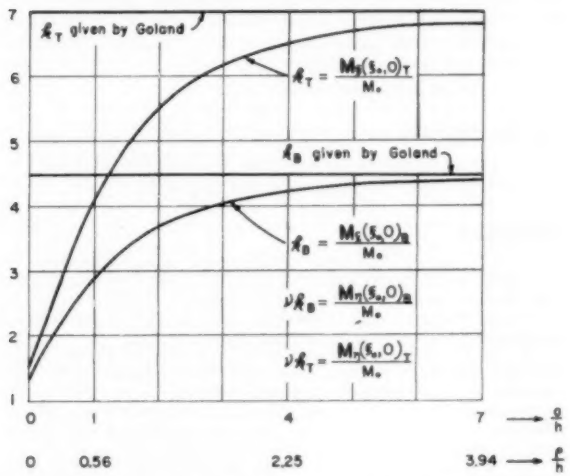

Fig. 1 Stress-concentration factors versus ratio of semimajor axis of rigid elliptic inclusion to plate thickness for both plain bending and pure twist; $\beta = 3/4$ and $\nu = 1/3$, where ρ = radius of curvature of ellipse at end of major axis = $(9/16)a$

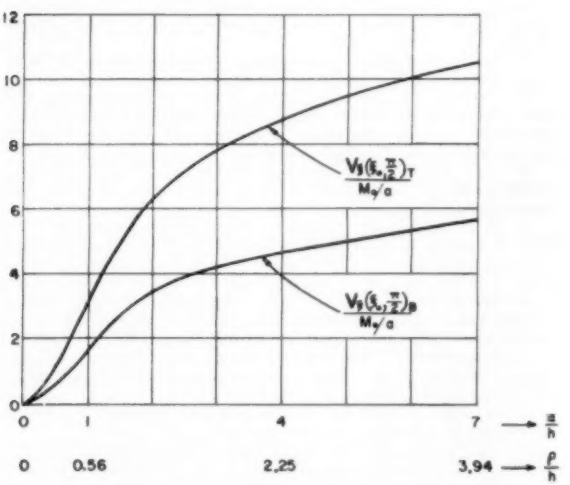

Fig. 2 Edge shear-stress resultants versus ratio of semimajor axis of rigid elliptic inclusion to plate thickness for both plain bending and pure twist; $\beta = 3/4$ and $\nu = 1/3$, where ρ = radius of curvature of ellipse at end of major axis = $(9/16)a$

Table 1

$\frac{a}{h}$	Stress-concentration factor — This paper	Stress-concentration factor — Classical theory	Per cent difference
0.5	2.195	4.5	104.5
1	2.885	4.5	56.0
7	4.391	4.5	2.5

Figs. 3 and 4 (references [3, 4]) show plottings of the stress-concentration factors around the inclusion for both plain bending and pure twist. In both cases $\nu = 1/3$. In Fig. 3, $2\rho/h$ is assumed equal to unity, $\beta = 3/4$, then $a/h = 3/2$. In Fig. 4, $2a/h$ is assumed equal to unity. We have ρ = radius of curvature of the elliptic inclusion at the ends of the major axis = $9/16a$. Along the x-axis

$$\left[\frac{M_\xi(\xi_0, 0)_B}{M_0}\right]_{\frac{2\rho}{h}=1}$$

is 36.64 per cent higher than

$$\left[\frac{M_r(a, 0)_B}{M_0}\right]_{\frac{2a}{h}=1}$$

and

$$\left[\frac{M_\xi(\xi_0, 0)_T}{M_0}\right]_{\frac{2\rho}{h}=1}$$

is 66.18 per cent higher than

$$\left[\frac{M_r(a, 0)_T}{M_0}\right]_{\frac{2a}{h}=1}$$

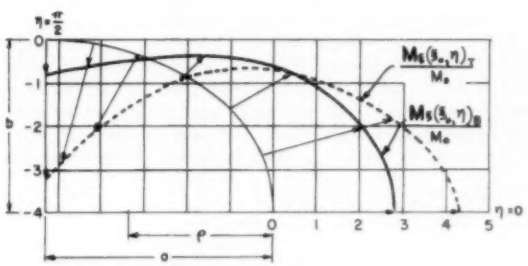

Fig. 3 Distribution of stress-concentration factors around rigid elliptic inclusion for plain bending and pure twist;

$$\beta = \tfrac{3}{4}, \quad \nu = \tfrac{1}{3}, \quad \frac{2\rho}{h} = 1, \quad \frac{a}{h} = \frac{9}{8}$$

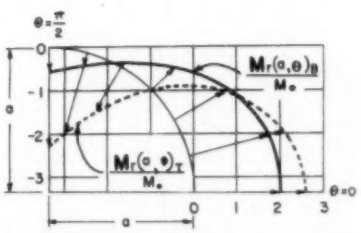

Fig. 4 Distribution of stress-concentration factors around rigid circular inclusion for both plain bending and pure twist;

$$\nu = \tfrac{1}{3} \quad \text{and} \quad \frac{2a}{h} = 1$$

although the radius of curvature is the same in the two cases.

In the calculations the values of the modified Mathieu function of the second kind Gek_2 and its first derivative for small values of their parameters were obtained directly from a suitable mathematical table [10, 11]. For values of the parameters q larger than 2.5, Gek_2 and Gek_2' were computed by means of the following series:

$$H_{\nu_2}^{(1)}(\xi_0, -q) = -\frac{i\sqrt{\frac{2}{\pi}}}{D_{0_2}} \sum_{m=0}^{\infty} D_{0_{2m}}[I_{m+1}(x) \cdot K_{m-1}(y) - I_{m-1}(x) \cdot K_{m+1}(y)] \quad (21)$$

$$H_{\nu_2}^{(1)\prime}(\xi_0, q) = \frac{i\sqrt{\frac{2}{\pi}}}{D_{0_2}} \sum_{m=0}^{\infty} D_{0_{2m}}\{y[I_{m+1}(x) \cdot K_{m-2}(y) - I_{m-1}(x) \cdot K_m(y)] + x[I_m(x) \cdot K_{m-1}(y) - I_{m-2}(x) \cdot K_{m+1}(y)] - 2[I_{m-1}(x) \cdot K_{m+1}(y) - I_{m+1}(x) \cdot K_{m-1}(y)]\} \quad (22)$$

$$\frac{Gek_2'}{Gek_2} = \frac{H_{\nu_2}^{(1)\prime}}{H_{\nu_2}^{(1)}} \left(\text{or} = \frac{Ne_2^{(1)\prime}}{N_{e2}^{(1)}}\right) \quad \text{(reference [8])} \quad (23)$$

where

$$x = \sqrt{|q|}e^{-i\eta} \qquad y = \sqrt{|q|}e^{i\eta} \quad (24)$$

and $H_{\nu_2}^{(1)}$ or $Ne_2^{(1)}$ = modified Mathieu function of the third kind (which were found in reference [8] article 13.41). I_2, K_2 were obtained from the suitable mathematical table [12]. B_{2m+2} or $BD_{0_{2m}}$ are the Fourier coefficients in the expansions of $se_2(\eta, -q)$ in sin 2η. For values of the parameter q smaller than 25, $D_{0_{2m}}$ were obtained directly from a suitable mathematical table [13]. For values of q larger than 25 $D_{0_{2m}}$ were computed with the help of references [13, 14, 15]. B is a constant.

For a vanishing elliptic inclusion, namely, $a/h \to 0$, it appears rather difficult to make direct computation owing to lack of information on the modified Mathieu functions of the second kind for very small parameters. However, since the ellipse becomes indistinguishable from a circle in the limit as $a/h \to 0$, we may make use of the following results for a rigid circular inclusion:

$$\lim_{u\to 0} \frac{M_r(a, 0)_B}{M_0} = \frac{5+\nu}{(1+\nu)(3-\nu)} = \frac{4}{3} = \left[\frac{M_\xi(\xi_0, 0°)_B}{M_0}\right]_{\frac{a}{h}=0} \quad (25)$$

$$\lim_{u\to 0} \frac{V_r\left(a, \frac{\pi}{2}\right)_B}{M_0/a} = 0 = \left[\frac{V_\xi\left(\xi_0, \frac{\pi}{2}\right)_B}{M_0/a}\right]_{\frac{a}{h}=0} \quad (26)$$

$$\lim_{u\to 0} \frac{M_r(a, 0)_T}{M_0} = \frac{4}{3-\nu} = \frac{3}{2} = \left[\frac{M_\xi(\xi_0, 0°)_T}{M_0}\right]_{\frac{a}{h}=0} \quad (27)$$

$$\lim_{u\to 0} \frac{V_r\left(a, \frac{\pi}{2}\right)_T}{M_0/a} = 0 = \left[\frac{V_\xi\left(\xi_0, \frac{\pi}{2}\right)_T}{M_0/a}\right]_{\frac{a}{h}=0} \quad (28)$$

where $\nu = 1/3$. Equations (25) and (26) for the bending case are taken from reference [3], and the twisting case is obtained from the bending one by superposition.

Discussion

The solution given here is approximate in the sense that equation (4) is not complete, as may be seen from the series expansion of $se_2(\eta, -q)$. For an exact solution of the problem, the stress function χ, given by equation (2) in reference [7] must include the entire second sum in equations (26) in reference [7], and this becomes progressively more important as the elliptic inclusion becomes more slender.

It is observed that, at the bond between the rigid inclusion and the plate, the shear-stress resultant in the tangential direction is equal to zero and the ratio between the stress couple in the tangential direction and that in the normal direction is equal to the Poisson ratio. These relations on the basis of Reissner's plate theory may be shown to be in general valid at the clamped boundary of a plate in the absence of lateral loading. The truth of the foregoing moment relation when the classical plate theory is employed has been known [9].

Acknowledgment

The author is indebted to his thesis adviser, Prof. Yi-Yuan Yu, for his invaluable encouragement and guidance.

References

1 E. Reissner, "The Effect of Transverse Shear Deformation on the Bending of Elastic Plates," JOURNAL OF APPLIED MECHANICS, vol. 12, TRANS. ASME, vol. 67, 1945, p. A-69.

2 E. Reissner, "On Bending of Elastic Plates," *Quarterly of Applied Mathematics*, vol. 5, 1947, pp. 55–68.

3 C. Pai, "Some Applications of a Theory of Plates Which Includes the Effect of Transverse Shear Deformation," MS thesis submitted to Massachusetts Institute of Technology, 1946.

4 R. A. Hirsch, "The Effect of a Rigid Circular Inclusion on the Bending of a Thick Elastic Plate," JOURNAL OF APPLIED MECHANICS, vol. 19, TRANS. ASME, vol. 74, 1952, pp. 28–32.

5 M. Goland, "The Influence of the Shape and Rigidity of an Elastic Inclusion on the Transverse Flexure of Thin Plates," JOURNAL OF APPLIED MECHANICS, vol. 10, TRANS. ASME, vol. 65, 1943, p. A-69.

6 J. N. Goodier, "The Influence of Circular and Eliptical Holes on the Transverse Flexure of Elastic Plates," *Philosophical Magazine*, series 7, vol. 22, 1936, pp. 69–80.

7 P. M. Naghdi, "The Effect of Elliptic Holes on the Bending of Thick Plates," JOURNAL OF APPLIED MECHANICS, vol. 22, TRANS. ASME, vol. 77, 1955, pp. 89–94.

8 N. W. McLachlan, "Theory and Application of Mathieu Functions," Oxford University Press, Oxford, England, 1947, p. 369.

9 Yi-Yuan Yu, Discussion of the paper "On Bending of a Flat Slab Supported by Square-Shaped Columns and Clamped," by S. Woinowsky-Krieger, JOURNAL OF APPLIED MECHANICS, vol. 22, TRANS. ASME, vol. 77, 1955, p. 152.

10 J. C. Wiltse and M. J. King, "Values of Mathieu Function," Technical Report No. AF-53, prepared by the Johns Hopkins University Radiation Laboratory, 1958.

11 M. J. King and J. C. Wiltse, "Derivatives, Zeros, and Other Data Pertaining to Mathieu Functions," Technical Report No. AF-57, prepared by the Johns Hopkins University Radiation Laboratory, 1958.

12 British Association for the Advancement of Science, Mathematical Tables, vol. 6, "Bessel Functions," published for The Royal Society at the University Press, Cambridge, England, 1950.

13 Computational Laboratory of the National Bureau of Standards "Tables Relating to Mathieu Functions," Columbia University Press, New York, N. Y., 1951.

14 G. Blanch, "On the Computation of Mathieu Function," *Journal of Mathematics and Physics*, vol. 25, 1946, pp. 1–20.

15 G. Blanch and I. Rhodes, "Table of Characteristic Values of Mathieu's Equation for Large Values of the Parameter," reprinted from *Journal of the Washington Academy of Sciences*, vol. 45, 1955, pp. 167–196.

T. R. KANE[2]

Professor of Engineering Mechanics, Stanford University, Stanford, Calif. Mem. ASME

An Addition to the Theory of Whirling[1]

Particular solutions of the equations of motion of a heavy disk attached at the center of a light, vertical, elastic shaft are used to describe a variety of forms of whirling. The stability of these motions is analyzed by a perturbation method.

THE first attempt to deal rationally with "whirling" of shafts was made nearly one hundred years ago by Rankine [1].[3] Since that time numerous theoretical and experimental investigations have been undertaken to improve understanding of this phenomenon. However, in separate papers published as late as 1956, Newkirk [2], who had been concerned for many years with the related (or identical, depending on definitions) problems of "oil whip," and Pinkus [3], whose paper contains a table comparing various investigators' results, demonstrated clearly that complete insight had not yet been attained. Hori's [4] "Theory of Oil Whip," as well as Poritzky's comments on a paper by Hull [5] indicate that even more recently a considerable amount of further work remained to be done.

The present paper is intended to close what may be regarded as a gap in the development of the theory of whirling, in the following sense: Early investigations were confined to highly idealized systems and led to theories which, while eminently successful in shedding light on some aspects of the problem, left others completely unexplained. The determination of the lowest critical speed of a rotating shaft (see e.g., [6], page 34) is a case in point. It leads to a satisfactory description of two forms of whirling, but, as pointed out by Timoshenko [6], contains no information about a whirling motion during which the plane of the bent shaft rotates at the critical speed of the shaft while the shaft itself rotates at a higher speed. In later theories, such specific difficulties were removed through consideration of previously neglected physical effects, such as, in the case just mentioned, imperfections in the elastic properties of the shaft. It is natural that this development has been accompanied by controversy regarding the assumptions made by various authors, and has led, at times, to contradictory results.

In what follows, the trend to analyze systems of ever greater physical complexity is reversed. The simplest system capable of exhibiting whirling motions is again studied, the analysis differing from earlier ones in that *all* descriptions of whirling satisfying the relevant differential equations are extracted from these equations. This leads to results which are more diverse and display better agreement with observed motions than might be expected in view of the simplicity of the underlying assumptions. However, many questions still remain unanswered. Thus the paper is presented with a twofold purpose: To give detailed descriptions of certain whirling motions and to establish possible points of departure for further study of others.

Analysis

In Fig. 1, which shows two views of the system under consideration, OX, OY, OZ are mutually perpendicular fixed lines, with OZ vertical. C is the geometric center and G the mass center of a circular disk, these being separated by a distance e, the "eccentricity." r measures the "lateral displacement," that is, the distance from C to line OZ; p the angle between the X-Z plane and the plane determined by the deformed center line of the shaft S; and q the angle between lines CG and OC (extended).

For motions during which the disk remains parallel to the X-Y plane, the angular speed w of the disk is given by

$$w = \dot{p} + \dot{q} \tag{1}$$

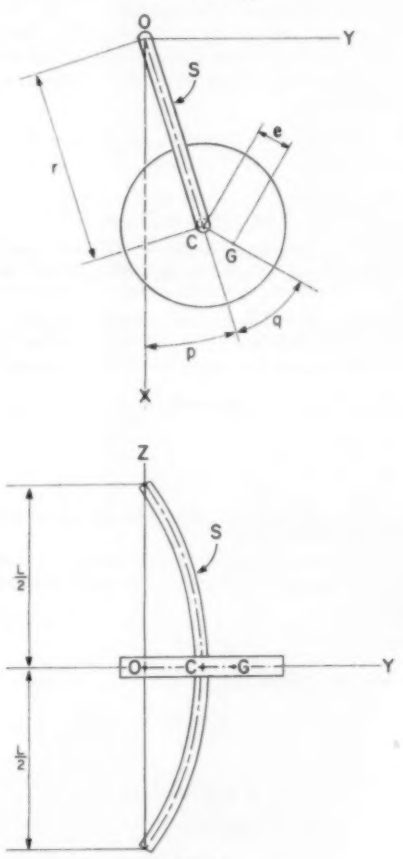

Fig. 1

[1] This paper was written while the author was a Visiting Lecturer at the College of Science and Technology, Manchester, England.

[2] Formerly, Associate Professor, University of Pennsylvania, Philadelphia, Pa.

[3] Numbers in brackets designate References at end of paper.

Presented at the West Coast Conference of the Applied Mechanics Division, Seattle, Wash., August 28–30, 1961, of THE AMERICAN SOCIETY OF MECHANICAL ENGINEERS.

Discussion of this paper should be addressed to the Editorial Department, ASME, United Engineering Center, 345 East 47th Street, New York 17, N. Y., and will be accepted until October 10, 1961. Discussion received after the closing date will be returned. Manuscript received by ASME Applied Mechanics Division, May 3, 1960. Paper No. 61—APMW-1.

and the velocity of G can be resolved into two components, parallel and perpendicular to line OC, whose magnitudes are

$$|\dot{r} - ew \sin q| \quad \text{and} \quad |r(w - \dot{q}) + ew \cos q|$$

Hence, if m is the mass and i the moment of inertia of the disk with respect to a line passing through G and parallel to OZ, the kinetic energy T of the disk is

$$T = \frac{1}{2} m\{[\dot{r} - ew \sin q]^2 + [r(w - \dot{q}) + ew \cos q]^2\} + \frac{1}{2} iw^2$$

Assume that the system of forces exerted on the disk by the shaft is equivalent to a "restoring" force, directed from C toward O and having a magnitude proportional to r, together with a couple whose moment about the Z-axis has a magnitude M. Then, if $\bar{w}$ denotes the circular frequency of free lateral vibrations (with $\dot{p} = \dot{q} = 0$), the restoring force has a magnitude $|m\bar{w}^2 r|$ (see reference [6], pages 34, 35) and the "generalized forces" F_p, F_q, F_r, associated with the "co-ordinates" p, q, r are

$$F_p = F_q = M, F_r = -m\bar{w}^2 r$$

Of the three Lagrange equations

$$\frac{d}{dt} \frac{\partial T}{\partial(\dot{p}, \dot{q}, \dot{r})} - \frac{\partial T}{\partial(p, q, r)} = F_p, F_q, F_r$$

governing all motions of the type under consideration, two (those for the co-ordinates p and q) involve M. One of these can therefore be used to eliminate M from the other. Furthermore, $\dot{p}$ can be eliminated from the remaining two by means of equation (1). For motions during which w remains constant, these two equations then become

$$\ddot{r} + [\bar{w}^2 - (w - \dot{q})^2]r - ew^2 \cos q = 0 \tag{2}$$

and

$$2\dot{r}(w - \dot{q}) - r\ddot{q} - ew^2 \sin q = 0 \tag{3}$$

(Once r and q have been found, either of the two Lagrange equations involving M can be used to find M such that w remains constant.)

From equation (3) it follows immediately that the "whirling speed" $\dot{p}$ cannot be permanently equal to zero unless the eccentricity e is equal to zero; for, equation (1) then becomes

$$\dot{q} = w \tag{4}$$

so that

$$q = wt + q_0$$

where q_0 is a constant, and this expression for q makes it impossible to satisfy equation (3).

One class of motions of special interest consists of those during which the whirling speed is equal to the angular speed of the disk; that is,

$$\dot{p} = w$$

in which case [see equation (1)]

$$\dot{q} = 0 \tag{5}$$

and

$$q = q_0, \text{ a constant} \tag{6}$$

Equations (2) and (3) then become

$$\ddot{r} + (\bar{w}^2 - w^2)r - ew^2 \cos q_0 = 0 \tag{7}$$

and

$$2\dot{r} - ew \sin q_0 = 0 \tag{8}$$

the second of which has the general solution

$$r = \frac{tew \sin q_0}{2} + r_0 \tag{9}$$

where r_0 is a constant, and substitution into equation (7) gives

$$tew(\bar{w}^2 - w^2) \sin q_0 + 2[(\bar{w}^2 - w^2)r_0 - ew^2 \cos q_0] = 0$$

which is satisfied for all values of t if and only if

$$(\bar{w}^2 - w^2) \sin q_0 = 0$$

and

$$(\bar{w}^2 - w^2)r_0 - ew^2 \cos q_0 = 0$$

The following possibilities thus present themselves: Either

$$\bar{w}^2 - w^2 = 0$$

and

$$q_0 = \pm \frac{\pi}{2}$$

or

$$q_0 = \frac{1 \pm 1}{2} \pi$$

while

$$(\bar{w}^2 - w^2)r_0 = \pm ew^2$$

In the first case, w has the "critical" value $\pm\bar{w}$ and the lateral deflection increases without limit, for, from equation (9),

$$r = \pm \frac{ew\bar{t}}{2} + r_0 \qquad \left(w = \pm\bar{w}, q = q_0 = \pm \frac{\pi}{2}\right) \tag{10}$$

In the second case, the lateral deflection remains constant, its magnitude depending on w:

$$r = \pm \frac{e}{1 - (\bar{w}/w)^2} \qquad \left(w \neq \bar{w}, q = q_0 = \frac{1 \pm 1}{2} \pi\right) \tag{11}$$

Equation (10) describes the well-known phenomenon of "resonance" and equation (11) the two most familiar forms of whirling.

Consider now the general case of whirling. This can be described by taking

$$\dot{q} = nw \tag{12}$$

where n is a constant, which, in view of equation (1), leads to whirling speeds

$$\dot{p} = (1 - n)w \tag{13}$$

As the motions associated with $n = 1$ and $n = 0$ have already been discussed [equations (4) and (5)], these values of n will be excluded from further consideration.

Integrate equation (12), and substitute into equations (2) and (3):

$$q = nwt + q_0 \tag{14}$$

$$\ddot{r} + [\bar{w}^2 - (1 - n)^2 w^2]r - ew^2 \cos(nwt + q_0) = 0 \tag{15}$$

$$2\dot{r}(1 - n) - ew \sin(nwt + q_0) = 0 \tag{16}$$

Equation (16) has the general solution

$$r = \frac{e}{2n(1-n)}\left[\cos q_0 - \cos\left(nwt + q_0\right)\right] + r_0 \qquad (17)$$

and substitution into equation (15) gives

$$\left[(1-2n)^2 - (\bar{w}/w)^2\right]\cos\left(nwt + q_0\right) = \frac{2n(1-n)}{e}\left[(1-n)^2 - (\bar{w}/w)^2\right]\left[r_0 + \frac{e\cos q_0}{2n(1-n)}\right]$$

which (excluding the cases $n = 0$ and $n = 1$) is satisfied for all values of t if and only if

$$(1-2n)^2 - (\bar{w}/w)^2 = 0$$

and

$$\left[(1-n)^2 - (\bar{w}/w)^2\right]\left[r_0 + \frac{e\cos q_0}{2n(1-n)}\right] = 0$$

From the first of these,

$$n = \tfrac{1}{2}\left(1 \pm \frac{\bar{w}}{w}\right) \qquad (18)$$

so that the second becomes

$$\left(1 \pm \frac{\bar{w}}{w}\right)\left(1 \mp 3\,\frac{\bar{w}}{w}\right)\left(r_0 + \frac{2e\cos q_0}{1 - \bar{w}^2/w^2}\right) = 0 \qquad (19)$$

which requires that either

$$\frac{\bar{w}}{w} = \pm\frac{1}{3} \qquad (20)$$

or

$$r_0 + \frac{2e\cos q_0}{1 - \bar{w}^2/w^2} = 0 \qquad (21)$$

or that equations (20) and (21) be satisfied simultaneously. In the first case it follows from equation (18) that

$$n = \tfrac{2}{3} \qquad (22)$$

and equations (13), (22), and (20) then lead to whirling speeds

$$\dot{p} = \pm\bar{w} \qquad (23)$$

while the lateral displacement, from equation (17), becomes

$$r = r_0 + \frac{9}{4}\,e[\cos q_0 - \cos\left(q_0 \pm 2\bar{w}t\right)] \qquad (24)$$

In the second case, the whirling speeds, obtained from equations (13) and (18), are

$$\dot{p} = \frac{w \pm \bar{w}}{2} \qquad (25)$$

and equations (17), (18), and (21) give for the associated lateral displacements

$$r = \frac{2ew^2}{\bar{w}^2 - w^2}\cos\left[q_0 + \tfrac{1}{2}(w \pm \bar{w})t\right] \qquad (26)$$

Finally, when equations (20) and (21) are satisfied simultaneously, the whirling speeds are again given by equation (23) and the lateral displacements become [equations (20) and (26)]

$$r = -\frac{9e}{4}\cos\left(q_0 \pm 2\bar{w}t\right) \qquad (27)$$

These results are summarized in Table 1. Note that they include whirling motions accompanied by lateral vibrations, whirling speeds below, above, and equal to either the critical speed ($\bar{w}$) or the angular speed (w), and motions during which the plane of the deformed shaft center line rotates in a sense opposite to that of the angular velocity of the disk, a phenomenon associated by Stodola [7] with gyroscopic effects.

As will be shown presently, not of all of the motions described in Table 1 are stable in the sense that they persist in essentially unaltered form subsequent to temporary action of small disturbing forces. This explains why certain forms of whirling occur frequently and others only under very special circumstances.

Let r_i and q_i, $i = 1, 2, \ldots, 5$, be pairs of functions which satisfy equations (2) and (3); r_i^* and q_i^*, $i = 1, 2, \ldots, 5$, "small" functions of time, such that r and q, given by

$$r = r_i + r_i^* \qquad (28)$$

and

$$q = q_i + q_i^* \qquad (29)$$

satisfy equations (2) and (3) to the first order of small quantities. Then, substituting from equations (28) and (29) into equations (2) and (3), dropping all terms of second or higher degree in starred quantities, and replacing w with w_i, the following equations, governing the "perturbations" r_i^* and q_i^*, are obtained:

$$\ddot{r}_i^* + (\bar{w}^2 - u_i^2)r_i^* + 2u_i\sigma_i\dot{q}_i^* + q_i^* e w_i^2 \sin q_i = 0 \qquad (30)$$

and

$$2u_i\dot{r}_i^* - 2\dot{r}_i\dot{q}_i^* - r_i\ddot{q}_i^* - r_i^*\ddot{q}_i - q_i^* e w_i^2\cos q_i = 0 \qquad (31)$$

where u_i is defined as

$$u_i = w_i - \dot{q}_i \qquad (32)$$

This pair of simultaneous equations (with variable coefficients,

Table 1 Description of whirling motions

i	Whirling speed ($\dot{p}$)	Lateral displacement (r)	Disk speed (w)	Initial valve of q (q_0)	References (equation numbers)
1	$w(=\pm\bar{w})$	$\pm\dfrac{e\bar{w}t}{2} + r_0$	$\pm\bar{w}$	$\pm\dfrac{\pi}{2}$	(10)
2	$w(\neq\pm\bar{w})$	$\dfrac{\pm ew^2}{w^2 - \bar{w}^2}$	$\neq\bar{w}$	$\dfrac{1\pm 1}{2}\,\pi$	(11)
3	$\pm\bar{w}\left(=\dfrac{w}{3}\right)$	$r_0 + \frac{9}{4}\,e[\cos q_0 - \cos\left(q_0 \pm 2\bar{w}t\right)]$	$\pm 3\bar{w}$	Unrestricted	(20, 23, 24)
4	$\dfrac{w \mp \bar{w}}{2}$	$\dfrac{2ew^2}{\bar{w}^2 - w^2}\cos[q_0 + \frac{1}{2}(w \pm \bar{w})t]$	$\neq\pm\bar{w}$	$\arccos\dfrac{r_0(\bar{w}^2 - w^2)}{2ew^2}$	(21, 25, 26)
5	$\pm\bar{w}\left(=\dfrac{w}{3}\right)$	$-\frac{9}{4}\,e\cos\left(q_0 \pm 2\bar{w}t\right)$	$\pm 3\bar{w}$	$\arccos\left(-4r_0/9e\right)$	(20, 21, 23, 27)

because r_i and q_i are functions of time) may be brought into more tractable form by noting that, from equations (2), (3), and (32),

$$ew_i^2 \cos q_i = \ddot{r}_i + (\bar{w}^2 - u_i^2)r_i$$

and

$$ew_i^2 \sin q_i = 2u_i\dot{r}_i - r_i\dot{q}_i$$

which, after defining f_i^* as

$$f_i^* = q_i^* r_i \tag{33}$$

permits one to replace equations (30) and (31) with

$$\ddot{r}_i^* + (\bar{w}^2 - u_i^2)r_i^* + 2u_i\dot{f}_i^* - \dot{q}_i f_i^* = 0$$

and

$$\dot{f}_i^* + (\bar{w}^2 - u_i^2)f_i^* - 2u_i\dot{r}_i^* + \dot{q}_i r_i^* = 0$$

Furthermore, as $\dot{q}_i$ is a constant for all motions under consideration, the perturbations r_i^* and f_i^* are then seen to be governed by the following equations with constant coefficients [see equation (32)]:

$$\ddot{r}_i^* + (\bar{w}^2 - u_i^2)r_i^* + 2u_i\dot{f}_i^* = 0$$

and

$$\dot{f}_i^* + (\bar{w}^2 - u_i^2)f_i^* - 2u_i\dot{r}_i^* = 0$$

The general solution of these is

$$r_i^* = A_i \sin(\bar{w} + u_i)t + B_i \cos(\bar{w} + u_i)t + C_i \sin(\bar{w} - u_i)t + D_i \cos(\bar{w} - u_i)t \tag{34}$$

$$f_i^* = B_i \sin(\bar{w} + u_i)t - A_i \cos(\bar{w} + u_i)t - D_i \sin(\bar{w} - u_i)t + C_i \cos(\bar{w} - u_i)t \tag{35}$$

where $A_i, B_i, C_i, D_i, i = 1, 2, \ldots, 5$, are constants whose values depend on the disturbance to which the system is subjected when performing the motion described by a pair of functions r_i and q_i.

Equations (32–35) yield the following information about the stability of the motions listed in Table 1:

With $i = 1$, there are two possibilities. From equation (5), $\bar{w} + u_i$ and $\bar{w} - u_i$ become either

$$\bar{w} + u_1 = 2\bar{w} \quad \text{and} \quad \bar{w} - u_1 = 0$$

or

$$\bar{w} + u_1 = 0 \quad \text{and} \quad \bar{w} - u_1 = 2\bar{w}$$

The perturbation r_1^* is thus given by an expression of the form

$$r_1^* = A \sin 2\bar{w}t + B \cos 2\bar{w}t + D$$

in either case, and the corresponding perturbation q_1^* by one of two expressions,

$$q_1^* = \frac{f_1^*}{r_1} = \frac{B \sin 2\bar{w}t - A \cos 2\bar{w}t + C}{\frac{e\bar{w}t}{2} \pm r_0}$$

This shows that the motion in question is stable as regards the lateral displacement (r) and may be either stable or unstable as regards the whirling speed ($\dot{p}$), depending on the value of r_0. It must be stressed that the phrase "stable as regards the lateral displacement" is *not* synonymous with "a stable motion of the disk." As the lateral deflection increases without limit, the motion of the disk is, of course, highly unstable. What may be inferred, and this is of practical interest, is that this unstable motion cannot be readily arrested or even altered.

With $i = 2$, $\bar{w} + u_i$ and $\bar{w} - u_i$ take on the values

$$\bar{w} + u_2 = \bar{w} + w \quad \text{and} \quad \bar{w} - u_2 = \bar{w} - w$$

and the perturbations r_2^* and q_2^* become

$$r_2^* = A_2 \sin(\bar{w} + w)t + B_2 \cos(\bar{w} + w)t + C_2 \sin(\bar{w} - w)t + D_2 \cos(\bar{w} - w)t$$

and

$$q_2^* = \pm \frac{w^2 - \bar{w}^2}{ew^2} \begin{bmatrix} B_2 \sin(\bar{w} + w)t - A_2 \cos(\bar{w} + w)t \\ -D_2 \sin(\bar{w} - w)t + C_2 \cos(\bar{w} - w)t \end{bmatrix}$$

from which it can be seen that line 2 of Table 1 describes two thoroughly stable motions.

With $i = 3$, it is again necessary to consider two possibilities. Either

$$\bar{w} + u_3 = 2\bar{w} \quad \text{and} \quad \bar{w} - u_3 = 0$$

or

$$\bar{w} + u_3 = 0 \quad \text{and} \quad \bar{w} - u_3 = 2\bar{w}$$

Consequently

$$r_3^* = A \sin 2\bar{w}t + B \cos 2\bar{w}t + D$$

and

$$q_3^* = \pm \frac{B \sin 2\bar{w}t - A \cos 2\bar{w}t + C}{r_0 + \frac{9}{4} e[\cos q_0 - \cos(q_0 \pm 2\bar{w}t)]}$$

which shows that the two motions corresponding to line 3 of Table 1 are stable as regards r and either stable or unstable as regards $\dot{p}$, according as $|r_0 + (9/4)e \cos q_0|$ is greater or smaller than $(9/4)e$. As the requirements for stability can thus be fulfilled in a variety of ways, these motions may be expected to occur in practice. Note that the relationship between the whirling speed and the angular speed of the disk (which, for a shaft possessing sufficient torsional rigidity, is equal to the "shaft speed") is here precisely that mentioned in the introductory statement; also, that increased stability (that is, $|r_0 + (9/4)e \cos q_0|$ large in comparison with $(9/4)e$) is accompanied by diminished relative importance of the time-dependent portion in the expression for r, equation (24), so that, when this motion is observed experimentally, the lateral deflection may be expected to remain very nearly constant.

Proceeding as in the foregoing, one finds that lines 4 and 5 of Table 1 describe motions which are stable as regards r, unstable as regards $\dot{p}$. Accordingly, it is concluded that two whirling speeds play a predominant role: w and $\bar{w}$.

References

1 W. J. Macquorn Rankine, "On the Centrifugal Force of Rotating Shafts," *The Engineer*, vol. 28, 1869, p. 249.

2 B. L. Newkirk, "Varieties of Shaft Disturbances Due to Fluid Films in Journal Bearings," TRANS. ASME, vol. 78, 1956, pp. 985–988.

3 Oscar Pinkus, "Experimental Investigation of Resonant Whip," TRANS. ASME, vol. 78, 1956, pp. 975–983.

4 Yukio Hori, "A Theory of Oil Whip," JOURNAL OF APPLIED MECHANICS, vol. 26, TRANS. ASME, vol. 81, Series E, 1959, pp. 189–198.

5 E. H. Hull, "Oil-Whip Resonance," TRANS. ASME, vol. 80, 1958, pp. 1490–1496.

6 S. Timoshenko, "Vibration Problems in Engineering," D. Van Nostrand Company, Inc., New York, N. Y., 1955, p. 227.

7 A. Stodola, "Steam and Gas Turbines," vol. 1, McGraw-Hill Book Company, Inc., New York, N. Y., 1927, p. 431.

Bending of a Cantilever Plate Supported From an Elastic Half Space[1]

N. C. SMALL[2]
Associate Professor,
Department of Mechanical Engineering,
University of Pittsburgh,
Pittsburgh, Pa.
Assoc. Mem. ASME

A solution is obtained for an infinitely long cantilever plate supported from an elastic half space. The junction conditions between the elasticity approach for the half space and the classical plate theory (no-shear) approach for the plate are based upon the use of assumed equilibrium surface tractions for the half space. The formal Fourier integral results for the example of a concentrated free-edge load are evaluated using an IBM 704 computer. The correlation with the deflection results of a steel model test is shown to be very good. The small deviations from the theoretical values are primarily due to shear effects in the model. It is also shown that, except for very stubby plates, it is sufficiently accurate to neglect the shear effects along the half space, and to assume that the rotation is proportional to the moment in the conventional "Winkler" sense.

1 Introduction

A HELICAL gear tooth is often represented, for purposes of analysis, as a long cantilever plate. This is clearly a broad idealization as is indicated by deflection measurements on actual gear teeth which show that this theory gives results which are low by about a factor of 2. It was suspected that a large part of this discrepancy could be accounted for by considering the flexibility of the gear body. The author was thus led to replacing the perfectly clamped classical edge conditions in the cantilever plate theory by the restraint offered by an elastic half space. In the present work an approximate analytical solution is obtained for this more realistic edge condition for arbitrary transverse loading by replacing the actual half-space surface stresses by an assumed equilibrium distribution. Classical thin-plate theory (no shear effects) is employed, and the formal Fourier integral results for the example of a concentrated transverse free edge load are evaluated using an IBM 704 computer. For this particular loading, an experiment was carried out using a steel model, and the test results are compared with corresponding values from the present theory.

Before embarking on the solution of the actual plate problem, we consider in the next section the definition of a suitable average rotation and displacement for the half space corresponding to assumed distributions of surface tractions. In Section 3 these generalized displacements are represented explicitly in integral form for subsequent matching with the corresponding plate quantities along the "clamped" edge. The plate problem is formulated and formally solved in Section 4 in terms of Fourier integrals. Section 5 deals with the numerical example of a concentrated free edge load, and the corresponding experimental work for a steel model is described in Section 6. The theoretical and test results are compared and discussed in Section 7, followed in the Appendix by consideration of some of the more lengthy theoretical details.

The transverse bending of an infinitely long, thin cantilever plate of finite width with one long edge *perfectly* clamped has been considered by several investigators. The case of a concentrated

[1] This paper is based upon a thesis presented by the author to Brown University, Providence, R. I., in partial fulfillment of the requirements for the degree of Doctor of Philosophy.

[2] Formerly, Research Engineer, Westinghouse Research Laboratories, Pittsburgh, Pa.

Presented at the Summer Conference of the Applied Mechanics Division, Chicago, Ill., June 14–16, 1961, of THE AMERICAN SOCIETY OF MECHANICAL ENGINEERS.

Discussion of this paper should be addressed to the Editorial Department, ASME, United Engineering Center, 345 East 47th Street, New York 17, N. Y., and will be accepted until October 10, 1961. Discussion received after the closing date will be returned. Manuscript received by ASME Applied Mechanics Division, May 27, 1960. Paper No. 61—APM-11.

Nomenclature

The subscript c is used for results associated with the perfectly clamped plate while the subscript f is used to indicate additional contributions due to the elasticity of the half space only. Total values, i.e., the sum of the f and c quantities, are shown with the subscript t.

a = plate width (Fig. 3)
$\bar{a}$ = a/h_0
b_0 = $h_0/2$ (Fig. 1)
D = $\dfrac{Eh^3}{12(1-\nu^2)}$
D_0 = $\dfrac{E_0h_0^3}{12(1-\nu_0^2)}$
E_0 = Young's modulus for half space
E = Young's modulus for plate
h_0 = plate thickness along clamped edge only (Fig. 1) (could include effect of fillets)
h = plate thickness
ln = natural logarithm
M = bending moment, per unit of length y
P = concentrated transverse edge load (Fig. 3)
q = transverse surface loading per unit of plate area (Fig. 3)
V = total shearing force, per unit of length y
w = lateral plate deflection (Fig. 3)
W_0 = average deflection of half space
x, y = co-ordinates of points in mid plane of plate (Fig. 3)
$\bar{x} = x/h_0$, $\bar{y} = y/h_0$ } dimensionless plate co-ordinates
Θ_0 = average rotation of half space
σ = normal (bending) stress on half space (Fig. 1)
τ = shear stress on half space (Fig. 2)
ν_0 = Poisson's ratio for half space
ν = Poisson's ratio for plate
$\nabla^4 = \dfrac{\partial^4}{\partial x^4} + \dfrac{2\partial^4}{\partial x^2\partial y^2} + \dfrac{\partial^4}{\partial y^4}$
η, ζ = dummy variables in the y and z-directions (Figs. 1, 2)
$\xi = y - \eta$

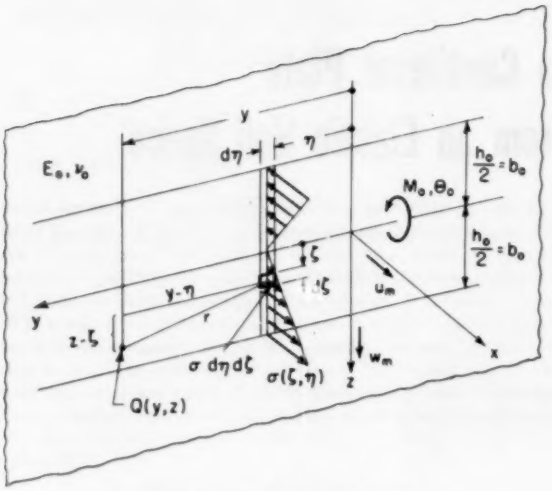

Fig. 1 Moment loading of half space

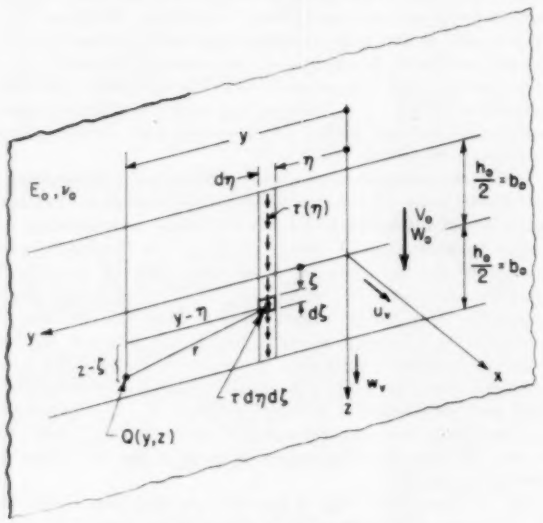

Fig. 2 Shear loading of half space

edge load was initially solved by MacGregor [1][a] in terms of Fourier integrals which were evaluated numerically. Holl [2] considered the same problem for a plate of finite length and obtained approximate results by using finite-difference techniques. In the course of a more general Fourier-integral analysis of infinite strips with various edge conditions, Hopkins [3] recalculated MacGregor's results (for a Poisson's ratio of $\nu = 0.25$) and included the computation of the transverse shear along the clamped edge. Jaramillo [4] considered the more general problem of a concentrated transverse load at any location on the plate surface. His results were obtained by using contour integration to evaluate the necessary Fourier integrals. All of the foregoing analyses apply to the case of a plate of uniform thickness. A special case of the variable-thickness problem has been treated by Conway [5] for harmonic edge loading.

In the present problem a thin plate is considered which has a constant thickness h and is infinitely long with a finite width a, Fig. 3. The plate carries arbitrary transverse loading and is supported along the clamped edge by an elastic half space. Both

[a] Numbers in brackets designate References at end of paper.

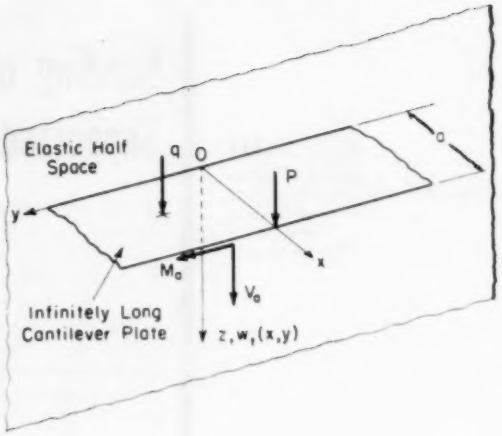

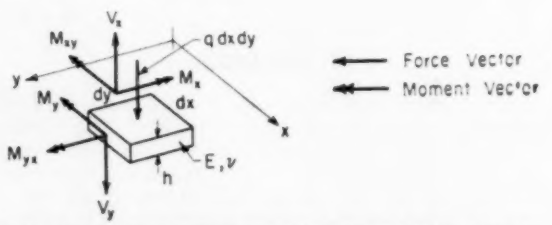

Fig. 3 Long cantilever plate supported from elastic half space showing sign convention for stress resultants

the displacement and rotational flexibility of this half space are considered. The present treatment differs from the usual Winkler type of elastic support in that mutual coupling effects are considered between the deformations at adjacent points along the half-space. The solution is approximate in that point wise compatibility across the plate thickness is neglected along the clamped edge. In its place, in the spirit of thin-plate theory, we consider only the compatibility of suitably defined average rotations and displacements. In the calculation of these latter quantities it is assumed for the half space that the normal (bending) stress σ varies linearly over the plate thickness, Fig. 1, and the shear stress is taken to be constant, Fig. 2. The formal Fourier integral results for the present flexible problem are presented in terms of the corresponding perfectly clamped solution.

2 Rotation and Displacement of Half Space

In formulating the boundary conditions for the classical plate problem the slope and deflection along the clamped edge must be matched with the same quantities for the half space. Since we intend to use elasticity theory for the half space and classical plate theory for the plate, it is necessary to define an appropriate average rotation Θ_0 and displacement W_0. It is reasonable to define these quantities so that the surface work E_s corresponding to the assumed stress distributions, per unit of length y, may be represented in the form

$$2E_s = M_0\Theta_0 + V_0W_0 \tag{1}$$

where M_0 and V_0 are the bending moment and shearing force, Figs. 1, 2. The actual work of the surface tractions depends to some extent on their (unknown) distribution across the thickness h_0. However, for realistic stress distributions it is reasonable to expect that this dependence will be weak. In order to check this point, an analysis was made of an analogous plane problem with a resultant moment M_0 (only) applied to the edge. Several dif-

ferent stress distributions were considered, and it was shown that the value of E_s for the linear distribution of normal stress $\sigma = 6M_0\rho/h_0^2$ was only 8 per cent higher than for the more realistic cubic distribution $\sigma = 10M_0\rho^3/h_0^2$, where $\rho = 2z/h_0$.

Thus the definition of Θ_0 and W_0 in (1) is by no means unique, but it does appear to be relatively insensitive to the assumed stress distributions. In addition, this type of definition satisfies the physical requirement that no net work be done at the clamped edge of the attached plate, and, as we shall see later, allows the use of reciprocity relations among the influence functions for the half space. A further advantage is the possibility of discussing the results in terms of the minimum complementary energy theorem. A consistent equilibrium solution for the moment and shear forces in the plate and stresses in the half space gives an upper bound on the deflection under a single concentrated load. In classical thin-plate theory the contribution of shear to deflection is ignored. The upper bound which is obtained with this idealization is, therefore, not truly an upper bound on the maximum deflection of the real plate. This question will be returned to later in a discussion of the final results (Fig. 6).

In an attempt to be somewhat consistent with thin-plate theory while retaining as much simplicity as possible, the normal stress σ is thus assumed to vary linearly, Fig. 1, over the thickness h_0 while the shear stress τ is taken to be constant, Fig. 2. Classical plate theory (which neglects shear) does not prescribe the distribution of shear stress. A parabolic distribution of this stress seems quite unrealistic at the clamped edge because of the restraint of the half space which limits the required warping of the cross section.

Θ_0 and W_0 are now determined by using equation (1). The surface work E_s is given by

$$2E_s = \int_{-b_0}^{b_0} \sigma(u_m + u_v)dz + \int_{-b_0}^{b_0} \tau(w_m + w_v)dz \qquad (2)$$

where u_m, w_m are the x and z-displacements due to the moment distribution M_0, and u_v, w_v are the correspondng displacement components for the shearing force V_0, Figs. 1, 2. The values of u_m and w_m are determined by using the classical Boussinesq result [6] for the displacements at an arbitrary point $Q(y, z)$, due to a concentrated normal load $\sigma\, d\eta\, d\zeta$ located at the point η, ζ, Fig. 1. Introducing the resultant moment M_0 and integrating the resulting Boussinesq expression first on ζ and then on η we obtain

$$u_m(y, z) = \frac{1}{\pi D_0}\int_{-\infty}^{\infty} f_{um}(y - \eta, z)M_0(\eta)d\eta \qquad (3)$$

$$w_m(y, z) = \frac{1 - 2\nu_0}{2\pi D_0(1 - \nu_0)}\int_{-\infty}^{\infty} f_{wm}(y - \eta, z)M_0(\eta)d\eta \qquad (4)$$

The Cerutti solution [7] for the shear force $\tau\, d\eta\, d\zeta$ is used in the same manner to obtain u_v and w_v, Fig. 2. The results are

$$u_v(y, z) = \frac{-(1 - 2\nu_0)(1 + \nu_0)}{2\pi E_0 h_0}\int_{-\infty}^{\infty} f_{uv}(y - \eta, z)V_0(\eta)d\eta \qquad (5)$$

$$w_v(y, z) = \frac{1 + \nu_0}{\pi E_0 h_0}\int_{-\infty}^{\infty} f_{wv}(y - \eta, z)V_0(\eta)d\eta \qquad (6)$$

The influence functions f_{um}, f_{wm}, f_{uv}, f_{wv} are obtained from the first integration on ζ by the use of elementary quadrature formulas (see Appendix). Now substitute $\sigma = 12M_0z/h_0^3$ and $\tau = V_0/h_0$ together with equations (3) to (6) into equation (2). After interchanging the order of the integration the result may be put in the form of equation (1), if Θ_0 and W_0 are taken as

$$\Theta_0 = \Theta_v + \Theta_m \qquad (7)$$

$$W_0 = W_v + W_m \qquad (8)$$

where

$$\Theta_m(y) = \int_{-\infty}^{\infty} G_{\theta m}(y - \eta)M_0(\eta)d\eta \qquad (9)$$

$$\Theta_v(y) = \int_{-\infty}^{\infty} G_{\theta v}(y - \eta)V_0(\eta)d\eta \qquad (10)$$

$$W_m(y) = \int_{-\infty}^{\infty} G_{wm}(y - \eta)M_0(\eta)d\eta \qquad (11)$$

$$W_v(y) = \int_{-\infty}^{\infty} G_{wv}(y - \eta)V_0(\eta)d\eta \qquad (12)$$

The influence functions G are obtained by integrating the f-functions of equations (3) to (6) with respect to z (see Appendix). It can be shown by the use of Maxwell's reciprocal theorem that $G_{wm} = G_{\theta v}$, which is henceforth denoted by the single symbol G_0. Further, this reciprocity relation is not peculiar to the particular stress distributions assumed, but is a consequence of the definitions following from equation (1).

3 Integral Representations for M_0, V_0, Θ_0, W_0

In order to satisfy the junction conditions along the clamped edge of the plate it is necessary to obtain explicit integral forms for M_0 and V_0. To accomplish this the integral equations (9) to (12) must be inverted. This would be a very formidable process were it not for the fact that all of the kernels ($G_{\theta m}$, and so on) in these equations are of the Wiener-Hopf type, i.e., functions of only $(y - \eta)$. Using this fact we proceed as follows [8]: The complex Fourier transform of $\Theta_m(y)$ is

$$\phi_m(\lambda) = \frac{1}{2\pi}\int_{-\infty}^{\infty} \Theta_m(y)e^{-iy\lambda}dy$$

After substitution of equation (9), this expression may be put in the form

$$\phi_m = \frac{1}{2\pi}\int_{-\infty}^{\infty} M_0(\eta)e^{-i\lambda\eta}d\eta \int_{-\infty}^{\infty} G_{\theta m}(\xi)e^{-i\lambda\xi}d\xi \qquad (13)$$

where $\xi = y - \eta$. With the definition

$$g_{\theta m}(\lambda) = \frac{1}{2\pi}\int_{-\infty}^{\infty} G_{\theta m}(\xi)e^{-i\lambda\xi}d\xi \qquad (14)$$

we may write

$$\int_{-\infty}^{\infty} M_0(\eta)e^{-i\lambda\eta}d\eta = \frac{\phi_m}{g_{\theta m}}$$

Using the inversion theorem for Fourier integrals [8] and replacing the dummy variable η by y, we obtain

$$M_0(y) = \frac{1}{2\pi}\int_{-\infty}^{\infty} \frac{\phi_m}{g_{\theta m}}\, e^{i\lambda y}d\lambda \qquad (15)$$

The remaining equations (10) to (12) are used in the same manner to give

$$V_0(y) = \frac{1}{2\pi}\int_{-\infty}^{\infty} \frac{\phi_v}{g_0}\, e^{i\lambda y}d\lambda \qquad (16)$$

$$M_0(y) = \frac{1}{2\pi}\int_{-\infty}^{\infty} \frac{\bar{\omega}_m}{g_0}\, e^{iy\lambda}d\lambda \qquad (17)$$

$$V_0(y) = \frac{1}{2\pi}\int_{-\infty}^{\infty} \frac{\bar{\omega}_v}{g_{wv}}\, e^{iy\lambda}d\lambda \qquad (18)$$

where ϕ_v, $\bar{\omega}_m$, and $\bar{\omega}_v$ are the complex Fourier transforms of Θ_v, W_m, and W_v respectively, and

$$g_0(\lambda) = \frac{1}{2\pi}\int_{-\infty}^{\infty} G_0(\xi)e^{-i\lambda\xi}d\xi \qquad (19)$$

$$g_{wv}(\lambda) = \frac{1}{2\pi}\int_{-\infty}^{\infty} G_{wv}(\xi)e^{-i\lambda\xi}d\xi \tag{20}$$

The corresponding integral expressions for V_0 and M_0 are now equated to give

$$\phi_v = \frac{\tilde{\omega}_v g_0}{g_{wv}} \tag{21}$$

$$\tilde{\omega}_m = \frac{\phi_m g_0}{g_{\theta m}} \tag{22}$$

Invert the Fourier transforms ϕ_m, ϕ_v, $\tilde{\omega}_m$, and $\tilde{\omega}_v$ and eliminate ϕ_v and $\tilde{\omega}_m$ by use of equations (21) and (22). Equations (7) and (8) are now used to give

$$\Theta_0(y) = \int_{-\infty}^{\infty}\left[\phi_m + \frac{\tilde{\omega}_v g_0}{g_{wv}}\right]e^{i\lambda y}d\lambda \tag{23}$$

$$W_0(y) = \int_{-\infty}^{\infty}\left[\tilde{\omega}_v + \frac{\phi_m g_0}{g_{\theta m}}\right]e^{i\lambda y}d\lambda \tag{24}$$

Thus the four junction quantities M_0, V_0, Θ_0, and W_0 are expressed explicitly by equations (15), (18), (23), and (24) in terms of only two unknown functions, ϕ_m and $\tilde{\omega}_v$.

4 Formulation and Solution of Plate Problem

We pass now to the formulation of the boundary-value problem for the plate, Fig. 3. The deflected surface of the plate w_t satisfies the well-known equation

$$\nabla^4 w_t(x, y) = q/D \tag{25}$$

for $0 \leq x \leq a$, and all y. For convenience we take w_t in the form

$$w_t = w_c + w_f \tag{26}$$

where w_c is the particular solution of equation (25) which corresponds to the given loading and a *perfectly* clamped edge at $x = 0$; w_f is the additional deflection due to the flexibility of the elastic half space. Thus w_c satisfies equation (25) together with the following boundary conditions for all y:

$$w_c = \frac{\partial w_c}{\partial x} = 0; \quad x = 0 \tag{27}$$

$$\left.\begin{aligned}\frac{\partial^2 w_c}{\partial x^2} + \nu\frac{\partial^2 w_c}{\partial y^2} &= -\frac{M_a(y)}{D}\\ \frac{\partial^3 w_c}{\partial x^3} + (2-\nu)\frac{\partial^3 w_c}{\partial x\,\partial y^2} &= -\frac{V_a}{D}\end{aligned}\right\} \quad x = a \tag{28}$$

where M_a and V_a are the prescribed edge moment and shear force, respectively; w_f satisfies the biharmonic equation

$$\nabla^4 w_f = 0 \tag{29}$$

over the surface of the plate and the following free edge conditions for all y:

$$\left.\begin{aligned}\frac{\partial^2 w_f}{\partial x^2} + \nu\frac{\partial^2 w_f}{\partial y^2} &= 0\\ \frac{\partial^3 w_f}{\partial x^3} + (2-\nu)\frac{\partial^3 w_f}{\partial x\,\partial y^2} &= 0\end{aligned}\right\} \quad x = a \tag{30}$$

Along the flexibly supported edge, $x = 0$, the total deflection w_t must satisfy the junction conditions below for all y:

$$\left.\begin{aligned}M_x &= M_0\\ V_x &= V_0\\ \frac{\partial w_t}{\partial x} &= -\Theta_0\\ w_t &= W_0\end{aligned}\right\} \quad x = 0 \tag{31}$$

where

$$\begin{aligned}M_x = M_t &= -D\left[\frac{\partial^2 w_t}{\partial x^2} + \nu\frac{\partial^2 w_t}{\partial y^2}\right]_{x=0}\\ V_x = V_t &= -D\left[\frac{\partial^3 w}{\partial x^3} + (2-\nu)\frac{\partial^3 w_t}{\partial x\,\partial y^2}\right]_{x=0}\end{aligned} \tag{32}$$

Thus $w_t = w_a + w_f$ is the required solution since it satisfies equation (25) together with the conditions (28) and (31).

The determination of w_c is a solved problem for certain types of loading (see Introduction). In any case, it may always be considered separately since it does not contain any effects of the elastic half space. Thus we assume that w_c is known, and that the corresponding total shearing force V_c and bending moment M_c along the clamped edge, $x = 0$, may be expressed in Fourier-integral form as follows:

$$\begin{aligned}M_c(y) &= \int_{-\infty}^{\infty} m_c(\lambda)e^{i y\lambda}d\lambda\\ V_c(y) &= \int_{-\infty}^{\infty} v_c(\lambda)e^{i y\lambda}d\lambda\end{aligned} \tag{33}$$

The quantities M_c and V_c are defined by equations (32), with the subscript c in place of t. The analogous notation M_f and V_f is used to denote the change in the clamped edge moment and total shear force produced by the elastic half space.

The additional deflection w_f satisfies the biharmonic equation (29); hence it may be taken in the general Fourier-integral form

$$w_f(x, y) = \int_{-\infty}^{\infty}\{(\alpha_f + x\lambda\beta_f)C + (\gamma_f + x\lambda\delta_f)S\}e^{i y\lambda}d\lambda \tag{34}$$

where α_f, β_f, γ_f, and δ_f are arbitrary functions of λ; $S = \sinh\lambda x$ and $C = \cosh\lambda x$. Formally substitute equations (23), (24), (26), and (34) into the boundary conditions (30) and (31); use the definitions of M_c and V_c as well as equations (33). The resulting six linear algebraic equations determine the six functions α_f, β_f, γ_f, δ_f, ϕ_m, and $\tilde{\omega}_v$. (Note that the last two functions do not enter explicitly in the solution.) These equations were solved by successive elimination of the variables, but the algebra is too lengthy to be included here.

Thus the formal solution for w_f (and hence w_t) is complete in terms of the assumed known perfectly clamped result w_c and the associated transform functions m_c and v_c. The integration indicated in equation (34) was carried out numerically for the example described in the following text.

5 Numerical Example: Concentrated Edge Load

As an illustration of the present theory we consider the case of a concentrated transverse load P located on the edge at $x = a$, $y = 0$, Fig. 3. The perfectly clamped version of this problem was first solved by MacGregor [1] using a method similar to that described previously. His results are in the desired Fourier integral form, and it is an easy task to identify the functions m_c and v_c in equations (33). The results are

$$m_c(\lambda) = -\left[\frac{P}{\pi\lambda}\right]\frac{(1+\nu)\sinh\lambda a + (1-\nu)\lambda a\cosh\lambda a}{4\cosh^2\lambda a + (1-\nu)^2\lambda^2 a^2 - (1+\nu)^2\sinh^2\lambda a} \tag{35}$$

$$v_c(\lambda) = \left[\frac{P}{\pi}\right]\frac{2\cosh\lambda a + (1-\nu)\lambda a\sinh\lambda a}{4\cosh^2\lambda a + (1-\nu)^2\lambda^2 a^2 - (1+\nu)^2\sinh^2\lambda a} \tag{36}$$

The central numerical problem is clearly the evaluation of Fourier integrals. Because the G-functions are all even, and the applied load is symmetrical, these integrals all reduce to real cosine form. The g-functions have the general form

$$g(\kappa) = \int_0^\infty G(p) \cos \kappa p \, dp \tag{37}$$

while expressions like

$$w(\bar{x}, \bar{y}) = \int_0^\infty R[\bar{x}, \bar{a}, \kappa, g(\kappa)] \cos \kappa \bar{y} \, d\kappa \tag{38}$$

are obtained for the final deflection, moment, and so on. For convenience, the symbols $\kappa = \lambda h_0$ and $p = \xi/h_0$ were introduced together with $\bar{x} = x/h_0$, $\bar{y} = y/h_0$, and $\bar{a} = a/h_0$. Although contour integration techniques could have been employed it was more expedient to resort to numerical methods in view of the availability of a high-speed digital computing facility. Thus all of the computations were carried out on an IBM 704 computer. In some instances the integrands contained logarithmic singularities at the origin. Hence, in each case the total range of integration was divided into at least two, and where necessary three, intervals, say: $0 \leq p \leq \lambda_1$, $\lambda_1 \leq p \leq \lambda_2$, and $\lambda_2 \leq p$ for the g-functions. The values λ_1 and λ_2 were chosen so that over the lower and upper ranges the integrands could be approximated with sufficient accuracy and integrated exactly by elementary means. For the final integrals (38) the lower end of the upper range, say κ_2, was chosen sufficiently large that the integration from κ_2 to infinity could be neglected. The major portion of the integration over the intermediate range [for both forms (37) and (38)] was then carried out numerically using a modified version of Simpson's rule due to Filon [9]. The general approach was first to determine the necessary extent of the intermediate integration interval, $\kappa_1 \leq \kappa \leq \kappa_2$, in the final forms (38) by means of trial machine calculations. The g-functions were then calculated at 200 equally spaced points in this interval, and used as required (without the need for interpolation) in the calculation of the final integrand functions R.

The results for the corresponding perfectly clamped case were also calculated, primarily as a check against Jaramillo's values [4]. Agreement with the present calculations was obtained to within about 2 in the fourth significant figure.[4] The computational errors resulting from numerical integration, "truncation" [neglecting the integration from κ_2 to infinity in the forms (38)], and the use of approximate integrands were carefully considered. Because of the large number of cases involved it is difficult to make a blanket statement concerning error. However, on the basis of several cases which were checked carefully, the over-all computational error in the final results for w_f, M_f, V_f, and Θ_0 is estimated to be less than 0.25 per cent.

[4] In the vicinity of the load this agreement dropped to 3 figures due to the present larger truncation error of about 1 per cent for this case.

6 Description of Experiment

In order to verify the theory for the case of a concentrated edge load, a steel model 18 in. long with a plate width of $1^1/_8$ in. was constructed and tested as indicated in Fig. 4. Since the plate deflection becomes essentially zero for $y/a > 3$, the 18-in. length is more than adequate to represent the infinite case. The entire model was machined from a single bar of heat-treated USS T-1 steel with a Young's modulus of 30×10^6 psi and a yield point of 84,000 psi. This modulus value is the average of six determinations made on two tension specimens with a Heiser-Martens extensometer. The gage length was 5 in. and the total spread in the results was about 0.5×10^6 psi; thus an error of about 1 per cent is indicated. A load of 400.3 lb (including the tare weight of the beam system) was applied to the model by hanging 500 lb of dead weight on a 3-in-deep I-beam as shown in Fig. 4. The load was applied to the exact edge of the model through a hardened steel point ($^1/_{32}$-in. tip radius) by machining a small semicircular projection ($^8/_{64}$-in. radius) on the edge of the plate. Horizontal thrust in the beam was eliminated by supporting it on a roller at the right end. Earlier tests in which the load was applied by a testing machine through a relatively rigid symmetrical yoke gave low deflections, and demonstrated the importance of avoiding lateral constraint in the loading system. As a check that the full deflection is produced with the present scheme, the roller was replaced by a flexible vertical cable attached to the ceiling and several deflection readings were reproduced within the accuracy of the measuring system (see following text). An additional verification was obtained by the direct application of the 50-lb dead weight of a piece of steel bar stock through the same hardened steel point on the top of the plate. The bar was guided to keep it vertical, and again several readings were reproduced along the edge of the plate.

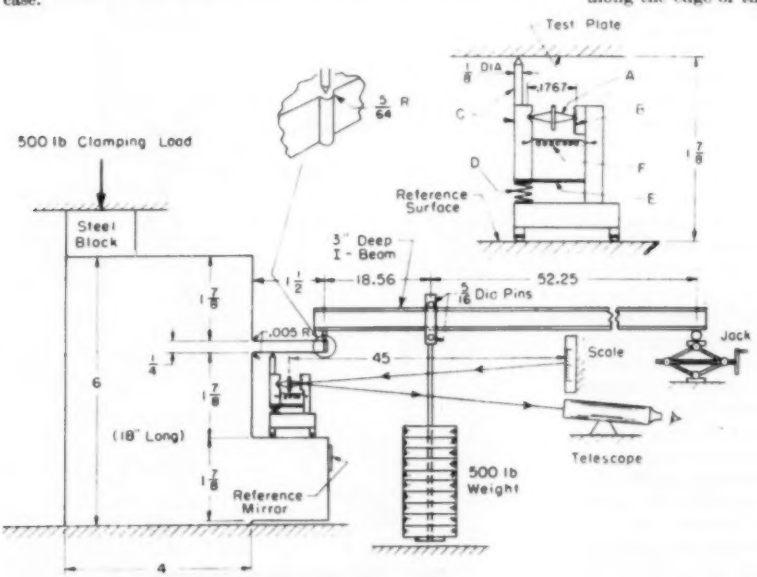

Fig. 4 Test setup for steel model

Deflections were measured accurately by means of the optical device shown in Fig. 4. A Marten's mirror and rhombus toggle A were mounted with one vertex of the rhombus held by the light tension spring F against a hardened serrated block B attached to the reference stand; the opposite vertex of the rhombus was seated in a V-groove attached to the movable indicator rod C. A light compression spring D holds the indicator rod against the underside of the test plate, while the strip of shim stock E stabilizes the rod and restricts it to vertical motion The 3 feet of the reference stand were held securely against the reference surface of the model by a permanent magnet (not shown). Deflection of the plate causes the mirror to rotate which is indicated by a change in scale reading through the telescope. This scale reading is easily converted into the desired plate deflection from a knowledge of the distances involved. The actual deflections are thus magnified by a factor of about 500. (This factor was slightly different for each reading because of the varying mirror-to-scale distance.) A small mirror was also mounted on the end of the reference surface, as shown in Fig. 4. Readings taken with this reference mirror and a separate scale and telescope showed that when the load is applied the reference surface rotates clockwise (in Fig. 4) a small constant amount, due, probably, to the more firm seating of front edge of the large block against the supporting surface. All of the readings were corrected for this effect which was equivalent to a plate deflection of about 25×10^{-6} in. (as compared, for example, to the maximum plate deflection of 4190×10^{-6} in.).

The accuracy of the measuring system was checked by measuring the small deflection near the fixed knife-edge fulcrum of a long lever, the opposite end of which was moved a known distance by means of a micrometer screw. The actual deflections calculated from the lever distances were reproduced within about 5×10^{-6} in. in the microin. range, while larger errors up to 30 microin. were observed when the measured deflection was of the order of mils. A deflection error of about 5×10^{-6} in. can be accounted for in reading the scale which was graduated in increments of 0.01 in. and could be read to within about ± 0.0025 in. Thus in the mid-plane of the plate ($y = 0$) the measurement error in the smallest reading of 66×10^{-6} in. is less than 10 per cent, while the measured maximum deflection of 4190×10^{-6} in. is accurate to within 1 per cent.

A zero reading was taken before and after the load application by lowering the motor-driven jack until the weights rested on the floor and the beam was supported on the lower $^{5}/_{16}$-in. diam pin, thus completely removing the load on the plate. With the use of a stress-concentration factor of 3.4 for the 0.005-in. fillet radius, the calculated maximum bending stress for the 400.3-lb test load is 66,000 psi, and thus no yielding occurs. This was verified by the consistency of the zero readings before and after the load application.

7 Discussion of Results

Figs. 5 and 6 show the good agreement of the deflection test results with the present theory. If the experimental model were constructed of the idealized material governed by classical plate theory we should expect the present approximate theory to be an upper bound on the test values (see Section 2). The presence of shear effects in the actual model, however, tends to raise the larger test values slightly above the theory. In fact, it may appear at first sight that the maximum test deflection should be even higher because of the influence of local shear under the point load. Examination of the magnitude of the load and the area of contact, however, shows that we do not actually have point contact, and that the local shear stress is relatively low (about 10,000 psi). Estimates of the relative magnitude of the "beam" shear deflection based on an end-loaded cantilever beam indicate that this effect accounts for a large part of the difference in question. Away from the vicinity of the load, i.e., for $y/a \geq 1$ or $x/a \leq \frac{1}{2}$, it is probable that the correlation more nearly reflects the error in the present theory owing to the use of the assumed equilibrium surface tractions on the half space. In this region the additional deflection due to the elasticity of the half space is high, as expected, by about 10 per cent. This value is in good agreement with estimates obtained from an analogous plane problem (see Section 2).

In the mid-plane, Fig. 6, the slopes were estimated from the deflection data and extrapolated back to the origin. The resulting slope at $x = 0$ was about 4×10^{-4} radians. This is about 12 per cent below the theoretical prediction, and is thus of the correct order of magnitude to account for the foregoing observed difference between theory and test away from the vicinity of the load. A similar extrapolation of the actual deflections in the mid-plane indicates a clamped-edge deflection of about 35×10^{-6} in. which is about 30 per cent larger than the theoretical value. Whether this increase of test result over theory is real or not is questionable due to the extrapolation and measurement errors.

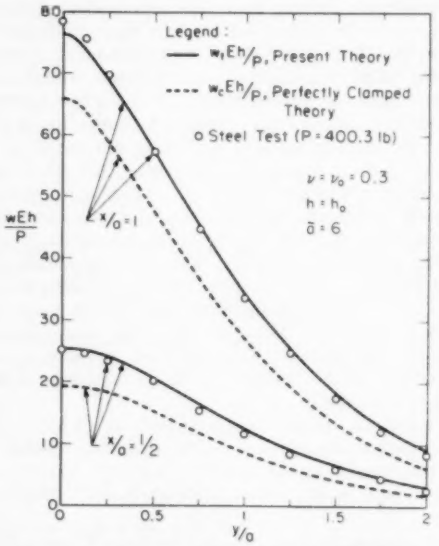

Fig. 5 Total deflection profiles along length of plate

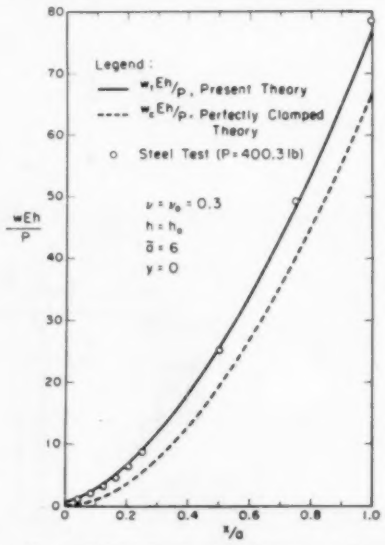

Fig. 6 Total deflection in mid-plane $y = 0$

Figs. 7 and 8 indicate that, except for a small smoothing effect, the moment and shear distributions along the clamped edge are relatively unchanged by the presence of the half-space flexibility (for $a/h = 6$). Fig. 7 also gives the distribution of the slope along $x = 0$.

In Fig. 9 the ratio of the half-space rotation Θ_0 (which includes shear effects) to the corresponding moment M_t is compared to the analogous plane-strain result for moment only. This figure shows that, except for very stubby plates, where coupling effects become more important, it is a good assumption to neglect the shear effects along the clamped edge, and to use the conventional Winkler type of elastic restraint with c_0 as the proportionality constant between moment and rotation.

Fig. 10 shows the ratio of the half-space effects (only) to the corresponding perfectly clamped maximum deflections and moments for various relative widths a/h. As expected, the influence of the half space becomes larger for small values of a/h. (This is useful for obtaining better estimates of the gear-tooth deflections mentioned in the Introduction.) For large values of

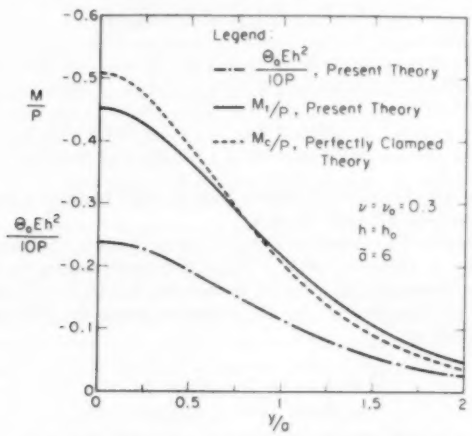

Fig. 7 Slope and bending moment along clamped edge

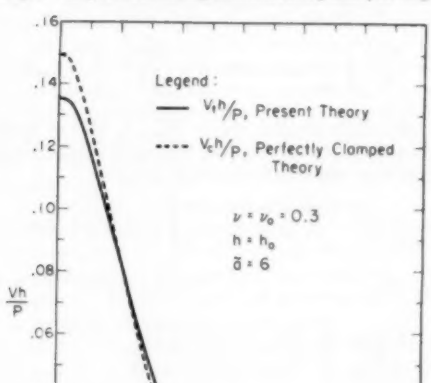

Fig. 8 Shearing force along clamped edge

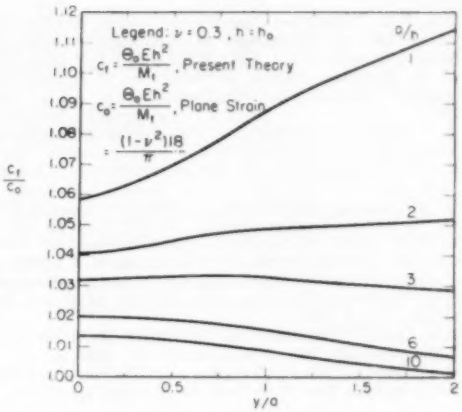

Fig. 9 Error in using simplified plane-strain elastic restraint

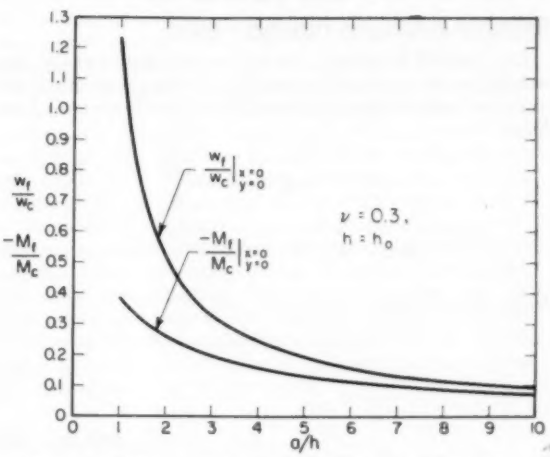

Fig. 10 Relative effect of support flexibility for different a/h

a/h the moment M_t becomes close to M_c, the perfectly clamped value, for which the rotation Θ_0 remains finite. It follows that the ratio w_f/w_c remains finite, and the moment is smoothed as shown in Fig. 7.

In conclusion, the present theory is in good agreement with the deflection test results. In the regions where the shear effects are small it overestimates the deflection due to the half space by about 10 per cent. This is in line with the upper-bound expectation from the minimum complementary energy theorem and estimates of the magnitude based on an analogous plane problem. In the vicinity of the load, shear effects account for the observed small increase of the test values above the theory.

Acknowledgments

The author wishes to express his appreciation to Dr. D. C. Drucker of Brown University for his helpful suggestions and capable direction during the course of the present work. Thanks are also due for the valuable assistance of Mr. George Killinger in the programming of the computer computations, and Mr. John R. McDowell in the instrumentation of the steel model. Both Mr. Killinger and Mr. McDowell are with the Westinghouse Electric Corporation.

References

1 C. W. MacGregor, "Deflection of a Long Helical Gear Tooth," *Mechanical Engineering*, vol. 57, 1935, pp. 225–227.

2 D. L. Holl, "Cantilever Plate With a Concentrated Edge Load," JOURNAL OF APPLIED MECHANICS, vol. 4, TRANS. ASME, vol. 59, 1937, pp. A-8 to A-10.
3 H. G. Hopkins, "Elastic Deformations of Infinite Strips," *Proceedings of The Cambridge Philosophical Society*, vol. 46, 1950, pp. 164–218.
4 T. J. Jaramillo, "Deflections and Moments Due to a Concentrated Load on a Cantilever Plate of Infinite Length," JOURNAL OF APPLIED MECHANICS, vol. 17, TRANS. ASME, vol. 72, 1950, pp. 67–72.
5 H. D. Conway, "The Flexure of Infinite Rectangular Plates of Varying Thickness," *Ingenieur-Archiv*, vol. 26, 1958, pp. 143–145.
6 A. E. H. Love, "A Treatise on the Mathematical Theory of Elasticity," Dover Publications, Inc., New York, N. Y., 1927, p. 191.
7 F. Vogt, "Uber die Berechnung der Fundamentdeformation," Norwegian Academy of Sciences, Oslo, Norway, Math and Sciences Classification, No. 2, 1925.
8 L. P. Smith, "Mathematical Methods for Scientists and Engineers," Prentice-Hall, Inc., New York, N. Y., 1953, p. 362, 376.
9 C. J. Tranter, "Integral Transforms in Mathematical Physics," John Wiley & Sons, Inc., New York, N. Y., 1951, pp. 67–72.

APPENDIX

Derivation of Influence Functions *f* and *G*

The classical Boussinesq results for the displacements Δu_m and Δw_m in the x and z-directions at an arbitrary point $Q(y, z)$ due to a concentrated normal load $\sigma\, d\eta\, d\zeta$ located at the point η, ζ are, Fig. 1,

$$\Delta u_m = A_{um}[M_0(\eta)d\eta]\,\frac{\zeta d\zeta}{r} \tag{39}$$

$$\Delta w_m = B_{wm}[M_0(\eta)d\eta]\,\frac{\zeta(z-\zeta)d\zeta}{r^2} \tag{40}$$

where we have used $\sigma = 12M_0\zeta/h_0^3$ and

$$r^2 = (z-\zeta)^2 + (y-\eta)^2$$

$$A_{um} = \frac{1}{\pi D_0}$$

$$B_{wm} = \frac{(1-2\nu_0)}{2\pi D_0(1-\nu_0)}$$

The corresponding displacements du_m and dw_m resulting from the moment $M_0 d\eta$ are obtained by integration on ζ by means of elementary quadrature formulas. The results are

$$du_m = A_{um} f_{um}(\xi, z)M_0(\eta)d\eta \tag{41}$$

$$dw_m = B_{wm} f_{wm}(\xi, z)M_0(\eta)d\eta \tag{42}$$

where $\xi = (y-\eta)$ and[6]

$$f_{um} = z\ln\left\{\frac{z+b_0+[\xi^2+(z+b_0)^2]^{1/2}}{z-b_0+[\xi^2+(z-b_0)^2]^{1/2}}\right\} + [\xi^2+(z-b_0)^2]^{1/2} - [\xi^2+(z+b_0)^2]^{1/2} \tag{43}$$

$$f_{wm} = \frac{z}{2}\ln\left\{\frac{\xi^2+(z+b_0)^2}{\xi^2+(z-b_0)^2}\right\} + \xi\left[\tan^{-1}\frac{(z+b_0)}{\xi} - \tan^{-1}\frac{(z-b_0)}{\xi}\right] - 2b_0 \tag{44}$$

The integration of equations (41) and (42) on η yields equations (3) and (4) of Section 2.

For the concentrated shear load $\tau\, d\eta\, d\zeta$ the Cerutti solutions corresponding to equations (39) and (40) are. Fig. 2,

$$\Delta w_v = A_{wv}[V_0(\eta)d\eta]\left[\frac{1}{r} - \frac{\nu_0(y-\eta)^2}{r^3}\right]d\zeta \tag{45}$$

$$\Delta u_v = -B_{uv}[V_0(\eta)d\eta]\,\frac{(z-\zeta)}{r^2}\,d\zeta \tag{46}$$

where $\tau = V_0/h_0$ has been used and

$$A_{wv} = \frac{(1+\nu_0)}{\pi E_0 h_0}$$

$$B_{uv} = \frac{(1-2\nu_0)(1+\nu_0)}{2\pi E_0 h_0}$$

Integrating on ζ, as before, we obtain

$$du_v = -B_{uv} f_{uv}(\xi, z)V_0 d\eta \tag{47}$$

$$dw_v = A_{wv} f_{wv}(\xi, z)V_0 d\eta \tag{48}$$

where

$$f_{uv} = \frac{1}{2}\ln\left[\frac{\xi^2+(z+b_0)^2}{\xi^2+(z-b_0)^2}\right] \tag{49}$$

$$f_{wv} = \ln\left[\frac{(z+b_0)+[\xi^2+(z+b_0)^2]^{1/2}}{(z-b_0)+[\xi^2+(z-b_0)^2]^{1/2}}\right] + \frac{\nu_0(z-b_0)}{[\xi^2+(z-b_0)^2]^{1/2}} - \frac{\nu_0(z+b_0)}{[\xi^2+(z+b_0)^2]^{1/2}} \tag{50}$$

Equations (5) and (6) of Section 2 are obtained by the integration of equations (47) and (48) on η.

Substituting equations (3) to (6), inclusive, into equation (2), using $\sigma = 12M_0 z/h_0^3$ and $\tau = V_0/h_0$, and interchanging the order of the integration, we obtain E_z in the form (1). Θ_0 and W_0 are defined by equations (7) to (12), inclusive, where the G-functions are given by

$$G_{\theta m}(\xi) = \frac{12A_{um}}{h_0^2}\int_{-b_0}^{+b_0} f_{um}(\xi, z)z\,dz$$

$$G_{wv}(\xi) = \frac{A_{wv}}{h_0}\int_{-b_0}^{+b_0} f_{wv}(\xi, z)dz$$

$$G_0(\xi) = \frac{B_{wm}}{h_0}\int_{-b_0}^{b_0} f_{wm}(\xi, z)dz = \frac{-12B_{uv}}{h_0^3}\int_{-b_0}^{b_0} f_{uv}(\xi, z)z\,dz$$

and the reciprocity relation $G_{\theta v} = G_{um} = G_0$ has been used. Substitution of equations (43), (44), (49), and (50) and integration by elementary quadrature formulas produces

$$G_{\theta m}(p) = \frac{1}{\pi D_0}\left\{\ln\left[\frac{(1+p^2)^{1/2}+1}{(1+p^2)^{1/2}-1}\right] + 6|p|(1+\tfrac{4}{6}p^2) - \tfrac{1.4}{3}(1+p^2)^{1/2}(1+\tfrac{4}{7}p^2)\right\}$$

$$G_{wv}(p) = \frac{(1+\nu_0)}{\pi E_0 h_0}\left\{\ln\left[\frac{(1+p^2)^{1/2}+1}{(1+p^2)^{1/2}-1}\right] + 2(1+\nu_0)[|p| - (1+p^2)^{1/2}]\right\}$$

$$G_0(p) = \frac{(1-2\nu_0)h_0}{4\pi D_0(1-\nu_0)}\left\{-p^2\ln\left(1+\frac{1}{p^2}\right) + 2p\tan^{-1}\left(\frac{1}{p}\right) - 1\right\}$$

where

$$p = \xi/h_0 \text{ and } G_{\theta m}(p) \equiv G_{\theta m}[\xi(p)], \text{ etc.}$$

[6] The exponent $^1/_2$ indicates the positive square root in all cases.

The Elastic, Plastic Bending of a Simply Supported Plate

G. EASON
Lecturer,
King's College,
Department of Mathematics,
Newcastle upon Tyne,
England

In this paper the problem of the elastic, plastic bending of a circular plate which is simply supported at its edge and carries a constant load over a central circular area is considered. The von Mises yield condition and the associated flow rule are assumed and the material of the plate is assumed to be nonhardening, elastic, perfectly plastic, and compressible. Stress fields are obtained in all cases and a velocity field is presented for the case of point loading. Some numerical results are given comparing the results obtained here with those obtained when the Tresca yield condition is assumed.

In the theory of plasticity there are two commonly accepted conditions of yielding—those due to Tresca and von Mises. Mathematically, the Tresca yield condition is the more tractable, and as a result it has received more attention in recent years than the more acceptable von Mises yield condition. Few problems have been solved for both the Tresca and von Mises yield conditions and as a result there is little evidence of the effect of choosing one yield condition rather than the other in a particular problem for which the solutions for the two yield conditions differ. Solutions to problems which have been obtained for both the Tresca and von Mises yield conditions include those of the elastic-plastic wedge [1, 2, 3],[1] and the elastic-plastic bending of a curved bar [4]. In both problems plane-stress conditions were assumed. In both [3] and [4] direct comparison was made between the Tresca and von Mises yield conditions. The results obtained here for the von Mises yield condition are compared with those for the Tresca yield condition.

The Tresca yield condition and the associated flow rule were used to consider fully plastic circular plates by Hopkins and Prager [5]. The von Mises yield condition and the associated flow rule were used for the same problem by Hopkins and Wang [6], and velocity fields for this yield condition were obtained by Eason [7]. Tekinalp [8, 9] has considered the elastic-plastic bending of a uniformly loaded circular plate which is simply supported or built in at its edge and obeys the Tresca yield condition. In both cases the material of the plate was assumed incompressible. Further problems of this type in which the material is compressible and obeys the Tresca yield condition have been considered by Haythornthwaite [10] and Hodge [11, 12]. None of these authors considers the precise problem treated here in the case of the Tresca yield condition, but results may be obtained in a straightforward manner by applying their methods. In view of this situation no algebraic results are given for the Tresca yield condition, numerical results only being quoted.

The problem to be considered here is that of a simply supported circular plate of nonhardening, perfectly plastic, compressible material which carries a constant load over a central circular area and is simply supported at its edge. An element of the plate is assumed to be either completely elastic or completely plastic. This approximation has been used previously in [8, 9, 10, 11, 12] for circular-plate problems with the Tresca yield condition. These conditions are most nearly satisfied in practice by a sandwich plate. For a solid plate a much greater degree of appproximation is involved. It is assumed throughout that the curvature and deflection of the plate remain small. Values of the bending moments are obtained for the von Mises yield condition for all the cases which occur. The equations for the velocity fields associated with the von Mises yield condition are not easy to solve, and only the case of point loading is treated in detail here.

Some numerical results are presented comparing the two yield conditions for the same value of applied load in the cases of point loading and uniform loading. It is found that for the same value of the applied load the area of the plate which is plastic may differ considerably even though the bending moments do not differ significantly. The numerical work was carried out on the high-speed digital computer FERDINAND.

Basic Equations

Let r, ϕ, z be cylindrical co-ordinates with the z-axis pointing downward. The plate is assumed to lie in the r, ϕ-plane so that, for an applied load which has axial symmetry, all quantities are functions of r alone. Let the plate have thickness h and radius R. The equations of equilibrium for an applied load which has axial symmetry are

$$\frac{d}{dr}(rQ) + rp = 0, \tag{1}$$

$$\frac{d}{dr}(rM) - N = rQ, \tag{2}$$

where M is the radial bending moment, N is the circumferential bending moment, Q is the shear force, and p the applied load, considered positive when its acts vertically downward. In the problems considered here the applied load p is constant over a central circular region of radius a and zero elsewhere so that (1) gives

$$rQ = \begin{cases} -\frac{1}{2}pr^2, & 0 \leqslant r \leqslant a, \\ -\frac{1}{2}pa^2 & a \leqslant r \leqslant R \end{cases} \tag{3}$$

The radial curvature κ and the circumferential curvature λ are related to the downward deflection of the plate w by the equations

$$\kappa = -\frac{d^2w}{dr^2}, \qquad \lambda = -\frac{1}{r}\frac{dw}{dr} \tag{4}$$

[1] Numbers in brackets designate References at end of paper.

Presented at the Summer Conference of the Applied Mechanics Division, Chicago, Ill., June 14–16, of The American Society of Mechanical Engineers.

Discussion of this paper should be addressed to the Editorial Department, ASME, United Engineering Center, 345 East 47th Street, New York 17, N. Y., and will be accepted until October 10, 1961. Discussion received after the closing date will be returned. Manuscript received by ASME Applied Mechanics Division, April 25, 1960. Paper No. 61—APM-18.

Throughout this paper a single prime will be used to denote the elastic component of the curvature and a double prime to denote the plastic component, so that in a plastic region

$$\kappa = \kappa' + \kappa'', \qquad \lambda = \lambda' + \lambda'' \tag{5}$$

The equations relating the bending moments and the elastic components of curvature are

$$\kappa' D(1 - \nu^2) = M - \nu N, \tag{6}$$

$$\lambda' D(1 - \nu^2) = N - \nu M, \tag{7}$$

where

$$D = Eh^3/12(1 - \nu^2), \tag{8}$$

E is Young's modulus and ν is Poisson's ratio. In a region which is elastic, equations (6) and (7) are the usual bending moment-curvature relationships, since the curvature is then purely elastic.

Hopkins and Wang [6] formulated the von Mises yield condition for circular plates. This yield condition has the form

$$f = M^2 - MN + N^2 - 3Y^2 = 0, \tag{9}$$

where $Y\sqrt{3}$ is the fully plastic bending moment. The flow rule associated with this yield condition leads to equations for the plastic components of the curvature rates of the form

$$\dot{\kappa}'' = \mu \frac{\partial f}{\partial M} = \mu(2M - N), \tag{10}$$

$$\dot{\lambda}'' = \mu \frac{\partial f}{\partial N} = \mu(2N - M), \tag{11}$$

where μ is a nonnegative parameter. These equations combine to give

$$\dot{\kappa}''(2N - M) = \dot{\lambda}''(2M - N) \tag{12}$$

The yield condition (9) is satisfied by the relations

$$M = -2Y \sin(\tfrac{1}{6}\pi - \theta), \quad N = 2Y \sin(\tfrac{1}{6}\pi + \theta), \tag{13}$$

where the parameter θ is taken to have the value $\frac{1}{3}\pi$ when $M = N = Y\sqrt{3}$. Substituting from (13) into (2) and (12) results in the equations

$$r \cos(\tfrac{1}{6}\pi - \theta) \frac{d\theta}{dr} - \cos\theta = \frac{rQ}{2Y}, \tag{14}$$

$$\dot{\kappa}'' \cos(\tfrac{1}{6}\pi - \theta) + \dot{\lambda}'' \cos(\tfrac{1}{6}\pi + \theta) = 0 \tag{15}$$

Equations (6) and (7) combine to give

$$\dot{\kappa}' \cos(\tfrac{1}{6}\pi - \theta) + \dot{\lambda}' \cos(\tfrac{1}{6}\pi + \theta) = \frac{Y\dot{\theta}}{D(1 - \nu^2)} \{(2 - \nu) + (1 - 2\nu)\cos 2\theta\}, \tag{16}$$

so that with (15) we have

$$\frac{d^2v}{dr^2} \cos(\tfrac{1}{6}\pi - \theta) + \frac{1}{r}\frac{dv}{dr} \cos(\tfrac{1}{6}\pi + \theta) = -\frac{Y\dot{\theta}}{D(1 - \nu^2)} \{(2 - \nu) + (1 - 2\nu)\cos 2\theta\}, \tag{17}$$

where v is the velocity of the plate so that

$$v = \dot{w} \tag{18}$$

For both the Tresca and von Mises yield conditions the general form of the deformation is the same. Initially the whole plate is elastic and the well-known solution to be found in [13] applies. As the applied load is increased in magnitude a plastic region develops at the center of the plate. This plastic region spreads outward from the center with increasing applied load. Let ρ be the radius of the elastic-plastic boundary. Two elastic-plastic cases are possible and in both of these the regions $0 \leqslant r \leqslant \rho$ and $\rho < r \leqslant R$ are plastic and elastic, respectively, but in the first case $\rho \leqslant a$ and in the second case $\rho \geq a$. The second case applies until $\rho = R$ and the entire plate is plastic.

The conditions to be satisfied at the plate edge, $r = R$, are $M = 0$ and $w = 0$. At the center of the plate w and M must be finite. The quantities M, N, Q, w, and dw/dr are continuous at the edge of the loaded area, $r = a$. At an elastic-plastic boundary M, Q, w, and dw/dr are continuous and the material on the elastic side of the boundary must be about to yield. For the form of the von Mises yield condition needed here, this last condition implies that N is continuous at an elastic-plastic boundary.

The Elastic Solution

The elastic solution for a plate which is loaded over a central region of radius a is well known [13]. It is obtained by solving equations (2), (4), (6), and (7) together with (3). The general solutions of these equations are found to be

$$\left.\begin{aligned} M &= -\tfrac{1}{16}pr^2(3 + \nu) + A + B/r^2, \\ N &= -\tfrac{1}{16}pr^2(1 + 3\nu) + A - B/r^2, \\ wD(1 - \nu^2) &= \tfrac{1}{64}pr^4(1 - \nu^2) - \tfrac{1}{2}Ar^2(1 - \nu) \\ &\quad + B(1 + \nu)\log r + C; \end{aligned}\right\} r \leqslant a, \tag{19}$$

$$\left.\begin{aligned} M &= -\tfrac{1}{4}pa^2(1 + \nu)\log r - \tfrac{1}{8}pa^2(1 - \nu) \\ &\quad + F + G/r^2, \\ N &= -\tfrac{1}{4}pa^2(1 + \nu)\log r + \tfrac{1}{8}pa^2(1 - \nu) \\ &\quad + F - G/r^2, \\ wD(1 - \nu^2) &= \tfrac{1}{8}pa^2(1 - \nu^2)r^2(\log r - 1) \\ &\quad - \tfrac{1}{2}F(1 - \nu)r^2 \\ &\quad + G(1 + \nu)\log r + H; \end{aligned}\right\} a \leqslant r \leqslant R, \tag{20}$$

where A, B, C, F, G, H are constants.

The particular results required here are for a simply supported plate when the bending moments are found to be

$$\left.\begin{aligned} M &= \tfrac{1}{4}pa^2(1 + \nu)\log(R/a) + \tfrac{1}{4}pa^2 \\ &\quad - \frac{pa^4}{16R^2}(1 - \nu) - \frac{pr^2}{16}(3 + \nu), \\ N &= \tfrac{1}{4}pa^2(1 + \nu)\log(R/a) + \tfrac{1}{4}pa^2 \\ &\quad - \frac{pa^4}{16R^2}(1 - \nu) - \frac{pr^2}{16}(1 + 3\nu); \end{aligned}\right\} 0 \leqslant r \leqslant a, \tag{21}$$

$$\left.\begin{aligned} M &= \tfrac{1}{4}pa^2(1 + \nu)\log(R/r) \\ &\quad + \frac{pa^4}{16}(1 - \nu)\left(\frac{1}{r^2} - \frac{1}{R^2}\right), \\ N &= \tfrac{1}{4}pa^2(1 + \nu)\log(R/r) + \tfrac{1}{4}pa^2(1 - \nu) \\ &\quad - \frac{pa^4}{16}(1 - \nu)\left(\frac{1}{r^2} + \frac{1}{R^2}\right). \end{aligned}\right\} a \leqslant r \leqslant R \tag{22}$$

Expressions for the deflection may be obtained in a straightforward manner from the results in (19) and (20). In the case of point loading for which $\pi pa^2 \to P$ as $a \to 0$, it is seen that the plate is plastic at its center for any value of P. For both the Tresca and von Mises yield conditions the plate first becomes plastic at the center in all cases. That this was so was checked numerically for several values of ν and a/R.

Bending Moments

(a) First elastic-plastic stage, $\rho \leqslant a$. The plate first becomes plastic at the center with $M = N = Y\sqrt{3}$ so that $\theta = \frac{1}{6}\pi$ there. It is to be expected that as the applied load is increased a central region of the plate will become plastic and that this region will spread outward to the plate edge. In the region $0 \leqslant r \leqslant \rho$ the plate is plastic and the parameter θ is determined by (3) and (14). For a loaded plastic region these equations combine to give

$$(\cos\theta - t)\frac{dt}{d\theta} = 2t\cos(\tfrac{1}{6}\pi - \theta), \tag{23}$$

with

$$F = pR^2/4Y, \quad s = r^2/R^2, \quad t = Fs \tag{24}$$

Equation (23) has to be integrated numerically with the starting values $t = 0$, $\theta = \frac{1}{2}\pi$. The plastic region ends when $r = \rho$, $\theta = \alpha$, and $t = t_1$.

The method of solution for α, ρ, and p was to assume α so that t_1 was known. This gives one relationship between p and ρ, the second equation being equation (25) obtained later. The values of the bending moments are then given by the numerical solution of (23) together with (13).

Expressions for the bending moments in the elastic region, $\rho < r \leqslant R$, follow in a straightforward manner from (19) and (20) and are found to be

$$\left.\begin{aligned} M &= -\tfrac{1}{16}pr^2(3+\nu) + \tfrac{1}{8}p\rho^2(1+\nu) + Y\sqrt{3}\sin\alpha \\ &\quad + \frac{\rho^2}{r^2}\{\tfrac{1}{16}p\rho^2(1-\nu) - Y\cos\alpha\}, \\ N &= -\tfrac{1}{16}pr^2(1+3\nu) + \tfrac{1}{8}p\rho^2(1+\nu) \\ &\quad + Y\sqrt{3}\sin\alpha - \frac{\rho^2}{r^2}\{\tfrac{1}{16}p\rho^2(1-\nu) - Y\cos\alpha\}, \end{aligned}\right\} \rho \leqslant r \leqslant a,$$

$$\left.\begin{aligned} M &= -\tfrac{1}{4}pa^2(1+\nu)\log(r/a) - \tfrac{1}{4}pa^2 \\ &\quad + \tfrac{1}{8}p\rho^2(1+\nu) + Y\sqrt{3}\sin\alpha \\ &\quad + \frac{a^2}{r^2}\left\{\tfrac{1}{16}pa^2(1-\nu) + \frac{\rho^2}{a^2}\left[\frac{p\rho^2}{16}(1-\nu) - Y\cos\alpha\right]\right\}, \\ N &= -\tfrac{1}{4}pa^2(1+\nu)\log(r/a) - \tfrac{1}{4}\nu pa^2 \\ &\quad + \tfrac{1}{8}p\rho^2(1+\nu) + Y\sqrt{3}\sin\alpha \\ &\quad - \frac{a^2}{r^2}\left\{\tfrac{1}{16}pa^2(1-\nu) + \frac{\rho^2}{a^2}[\tfrac{1}{16}p\rho^2(1-\nu) - Y\cos\alpha]\right\}; \end{aligned}\right\} a \leqslant r \leqslant R,$$

together with the equation

$$-\tfrac{1}{4}pa^2(1+\nu)\log(R/a) - \tfrac{1}{4}pa^2 + \tfrac{1}{8}p\rho^2(1+\nu) + Y\sqrt{3}\sin\alpha + \frac{pa^4}{16R^2}(1-\nu) + \frac{\rho^2}{R^2}\left\{\frac{p\rho^2}{16}(1-\nu) - Y\cos\alpha\right\} = 0 \tag{25}$$

The foregoing equations hold until $a = \rho$.

(b) Second elastic-plastic stage, $\rho \geqslant a$. Within the loaded region of the plate, (23) and (24) still determine the relationship between t and θ so that once θ is known, (13) determine the bending moments. Within the region $a \leqslant r \leqslant \rho$ the plate is plastic but unloaded. The parameter θ is determined by (3) and (14) which together give

$$2s\cos(\tfrac{1}{6}\pi - \theta)\frac{d\theta}{ds} - \cos\theta = -Fa^2/R^2 = -G. \tag{26}$$

where F and s are defined by (24), and G is the value of t at $r = a$. This equation may be partially integrated to give

$$\frac{r^2}{a^2} = \frac{G - \cos\beta}{G - \cos\theta}\exp\left\{\sqrt{3}\int_\theta^\beta \frac{\cos\theta\, d\theta}{G - \cos\theta}\right\}, \tag{27}$$

where β is the value of θ at $r = a$. The integral appearing in (27) may be evaluated in terms of elementary functions by the substitution $t = \tan(\frac{1}{2}\theta)$, but it is usually simpler to integrate numerically. This region ends when $r = \rho$ and $\theta = \alpha$.

In the elastic region of the plate, $\rho < r \leq R$, it is found that

$$\begin{aligned} M &= -\tfrac{1}{4}pa^2(1+\nu)\log(r/\rho) - \tfrac{1}{8}pa^2(1-\nu) \\ &\quad + Y\sqrt{3}\sin\alpha + \frac{\rho^2}{r^2}\{\tfrac{1}{8}pa^2(1-\nu) - Y\cos\alpha\}, \\ N &= -\tfrac{1}{4}pa^2(1+\nu)\log(r/\rho) + \tfrac{1}{8}pa^2(1-\nu) \\ &\quad + Y\sqrt{3}\sin\alpha - \frac{\rho^2}{r^2}\{\tfrac{1}{8}pa^2(1-\nu) - Y\cos\alpha\} \end{aligned}$$

One equation connecting p, ρ, and α is

$$\sqrt{3}\sin\alpha - G(1+\nu)\log(R/\rho) - \tfrac{1}{2}G(1-\nu) + \frac{\rho^2}{R^2}\{\tfrac{1}{2}G(1-\nu) - \cos\alpha\} = 0, \tag{28}$$

the other required equation being (27) with $r = \rho$ when $\theta = \alpha$. The simplest method of solving the equations connecting α, β, ρ, a, and p is to assume α and β so that from the integrated form of (23) the value of G is known. Equation (28) then gives ρ/R and (27) with $\theta = \alpha$ and $r = \rho$ gives ρ/a. The value of p is then obtained from the value of G. This stage ends when $\rho = R$, $\alpha = \frac{1}{6}\pi$, and the whole plate is plastic.

The results for point loading in which $\pi pa^2 \to P$ as $a \to 0$ are a special case of the foregoing. It is found that the bending moments are constant in the plastic region for any given value of P. This result is also true for the Tresca yield condition. The resulting expressions are

$$M = -2Y\sin(\tfrac{1}{6}\pi - \alpha), \quad N = 2Y\sin(\tfrac{1}{6}\pi + \alpha); \quad 0 \leqslant r \leqslant \rho, \tag{29}$$

$$\left.\begin{aligned} M &= Y\sqrt{3}\sin\alpha - \frac{P}{4\pi}(1+\nu)\log(r/\rho) \\ &\quad - \frac{P}{8\pi}(1-\nu) + \frac{\rho^2}{r^2}\left\{\frac{P(1-\nu)}{8\pi} - Y\cos\alpha\right\}, \\ N &= Y\sqrt{3}\sin\alpha - \frac{P}{4\pi}(1+\nu)\log(r/\rho) \\ &\quad + \frac{P}{8\pi}(1-\nu) - \frac{\rho^2}{r^2}\left\{\frac{P(1-\nu)}{8\pi} - Y\cos\alpha\right\}; \end{aligned}\right\} \rho \leqslant r \leqslant R, \tag{30}$$

and the equations connecting P and α are

$$4\pi Y\sqrt{3}\sin\alpha - P(1+\nu)\log(R/\rho) - \tfrac{1}{2}P(1-\nu) + \frac{\rho^2}{R^2}\{\tfrac{1}{2}P(1-\nu) - 4\pi Y\cos\alpha\} = 0, \tag{31}$$

$$P = 4\pi Y \cos \alpha \tag{32}$$

For a fully plastic plate, when $\rho = R$, the parameter θ is determined by (23) and (27). The results for this case have been given previously in [6] and [7].

Deflection for von Mises Yield Condition

Distributed loading. The deflection in an elastic region of the plate for distributed loading is obtained as the solution of (7) and the second of equations (4), with the condition $w = 0$ at $r = R$. In the case of distributed loading the solution for a plastic region of the plate is not easy to obtain. It is expected to be a solution of (17) with suitable continuity conditions at $r = \rho$. A solution could be obtained numerically, and there can be little doubt that the solution so obtained would satisfy the conditions implied in (10) and (11). The solution given here for point loading certainly satisfies these conditions, and the velocity fields given in [7] for a fully plastic plate can also be shown to satisfy the conditions. Thus there can be little doubt that the solutions presented here for the bending moments are the correct ones for a partially plastic plate.

Point loading. In the case of point loading the deflection in the elastic region of the plate, $\rho < r \leqslant R$, associated with the bending moments (30) is found to be

$$\begin{aligned} wD(1-\nu^2) &= (R^2 - r^2)\{\tfrac{1}{2}Y(1-\nu^2)\cos\alpha \\ &\quad + \tfrac{1}{2}(1-\nu)Y\sqrt{3}\sin\alpha\} \\ &\quad + (1+\nu)Y\rho^2\cos\alpha\log(R/r) \\ &\quad + \tfrac{1}{2}Y(1-\nu^2)\cos\alpha\{r^2\log(r/\rho) - R^2\log(R/\rho) \\ &\quad - \rho^2\log(R/r)\} \end{aligned}$$

Within the plastic region of the plate the parameter α appearing in (29) does not depend on r but does depend on ρ. Equation (17) may now be written

$$\frac{d^2v}{dr^2}\cos(\tfrac{1}{6}\pi - \alpha) + \frac{1}{r}\frac{dv}{dr}\cos(\tfrac{1}{6}\pi + \alpha) = -\frac{Y\Phi}{D(1-\nu^2)}\cos(\tfrac{1}{6}\pi - \alpha), \tag{33}$$

where

$$\Phi = \dot{\alpha}\{(2-\nu) + (1-2\nu)\cos 2\alpha\}\sec(\tfrac{1}{6}\pi - \alpha)$$

Equation (33) may be integrated to give

$$D(1-\nu^2)\frac{dv}{dr} = -\frac{Y\Phi r}{1+\gamma} + A(1-\gamma)r^{-\gamma} \tag{34}$$

where γ is defined by

$$\gamma = \cos(\tfrac{1}{6}\pi + \alpha)\sec(\tfrac{1}{6}\pi - \alpha),$$

and A is a constant of integration. It is seen from equation (34) that if γ is negative ($\frac{1}{3}\pi < \alpha \leqslant \frac{1}{2}\pi$) then dv/dr is zero at the origin whereas if γ is positive ($\frac{1}{6}\pi \leqslant \alpha < \frac{1}{3}\pi$) then dv/dr becomes infinite at the origin. Integration of (34) leads to the result

$$D(1-\nu^2)v = -\frac{Y\Phi r^2}{2(1+\gamma)} + Ar^{1-\gamma} + B, \tag{35}$$

where B is a constant of integration. The quantities A and B (which depend on ρ) are determined by the continuity of v and dv/dr at $r = \rho$. Treating differentiation with respect to time as differentiation with respect to ρ it is found that

$$\begin{aligned} A(1-\gamma) &= Y\rho^{\gamma}\left\{\frac{\Phi\rho}{1+\gamma} - \dot{\alpha}\rho(1-\nu)\sqrt{3}\cos\alpha \right. \\ &\quad \left. - (1+\nu)(2\cos\alpha - \rho\dot{\alpha}\sin\alpha)\right\}, \end{aligned} \tag{36}$$

$$\begin{aligned} B &= \frac{Y\rho^2\Phi}{2(1+\gamma)} \quad A\rho^{\gamma} \\ &\quad + \tfrac{1}{2}Y\dot{\alpha}(R^2-\rho^2)[(1-\nu)\sqrt{3}\cos\alpha - (1-\nu^2)\sin\alpha] \\ &\quad + Y(1+\nu)\log(R/\rho)[2\rho\cos\alpha - \rho^2\dot{\alpha}\sin\alpha] \\ &\quad + \tfrac{1}{2}Y(1-\nu^2)\dot{\alpha}(R^2+\rho^2)\sin\alpha\log(R/\rho) \\ &\quad + \tfrac{1}{2}Y(1-\nu^2)\cos\alpha\left[\frac{R^2}{\rho} - \rho - 2\rho\log(R/\rho)\right]. \end{aligned} \tag{37}$$

Combining equations (35), (36), and (37) results in an expression for the velocity v in terms of ρ. By integrating numerically with respect to ρ values for the deflection of the plate may be calculated.

It remains to be shown that the parameter μ appearing in (10) and (11) is nonnegative. Equation (11) may be written in the form

$$\dot{\lambda}'' = 2\mu Y\sqrt{3}\cos(\tfrac{1}{6}\pi - \theta),$$

and since $\frac{1}{6}\pi \leqslant \theta = \alpha \leqslant \frac{1}{2}\pi$ here, μ will be nonnegative if $\dot{\lambda}''$ is nonnegative. Now

$$\begin{aligned} D(1-\nu^2)\dot{\lambda}'' &= -D(1-\nu^2)\left(\frac{1}{r}\frac{dv}{dr} + \dot{\lambda}'\right) \\ &= Y(1+\nu)\left\{\frac{2}{\rho}\left(\frac{\rho}{r}\right)^{1+\gamma}\cos\alpha \right. \\ &\quad \left. - \dot{\alpha}\left[\left(\frac{\rho}{r}\right)^{1+\gamma} - 1\right]\sin\alpha\left(1 + \frac{1}{\sqrt{3}}\tan\alpha\right)\right\}, \end{aligned}$$

and since $\rho \geqslant r$ and $\dot{\alpha} \leqslant 0$ the condition on $\dot{\lambda}''$ is satisfied and the solution presented is satisfactory.

Discussion of Results

The object of this paper has been to compare the results obtained by assuming the Tresca and von Mises yield conditions in turn for the same problem. The two most important special cases of the present problem are those of uniform loading and point loading and the numerical work has been confined to these cases. In the following, $2k$ is the fully plastic bending moment for the Tresca yield condition. The yield conditions have been chosen such that $2k \equiv Y\sqrt{3}$, that is, the Tresca yield curve lies entirely within the von Mises yield curve.

Fig. 1 shows the variation of ρ/R with the applied load for uniform loading ($a = R$) and two values of Poisson's ratio. The applied load appears as the quantity H where

$$H \equiv pR^2/2k \equiv pR^2/Y\sqrt{3}$$

As might be expected, for a plate which is almost entirely elastic, variation in ν can have as much effect as variation in yield condition, although this is no longer true for an almost entirely plastic plate. The variation of the circumferential bending moment, N, with r/R for uniform loading, $\nu = 0.5$, and several values of H is shown in Fig. 2. Again, the greatest differences are for an almost entirely plastic plate although even then the curves for the two yield conditions are quite similar. Variation of N with r/R for other values of ν is much the same. The values of the radial bending moment M corresponding to the values of N shown in Fig. 2 are given in Tables 1 and 2. The variation of M with r/R seems to be most insensitive to variation in yield condition, applied load, or Poisson's ratio. For values of H such that $5.7 < H < 6.0$ approximately, the distribution of the bending moments for the two yield conditions does not differ greatly, although the area of the plate which is plastic may differ by more than half the area of the plate.

The variation of ρ/R with applied load for point loading and

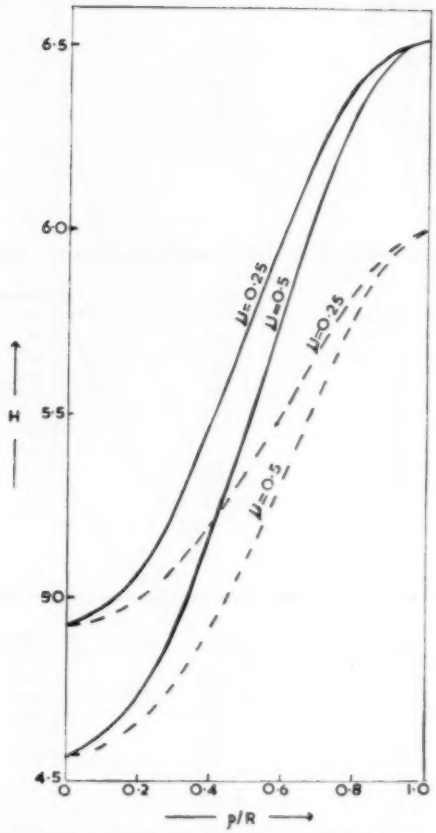

Fig. 1 Variation of ρ/R with H for uniform loading ($a = R$). Tresca - - - -, von Mises———.

Table 1 Variation of radial bending moment M with r/R for $H = 5.09$, $\nu = 0.5$, and $a = R$

r/R	Tresca $M/2k$	von Mises $M/Y\sqrt{3}$
0	1.0	1.0
0.127	0.986	0.990
0.221	0.959	0.968
0.317	0.915	0.934
0.369	0.884	0.910
0.40	0.864	0.892
0.50	0.788	0.810
0.60	0.685	0.698
0.70	0.551	0.559
0.80	0.392	0.396
0.90	0.208	0.209
1.0	0	0

Table 2 Variation of radial bending moment M with r/R for $H = 5.79$, $\nu = 0.5$, and $a = R$

r/R	Tresca $M/2k$	von Mises $M/Y\sqrt{3}$
0	1.0	1.0
0.119	0.986	0.990
0.207	0.959	0.968
0.297	0.915	0.934
0.390	0.853	0.885
0.487	0.771	0.816
0.603	0.649	0.711
0.70	0.527	0.589
0.80	0.382	0.425
0.90	0.210	0.228
1.0	0	0

$\nu = 0.5$ is shown in Fig. 3. The quantity L which appears her is defined by

$$L \equiv P/4\pi k \equiv P/2\pi Y\sqrt{3}$$

Change in yield condition produces little change in these curves. Results for other values of Poisson's ratio are also quite similar to those shown here for incompressible material. Fig. 4 shows the variation of N with r/R in the case of point loading for

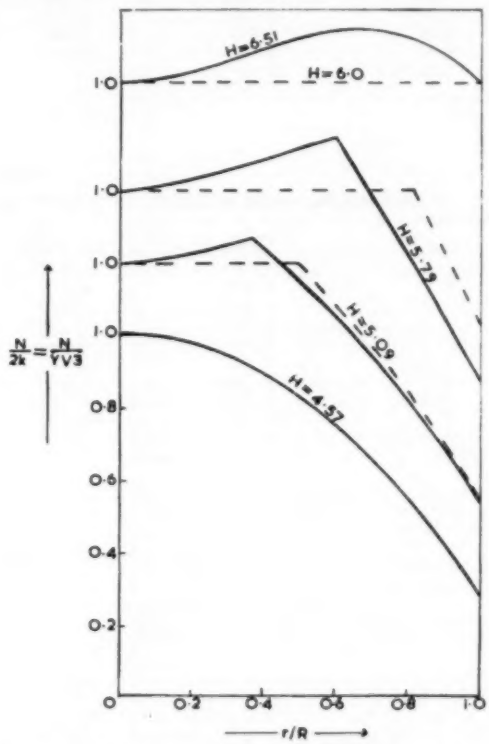

Fig. 2 Variation of circumferential bending moment with r/R for uniform loading and $\nu = 0.5$. For convenience, some of the curves have been raised. Tresca- - - -, von Mises———.

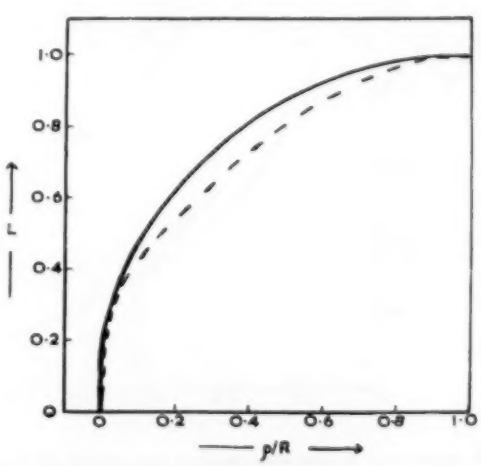

Fig. 3 Variation of ρ/R with L for point loading and $\nu = 0.5$. Tresca - - - -, von Mises———.

Table 3 Variation of radial bending moment M with r/R for $L = 0.488$, $\nu = 0.5$, and $a = 0$

r/R	Tresca $M/2k$	von Mises $M/Y\sqrt{3}$
0	0.512	0.662
0.1	0.512	0.662
0.2	0.486	0.545
0.3	0.398	0.422
0.4	0.313	0.326
0.5	0.241	0.248
0.6	0.180	0.184
0.7	0.126	0.129
0.8	0.079	0.081
0.9	0.038	0.038
1.0	0	0

Table 4 Variation of radial bending moment M with r/R for $L = 0.730$, $\nu = 0.5$, and $a = 0$

r/R	Tresca $M/2k$	von Mises $M/Y\sqrt{3}$
0	0.270	0.410
0.3	0.270	0.410
0.4	0.270	0.372
0.5	0.247	0.306
0.6	0.201	0.236
0.7	0.149	0.170
0.8	0.097	0.108
0.9	0.047	0.052
1.0	0	0

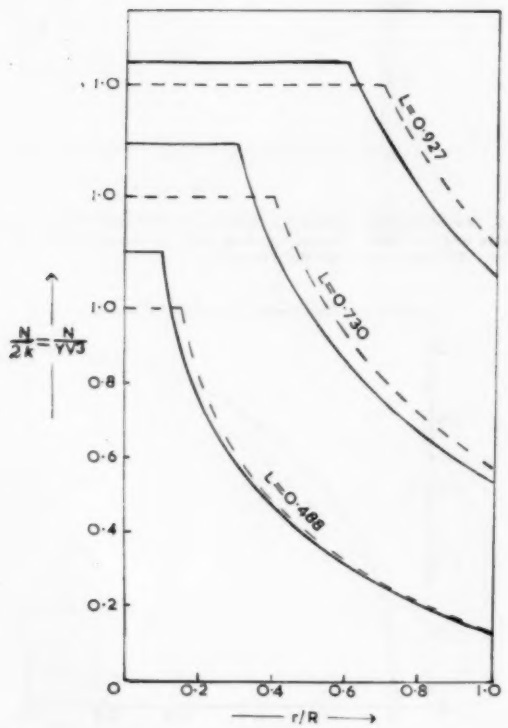

Fig. 4 Variation of circumferential bending moment with r/R for point loading and $\nu = 0.5$. For convenience some of the curves have been raised. Tresca – – –, von Mises———.

Table 5 Variation of radial bending moment M with r/R for $L = 0.927$, $\nu = 0.5$, and $a = 0$

r/R	Tresca $M/2k$	von Mises $M/Y\sqrt{3}$
0	0.073	0.133
0.6	0.073	0.133
0.7	0.073	0.118
0.8	0.061	0.085
0.9	0.034	0.044
1.0	0	0

Table 6 Variation of w with r/R for point loading with $L = 0.624$ and $\nu = 0.5$

r/R	Tresca $Dw/2kR^2$	von Mises $Dw/YR^2\sqrt{3}$
0	0.298	0.246
0.1	0.264	0.222
0.2	0.231	0.198
0.3	0.200	0.174
0.4	0.170	0.150
0.5	0.140	0.125
0.6	0.111	0.099
0.7	0.082	0.074
0.8	0.054	0.049
0.9	0.026	0.024
1.0	0	0

Table 7 Variation of w with r/R for point loading with $L = 0.814$ and $\nu = 0.5$

r/R	Tresca $Dw/2kR^2$	von Mises $Dw/YR^2\sqrt{3}$
0	0.633	0.529
0.1	0.553	0.449
0.2	0.476	0.384
0.3	0.404	0.326
0.4	0.336	0.273
0.5	0.272	0.223
0.6	0.212	0.175
0.7	0.155	0.129
0.8	0.101	0.084
0.9	0.049	0.041
1.0	0	0

Table 8 Variation of w with r/R for point loading with $L = 0.927$ and $\nu = 0.5$

r/R	Tresca $Dw/2kR^2$	von Mises $Dw/YR^2\sqrt{3}$
0	1.009	0.987
0.1	0.883	0.793
0.2	0.763	0.664
0.3	0.648	0.554
0.4	0.539	0.456
0.5	0.436	0.367
0.6	0.338	0.285
0.7	0.246	0.208
0.8	0.159	0.135
0.9	0.078	0.066
1.0	0	0

Table 9 Variation of w with r/R for point loading with $L = 1.0$ and $\nu = 0.5$.

r/R	Tresca $Dw/2kR^2$	von Mises $Dw/YR^2\sqrt{3}$
0	1.667	2.394
0.1	1.470	1.771
0.2	1.280	1.454
0.3	1.097	1.198
0.4	0.920	0.977
0.5	0.750	0.780
0.6	0.587	0.601
0.7	0.430	0.436
0.8	0.280	0.282
0.9	0.137	0.137
1.0	0	0

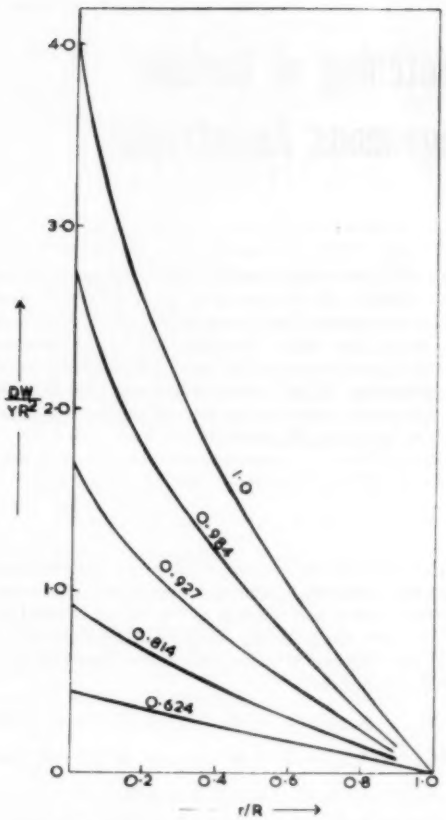

Fig. 5 Variation of deflection with r/R for point loading and $\nu = 0.5$ (von Mises yield condition)

$\nu = 0.5$ and several values of L. Tables 3, 4, and 5 give the values of M corresponding to these values of N. In the case of point loading the stress distribution is quite insensitive to both yield condition and the value of Poisson's ratio. This result is due in part to the fact that the stress distribution for a fully plastic plate is the same for both yield conditions.

Fig. 5 shows the development of the plate deflection in the case of point loading with $\nu = 0.5$ and the assumption of the von Mises yield condition. For all values of L less than about 0.8 the deflection is nearly linear. The curves indicate that for increasing applied load most of the plastic deformation takes place during the final stages of the loading. Tables 5, 6, 7, and 8 give a comparison of the deflection due to point loading for the two yield conditions with $\nu = 0.5$ and selected values of L.

Conclusion

In conclusion, it would seem that the stress distribution for a given problem is relatively insensitive to the yield condition. The volume of a given body which is plastic for a given load is likely to be much more sensitive to the choice of yield condition. In the problem considered here the uniformly loaded plate is much more sensitive to change of yield condition than the plate subjected to point loading.

References

1 P. M. Naghdi, "On Plane Stress Solution of Elastic, Perfectly Plastic Wedge," JOURNAL OF APPLIED MECHANICS, vol. 25, TRANS. ASME, vol. 80, 1958, pp. 407–410.

2 L. M. Kachanov, "Elastic-Plastic Equilibrium of a Wedge in Plane Stress State," *Prikladnaya Matematika i Mekhanika*, vol. 21, 1957, pp. 413–418.

3 A. Kalnins, "On Plane-Stress Solution of a Compressible Wedge With the Use of Mises Yield Condition," JOURNAL OF APPLIED MECHANICS, vol. 26, TRANS. ASME, Series E, vol. 81, 1959, pp. 676–678.

4 G. Eason, "The Elastic-Plastic Bending of a Curved Bar by End Couples in Plane Stress," *Quarterly Journal of Mechanics and Applied Mathematics*, vol. 13, 1960, pp. 334–358.

5 H. G. Hopkins and W. Prager, "The Load Carrying Capacities of Circular Plates," *Journal of the Mechanics and Physics of Solids*, vol. 2, 1953, pp. 1–13.

6 H. G. Hopkins and A. J. Wang, "Load-Carrying Capacities for Circular Plates of Perfectly-Plastic Material With Arbitrary Yield Condition," *Journal of the Mechanics and Physics of Solids*, vol. 3, 1954, pp. 117–129.

7 G. Eason, "Velocity Fields for Circular Plates With the von Mises Yield Condition," *Journal of the Mechanics and Physics of Solids*, vol. 6, 1959, pp. 231–235.

8 B. Tekinalp, "Elastic-Plastic Bending of a Simple Supported Circular Plate Under a Uniformly Distributed Load," Brown University Report C11-6, 1956.

9 B. Tekinalp, "Elastic-Plastic Bending of a Built-In Circular Plate Under a Uniformly Distributed Load," *Journal of the Mechanics and Physics of Solids*, vol. 5, 1957, 135–142.

10 R. M. Haythornthwaite, "The Deflection of Plates in the Elastic-Plastic Range," *Proceedings of the Second U. S. National Congress of Applied Mechanics*, 1955, pp. 521–526.

11 P. G. Hodge, Jr., "Elasticity-Plasticity," part 2, section 15, John Wiley & Sons, Inc., New York, N. Y., 1958.

12 P. G. Hodge, Jr., "Plastic Analysis of Plates," section 10-4, McGraw-Hill Book Company, Inc., New York, N. Y., 1959.

13 S. Timoshenko, "Theory of Plates and Shells," McGraw-Hill Book Company, Inc., New York and London, 1940.

E. REISSNER
Professor of Mathematics
Massachusetts Institute of Technology,
Cambridge, Mass.
Mem. ASME

Y. STAVSKY
Assistant Professor
of Civil Engineering,
Massachusetts Institute
of Technology,
Cambridge, Mass.

Bending and Stretching of Certain Types of Heterogeneous Aeolotropic Elastic Plates[1]

The class of plates with which this paper is concerned includes as an important special case plates consisting of two orthotropic sheets of equal thickness which are laminated in such a way that the axes of elastic symmetry enclose an angle $+\theta$ with the x, y-axes in one sheet and an angle $-\theta$ in the other sheet. For plates of this type there occurs a coupling phenomenon between in-plane stretching and transverse bending which does not occur in the theory of homogeneous plates and which has not been considered in earlier work for such plates. The general results of the present paper are illustrated by means of explicit solutions for two specific plate problems.

In order to indicate the types of plates with which we are concerned in what follows, we specifically mention the following case. Two orthotropic sheets of equal thickness are laminated in such a way that the axes of elastic symmetry enclose an angle $+\theta$ with the x, y-axes in one sheet and an angle $-\theta$ in the other sheet. If z is a third co-ordinate normal to the plane of the undeflected sheets, measured from the interface of the two sheets, we then have the following system of stress-strain relations for the composite plate:

$$\begin{bmatrix} \tau_x \\ \tau_y \\ \tau_{xy} \end{bmatrix} = \begin{bmatrix} E_{11} & E_{12} & \text{sig } (z)E_{13} \\ E_{12} & E_{22} & \text{sig } (z)E_{23} \\ \text{sig } (z)E_{13} & \text{sig}(z)\ E_{23} & E_{33} \end{bmatrix} \begin{bmatrix} \epsilon_x \\ \epsilon_y \\ \epsilon_{xy} \end{bmatrix}$$

in which the E_{jk} are constants and sig(z) is $+1$ when $z > 0$ and -1 when $z < 0$.

We will show that for plates of this type there occurs a coupling phenomenon between in-plane stretching and transverse bending which does not occur in the theory of homogeneous plates, and which may be of practical importance. Our attention to this problem was drawn by an earlier publication on the subject of such plates,[3] which is also reported by Lekhnitsky,[4] and which does not take account of the coupling between stretching and bending with which we are concerned in the present treatment.

Formulation of Problem. Defining stress resultants, stress couples, mid-surface strains, and bending curvatures as is usual in plate theory, we have the following equilibrium relations and strain-displacement relations of linear plate theory, based on the Euler-Bernoulli hypothesis:

$$N_{x,x} + N_{xy,y} + p_x = 0, \quad N_{xy,x} + N_{y,y} + p_y = 0 \tag{1}$$

$$M_{x,x} + M_{xy,y} - Q_x = 0, \quad M_{xy,x} + M_{y,y} - Q_y = 0 \tag{2}$$

$$Q_{x,x} + Q_{y,y} + p = 0 \tag{3}$$

$$\epsilon_x = \epsilon_x^0 + z\kappa_x, \quad \epsilon_y = \epsilon_y^0 + z\kappa_y, \quad \epsilon_{xy} = \epsilon_{xy}^0 + z\kappa_{xy} \tag{4}$$

$$\epsilon_x^0 = u_{,x}, \quad \epsilon_y^0 = v_{,y}, \quad \epsilon_{xy}^0 = u_{,y} + v_{,x} \tag{5}$$

$$\kappa_x = -w_{,xx}, \quad \kappa_y = -w_{,yy}, \quad \kappa_{xy} = -2w_{,xy} \tag{6}$$

The components of strain according to (4) define components of stress through strain-strain relations which we write in matrix notation, and with a notation for moduli which we have found convenient, as follows:

$$\begin{bmatrix} \tau_x \\ \tau_y \\ \tau_{xy} \end{bmatrix} = \begin{bmatrix} E_{xx} & E_{xy} & E_{xs} \\ E_{yx} & E_{yy} & E_{ys} \\ E_{sx} & E_{sy} & E_{ss} \end{bmatrix} \begin{bmatrix} \epsilon_x \\ \epsilon_y \\ \epsilon_{xy} \end{bmatrix} \tag{7}$$

We assume the symmetry relations $E_{xy} = E_{yx}$, $E_{xs} = E_{sx}$, $E_{ys} = E_{sy}$ and we assume, furthermore, that E_{xx}, E_{xy}, E_{yy}, E_{ss} are *even* functions of z and E_{xs}, E_{ys} are *odd* functions of z.

In order to obtain a complete system of plate equations we introduce (7) into the definitions

$$N_x = \int_{-h/2}^{h/2} \tau_x dz, \quad M_x = \int_{-h/2}^{h/2} \tau_x z dz,$$

and so on, for resultants and couples. We thereby obtain a system of plate stress-strain relations of the following form:

$$\left[\begin{array}{c} N_x \\ N_y \\ N_{xy} \\ M_x \\ M_y \\ M_{xy} \end{array}\right] = \left[\begin{array}{ccc:ccc} A_{xx} & A_{xy} & 0 & 0 & 0 & B_{xs} \\ A_{yx} & A_{yy} & 0 & 0 & 0 & B_{ys} \\ 0 & 0 & A_{ss} & B_{sx} & B_{sy} & 0 \\ \hdashline 0 & 0 & B_{xs} & D_{xx} & D_{xy} & 0 \\ 0 & 0 & B_{ys} & D_{yx} & D_{yy} & 0 \\ B_{sx} & B_{sy} & 0 & 0 & 0 & D_{ss} \end{array}\right] \left[\begin{array}{c} \epsilon_x^0 \\ \epsilon_y^0 \\ \epsilon_{xy}^0 \\ \kappa_x \\ \kappa_y \\ \kappa_{xy} \end{array}\right] \tag{8}$$

---

[1] This is a report on work supported in part by the Office of Naval Research of the United States Navy, and in part by the Air Research and Development Command of the United States Air Force. Some of the results of this paper are taken from a chapter of the Doctoral dissertation[2] of the second named author. The second named author is indebted to Prof. S. Namyet for helpful discussions of the matrix algebra of this paper.

[2] Y. Stavsky, "On the Theory of Heterogeneous Anisotropic Plates," Doctor's thesis, Massachusetts Institute of Technology, Cambridge, Mass., September, 1959.

[3] C. B. Smith, "Some New Types of Orthotropic Plates Laminated of Orthotropic Material," JOURNAL OF APPLIED MECHANICS, vol. 20, TRANS. ASME, vol. 75, 1953, pp. 286–288.

[4] S. G. Lekhnitsky, "Anisotropic Plates," second edition, Moscow, Russia, *Gosud. Izdat. Tekh.-Teor. Lit.*, 1957, pp. 270–271 (in Russian).

Presented at the Summer Conference of the Applied Mechanics Division, Chicago, Ill., June 14–16, 1961, of THE AMERICAN SOCIETY OF MECHANICAL ENGINEERS.

Written discussion on this paper should be addressed to the Editorial Department, ASME, United Engineering Center, 345 East 47th Street, New York 17, N. Y., and will be accepted until October 10, 1961. Discussion received after the closing date will be returned. Manuscript received by ASME Applied Mechanics Division, September 8, 1960. Paper No. 61—APM-21.

The quantities A_{xx}, B_{xx}, D_{xx}, and so on are given by

$$(A_{xx}, B_{xx}, D_{xx}) = \int_{-h/2}^{h/2} (1, z, z^2) E_{xx} dz, \text{ etc.} \tag{9}$$

Equations (8) may also be written with the help of appropriate auxiliary matrices in the form

$$\begin{bmatrix} N \\ M \end{bmatrix} = \left[\begin{array}{c:c} A & B \\ \hdashline B & D \end{array}\right] \begin{bmatrix} \epsilon^0 \\ \kappa \end{bmatrix} \tag{8a}$$

Equations (1) to (3) together with (8) represent a system of eleven equations for eleven unknowns N_x, N_y, N_{xy}, Q_x, Q_y, M_x, M_y, M_{xy}, u, v, w. This system may be reduced to three simultaneous equations for u, v, w by introducing (8) into the two equations (1) and into a third equation which follows upon introducing equations (2) into equation (3). However, in order to see the relations of the present problem to the usual problems of stretching and bending of homogeneous plates, it is preferable to carry out a reduction to two simultaneous equations, in terms of w and in terms of an Airy stress function F.

Reduction to Two Simultaneous Equations. In order to obtain the required reduction we combine equation (2) and (3) in the form

$$M_{x,xx} + 2M_{xy,xy} + M_{y,yy} + p = 0 \tag{10}$$

and we also utilize the compatibility relation

$$\epsilon_{x,yy}{}^0 + \epsilon_{y,xx}{}^0 = \epsilon_{xy,xy}{}^0 \tag{11}$$

which is a consequence of equation (6).

We next satisfy the equilibrium equations (1) by means of an Airy stress function F, where we will assume that the body force components p_x and p_y are restricted so as to be derivable from a potential Ω as $p_x = -\Omega_{,x}$, $p_y = -\Omega_{,y}$, by setting

$$N_x = F_{,yy} + \Omega, \quad N_y = F_{,xx} + \Omega, \quad N_{xy} = -F_{,xy} \tag{12}$$

In order to obtain the final system for w and F we must write the system of stress-strain relations (8) in such a manner that $\epsilon_x{}^0$, $\epsilon_y{}^0$, $\epsilon_{xy}{}^0$, M_x, M_y, M_{xy} are given as functions of N_x, N_y, N_{xy}, κ_x, κ_y, κ_{xy}. Solving the first three of equations (8) for $\epsilon_x{}^0$, $\epsilon_y{}^0$, $\epsilon_{xy}{}^0$ in terms of N_x, N_y, N_{xy}, κ_x, κ_y, κ_{xy} and introducing the result into the remaining three equations, we arrive at a system of stress-strain relations which may be written in a form corresponding to (8a) as follows:

$$\begin{bmatrix} \epsilon^0 \\ M \end{bmatrix} = \left[\begin{array}{c:c} A^* & B^* \\ \hdashline C^* & D^* \end{array}\right] \begin{bmatrix} N \\ \kappa \end{bmatrix} \tag{13}$$

The starred matrices are given in terms of the unstarred matrices and in terms of their inverse as follows

$$[A^*] = [A^{-1}], \quad [B^*] = -[A^{-1}][B], \quad [C^*] = [B][A^{-1}].$$
$$[D^*] = [D] - [B][A^{-1}][B] \tag{14}$$

It is noted that while A^* and D^* are symmetric matrices, the same need not be true for B^* and C^*.

We now introduce (6) and (12) on the right of (13) and then introduce the appropriate portions of (13) into (10) and (11). In this way we obtain the following system of simultaneous fourth-order equations:

$$L_1 w - L_2 F = p - 2(B_{xs}{}^* + B_{ys}{}^*)\Omega_{,xy} \tag{15}$$

$$L_2 F + L_3 w = -(A_{xy}{}^* + A_{yx}{}^*)\Omega_{,xx} - (A_{xx}{}^* + A_{xy}{}^*)\Omega_{,yx} \tag{16}$$

The operators L_i are as follows

$$L_1 = D_{xx}{}^*(\ )_{,xxxx} + 2(D_{xy}{}^* + 2D_{ss}{}^*)(\ )_{,xxyy} + D_{yy}{}^*(\ )_{,yyyy} \tag{17}$$

$$L_2 = A_{yy}{}^*(\ )_{,xxxx} + 2(2A_{xy}{}^* + A_{ss}{}^*)(\ )_{,xxyy} + A_{xx}{}^*(\ )_{,yyyy} \tag{18}$$

$$L_3 = (B_{xx}{}^* - 2B_{ys}{}^*)(\ )_{,xxxy} + (B_{xy}{}^* - 2B_{xs}{}^*)(\ )_{,xyyy} \tag{19}$$

Equations (15) to (19) are remarkable for two specific properties:

1 There is a coupling between transverse bending and in-plane stretching effects, which is governed by the L_3-operator, the structure of which is connected with the B-matrix in the stress-strain relations (8).

2 The operator L_1 involves the elements of the matrix D^* rather than the elements of the matrix D.

Associated with the differential equations (15) and (16) are boundary conditions which, because of the coupling effect between the two equations, each time require consideration of in-plane and transverse effects simultaneously. This means, for instance, that if in a problem of transverse bending we have prescribed values of M_x and $R_x = Q_x + M_{xy,y}$ at an edge $x = \text{const}$, we must at the same time formulate conditions pertaining to N_x and N_{xy} (or pertaining to u and v).

Expressions for Stresses in Terms of Stress Resultants and Stress Couples. We obtain stresses in terms of resultants and couples if we transform the stress-strain relations (7) appropriately. Combination of (7) and (4) leads to a formula which, in matrix notation is

$$[\tau] = [E][\epsilon^0] + z[E][k] \tag{20}$$

We next invert equations (8) in the form

$$\begin{bmatrix} \epsilon_x{}^0 \\ \epsilon_y{}^0 \\ \epsilon_{xy}{}^0 \\ \kappa_x \\ \kappa_y \\ \kappa_{xy} \end{bmatrix} = \left[\begin{array}{ccc:ccc} a_{xx} & a_{xy} & 0 & 0 & 0 & b_{xs} \\ a_{yx} & a_{yy} & 0 & 0 & 0 & b_{ys} \\ 0 & 0 & a_{ss} & b_{sx} & b_{sy} & 0 \\ \hdashline 0 & 0 & c_{xs} & d_{xx} & d_{xy} & 0 \\ 0 & 0 & c_{ys} & d_{yx} & d_{yy} & 0 \\ c_{sx} & c_{sy} & 0 & 0 & 0 & d_{ss} \end{array}\right] \begin{bmatrix} N_x \\ N_y \\ N_{xy} \\ M_x \\ M_y \\ M_{xy} \end{bmatrix} \tag{21}$$

Introduction of (21) into (20) leads to a matrix relation of the form

$$\begin{bmatrix} \tau_x \\ \tau_y \\ \tau_{xy} \end{bmatrix} = \left[\begin{array}{ccc:ccc} e_{xx} & e_{xy} & e_{xs} & f_{xx} & f_{xy} & f_{xs} \\ e_{yx} & e_{yy} & e_{ys} & f_{yx} & f_{yy} & f_{ys} \\ e_{sx} & e_{sy} & e_{ss} & f_{sx} & f_{sy} & f_{ss} \end{array}\right] \begin{bmatrix} N_x \\ N_y \\ N_{xy} \\ M_x \\ M_y \\ M_{xy} \end{bmatrix} \tag{22}$$

where $e_{xx} = e_{xx}{}^0 + ze_{xx}{}'$, and so on, and where

$$[e^0 | f^0] = [E][a | b], \quad [e' | f'] - [E][c | d] \tag{23}$$

Equation (22) indicates the remarkable fact that, in general, τ_x depends not only on N_x and M_x but also on N_y, M_y, N_{xy}, M_{xy}, and that an analogous "cross elasticity" effect is encountered in the expressions for τ_y and τ_{xy}.

Uniform Distributions of Stress Resultants and Couples. Insight, in a relatively simple manner, into some of the consequences of elastic heterogeneity of the kind considered here may be obtained by determining the state of stress and deformation associated with resultants N and couples M which are independent of x, y.

In view of (12) we have, when N_x, N_y, N_{xy} have constant values n_x, n_y, n_{xy} and there are no body forces p_x, p_y,

$$F = \tfrac{1}{2} n_x y^2 + \tfrac{1}{2} n_y x^2 - n_{xy} xy \tag{24}$$

In order that M_x, M_y, M_{xy} at the same time have constant values m_x, m_y, m_{xy} it is necessary, in view of (13), that κ_x, κ_y, κ_{xy} have constant values k_x, k_y, k_{xy}. Accordingly, the deflection function w must be of the form

$$w = \tfrac{1}{2}k_x x^2 + \tfrac{1}{2}k_y y^2 + k_{xy}xy \tag{25}$$

and we have then that the differential equations (15) and (16), with $p = \Omega = 0$, are automatically satisfied.

Consideration of the stress-strain relations (21) indicates that in-plane forces are associated with in-plane deformations *and* transverse deflections of the plate. Similarly, bending and twisting couples are associated with transverse deflections *and* in-plane deformations of the plate. Specifically, when $m_x = m_y = m_{xy} = 0$ then

$$[\epsilon^0] = [a][n], \quad [k] = [c][n] \tag{26}$$

and when $n_x = n_y = n_{xy} = 0$, then

$$[\epsilon^0] = [b][m], \quad [k] = [d][m] \tag{27}$$

Corresponding formulas for stresses are

$$[\tau] = [e][n], \quad [\tau] = [f][m] \tag{28}$$

Sinusoidal Deflection of Infinite Plate Due to Sinusoidal Transverse Load Distributions. We now assume that the plate is subjected to a transverse load distribution of the form $p = p_0 \sin \alpha x \sin \beta y$ where p_0, α, β are constants. We also assume $p_x = p_y = 0$ so that $\Omega = 0$ in (15) and (16). Equations (15) and (16) then have solutions of the form

$$w = W_0 \sin \alpha x \sin \beta y, \quad F = F_0 \cos \alpha x \cos \beta y \tag{29}$$

and the constants W_0 and F_0 are determined from

$$[\alpha^4 D_{xx}^* + 2\alpha^2\beta^2(D_{xy}^* + 2D_{ss}^*) + \beta^4 D_{yy}^*]W_0 + [\alpha^3\beta(B_{xx}^* - 2B_{ys}^*) + \alpha\beta^3(B_{xy}^* - 2B_{xs}^*)]F_0 = p_0 \tag{30}$$

$$[\alpha^4 A_{yy}^* + 2\alpha^2\beta^2(2A_{xy}^* + A_{ss}^*) + \beta^4 A_{xx}^*]F_0 - [\alpha^3\beta(B_{xx}^* - 2B_{ys}^*) + \alpha\beta^3(B_{xy}^* - 2B_{xs}^*)]W_0 = 0 \tag{31}$$

in the form

$$\frac{W_0}{p_0} = \left\{\alpha^4 D_{xx}^* + 2\alpha^2\beta^2(D_{xy}^* + 2D_{ss}^*) + 2D_{yy}^* + \frac{[\alpha^3\beta(B_{xx}^* - 2B_{ys}^*) + \alpha\beta^3(B_{xy}^* - 2B_{xs}^*)]^2}{\alpha^4 A_{yy}^* + 2\alpha^2\beta^2(2A_{xy}^* + A_{ss}^*) + \beta^4 A_{xx}^*}\right\}^{-1} \tag{32}$$

$$\frac{F_0}{W_0} = \frac{\alpha^3(B_{xx}^* + 2B_{ys}^*) + \alpha\beta^3(B_{xy}^* - 2B_{xs}^*)}{\alpha^4 A_{yy}^* + 2\alpha^2\beta^2(2A_{xy}^* + A_{ss}^*) + \beta^4 A_{xx}^*} \tag{33}$$

Having W_0 and F_0 we find stress resultants from

$$N_x = -\beta^2 F_0 \cos \alpha x \cos \beta y, \quad N_y = \alpha^2\beta^{-2}N_x, \quad N_{xy} = -\alpha\beta F_0 \sin \alpha x \sin \beta y \tag{34}$$

In order to determine stress couples we first calculate

$$\kappa_x = \alpha^2 W_0 \sin \alpha x \sin \beta y, \quad \kappa_y = \beta^2\alpha^{-2}\kappa_x, \quad \kappa_{xy} = -2\alpha\beta W_0 \cos \alpha x \cos \beta y \tag{35}$$

and then substitute the result into the matrix formula

$$\begin{bmatrix} M_x \\ M_y \\ M_{xy} \end{bmatrix} = \left[\begin{array}{ccc:ccc} 0 & 0 & C_{xs}^* & D_{xx}^* & D_{xy}^* & 0 \\ 0 & 0 & C_{ys}^* & D_{yx}^* & D_{yy}^* & 0 \\ C_{xx}^* & C_{xy}^* & 0 & 0 & 0 & D_{ss}^* \end{array}\right] \begin{bmatrix} N_x \\ N_y \\ N_{xy} \\ \kappa_x \\ \kappa_y \\ \kappa_{xy} \end{bmatrix} \tag{36}$$

We note that the presence of the numerous zeros in the coefficient matrix in (36) is due to the symmetry properties of the material which we have assumed in so far as the coefficient matrix in the stress-strain relation (7) is concerned. If some or all of these properties are not assumed, then none of the coefficients in $[C^*]$ and $[D^*]$ necessarily vanishes.

Numerical Examples. We consider a plate consisting of two identical orthotropic layers of thickness $\frac{1}{2}h$. We assume that the axes of elastic symmetry of the layer $0 < z \leq \frac{1}{2}h$ enclose an angle $+\theta$ with the x,y-axes and of the layer $-\frac{1}{2}h \leq z < \theta$ an angle $-\theta$. We assume further that the stress-strain relations with reference to the axes of elastic symmetry x', y' are of the form

$$\begin{bmatrix} \tau_{x'} \\ \tau_{y'} \\ \tau_{x'y'} \end{bmatrix} = \begin{bmatrix} E_{xx}' & 0 & 0 \\ 0 & E_{yy}' & 0 \\ 0 & 0 & E_{ss}' \end{bmatrix} \begin{bmatrix} \epsilon_{x'} \\ \epsilon_{y'} \\ \epsilon_{x'y'} \end{bmatrix} \tag{37}$$

Rotation by angles $\pm\theta$ leads to the following values of E_{xx}, and so on, in (7) for $z = \gtrless 0$:

$$E_{xx} = E_{xx}' \cos^4\theta + E_{yy}' \sin^4\theta + 4E_{ss}' \sin^2\theta \cos^2\theta \tag{38}$$

$$E_{xy} = E_{yx} = (E_{xx}' + E_{yy}' - 4E_{ss}') \sin^2\theta \cos^2\theta \tag{39}$$

$$E_{yy} = E_{xx}' \sin^4\theta + E_{yy}' \cos^4\theta + 4E_{ss}' \sin^2\theta \cos^2\theta \tag{40}$$

$$E_{ss} = (E_{xx}' + E_{yy}') \sin^2\theta \cos^2\theta + E_{ss}'(\cos^2\theta - \sin^2\theta)^2 \tag{41}$$

$$E_{xs} = E_{sx} = \operatorname{sig}(z)[E_{xx}' \cos^3\theta \sin\theta - E_{yy}' \sin^3\theta \cos\theta - 2E_{ss}' \sin\theta \cos\theta (\cos^2\theta - \sin^2\theta)] \tag{42}$$

$$E_{ys} = E_{sy} = \operatorname{sig}(z)[E_{xx}' \sin^3\theta \cos\theta - E_{yy}' \cos^3\theta \sin\theta - 2E_{ss}' \sin\theta \cos\theta (\cos^2\theta - \sin^2\theta)] \tag{43}$$

We note that E_{xx}, E_{xy}, E_{yy}, E_{ss} are independent of z but E_{xs}, E_{ys} change sign as z changes sign.

Equations (38) to (43) define the E-matrix in (7), and using equations (9) the A, B, D matrices are readily obtained. The starred matrices in (13), (14) are given in terms of the unstarred matrices and so the functional operators (17), (18), (19) are defined in terms of the basic E' matrix in (37).

To obtain a quantitative insight into the results which apply for problems with uniform distributions, we consider an aeolotropic material with

$$E_{xx}' = 5E_{yy}' = (^{10}/_3)E_{ss}' \tag{44}$$

We assume further that $\theta = 45°$ and have then that the stress-strain relations (7) assume the form

$$\begin{bmatrix} \tau_x \\ \tau_y \\ \tau_{xy} \end{bmatrix} = E_{xx}' \begin{bmatrix} \frac{3}{5} & 0 & \frac{1}{5}\operatorname{sig}(z) \\ 0 & \frac{3}{5} & \frac{1}{5}\operatorname{sig}(z) \\ \frac{1}{5}\operatorname{sig}(z) & \frac{1}{5}\operatorname{sig}(z) & \frac{1}{10} \end{bmatrix} \tag{45}$$

We now consider a rectangular plate subject to:

(*a*) A uniform axial force N_x.
(*b*) A pure bending moment M_x.

Expressions for the transverse deflection of the plate and for the strain and stress components are obtained by using equations (24) to (28), (4) to (6), and (45).

We find the following results for the case of a uniform axial force N_x:

$$w = \frac{3}{2}\frac{N_x}{E_{xx}h^2}xy \tag{46}$$

$$\begin{bmatrix} \epsilon_x \\ \epsilon_y \\ \epsilon_{xy} \end{bmatrix} = \frac{N}{E_{xx}h} \begin{bmatrix} \frac{5}{4} \\ \frac{1}{4} \\ -\frac{3}{2}\frac{z}{h/2} \end{bmatrix} \tag{47}$$

$$\begin{bmatrix} \tau_x \\ \tau_y \\ \tau_{xy} \end{bmatrix} = \frac{N_x}{h} \begin{bmatrix} \frac{5}{4} - \frac{|z|}{h} \\ \frac{1}{4} - \frac{|z|}{h} \\ \frac{1}{2}\frac{z}{|z|} - \frac{3}{4}\frac{z}{h/2} \end{bmatrix} \tag{48}$$

The corresponding results according to Stavsky[2] are of the form

$$w^s = 0 \tag{49}$$

$$\begin{bmatrix} \epsilon_x{}^s \\ \epsilon_y{}^s \\ \epsilon_{xy}{}^s \end{bmatrix} = \frac{N_x}{E_{xx}h} \begin{bmatrix} 1 \\ 0 \\ 0 \end{bmatrix} \tag{50}$$

$$\begin{bmatrix} \tau_x{}^s \\ \tau_y{}^s \\ \tau_{xy}{}^s \end{bmatrix} = \frac{N_x}{h} \begin{bmatrix} 1 \\ 0 \\ \frac{1}{3}\frac{z}{|z|} \end{bmatrix} \tag{51}$$

A graphical representation of these results is given in Fig. 1.

Analogous results for the case of a uniform bending moment M_x are

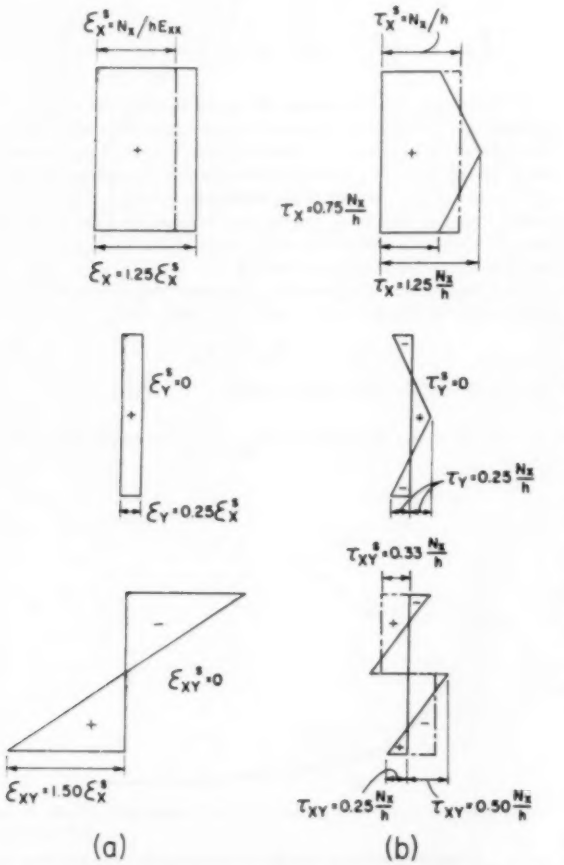

Fig. 1 Stress and strain components in a 2-layer plate subjected to uniform axial tension N_x when $E_{xx}' = 5E_{yy}' = \frac{10}{3}E_{zz}'$ and $\theta = 45°$. Quantities with superscript s are those corresponding to theory of Smith.[3]

$$w = -\frac{6M_x}{E_{xx}h^3}\left(\frac{5}{4}x^2 + \frac{1}{4}y^2\right) \tag{52}$$

$$\begin{bmatrix} \epsilon_x \\ \epsilon_y \\ \epsilon_{xy} \end{bmatrix} = \frac{3M_x}{E_{xx}h^2} \begin{bmatrix} \frac{5}{4}\frac{z}{h/2} \\ \frac{1}{4}\frac{z}{h/2} \\ \frac{1}{2} \end{bmatrix} \tag{53}$$

$$\begin{bmatrix} \tau_x \\ \tau_y \\ \tau_{xy} \end{bmatrix} = \frac{6M_x}{h^2} \begin{bmatrix} \frac{1}{6}\frac{z}{|z|} + \frac{5}{4}\frac{z}{h/2} \\ \frac{1}{6}\frac{z}{|z|} + \frac{1}{4}\frac{z}{h/2} \\ \frac{1}{4} + \frac{|z|}{h} \end{bmatrix} \tag{54}$$

We list again the corresponding results according to Smith[3]

$$w^o = -\frac{6M_x}{E_{xx}h^3}x^2 \tag{55}$$

$$\begin{bmatrix} \epsilon_x{}^o \\ \epsilon_y{}^o \\ \epsilon_{xy}{}^o \end{bmatrix} = \frac{6M_x}{E_{xx}h^3} \begin{bmatrix} \frac{z}{h/2} \\ 0 \\ 0 \end{bmatrix} \tag{56}$$

$$\begin{bmatrix} \tau_x{}^o \\ \tau_y{}^o \\ \tau_{xy}{}^o \end{bmatrix} = \frac{6M_x}{h^3} \begin{bmatrix} \frac{z}{h/2} \\ 0 \\ \frac{1}{5}\frac{|z|}{h/2} \end{bmatrix} \tag{57}$$

A graphical representation of these results is given in Fig. 2.

We note that in case (*a*) the axial tension deforms the flat plate into a hyperbolic paraboloid surface. The coupling of stretching and bending is clearly indicated by equations (47) and the cross elasticity effect is shown in equation (48).

No transverse deflection is predicted in Smith,[3] and the strain and stress distribution according to (50), (51) differs qualitatively and quantitatively from the results in (47), (48).

Note that the stress distribution (51) has as a resultant not only an axial force N_x, but a twisting couple as well.

In case (*b*) (52) yields larger deflections than (55) does, and the strain and stress components in (53), (54) are entirely different from those in (56), (57).

For any other value of θ in the transformation equations (38) to (43) we would get all the terms in the E-matrix in (7), but qualitatively the previous results are still valid.

To illustrate the results for the problem of the infinite plate with sinusoidal transverse load, we consider further the special case of this problem where we have equal wave lengths, $\beta = \alpha$, in equations (29).

We consider three different solutions given by the following:

1 The approach of Smith[3] (indicated again by a superscript *s*).
2 Neglecting the coupling terms L_3 in the differential equation (15), (16) (indicated by a superscript 0).
3 The complete system (15) and (16).

We will see that for the present problem the case $\theta = 45°$ is associated with rather special properties of the solution. Setting $\theta = 45°$ in equations (38) to (42) and observing (32), (33), and (14) we find that the shear rigidity constant E_{zz}' does not enter into the expressions for the composite plate.

Setting $E_{yy}'/E_{xx}' = k$ we obtain the following expressions for deflections, stress resultants, stress couples, strains and stresses:

$$(w^s, w) = \left(\frac{1}{2(1+k)}, \frac{2(1+k)}{4(1+k)^2 - 3(1-k)^2}\right) \frac{12p_0h}{E_{xx}'\alpha^4h^4} \sin \alpha x \sin \alpha y \quad (58)$$

$$(M_x^s, M_x) = (M_y^s, M_y) = \frac{p_0}{4\alpha^2} \sin \alpha x \sin \alpha y \quad (59)$$

$$(M_{xy}^s, M_{xy}) = -\frac{p_0}{4\alpha^2} \cos \alpha x \cos \alpha y \quad (60)$$

$$(N_x^s, N_x, N_y^s, N_y, N_{xy}^s, N_{xy}) = 0 \quad (61)$$

$$(\epsilon_x^s, \epsilon_z) = (\epsilon_y^s, \epsilon_y) = \frac{6p_0}{E_{xx}'\alpha^2h^2} \left\{\left(\frac{1}{2(1+k)}, \frac{2(1+k)}{4(1+k)^2 - 3(1-k)^2}\right) \frac{z}{h/2} \sin \alpha x \sin \alpha y + \left(0, \frac{(1-k)}{4(1+k)^2 - 3(1-k)^2}\right) \cos \alpha x \cos \alpha y \right. \quad (62)$$

$$(\epsilon_{xy}^s, \epsilon_{xy}) = \frac{12p_0}{E_{xx}'\alpha^2h^2} \left\{0, -\frac{(1-k)}{4(1+k)^2 - 3(1-k)^2}\right) \sin \alpha x \sin \alpha y - \left(\frac{1}{2(1+k)}, \frac{2(1+k)}{4(1+k)^2 - 3(1-k)^2}\right) \frac{z}{h/2} \cos \alpha x \cos \alpha y \right\} \quad (63)$$

$$\tau_x^s = \tau_y^s = \frac{3}{2} \frac{p_0}{\alpha^2h^2} \left\{\frac{z}{h/2} \sin \alpha x \sin \alpha y - \frac{1-k}{1+k} \frac{|z|}{h/2} \cos \alpha x \cos \alpha y \right\} \quad (64)$$

$$\tau_x = \tau_y = \frac{3p_0}{2\alpha^2h^2[4(1+k)^2 - 3(1-k)^2]} \left\{\left((4(1+k)^2 \frac{z}{h/2} - 2(1-k)^2 \frac{z}{|z|}\right) \sin \alpha x \sin \alpha y + 2(1-k^2)\left(1 - 2\frac{|z|}{h/2}\right) \cos \alpha x \cos \alpha y \right\} \quad (65)$$

$$\tau_{xy}^s = \frac{3}{2} \frac{p_0}{\alpha^2h^2} \left\{\frac{1-k}{1+k} \frac{|z|}{h/2} \sin \alpha x \sin \alpha y - \frac{z}{h/2} \cos \alpha x \cos \alpha y \right\} \quad (66)$$

$$\tau_{xy} = \frac{3p_0}{2\alpha^2h^2[4(1+k)^2 - 3(1-k)^2]} \left\{2(1-k^2)\left(2\frac{|z|}{h/2} - 1\right) \sin \alpha x \sin \alpha y + \left(2(1-k)^2 \frac{z}{|z|} - 4(1+k)^2 \frac{z}{h/2}\right) \cos \alpha x \cos \alpha y \right\} \quad (67)$$

We note that the expressions for stress couples and stress resultants are the same as those for homogeneous isotropic plates. The remaining expressions for deflections, strains, and stresses show the effect of heterogeneity through the appearance of the parameter k. The nature of the difference between the present results and the results of Smith[2] is indicated in Fig. 3 which represents certain deflection and strain deflection and strain ratios as a function of the parameter k.

For a more detailed discussion of stresses and strains we consider a case for which $\theta = 30°$ and

$$E_{xx}' = 10E_{yy}' = E_{zz}' \quad (68)$$

We now obtain the following formulas:

$$(w^s, w^0, w) = (4.100, 7.200, 6.750) \frac{p_0h}{E_{xx}'\alpha^4h^4} \sin \alpha x \sin \alpha y \quad (69)$$

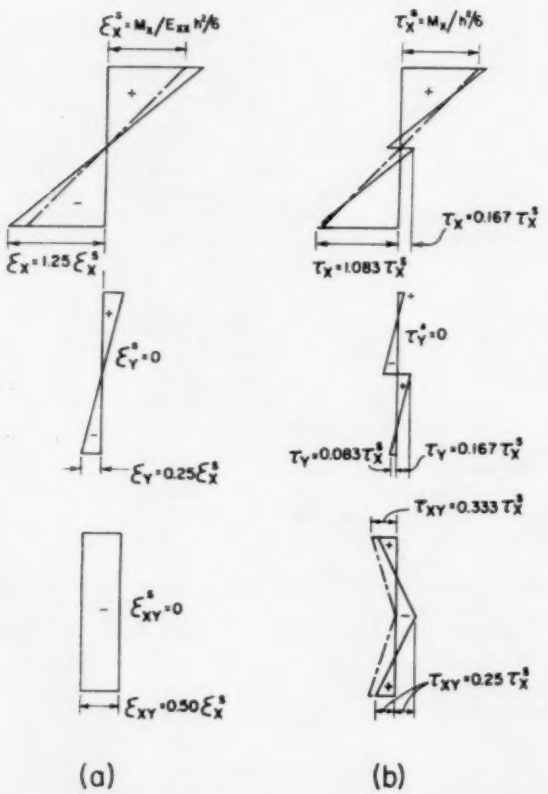

Fig. 2 Stress and strain components in a 2-layer plate subjected to pure bending M_x, when $E_{xx}' = 5E_{yy}' = \frac{10}{3} E_{xy}'$ and $\theta = 45°$. Quantities with superscript s are those corresponding to theory of Smith.[2]

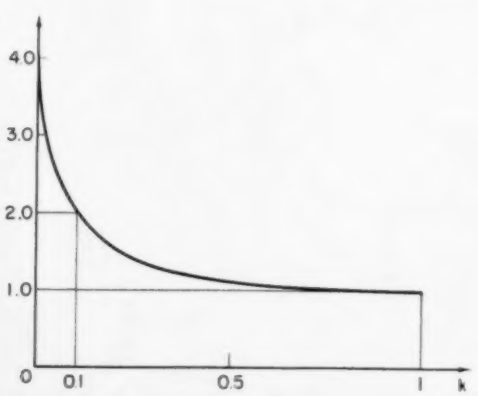

Fig. 3 Values of $w/w^s = \epsilon_z/\epsilon_z^s = \epsilon_y/\epsilon_y^s$ for $\alpha x = \alpha y = \frac{1}{2}\pi$ as a function of $k = E_{yy}'/E_{xx}'$ when $\theta = 45°$

$$(M_x^s, M_x^0, M_x) = (0.264, 0.476, 0.494)\frac{p_0}{\alpha^2}\sin\alpha x\sin\alpha y \quad (70)$$

$$(M_y^s, M_y^0, M_y) = (0.101, -0.003, -0.079)\frac{p_0}{\alpha^2}\sin\alpha x\sin\alpha y \quad (71)$$

$$(M_{xy}^s, M_{xy}^0, M_{xy}) = (-0.312, -0.228, -0.291)\frac{p_0}{\alpha^2}\cos\alpha x\cos\alpha y \quad (72)$$

$$\begin{bmatrix} N_x^s, & N_x^0, & N_x \\ N_y^s, & N_y^0, & N_y \\ N_{xy}^s, & N_{xy}^0, & N_{xy} \end{bmatrix} = (0, 0, 0.274)\frac{p_0 h}{\alpha^2 h^2}\begin{bmatrix} \cos\alpha x\cos\alpha y \\ \cos\alpha x\cos\alpha y \\ \sin\alpha x\sin\alpha y \end{bmatrix} \quad (73)$$

$$(\epsilon_x^s, \epsilon_x^0, \epsilon_x) = (0, 0.734, 0.232)\frac{p_0}{E_{zz}'\alpha^2 h^2}\cos\alpha x\cos\alpha y + (2.050, 3.600, 3.380)\frac{z}{h/2}\frac{p_0}{E_{zz}'\alpha^2 h^2}\sin\alpha x\sin\alpha y \quad (74)$$

$$(\epsilon_y^s, \epsilon_y^0, \epsilon_y) = (0, 0.207, 1.810)\frac{p_0}{E_{zz}'\alpha^2 h^2}\cos\alpha x\cos\alpha y + (2.050, 3.600, 3.380)\frac{p_0}{E_{zz}'\alpha^2 h^2}\sin\alpha x\sin\alpha y \quad (75)$$

$$(\epsilon_{xy}^s, \epsilon_{xy}^0, \epsilon_{xy}) = (0, -1.540, -2.040)\frac{p_0}{E_{zz}'\alpha^2 h^2}\sin\alpha x\sin\alpha y + (-4.100, -7.200, -6.750)\frac{z}{h/2}\frac{p_0}{E_{zz}'\alpha^2 h^2}\cos\alpha x\cos\alpha y \quad (76)$$

$$(\tau_x^s, \tau_x^0, \tau_x) = \left(\left[1.590\frac{z}{h/2}\right], \left[2.800\frac{z}{h/2} - 0.1830\frac{z}{|z|}\right], \left[2.620\frac{z}{h/2} - 0.243\frac{z}{|z|}\right]\right)\frac{p_0}{\alpha^2 h^2}\sin\alpha x\sin\alpha y + \left(\left[-0.492\frac{|z|}{h/2}\right], \left[-0.860\frac{|z|}{h/2} - 0.427\right], \left[-0.810\frac{|z|}{h/2} - 0.679\right]\right)\frac{p_0}{\alpha^2 h^2}\cos\alpha x\cos\alpha y \quad (77)$$

$$(\tau_y^s, \tau_y^0, \tau_y) = \left(\left[0.670\frac{z}{h/2}\right], \left[1.220\frac{z}{h/2} + 0.780\frac{z}{|z|}\right],$$

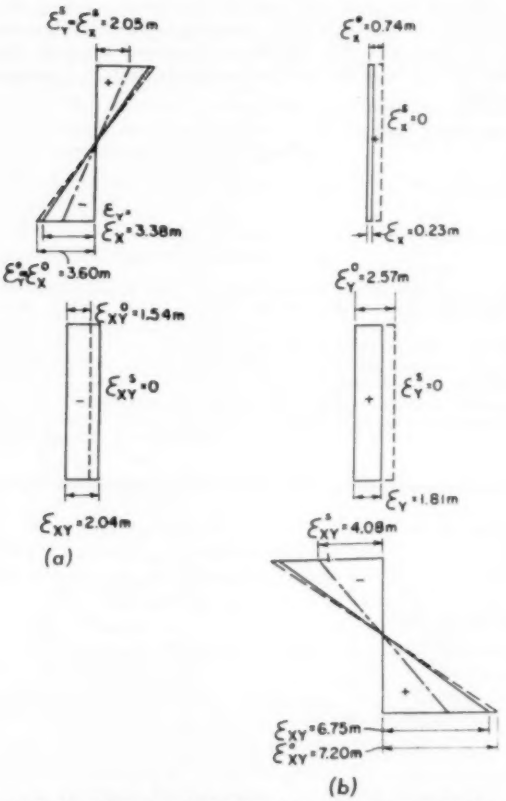

Fig. 4 Strain distributions in infinite plate with transverse load $p_0 \sin \alpha x \sin \alpha y$ for:

(a) $\alpha x = \alpha y = \pm\frac{1}{2}\pi, \pm\frac{5}{2}\pi, \ldots$ (b) $\alpha x = \alpha y = 0, \pm 2\pi, \ldots$ when $E_{zz}' = 10E_{yy}' = E_{xx}', \theta = 30°$ in units of $m = p_0/E_{zz}'\alpha^2 h^2$.

Solid lines indicate results of present theory. Dashed and dot-dashed lines indicate results of theories without consideration of cross-coupling terms.

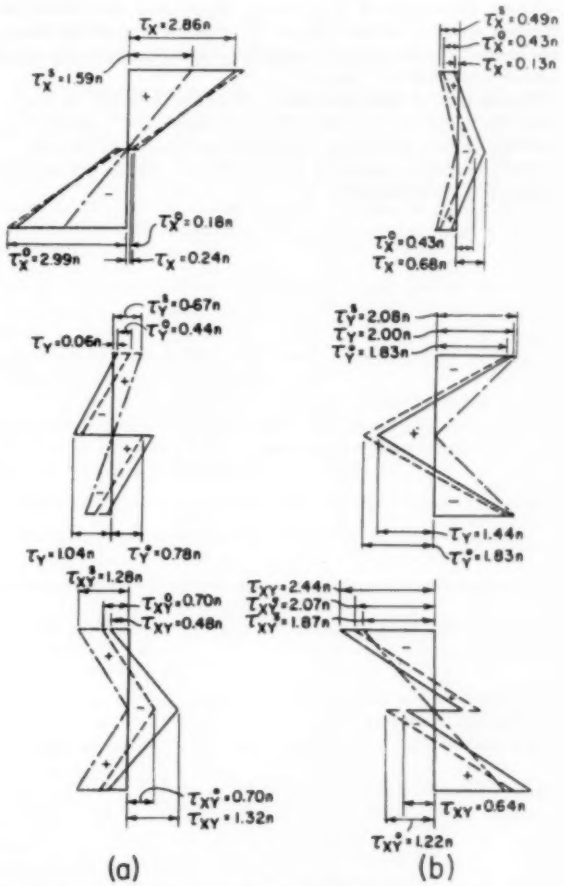

Fig. 5 Stress distribution in infinite plate with transverse load $p_0 \sin \alpha x \sin \alpha y$ for:

(a) $\alpha x = \alpha y = \pm\frac{1}{2}\pi, \pm\frac{5}{2}\pi, \ldots$, (b) $\alpha x = \alpha y = 0, \pm 2\pi, \ldots$ when $E_{zz}' = 10\,E_{yy}' = E_{xx}', \theta = 30°$ in units of $n = p_0/\alpha^2 h^2$. Solid lines indicate results of present theory Dashed and dot-dashed lines indicate results of theories without consideration of cross-coupling terms.

$$\left[1.100\,\frac{z}{h/2} + 1.040\,\frac{z}{|z|}\right]\frac{p_0}{\alpha^2 h^2}\sin\alpha x \sin\alpha y + \left(\left[2.080\,\frac{|z|}{h/2}\right], \left[3.670\,\frac{|z|}{h/2} + 1.830\right], \left[3.440\,\frac{|z|}{h/2} + 1.440\right]\right)\frac{p_0}{\alpha^2 h^2}\cos\alpha x \cos\alpha y \quad (78)$$

$$(\tau_{xy}^0, \tau_{xy}^0, \tau_{xy}) = \left(\left[-1.290\,\frac{|z|}{h/2}\right], \left[-1.400\,\frac{|z|}{h/2} - 0.695\right], \left[-1.320\,\frac{|z|}{h/2} - 0.931\right]\right)\frac{p_0}{\alpha^2 h^2}\sin\alpha x \sin\alpha y + \left(\left[-1.870\,\frac{z}{h/2}\right], \left[-3.290\,\frac{z}{h/2} - 1.220\,\frac{z}{|z|}\right], \left[-3.080\,\frac{z}{h/2} - 0.641\,\frac{z}{|z|}\right]\right)\frac{p_0}{\alpha^2 h^2}\cos\alpha x \cos\alpha y \quad (79)$$

The results of equations (74) to (79) are indicated graphically in Figs. 4 and 5. It is apparent that considerable differences exist between the results of the present theory and the results of theories which do not consider all the cross-coupling terms which are associated with the particular kind of nonisotropy and heterogeneity which has been assumed.

Consideration of Finite Deflections. We indicate briefly in which way the linear theory with which we have been concerned is modified if finite transverse deflections are taken into account.

The equilibrium equations (1) and (2) are valid as before, but equation (3) is replaced by

$$[Q_x + N_x w_{,x} + N_{xy} w_{,x}]_{,x} + [Q_y + N_{xy} w_{,x} + N_y w_{,y}]_{,y} + p = 0 \quad (80)$$

The strain-displacement relations (5) are replaced by

$$\epsilon_x^0 = u_{,x} + \tfrac{1}{2} w_{,x}^2, \quad \epsilon_y^0 = v_{,y} + \tfrac{1}{2} w_{,y}^2, \quad \epsilon_{xy}^0 = u_{,y} + v_{,x} + w_{,x} w_{,y} \quad (81)$$

and equations (4) and (6) remain unchanged.

The plate stress-strain relations (8) remain valid which means that together with equations (1), (2), and (80) we have again a system of eleven equations for eleven unknowns N_x, N_y, N_{xy}, Q_x, Q_y, M_x, M_y, M_{xy}, u, v, w.

This system is reduced to two simultaneous equations by using equation (10) and the modified compatibility relation

$$\epsilon_{x,yy}^0 + \epsilon_{y,xx}^0 - \epsilon_{xy,xy}^0 = w_{,xy}^2 - w_{,xx} w_{,yy} \quad (82)$$

which is a consequence of equation (81).

Following the same procedure as before, we use equations (12), (13), (14) in (80) and (82) to get

$$L_1 w - L_2 F = p - 2(B_{xx}^* + B_{yx}^*)\Omega_{,xy} + \Omega_{,x} w_{,x} + \Omega_{,y} w_{,y} + \Omega(w_{,xx} + w_{,yy}) + F_{,yy} w_{,xx} - 2F_{,xy} w_{,xy} + F_{,xx} w_{,yy} \quad (83)$$

$$L_2 F + L_1 w = -(A_{xy}^* + A_{yy}^*)\Omega_{,xx} - (A_{xx}^* + A_{xy}^*)\Omega_{,yy} + w_{,xy}^2 - w_{,xx} w_{,yy} \quad (84)$$

Equations (83) and (84) combine the linear coupling effect which is a characteristic of the heterogeneity which has been assumed here with the well-known nonlinear coupling effect which is seen to be of the same form as for the isotropic homogeneous plate.

W. G. FLIEDER
Staff Engineer,
Arthur D. Little, Inc.,
Santa Monica, Calif.

J. C. LORIA
Staff Engineer,
Arthur D. Little, Inc.,
Cambridge, Mass.

W. J. SMITH
Staff Engineer,
Arthur D. Little, Inc.,
Santa Monica, Calif.

Bowing of Cryogenic Pipelines

The design of propellant loading systems for present-day missiles involves the design of pipelines that can carry cryogenic fluids and requires an additional consideration beyond the conventional analyses for flexibility and dead weight. Because of varying flow conditions and boil-off, these cryogenic lines experience varying fill levels and concomitant temperature gradients which cause these lines to bow; i.e., to assume a uniform curvature of circular arc. If constrained, the thermal-stress distributions which are generated by the temperature gradients will have superposed on them additional stresses, which result from the action of the support constraints. This combination of stresses may be critical and/or the loads on the supports may be excessive. The following analysis investigates these bowing effects, thermal stresses, and indicates the support problems entailed.

A LOW-TEMPERATURE liquid flowing at varying levels in a horizontal pipeline acts as a heat sink and induces transient temperature gradients over the cross section of the pipe and across its thickness. In contrast with the situation that exists when a hot fluid flows at a certain level in a pipeline, the temperature gradients are intensified rather than alleviated. This intensification is explained by the following factors:

1 The thermal conductivity of the pipe material is reduced at low temperatures; this reduces the heat transfer by conduction.

2 The external convective heat-flow pattern is downward, because of gravity; this tends to maintain the upper side of the pipe at ambient temperature.

3 The internal convective heat flow is minimized since, again, the low-temperature vapor formed above the fluid vapor tends to fall rather than rise because of gravity.

These temperature gradients in the pipe have the following important effects:

1 Transient thermal stresses are induced by differential contractions over the pipe cross-sectional area.

Presented at the West Coast Conference of the Applied Mechanics Division, Seattle, Wash., August 28–30, 1961, of THE AMERICAN SOCIETY OF MECHANICAL ENGINEERS.

Discussion of this paper should be addressed to the Editorial Department, ASME, United Engineering Center, 345 East 47th Street, New York 17, N. Y., and will be accepted until October 10, 1961. Discussion received after the closing date will be returned. Manuscript received by ASME Applied Mechanics Division, September 2, 1960. Paper No. 61—APMW-7.

2 The strength and modulus of elasticity of the material are changed at low temperatures.

3 The pipe tends to bow into a circular arc, and large reaction forces and moments may result at anchors and intermediate supports.

Basic Thermoelastic Relationships [1–4] [1]

If the structure behaves elastically and if the temperature distribution is known, then the stresses can be calculated in the following manner. In this analysis, it is assumed that the temperature gradient at any cross section of the pipe is the same at any specific time, and that the pipe thickness is small enough that radial temperature gradients through the pipe wall may be ignored safely. The following assumptions are necessary to proceed with this analysis:

1 Only the lengthwise distortions and stresses in the pipe structure are important to the establishment of the bowing effect.

2 Plane cross sections remain plane after distortion.

3 There is no end constraint.

4 In accordance with Saint Venant's principle, the internal thermoelastic stress pattern exists uniformly throughout the pipe length, except for a short distance from the free ends of the pipe. A typical section of pipe is shown in Fig. 1.

Although a pipe is a perfectly symmetrical element about its

[1] Numbers in brackets designate References at end of paper.

Nomenclature

d = pipe diameter, in.
E = modulus of elasticity, psi
e = integrated coefficient of thermal expansion, in./in.
F = force, lb
I = moment of inertia of pipe section, in.^{4}
i = element number measured from top of pipe
K = factor relating bowing curvature to temperature gradient, dimensionless
k_1, k_2, k_3 = coefficients used to specify total strain
L = distance between supports, in.
M = bending moment, in-lb
m = number of elements into which pipe section is divided
$P_0, P_1,$ etc. = support loads, lb
R = radius of curvature of bowing, in.
r = pipe radius, in.
T, T_1, T_2 = temperature, deg F
t = pipe thickness, in.
u = displacement in x-axis, in.
x, y, z = pipe co-ordinates, in.
y_i, z_i = pipe co-ordinates measured from centroidal axis to ith element, in.
$\bar{y}, \bar{z}$ = displacement of neutral axis from centroidal axis, in.
z', z_i' = vertical pipe co-ordinates measured from neutral axis, in.
$\bar{z}_i, \bar{z}_i', \bar{\bar{z}}$ = normalized vertical pipe co-ordinates, dimensionless
ΔT = temperature differential, deg F
α = thermal coefficient of expansion (contraction), in/in/deg F
δ = displacement, in.
ϵ = elastic strain, in/in.
ϵ_{tot} = total strain, in/in.
ϵ_t = thermal strain, in/in.
θ = vertical pipe co-ordinate in polar form, deg
θ_1 = fill level in polar form, deg
σ = stress, psi

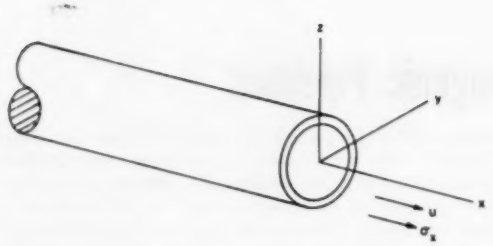

u = AXIAL DISPLACEMENT

σ_x = AXIAL STRESS

Fig. 1 Typical section of pipe

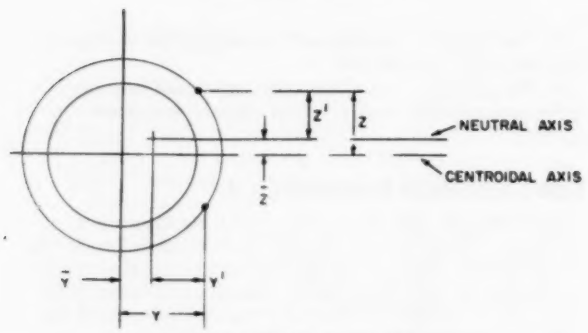

Fig. 2 Typical cross section

center lines, the modulus of elasticity varies with temperature and causes displacement of the neutral axes of the pipe with respect to the centroidal axes. A typical cross section is shown in Fig. 2. In the figure,

y, z = distance measured from centroidal axis

y', z' = distance measured from neutral axis

$\bar{y}, \bar{z}$ = displacement of neutral axis

Then, by definition of the neutral axis,

$$z' = z - \bar{z} \tag{1}$$

$$\int_A Ez'dA = 0 \tag{2}$$

From Equations (1) and (2),

$$\bar{z} = \frac{\int_A E\,z\,dA}{\int_A EdA} \tag{3}$$

Similarly,

$$\bar{y} = \frac{\int_A E\,y\,dA}{\int_A EdA} \tag{4}$$

The total strain of any point on the cross section may now be specified as

$$\epsilon_{tot} = \frac{du}{dx} = (k_1y' + k_2z' + k_3) \tag{5}$$

A portion of the total strain is attributed to thermal strain:

$$\epsilon_t = \alpha\Delta T(y, z), \tag{6}$$

where

α = average expansion coefficient for temperature change

ΔT = temperature differential

The difference between equations (5) and (6) is elastic strain ϵ, and the axial stress at any point is

$$\sigma_x = E\epsilon = E\left[\frac{du}{dx} - \alpha\Delta T\right]$$

$$= E(k_1y' + k_2z' + k_3) - E\alpha\Delta T \tag{7}$$

Now the condition of zero end constraint implies the following expressions:

$$\Sigma\ F = 0, \int_A \sigma_x dA = 0$$

$$\Sigma M_z = 0, \int_A \sigma_x y'dA = 0 \tag{8}$$

$$\Sigma M_y = 0, \int_A \sigma_x z'dA = 0$$

And by substitution of equations (2) and (7) into equation (8),

$$k_1 = \frac{\int_A Ey'\alpha\Delta T\,dA}{\int_A Ey'^2dA}$$

$$k_2 = \frac{\int_A Ez'\alpha\Delta T\,dA}{\int_A Ez'^2dA} \tag{9}$$

$$k_3 = \frac{\int_A E\alpha\Delta T\,dA}{\int_A E\,dA}$$

If we place the results from equation (9) into equation (7), a general equation for stress at any point in the pipe section can then be determined as follows:

$$\sigma_x(y, z) = E\left[\frac{y\int_A Ey'\alpha\Delta T\,dA}{\int_A Ey'^2dA} + \frac{z\int_A Ez'\alpha\Delta T\,dA}{\int_A Ez'^2dA} + \frac{\int_A E\alpha\Delta T dA}{\int_A E\,dA}\right] - E\alpha\Delta T \tag{10}$$

The temperature distribution will always be symmetrical with respect to the z-axis of Fig. 1, which means that $\bar{y} = 0$ and $k_1 = 0$. The numerator of the k_2-term in this expression is equal to the bending moment that would be developed if bowing were prevented by end moments, and the denominator is equal to the rigidity of the cross section. Thus k_2 is identically equal to the bowing curvature that would be produced in the unconstrained pipe; i.e., $k_2 = 1/R$. The value of k_3 is equal to the average total strain for the cross section.

These expressions are entirely general, and no restriction has been placed upon the variation of expansion coefficients and modulus of elasticity as a function of temperature.

Effect of Temperature Distribution on Bowing

General Analysis. The following general analysis yields some insight into the effect of temperature distribution on bowing.

Two additional basic assumptions were employed to reduce the mathematical complexity without sacrificing the validity of the results:

1 The modulus of elasticity is invariant with temperature.

2 The thermal-expansion coefficient is a constant over the temperature range.

A thin, uninsulated pipe partly filled with liquid oxygen or liquid nitrogen is at the liquid temperature to the fill level, whereas the top fibers are much warmer. The temperature distribution across the pipe is shown in Fig. 3. From the figure, taking the elemental area

$$dA = t\,\frac{d}{2}\,d\theta, \quad z = \frac{d}{2}\cos\theta,$$

and applying these assumptions to equation (10) yields

$$\sigma_x(\theta) = \frac{E\alpha}{\pi}\left[2\cos\theta\int_0^\pi \Delta T(\theta)\cos\theta d\theta + \int_0^\pi \Delta T(\theta)d\theta - \pi\Delta T(\theta)\right] \tag{11}$$

Also, the terms k_2 and k_3 in equation (9) reduce to

$$k_2 = \frac{4\alpha}{\pi d}\int_0^\pi \Delta T(\theta)\cos\theta d\theta$$
$$k_3 = \frac{\alpha}{\pi}\int_0^\pi \Delta T(\theta)d\theta \tag{12}$$

For this analysis, the three simple temperature distributions shown in Fig. 4 will be assumed. The temperature T_2 will depend on the fill level, the pipe diameter, ambient conditions, and the pipe-material properties.

Case 1. Linear Temperature Distribution. The temperature differential from T_2 at any point in the pipe is

$$\Delta T(\theta) = \frac{T_1 - T_2}{2}\,[\cos\theta - 1] \tag{13}$$

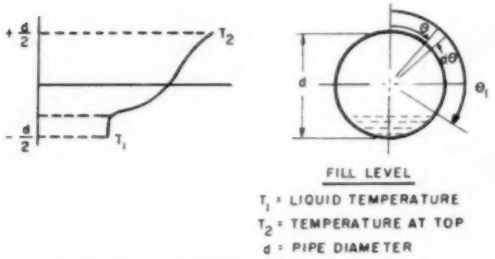

Fig. 3 Typical temperature distribution

By substitution in equation (11), the well-known fact follows that the thermal stresses resulting from a linear gradient are zero:

$$\sigma_x(\theta) = 0 \tag{14}$$

The solution of equation (12) yields

$$k_2 = \frac{\alpha(T_1 - T_2)}{d}, \tag{15}$$

and since

$$k_2 = 1/R \tag{16}$$

and

$$e = \alpha(T_1 - T_2), \tag{17}$$

then

$$R = d/e \tag{18}$$

Taking the curvature for the linear gradient as a standard, we can define the factor K to compare the change in curvature resulting from other gradients; that is,

$$\frac{1}{R} = K\,\frac{e}{d}$$

Thus, for the linear gradient, $K = 1.0$.

Case 2. Step Temperature Change at Fill Level. For a step temperature condition:

$$\Delta T(\theta) = 0 \qquad 0 \le \theta \le \theta_1$$
$$\Delta T(\theta) = T_2 - T_1 \qquad \theta_1 \le \theta \le \pi \tag{19}$$

Through the use of equation (11), the stress can be expressed as

$$\sigma_x(\theta) = \frac{Ee}{\pi}(2\sin\theta_1\cos\theta + \theta_1 - \pi) \qquad 0 \le \theta \le \theta_1$$
$$\sigma_x(\theta) = \frac{Ee}{\pi}(2\sin\theta_1\cos\theta + \theta_1) \qquad \theta_1 \le \theta \le \pi \tag{20}$$

and,

$$R = \frac{\pi}{4\sin\theta_1}\,\frac{d}{e} \tag{21}$$

Case 3. Constant Temperature to Fill Line and Linear Temperature Rise. The temperature differential at any point in the pipe is

$$\Delta T(\theta) = (T_2 - T_1)\left[\frac{1 - \cos\theta}{1 - \cos\theta_1}\right] \qquad 0 \le \theta \le \theta_1$$
$$\Delta T(\theta) = T_2 - T_1 \qquad \theta_1 \le \theta \le \pi \tag{22}$$

Again, by the use of equation (11),

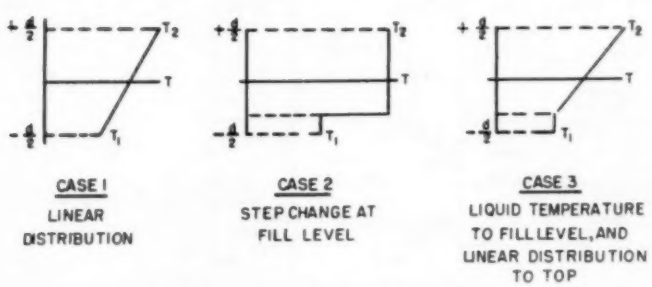

Fig. 4 Temperature distribution in vertical axis

$$\sigma_x(\theta) = \frac{Ee}{\pi(1 - \cos\theta_1)} [(\theta_1 - \pi - \sin\theta_1 \cos\theta_1)\cos\theta - (\theta_1 - \pi)\cos\theta_1 + \sin\theta_1] \quad 0 \le \theta \le \theta_1$$

$$\sigma_x(\theta) = \frac{Ee}{\pi(1 - \cos\theta_1)} [(\theta_1 - \sin\theta_1 \cos\theta_1)\cos\theta - \theta_1 \cos\theta_1 + \sin\theta_1] \quad \theta_1 \le \theta \le \pi \tag{23}$$

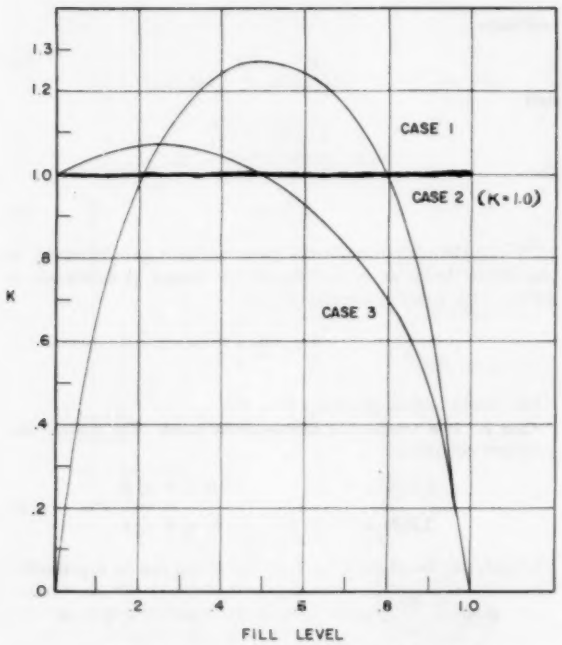

Fig. 5 K versus fill level for Cases 1, 2, and 3

and

$$R = \frac{\pi(1 - \cos\theta_1)}{2\theta_1 - \sin 2\theta_1} \left(\frac{d}{e}\right) \tag{24}$$

Comparison of Three Cases. For each of the three cases, the variation of the factor K with fill level is given in Fig. 5.

The maximum possible value for K is 1.273. Over the range $^1/_4$ to $^3/_4$ full, the step in temperature would cause a large pipe curvature, and the maximum possible value is 27 per cent in excess of the curvature indicated by a linear gradient.

The actual stress patterns set up in an unconstrained pipe are very strongly influenced by the temperature distribution across the pipe section. The stresses developed in the pipe for Cases 1, 2, and 3 are summarized in Fig. 6.

Stress Analysis in a 12-In. Line

It may be essential to evaluate internal stresses in pipes for known temperature distributions that cannot be resolved into simple mathematical formulations. Experimental data obtained on 8 and 12-in. stainless-steel pipes for a half-full condition yielded the steady-state temperature distributions shown in Fig. 7. The ambient temperature was 80 F during this experiment, and the temperature at the top fibers of the pipe was 35 F, which confirms the introductory statements.

We can make an accurate stress analysis by breaking the pipe area into small elements and performing numerical summations in place of the integrations indicated in equations (1–12). We can also take into account the variation in elastic modulus and expansion coefficient as a function of temperature. Because the pipe is symmetrical, these operations need be performed for only one half the pipe cross section. For a half section divided into m equal elements of area, the data shown in Fig. 8 apply. In the figure,

i = element number measured from top
A_i = cross-sectional area of ith element
z_i = distance from y-axis to centroid of ith element

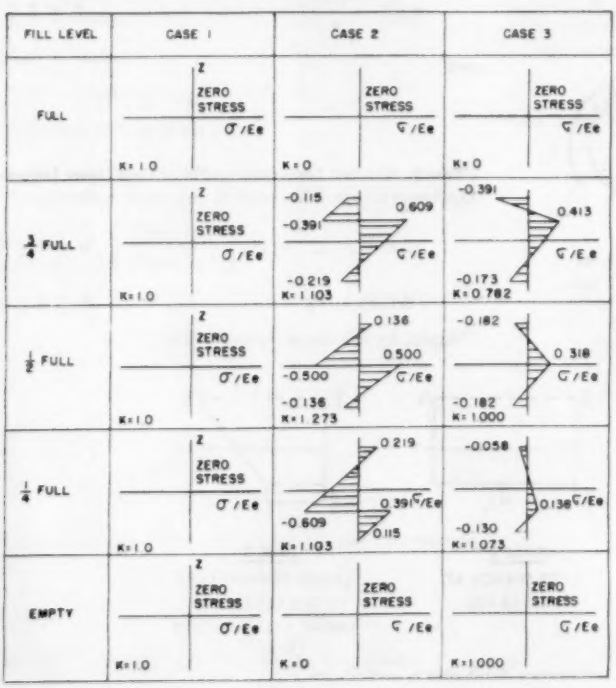

Fig. 6 Internal stresses in unconstrained pipe

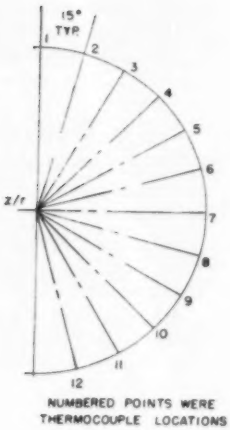

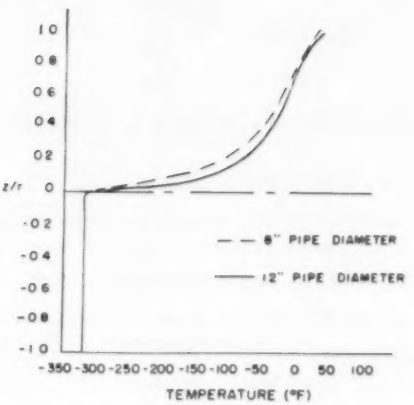

Fig. 7 Temperature-shock data for pipe half filled with liquid nitrogen

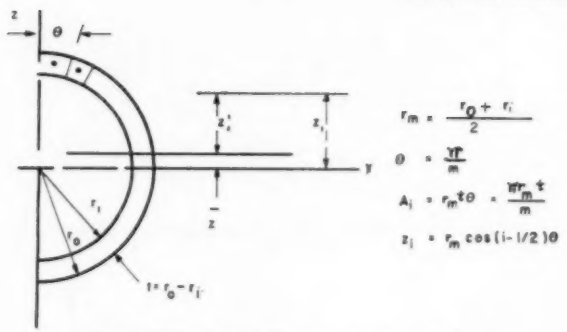

Fig. 8 Elemental presentation of pipe cross section

z_i' = distance from neutral axis to centroid of ith element

$z_i' = z_i - \bar{z}$

The modified form for Equation (3) becomes

$$\bar{z} = \frac{\sum_{i=1}^{m} E_i z_i A_i}{\sum_{i=1}^{m} E_i A_i} = \frac{\sum_{i=1}^{m} E_i z_i}{\sum_{i=1}^{m} E_i} \tag{25}$$

From Equation (9)

$$k_1 = 0$$

$$k_2 = \frac{\sum_{i=1}^{m} E_i \alpha_i \Delta T_i z_i'}{\sum_{i=1}^{m} E_i z_i'^2} \tag{26}$$

$$k_3 = \frac{\sum_{i=1}^{m} E_i \alpha_i \Delta T_i}{\sum_{i=1}^{m} E_i}$$

And applying this result to equation (7) yields

$$\sigma_i = -E_i \alpha_i \Delta T_i + \frac{E_i z_i' \sum_{i=1}^{m} E_i \alpha_i \Delta T_i z_i'}{\sum_{i=1}^{m} E_i z_i^2} + \frac{E_i \sum_{i=1}^{m} E_i \alpha_i \Delta T_i}{\sum_{i=1}^{m} E_i} \tag{27}$$

By direct substitutions

$$z_i' = z_i - \bar{z} = r_m \left[\cos(i - \tfrac{1}{2})\theta - \frac{\sum_{i=1}^{m} E_i \cos(i - \tfrac{1}{2})\theta}{\sum_{i=1}^{m} E_i} \right] \tag{28}$$

The solution will be facilitated if we normalize as follows:

$$\bar{z}_i = \frac{z_i}{r_m} = \cos(i - \tfrac{1}{2})\theta$$

$$\bar{z}_i' = \frac{z_i'}{r_m} \tag{29}$$

$$\bar{z} = \frac{\bar{z}}{r_m}$$

$$\bar{z}_i' = \bar{z}_i - \bar{z}$$

Hence equations (25), (26), (27), and (28) become, respectively,

$$\bar{z} = \frac{\sum_{i=1}^{m} E_i \cos(i - \tfrac{1}{2})\theta}{\sum_{i=1}^{m} E_i} \tag{30}$$

$$\frac{1}{R} = k_2 = \frac{1}{r_m} \frac{\sum_{i=1}^{m} E_i \alpha_i \Delta T_i \bar{z}_i'}{\sum_{i=1}^{m} E_i \bar{z}_i'^2} \tag{31}$$

$$k_3 = \frac{\sum_{i=1}^{m} E_i \alpha_i \Delta T_i}{\sum_{i=1}^{m} E_i}$$

$$\sigma_i = -E_i \alpha_i \Delta T_i + \frac{E_i \bar{z}_i' \sum_{i=1}^{m} E_i \alpha_i \Delta T_i \bar{z}_i'}{\sum_{i=1}^{m} \bar{z}_i' E_i} + \frac{E_i \sum_{i=1}^{m} E_i \alpha_i \Delta T_i}{\sum_{i=1}^{m} E_i} \tag{32}$$

$$z_i' = \cos\left(i - \tfrac{1}{2}\right)\theta - \frac{\sum_{i=1}^{m} E_i \cos\left(i - \tfrac{1}{2}\right)\theta}{\sum_{i=1}^{m} E_i} \tag{33}$$

Through the employment of a grid system of 36 elements ($m = 36$),

$$\theta = \pi/36 = 0.0874 \text{ radians} = 5 \text{ deg}$$

Taking the variation of E with T over the low-temperature range as

$$E(T) = (28.0 + A\Delta T)(10)^6$$

$$\Delta T = T - T_{rt}$$

with the conditions that

$$E(-320°) = 30(10)^6$$

$$T_{rt} = 80 \text{ deg}$$

yields

$$E(T) = (28.0 - 0.005\Delta T)(10)^6$$

We determined $\alpha_i \Delta T_i$ by referring to published data [5]; the reference temperature was taken to be 35 F. The required computations were then carried out as indicated by equations (25) through (33). The thermal-stress distribution is shown in Fig. 9.

The axial-stress distribution shown in Fig. 9 indicates that the most serious stresses occur near the liquid level. These stresses are high (but not excessive) and of a very local character.

The radius of bowing curvature was found to be

$$R = \frac{d_m}{27.91 \times 10^{-4}}$$

Since $e = 24.90 \times 10^{-4}$, the coefficient K is determined as

$$K = 1.12$$

Fig. 5 indicates that this value of K lies between the values for Cases 2 and 3, and that the bowing curvature is less severe than that predicted by Case 2.

A further point of interest is the magnitude of the bowing deflection. Consider a 50-ft run of pipe simply supported at its ends, Fig. 10. For small angles,

$$\alpha = \frac{L}{2R}$$

$$\cos\alpha = \frac{[R^2 - (L/2)^2]^{1/2}}{R} = 1 - \frac{1}{2}\left(\frac{L}{2R}\right)^2$$

Then,

$$\delta = L^2/8R$$

Hence,

$$\delta = \frac{(600)^2}{(8)(4750)} = 9.5 \text{ in}$$

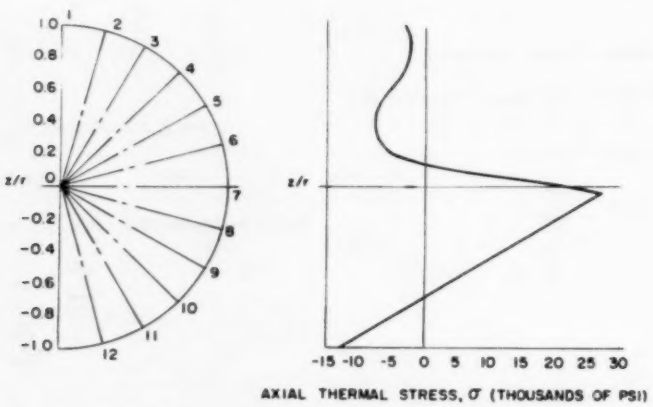

Fig. 9 Thermal-stress distribution for pipe half filled with liquid nitrogen

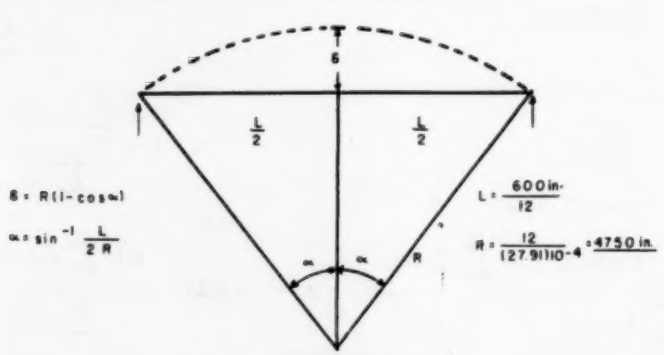

Fig. 10 Bowed length of pipe

Since pipe motions of this amount are rarely permissible at plant installations, it is evident that a definite restriction must be placed upon the lengths of pipe that undergo bowing; i.e., the rigidity of the line must be broken by the use of hinged-type expansion joints.

Effect of Bowing on Support Loads and Pipe Stress [6]

The support loads at anchors and hangers, as well as the added component of pipe stress caused by bowing, are of primary interest. Consider the case of a pipe simply supported at its ends and with a single central hanger support, Fig. 11.

This situation might arise in a long U-bend. The hanger spacing L is computed from the dead weight of the pipe plus that of the fluid.

Hanger loads are computed by superposition. With P_1 removed, the pipe would bow upward a distance δ_1, Fig. 12. The load P_1 opposes this deflection:

$$-\delta_1 = \frac{P_1 L^3}{6EI}$$

Then,

$$P_1 = -\frac{3EI}{LR} = -\frac{3KEeI}{Ld} \text{ (compressive force)}$$

$$P_0 = P_2 = -\frac{P_1}{2} = \frac{3EI}{2LR} = \frac{3KEeI}{2Ld}$$

The bending moment along the length of pipe is shown in Fig. 13.

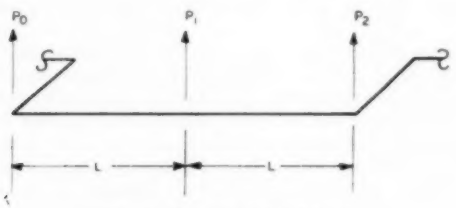

Fig. 11 Pipe expansion U-bend

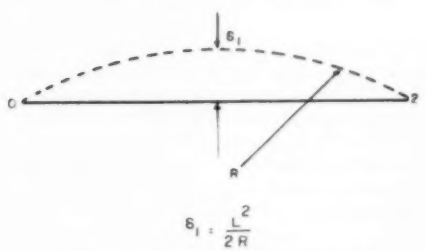

$$\delta_1 = \frac{L^2}{2R}$$

Fig. 12 Unconstrained bowing of line

Maximum pipe stress is at support point No. 1.

$$\sigma = \frac{Mz}{I} = -\tfrac{3}{4} KEe \frac{z}{d/2}$$

$$\sigma_{max} = \mp \tfrac{3}{4} KEe$$

If ceiling hangers are assumed, the center hanger undergoes a compressive load P_B as the result of bowing:

$$P_B = -\frac{3KEeI}{Ld}$$

The hanger load caused by dead weight, P_w, in this case is $P_w = \frac{5}{4} wL$ (w = weight per unit length of pipe and liquid). But the spacing of hangers is known, and the stress caused by dead weight in this arrangement is

$$\sigma_{all} = \frac{wL^2}{8} \frac{d/2}{I}$$

Thus,

$$\frac{P_B}{P_w} = -\frac{12KEeI}{5wL^2 d} = \frac{3KEe}{20\sigma_{all}}$$

The following probable values are employed:

$K = 1.2$
$E = 30 \times 10^6$
$e = 25 \times 10^{-4}$ (300-deg temperature differential)
$\sigma_{all} = 6000$ psi (dead-weight stress only)

from which

$$P_B = 2.25 P_w$$

The net load on the hanger is

$$P_{net} = -1.25 P_w = 1.56wL \text{ (compressive load on hanger).}$$

The two end hangers normally carry a load of $P = 0.375wL$. The bowing load adds to this value by

$$\left(\frac{2.25}{2}\right) \tfrac{5}{4} wL$$

The net load is therefore

$$P_{net} = (0.375 + 1.41)wL = 1.78wL$$

Hence the bowing loads cannot be ignored in the design of supports, particularly in the foregoing case, because they result in buckling loads on the center hanger.

Conclusion

The foregoing analysis has indicated the nature and magnitude of the bowing problem in pipelines carrying cryogenic fluids. The thermal stresses generated in these lines are very sensitive

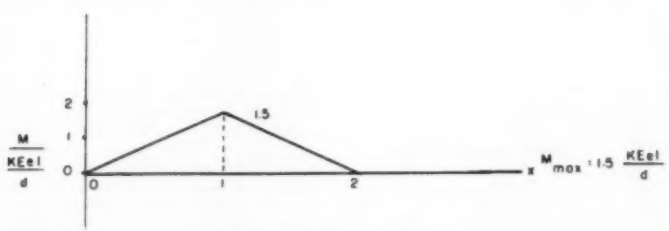

Fig. 13 Loads and moment diagram

to the temperature gradient, whereas the curvature of the lines is relatively insensitive and can be predicted in a conservative manner by a simple approximation. The magnitude of the stresses, bowing deflections, and loads on restraints require that these conditions be considered in design.

References

1 R. L. Bisplinghoff, "Three-Dimensional Equations of Linear Thermoelasticity," Notes from a Special Summer Program in Aerodynamic Heating of Aircraft Structures in High-Speed Flight, Department of Aeronautical Engineering, Massachusetts Institute of Technology, Cambridge, Mass., chapter 8, July, 1956.

2 S. Timoshenko and J. N. Goodier, "Theory of Elasticity," McGraw-Hill Book Company, Inc., New York, N. Y., 1934.

3 "The Effects of Thermal Radiation on Aircraft Structures, Part II: The Response of a Simple Structure to Radiant Heating," WADC TR 54-384, February, 1955.

4 E. S. Criscione, "The Combined Effects of Short Duration Heat Input on a One Cell Box Beam," SM thesis, Massachusetts Institute of Technology, Cambridge, Mass., 1953.

5 D. E. Furman, "Thermal Expansion Characteristics of Stainless Steels Between −300° and 1000°F," *Journal of Metals*, vol. 2, 1950, pp. 688–691.

6 W. G. Flieder, W. J. Smith, and K. R. Wetmore, "Flexibility Considerations for the Design of Cryogenic Transfer Lines," *Proceedings of the 1959 Cryogenic Engineering Conference*, Plenum Press, Inc., New York, N. Y., 1960, pp. 111–119.

Dynamic Membrane Stresses in a Circular Elastic Shell

R. G. PAYTON
Staff Scientist,
Avco Research and Advanced Development, Wilmington, Mass.

The dynamic membrane stress for a thin, infinitely long, circular, elastic shell is obtained for a point impulse, a distributed impulse, and a moving pressure load. These solutions, based on a method due principally to Friedlander, give new solutions to the problems mentioned.

MANY dynamic circular elastic-shell problems can, because of symmetry, be reduced to the solution of partial differential equations which depend on but two independent variables; the angular coordinate θ and the time t. The time-honored way of solving such problems is to assume a product solution of a function of θ times a function of time. While this method has many advantages in simplicity, it suffers from one major disadvantage in that it effectively dictates the form of solution instead of allowing this to evolve in a more natural way from the problem itself. The product solution usually leads to infinite series, all terms of which must be included if the solution is to be evaluated at a particular time. Convergence difficulties can arise in certain portions of the (θ, t) plane and a great number of terms in the series may be needed in order to obtain a good approximation to the true answer. The need for other forms of solutions is apparent.

One of the first attempts to recast product solutions in a different form was given by Watson [1][1] in a classic paper concerned with the propagation of high-frequency radio waves about the earth's surface. Indeed, practically all the work in this area has been done by electromagnetic engineers. Recently, the method has been applied to time-dependent problems by Friedlander [2] in connection with sound diffraction. Gilbert and Knopoff [3] have considered the scattering of elastic waves by a rigid cylinder. These problems serve to illustrate the power of the method but the results are somewhat obscured by the complexity of the mathematics.

In this paper three examples of the dynamic response of a circular elastic shell are considered in detail. In the first example, the dynamic response to a point impulse is found in closed form. Next, a distributed impulse and finally a moving pressure load are considered. These problems are solved within the framework of linear membrane-shell theory. It should be mentioned that no theoretical difficulties are added by the inclusion of bending terms, however, the resulting mathematics becomes more tedious.

Equation of Motion

The dynamic differential equations describing the membrane motion of a thin, infinitely long, circular elastic shell, Fig. 1, can be found in [4]. They are,

Equilibrium

$$\sigma' - \frac{E}{1-\nu^2}\ddot{V} = 0 \tag{1}$$

and

$$\sigma = -\frac{E}{1-\nu^2}\ddot{W} - \frac{a}{h}P \tag{2}$$

Strain-Displacement

$$\epsilon = V' + W \tag{3}$$

Stress-Strain

$$\sigma = \frac{E}{1-\nu^2}\epsilon \tag{4}$$

where

σ = shell stress, considered constant through shell thickness
ϵ = strain
ρ = shell density
E = Young's modulus
ν = Poisson's ratio
aW = radial displacement
aV = tangential displacement
P = applied pressure
a = shell radius
h = shell thickness

Primes denote θ derivatives and dots denote differentiation with respect to τ, a dimensionless time given by

$$\tau = \frac{t}{a}\left[\frac{E}{\rho(1-\nu^2)}\right]^{1/2} \equiv \frac{ct}{a}$$

where c is the speed at which disturbances propagate in the shell and t is a real time.

Differentiating equation (1) with respect to θ and using equation (2) gives

$$\sigma'' - \sigma - \frac{E}{1-\nu^2}(\ddot{V}' + \ddot{W}) = \frac{a}{h}P \tag{5}$$

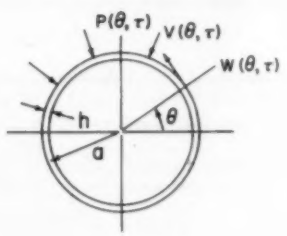

Fig. 1 Circular shell

[1] Numbers in brackets designate References at end of paper.

Presented at the West Coast Conference of the Applied Mechanics Division, Seattle, Wash., August 28–30, 1961, of THE AMERICAN SOCIETY OF MECHANICAL ENGINEERS.

Discussion of this paper should be addressed to the Editorial Department, ASME, United Engineering Center, 345 East 47th Street, New York 17, N. Y., and will be accepted until October 10, 1961. Discussion received after the closing date will be returned. Manuscript received by ASME Applied Mechanics Division, September 20, 1960. Paper No. 61—APMW-10.

or, from (3) and (4)

$$-\sigma'' + \sigma + \ddot{\sigma} = -\frac{a}{h} P \tag{6}$$

It is required that σ be periodic in θ with period 2π, and that σ and its first time derivative to be initially zero.

Following Friedlander [2], a solution to equation (6) will be assumed in the form

$$\sigma(\theta, \tau) = \sum_{n=-\infty}^{+\infty} \psi(\theta + 2n\pi, \tau) \tag{7}^{2}$$

This form of solution removes any periodicity requirement on $\psi(\theta, \tau)$ and allows the range of θ to be extended to the interval $-\infty < \theta < +\infty$. In this new notation equation (6) becomes

$$-\psi'' + \psi + \ddot{\psi} = -\sigma_0 f(\theta, \tau) \tag{8}$$

where

$$f(\theta, \tau) = \begin{cases} \dfrac{P}{P_0} \text{ for } |\theta| < \pi \\ \\ 0 \text{ for } |\theta| > \pi \end{cases}, \quad \sigma_0 = \frac{a}{h} P_0, \quad \tau > 0,$$

$-\infty < \theta < +\infty$ and P_0 is a characteristic measure of the applied pressure.

It is now convenient to introduce Fourier and Laplace transforms. Thus,

$$\bar{\psi}(\theta, s) = \int_0^\infty \psi(\theta, \tau) e^{-s\tau} d\tau \quad \text{and}$$

$$\psi(\theta, \tau) = \frac{1}{2\pi i} \int_c \bar{\psi}(\theta, s) e^{s\tau} ds \tag{9}$$

$$\bar{\psi}^*(\xi, s) = \int_{-\infty}^{+\infty} \bar{\psi}(\theta, s) e^{-i\xi\theta} d\theta \quad \text{and}$$

$$\bar{\psi}(\theta, s) = \frac{1}{2\pi} \int_\Gamma \bar{\psi}^*(\xi, s) e^{i\xi\theta} d\xi \tag{10}$$

Equation (8) now transforms to

$$(\xi^2 + s^2 + 1)\bar{\psi}^* = -\sigma_0 \bar{f}^*(\xi, s) \tag{11}$$

with

$$\bar{f}^*(\xi, s) = \frac{1}{P_0} \int_{-\pi}^{+\pi} \int_0^\infty P(\theta, \tau) e^{-s\tau - i\xi\theta} d\tau d\theta \tag{12}$$

The solution to equation (11) will now be obtained for three different loading pressures P.

Examples

Example 1

$$P(\theta, \tau) = P_0 \delta(\theta) \delta(\tau)$$

(δ is the Dirac delta function) so that

$$\bar{f}^*(\xi, s) = 1$$

This corresponds to suddenly applying an impulse of strength P_0 per unit area to the shell at $\theta = 0$, and then releasing the load. For this example equations (10) and (11) give

$$\frac{\bar{\psi}}{\sigma_0} = -\frac{1}{2\pi} \int_{-\infty}^{+\infty} \frac{e^{i\xi\theta}}{\xi^2 + s^2 + 1} d\xi = -\frac{e^{-|\theta|(s^2+1)^{1/2}}}{2(s^2+1)^{1/2}} \tag{13}$$

where Γ, the integration path in the ξ-plane, has been taken along the real axis. The inverse Laplace transform [5] results in

$$\frac{\psi}{\sigma_0} = -\frac{1}{2} J_0[(\tau^2 - |\theta|^2)^{1/2}] H(\tau - |\theta|) \tag{14}$$

The hoop membrane stress is now found by summation

$$\sigma(\theta, \tau) = \sum_{n=-\infty}^{+\infty} \psi(\theta + 2n\pi, \tau) = -\frac{\sigma_0}{2} \sum_{n=-\infty}^{+\infty} J_0[(\tau^2 - |\theta + 2n\pi|^2)^{1/2}] H(\tau - |\theta + 2n\pi|) \tag{15}$$

where H, the Heaviside unit step function, is unity for a positive argument and zero otherwise. J_0 is the Bessel function of zero order.

It should be noted that for any particular time only a finite number of terms in the series (14) give contributions to the membrane stress. As has been pointed out by Friedlander [2], the terms in the series (15) correspond to waves encircling the shell in both the positive and negative θ-directions. A plot of the membrane stress at $\theta = 0$ is shown in Fig. 2.

This example probably does not have too much physical significance owing to the exclusion of bending. It does, however, furnish a Green's function for the operator

$$L(\ ) = -(\ )'' + (\ ) + (\ddot{\ }) \tag{16}$$

which can be used to generate other (and more meaningful solutions.

Example 2

$$P(\theta, \tau) = P_0 \delta(\tau) \begin{cases} \cos\theta \text{ for } |\theta| < \pi/2 \\ 0 \quad \text{for } \pi/2 < |\theta| < \pi \end{cases}$$

In this example the impulse is applied as a cosine distribution over one half of the shell. The transform of the impulse is easily found to be

$$\bar{f}^*(\xi, s) = \frac{1}{2}\left[-\frac{e^{-i\xi\pi/2}}{\xi - 1} - \frac{e^{i\xi\pi/2}}{\xi - 1} + \frac{e^{-i\xi\pi/2}}{\xi + 1} + \frac{e^{i\xi\pi/2}}{\xi + 1} \right] \tag{17}$$

From (11), (17), and (10)

$$\bar{\psi}(\theta, s) = \frac{1}{2\pi} \int_\Gamma -\frac{\sigma_0}{2} \left[-\frac{e^{-i\xi\pi/2}}{\xi - 1} - \frac{e^{i\xi\pi/2}}{\xi - 1} + \frac{e^{-i\xi\pi/2}}{\xi + 1} + \frac{e^{i\xi\pi/2}}{\xi + 1} \right] \frac{e^{i\xi\theta}}{\xi^2 + s^2 + 1} d\xi \tag{18}$$

where the integration path Γ (chosen so as to insure that no disturbance reaches the backside of the shell until after $\tau = 0$) is

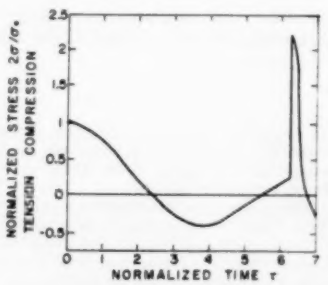

Fig. 2 Stress at $\theta = 0$ resulting from a point impulse

[2] Note that any periodic function of θ, $\sigma(\theta, \tau)$, defined in the interval $-\pi < \theta < +\pi$ can always be written in this way simply by taking

$$\psi(\theta, \tau) = \begin{cases} \sigma(\theta, \tau) & \text{for} \quad |\theta| < \pi \\ 0 & \text{for} \quad |\theta| > \pi \end{cases}$$

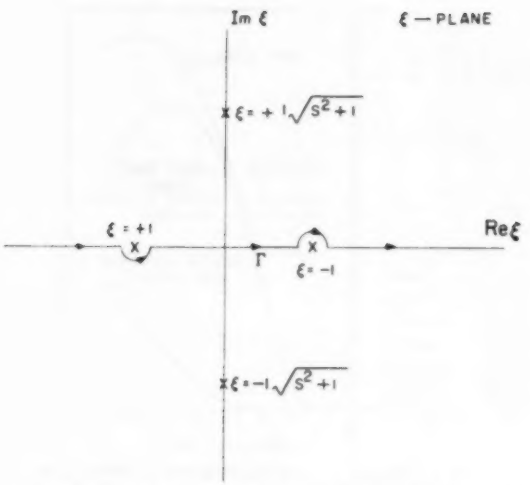

Fig. 3 Integration path Γ for inverse Fourier transform (NOTE: Second and fourth lines should read: $x\xi = +i$ and $x\xi = -i$, etc.)

shown in Fig. 3. The integrand of (18), regarded as a function of the complex variable ξ, has simple poles at $\xi = \pm 1$ and $\xi = \pm i(s^2 + 1)^{1/2}$. Evaluating this integral by residues gives

$$\bar{f}(\theta, s) = -\frac{\sigma_0}{2}\left[\frac{2\cos\theta}{s^2+2}H(\pi/2 - |\theta|) + \frac{e^{-|\theta-\pi/2|(s^2+1)^{1/2}}}{(s^2+2)(s^2+1)^{1/2}} + \frac{e^{-|\theta+\pi/2|(s^2+1)^{1/2}}}{(s^2+2)(s^2+1)^{1/2}}\right] \quad (19)$$

The relation (19) must now be inverted in the complex s-plane where $\bar{f}(\theta, s)$ has simple poles at $s = \pm i\sqrt{2}$ and branch points at $s = \pm i$. It does not seem possible to determine $\psi(\theta, \tau)$ in closed form; however, by the use of the convolution theorem $\psi(\theta, \tau)$ can be expressed in terms of a real integral. Thus,

$$\psi(\theta, \tau) = -\frac{\sigma_0}{2}\left[\sqrt{2}\cos\theta \sin\sqrt{2}\,\tau\, H(\pi/2 - |\theta|)H(\tau) + \frac{1}{\sqrt{2}}H(\tau - |\theta - \pi/2|)\int_{|\theta-\pi/2|}^{\tau} J_0[(x^2 - |\theta - \pi/2|^2)^{1/2}] \sin\sqrt{2}(\tau - x)dx + \frac{1}{\sqrt{2}}H(\tau - |\theta + \pi/2|)\int_{|\theta+\pi/2|}^{\tau} J_0[(x^2 - |\theta + \pi/2|^2)^{1/2}] \sin\sqrt{2}\,(\tau - x)dx\right] \quad (20)$$

It will be recognized from (7) and the wave character of (20) that the only nonzero term in the summation (7), prior to the arrival of the second wave front at any point on the shell, is $\psi(\theta, \tau)$. In particular, at $\theta = 0$ and π, $\sigma(\theta, \tau) = \psi(\theta, \tau)$ for $0 < \tau < 3\pi/2$. For later times than these we simply add on more and more terms in the summation (7). A plot of the stress at $\theta = 0$ and $\theta = \pi$ is shown in Fig. 4.[3]

Example 3

$$P(\theta, \tau) = P_0 H[\tau - \alpha(1 - \cos\theta)]$$

where $\alpha = C/V_0$. This represents a moving pressure load which engulfs the shell with the constant velocity (along the x-axis) V_0.

From (9) and (10)

[3] The results of this example and the next were obtained from the IBM 704 computer by J. Connors and M. Bower of the AVCO Mathematics Section.

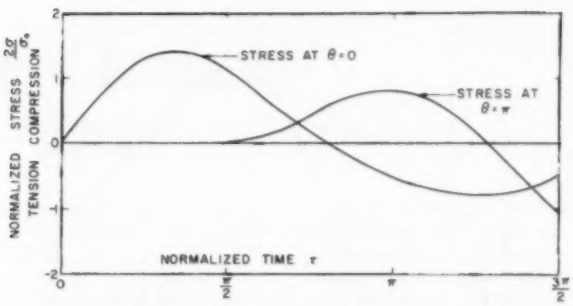

Fig. 4 Stress resulting from a cosine impulse

$$\bar{f}^*(\xi, s) = \frac{1}{s}\int_{-\pi}^{+\pi} e^{-i\xi\eta - \alpha s(1-\cos\eta)}d\eta \quad (21)$$

so that

$$\frac{\bar{\psi}^*}{\sigma_0} = -\int_{-\pi}^{+\pi}\frac{e^{-i\xi\eta - \alpha s(1-\cos\eta)}}{s(\xi^2 + s^2 + 1)}\,d\eta \quad (22)$$

Taking the inverse Fourier transform path along the real ξ-plane axis gives

$$\frac{\bar{\psi}}{\sigma_0} = -\frac{1}{2\pi}\int_{-\infty}^{+\infty}\int_{-\pi}^{+\pi}\frac{e^{i\xi(\theta-\eta) - \alpha s(1-\cos\eta)}}{s(\xi^2 + s^2 + 1)}d\eta d\xi = -\frac{1}{2}\int_{-\pi}^{+\pi}\frac{e^{-|\theta-\eta|(s^2+1)^{1/2} - \alpha s(1-\cos\eta)}}{s(s^2+1)^{1/2}}\,d\eta \quad (23)$$

where the orders of integration have been interchanged.

It is now necessary to distinguish between two possible cases depending upon whether $0 \le \theta \le \theta_0$ or $\theta_0 \le \theta < \pi$, where $\sin\theta_0 = 1/\alpha$, and $0 < \theta_0 < \pi/2$. In order for θ_0 to be real it is required that $\alpha \ge 1$; i.e., that the engulfing pressure wave velocity is equal to or less than the elastic wave velocity. To simplify things further it is assumed that $\alpha > 1.39$. Physically, θ_0 locates the point on the shell at which the x-component of the elastic wave velocity becomes equal to the pressure-wave velocity. Thus for values of $\theta > \theta_0$ there will be a stress prior to the arrival of the external pressure wave. The condition that α be greater than 1.39 prevents the pressure wave from overtaking the elastic disturbance. Neither of the requirements $\alpha > 1$ nor $\alpha > 1.39$ is necessary to the analysis but they seem to lead to the most interesting practical cases.

Performing the Laplace inversion on (23) gives,

Case 1. $0 \le \theta \le \theta_0$

$$\frac{\psi}{\sigma_0} = -\frac{1}{2}H[\tau - \alpha(1 - \cos\theta)]\int_{-\pi}^{\theta} f_1(\eta, \theta, \tau)H[\tau - \alpha(1 - \cos\eta) - \theta + \eta]d\eta - \tfrac{1}{2}H[\tau - \alpha(1 - \cos\theta)]\int_{\theta}^{\pi} f_1(-\eta, -\theta, \tau)H[\tau - \alpha(1 - \cos\eta) - \eta + \theta]d\eta \quad (24)$$

Case 2. $\theta_0 \le \theta < \pi$

$$\frac{\psi}{\sigma_0} = -\tfrac{1}{2}H[\tau - \tau_0 + \theta_0 - \theta]\int_{-\pi}^{\theta} f_1(\eta, \theta, \tau)H[\tau - \alpha(1 - \cos\eta) - \theta + \eta]d\eta - \tfrac{1}{2}H[\tau - \alpha(1 - \cos\theta)]\int_{\theta}^{\pi} f_1(-\eta, -\theta, \tau)H[\tau - \alpha(1 - \cos\eta) - \eta + \theta]d\eta \quad (25)$$

with $\tau_0 = \alpha(1 - \cos\theta_0)$ and

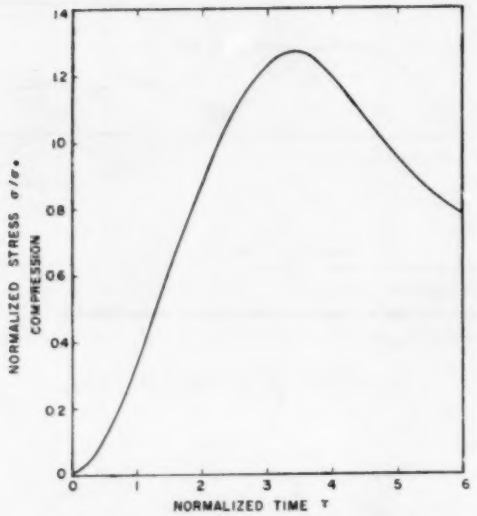

Fig. 5 Stress at $\theta = 0$ resulting from a moving load

$$f_1(\eta, \theta, \tau) = \int_{\theta-\eta+\alpha(1-\cos\eta)}^{\tau} J_0\left[\left\{[x - \alpha(1 - \cos\eta)]^2 - (\theta - \eta)^2\right\}^{1/2}\right] dx$$

A plot of the stress versus time is shown in Fig. 5 at $\theta = 0$ for $\alpha = 2$. Fig. 6 shows the stress at $\theta = \pi/2$, also for $\alpha = 2$. In Fig. 6 the separate results of the elastic wave, the first term in equation (25), and the moving pressure load, the second term in equation (25), are shown separately.

The foregoing illustrations by no means exhaust the number of circular shell problems whose solutions exist in the form (7). It is hoped, however, that his paper will acquaint the reader with the flexibility of the method.

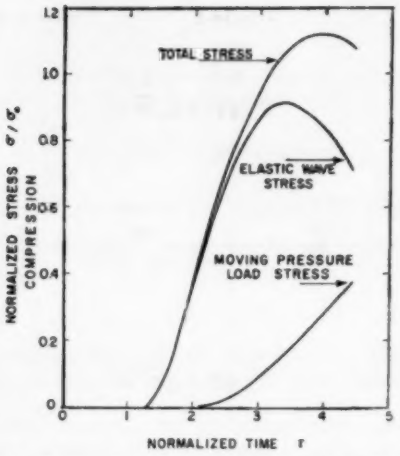

Fig. 6 Stress at $\theta = \pi/2$ resulting from a moving load

Acknowledgment

This work was jointly supported by AFSWC under Air Force Contract Number AF 29 (601)-2560 and by AFBMD under Air Force Contract Number AF 04 (647)-258.

References

1 G. N. Watson, "The Diffraction of Electrical Waves by the Earth," *Proceedings of The Royal Society*, London, England, series A, vol. 95, 1918, p. 83.

2 F. G. Friedlander, "Sound Pulses," Cambridge University Press, Cambridge, England, 1958.

3 F. Gilbert and L. Knopoff, "Scattering of Impulsive Elastic Waves by a Rigid Cylinder," *Journal of the Acoustical Society of America*, vol. 31, 1959, p. 1169.

4 V. V. Novozhilov, "The Theory of Thin Shells," P. Noordhoff Limited, Groningen, The Netherlands, 1959.

5 A. Erdelyi, et al., "Tables of Integral Transforms," vol. 1, McGraw-Hill Book Company, Inc., New York, N. Y., 1954.

An Extension of Duhamel's Analogy to Plasticity[1]

S. A. MURCH
Institute of Engineering Research,
University of California,
Berkeley, Calif.
Assoc. Mem. ASME

It is shown that the Duhamel analogy of classical elasticity theory may be extended without modification to the incremental theory of plasticity, when the loading function is temperature independent. For a class of temperature-dependent loading functions the analogy of the Duhamel type is shown to hold: (a) When the temperature field is stationary; (b) for problems in which the elastic and plastic components of strain individually satisfy compatibility; or (c) when the material is rigid plastic, provided the medium is interpreted as nonhomogeneous. Examples of particular correspondences are discussed. It is also noted that for linear viscoelastic materials in which volume changes are purely thermoelastic the transformations in the analogy are identical to those for elasticity.

When dealing with the deformation of continuous media, it is often possible to find a correspondence between the solutions to boundary-value problems of neighboring disciplines that relates the solution of one problem, through an appropriate transformation, to the solution of the corresponding problem. For example, the correspondence principle of viscoelasticity relates the disciplines of linear viscoelasticity and classical elasticity. A well-known analogy, referred to here (following Morgan [1][2]) as the Duhamel analogy, establishes a correspondence between the theory of thermoelasticity and isothermal elasticity. While analogies in elasticity are numerous, relatively few have arisen in plasticity. A discussion of some such correspondences, exact and partial, for elastic as well as inelastic solids may be found in the survey [2] by Hill.

It is the intention here to examine the Duhamel analogy and determine the circumstances under which it may be extended to include the incremental theory of plasticity. Practical interest in the analogy stems from the alternate viewpoint that it places on a given problem. Its more theoretical value is derived from the fact that variational and uniqueness theorems proved previously for isothermal theory then hold automatically for nonisothermal theory.

Specifically, following some preliminary background, it is shown that the Duhamel analogy may be incorporated into incremental plasticity theory without modification for temperature-independent loading functions and with modification for a class of temperature-dependent loading functions. As examples, the analogy is used to draw a correspondence (*a*) between the thermal problem of the solid-cylindrical, nuclear-reactor fuel element and the isothermal problem of a rotating cylindrical shaft, and (*b*) between the problem of a hollow sphere with uniform heat source and the isothermal problem of a hollow sphere under the mutual gravitation of its parts. Although in the main, attention is confined to regular loading functions, the extension to loading functions with singular regimes is discussed briefly.

The analogy, as it is presently given in the literature,[3] relates the solution of a given (mixed) boundary-value problem of linear thermoelasticity (referred to here as problem I) to the solution of a specific problem (problem II) in isothermal elasticity for a body geometrically and physically identical to the first but subjected to different body forces and surface tractions. If θ is the change in temperature from the unstrained state in body I and E, ν, and α are the temperature-independent Young's modulus, Poisson's ratio, and the linear thermal coefficient of expansion, respectively, the Duhamel analogy may be stated as follows:

The original field equations and boundary conditions of a problem in thermoelasticity are reducible to the field equations of an associated problem in the isothermal theory. The stress field σ_{ij}^{I} and the strains $\epsilon_{ij}^{\mathrm{I}}$ in the thermally stressed body I are related to the stress field $\sigma_{ij}^{\mathrm{II}}$ and the strains $\epsilon_{ij}^{\mathrm{II}}$ in the corresponding isothermal problem through

$$\sigma_{ij}^{\mathrm{II}} = \sigma_{ij}^{\mathrm{I}} + \frac{\alpha E}{1-2\nu}\theta\delta_{ij} \tag{1a}$$

$$\epsilon_{ij}^{\mathrm{II}} = \epsilon_{ij}^{\mathrm{I}} \tag{1b}$$

provided that the body force F_i^{I} and the surface traction T_i^{I} of the thermal problem are related to the body forces F_i^{II} and surface tractions T_i^{II} of the corresponding isothermal problem by

$$F_i^{\mathrm{II}} = F_i^{\mathrm{I}} - \frac{\alpha E}{1-2\nu}\frac{\partial\theta}{\partial x_i} \tag{2a}$$

$$T_i^{\mathrm{II}} = T_i^{\mathrm{I}} + \frac{\alpha E}{1-2\nu}\theta\alpha_i \tag{2b}$$

where the α_i are the direction cosines of the unit normal to the boundary.

The converse also holds; namely, that through (1) and (2) to every isothermal problem there exists a corresponding thermoelastic problem for a given temperature field.

That the correspondence holds is easily demonstrated by substitution of the quantities denoted with superscript I as given by (1) and (2) into the field equations of thermoelasticity; for example, the Duhamel-Neumann stress-strain law

$$\epsilon_{ij}^{\mathrm{I}} = \frac{1+\nu}{E}\sigma_{ij}^{\mathrm{I}} - \left[\frac{\nu}{E}\sigma_{kk}^{\mathrm{I}} - \alpha\theta\right]\delta_{ij} \tag{3}$$

---

[1] The results presented here were obtained in the course of research sponsored by the Office of Naval Research, under Contract Nonr-222(69), Project NR 064-436, with the University of California, Berkeley, Calif.

[2] Numbers in brackets designate References at end of paper.

Presented at the Summer Conference of the Applied Mechanics Division, Chicago, Ill., June 14–16, 1961, of The American Society of Mechanical Engineers.

Discussion of this paper should be addressed to the Editorial Department, ASME, United Engineering Center, 345 East 47th Street, New York 17, N. Y., and will be accepted until October 10, 1961. Discussion received after the closing date will be returned. Manuscript received by ASME Applied Mechanics Division, September 8, 1960. Paper No. 61—APM-9.

[3] For example, reference [3], p. 77.

upon substitution from (1*a*) and (1*b*) reduces to the generalized Hooke's law,

$$\epsilon_{ij}^{II} = \frac{1+\nu}{E}\sigma_{ij}^{II} - \frac{\nu}{E}\sigma_{kk}^{II}\delta_{ij} \tag{4}$$

applicable to problem II. In a similar manner (2*a*) and (2*b*) relate, respectively, the equations of equilibrium and the stress boundary conditions of the two problems. The displacement boundary conditions, being unaffected by the transformations (1) and (2), are identical.

It may be observed from (1) and (2) that the analogy must fail, if Poisson's ratio is one half. The reason for this is immediately evident, when one considers that by (1*a*) the corresponding dilatations must be the same in problems I and II; yet $\nu = 1/2$ implies an incompressible material ($\epsilon_{ii}^{II} = 0$) for problem II which is clearly incompatible with thermal expansion [$\epsilon_{ii}^{I} = (3\alpha\theta/E)$] for problem I.

Should an isotropic, nonhomogeneous material be considered, i.e., if α, E, and ν vary with position, then instead of (2*a*)

$$F_i^{II} = F_i^{I} - \frac{\partial}{\partial x_i}\left\{\frac{\alpha(x)E(x)}{1-2\nu(x)}\theta\right\} \tag{5}$$

It may also be observed that the analogy is not restricted to quasistatic problems, since the body force may include inertia terms. Only the uncoupled thermoelastic problem, however, can be treated, since the transformations (1) and (2) depend upon the temperature field being known in advance.

In passing we note that, in view of the correspondence principle, the Duhamel analogy is immediately extendable to linear viscoelastic media through the relations

$$2G = \frac{P_2(p)}{P_1(p)}, \qquad 3K = \frac{P_3(p)}{P_4(p)} \tag{6}$$

where G and K are the shear and bulk moduli of elasticity, respectively, and the $P_i(p)$ [$i = 1, 2, 3, 4$] are the Laplace transforms with respect to the time variable t of the linear operators

$$P_m(D) = \sum_{n=0}^{N_m} C_m^{(n)} D^n, \qquad D^n \equiv \frac{\partial^n}{\partial t^n} \tag{7}$$

appearing in the stress-strain relations of linear viscoelasticity, modified to account for thermal effects as given, for example, by Sternberg [4],

$$P_1 s_{ij} = P_2 e_{ij} \tag{8a}$$

$$P_3 s = P_4(e - \alpha\theta) \tag{8b}$$

where s_{ij} is the deviatoric stress, e_{ij} is the deviatoric strain, s is the mean normal stress, and e is the mean normal strain. Making the appropriate substitution from (6) into the Laplace transforms of (1) and (2), followed by taking the inverse transforms, it is found that for linear viscoelasticity the Duhamel analogy holds, if in the transformations (1) and (2) the coefficient $(E/1-2\nu)$ is replaced by the operator $P_3^{-1}(D)P_4(D)$. It is particularly significant that only the operators $P_3(D)$ and $P_4(D)$ enter into the transformation; thus, for viscoelastic materials which are thermoelastic dilatational,[4] i.e., materials for which (8*b*) is replaced by

$$s = 3K(e - \alpha\theta) \tag{9}$$

the transformations of the Duhamel analogy are identical to (1) and (2) for an elastic material.

General Background

During any given state of deformation in the solution to a problem in plasticity, the body in question consists of a number of elastic and plastic domains. Given the state variables σ_{ij}, ϵ_{ij}^{p}, θ, and α, where α is a nondecreasing measure of work-hardening given by

$$\alpha = \int_0^t \sigma_{ij}\dot{\epsilon}_{ij}^{p}dt \tag{10}$$

a function f of these variables is assumed to exist which specifically defines the regions; if $f < 0$, the state is elastic, while if $f = 0$, the state is plastic. The function f, called the loading function, is regular, convex, and is assumed to be independent of hydrostatic pressure; hence it may be written as follows in terms of the stress deviation:

$$f = f(s_{ij}, \epsilon_{ij}^{p}, \theta, \alpha) \tag{11}$$

In the elastic regions the equations of thermoelasticity continue to hold; in the plastic regions, however, the total strain is assumed to be the sum of two components

$$\epsilon_{ij} = \epsilon_{ij}' + \epsilon_{ij}^{p} \tag{12}$$

into which the thermal component of strain is already assumed to be incorporated. The elastic component ϵ_{ij}' continues to obey the Duhamel-Neumann equation (3). The plastic component ϵ_{ij}^{p} on the other hand is taken to obey the constitutive equations proposed by Prager [6] for the nonisothermal deformation of a rigid, work-hardening material:

$$\dot{\epsilon}_{ij}^{p} = \begin{cases} 0 & \text{if } f < 0 \\ \dfrac{1}{D}\dfrac{\partial f}{\partial \sigma_{ij}}\left[\dfrac{\partial f}{\partial \theta}\dot{\theta} + \dfrac{\partial f}{\partial \sigma_{kl}}\dot{\sigma}_{kl}\right] & \text{if } f = 0 \end{cases} \tag{13a}$$

where dot denotes differentiation with respect to time and

$$D = -\left(\frac{\partial f}{\partial \epsilon_{ij}^{p}} + \frac{\partial f}{\partial \alpha}\sigma_{ij}\right)\frac{\partial f}{\partial \sigma_{ij}} \tag{13b}$$

The symbolic notation $[x]$ is defined by

$$[x] = \begin{cases} 0 & \text{if } x \leqq 0 \\ x & \text{if } x > 0 \end{cases} \tag{13c}$$

and incorporates the definition of loading into (13*a*).

The Duhamel Analogy for Thermoplasticity

As in the case of an elastic material, the procedure used to demonstrate the validity of the Duhamel analogy for plasticity consists in replacing the quantities σ_{ij}^{I}, ϵ_{ij}^{I}, F_i^{I}, and T_i^{I}, appearing in the field equations and boundary conditions of the thermoelastic-plastic problem, by expressions such as (1) and (2), written in terms of σ_{ij}^{II}, ϵ_{ij}^{II}, F_i^{II}, T_i^{II}, and θ, and observing the reduction to the field equations and boundary conditions of an associated isothermal problem. In plasticity, however, the elastic and plastic domains require separate consideration, and the boundary conditions must be augmented by the continuity conditions at the elastic-plastic interfaces. The latter are automatically satisfied, since the continuity of θ with co-ordinates together with its continuous entry into relations such as (1*a*) insures that quantities continuous across the elastic-plastic boundary in one problem are necessarily continuous in the corresponding problem. As seen in the preceding section, the effect of temperature is incorporated into the theory of plasticity in two ways: (*a*) Through the Duhamel-Neumann equation (3), and (*b*) through the loading function into the associated flow rule (13). In the following, temperature-independent and temperature-dependent loading functions are considered separately. Since the extension of the Duhamel analogy for the former case may be

[4] Reference [5], pp. 48–50.

considered elementary, it is considered first to illustrate the method of approach.

(a) Temperature-Independent Loading Function. The class of loading functions which has received the widest application is that in which the loading function does not depend on θ; i.e.,

$$f(s_{ij}, \epsilon_{ij}^{\ p}, \alpha) = 0 \tag{14}$$

The thermal effect thus enters only through the Duhamel-Neumann relations (3).

As in the purely elastic case [3], F_i^{II} and T_i^{II} are chosen to satisfy equilibrium and the stress boundary conditions, giving rise to (2*a*) and (2*b*), respectively. It is thus clear with the aid of (1*a*) that the field equations for the elastic domain undergo the foregoing reduction exactly as in the purely elastic case. We may thus confine our attention to the plastic domain and in particular to the loading function and its associated flow rule.

Since for an analogy of the Duhamel type the total strains in the corresponding problems agree, i.e., $\epsilon_{ij}^{\text{I}} = \epsilon_{ij}^{\text{II}}$, and since it can be shown through (1*a*), (3), and (4) in a manner identical to that for the elastic domain that the elastic components of strain in the plastic regions are the same, it follows from (12) that the plastic components of strain in the corresponding problems must also agree; i.e.,

$$\epsilon_{ij}^{\ p\text{I}} = \epsilon_{ij}^{\ p\text{II}} \tag{15}$$

An immediate consequence of (15) is the coincidence of the corresponding elastic and plastic regions; thus, using the same functional form of the loading function for each problem, the identity

$$f(s_{ij}^{\text{I}}, \epsilon_{ij}^{\ p\text{I}}, \alpha^{\text{I}}) = f(s_{ij}^{\text{II}}, \epsilon_{ij}^{\ p\text{II}}, \alpha^{\text{II}}) \tag{16}$$

must hold throughout the plastic domain. That this is indeed the case is seen from (15) and the identities

$$s_{ij}^{\text{I}} = s_{ij}^{\text{II}} \tag{17}$$

$$\alpha^{\text{II}} = \int_0^t \sigma_{ij}^{\text{II}} \dot{\epsilon}_{ij}^{\ p\text{II}} dt = \int_0^t \left(\sigma_{ij}^{\text{I}} + \frac{\alpha E}{1 - 2\nu}\, \theta\delta_{ij} \right) \dot{\epsilon}_{ij}^{\ p\text{I}} dt = \alpha^{\text{I}} \tag{18}$$

which follow from (1*a*) and (15).

Turning now to the constitutive equation (13) associated with f, it remains to verify the relation

$$\left\{ \left(\frac{\partial f}{\partial \epsilon_{ij}^{\ p\text{I}}} + \frac{\partial f}{\partial \alpha^{\text{I}}} \sigma_{ij}^{\text{I}} \right) \frac{\partial f}{\partial \sigma_{ij}^{\text{I}}} \right\}^{-1} \left[\frac{\partial f}{\partial \sigma_{mn}^{\text{I}}} \dot{\sigma}_{mn}^{\text{I}} \right] \frac{\partial f}{\partial \sigma_{kl}^{\text{I}}} = \left\{ \left(\frac{\partial f}{\partial \epsilon_{ij}^{\ p\text{II}}} + \frac{\partial f}{\partial \alpha^{\text{II}}} \sigma_{ij}^{\text{II}} \right) \frac{\partial f}{\partial \sigma_{ij}^{\text{II}}} \right\}^{-1} \left[\frac{\partial f}{\partial \sigma_{mn}^{\text{II}}} \dot{\sigma}_{mn}^{\text{II}} \right] \frac{\partial f}{\partial \sigma_{kl}^{\text{II}}} \tag{19}$$

obtained by equating the corresponding plastic strain rates. By (1*a*)

$$\frac{\partial f}{\partial \sigma_{ij}^{\text{II}}} = \frac{\partial f}{\partial \sigma_{kl}^{\text{I}}} \frac{\partial \sigma_{kl}^{\text{I}}}{\partial \sigma_{ij}^{\text{II}}} = \frac{\partial f}{\partial \sigma_{ij}^{\text{I}}}, \tag{20}$$

$$\frac{\partial f}{\partial \sigma_{ij}^{\text{II}}} \dot{\sigma}_{ij}^{\text{II}} = \frac{\partial f}{\partial \sigma_{ij}^{\text{I}}} \left\{ \dot{\sigma}_{ij}^{\text{I}} + \frac{\alpha E}{1 - 2\nu}\, \dot{\theta}\delta_{ij} \right\} = \frac{\partial f}{\partial \sigma_{ij}^{\text{I}}} \dot{\sigma}_{ij}^{\text{I}} \tag{21}$$

and the expressions for the loading criterion (13*c*) in the brackets of (19) are identical. This essential part of the stress-strain relations insures that the elastic and plastic domains coincide not only at the time considered but throughout the duration of the loading. Since in addition to (20) and (21) it can be shown in a similar manner that

$$\frac{\partial f}{\partial \alpha^{\text{I}}} = \frac{\partial f}{\partial \alpha^{\text{II}}} \frac{\partial f}{\partial \sigma_{ij}^{\text{I}}} \sigma_{ij}^{\text{I}} = \frac{\partial f}{\partial \sigma_{ij}^{\text{II}}} \sigma_{ij}^{\text{II}}, \frac{\partial f}{\partial \epsilon_{ij}^{\ p\text{I}}} = \frac{\partial f}{\partial \epsilon_{ij}^{\ p\text{II}}} \tag{22}$$

(19) is established.

Hence for temperature-independent yield conditions the Duhamel analogy holds for plasticity in a manner identical to that for elasticity with the transformations again given by (1) and (2), and in addition by (15) and (18). For nonhomogeneous materials, (5) replaces (2*a*) as in the case of an elastic material.

(b) Temperature-Dependent Loading Function. With the entry of θ into the loading function, the procedure necessary to show that an analogy of the Duhamel type holds ceases to be as straightforward as in the temperature-independent case. Modification of the transformations (1) and (2) along with reinterpretation of the resulting system of equations must be made, in order that f and its associated flow rule (13) may assume isothermal forms. The possibility of a transformation that reduces (11) to an isothermal form is suggested from the known phenomenon[5] that a nonhomogeneous temperature field may give rise to plastic nonhomogeneity. With this in mind, the most obvious attack is to replace θ in (11) by its functional form in terms of position and time, as determined from the heat equation, the intention being to regard the corresponding isothermal problem as applying to a nonhomogeneous material, since now the loading function and its associated flow rule would vary from point to point within the body. Such a loading function, however, could at most apply to plastic flow in the presence of a steady-state temperature field, since a loading function cannot vary explicitly with time but only implicitly through the state variables.

As long as the form of the loading function is unspecified, little can be said of any generality regarding the removal of θ from (11) to obtain an equation of the type (14). There are, however, special classes of loading functions in which θ appears in combination with certain other of the variables in f. Such a class of loading functions that lends itself to treatment by the Duhamel analogy is the one in which the temperature enters only in conjunction with the components of the stress deviation, i.e.,

$$f\{g(\theta)s_{ij}, \epsilon_{ij}^{\ p}\} = 0 \tag{23}$$

Loading functions of this type[6] include the generalization to admit thermal effects of the familiar single parameter isotropic loading functions

$$f = F(J_2, J_3) - p(\theta)c \tag{24}$$

as well as the more general form

$$f = F(s_{ij}, \epsilon_{ij}^{\ p}) - p(\theta)c \tag{25}$$

where in both (24) and (25) F is homogeneous in s_{ij} and c depends on the strain history. For example, the generalized Mises yield condition[7]

$$f = \tfrac{1}{2} s_{ij}s_{ij} - k^2(\theta) \tag{26}$$

where $k(\theta)$ is the temperature-dependent yield limit in simple shear, may be written in the form (23); i.e.,

$$\{g(\theta)s_{ij}\}\{g(\theta)s_{ij}\} - 1 = 0, \tag{27}$$

where in this case $gk = 1$.

[5] Reference [7], p. 263.

[6] Prager [6] has shown this class of loading functions leads to constitutive equations identical in form to isothermal relations derived previously [8], also by Prager, but in which $\tau_{ij} = g(\theta)\sigma_{ij}$, referred to as the "effective stress," replaces σ_{ij}. This suggests that the transformation $\sigma_{ij}^{\text{II}} = g(\theta)\sigma_{ij}^{\text{I}}$ be used in place of (1*a*). The fictitious body force introduced, if such a transformation is made, however, depends upon the stress field, thus greatly limiting the range of application of the analogy.

[7] A discussion of (26) and a similar generalization of the Tresca yield condition for perfectly plastic materials appears in [3].

In the following, it is necessary to make the further restriction that the time function contained in $g(\theta)$ is separable, i.e.,

$$g[\theta(x, t)] = a(t)p(x), \tag{28}$$

so that f may be written as

$$f\{p(x)a(t)s_{ij}, \epsilon_{ij}^{p}\} = 0 \tag{29}$$

If the transformation (1) is modified to include the function $a(t)$,

$$\sigma_{ij}^{II} = a(t)\sigma_{ij}^{I} + \frac{\alpha E}{1 - 2\nu} a(t)\theta\delta_{ij} \tag{30}$$

and it follows that

$$s_{ij}^{II} = a(t)s_{ij}^{I} \tag{31}$$

Through the form (31) it is seen that the time function $a(t)$, entering explicitly into (29), has been incorporated into the stress deviation; thus, for the corresponding isothermal problem II, the loading function may be taken as

$$f\{p(x)s_{ij}^{II}, \epsilon_{ij}^{pII}\} = 0 \tag{32}$$

With the space-dependent parameter $p(x)$ as part of the loading function, the material so described must be regarded as nonhomogeneous. Two such loading functions (generalizations of the Mises and Tresca yield conditions) for nonhomogeneous materials that may be readily put in the form (32) have been given by Olszak [9].

Before proceeding, it should be mentioned that if the temperature θ in (23) appears in such a manner that each component of s_{ij} is multiplied by a different function of θ, the procedure used here is unaltered, provided the time function $a(t)$ is removable. The resulting class of isothermal loading functions includes the form

$$\psi = \tfrac{1}{2} H_{ijkl}(x)\sigma_{ij}\sigma_{kl}$$

discussed by Olszak and Urbanowski [7].

That the equations for the elastic-plastic boundaries in the corresponding problems are the same may be seen by setting $\epsilon_{ij}^{p} = 0$ in (23) and (32); the problems I and II, thus are again geometrically identical. Equality of the plastic strain rates follows from the constitutive equations associated with (23) and (32) provided

$$\left\{\frac{\partial f}{\partial \epsilon_{kl}^{pI}} \frac{\partial f}{\partial \sigma_{kl}^{I}}\right\}^{-1} \frac{\partial f}{\partial \sigma_{ij}^{I}} \left[\frac{\partial f}{\partial \sigma_{mn}^{I}} \dot{\sigma}_{mn}^{I} + \frac{\partial f}{\partial \theta} \dot{\theta}\right] = \left\{\frac{\partial f}{\partial \epsilon_{kl}^{pII}} \frac{\partial f}{\partial \sigma_{kl}^{II}}\right\}^{-1} \frac{\partial f}{\partial \sigma_{kl}^{II}} \left[\frac{\partial f}{\partial \sigma_{mn}^{II}} \dot{\sigma}_{mn}^{II}\right] \tag{33}$$

It may be verified from (23) and (32) that

$$\frac{\partial f}{\partial \sigma_{ij}^{II}} \dot{\sigma}_{ij}^{II} = \frac{\partial f}{\partial \sigma_{ij}^{I}} \dot{\sigma}_{ij}^{I} + \frac{\partial f}{\partial \theta} \dot{\theta} \tag{34}$$

so that the loading criterions for the corresponding problems are identical; furthermore, by the identities

$$\frac{\partial f}{\partial \epsilon_{ij}^{pII}} = \frac{\partial f}{\partial \epsilon_{ij}^{pI}}$$
$$a \frac{\partial f}{\partial \sigma_{ij}^{II}} = \frac{\partial f}{\partial \sigma_{ij}^{I}} \tag{35}$$

equation (33) holds. For completeness we record also

$$F_i^{II} = aF_i^{I} - \frac{\alpha E}{1 - 2\nu} a \frac{\partial \theta}{\partial x_i}$$
$$T_i^{II} = aT_i^{I} + \frac{\alpha E}{1 - 2\nu} a\theta\alpha_i \tag{36}$$

obtained from the equations of equilibrium and stress boundary conditions, respectively. Elastically nonhomogeneous materials or any material in the C-classification discussed in [7] may be treated by replacing (2a) by (5) or the first of (36) by

$$F_i^{II} = aF_i^{I} - a \frac{\partial}{\partial x_i} \left(\frac{\alpha(x)E(x)}{1 - 2\nu(x)} \theta\right) \tag{37}$$

Although the equality of the plastic strains (15) is again part of the extended analogy, it may be seen by (3) and (4) that (30), relating the corresponding stress fields, gives rise to

$$\epsilon_{ij}^{pII} = a(t)\,\epsilon_{ij}^{pI} \tag{38}$$

Hence additional restrictions on the applicability of the analogy must be imposed, since in general the compatibility of the strains in one problem does not imply the compatibility of the strains in the other, when the corresponding total strains are not equal. Three exceptions present themselves, however, for which compatibility *is* implied.

1 If $a(t)$ is unity, the problem I becomes that of plastic flow in the presence of a steady-state temperature field. The transformations (30), (36), and (38) reduce to the corresponding equations (1a) to (2b) for a temperature-independent yield condition. The material of the isothermal problem II, however, must still be regarded as nonhomogeneous. As observed earlier, if θ is not time dependent, restriction to the form (23) need not be made.

2 If the strains are such that the elastic and plastic components satisfy compatibility independently in one problem, it then follows that the total strains though unequal are compatible in both problems; the analogy is then given through the transformations (15), (30), (36), and (37).

3 If the material is rigid plastic, i.e., if the elastic components of the total strain may be neglected in comparison to the plastic components, the correspondence between the total strains is given by (15), and the analogy again holds.

The hardening parameter α was not included in the loading function (23), since the analogy cannot be shown to hold unless the function $g(\theta)$ also appears in combination with σ_{ij} under the integral sign in (10). The analogy can be shown to hold, however, if the equivalent plastic strain rate

$$\dot{\bar{\epsilon}} = (\tfrac{2}{3})^{1/2}(\dot{\epsilon}_{ij}^{p}\dot{\epsilon}_{ij}^{p})^{1/2}$$

is used instead as a measure of work-hardening.

In regard to perfectly plastic materials, if we adopt the procedure used by Boley and Weiner,[8] the stress-strain relations for a perfectly plastic material may be obtained from those of a work-hardening material by replacing ϵ_{ij}^{p} in f by $c\epsilon_{ij}^{p}$ and taking the limit as $c \to 0$ in the resulting constitutive equations. Hence the Duhamel analogy subject to the same limitations, as described for a hardening material, may be shown to hold also for perfectly plastic materials.

Examples

As mentioned earlier, one way that the Duhamel analogy may be utilized in obtaining the solution of a particular problem is by providing an alternative viewpoint. In way of demonstration consider a special case of the problem discussed in [10], namely, the axisymmetric deformation of an elastic-plastic cylinder with a radially distributed temperature distribution, obeying Tresca's temperature-independent yield condition. For present purposes the material is assumed to be elastic, perfectly plastic, and deformed in the state of plane strain. As shown in [10], the state of stress in the plastic domain may lie on any side or on any edge of Tresca's yield hexagon, depending upon the loading and

[8] Reference [3], p. 473.

temperature distribution. The analogy may be demonstrated for all such regimes, but the discussion will be limited here to the plastic region in the cylinder for which, referring to cylindrical polar co-ordinates (r, θ, z),

$$\sigma_\theta - \sigma_z = 2k_0 \tag{39}$$

where k_0 is constant, and the radial component of stress σ_r is the intermediate principal stress. The extended Duhamel analogy may now be used to approach the problem as one in isothermal plasticity. In the absence of body forces in the thermal problem I, the fictitious body force[9] in the corresponding problem II is by

$$F_r^{II} = \frac{-\alpha E}{1-2\nu}\frac{\partial \theta}{\partial r} \tag{40}$$

$$F_\theta^{II} = F_z^{II} = 0$$

Through the condition of plane strain, and the flow rule

$$\epsilon_r^{\,p} = 0$$

$$\epsilon_\theta^{\,p} = \epsilon_z^{\,p}$$

$$\epsilon_z^{\,p} = -\epsilon_z^{\,\prime} \tag{41}$$

so that the total strains are

$$\epsilon_r = \epsilon_r^{\,\prime} = \frac{1}{E}\left\{\sigma_r^{II} - \nu(\sigma_\theta^{II} + \sigma_z^{II})\right\}$$

$$\epsilon_\theta = \epsilon_\theta^{\,\prime} + \epsilon_z^{\,\prime} = \frac{1}{E}\left\{\sigma_\theta^{II} + \sigma_z^{II} - \nu(2\sigma_r^{II} + \sigma_z^{II} + \sigma_\theta^{II})\right\} \tag{42}$$

By equilibrium and the yield condition (39) σ_θ and σ_z may be expressed as

$$\sigma_\theta^{II} = \frac{\partial}{\partial r}(r\sigma_r^{II}) + rF_r^{II}$$

$$\sigma_z^{II} = \frac{\partial}{\partial r}(r\sigma_r^{II}) + rF_r^{II} - 2k_0 \tag{43}$$

Substitution of (42) into the compatibility equation

$$r\frac{\partial \epsilon_\theta}{\partial r} + \epsilon_\theta - \epsilon_r = 0 \tag{44}$$

followed by the replacement of σ_θ^{II} and σ_z^{II} through (43) results in

$$2(1-\nu)r^2\frac{\partial^2\sigma_r^{II}}{\partial r^2} + 6(1-\nu)r\frac{\partial \sigma_r^{II}}{\partial r} + (1-2\nu)\sigma_r^{II} = \frac{2(1-\nu)}{1-2\nu}r^2\alpha E\frac{\partial^2\theta}{\partial r^2} + \frac{2(2-\nu)}{1-2\nu}r\alpha E\frac{\partial \theta}{\partial r} + 2k_0 \tag{45}$$

where (40) has also been employed.

The solution of (45) leads through (43) to the stress field of the isothermal problem II, corresponding to the original thermal problem I. To obtain the stress field for body I the transformation (1a) is employed. A check on equation (45) is provided through the relation (1a) which, if substituted in (45), results in

$$2(1-\nu)r^2\frac{\partial^2\sigma_r^{I}}{\partial r^2} + 6(1-\nu)r\frac{\partial \sigma_r^{I}}{\partial r} + (1-2\nu)\sigma_r^{I} = 2k_0 - 2\alpha E r\frac{\partial \theta}{\partial r} - \alpha E\theta \tag{46}$$

which is precisely the governing equation for the state of plane strain, derived in [10], for problem I.

Besides providing an alternate approach to a given problem, the Duhamel analogy through the correspondence may be used to obtain new solutions from those previously existing. In this regard it is found that a temperature field of particular interest arises, when the distributed heat source Q is constant in the thermoelastic-plastic problem discussed in the foregoing. The temperature field in this case becomes

$$T = -\frac{Qr^2}{4K} + T(0) \tag{47}$$

where K is the thermal conductivity. In the corresponding isothermal problem the body force by (2) is

$$F_r^{II} = \frac{\alpha E}{1-2\nu}\frac{Q}{2K}r, \tag{48}$$

the form of which is immediately recognized as that due to centrifugal force in a cylinder rotating with angular velocity ω. We need only identify Q with ω through

$$\rho\omega^2 = \frac{\alpha E}{1-2\nu}\frac{Q}{2K} \tag{49}$$

where ρ is the density of the material.

In a similar manner it can be shown that the related problem of a hollow sphere of inner radius a and outer radius b with a uniformly distributed heat source[10] has, as its Duhamel analog, a problem which is of interest from a geophysical standpoint; namely, that of a hollow sphere reacting under the mutual gravitation of its parts, the body force for which is given by

$$F_r = -g\frac{r}{b}\frac{\left(1-\frac{a^3}{r^3}\right)}{\left(1-\frac{a^3}{b^3}\right)} \tag{50}$$

where g is the acceleration due to gravity at the outer radius $r = b$.

Concluding Remarks

Until this section the loading function was assumed regular; in general, however, $f = 0$ is only piecewise regular being composed of a number of surfaces $f^{(p)}$ which meet to form singular regimes, where a unique normal is not defined and where the flow rule (13a) does not hold. By use of a concept due to Koiter [12], if the $f^{(n)}$ act independently, the plastic strain rate at singular regimes may be taken as the sum of contributions from the individual $f^{(n)}$; i.e.,

$$\dot{\epsilon}_{ij}^{\,p} = \sum_{m=1}^{n} D_{(m)}\frac{\partial f^{(m)}}{\partial \sigma_{ij}}\left[\frac{\partial f^{(m)}}{\partial \sigma_{kl}}\dot{\sigma}_{kl} + \frac{\partial f}{\partial \theta}\dot{\theta}\right] \tag{51}$$

where the loading criterion has again been incorporated through

[9] In addition to F_r^{II} a uniform surface pressure

$$\sigma_r(a) = \frac{\alpha E}{1-2\nu}\theta(a)$$

is also imposed by (2b); one way that this pressure may be removed is by letting

$$T_r^{I} = -\frac{\alpha E}{1-2\nu}\theta(a)$$

in the thermal problem so that by (2b) $T_s^{II} = 0$.

[10] This problem may be solved with some modification along the same lines as in [10] for the cylinder. A solution, using deformation theory and a parabolically distributed heat source, has been obtained by Johnson [11] with application to a reactor pressure shell for a nuclear rocket.

(13c). The invariants $D_{(m)}$ are determined by substitution of (51) into the system

$$\dot{f}^{(m)} = 0 \tag{52}$$

composed of those $f^{(m)}$ contributing to $\dot{\epsilon}_{ij}{}^{p}$.

The extended Duhamel analogy may be demonstrated for the constitutive equations (51) in the same manner as described earlier, provided each of the $f^{(m)}$ can be written in the form (23) with the same separable function of time $a(t)$. Again the plastic strains in the corresponding problem agree (15); indeed, it can be shown that the individual contributions $\dot{\epsilon}_{ij}{}^{p(m)}$ of each $f^{(m)}$ to $\dot{\epsilon}_{ij}{}^{p}$ also correspond.

It is clear through the Duhamel analogy, as extended here to include materials obeying (14) and (23) under the conditions described, that uniqueness theorems for the stress rate, strain rate, and stresses as well as the minimum principles such as those discussed in [13] may be shown to hold. Recall [6] that in the case of a rigid plastic material only the scalar $(\partial f/\partial \sigma_{ij})\dot{\sigma}_{ij}$ is unique and not the individual components of the stress rate.

References

1 A. J. A. Morgan, "A Proof of Duhamel's Analogy for Thermal Stresses," *Journal of the Aero/Space Sciences*, vol. 25, 1958, pp. 466–467.

2 R. Hill, "New Horizons in the Mechanics of Solids," *Journal of the Mechanics and Physics of Solids*, vol. 5, 1956, pp. 66–74.

3 B. A. Boley and J. H. Weiner, "Theory of Thermal Stresses," John Wiley & Sons, New York, N. Y., 1960.

4 E. Sternberg, "On Transient Thermal Stresses in Linear Viscoelasticity," *Proceedings of The Third U. S. National Congress of Applied Mechanics*, ASME, 1958, pp. 673–683.

5 D. R. Bland, "The Theory of Linear Viscoelasticity," Pergamon Press, New York, N. Y., 1960.

6 W. Prager, "Non-Isothermal Plastic Deformation," *Proceedings Nederlandse Akademie Van Wetenshappen*, series B, vol. 61, 1958, pp. 176–192.

7 W. Olszak and W. Urbanowski, "Plastic Non-Homogeneity: A Survey of Theoretical and Experimental Research," *Proceedings of The IUTAM Symposium for Non-Homogeneity in Elasticity and Plasticity*, Pergamon Press, New York, N. Y., 1959, pp. 259–298.

8 W. Prager, "Recent Developments in the Mathematical Theory of Plasticity," *Journal of Applied Physics*, vol. 20, 1949, pp. 235–241.

9 W. Olszak, "On the Foundations of the Theory of Non-Homogeneous Elastoplastic Bodies (II)," *Bulletin de L'Academie Polonaise des Sciences*, vol. 3, 1955, pp. 111–117.

10 T. B. Kammash, S. A. Murch, and P. M. Naghdi, "The Elastic-Plastic Cylinder Subjected to Radially Distributed Heat Source, Lateral Pressure, and Axial Force with Application to Nuclear Reactor Fuel Elements," *Journal of the Mechanics and Physics of Solids*, vol. 8, 1960, pp. 1–25.

11 D. F. Johnson, "Analysis of Elastic-Plastic Stress Distribution in Thin-Walled Cylinders and Spheres Subjected to Internal Pressure and Nuclear Radiation Heating," NASA TN D 271, 1960.

12 W. T. Koiter, "Stress-Strain Relations, Uniqueness and Variational Theorems for Elastic-Plastic Material With a Singular Yield Surface," *Quarterly of Applied Mathematics*, vol. 11, 1953, pp. 350–354.

13 W. T. Koiter, "General Theorems for Elastic-Plastic Solids," Progress in Solid Mechanics, vol. 1, North-Holland Publishing Company, Amsterdam, Holland, 1960, pp. 165–221.

H. R. MECK
Design Engineer,
Pratt & Whitney Aircraft,
Connecticut Aircraft
Nuclear Engine Laboratory,
Middletown, Conn.

Bending of a Thin Cylindrical Shell Subjected to a Line Load Around a Circumference

An analysis is developed for bending of a thin circular cylindrical shell under a varying radial line load distributed around the circumference at the center section. The problem is solved by reducing the eighth-order differential equation of thin-shell theory to two approximate fourth-order equations. Deflections, bending stresses, and membrane stresses are evaluated. Both simply supported and clamped ends are considered.

Introduction and Basic Equations

THIS paper considers the deflections and stresses in a thin circular elastic cylinder subjected to a radial line load sinusoidally distributed around the circumference at the center section. Related problems have been investigated in several papers. Cylinders subjected to point loads have been analyzed in references [4, 7, 8].[1] Line loads distributed along axial generatrices have been considered in [11]. General solutions have been developed in [5, 6], but have not been applied to specific problems. The methods of references [4, 8, 13] can be applied to the present problem, but are limited to the case of an infinite cylinder or simply supported ends. Reference [7] can be used to evaluate displacements, but not stresses.

The basic differential equation of a thin circular cylinder subjected to a distributed radial load p is

$$\nabla^8 w + \frac{2}{a^8}\frac{\partial^6 w}{\partial\theta^6} + \frac{1}{a^8}\frac{\partial^4 w}{\partial\theta^4} + \frac{12(1-\nu^2)}{a^2h^2}\frac{\partial^4 w}{\partial x^4} = \frac{\nabla^4 p}{D} \quad (1)$$

This result is due to Donnell [1]. The equation usually known as Donnell's equation is a simplified form of that shown, valid in special cases [2].

In order to evaluate the bending moments, the following equations may be used:

$$M_x = D(\kappa_x + \nu\kappa_\theta) \qquad M_\theta = D(\kappa_\theta + \nu\kappa_x) \quad (2)$$

[1] Numbers in brackets designate References at end of paper.

Presented at the Summer Conference of the Applied Mechanics Division, Chicago, Ill., June 14–16, 1961, of THE AMERICAN SOCIETY OF MECHANICAL ENGINEERS.

Discussion of this paper should be addressed to the Editorial Department, ASME, United Engineering Center, 345 East 47th Street, New York 17, N. Y., and will be accepted until October 10, 1961. Discussion received after the closing date will be returned. Manuscript received by ASME Applied Mechanics Division, May 23, 1960. Paper No. 61—APM-15.

where

$$\kappa_x = \frac{\partial^2 w}{\partial x^2} \qquad \kappa_\theta = \frac{1}{a^2}\left(\frac{\partial^2 w}{\partial\theta^2} + w\right) \quad (3)$$

The bending stresses are

$$\sigma_x = \frac{6M_x}{h^2} \qquad \sigma_\theta = \frac{6M_\theta}{h^2} \quad (4)$$

Two methods of solution will be used for equation (1). The first method is to represent the applied load by a Fourier series in x and solve for w and its derivatives. The second method consists of reducing the eighth-order differential equation to an approximate fourth-order equation and solving in closed form. This procedure is applied separately to the limiting cases of a very short and a very long cylinder, and a general solution is then deduced. For convenience it is assumed that the load is sinusoidally distributed around the circumference. A problem involving a non-sinusoidal load can be analyzed by expanding the load in a Fourier series in θ and superposing sinusoidal solutions.

Deflections and Bending Stresses

Series Solution. A cylindrical shell is subjected to a sinusoidally distributed line load $P\cos n\theta$ at the center section, Fig. 1. The plane $x = 0$ is taken at the center, and the case of simply supported ends is first considered. At $x = \pm L/2$ the boundary conditions are

$$w = 0, \quad M_x = 0$$

At a section where $w = 0$ for all values of θ,

$$\partial w/\partial\theta = \partial^2 w/\partial\theta^2 = 0$$

Then $\kappa_\theta = 0$, and

$$M_x = D\frac{\partial^2 w}{\partial x^2}$$

Nomenclature

a = mean radius of shell
h = thickness
L = length
x = axial co-ordinate
θ = circumferential co-ordinate (angular)
P = maximum line load
p = distributed load
M = bending moment per unit length
N = membrane force per unit length
E = modulus of elasticity
ν = Poisson's ratio
$D = \dfrac{Eh^3}{12(1-\nu^2)}$
$\nabla^2 = \dfrac{\partial^2}{\partial x^2} + \dfrac{1}{a^2}\dfrac{\partial^2}{\partial\theta^2}$
u = axial displacement
v = circumferential displacement
w = radial displacement (positive outward)
κ = curvature
ϵ = strain
σ = stress
m = number of lobes of axial bending
n = number of lobes of circumferential bending

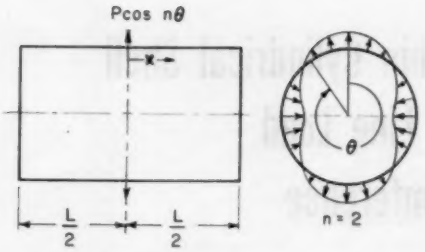

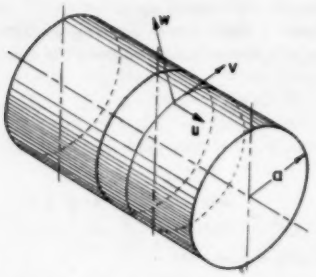

Fig. 1 Reference co-ordinates and dimensions

Hence the required end conditions can be expressed by the equations $w = 0$ and $\partial^2 w/\partial x^2 = 0$. The first method to be used is similar to that of reference [4]. The load is considered to be a distributed pressure on a circumferential strip of width Δ, and is expressed as a Fourier series:

$$p = \frac{4P}{\pi\Delta} \cos n\theta \sum_{m=1,\,3,\,5}^{\infty} \frac{1}{m} \sin \frac{m\pi\Delta}{2L} \cos \frac{m\pi x}{L}$$

By substituting this expression in equation (1), solving for w, and taking the limit as $\Delta \to 0$, the radial displacement is found:

$$w = \frac{2P}{DL} \cos n\theta \sum_{m=1,\,3,\,5}^{\infty} \frac{\left(\frac{n^2}{a^2} + \frac{m^2\pi^2}{L^2}\right)^2 \cos \frac{m\pi x}{L}}{\left(\frac{n^2}{a^2} + \frac{m^2\pi^2}{L^2}\right)^4 - 2\frac{n^6}{a^6} + \frac{n^4}{a^4} + \frac{12(1-\nu^2)}{a^2h^2}\left(\frac{m\pi}{L}\right)^4} \quad (5)$$

The slope and curvatures are

$$\frac{\partial w}{\partial x} = -\frac{2P}{DL} \cos n\theta \sum_{m=1,\,3,\,5}^{\infty} \frac{\left(\frac{m\pi}{L}\right)\left(\frac{n^2}{a^2} + \frac{m^2\pi^2}{L^2}\right)^2 \sin \frac{m\pi x}{L}}{\left(\frac{n^2}{a^2} + \frac{m^2\pi^2}{L^2}\right)^4 - 2\frac{n^6}{a^6} + \frac{n^4}{a^4} + \frac{12(1-\nu^2)}{a^2h^2}\left(\frac{m\pi}{L}\right)^4} \quad (6)$$

$$\kappa_x = \frac{\partial^2 w}{\partial x^2} = -\frac{2P}{DL} \cos n\theta \cdot \sum_{m=1,\,3,\,5}^{\infty} \frac{\left(\frac{m\pi}{L}\right)^2\left(\frac{n^2}{a^2} + \frac{m^2\pi^2}{L^2}\right)^2 \cos \frac{m\pi x}{L}}{\left(\frac{n^2}{a^2} + \frac{m^2\pi^2}{L^2}\right)^4 - 2\frac{n^6}{a^6} + \frac{n^4}{a^4} + \frac{12(1-\nu^2)}{a^2h^2}\left(\frac{m\pi}{L}\right)^4} \quad (7)$$

$$\kappa_\theta = \frac{1}{a^2}\left(\frac{\partial^2 w}{\partial\theta^2} + w\right) = -(n^2 - 1)\frac{w}{a^2} \quad (8)$$

It can be seen that the required end conditions are satisfied. The bending moments can be obtained from equations (2), (7), and (8).

Although the differential equation (1) is of eighth order, only four boundary conditions have been specified (w and M_x equal to zero at each end). A complete examination of the present solution shows that the end conditions $N_x = 0$ and $v = 0$ are also implied. In principle, any set of eight boundary conditions could be imposed, but with the series method of solution this would lead to considerable mathematical difficulty. In fact, the foregoing conditions (simply supported ends) are the only ones which can conveniently be handled by the present method. The series solution has one other undesirable feature. Although the convergence of series (5) may be satisfactory, that of (7) is usually very poor. A more satisfactory procedure will be developed which gives results in closed form and is valid for either simply supported or clamped ends.

Short Cylinder. In the case of a short cylinder, $(L/a) \ll 1$. Hence equation (5) reduces to

$$w = \frac{2P}{DL} \cos n\theta \sum_{m=1,\,3,\,5}^{\infty} \frac{\cos \frac{m\pi x}{L}}{\left(\frac{m\pi}{L}\right)^4 + \frac{12(1-\nu^2)}{a^2h^2}} \quad (9)$$

The last term in the denominator is retained because the assumption that $(L/a) \ll 1$ does not necessarily imply that $[L/(ah)^{1/2}] \ll 1$. This series can be summed directly for maximum deflection [12] but a different procedure is more advantageous. The simplification from equation (5) to equation (9) is equivalent to replacing (1) by

$$\frac{\partial^4 w}{\partial x^4} + \frac{12(1-\nu^2)}{a^2h^2} w = \frac{p}{D} \quad (10)$$

A solution was obtained previously by expanding p in a Fourier series and inserting the result in equation (1). An alternate procedure is to set $p = 0$ everywhere in a half cylinder of length $L/2$ and impose appropriate boundary conditions at the ends. The second method will now be used. Setting $p = 0$ in equation (10), a product solution is assumed:

$$w = X \cos n\theta$$

where X is a function of x only, to be determined from the equation

$$X^{IV} + 4\alpha^4 X = 0 \qquad \alpha^4 = \frac{3(1-\nu^2)}{a^2h^2} \quad (11)$$

Superscripts denote differentiation with respect to x. The solution is

$$X = A_1 e^{\alpha x} \cos \alpha x + A_2 e^{\alpha x} \sin \alpha x + A_3 e^{-\alpha x} \cos \alpha x + A_4 e^{-\alpha x} \sin \alpha x \quad (12)$$

Considering first the case of simply supported ends, the boundary conditions are

$$x = \frac{L}{2}: \qquad w = 0 \qquad \frac{\partial^2 w}{\partial x^2} = 0$$

and at the center, from symmetry

$$x = 0: \qquad \frac{\partial w}{\partial x} = 0$$

The remaining boundary condition is satisfied by equating the shearing traction V_x at $x = 0$ to the applied load. In a short cylinder, V_x is given with negligible error by the expression $V_x = D(\partial^3 w/\partial x^3)$. Then the fourth boundary condition is

$$x = 0: \quad V_x = D\frac{\partial^3 w}{\partial x^3} = \frac{P}{2}\cos n\theta$$

$$X''' = \frac{P}{2D}$$

It can be seen that the general solution (12) and associated boundary conditions are identical to those for a symmetrically loaded circular cylinder or beam on elastic foundation. From section 20a of reference [3] or directly, w is found

$$w = \tfrac{1}{2}[3(1-\nu^2)]^{1/4}\frac{P}{E}\left(\frac{a}{h}\right)^{3/2}\left[e^{-\alpha x}(\cos\alpha x + \sin\alpha x) - \frac{e^{-\alpha L} + \cos\alpha L + \sin\alpha L}{\cosh\alpha L + \cos\alpha L}\cosh\alpha x\cos\alpha x + \frac{e^{-\alpha L} + \cos\alpha L - \sin\alpha L}{\cosh\alpha L + \cos\alpha L}\sinh\alpha x\sin\alpha x\right]\cos n\theta \quad (13)$$

The maximum deflection and curvature occur at the point $x = 0$, $\theta = 0$:

$$w_0 = \tfrac{1}{2}[3(1-\nu^2)]^{1/4}\frac{P}{E}\left(\frac{a}{h}\right)^{3/2}\frac{\sinh\alpha L - \sin\alpha L}{\cosh\alpha L + \cos\alpha L} \quad (14)$$

$$\left(\frac{\partial^2 w}{\partial x^2}\right)_0 = -[3(1-\nu^2)]^{3/4}\frac{P}{Eh^2}\left(\frac{a}{h}\right)^{1/2}\frac{\sinh\alpha L + \sin\alpha L}{\cosh\alpha L + \cos\alpha L} \quad (15)$$

The case of a short cylinder with clamped ends can be solved by an analogous procedure. In this case the boundary conditions are:

$$x = \frac{L}{2}: \qquad w = 0 \qquad \frac{\partial w}{\partial x} = 0$$

$$x = 0: \qquad \frac{\partial w}{\partial x} = 0 \qquad V_x = D\frac{\partial^3 w}{\partial x^3} = \frac{P}{2}\cos n\theta$$

The solution is (using reference [3], section 21a)

$$w = \tfrac{1}{2}[(1-\nu^2)]^{1/4}\frac{P}{E}\left(\frac{a}{h}\right)^{3/2}\left[e^{-\alpha x}(\cos\alpha x + \sin\alpha x) - \frac{2 - e^{-\alpha L} - \cos\alpha L + \sin\alpha L}{\sinh\alpha L + \sin\alpha L}\cosh\alpha x\cos\alpha x + \frac{-e^{-\alpha L} + \cos\alpha L + \sin\alpha L}{\sinh\alpha L + \sin\alpha L}\sinh\alpha x\sin\alpha x\right]\cos n\theta \quad (16)$$

$$w_0 = \tfrac{1}{2}[3(1-\nu^2)]^{1/4}\frac{P}{E}\left(\frac{a}{h}\right)^{3/2}\frac{\cosh\alpha L + \cos\alpha L - 2}{\sinh\alpha L + \sin\alpha L} \quad (17)$$

$$\left(\frac{\partial^2 w}{\partial x^2}\right)_0 = -[3(1-\nu^2)]^{3/4}\frac{P}{Eh^2}\left(\frac{a}{h}\right)^{1/2}\frac{\cosh\alpha L - \cos\alpha L}{\sinh\alpha L + \sin\alpha L} \quad (18)$$

The foregoing equations completely define the bending of a short cylinder. The bending moments are found by substituting these results in equations (2), (3), and (8).

The simplification from equation (1) to (10) involves several limitations. Physically this approximation amounts to neglecting terms which represent circumferential bending. Equation (10) applies to a short cylinder with clamped or simply supported ends, but would not apply to a cylinder with free ends. Also, it can be seen by comparison of equations (5) and (9) that (10) is not correct for large values of n. This point is discussed later under "Validity of the Approximations."

It was remarked before that the series method does not lend itself to use of the full eight boundary conditions permitted by equation (1). The second method, although more general, is still restricted to four boundary conditions because of the reduction of order in obtaining equation (10). Only conditions involving w and M_x can be specified, whereas a more rigorous solution would also satisfy conditions involving u, v, N_x, and $N_{x\theta}$ at the edge. In the present problem the latter boundary conditions are much less important than the former, so that this limitation is not serious.

Long Cylinder. In this case equation (5) is a satisfactory starting point. Since $L/a \gg 1$, terms of order a/L may be neglected. It does not follow rigorously from this that terms of order ma/L may be neglected. This will be assumed for the present, but the point will be discussed later. With this simplification, equation (5) reduces to

$$w = \frac{2Pn^4a^2}{EhL}\cos n\theta \sum_{m=1,3,5}^{\infty}\frac{\cos\dfrac{m\pi x}{L}}{\dfrac{n^4(n^2-1)^2}{12(1-\nu^2)}\left(\dfrac{h}{a}\right)^2 + \left(\dfrac{m\pi a}{L}\right)^4} \quad (19)$$

This can be evaluated in closed form in the limit $L/a \to \infty$. Substituting

$$\beta^4 = \frac{n^4(n^2-1)^2}{48(1-\nu^2)}\cdot\frac{h^2}{a^6} \qquad Q = \frac{m\pi}{L} \qquad \Delta Q = \frac{2\pi}{L}$$

leads to

$$w = \frac{Pn^4}{\pi Ea^2 h}\cos n\theta \sum_{m=1,3,5}^{\infty}\frac{\cos Qx\,\Delta Q}{Q^4 + 4\beta^4}$$

In the limit $L/a \to \infty$ the foregoing summation becomes an integral which can easily be evaluated by residue theory [12]. Then one obtains

$$w = \frac{Pn^4}{\pi Ea^2 h}\int_0^{\infty}\frac{\cos Qx\,dQ}{Q^4 + 4\beta^4}\cos n\theta = [3(1-\nu^2)]^{3/4}\frac{n}{(n^2-1)^{3/2}}\frac{P}{E}\left(\frac{a}{h}\right)^{3/2} e^{-\beta x}(\cos\beta x + \sin\beta x)\cos n\theta \quad (20)$$

$$0 \le x \le \frac{L}{2}$$

A long but finite cylinder with simply supported ends could be analyzed by replacing the finite cylinder with an infinite cylinder and an infinite set of images [8]. However, in the case of clamped ends, this leads to serious difficulties. It is preferable to adopt the second method at this point. Equation (20) may be used with correction terms for the end moments and forces. This is similar to the procedure used in [7]. To evaluate the effect of the end restraints it may be observed that equation (19) is the

solution which would be obtained from the equation[2]

$$\frac{\partial^8 w}{\partial \theta^8} + 2\frac{\partial^6 w}{\partial \theta^6} + \frac{\partial^4 w}{\partial \theta^4} + 12(1-\nu^2)\frac{a^6}{h^2}\frac{\partial^4 w}{\partial x^4} = \frac{a^4}{D}\frac{\partial^4 p}{\partial \theta^4} \tag{21}$$

In considering end tractions, $p = 0$ everywhere on the cylinder. A product solution may be assumed for equation (21):

$$w = X\cos n\theta$$

A fourth-order differential equation is again obtained:

$$X^{IV} + 4\beta^4 X = 0 \tag{22}$$

The solution is

$$X = B_1 e^{\beta x}\cos\beta x + B_2 e^{\beta x}\sin\beta x + B_3 e^{-\beta x}\cos\beta x + B_4 e^{-\beta x}\sin\beta x \tag{23}$$

It is clear that the end correction must be an even function of x. Then the deflection of a long but finite cylinder is

$$w = \left\{[3(1-\nu^2)]^{3/4}\frac{n}{(n^2-1)^{3/2}}\frac{P}{E}\left(\frac{a}{h}\right)^{5/2} e^{-\beta x}(\cos\beta x + \sin\beta x) + B_1\cosh\beta x\cos\beta x + B_2\sinh\beta x\sin\beta x\right\}\cos n\theta$$

For a cylinder with simply supported ends the boundary conditions are

$$x = \frac{L}{2}: \qquad w = 0 \qquad \frac{\partial^2 w}{\partial x^2} = 0$$

The radial deflection is

$$w = [3(1-\nu^2)]^{3/4}\frac{n}{(n^2-1)^{3/2}}\frac{P}{E}\left(\frac{a}{h}\right)^{5/2}\cdot\left[e^{-\beta x}(\cos\beta x + \sin\beta x) - \frac{e^{-\beta L} + \cos\beta L + \sin\beta L}{\cosh\beta L + \cos\beta L}\cosh\beta x\cos\beta x + \frac{e^{-\beta L} + \cos\beta L - \sin\beta L}{\cosh\beta L + \cos\beta L}\sinh\beta x\sin\beta x\right]\cos n\theta \tag{24}$$

The maximum deflection occurs at the point $x = 0$, $\theta = 0$:

$$w_0 = [3(1-\nu^2)]^{3/4}\frac{n}{(n^2-1)^{3/2}}\frac{P}{E}\left(\frac{a}{h}\right)^{5/2}\frac{\sinh\beta L - \sin\beta L}{\cosh\beta L + \cos\beta L} \tag{25}$$

In the case of clamped ends, the corresponding result is

$$w_0 = [3(1-\nu^2)]^{3/4}\frac{n}{(n^2-1)^{3/2}}\frac{P}{E}\left(\frac{a}{h}\right)^{5/2}\frac{\cosh\beta L + \cos\beta L - 2}{\sinh\beta L + \sin\beta L} \tag{26}$$

In order to continue the solution to the long-cylinder problem, it is necessary to obtain expressions for the bending moments and stresses. This reduces to a problem of evaluating the curvatures κ_θ and κ_x. The maximum values occur at the point $x = 0$, $\theta = 0$. The circumferential curvature can be found by substituting the foregoing results in equation (8). It appears offhand that the maximum axial curvature $(\partial^2 w/\partial x^2)_0$ could be obtained by differentiating the equation for the deflection curve, e.g., equation (24) for simply supported ends, twice with respect to x. However, the result obtained by doing this turns out to be incorrect. In deriving equation (19) from equation (5), it was assumed that terms of order ma/L may be neglected, but the only statement that can be made reliably is that a/L is small. No significant error occurs in the case of deflection, but a very serious error occurs in the case of axial curvature in the neighborhood of the applied load. The evaluation of curvature by differentiation of equation (24) implies that equation (7) may be simplified in the same way as equation (5). This is not true, since the terms in the series (7) contain a factor of m^2 which greatly magnifies the importance of higher axial harmonics of large m, which are falsified by this approximation. The correct results for axial curvature will be found in the next section.

It was because of the foregoing difficulty that the boundary conditions at $x = 0$ could not be satisfied by the simpler method used for the short cylinder. All derivatives of w obtained by differentiating equation (24) are unreliable. It will be seen in the next section that this behavior occurs only locally near $x = 0$. Elsewhere the results obtained by formal differentiation of the long cylinder deflection equation are correct. Hence the assumption which was implied in satisfying the foregoing boundary conditions, that $\partial w/\partial x$ and $\partial^2 w/\partial x^2$ were known at $x = L/2$, remains valid. The present method does not apply to a long cylinder with free ends, since the boundary conditions are more complicated in this case. This discussion differs from the viewpoint on boundary conditions given in reference [7], which appears to be unsound.

Cylinder of any Length. If a cylinder is neither very short nor very long, the eighth-order differential equation (1) cannot be reduced to a fourth-order equation, and a more general solution must be obtained. This can be done by assuming a solution of the form

$$w = Ce^{\psi(x/a)}\cos n\theta$$

Substituting this result in (1), an algebraic equation is obtained for ψ:

$$(\psi^2 - n^2)^4 + 4\lambda^4\psi^4 - 2n^6 + n^4 = 0 \qquad \lambda = \alpha a \tag{27}$$

It can be seen by inspection that, since λ^4 is a very large number, equation (27) has four very large roots and four very small roots. The large roots are given approximately by the equation

$$(\psi^2 - n^2)^4 + 4\lambda^4\psi^4 \approx 0$$

$$\psi^4 + 4\lambda^4 \approx 0$$

$$\psi = (1+i)\lambda, \quad (1-i)\lambda, \quad (-1+i)\lambda, \quad (-1-i)\lambda$$

The small roots are given approximately by the equation

$$4\lambda^4\psi^4 + n^8 - 2n^6 + n^4 \approx 0$$

$$\psi = (1+i)\frac{n(n^2-1)^{1/2}}{2\lambda}, (1-i)\frac{n(n^2-1)^{1/2}}{2\lambda} \qquad (-1+i)\frac{n(n^2-1)^{1/2}}{2\lambda}, \quad (-1-i)\frac{n(n^2-1)^{1/2}}{2\lambda}$$

Transforming to real variables, the general solution to equation (1) becomes

$$w = [A_1 e^{\alpha x}\cos\alpha x + A_2 e^{\alpha x}\sin\alpha x + A_3 e^{-\alpha x}\cos\alpha x + A_4 e^{-\alpha x}\sin\alpha x + B_1 e^{\beta x}\cos\beta x + B_2 e^{\beta x}\sin\beta x + B_3 e^{-\beta x}\cos\beta x + B_4 e^{-\beta x}\sin\beta x]\cos n\theta \tag{28}$$

where α and β have the same meanings as before.

Eight independent functions appear in the general solution, and in principle eight boundary conditions are necessary to evaluate

[2] Equations similar to (10) and (21) have been obtained from a different viewpoint by Reissner for the case of a semi-infinite cylinder loaded at the end. See equations 14.11 and 14.16 of [14].

the constants. For practical purposes the work can be greatly simplified by the following observation: The constant β is much smaller than α, by a factor of h/a. Thus the terms involving α represent deformations varying rapidly in the axial direction, while those involving β represent deformations varying slowly in the axial direction. In the case of a very short cylinder, the solution must be given by the first four terms on the right-hand side of equation (28). This solution has been found previously, hence the A's here are the same A's which appeared in equation (12) for the short-cylinder case. Likewise, in the case of a very long cylinder the last four terms must predominate, and the B's here are the same B's which appeared in the long-cylinder solution, equation (23). This indicates that the general solution can be obtained by simple addition of the appropriate short-cylinder and long-cylinder solutions. Thus, in the case of simply supported ends, it follows from equations (13) and (24) that

$$w = \tfrac{1}{2}\,[3(1-\nu^2)]^{1/4}\,\frac{P}{E}\left(\frac{a}{h}\right)^{3/2}\left[e^{-\alpha x}(\cos\alpha x+\sin\alpha x) - \frac{e^{-\alpha L}+\cos\alpha L+\sin\alpha L}{\cosh\alpha L+\cos\alpha L}\cosh\alpha x\cos\alpha x + \frac{e^{-\alpha L}+\cos\alpha L-\sin\alpha L}{\cosh\alpha L+\cos\alpha L}\sinh\alpha x\sin\alpha x\right]\cos n\theta$$
$$+\,[3(1-\nu^2)]^{3/4}\frac{n}{(n^2-1)^{3/2}}\,\frac{P}{E}\left(\frac{a}{h}\right)^{3/2}\left[e^{-\beta x}(\cos\beta x+\sin\beta x) - \frac{e^{-\beta L}+\cos\beta L+\sin\beta L}{\cosh\beta L+\cos\beta L}\cosh\beta x\cos\beta x + \frac{e^{-\beta L}+\cos\beta L-\sin\beta L}{\cosh\beta L+\cos\beta L}\sinh\beta x\sin\beta x\right]\cos n\theta \quad (29)$$

The deflection at the center is

$$w_0 = \tfrac{1}{2}\,[3(1-\nu^2)]^{1/4}\,\frac{P}{E}\left(\frac{a}{h}\right)^{3/2}\frac{\sinh\alpha L-\sin\alpha L}{\cosh\alpha L+\cos\alpha L} + [3(1-\nu^2)]^{3/4}\frac{n}{(n^2-1)^{3/2}}\,\frac{P}{E}\left(\frac{a}{h}\right)^{3/2}\frac{\sinh\beta L-\sin\beta L}{\cosh\beta L+\cos\beta L} \quad (30)$$

In the case of a very long cylinder both transcendental fractions approach unity, and the deflection reduces to that of equation (25) at $x = 0$, $\theta = 0$. In the case of a very short cylinder, the fractions approach $\alpha^3L^3/6$ and $\beta^3L^3/6$, respectively, so that the second term is negligible in comparison with the first by a factor of $(h/a)^2$. This also agrees with the previous result, equation (14).

By differentiating equation (29) twice with respect to x and substituting $x = 0$, $\theta = 0$, the expression for axial curvature at the center is obtained:

$$\left(\frac{\partial^2 w}{\partial x^2}\right)_0 = -[3(1-\nu^2)]^{3/4}\,\frac{P}{Eh^2}\left(\frac{a}{h}\right)^{1/2}\frac{\sinh\alpha L+\sin\alpha L}{\cosh\alpha L+\cos\alpha L} - \tfrac{1}{2}\,[3(1-\nu^2)]^{1/4}\,\frac{n^2}{(n^2-1)^{1/2}}\,\frac{P}{Eh^2}\left(\frac{h}{a}\right)^{1/2}\frac{\sinh\beta L+\sin\beta L}{\cosh\beta L+\cos\beta L} \quad (31)$$

The foregoing result clarifies the fact which has been mentioned previously about a long cylinder. Although the second term in the deflection solution is of higher order of magnitude than the first, two differentiations with respect to x have the effect of an algebraic multiplication by α^2 on the first term and β^2 on the second term. Thus in the expression for $(\partial^2 w/\partial x^2)_0$ the first term predominates regardless of whether the cylinder is short or long.

In the case of clamped ends, the corresponding formulas for maximum deflection and axial curvature are

$$w_0 = \tfrac{1}{2}\,[3(1-\nu^2)]^{1/4}\,\frac{P}{E}\left(\frac{a}{h}\right)^{3/2}\frac{\cosh\alpha L+\cos\alpha L-2}{\sinh\alpha L+\sin\alpha L} + [3(1-\nu^2)]^{3/4}\frac{n}{(n^2-1)^{3/2}}\,\frac{P}{E}\left(\frac{a}{h}\right)^{3/2}\frac{\cosh\beta L+\cos\beta L-2}{\sinh\beta L+\sin\beta L} \quad (32)$$

$$\left(\frac{\partial^2 w}{\partial x^2}\right)_0 = -[3(1-\nu^2)]^{3/4}\,\frac{P}{Eh^2}\left(\frac{a}{h}\right)^{1/2}\frac{\cosh\alpha L-\cos\alpha L}{\sinh\alpha L+\sin\alpha L} - \tfrac{1}{2}\,[3(1-\nu^2)]^{1/4}\,\frac{n^2}{(n^2-1)^{1/2}}\,\frac{P}{Eh^2}\left(\frac{h}{a}\right)^{1/2}\frac{\cosh\beta L-\cos\beta L}{\sinh\beta L+\sin\beta L} \quad (33)$$

and the same remarks apply as before.

In an infinite cylinder the deflection at any point is

$$w = \frac{P}{E}\left\{\tfrac{1}{2}\,[3(1-\nu^2)]^{1/4}\left(\frac{a}{h}\right)^{3/2}e^{-\alpha x}(\cos\alpha x+\sin\alpha x) + [3(1-\nu^2)]^{3/4}\frac{n}{(n^2-1)^{3/2}}\left(\frac{a}{h}\right)^{3/2}e^{-\beta x}(\cos\beta x+\sin\beta x)\right\}\cos n\theta \quad (34)$$

and the curvature is

$$\frac{\partial^2 w}{\partial x^2} = -\frac{P}{Eh^2}\left\{[3(1-\nu^2)]^{3/4}\left(\frac{a}{h}\right)^{1/2}e^{-\alpha x}(\cos\alpha x-\sin\alpha x) + \tfrac{1}{2}\,[3(1-\nu^2)]^{1/4}\frac{n^2}{(n^2-1)^{1/2}}\left(\frac{h}{a}\right)^{1/2}e^{-\beta x}(\cos\beta x-\sin\beta x)\right\}\cos n\theta \quad (35)$$

It is desirable to examine the axial distribution of w and $\partial^2 w/\partial x^2$ in a long cylinder. From equation (29) or (34) it can be seen that the deflection in a long cylinder is felt for a distance from the applied load of order $a(a/h)^{1/2}$. This is entirely different from behavior under symmetrical loading, where the deflection decays within a distance of order $(ah)^{1/2}$. The distribution of circumferential curvature is identical to that of w, equation (8). It can be seen by differentiating equation (29) twice with respect to x or from equation (35) that the high value of axial curvature due to

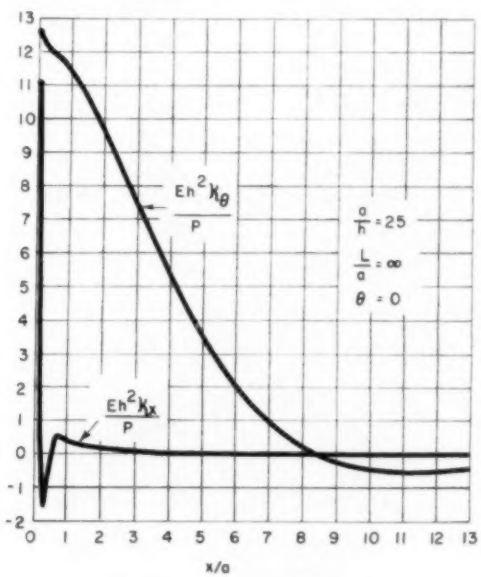

Fig. 2 Axial distribution of χ_θ and χ_x

the α-part of the solution is localized in a small area near the applied load. Away from the origin the β-part of the solution determines the axial curvature. The same conclusions apply qualitatively to a long cylinder with simply supported or clamped ends. Axial distributions of κ_θ and κ_x are plotted in Fig. 2 for an infinite cylinder with $a/h = 25$.

Membrane Stresses

For a complete analysis of the stresses in the cylinder, it is necessary to consider the membrane tensions as well as the bending stresses investigated previously. In applying the present method it is convenient to have expressions for N_θ and N_x in terms of w only. Starting with N_θ, the required result can be obtained from the equation of equilibrium of a differential element [9, 10]

$$N_\theta = -a\left(\frac{\partial^2 M_x}{\partial x^2} + \frac{1}{a}\frac{\partial^2 M_{\theta x}}{\partial x\,\partial\theta} + \frac{1}{a}\frac{\partial^2 M_{x\theta}}{\partial\theta\,\partial x} + \frac{1}{a^2}\frac{\partial^2 M_\theta}{\partial\theta^2}\right) + pa \quad (36)$$

Equations (2) and (3) may be used together with the equation

$$M_{x\theta} = M_{\theta x} = (1-\nu)\frac{D}{a}\frac{\partial}{\partial x}\left(\frac{\partial w}{\partial\theta} - v\right) \quad (37)$$

With these substitutions, equation (36) becomes, after dropping negligible terms and setting $p = 0$

$$N_\theta = -Da\left(\nabla^4 w + \frac{1}{a^4}\frac{\partial^2 w}{\partial\theta^2}\right) \quad (38)$$

Sign conventions are defined by Fig. 3. Moments are represented vectorially according to the right-hand rule.

To evaluate N_θ in specific cases it may be observed that all the equations for deflection derived in this paper are of the form

$$w = [X(\alpha) + X(\beta)]\cos n\theta$$

where $X(\alpha)$ is a function of α and x, and $X(\beta)$ is a function of β and x. Substituting the foregoing expression in equation (38),

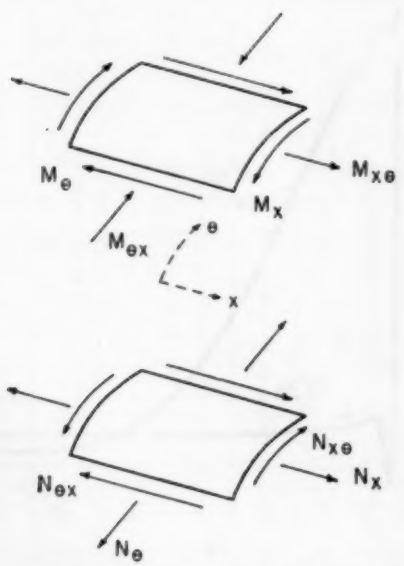

Fig. 3 Sign conventions for moments and membrane forces

and again omitting negligible terms, the following formula for N_θ is obtained:

$$N_\theta = -Da\left[X^{IV}(\alpha) + \frac{n^2(n^2-1)}{a^4}X(\beta)\right]\cos n\theta$$

Using equation (11), this reduces to

$$\frac{N_\theta}{E} = \left[\left(\frac{h}{a}\right)X(\alpha) - \frac{n^2(n^2-1)}{12(1-\nu^2)}\left(\frac{h}{a}\right)^3 X(\beta)\right]\cos n\theta \quad (39)$$

The X's can be taken from the preceding section for the appropriate boundary conditions. The maximum value of N_θ occurs at $x = 0$, $\theta = 0$, and is approximately

$$N_{\theta 0} = E\frac{h}{a}X(\alpha) \quad (40)$$

The axial membrane tension N_x must also be evaluated. This can be done by using the two equations

$$\frac{\partial N_x}{\partial x} + \frac{1}{a}\frac{\partial N_{\theta x}}{\partial\theta} = 0$$

$$\frac{1}{a}\frac{\partial N_\theta}{\partial\theta} + \frac{\partial N_{x\theta}}{\partial x} = \frac{1}{a^2}\frac{\partial M_\theta}{\partial\theta} + \frac{1}{a}\frac{\partial M_{x\theta}}{\partial x}$$

Using the fact that $N_{x\theta} = N_{\theta x}$, these equations lead to

$$\frac{\partial^2 N_x}{\partial x^2} = \frac{1}{a^2}\frac{\partial^2 N_\theta}{\partial\theta^2} - \frac{1}{a^3}\frac{\partial^2 M_\theta}{\partial\theta^2} - \frac{1}{a^2}\frac{\partial^2 M_{x\theta}}{\partial x\,\partial\theta} \quad (41)$$

All the terms on the right-hand side of equation (41) have been evaluated previously, and substitution of their values gives, after dropping negligible terms

$$\frac{\partial^2 N_x}{\partial x^2} = -\frac{D}{a}\frac{\partial^2}{\partial\theta^2}\left[\nabla^4 w + \frac{2}{a^4}\frac{\partial^2 w}{\partial\theta^2} + \frac{w}{a^4}\right] = \frac{n^2 D}{a}\left[X^{IV}(\alpha) + \frac{(n^2-1)^2}{a^4}X(\beta)\right]\cos n\theta$$

Using equation (22), N_x is found:[3]

$$\frac{N_x}{E} = \left[\frac{n^2h^2}{12(1-\nu^2)a}X''(\alpha) - \frac{ah}{n^2}X''(\beta)\right]\cos n\theta \quad (42)$$

The detailed solution will be worked out for an infinite cylinder In this case the X's are, from equation (34)

$$X(\alpha) = \tfrac{1}{2}[3(1-\nu^2)]^{1/4}\frac{P}{E}\left(\frac{a}{h}\right)^{1/2}e^{-\alpha x}(\cos\alpha x + \sin\alpha x)$$

$$X(\beta) = [3(1-\nu^2)]^{3/4}\frac{n}{(n^2-1)^{1/2}}\frac{P}{E}\left(\frac{a}{h}\right)^{1/2} e^{-\beta x}(\cos\beta x + \sin\beta x)$$

Substituting in equation (39):

$$N_\theta = P\left\{\tfrac{1}{2}[3(1-\nu^2)]^{1/4}\left(\frac{a}{h}\right)^{1/2}e^{-\alpha x}(\cos\alpha x + \sin\alpha x) - \frac{1}{4[3(1-\nu^2)]^{1/4}}\frac{n^2}{(n^2-1)^{1/2}}\left(\frac{h}{a}\right)^{1/2}e^{-\beta x}(\cos\beta x + \sin\beta x)\right\}\cos n\theta \quad (43)$$

and from equation (42)

[3] In deriving equation (42), negligible terms have been dropped at each step. It is conceivable that this procedure could introduce errors through cancellation of first-order terms [1], but the present result can be verified by retaining all terms until the last step and then simplifying.

$$N_x = \tfrac{1}{2}\,[3(1-\nu^2)]^{1/4}\,\frac{n}{(n^2-1)^{1/4}}\,P\left(\frac{a}{h}\right)^{1/2} e^{-\beta x}(\cos\beta x - \sin\beta x)\cos n\theta \quad (44)$$

A complete stress analysis is now possible for any of the cases considered in the foregoing. The complete expression for deflection is first found, as in equation (29) or (34). The bending stresses are then found from equations (2), (3), (4), and (8). The membrane stresses N_θ/h and N_x/h are found from equations (39) and (42) and are added to the bending stresses. Since the maximum stresses occur at the point $x = 0$, $\theta = 0$, $M_{x\theta}$ and $N_{x\theta}$ are zero from symmetry, so that σ_θ and σ_x are the principal stresses.

Validity of the Approximations

A number of errors of order h/a have been introduced in the present analysis. The basic differential equation (1) involves the neglect of terms of order h/a in its derivation. Further errors are introduced in the various approximations, and the results are not entirely consistent. For example, the results for deflection of a long cylinder with simply supported ends given by equations (5), (24), and (29) all differ slightly. Discrepancies of this type are trivial unless the shell is thick, in which case no satisfactory result can be obtained by conventional thin-shell analysis.

The errors in the series solution are all of order h/a, but some of the approximations in closed form contain errors of another type which depend upon m and n as well as a/h. For example, it was found that the simple long-cylinder solution falsifies terms of large m and is not correct for axial bending, although it is correct for deflection. General solutions such as equation (29) are correct for all values of m.

The magnitude of n also has a marked effect upon the validity of the approximations. For large values of n the modified Donnell equation (1) is equivalent to the simple Donnell equation [2]:

$$\nabla^8 w + \frac{12(1-\nu^2)}{a^2h^2}\,\frac{\partial^4 w}{\partial x^4} = \frac{\nabla^4 p}{D} \quad (45)$$

A solution to equation (45) has been derived in reference [6]. This may lead to serious errors if n is small. The present analysis is free from this limitation, but an error was introduced by reducing the correct eighth-order differential equation (1) to two fourth-order equations or, equivalently, by the approximation made in solving the characteristic equation (27). A careful examination shows that this approximation is valid only if $a/h \gg n^2$, so that the present solutions are not correct for large values of n.

A load having a nonsinusoidal circumferential distribution may be represented by a double Fourier series in x and θ as in reference [4], or by a single Fourier series in θ of which each term is a solution of the type developed in this paper. The second method has been applied in reference [7] to a long cylinder subjected to concentrated loads. Although this solution is not valid for either large m or large n, no significant error occurs in the resulting deflection. Curvatures and bending stresses cannot be calculated by this method because of the importance of higher harmonics in the derivatives of w. If an attempt is made to evaluate deflection due to concentrated loads on a short cylinder by an analogous procedure, the result is a series which diverges. An exact solution to equation (27) shows a variation of α which is important for large values of n and causes the series to converge. Unfortunately, the exact solution is considerably more complicated than the present analysis.

One further limitation may be noted. Large values of m and n represent higher harmonics of short wave length. For very large values, the wave lengths approach the same order of magnitude as the thickness of the shell. In this case the basic thin-shell equation (1) breaks down. Thus the series summations do not remain strictly valid as $m \to \infty$. In the case of deflection this has no appreciable effect on the result, but in the case of curvature, where the series converges much more slowly, some rounding of the κ_x curve could be expected at the origin, Fig. 2. The same remarks apply to both the series and the closed-form solutions. This point probably is not a major source of error. The same effect occurs in a symmetrically loaded cylinder, and is not usually considered.

The present paper contains only theoretical results, but it may be mentioned that this investigation was made in response to a practical problem in shell design. Strain gage tests carried out by the author and coworkers have substantiated the analysis for a case similar to that shown in Fig. 2.

Acknowledgment

This work was supported by the U. S. Atomic Energy Commission under contract AT(11-1)-229.

References

1 L. H. Donnell, "A Discussion of Thin Shell Theory," *Proceedings of the Fifth International Congress for Applied Mechanics*, John Wiley & Sons, New York, N. Y., 1938, pp. 66–70.

2 L. H. Donnell, "Stability of Thin-Walled Tubes Under Torsion," NACA Report No. 479, 1933.

3 M. Hetényi, "Beams on Elastic Foundation," University of Michigan Press, Ann Arbor, Mich., 1946.

4 P. P. Bijlaard, "Stresses From Local Loadings in Cylindrical Pressure Vessels," TRANS. ASME, vol. 77, 1955, pp. 805–816.

5 L. S. D. Morley, "An Improvement on Donnell's Approximation," *Quarterly Journal of Mechanics and Applied Mathematics*, vol. 12, part 1, 1959, pp. 89–99.

6 N. J. Hoff, "Boundary Value Problems of the Thin-Walled Circular Cylinder," JOURNAL OF APPLIED MECHANICS, vol. 21, TRANS. ASME, vol. 76, 1954, pp. 343–350.

7 L. Ting and S. W. Yuan, "On Radial Deflection of a Cylinder of Finite Length With Various End Conditions," *Journal of the Aeronautical Sciences*, vol. 25, 1958, pp. 230–234.

8 S. W. Yuan and L. Ting, "On Radial Deflection of a Cylinder Subjected to Equal and Opposite Concentrated Radial Loads," JOURNAL OF APPLIED MECHANICS, vol. 24, TRANS. ASME, vol. 79, 1957, pp. 278–282.

9 S. P. Timoshenko and S. Woinowsky-Krieger, "Theory of Plates and Shells," second edition, McGraw-Hill Book Company, Inc., New York, N. Y., 1959.

10 W. Flugge, "Stresses in Shells," Springer-Verlag, Berlin, Germany, 1960, chapter 5.

11 J. Kempner, "Derivation of Generalized Donnell-Type Equations for Circular Cylindrical Shells With Application to Shells With Line Loads Along Generatrices," Knolls Atomic Power Laboratory, Report No. 926, 1953.

12 E. G. Phillips, "Functions of a Complex Variable," seventh edition, Oliver and Boyd, London, England, 1951, chapter 5.

13 L. S. D. Morley, "The Thin-Walled Circular Cylinder Subjected to Concentrated Radial Loads," *Quarterly Journal of Mechanics and Applied Mathematics*, vol. 13, part 1, 1960, pp. 24–37.

14 E. Reissner, "On Some Problems in Shell Theory," *Proceedings of the First Symposium on Naval Structural Mechanics*, Pergamon Press, London and New York, 1960, pp. 74–114.

The Stresses in an Elastoplastic Bar Subjected to a Sudden Change of Surface Temperature[1]

E. W. PARKES[2]
Professor,
University of Leicester,
Department of Engineering,
Leicester, England

An analysis is given for the stress history in an elastoplastic bar subjected to a sudden change of surface temperature. The type of behavior is found to depend on the ratio of thermal strain (αV) to yield strain (σ_y/E). For $E\alpha V/\sigma_y < 1$, the stresses are entirely elastic. For $1 < E\alpha V/\sigma_y < 2.04$ there are two transient zones of compressive yielding. For $2.04 < E\alpha V/\sigma_y < 4.4$ there are two transient zones of compressive yielding and two enduring zones of tensile yielding. For $E\alpha V/\sigma_y > 4.4$ there are two transient zones of compressive yielding, one transient zone of tensile yielding, and two enduring zones of tensile yielding. The investigation is restricted to the range $0 \leqslant E\alpha V/\sigma_y \leqslant 5$ and the particular case $E\alpha V/\sigma_y \to \infty$. Detailed solutions are given for $E\alpha V/\sigma_y = 1, 2, 3, 4, 5$, and ∞.

In previous papers [1, 2][3] the author has considered the elastic behavior of solid and cellular structures subjected to changes of environmental temperature, and the alleviation of the thermal effects which may occur because of the use of insulation or suitable choice of materials. He has also considered the behavior of a cellular structure when the stresses are allowed to exceed the elastic limit [3, 4]. The present paper represents the first stage of a similar investigation for a solid structure.

The problem considered is that of a long elastoplastic bar initially in equilibrium at datum temperature. Two opposite faces of the bar are suddenly raised to temperature V and subsequently maintained there, all other faces of the bar being insulated. The stress history of the bar is determined for various values of the ratio $E\alpha V/\sigma_y$, where E is Young's modulus, α is the coefficient of expansion, and σ_y is the yield stress, all supposedly independent of temperature.

The problem is complementary to two which have been solved by J. H. Weiner. In [5] Weiner solved the problem of a plate subjected to a slowly varying heat-input flux on one face. The analysis is inapplicable to our present problem where the initial variation of heat-input flux is infinite. In [6], Landau and Weiner solved our present problem with a heat-transfer coefficient h on the surfaces. They obtained solutions for $E\alpha V/\sigma_y = 5$ with $hL/K = 3$, 5, and 10, and also for $E\alpha V/\sigma_y = 4$, 5, and 6.7 with $hL/K = 2$, where $2L$ is the thickness of the slab and K is the conductivity. Certain approximations were made to speed the later stages of the calculations and the authors state that these approximations would not be valid for high heating rates (such as we have).[4]

The paper is divided into two main parts—the theoretical analysis and the numerical results for $E\alpha V/\sigma_y = 1, 2, 3, 4, 5$, and ∞. The analysis and results for $E\alpha V/\sigma_y = 1, 2, 3, 4$, and ∞ were obtained by the author. M. J.-P. Lacaze extended the analysis to cover the new type of behavior which occurs beyond $E\alpha V/\sigma_y = 4.4$, and calculated the results for $E\alpha V/\sigma_y = 5$.

Analysis

Consider a long bar of unit thickness and width $2L$, as shown in Fig. 1. The material of the bar will be assumed to be elastoplastic, having Young's modulus E and yield stress in tension and compression σ_y. The coefficient of linear expansion of the bar will be denoted by α and its diffusivity by κ. E, σ_y, α, and κ are assumed to be independent of temperature.

[1] The work here presented was supported in whole by the United States Air Force under Contract No. AF49(638)-223 monitored by the Air Force Office of Scientific Research of the Air Research and Development Command. Reproduction in whole or in part is permitted for any purpose of the United States Government.

[2] Presently, Visiting Professor, Department of Aeronautical Engineering, Stanford University, Stanford, Calif.

[3] Numbers in brackets designate References at end of paper.

Presented at the Summer Conference of the Applied Mechanics Division, Chicago, Ill., June 14–16, 1961, of The American Society of Mechanical Engineers.

Discussion of this paper should be addressed to the Editorial Department, ASME, United Engineering Center, 345 East 47th Street, New York 17, N. Y., and will be accepted until October 10, 1961. Discussion received after the closing date will be returned. Manuscript received by ASME Applied Mechanics Division, August 31, 1960. Paper No. 61—APM-16.

[4] The results for $\kappa t/L^2 = \infty$ from our Fig. 11 can be directly superimposed on Fig. 3 of [6]. If this is done it will be seen that our results and those of Landau and Weiner form a regular series. A similar consistency is found between our Fig. 12 (for $E\alpha V/\sigma_y = 5$) and their Fig. 1.

Nomenclature

b = value of x at inner edge of compressive yield zone
c = value of x at outer edge of compressive yield zone
d = value of x at inner edge of tensile yield zone
E = Young's modulus
h = heat-transfer coefficient
K = thermal conductivity
L = half thickness of bar
n = integer taking all values from 0 to ∞
R = radius of curvature of half bar
t = time
v = temperature
V = temperature at $x = \pm L$
x = co-ordinate measured from center of bar
α = coefficient of linear expansion
ϵ = longitudinal strain
ϵ_r = residual strain
σ = longitudinal stress
σ_y = yield stress
κ = thermal diffusivity

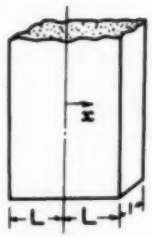

Fig. 1 Long bar

The bar is supposed to be initially unstressed at datum temperature when at time $t = 0$ the faces $x = \pm L$ are subjected to a temperature rise V, subsequently maintained constant. Then if we assume that all other faces of the bar are insulated, so that the heat flow is one-dimensional, and that we may ignore the stress contribution to the heat-conduction equation, the temperature v at x at time t is given [7] by

$$\frac{v}{V} = 1 - \frac{4}{\pi} \sum_{0}^{\infty} \frac{(-1)^n}{2n+1} e^{-\frac{(2n+1)^2\pi^2}{4} \frac{\kappa t}{L^2}} \cdot \cos \frac{(2n+1)\pi x}{2L} \quad (1)$$

Because of the temperature rise in the bar, it expands and there is thus a longitudinal strain ϵ. Since the bar is long, plane sections will remain plane and ϵ will be independent of x. Provided the material remains elastic, the longitudinal stress at x will be given by

$$\sigma = E(\epsilon - \alpha v) \quad (2)$$

and all other stresses will be zero. The condition for equation (2) to apply for all x and t may be obtained by considering the outer fibers of the bar when V is applied. For an unloaded bar, $\epsilon = 0$ when $t = 0$ and so the initial stress in the outer fibers is $-E\alpha V$. This stress must not exceed the compressive yield stress $-\sigma_y$, so we have as our condition that

$$\frac{E\alpha V}{\sigma_y} \leqslant 1 \quad (3)$$

For $t > 0$, ϵ is positive and $0 < v < V$ so that equation (3) still insures that the stresses given by equation (2) are everywhere elastic.

If equation (3) does not hold, the outer fibers of the bar yield in compression at $t = 0$. For $t > 0$, the stress in the outer fibers is again elastic, since they are at constant temperature V and ϵ is increasing; a short distance inside the bar, the fibers are yielding in compression because v is increasing rapidly and ϵ only slowly. Conditions now are shown in Fig. 2. From $x = b$ to $x = c$, the bar is yielding in compression. Between $x = 0$ and b, the bar is elastic. Between $x = c$ and L, the bar is behaving elastically, having previously yielded in compression. The stresses in the three zones are as follows:

$$\left.\begin{array}{ll} 0 < x < b & \sigma = E(\epsilon - \alpha v) \\ b < x < c & \sigma = -\sigma_y \\ c < x < L & \sigma = -\sigma_y + E(\epsilon - \alpha v) - E(\epsilon - \alpha v)_c \end{array}\right\} \quad (4)$$

where the subscript c denotes the value when the fiber concerned was fiber c.

The points b and c are defined by the conditions

$$E(\epsilon - \alpha v_b) = -\sigma_y \quad (5)$$

and

$$\frac{\partial}{\partial t}(\epsilon - \alpha v_c) = 0 \quad (6)$$

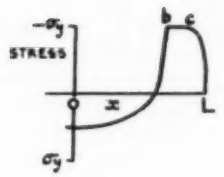

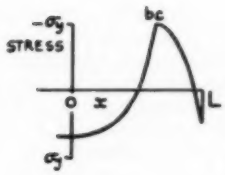

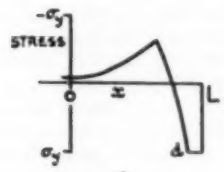

Figs. 2, 3, 4 Stress distributions

where v_c in equation (6) means the temperature of that fixed point which is instantaneously the point c.

For an unloaded bar, we have in addition the equilibrium condition

$$\int_0^b E(\epsilon - \alpha v)dx + \int_c^L E(\epsilon - \alpha v)dx - \int_c^L E(\epsilon - \alpha v)_c dx - \sigma_y(L - b) = 0 \quad (7)$$

If we differentiate equation (7) with respect to time we get

$$\int_0^b \frac{\partial}{\partial t} E(\epsilon - \alpha v)dx + \int_c^L \frac{\partial}{\partial t} E(\epsilon - \alpha v)dx = 0 \quad (8)$$

Equations (5), (6), and (8) are best expressed nondimensionally as

$$\frac{v_b}{V} = \frac{\epsilon}{\alpha V} + \frac{\sigma_y}{E\alpha V} \quad (9)$$

$$\frac{\partial(v_c/V)}{\partial(\kappa t/L^2)} = \frac{\partial(\epsilon/\alpha V)}{\partial(\kappa t/L^2)} \quad (10)$$

$$\frac{\partial(\epsilon/\alpha V)}{\partial(\kappa t/L^2)} \left\{1 + \frac{b}{L} - \frac{c}{L}\right\} = \int_0^{b/L} \frac{\partial(v/V)}{\partial(\kappa t/L^2)} d(x/L) + \int_{c/L}^1 \frac{\partial(v/V)}{\partial(\kappa t/L^2)} d(x/L) \quad (11)$$

where v/V is a known function of x/L and $\kappa t/L^2$ from equation (1).

These equations can be solved numerically as follows. At a given value of $\kappa t/L^2$, $\epsilon/\alpha V$ is supposed known. From equation (9), b/L can be found. Equations (10) and (11) can then be solved simultaneously to find c/L and $\partial(\epsilon/\alpha V)/\partial(\kappa t/L^2)$. The last quantity can be used to predict $\epsilon/\alpha V$ at a later value of $\kappa t/L^2$. The initial conditions are $b/L = c/L = 1$ and $\epsilon/\alpha V = 0$ at $\kappa t/L^2 = 0$, and it is necessary to guess a value for $\epsilon/\alpha V$ for the first interval, and then improve the guess from the calculated value of $\partial(\epsilon/\alpha V)/\partial(\kappa t/L^2)$.

To perform the calculation, tables of v/V and the following functions are needed:

$$\frac{\partial(v/V)}{\partial(\kappa t/L^2)} = \pi \sum_0^\infty (-1)^n(2n+1)e^{-\frac{(2n+1)^2\pi^2}{4}\cdot\frac{\kappa t}{L^2}}\cos\frac{(2n+1)\pi x}{2L} \tag{12}$$

$$\int_0^{x/L} \frac{\partial(v/V)}{\partial(\kappa t/L^2)}\,d\left(\frac{x}{L}\right) = 2\sum_0^\infty (-1)^n e^{-\frac{(2n+1)^2\pi^2}{4}\cdot\frac{\kappa t}{L^2}}\sin\frac{(2n+1)\pi x}{2L} \tag{13}$$

These were computed on EDSAC in Cambridge for $x/L = 0(0.02)1$ and $\kappa t/L^2 = 0$ (various intervals)2.

As t increases, b and c decrease until a time is reached at which either the center of the bar yields in tension (a condition we shall for the present ignore) or c coincides with b, Fig. 3. After the coincidence of b and c, the compressive stresses become elastic, and all the stresses may remain elastic thereafter. The stresses can be determined from equations (4) and (8) if we remember that $b = c$, a known fixed position.

If $E\alpha V/\sigma_y$ is sufficiently large, however, the stresses do not remain elastic after b and c coincide. The outer fiber stress may become sufficiently large for tensile yield to occur at $x = L$. A tensile yield zone then spreads into the bar, Fig. 4. The condition for this to occur can be found as follows: The maximum tensile stress at $x = L$ occurs for $t \to \infty$ and is given by $E\epsilon_{(t\to\infty)} - \sigma_y$. The strain $\epsilon_{(t\to\infty)}$ can conveniently be written as $\alpha V + \epsilon_r$, where ϵ_r is the amount by which the strain is more than that which would occur at the end of a purely elastic thermal expansion (ϵ_r in fact is negative). If tensile yield is to occur we have

$$E\epsilon_{(t\to\infty)} - \sigma_y = E\alpha V + E\epsilon_r - \sigma_y = \sigma_y$$

or

$$\frac{E\epsilon_r}{\sigma_y} = 2 - \frac{E\alpha V}{\sigma_y} \tag{14}$$

Fig. 13 shows $E\epsilon_r/\sigma y$ plotted against $E\alpha V/\sigma_y$, together with the line of equation (14). It will be seen that they intersect where $E\alpha V/\sigma_y = 2.04$. The condition for tensile yield in the outer fibers is thus

$$\frac{E\alpha V}{\sigma_y} > 2.04 \tag{15}$$

If we denote the inner edge of the tensile yield zone by $x = d$, then the time differential of the equilibrium condition can be shown to be

$$\int_0^d \frac{\partial}{\partial t}\,E(\epsilon - \alpha v)dx = 0 \tag{16}$$

The condition at d is

$$E(\epsilon - \alpha v_d) - E(\epsilon - \alpha v_d)_e = 2\sigma_y \tag{17}$$

Equations (16) and (17) are sufficient for the determination of the stresses during the period of tensile yielding, which continues until $t \to \infty$.

The regime described in the foregoing will obtain unless $E\alpha V/\sigma_y$ is sufficiently large that tensile yielding occurs first at the center of the bar. Fig. 5 shows the stress at the center of the bar as a fraction of the yield stress, plotted against $E\alpha V/\sigma_y$. It will be seen that tensile yield occurs at the center provided

$$\frac{E\alpha V}{\sigma_y} > 4.4 \tag{18}$$

For values of $E\alpha V/\sigma_y$ in excess of 4 it is unlikely that our analysis

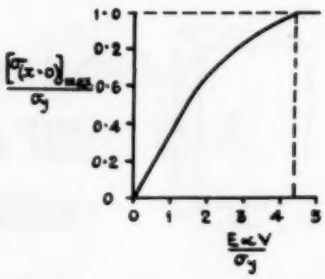

Fig. 5 Maximum stress at center of bar

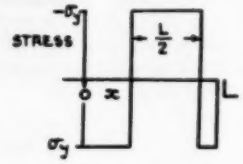

Fig. 6 Stress distribution for $E\alpha V/\sigma_y \to \infty$

will have practical application, since the conditions on which it depends (constancy of E, σ_y, α, and κ) will not be satisfied with sufficient accuracy. Nevertheless, since there is a new regime of behavior for $E\alpha V/\sigma_y > 4.4$, M. J.-P. Lacaze has, at the author's suggestion, investigated the case $E\alpha V/\sigma_y = 5$. He finds that a small tensile yield zone forms at the center of the bar and then disappears again before b and c coincide; tensile yielding of the outer fibers of the bar occurs after the coincidence of b and c (Fig. 11).

The solution for $E\alpha V/\sigma_y \to \infty$ may readily be determined, since the elastic zones become infinitesimally small. At $x = L$, for $t > 0$ there is tensile yielding. The tensile yield zone extends into the bar so long as $\partial\epsilon/\partial t > \partial\alpha v/\partial t$. For values of x less than that at which $\partial\epsilon/\partial t = \partial\alpha v/\partial t$ there will be compressive yielding so long as $\partial\epsilon/\partial t < \partial\alpha v/\partial t$. Inside the section at which $\partial\epsilon/\partial t$ is again equal to $\partial\alpha v/\partial t$ there will be a further zone of tensile yield. This situation is shown in Fig. 6. For longitudinal equilibrium, the compressive yield zone must be $0.5L$ long. We thus have to determine, using the table of equation (12), the solution of

$$\left(\frac{\partial v}{\partial t}\right)_x = \left(\frac{\partial v}{\partial t}\right)_{x+0.5L} \tag{19}$$

The results are shown in Fig. 12. It will be seen that for $\kappa t/L^2 > 0.145$, no solution of equation (19) is possible and we have two zones only, with $\partial\epsilon/\partial t = \partial\alpha v/\partial t$ at $x = 0.5L$.

The foregoing analysis has been developed for an unloaded bar. However, it may be used unchanged for a loaded bar, provided an appropriate initial value of ϵ is inserted. The analysis refers only to a step-function temperature change on the surface and it is not possible to use Duhamel's theorem [8] to derive the results for other temperature variations, since the elastoplastic equations are nonlinear.

With slight modification in the meaning of symbols, the results are also applicable to an elastoplastic plate.

Results

The stress distributions at various times, computed according to the foregoing analysis are shown for $E\alpha V/\sigma_y = 1, 2, 3, 4$, and 5 in Figs. 7 to 11. It will be seen that for $E\alpha V/\sigma_y = 1$ the stresses are elastic at all times. For $E\alpha V/\sigma_y = 2$, a compressive yield zone moves in from the outer edge until $\kappa t/L^2 = 0.051$, when it

disappears at $b/L = c/L = 0.895$. The stresses are subsequently elastic.

For $E\alpha V/\sigma_y = 3$, the compressive yield zone moves in from the outer edge until $\kappa t/L^2 = 0.093$ when it disappears at $b/L = c/L = 0.790$. It is followed by a tensile zone starting from the outer edge at $\kappa t/L^2 = 0.430$ and spreading to $d/L = 0.948$ as $t \to \infty$.

For $E\alpha V/\sigma_y = 4$, the compressive yield zone moves in from the outer edge until $\kappa t/L^2 = 0.123$ when it disappears at $b/L = c/L = 0.718$. It is followed by a tensile zone starting at $\kappa t/L^2 = 0.260$ and eventually extending to $d/L = 0.903$.

For $E\alpha V/\sigma_y = 5$, the compressive yield zone moves in from the outer edge until $\kappa t/L^2 = 0.145$ when it disappears at $b/L = c/L = 0.664$. During this period a tensile yield zone forms at the center of the bar at $\kappa t/L^2 = 0.076$, extends to $x/L = 0.140$ at $\kappa t/L^2 = 0.102$, and then disappears by $\kappa t/L^2 = 0.108$. A tensile zone starts at the edge at $\kappa t/L^2 = 0.190$ and extends to $d/L = 0.842$ as $t \to \infty$.

The formation and disappearance of the yield zones is shown in a separate diagram in Fig. 12. This diagram also gives the results of the calculations for $E\alpha V/\sigma_y \to \infty$.

An important effect of the thermal shock applied to the bar is the permanent dimensional change which it produces. If we suppose that after thermal equilibrium at V has been reached, the bar is slowly cooled to its original datum temperature, so that the stress distribution remains unchanged, then the length of the bar will have changed from its original value. If we denote the change in strain by ϵ_r, then

$$\epsilon_r = \epsilon_{(t\to\infty)} - \alpha V \tag{20}$$

$E\epsilon_r/\sigma_y$ is plotted against $E\alpha V/\sigma_y$ in Fig. 13.

A measure of the variation of stress across the section is the radius of curvature, R, which each half of the bar would take up if it were split along the line $x = 0$. $EL/\sigma_y R$ is plotted against

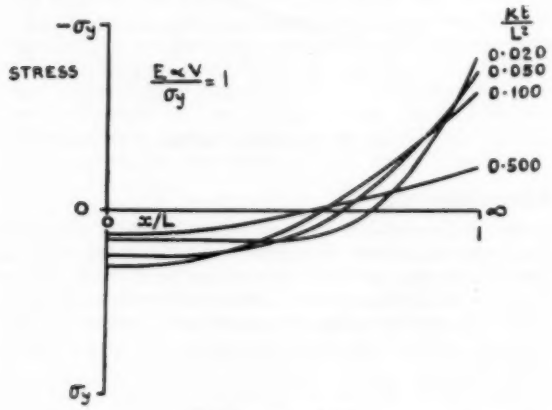

Fig. 7 Stress history

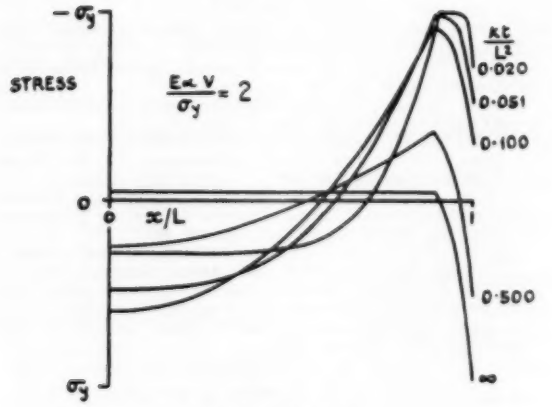

Fig. 8 Stress history

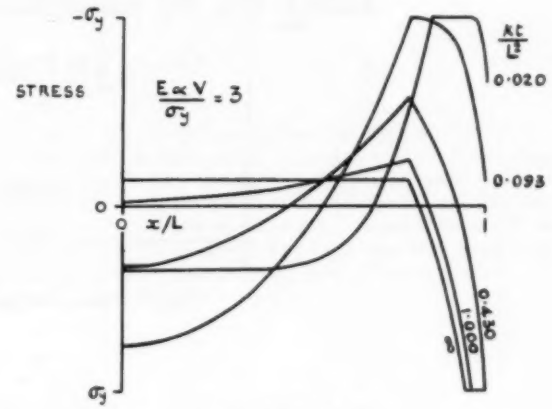

Fig. 9 Stress history

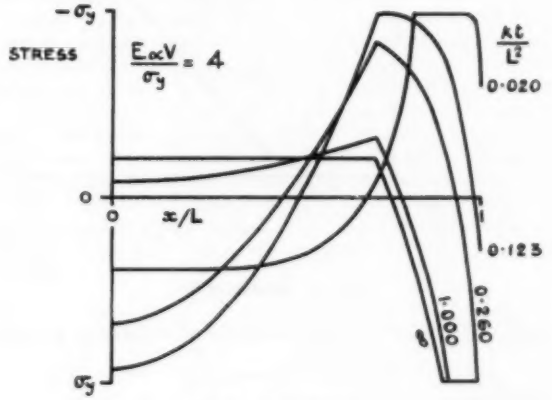

Fig. 10 Stress history

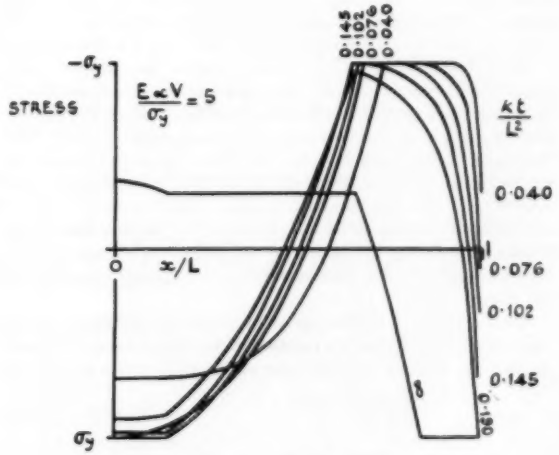

Fig. 11 Stress history

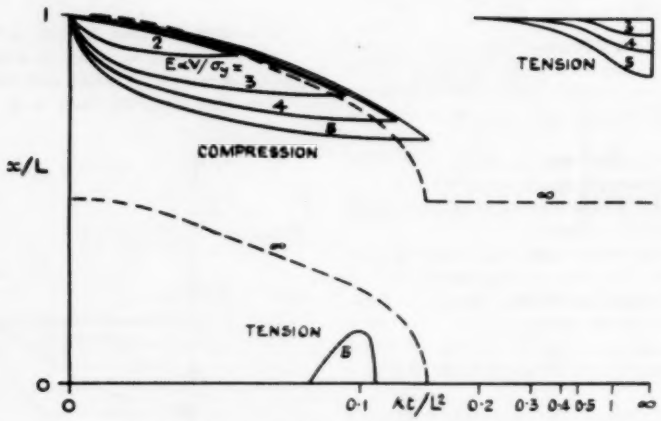

Fig. 12 Growth and disappearance of yield zones

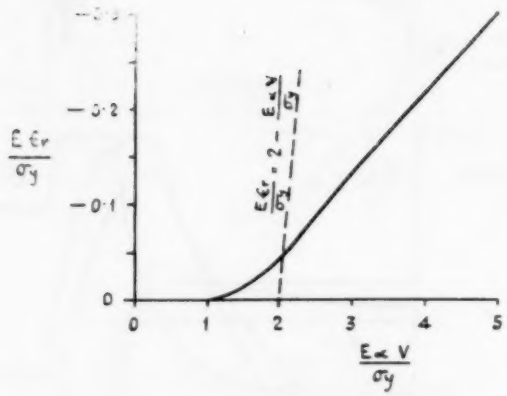

Fig. 13 Residual strain

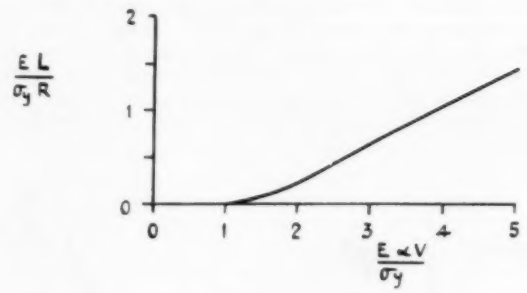

Fig. 14 Curvature of half bar

$E\alpha V/\sigma_y$ in Fig. 14: for very large values of $E\alpha V/\sigma_y$, $EL/\sigma_y k \to 3$.

Conclusions

An analysis has been given for the stress-time history in an elastoplastic bar subjected to a sudden change of surface temperature. Detailed results have been calculated for $E\alpha V/\sigma_y = 1$, 2, 3, 4, 5, and ∞. It is found that, for $E\alpha V/\sigma_y < 1$, the behavior is always elastic. For $1 < E\alpha V/\sigma_y < 2.04$, two zones of compressive yield move into the bar from the faces and eventually disappear, the subsequent behavior being elastic. For $2.04 < E\alpha V/\sigma_y < 4.4$, the compressive yield zones again move in from the edges and disappear; there is then a period of elastic behavior followed by the formation of two tensile yield zones which extend into the bar from the edges. For $E\alpha V/\sigma_y > 4.4$, a tensile yield zone forms at the center of the bar and then disappears again during the period of compressive yielding; there is then a period of elastic behavior followed by tensile yielding from the edges.

For $E\alpha V/\sigma_y > 1$, the bar is permanently deformed by the thermal shock. There is a residual strain which varies from zero at $E\alpha V/\sigma_y = 1$ to -30 per cent of the yield strain at $E\alpha V/\sigma_y = 5$.

Acknowledgments

The author would like to thank Miss G. Christ of Cambridge University Engineering Laboratory, who programmed the expressions of equations (1), (12), and (13) for EDSAC and who computed the necessary tables. He would also like to thank M. J.-P. Lacaze for extending the analysis and computation to the case $E\alpha V/\sigma_y = 5$ and for checking some of the earlier calculations.

References

1 E. W. Parkes, "The Alleviation of Thermal Stresses," *Aircraft Engineering*, vol. 25, 1953, pp. 51–53.

2 E. W. Parkes, "Transient Thermal Stresses in Wings," *Aircraft Engineering*, vol. 25, 1953, pp. 373–378.

3 E. W. Parkes, "Wings Under Repeated Thermal Stress," *Aircraft Engineering*, vol. 26, 1954, pp. 402–406.

4 E. W. Parkes, "Incremental Collapse Due to Thermal Stress," *Aircraft Engineering*, vol. 28, 1956, pp. 395–396.

5 J. H. Weiner, "An Elastoplastic Thermal-Stress Analysis of a Free Plate," JOURNAL OF APPLIED MECHANICS, vol. 23, TRANS. ASME, vol 78, 1956, pp. 395–402.

6 H. G. Landau and J. H. Weiner, "Transient and Residual Stresses in Heat-Treated Plates," JOURNAL OF APPLIED MECHANICS, vol. 25, TRANS. ASME, vol. 80, 1958, pp. 459–465.

7 H. S. Carslaw and J. C. Jaeger, "Conduction of Heat in Solids," second edition, Oxford University Press, Oxford, England, 1959.

8 J. M. C. Duhamel, "Mémoire sur la méthode générale relative au mouvement de la chaleur dans les corps solides plongés dans les milieux dont la température varie avec le temps," *Journal de l'Ecole Polytechnique*, Paris, France, 1833.

J. PARKER

J. KETTLEWELL

Lecturers in Mechanical Engineering, College of Science and Technology, University of Manchester, Manchester, England

Plastic Stress-Strain Relationships—Further Experiments on the Effect of Loading History

Further tests have been carried out on thin closed-ended tubes of alpha brass subjected to various combinations of torque and internal pressure. The effect of loading, unloading, and reloading along different paths has been investigated. The loading paths were based on a yield function which has previously been found to correlate initial radial loadings for this material, which possesses one degree of anisotropy. However, the results obtained from the second loadings suggest a cross effect which is greater than would be obtained from a nested set of yield surfaces of the foregoing form. There appears to be no evidence to support the presence of a corner in the yield surface.

EXPERIMENTS previously carried out on thin closed-ended tubes of alpha brass subjected to combinations of torque and internal pressure have already been reported [1].[1] Eleven specimens were previously tested and the loading paths which were followed were based on the assumption that the material would follow the von Mises-Hencky yield criterion $f = 2\bar{\sigma}^2$. However, the test specimens were found to be isotropic in the plane of the surface of the tube but anisotropic in a radial direction. A form of yield criterion $f = 2\sigma_R{}^2$ which possesses this one degree of anisotropy was deduced which enabled reasonable correlation of the initial loading paths on the basis of representative stress σ_R and corresponding representative plastic strain $\epsilon_R{}^p$.

The loading paths for the previous experiments [1] were based on the von Mises-Hencky yield criterion; i.e., the specimens were initially loaded in tension, torsion, or internal pressure to the same value of $\bar{\sigma}$, unloaded, then loaded in tension to the same value of $\bar{\sigma}$ followed by loading in either tension, torsion, or internal pressure. However, since the initial loadings showed that the material followed a yield criterion of the form $f = 2\sigma_R{}^2$, these latter loadings started from either inside or outside the loading surface rather than from a point lying in this surface as intended. A series of experiments similar to those reported in [1] but based on the yield criterion $f = 2\sigma_R{}^2$ are now described herein. Fig. 1 shows the test specimen which is of the same size as in the previous experiments [1] and produced in the same manner [2]. The specimens were machined from the same batch of material, the analysis being Cu 69.42, Zn 30.56, Fe 0.02 per cent, and a final heat-treatment was carried out as in [1]. The same test rig for applying the torque and internal pressure was used. The techniques used for the measurement of shear, longitudinal, and circumferential strains were also the same and have been described briefly [3]. All strain measurements are sensitive to 1×10^{-6}.

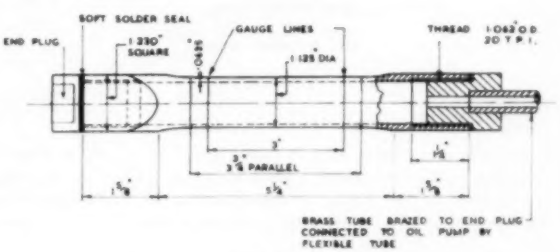

Fig. 1 Test specimen

[1] Numbers in brackets designate References at end of paper.

Presented at the Summer Conference of the Applied Mechanics Division, Chicago, Ill., June 14–16, 1961, of THE AMERICAN SOCIETY OF MECHANICAL ENGINEERS.

Discussion of this paper should be addressed to the Editorial Department, ASME, United Engineering Center, 345 East 47th Street, New York 17, N. Y., and will be accepted until October 10, 1961. Discussion received after the closing date will be returned. Manuscript received by ASME Applied Mechanics Division, July 20, 1960. Paper No. 61—APM-24.

Nomenclature

σ_z = longitudinal stress
σ_t = circumferential stress
τ = shear stress
ϵ_z = longitudinal strain
ϵ_t = circumferential strain
γ = shear strain
p = internal pressure
T = torque
d_i = internal diameter of specimen
d_m = mean diameter of specimen
t = wall thickness of specimen
σ_R = representative stress, given by [1]

$$2\sigma_R{}^2 = 2\sigma_t{}^2 + 2\sigma_z{}^2 - 1.552\sigma_z\sigma_t + 5.55\tau^2$$

f = yield criterion = $2\sigma_R{}^2$
$\bar{\sigma}$ = representative stress (von Mises-Hencky)
$\epsilon_R{}^p$ = representative plastic strain, given by [1]

$$d\epsilon_R{}^p = 0.767[2(d\epsilon_t{}^p)^2 + 2(d\epsilon_z{}^p)^2 + 1.552d\epsilon_t{}^p d\epsilon_z{}^p + 0.612(d\gamma^p)^2]^{1/2},$$

assuming no permanent volume change to obtain the increment of radial plastic strain from the measured values of $d\epsilon_t{}^p$ and $d\epsilon_z{}^p$. Superscript p denotes plastic part of strain component.

$$\tau = \frac{2T}{\pi d_m{}^2 t} = 9.022T$$

$$\sigma_t = \frac{pd_i}{2t} = 8p$$

$$\sigma_z = \frac{pd_i{}^2}{4d_m t} = 3.765p$$

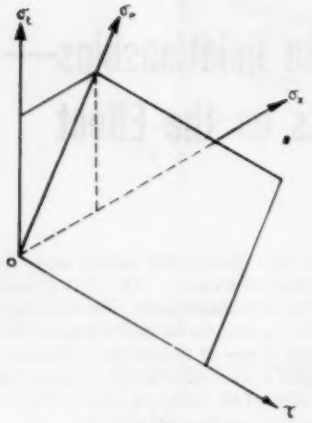

Fig. 2 Stress space

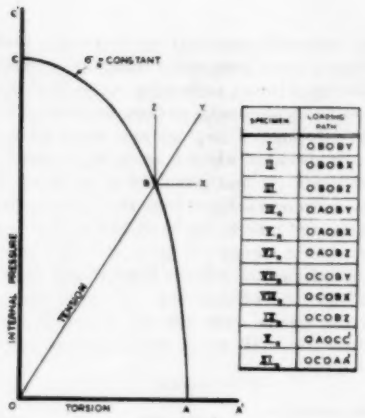

Fig. 3 Loading paths

Loading Paths

Let the co-ordinate axes in stress space be σ_t, σ_x, τ, Fig. 2. Loading in internal pressure gives $\sigma_t/\sigma_x = 2.124$; i.e., line $0\sigma_p$ which lies in plane $\sigma_t 0\sigma_x$. Hence all states of stress caused by torsion and internal pressure give points in the plane $\sigma_p 0\tau$ where

$$\sigma_p = (\sigma_t^2 + \sigma_x^2)^{1/2} = 2.348\sigma_x = 8.841p$$

A pure tensile stress in the plane of the surface of the tube at an angle of $55\frac{1}{2}$ deg to the tube axis is produced when the loading gives $\sigma_p/\tau = 1.61$ [1]. In what follows this is referred to as tension loading and is shown by the tension line in Fig. 3.

The loading paths of the eleven specimens are tabulated in Fig. 3. The curve ABC is the intersection by the $\sigma_p 0\tau$ plane of the yield surface $f = 2\sigma_R^2$; i.e.,

$$2\sigma_R^2 = 1.4\sigma_p^2 + 5.55\tau^2$$

The ellipse ABC in Fig. 3 is plotted for $\sigma_R = 13{,}000$ psi where point B on this ellipse is the same as point B in Fig. 3 in the previous paper [1]; i.e., the ellipses $\sigma_R = 13{,}000$ psi and $\bar{\sigma} = 13{,}000$ psi both pass through this point. Hence the loading paths for specimens I, II, III are the same as those for the same specimens in [1]. In fact it was not necessary to repeat these loadings and the results quoted herein for these specimens (I, II, III) are those obtained previously [1].

Test Procedure

In loading, the same procedure as in [1] was adopted to eliminate the effect of creep; i.e., after the application of an increment of load, creep was allowed to take place until the readings of the strain-measuring instruments were constant within the sensitivity of each instrument. The readings were then taken. Also, during pressure increments, the test specimen was rocked slightly to eliminate endwise friction on the torque-arm bearing.

Experimental Results

Figs. 4–9 show the main experimental results for the eleven specimens tested. The plots of $\sigma_R - \epsilon_R^p$ (representative stress and representative plastic strain based on the yield function $f = 2\sigma_R^2$) are shown in Figs. 4–7. The results shown in Fig. 4 for specimens I, II, and III, initially loaded in tension, are those shown in Fig. 8 in [1]. The curves of $\sigma_R - \epsilon_R^p$ for the specimens having the same initial loading again show sufficiently good agreement and consistency of mechanical properties (except at low strains) to justify the comparison of the effects of subsequent loading paths. The discrepancies at the low strains were obtained previously [1] and appear to be a feature of the material. The yield on initial loading is again very "sharp" but on second loading a "rounded" curve is obtained in all cases where the second loading is different from the first. It also should be pointed out that, in all cases during the unloading following the initial loading, small departures from the straight elastic stress-strain lines were recorded on the relevant strain-measuring equipment as the load approached zero; e.g., for specimens I, II, and III initially loaded in tension the values of γ, ϵ_t and ϵ_x obtained on unloading showed reductions greater than the straight-line elastic unloading values as shown in Fig. 10 for specimen I. This rounding of the unloading $\sigma_R - \epsilon_R^p$ line, which is very small, is not shown in Figs. 4–7.

Similarly, on all second loadings the measured strains showed increases greater than the straight-line elastic loading values. This effect commenced in all cases at a value of σ_R appreciably less than the initial loading value of $\sigma_R = 13{,}000$ psi. These are shown in Figs. 4–7 giving a rounded plot of $\sigma_R - \epsilon_R^p$ in all cases where the second loading was different from the initial. In the case of specimens I, II, and III, where the initial and second loadings were the same (tension), smaller values of ϵ_R^p were obtained up to $\sigma_R = 13{,}000$ psi and then an instantaneous yield occurred at this value of σ_R.

Fig. 8 gives the mean curves of $\sigma_R - \epsilon_R^p$ for the three initial loading paths. The correlation is not as good as that reported previously [1], the mean curve for the specimens loaded in torsion being slightly lower than those for tension and internal pressure. Note the agreement between the initial torsion loading for specimen X_R, Fig. 7, and those for specimens IV_R, V_R, VI_R, Fig. 5, and similarly for the initial internal pressure loading of specimen XI_R, Fig. 7, and those for specimens VII_R, $VIII_R$, IX_R, Fig. 6. These curves of $\sigma_R - \epsilon_R^p$ for the initial loadings also provide good agreement with those obtained for the previous specimens, Fig. 11(*b*) [1]. This again confirms the repeatability of the mechanical properties of the test specimens.

Fig. 9 shows the direction of the plastic-strain increment vectors for the loadings of the nine specimens $I–IX_R$ after their initial loading, unloading, and reloading in tension to point B, Fig. 3. The choice of the components of the plastic-strain increment vectors has been explained previously [1]; i.e., the increment of plastic work.

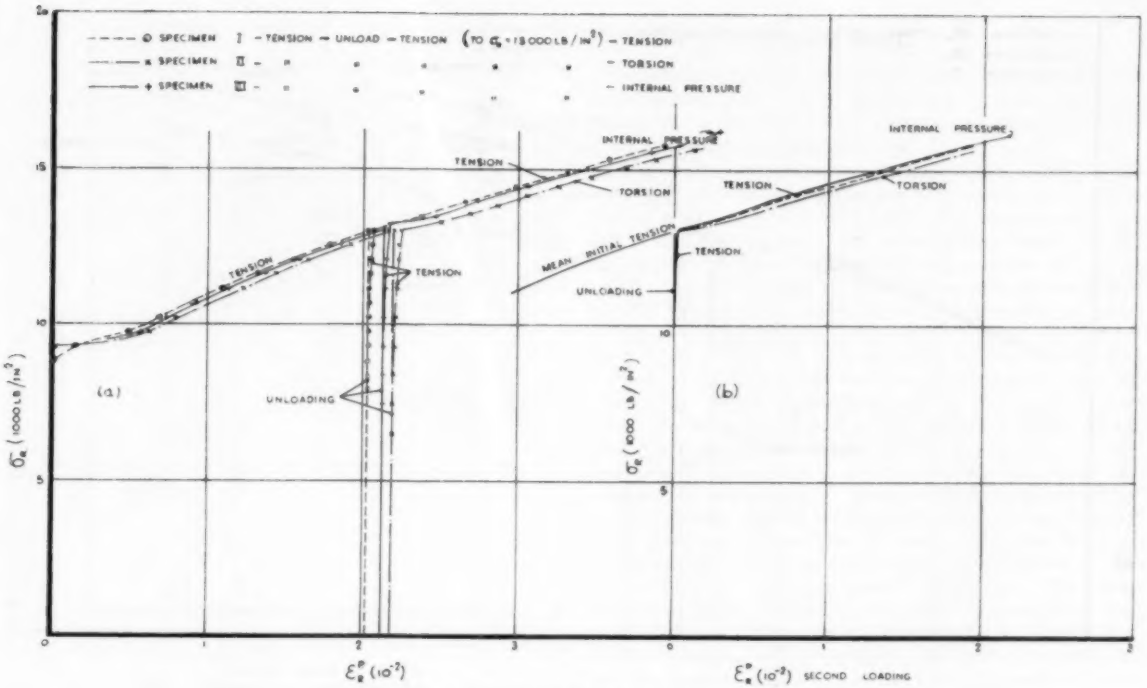
SPECIMEN I – TENSION → UNLOAD → TENSION (TO σ_z = 15 000 LB/IN^2) – TENSION
SPECIMEN II – " " " " " – TORSION
SPECIMEN III – " " " " " – INTERNAL PRESSURE
INTERNAL PRESSURE
TENSION
TORSION
MEAN INITIAL TENSION
UNLOADING
(a)
(b)
σ_z (1000 LB/IN^2)
ε_z^p (10^{-2})
ε_z^p (10^{-2}) SECOND LOADING

Fig 4 Representative stress-strain curves

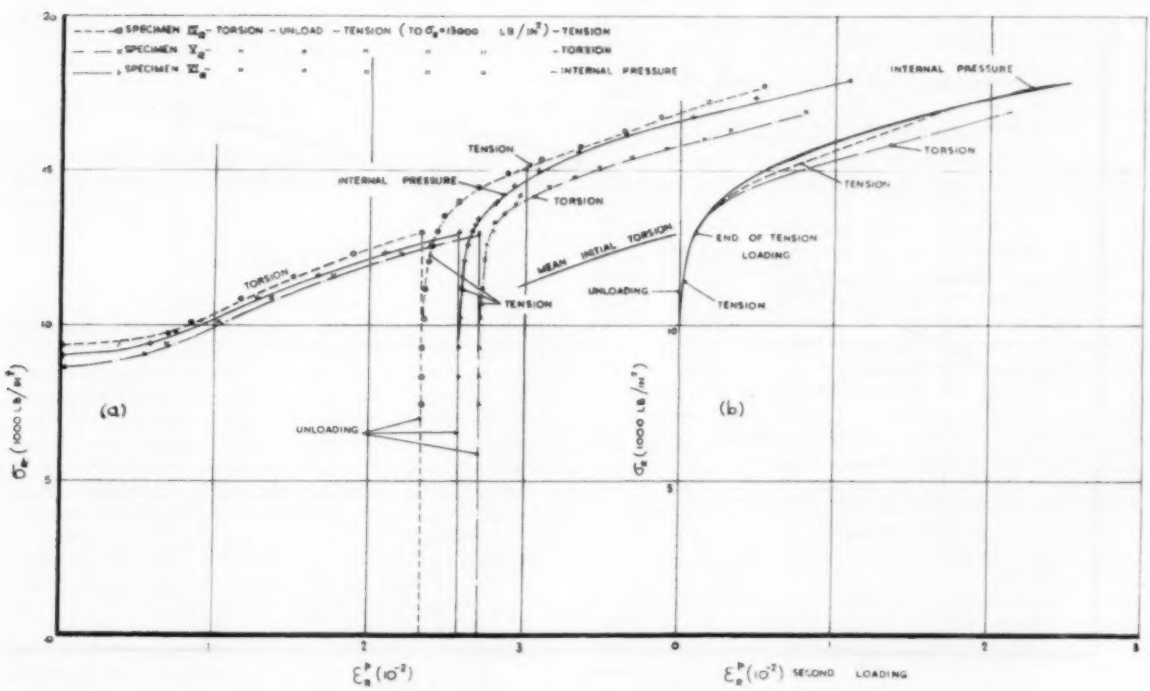
SPECIMEN II – TORSION → UNLOAD → TENSION (TO σ_z = 13000 LB/IN^2) – TENSION
SPECIMEN V – " " " " " – TORSION
SPECIMEN VI – " " " " " – INTERNAL PRESSURE
INTERNAL PRESSURE
TENSION
TORSION
MEAN INITIAL TORSION
END OF TENSION LOADING
UNLOADING
(a)
(b)
σ_z (1000 LB/IN^2)
ε_z^p (10^{-2})
ε_z^p (10^{-2}) SECOND LOADING

Fig. 5 Representative stress-strain curves

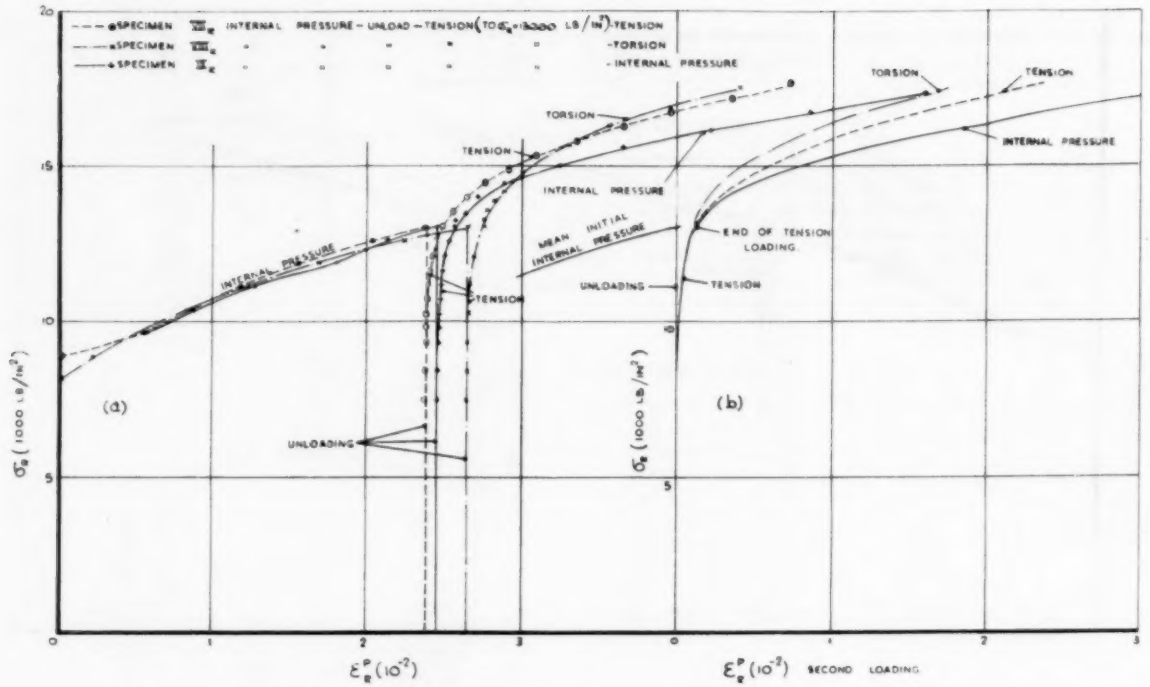

Fig. 6 Representative stress-strain curves

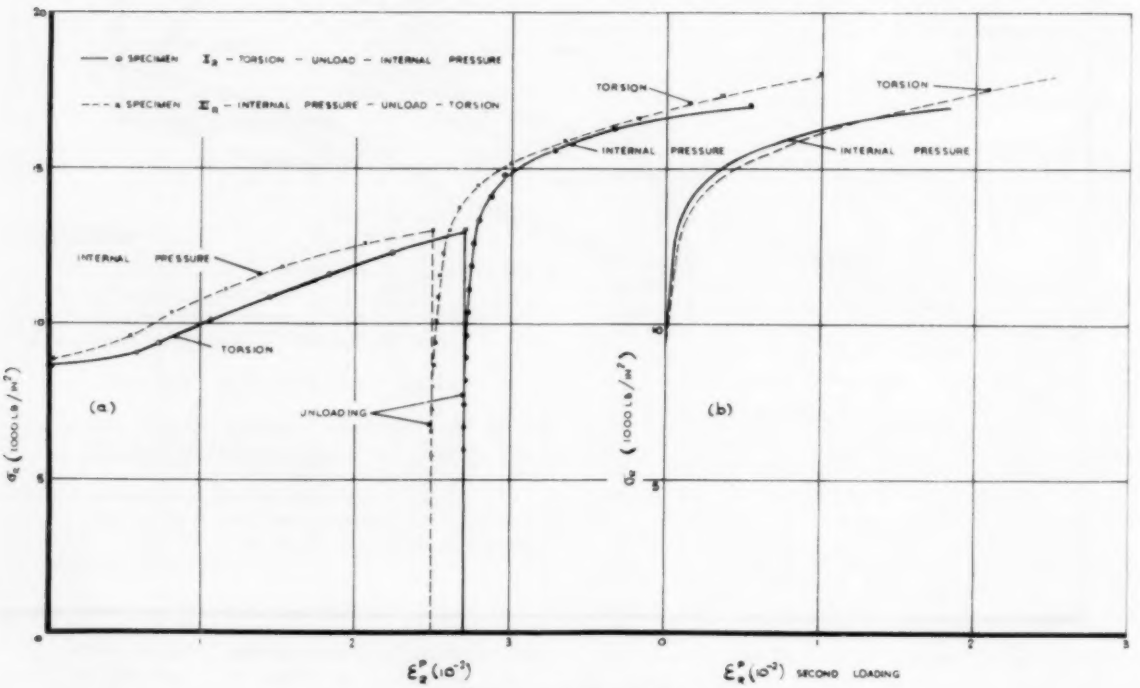

Fig. 7 Representative stress-strain curves

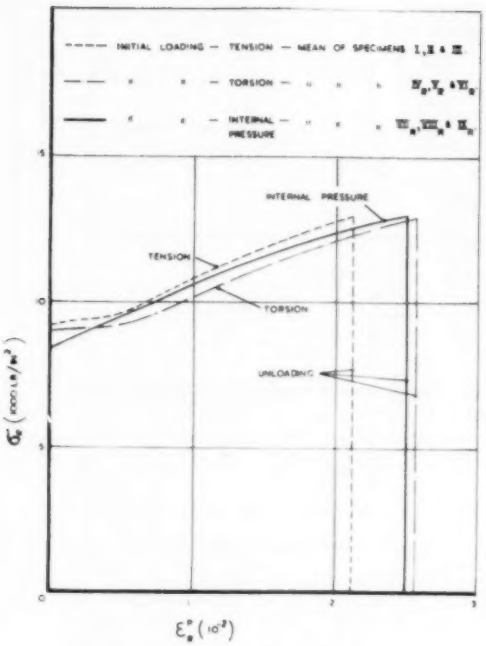

Fig. 8 Comparison of initial loadings

$$dW^p = \tau d\gamma^p + \sigma_z d\epsilon_z^p + \sigma_t d\epsilon_t^p$$

$$= \tau d\gamma^p + \frac{\sigma_p}{2.348}(d\epsilon_z^p + 2.124 d\epsilon_t^p)$$

$$= \tau d\gamma^p + \sigma_p d\epsilon_p^p$$

Hence in the two-dimensional section $\sigma_p 0\tau$ of the stress space the components of the plastic-strain increment vectors are $d\gamma^p$ and $d\epsilon_p^p$ where

$$d\epsilon_p^p = \frac{d\epsilon_z^p + 2.124 d\epsilon_t^p}{2.348}$$

and the direction of the plastic-strain increment vectors is given by $d\epsilon_p^p/d\gamma^p$. This choice of components is such that the vector represents a normal to the yield curve in the $\sigma_p 0\tau$ plane at that point of the loading path for the particular specimen [4].

In Fig. 9 the values of $d\epsilon_p^p/d\gamma^p$ are plotted as a function of σ_R and the points shown are given at the values of σ_R corresponding to the mid-points of the load increments. The small plastic strains obtained during the tension part of the second loading below $\sigma_R = 13{,}000$ psi and shown in Figs. 4, 5, and 6 are indicated by chain dotted lines in Fig. 9. Since these plastic-strain increments are very small the slopes $d\epsilon_p^p/d\gamma^p$ are very sensitive to small errors in either $d\epsilon_p^p$ or $d\gamma^p$, and the chain dotted line gives the mean value of $d\epsilon_p^p/d\gamma^p$ over this loading range.

The mean values of the slopes of the plastic-strain increment vectors for the initial tension loading of specimens I, II, and III are also shown in Fig. 9(*a*).

The full lines shown in Fig. 9 give the values of the slopes of the normals to the yield surface σ_R corresponding to the second loading paths of the nine specimens; i.e., the slopes of the normals to $2\sigma_R^2 = 1.4\sigma_p^2 + 5.55\tau^2$ which are given by $0.252\sigma_p/\tau$ and for tension loading is 0.406.

Discussion of Experimental Results

Consideration of the curves of $\sigma_R - \epsilon_R^p$ for the three different initial loading paths Fig. 8 and also Fig. 7 shows reasonable correlation on this basis of σ_R although the curves for initial loading in torsion are consistently low.

However, the curves of $\sigma_R - \epsilon_R^p$ for the second loadings of the eight specimens whose second loading is different from the initial loading, i.e., all specimens except I, II, and III, are quite definitely higher than continuation of the initial loading curves. If the yield surface produced by initial loading were one of a set of nested surfaces of the form σ_R, a sharp departure on second loading at a value of $\sigma_R = 13{,}000$ psi (the value attained on initial loading) would be expected; i.e., similar to that obtained for tension, Fig. 4, where the $\sigma_R - \epsilon_R^p$ curve for the second loading above $\sigma_R = 13{,}000$ psi is very nearly a continuation of that for the first loading. In fact, the curves of $\sigma_R - \epsilon_R^p$ for any second loading different to the first, Figs. 5, 6, and 7, all show a gradual rounding in the region of $\sigma_R = 13{,}000$ psi and there is no clearly defined point corresponding to the yield surface from which the specimen has been unloaded. However, the higher nature of the $\sigma_R - \epsilon_R^p$ curves obtained for each of these specimens, where the second loading is different from the first, suggests that the yield surface established by the initial loading is not attained at a value of $\sigma_R = 13{,}000$ psi but at a somewhat higher value. This higher value of σ_R might possibly be determined by considering that part of the $\sigma_R - \epsilon_R^p$ curve beyond the rounded portion obtained for second loading, and extrapolating this back to intersect the vertical unloading line. This is similar to the approach of Taylor and Quinney [5] although there is great difficulty in determining this point with any certainty.

If the points on the yield surfaces are tentatively defined as suggested in the foregoing, then very similar values of σ_R (for these points) are obtained for specimens IV_R to IX_R; i.e., those loaded initially in internal pressure or torsion, Figs. 5(*b*) and 6(*b*). However, for specimens X_R and XI_R, Fig. 7, the values of σ_R determined in the same manner, are somewhat higher than the foregoing values for specimens IV_R to IX_R. This suggests that the yield surfaces produced by initial loading in either torsion or internal pressure lie outside the surface corresponding to $\sigma_R = 13{,}000$ psi. Fig. 11(*a*) shows the suggested form produced by initial loading in torsion to $\sigma_R = 13{,}000$ psi, and Fig. 11(*b*) that produced by initial loading in internal pressure to $\sigma_R = 13{,}000$ psi. The earlier experiments [1] also gave higher $\sigma_R - \epsilon_R^p$ curves for any second loading which was different to the initial loading. All these results suggest that the yield function does not depend upon stress alone but is strongly influenced by the strain history. In fact, the foregoing suggests a cross effect which is greater than would be obtained if the yield surfaces produced by initial loading were a nested set of the form of σ_R.

This greater cross effect is at variance with the results of other investigators on different materials [6, 7] where the loading was a combination of longitudinal tension and torsion [6] and longitudinal tension and transverse tension [7]. In both these sections of stress space the subsequent yield surfaces showed either a complete absence of cross effect or even a reduction. However, these yield surfaces were obtained by tests which were terminated just beyond yield, this point being determined by the initial departure from linearity of the stress-strain curve. This differs from the procedure used for the tests reported herein in that for each of these specimens the second loading was continued until plastic strains of the order of 2 per cent were recorded, Figs. 4, 5, 6, 7. The significant feature of each of these $\sigma_R - \epsilon_R^p$ curves is the higher curve obtained for any second loading different from the initial loading, showing that in each case the material is "stiffer" for these second loadings, and the method given herein for determining the points on the yield sur-

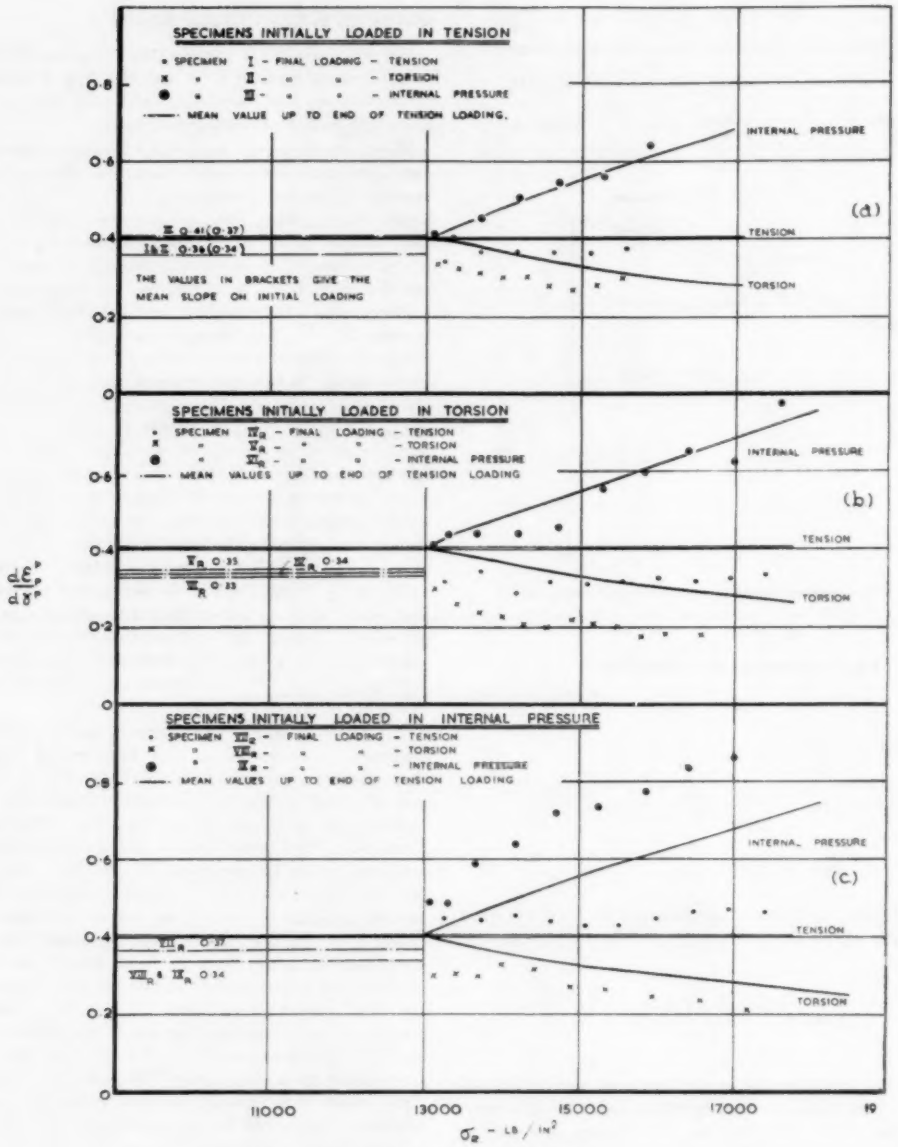

Fig. 9 Slopes of strain-increment vectors

face give correspondingly higher values. The plastic-stress-strain relationships based on this higher yield surface would be able to predict these higher curves for continued straining. If, however, the points on the yield surface were determined by the initial departure from linearity [6] much lower values of σ_R would be obtained, Fig. 4, 5, 6, 7, and the subsequent yield surface would lie well inside the σ_R-surface produced by initial loading. The method of determining the yield surface given herein gives a yield surface which implies the higher stress-strain curves for subsequent straining, although admittedly it does not define clearly the elastic-plastic boundary which is perhaps of secondary importance as compared with the predictions of the stress-strain relationships.

Now consider the direction of the plastic-strain increment vectors for the second loadings of the nine specimens I to IX_R as shown in Fig. 9. The values given in Fig. 9(*a*) are the same as those in Fig. 16(*b*) of the previous paper [1] and refer to specimens I, II, III initially loaded in tension. As discussed previously [1], the general trend of the slopes closely resembles that for the theoretical slopes of the normals if allowance is made for the lower values of the mean slope below σ_R = 13,000 psi for specimens I and II.

The results shown in Fig. 9(*b*) for specimens IV_R, V_R, VI_R initially loaded in torsion show the same general trends as those previously reported [1]. The slopes of the plastic-strain increment vectors for the tension loading up to σ_R = 13,000 psi are all slightly lower than the corresponding values for specimens I, II, III and the slopes above σ_R = 13,000 psi are also lower than the corresponding values for specimens I, II, and III although the difference between specimen VI_R and specimen III is very small.

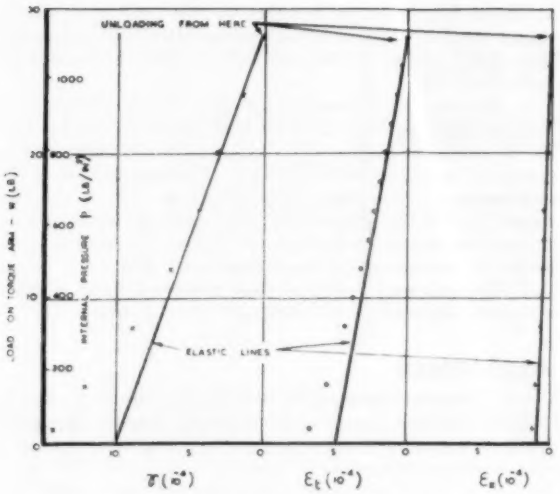

Fig. 10 Unloading curves for Specimen I

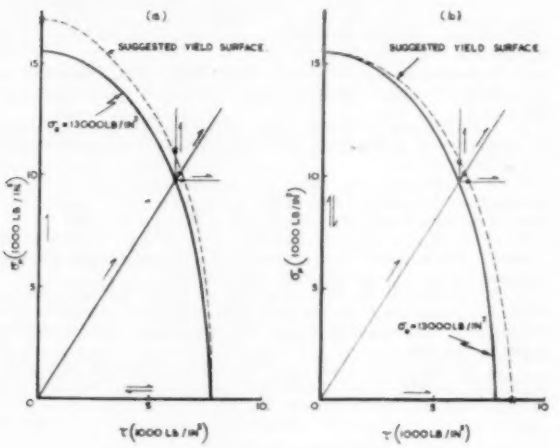

Fig. 11 Suggested form of yield surface

This tendency for the slopes of the plastic-strain increment vectors, after initial loading in torsion, to be lower than the theoretical values for a nested set of surfaces of the form σ_R is qualitatively in agreement with the suggested form of the yield surface produced by initial loading in torsion, Fig. 11(a), since the slopes of the normals to these suggested surfaces would be relatively smaller than those of the normals to a nested set of surfaces of the form σ_R.

Note that if the yield surface produced by initial loading in torsion is of the form suggested in Fig. 11(a) then the loading paths for specimens IV_R, V_R, VI_R would not reach the yield surface on second loading when the loading point reaches the end of the tension loading, Fig. 3. Thus the first part of the loadings along BX, BY, BZ, Fig. 3, will be inside the yield surface.

Refer now to Fig. 9(c) which shows the slopes of the plastic-strain increment vectors for specimens VII_R, $VIII_R$, IX_R initially loaded in internal pressure. Following the lower values obtained after initial torsion it might be expected that the mean values of the slopes of the vectors on the tension loading up to σ_R = 13,000 psi would be higher than the corresponding values for the specimens originally loaded in tension, but this is not so.

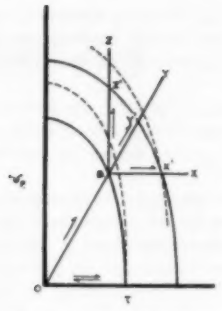

Fig. 12 Effect of suggested form of yield surface

However, the values of the slopes above σ_R = 13,000 psi for specimens VII_R and IX_R are significantly greater than the values for the specimens originally loaded in tension and even greater than the slope of the normals to successive σ_R surfaces. The slopes for specimen $VIII_R$ above σ_R = 13,000 psi, although greater than the corresponding values for specimen V_R, initially loaded in torsion, are not significantly greater than those for specimen II initially loaded in tension, and indeed are smaller than the slopes of the normals to surfaces of the form σ_R.

However, apart from this latter specimen the tendency for the slopes of the plastic-strain increment vectors, after initial loading in internal pressure, to be higher than the theoretical values for a nested set of σ_R yield surfaces is qualitatively in agreement with the previously suggested form of yield surface, Fig. 11(b); i.e., the slopes of the normals to these suggested surfaces are greater than those to surfaces of the form of σ_R.

Refer now to Figs. 5(b) and 6(b) showing the curves of $\sigma_R - \epsilon_R^p$ for the specimens initially loaded in torsion and internal pressure. In Fig. 5(b) for the three specimens initially loaded in torsion the curve for the second loading in tension-torsion of specimen V_R is below that for the tension loading of specimen IV_R which in turn is lower than that for the tension-internal pressure loading of specimen VI_R. Similarly in Fig. 6(b) for the second loadings of the three specimens initially loaded in internal pressure the internal pressure loading of specimen IX_R gives the lowest $\sigma_R - \epsilon_R^p$ curve, the tension loading of specimen VII_R gives an intermediate curve and the torsion loading of specimen $VIII_R$ the highest curve. This again can be qualitatively explained by a set of yield surfaces of the form produced by the initial loading in (a) torsion, Fig. 11(a); (b) internal pressure, Fig. 11(b).

Consider the loading paths of the three specimens initially loaded in torsion as shown in Fig. 12. Specimen V_R is loaded in torsion along BX and a point X' is where this loading path crosses a subsequent σ_R-surface. Similarly the loading paths for specimen IV_R and VI_R cross this σ_R-surface at Y' and Z', respectively. The dotted lines in Fig. 12 show the suggested shapes of subsequent yield surfaces produced by the initial loading, one of these surfaces being drawn to pass through X'. The points Y' and Z' however, lie progressively farther inside this suggested yield surface passing through X'. Hence, although the values of σ_R at the points X', Y', Z' are the same, the values of the representative stress as defined by the suggested surface, are progressively smaller at Y' and Z'. Thus, if correlation is obtained for the three loadings when plotted on the basis of the suggested representative stress, the three curves when plotted on the basis of $\sigma_R - \epsilon_R^p$ would be progressively higher for the three loading paths BX, BY, and BZ, which is the result obtained, Fig. 5(b). Similarly for the specimens VII_R, $VIII_R$, IX_R, initially loaded in internal pressure, the suggested shape of the yield surface produced by the initial loading, Fig. 11(b), predicts that the $\sigma_R - \epsilon_R^p$ curves for the second loadings in tension (specimen VII_R), tor-

sion (specimen $VIII_R$) will lie progressively higher than that for the internal pressure second loading (specimen IX_R). This qualitatively is in agreement with the experimental results, Fig. 6(*b*).

As found previously [1] any internal pressure loading appears to have a disproportionately large effect on this material which must be attributed to the one degree of anisotropy in the radial direction.

Some other points of interest in the experimental results which are not brought out by the data reported in the foregoing were observed and are identical with those obtained previously.[2]

Conclusions

1 The test specimens had repeatable mechanical properties on initial loading which justifies a comparison of the initial loadings with each other and also a comparison of the behavior of the specimens on the second loading.

2 The behavior of the specimens on initial loading can well be explained in the terms of a yield criterion σ_R of a material which possesses one degree of anisotropy in the radial direction [1].

3 For all second loading paths which differ from the initial loading, the curves of $\sigma_R - \epsilon_R{}^p$ are higher than the extrapolation of the initial loading curves, although in each case a slight "rounding" of the $\sigma_R - \epsilon_R{}^p$ curve is obtained before the value of σ_R at the end of the initial loading is attained. By extrapolating these second curves back to the vertical unloading line to define the point on the yield surface established by the initial loading, a suggested yield surface lying outside the σ_R surface is obtained. This suggests a very strong cross effect.

4 This method of obtaining points on the subsequent yield surface gives a yield surface which lies outside the σ_R surface defined by the initial loading and corresponds to the higher $\sigma_R - \epsilon_R{}^p$ curves obtained for any subsequent loading different to the initial loading. This differs from the "elastic-plastic boundary" yield surface as determined by other investigators [6, 7]. If the subsequent yield surface for the tests described herein was obtained in this latter manner it would lie well inside the σ_R surface established by the initial loading.

5 The $\sigma_R - \epsilon_R{}^p$ curves obtained for the second loadings of the specimens initially loaded in either internal pressure or torsion do not correlate, as do the initial loadings, but the differences can be explained qualitatively by yield surfaces of the shape suggested in the foregoing.

6 The slopes of the plastic-strain increment vectors on second loading which may be interpreted as normals to the yield surface at the particular loading point [4] are not consistent with a nested set of surfaces of the form σ_R. However, in general, the differences can be explained qualitatively in terms of the suggested shape of the yield surface produced by the initial loading. Even so the values obtained for the final second loadings in internal pressure do appear disproportionately high.

7 From the results obtained there appears to be no evidence to support the presence of a corner in the yield surface.

[2] See items 1, 2, 3, 4, Fig. 17, and Table 1 on page 86 of [1].

Acknowledgment

The authors wish to thank Dr. S. S. Gill, Prof. H. Wright Baker, Prof. W. Merchant, and Prof. D. C. Drucker for their invaluable advice and encouragement, and Mr. J. W. Flowett for his advice and practical assistance.

References

1 S. S. Gill and J. Parker, "Plastic Stress-Strain Relationships—Some Experiments on the Effect of Loading Path and Loading History," JOURNAL OF APPLIED MECHANICS, vol. 26, TRANS. ASME, vol. 81, Series E, 1959, pp. 77–87.

2 J. Parker, S. S. Gill, and J. W. Flowett, "The Production of Thin-Walled Tubular Test Specimens," *Microtecnic*, vol. 2, no. 2, 1957, pp. 82–85.

3 J. Parker and S. S. Gill, "Some Strain Measuring Techniques for Experiments in Plasticity," *British Journal of Applied Physics*, vol. 8, 1957, p. 309.

4 D. C. Drucker, "A More Fundamental Approach to Plastic Stress-Strain Relations," *Proceedings of the First U. S. National Congress of Applied Mechanics*, ASME, June, 1951, pp. 487–491.

5 G. I. Taylor and H. Quinney, "The Plastic Distortion of Metals," *Philosophical Transactions of The Royal Society*, London, England, series A, vol. 230, 1931, pp. 323–362.

6 P. M. Naghdi, F. Essenburg, and W. Koff, "An Experimental Study of Initial and Subsequent Yield Surfaces in Plasticity," JOURNAL OF APPLIED MECHANICS, vol. 25, TRANS. ASME, vol. 80, 1958, pp. 201–209.

7 L. W. Hu and J. F. Bratt, "The Effect of Tensile Plastic Deformation on the Yield Condition," JOURNAL OF APPLIED MECHANICS, vol. 25, TRANS. ASME, vol. 80, 1958, p. 411.

On the Dynamic Behavior of a Frank-Read Source

J. D. CAMPBELL[1]
J. A. SIMMONS[2]
J. E. DORN[3]

The equation of motion for a curved dislocation moving at high velocities in a slip plane is solved for a dislocation half-mill. It is found that the angular velocity of a dislocation half-mill about the pinning point is constant for constant stress. The solution is applied to a Frank-Read source to give the shape of the nucleating source and the time of activation. For Al, the time of nucleation of a Frank-Read source is about 9×10^{-10} *sec when the stress on the source is* $5 \times 10^{-4}G$.

THE propagation of plastic waves in crystalline solids is determined by the behavior of dislocations. Following application of stress there will be a period of acceleration of dislocations since dislocations possess a small effective mass. After a very short time interval dislocation interaction will be so great that the strain rate will level off and the material will work-harden. Finally, the solid will come to a quasi-static condition in which the plastic strain will be almost constant for a constant stress.

Von Karman [1],[4] Taylor [2], and Rakhmatulin [3] proposed a plastic-wave-propagation theory based on this latter quasi-static stress-strain curve. Discrepancies between their theory and experiment were found by Riparbelli [4], and Sternglass and Stuart [5]. Malvern [6] proposed a correction for the quasi-static theory by including a correction for strain rate. He used a quasi-viscous equation of the form

$$\frac{\partial \epsilon}{\partial t} = \frac{1}{E}\frac{\partial \sigma}{\partial t} + f(\sigma, \epsilon),$$

where f represents the plastic-strain rate.

It is the purpose of this paper to describe semiquantitatively the behavior of the Frank-Read dislocation source under shock stressing, thus determining the effect of dislocation inertia upon Malvern's strain-rate equation for plastic waves as well as giving information on the actual behavior of a dislocation in a nonsteady-state dynamic situation. It will be demonstrated that a typical Frank-Read source begins to multiply in about 5×10^{-3} microsec. At that time the estimated plastic strain in a typical metal will be only 0.003. Shortly following multiplication, it is expected that dislocations will begin to interact, causing initiation of decelerative processes. Thus, provided the initial accelerative portion of the dynamic behavior of dislocations can be neglected, the Malvern theory of plastic-wave propagation will, at least formally, describe the subsequent actual behavior of real crystalline materials.

The model to be used in this analysis is that given by F. C. Frank for a straight dislocation moving at constant velocity through a crystal [7]. In that case the dislocation has energy Γ/β per unit length where $\Gamma \cong Gb^2/2$ (b is the Burger's vector and G the shear modulus) while

$$\beta = \left[1 - \frac{v^2}{c^2}\right]^{1/2}$$

where v is the dislocation velocity,

$$c = \left[\frac{G}{\rho_0}\right]^{1/2}$$

is the velocity of an elastic shear wave, and ρ_0 is the density of the crystal.

1 Equation of Motion of a Dislocation

We shall consider a single half-infinite dislocation mill, as shown in Fig. 1, originally aligned along the x-axis and pinned at a nodal point at the origin. At time $t = 0$ an abrupt shock in shear stress, σ, will be applied to the slip plane and maintained thereafter. Consequently, a constant force, σb, will act normal to each unit length of the dislocation line. Under these conditions each segment of the dislocation will begin to accelerate in a direction normal to its arc; and each geometrical point on this dislocation will form a trajectory normal to the dislocation line itself. These trajectories shown in Fig. 1 will be represented in terms of a

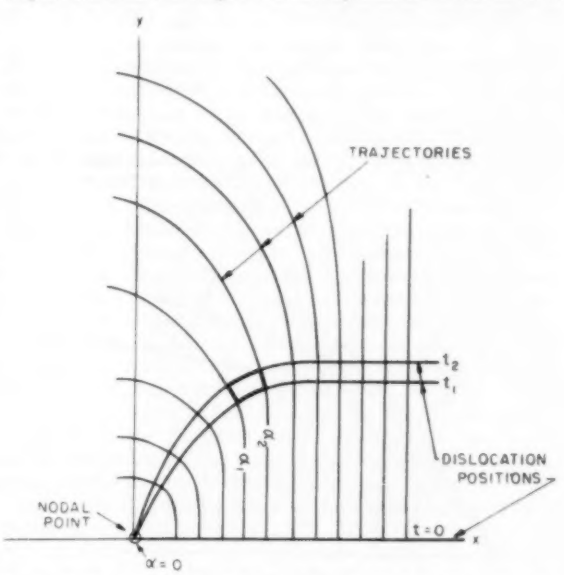

Fig. 1 Motion of a single dislocation showing trajectories in the slip plane

[1] Lecturer, Department of Engineering Science, Oxford University, Oxford, England.

[2] Research Mathematician, Institute of Engineering Research, University of California, Berkeley, Calif.

[3] Professor of Metallurgy, University of California, Berkeley, Calif.

[4] Numbers in brackets designate References at end of paper.

Contributed by the Applied Mechanics Division and presented at the Winter Annual Meeting, New York, N. Y., November 27–December 2, 1960, of THE AMERICAN SOCIETY OF MECHANICAL ENGINEERS.

Discussion of this paper should be addressed to the Editorial Department, ASME, United Engineering Center, 345 East 47th Street, New York 17, N. Y., and will be accepted until October 10, 1961. Discussion received after the closing date will be returned. Manuscript received at ASME Applied Mechanics Division, August 12, 1960. Paper No. 60—WA-204.

Lagrangian co-ordinate system α, t, where α will be taken as the x-co-ordinate of the trajectories at $t = 0$. The following analysis will be conducted in the α, t-plane. The length of the dislocation arc between α and $\alpha + d\alpha$ changes with time. We will denote the actual arc length ds by

$$ds = Ad\alpha \tag{1}$$

where A is a dimensionless factor. Similarly, the length along the trajectories is

$$vdt \tag{2}$$

where v denotes the velocity of the dislocation segment normal to itself.

The first equation of motion for a dislocation derives from the conservation of energy. The energy of a moving segment of a dislocation of length $ds = Ad\alpha$ will be taken to be $\Gamma Ad\alpha/\beta$. Since the work done on a dislocation is σb times the area swept out by the dislocation, the work done in time dt on the segment $d\alpha$ is $\sigma bvdtAd\alpha$. Consequently, the rate of work done on a dislocation segment between α_1 and α_2 is related to the rate of change of energy of the system according to

$$\int_{\alpha_1}^{\alpha_2} \sigma bAvd\alpha = \frac{\partial}{\partial t}\int_{\alpha_1}^{\alpha_2} \frac{\Gamma A}{\beta}\, d\alpha \tag{3}$$

or

$$\frac{1}{\rho}\int_{\alpha_1}^{\alpha_2} Avd\alpha = \frac{\partial}{\partial t}\int_{\alpha_1}^{\alpha_2} \frac{A}{\beta}\, d\alpha \tag{4}$$

where $\rho = \Gamma/\sigma b$ is the well-known expression for the radius of curvature of a dislocation for static equilibrium under the stress σ.

If we let $\alpha_1 \to \alpha_2$, equation (4) becomes

$$\frac{Av}{\rho} = \frac{1}{\beta}\frac{\partial A}{\partial t} + \frac{Av}{c^2\beta^3}\frac{\partial v}{\partial t} \tag{5}$$

The mechanical equation for propagation of a small shock in slope along the length of a dislocation, as shown in Fig. 2, will be useful to us presently and can be derived directly from (4).

Thus if $\alpha(t)$ gives the Lagrangian position of the shock front, the right-hand side of (4) becomes

$$\frac{\partial}{\partial t}\int_{\alpha_1}^{\alpha(t)} \frac{A}{\beta}\, d\alpha + \frac{\partial}{\partial t}\int_{\alpha(t)}^{\alpha_2} \frac{A}{\beta}\, d\alpha \tag{6}$$

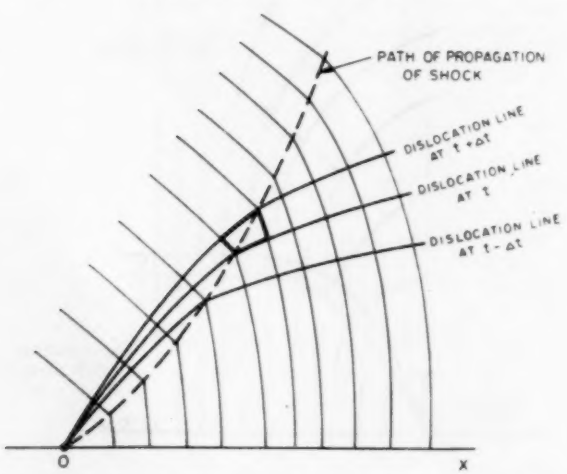

Fig. 2 Path of a small disturbance along a dislocation

Formula (6) may be rewritten as

$$\frac{d\alpha(t)}{dt}\left(\frac{A}{\beta}\right)_{\substack{\text{after}\\ \text{shock}}} + \int_{\alpha_1}^{\alpha(t)} \frac{\partial}{\partial t}\left(\frac{A}{\beta}\right) d\alpha + \int_{\alpha(t)}^{\alpha_2} \frac{\partial}{\partial t}\left(\frac{A}{\beta}\right) d\alpha - \frac{d\alpha(t)}{dt}\left(\frac{A}{\beta}\right)_{\substack{\text{before}\\ \text{shock}}} \tag{7}$$

Now letting $\alpha_1 \to \alpha_2 \to \alpha(t)$ with t constant equation (4) becomes

$$\Delta\left(\frac{A}{\beta}\right) = 0 \tag{8}$$

where Δ represents the jump across the shock front.

2 Shock Propagation Along a Dislocation and the Compatibility Equation

Two equations are needed to describe the motion of a dislocation. One is the mechanical equation derived in the preceding section. The second is the geometrical condition describing the fact that the dislocation must slip on its slip plane.

Thus, as shown in Fig. 3, if we define $\theta(\varphi)$ as the angle between the trajectory (dislocation line) and the x-axis so that

$$\theta + \varphi = \frac{\pi}{2},$$

then

$$d\theta + d\varphi = 0 \tag{9}$$

Defining R and R' as the radii of curvature of dislocation and trajectory, respectively,

$$Rd\theta = Ad\alpha \quad \text{along } t = \text{const} \tag{10}$$

and

$$R'd\varphi = vdt \quad \text{along } \alpha = \text{const} \tag{11}$$

Furthermore, by translating the α-trajectory to $\alpha + d\alpha$ one sees that

$$d\theta = \frac{A(t + dt)d\alpha - A(t)d\alpha}{vdt} = \frac{\dfrac{\partial A}{\partial t}\, d\alpha}{v} \tag{12}$$

and similarly

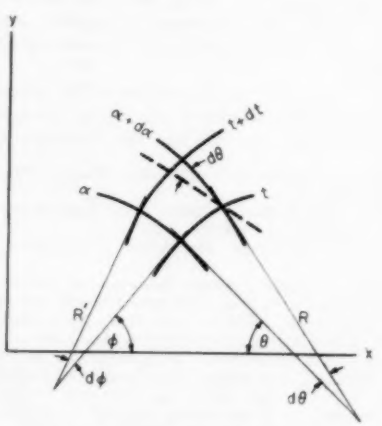

Fig. 3 Compatibility relationship

$$d\varphi = \frac{v(\alpha + d\alpha)dt - v(\alpha)dt}{A d\alpha} = \frac{\dfrac{\partial v}{\partial \alpha}\, dt}{A} \tag{13}$$

Combining equations (9) to (13) yields the following equations for the radii of curvature:

$$\frac{1}{R} = \frac{1}{A}\frac{\partial \theta}{\partial \alpha} = \frac{1}{Av}\frac{\partial A}{\partial t} \tag{14}$$

and

$$\frac{1}{R'} = \frac{1}{v}\frac{\partial \varphi}{\partial t} = \frac{1}{Av}\frac{\partial v}{\partial \alpha} \tag{15}$$

The geometrical condition that the dislocation remains in its slip plane is that

$$\frac{\partial^2 \theta}{\partial t \partial \alpha} = \frac{\partial}{\partial t}\left(\frac{1}{v}\frac{\partial A}{\partial t}\right)$$

and

$$\frac{\partial^2 \theta}{\partial \alpha \partial t} = \frac{\partial}{\partial \alpha}\left(\frac{\partial \theta}{\partial t}\right) = -\frac{\partial}{\partial \alpha}\left(\frac{\partial \varphi}{\partial t}\right) = -\frac{\partial}{\partial \alpha}\left(\frac{1}{A}\frac{\partial v}{\partial \alpha}\right)$$

are equal, so that

$$\frac{\partial}{\partial t}\left(\frac{1}{v}\frac{\partial A}{\partial t}\right) + \frac{\partial}{\partial \alpha}\left(\frac{1}{A}\frac{\partial v}{\partial \alpha}\right) = 0 \tag{16}$$

which is the desired compatibility equation.

From Fig. 4 which is the analog of Fig. 3 for a small shock we can derive the rate of shock propagation and uncover a linear equation which we can substitute to a good degree of accuracy for the nonlinear compatibility equation. The subscripts 1 and 2 will refer to values just to the left and just to the right of the shock front at constant t, and Δ will refer to the negative of the jump across the shock front. From Fig. 4 we obtain the two equations

$$A_1^2\, d\alpha^2 + v_1^2 dt^2 = A_2^2 d\alpha^2 + v_2^2 dt^2 \tag{17}$$

and

$$A_1^2 d\alpha^2 + v_1^2 dt^2 - 2A_1 v_1 d\alpha dt \cos\left(\frac{1}{2}\pi - \Delta\theta\right) = A_2^2 d\alpha^2 + v_1^2 dt^2 - 2A_2 v_1 d\alpha dt \cos\left(\frac{1}{2}\pi + \Delta\theta\right) \tag{18}$$

which become for small shocks

[where $\Delta(fg) \cong (\Delta f)g + f(\Delta g)$]

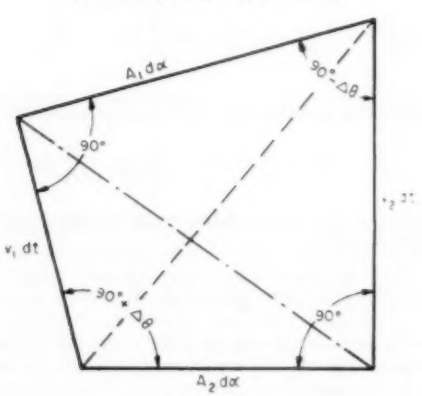

Fig. 4 Details at the shock front

$$\frac{d\alpha}{dt} = \pm\left(-\frac{\Delta v^2}{\Delta A^2}\right)^{1/2} = \pm\left(-\frac{v\Delta v}{A\Delta A}\right)^{1/2} \tag{19}$$

and

$$\Delta v = A\frac{d\alpha}{dt}\Delta\theta \tag{20}$$

Combining (19) and (20) with (8) gives

$$\frac{d\alpha}{dt} = \pm\frac{c\beta}{A} \tag{21}$$

and

$$\Delta v = c\beta\Delta\theta \tag{22}$$

Equation (22) yields a heuristic motivation for the introduction of the linear equation which we shall use to simplify the equation of compatibility. If in equation (22) we let Δv and $\Delta\theta$ become infinitesimals,

$$dv = \frac{\partial v}{\partial \alpha}\, d\alpha \quad \text{and} \quad d\theta = \frac{1}{v}\frac{\partial A}{\partial t}\, d\alpha,$$

the latter following from equation (12). Hence equation (22) becomes

$$v\frac{\partial v}{\partial \alpha} = \beta c\frac{\partial A}{\partial t} \tag{23}$$

This argument serves only as a motivation for the introduction of equation (23) rather than a derivation of it, since in letting Δv and $\Delta\theta$ become infinitesimal we have violated the assumptions used in deriving equation (17). The actual justification of equation (23) will follow in the next section where the problem of the motion of a dislocation half-mill will be solved.

3 Motion of a Dislocation Half-Mill

In this section we shall determine the motion of a dislocation half-mill using equations (23) and (5) for the equation of motion. As will be shown, when $v/c \ll 1$ so that $\beta \simeq 1$, equations (23) and (5) imply the compatibility equation (16) so that the solution obtained will be an exact one for nonrelativistic velocities. However, a straight dislocation achieves almost the speed of sound in the order of 10^{-9} sec, so that relativistic effects eventually must be taken into account. Since the compatibility conditions do not hold for the relativistic motion of a dislocation, the solution obtained may be envisioned as one in which the dislocation slips on a nonplanar surface. Since more of the work done by the stress goes into potential energy than would occur in planar motion, the potential energies of the relativistic approximation should then be somewhat higher and the velocities somewhat lower than in the real planar relativistic solution. The actual motion may be expected to lie somewhere between the relativistic and the nonrelativistic approximations when the undisturbed segments of the dislocation have traveled the same distance. We shall use this fact in the next section to delimit the time necessary to nucleate a Frank-Read source.

The method of solution used is the same for both the relativistic approximation and the nonrelativistic case. We shall work out only the nonrelativistic case, summarizing the results and showing a picture of the solution for the relativistic case.

In the nonrelativistic case, $\beta \simeq 1$ and equations (5) and (23) become

$$\frac{Av}{\rho} = \frac{\partial A}{\partial t} + \frac{Av}{c^2}\frac{\partial v}{\partial t} \tag{24}$$

and

$$c\frac{\partial A}{\partial t} = v\frac{\partial v}{\partial \alpha} \tag{25}$$

We will now show that equations (24) and (25) imply the compatibility relationship (16). Substituting equation (25) into (24) reveals that

$$\frac{1}{A}\frac{\partial v}{\partial \alpha} + \frac{1}{c}\frac{\partial v}{\partial t} = c/\rho \tag{26}$$

and differentiating this equation with respect to α yields

$$\frac{\partial}{\partial \alpha}\left(\frac{1}{A}\frac{\partial v}{\partial \alpha}\right) + \frac{\partial}{\partial \alpha}\left(\frac{1}{c}\frac{\partial v}{\partial t}\right) = 0 \tag{27}$$

However,

$$\frac{\partial}{\partial \alpha}\left(\frac{1}{c}\frac{\partial v}{\partial t}\right) = \frac{\partial}{\partial t}\left(\frac{1}{c}\frac{\partial v}{\partial \alpha}\right) = \frac{\partial}{\partial t}\left(\frac{1}{v}\frac{\partial A}{\partial t}\right) \tag{28}$$

as obtained from equation (25). Introducing equation (28) into (27) gives the compatibility expression of equation (16). Consequently, a solution of equations (24) and (25) is also a special solution of equations (24) and (16).

Application of the same procedure to the relativistic case, given by equations (5) and (22), yields the condition that

$$\frac{\partial}{\partial t}\left(\frac{1}{v}\frac{\partial A}{\partial t}\right) + \frac{\partial}{\partial \alpha}\left(\frac{1}{A}\frac{\partial v}{\partial \alpha}\right) = \frac{\partial}{\partial \alpha}\left(c\frac{\beta^2}{\rho}\right) = -\frac{2v}{\rho c}\frac{\partial v}{\partial \alpha} \tag{29}$$

Obviously, equations (5) and (22) do not satisfy the compatibility relationship given by equation (16) except in the limiting cases where either v or $\partial v/\partial \alpha$ approaches zero, as near the nodal point of the dislocation where $v \simeq 0$ or on the straight-line portion of the dislocation, where $\partial v/\partial \alpha = 0$. Thus, even for the relativistic case, equations (5) and (22) may be expected to give a reasonable approximation to the motion of a dislocation half-mill.

Equations (24) and (25) are sufficiently general to describe the nonrelativistic motion of a single mill. Consider a single mill with a nodal point at the origin of the α, t-plane. When a stress σ is applied, the dislocation accelerates but the end $\alpha = 0$ remains fixed. The disturbance produced by keeping this end fixed is propagated in the α, t-plane with velocity c/A as demonstrated by equation (21). Before this disturbance reaches a given point, the dislocation accelerates as though free. Therefore $\partial A/\partial t = \partial v/\partial \alpha = 0$, so that equation (24) may be integrated directly yielding

$$v = \frac{c^2 t}{\rho} \tag{30}$$

The distance y traveled by the dislocation in the x,y-plane is $c^2t^2/2\rho$ and the distance x traveled by the disturbance along the horizontal dislocation line is ct. Therefore the equation of the original disturbance line in the x,y-plane is

$$\left(\frac{x}{\rho}\right)^2 = 2\left(\frac{y}{\rho}\right) \tag{31}$$

Equations (30) and (31) describe completely the dislocation motion in the α, t-plane for $\alpha \geq ct$. To treat the solution in the region $\alpha \leq ct$ we employ characteristics.

We define

$$\frac{\partial}{\partial \xi} = \frac{c}{A}\frac{\partial}{\partial \alpha} + \frac{\partial}{\partial t} \tag{32}$$

and

$$\frac{\partial}{\partial \eta} = \frac{\partial}{\partial t} \tag{33}$$

Equations (26) and (24) may then be written

$$\frac{\partial v}{\partial \xi} = \frac{c^2}{\rho} \tag{34}$$

and

$$\frac{\partial\left(\ln A + \frac{v^2}{2c^2}\right)}{\partial \eta} = \frac{v}{\rho} \tag{35}$$

Equations (32) and (33) may be solved for differentials yielding

$$d\xi = \frac{A}{c}\,d\alpha \tag{36}$$

$$d\eta = dt - \frac{A}{c}\,d\alpha \tag{37}$$

Hence along the characteristic curves $d\eta = 0$, $dt = (A/c)d\alpha$ and equation (34) becomes

$$dv = \frac{c^2}{\rho}\,dt \tag{38}$$

We now define t_0 to be the time at which each characteristic curve $d\eta = 0$ intersects $\alpha = 0$ so that $t_0 = \text{const}$ on these characteristics. Since $v = 0$ along $\alpha = 0$, equation (38) can be integrated directly to yield

$$v = \frac{c^2}{\rho}(t - t_0) \tag{39}$$

Equation (39) derived for each characteristic curve is valid in the whole region $\alpha \leq ct$. The solutions of equations (34) and (35) may now be found by introducing v and t_0 as new independent variables.

We know

$$dv = \frac{\partial v}{\partial \xi}\,d\xi + \frac{\partial v}{\partial \eta}\,d\eta$$

and $\partial v/\partial \xi$ is given directly by equation (34). Using equations (24) and (14) we obtain

$$\frac{\partial v}{\partial \eta} = c^2\left(\frac{1}{\rho} - \frac{1}{R}\right)$$

Therefore

$$dv = \frac{c^2}{\rho}\,d\xi + c^2\left(\frac{1}{\rho} - \frac{1}{R}\right)d\eta = \frac{cA}{R}\,d\alpha + c^2\left(\frac{1}{\rho} - \frac{1}{R}\right)dt \tag{40}$$

Differentiating equation (39) and using equation (40),

$$dt_0 = dt - \frac{\rho}{c^2}\,dv = -\frac{\rho A}{cR}\,d\alpha + \frac{\rho}{R}\,dt \tag{41}$$

To show that v and t_0 are a nondegenerate co-ordinate system, we compute the Jacobian,

$$J = \left(\frac{v, t_0}{\alpha, t}\right) = \frac{cA\rho}{R^2} + \frac{cA}{R^2}(R - \rho) = \frac{cA}{R} \tag{42}$$

Therefore a solution will only be valid for the curved portion of the dislocation line where R is neither zero nor infinite. Since the solution for the straight-line portion of the dislocation has already been obtained, v and t_0 are satisfactory co-ordinates.

From equations (40) and (41) we see that

$$\frac{\partial}{\partial \alpha} = \frac{cA}{R}\frac{\partial}{\partial v} - \frac{\rho A}{cR}\frac{\partial}{\partial t_0} \tag{43}$$

and

$$\frac{\partial}{\partial t} = c^2\left(\frac{1}{\rho} - \frac{1}{R}\right)\frac{\partial}{\partial v} + \frac{\rho}{R}\frac{\partial}{\partial t_0} \tag{44}$$

In terms of v and t_0 equation (25) becomes

$$\frac{c^2(R-\rho)}{\rho A}\frac{\partial A}{\partial v} + \frac{\rho}{A}\frac{\partial A}{\partial t_0} = v \tag{45}$$

and the relation

$$\frac{\partial}{\partial \alpha}\left(\frac{\partial t_0}{\partial t}\right) = \frac{\partial}{\partial t}\left(\frac{\partial t_0}{\partial \alpha}\right)$$

becomes

$$\frac{\partial R}{\partial v} = \frac{(R-\rho)}{A}\frac{\partial A}{\partial v} + \frac{\rho^2}{c^2 A}\frac{\partial A}{\partial t_0} \tag{46}$$

Combining equations (45) and (46) we obtain

$$\frac{\partial R}{\partial v} = \frac{\rho v}{c^2} \tag{47}$$

which may be integrated directly along $t_0 = \text{const}$, starting from $\alpha = 0$ to give

$$R - R_0 = \frac{\rho v^2}{2c^2} - \frac{\rho v_0^2}{2c^2} \tag{48}$$

Along $\alpha = 0$, $v = 0$ so $v_0 = 0$. Also $t = t_0$, so that $\partial t_0/\partial t = 1$. From equation (41),

$$\frac{\partial t_0}{\partial t} = \frac{\rho}{R}, \quad \text{so} \quad R_0 = \rho$$

Hence

$$R = \rho\left(1 + \frac{v^2}{2c^2}\right) \tag{49}$$

We can now solve for A and α. Combining equations (14) and (49) and integrating along lines $\alpha = \text{const}$ starting from the leading characteristic $\alpha = ct$ yields

$$A = \frac{\rho^2 v^2}{c^2\alpha^2} \tag{50}$$

Now setting $dv = 0$ and integrating along $v = \text{const}$ from $\alpha = c$ gives

$$\frac{\rho}{\alpha} - \frac{c}{v} = \frac{ct_0}{2\rho} \tag{51}$$

This completes the nonrelativistic solution for the motion of a single mill. From equations (39), (49), (50), and (51) the quantities A, v, and R can be computed in the α, t-plane for $\alpha \leq ct$. The methods used for the relativistic approximation are the same as those of the nonrelativistic case, so we only summarize the results here.

Over the straight segment

$$v = \frac{c^2 l}{\rho}\left(1 + \frac{c^2 l^2}{\rho^2}\right)^{-1/2} \tag{52}$$

and the path of the initial disturbance is described by

$$\frac{ct}{\rho} = \sinh\frac{\alpha}{\rho} \tag{53}$$

in the α, t-plane and

$$\frac{y}{\rho} = \cosh\frac{x}{\rho} - 1 \tag{54}$$

in the x, y-plane.

This describes the solution over the region $ct/\rho \leq \sinh \alpha/\rho$. For $ct/\rho \geqslant \sinh \alpha/\rho$ we apply the same characteristic techniques as before using equations (23) and (5) to obtain

$$\frac{v}{\beta} = \frac{c^2}{\rho}(t - t_0) \tag{55}$$

$$R = \rho/\beta^2 \tag{56}$$

$$A = \frac{1-\beta}{1 - \operatorname{sech}(\alpha/\rho)} \tag{57}$$

$$\frac{ct_0}{\rho} = \operatorname{ctnh}\frac{\alpha}{2\rho} - \frac{\alpha}{\rho} + \tanh^{-1}\frac{v}{c} - \frac{v}{c(1-\beta)} \tag{58}$$

From the foregoing equations we can get a good picture of the motion of a single mill in the x, y-plane as illustrated in Fig. 5 using the dimensionless co-ordinates x/ρ, y/ρ.

Our solution gives an exact description of the motion of the dislocation in the straight segment beyond the initial disturbance and at the nodal point since at these points the compatibility equation is satisfied. Equation (54) gives us the shape of the initial disturbance curve and equation (56) tells us that along this curve

$$R = \rho\cosh^2\frac{x}{\rho}$$

which means that R suffers a steadily decreasing shock along the leading characteristic. At the nodal point $R = \rho$ and increases along the dislocation until one gets to the shock front.

As we shall show in the next section, $\partial\varphi/\partial t = c/\rho$ at the nodal point, where φ is, as before, the angle between the dislocation and the x-axis. The angular velocity, c/ρ, of the dislocation about the nodal point is therefore constant. Using this information we can fair in the dislocation curves in the x, y-plane, obtaining the approximate solution for the motion of a single mill.

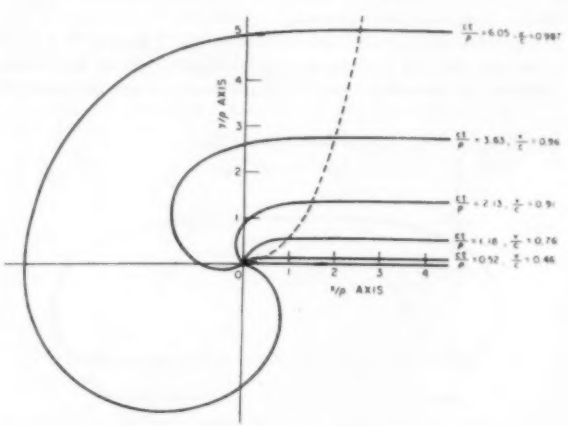

Fig. 5 Relativistic solution of a dislocation half-mill

Note that the equations

$$R = \frac{\rho}{\beta^2}, \quad R = \rho\left(1 + \frac{v^2}{2c^2}\right) \simeq \rho/\beta$$

do not agree for moderate to high velocities. This is because the relativistic approximation is describing nonplanar motion.

4 The Frank-Read Source

The strain suffered by a crystalline material immediately after application of stress may well be pictured as caused by nucleating Frank-Read sources. We may obtain the strain as a function of time for a nucleating Frank-Read source as well as the time for nucleation by using the dislocation half-mill solution of the preceding section.

We shall approximate the Frank-Read source by two single mill dislocations, as shown in Fig. 6. The equations for dislocation motion do not allow superposition to be applied, so that the single mill approximation can be used rigorously only over the time interval necessary for the initial disturbance to reach the center of the dislocation line. To ascertain this time we let the length of the Frank-Read source be $2\lambda\rho$, where λ is a dimensionless parameter. The center of the source is given by $\alpha = \lambda\rho$ and the time necessary for the initial disturbance to travel that far is given by

$$t = \frac{\rho\lambda}{c} \tag{59}$$

$$t = \frac{\rho}{c}\sinh\lambda \tag{60}$$

for the nonrelativistic and relativistic cases, respectively.

In order to discuss the motion of a Frank-Read source, we again introduce the angle φ between the dislocation and the x-axis. As seen from Section 3, equations (25) and (41),

$$d\varphi = -\frac{1}{v}\frac{\partial A}{\partial t}\,d\alpha + \frac{1}{A}\frac{\partial v}{\partial \alpha}\,dt \tag{61}$$

$$= \frac{c}{\rho}\,dt_0 \tag{62}$$

in the nonrelativistic case, and

$$d\varphi = \frac{c\beta^2}{\rho}\,dt_0 \tag{63}$$

in the relativistic approximation.

Equation (62) implies that at the nodal point where $\alpha = v = 0$, $\varphi = ct/\rho$ yielding a constant angular velocity about the nodal point, as mentioned in the preceding section. Using the example of Al, $G \simeq 2.7 \times 10^{11}$ dynes/cm^2, $\rho_0 \simeq 2.7$ g/cm^3, $b = 2.86 \times 10^{-8}$ cm, $c = 3.2 \times 10^5$ cm/sec, $\sigma\rho \simeq 3860$ dynes/cm and the angular velocity becomes 13.2 rev per sec per dyne/cm.^{2} Applying a small stress of $10^{-4}G$ will result in an angular velocity of about 36×10^7 rev per sec. The angular velocity of a free single mill is thus exceedingly fast under ordinary stress.

In order to compute the time necessary for the first loop to form from the source, we note that the leading edge of the loop is determined by the condition $\varphi = 3\pi/2$ as seen in Fig. 7, and its normal velocity v is the horizontal velocity of the leading edge. The distance traveled by the leading edge is therefore $\int v\,dt$ along the curve $\varphi = 3\pi/2$.

In the nonrelativistic case we have from equation (62) and (39)

$$v = \frac{c^2 t}{\rho} - \frac{3\pi c}{2} \tag{64}$$

along $\varphi = 3\pi/2$, $(t \geqslant 3\pi\rho/2c)$.

The first loop is generated by the Frank-Read source when the leading edge has traveled $\lambda\rho$. The time necessary to generate a loop computed as a function of λ is

$$t = \frac{\rho}{c}\left(\frac{3\pi}{2} + (2\lambda)^{1/2}\right) \tag{65}$$

When the time given in (65) is less than the time given in equation (59) then the single-mill approximation for the operation of a Frank-Read source is accurate and this is the case whenever

$$\lambda \geqslant 8.9 \tag{66}$$

The more realistic relativistic solution may be treated in a similar fashion integrating along the curve $d\varphi = 0$ with $\varphi = 3\pi/2$ at the origin. It should be remarked that in the relativistic solution, the compatibility equation does not hold and φ is not a well-defined angle away from the pinning point. Nonetheless, one can integrate along the curve using the equation

$$dv = \frac{Ac\beta}{R}\,d\alpha + \frac{c^2\beta^2}{\rho}\left(\frac{\beta R - \rho}{R}\right)dt \tag{67}$$

to obtain

$$t = \frac{\rho}{c}\left(\frac{3\pi}{2} + (\lambda^2 + 2\lambda)^{1/2}\right) \tag{68}$$

a formula for the nucleation time very near to that of the nonrela-

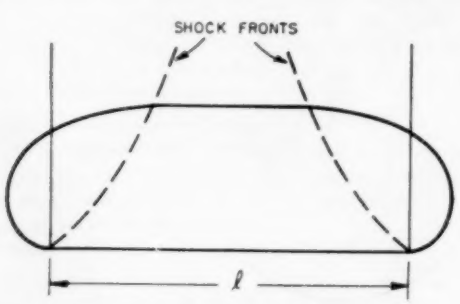

Fig. 6 Frank-Read source as two single mill dislocations

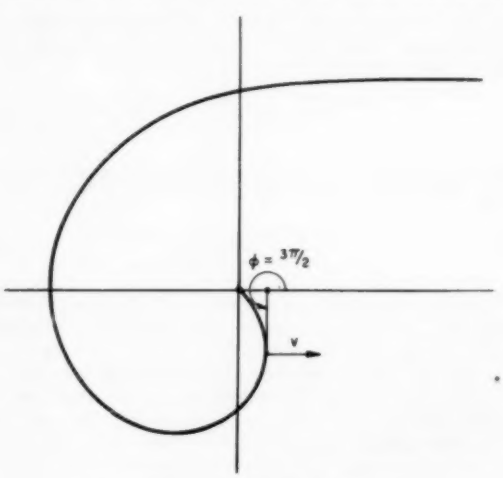

Fig. 7 Closing motion of a Frank-Read source

tivistic solution, being only a little longer. As mentioned earlier, the speed of the real planar dislocation is between that of the nonrelativistic and relativistic solutions, and probably much closer to the latter, especially when it is recalled that dissipative forces have been ignored in these solutions. Therefore the time to nucleate a Frank-Read source lies in value between the two times obtained in equations (65) and (68), probably closer to the latter, and is thus well pinpointed.

Equation (68) compared with (60) proves to be valid whenever $\lambda \geq 2.9$, yielding a greater range of validity than the preceding formula and one which is more correct since we know that equation (60) is an accurate expression for the time the initial shock takes to travel halfway between the nodal points. An attempt to extend the range of validity further by allowing the shock to travel all the way round to the leading edge of the dislocation results in an unimportant reduction of the value of λ. When λ is less than the critical amount, 2.9, the waves from both ends interact and when λ becomes less than 1, the solution to the dislocation motion must become a solution oscillating about the steady-state solution of a circular arc, since as noted earlier, ρ is the radius of a circular arc in equilibrium under the applied stress σ.

For a numerical example, if we are given a Frank-Read source of length 10^{-4} cm in Al, the single mill approximation could be assumed accurate for $\rho \leq 1.7 \times 10^{-6}$ cm or for $\sigma \geq 2.3 \times 10^{9}$ dynes/cm^2. The time to form the first loop from the Frank-Read source would be in this case about 4.5×10^{-10} sec using the relativistic formula.

We come finally to the question of the strain as a function of time during the initial instants after applying a stress σ. The correct value of the strain may be considered to lie between that given by the nonrelativistic and relativistic solutions and much nearer to the latter.

The element of area generated in time t before forming a Frank-Read loop is

$$2\int_0^t \int_{\alpha=0}^{\lambda\rho} A v d\alpha \, dt \tag{69}$$

The computation of this integral in the relativistic approximation yields the formula for the area generated by the loop in time t as

$$\rho^2 \left\{ 2\left(\left[1 + \frac{c^2t^2}{\rho^2}\right]^{1/2} - 1\right)\left(\lambda - \sinh^{-1}\frac{ct}{\rho}\right) + \left(\frac{ct}{\rho}\left[1 + \frac{c^2t^2}{\rho^2}\right]^{1/2} - \sinh^{-1}\frac{ct}{\rho}\right)\right\} \tag{70}$$

where

$$\lambda \geq 2.9, \quad 0 \leq t \leq \frac{\rho}{c}\left[\frac{3\pi}{2} + (\lambda^2 + 2\lambda)^{1/2}\right]$$

The strain may now be determined as a function of time if we assume, for example, 10^{13} Frank-Read sources all of length 2×10^{-4} cm per cc in a given planar direction. Then for $\lambda = 3.1$, $\rho = 3.2 \times 10^{-5}$ cm or $\sigma = 1.2 \times 10^{9}$ dynes/cm^2, and $c/\rho = 10^{10}$/sec. The strain is then given by the formula

$$\epsilon = 2.9 \times 10^{-32}(3.1 - \sinh^{-1} 10^{10}t)([1 + 10^{20}t^2]^{1/2} - 1) + (10^{10}t[1 + 10^{20}t^2)^{1/2} - \sinh^{-1}10^{10}t] \tag{71}$$

for $0 \leq t \leq 8.7 \times 10^{-10}$ sec. When $t = 8.7 \times 10^{-10}$ sec, $\epsilon = 2.2 \times 10^{-3}$.

The foregoing results for a typical case suggest that dislocations accelerate very rapidly. A Frank-Read source of usual length will begin to multiply in about 9×10^{-10} sec when subjected to a shock stress of about 5×10^{-3}G. At this time the plastic strain in a typical metal will be about 0.002 and the average strain rate will be approximately 3×10^{6}/sec. Since dislocation loops leaving the source will begin to apply back stresses on the source shortly following their nucleation, the resulting strain-hardening will soon cause the strain rate to diminish. Thus neglecting the accelerative period of about the first 10^{-9} sec, Malvern's type of analysis of plastic-wave propagation is at least qualitatively acceptable.

Conclusions

1 A complete solution is given for the nonrelativistic activation of a dislocation half-mill under shock stressing.

2 An approximate solution is given for the relativistic activation of a dislocation half-mill.

3 A typical Frank-Read source will begin to multiply in about 9×10^{-10} sec when the plastic strain is about 0.002.

Acknowledgments

The authors wish to express their appreciation to Convair Research Division of General Dynamics for their support of this investigation as part of their research program on Dynamic Stressing of Metals. They also wish to extend their thanks to Prof. James W. Mar for many helpful discussions and suggestions, and to Mrs. Erik Ellentuck for preparing the manuscript.

References

1 T. von Karman and P. Duwez, "Propagation of Plastic Deformation in Solids," *Journal of Applied Physics*, vol. 21, 1950, pp. 987–994.

2 G. I. Taylor, "Plastic Wave in a Wire Extended by an Impact Load," Scientific Papers, vol. 1, Cambridge University Press, Cambridge, England, 1957.

3 K. A. Rakhmatulin, "Deformation in Solids," ONR Translation No. 2, Brown University, Providence, R. I., November, 1948.

4 C. Riparbelli, "On the Relation Among Stress, Strain and Strain Rate in Copper Wires Submitted to Longitudinal Impact," Society for Experimental Stress Analysis, *Proceedings*, vol. 14, 1954, p. 55.

5 E. J. Sternglass and D. A. Stuart, "An Experimental Study of the Propagation of Transient Longitudinal Deformations in Elastoplastic Media," Journal of Applied Mechanics, vol. 20, Trans. ASME, vol. 75, 1953, p. 427.

6 L. E. Malvern, "The Propagation of Longitudinal Waves of Plastic Deformation in a Bar of Material Exhibiting Strain-Rate Effect," Journal of Applied Mechanics, vol. 18, Trans. ASME, vol. 73, 1951, pp. 203–208.

7 F. C. Frank, "On the Equations of Motion of Crystal Dislocations," *Proceedings of the Physical Society of London*, England, vol. 62, 1949, pp. 131–134.

Journal of APPLIED MECHANICS

Brief Notes

On the recommendation of the Executive Committee of the ASME Applied Mechanics Division, it was decided to initiate a section devoted to brief notes on technical matters in mechanics. These notes must not be longer than 750 words (about 2½ double-spaced typewritten pages, including figures) and will be subject to the usual review procedure prior to publication. After approval such notes will be published as soon as possible, normally in the next issue of the Journal. The notes should be submitted to the Technical Editors of the Journal of Applied Mechanics.

On Similarity Solutions for Free-Convection Flow Past Flat Plates

PAU-CHANG LU[1]

Introduction

RECENTLY, Yang [1][2] has given an extensive list of possible similarity solutions for laminar free-convection flow past flat plates. In the present note, the scope of reference [1] is extended to include (*a*) flow with energy dissipation, (*b*) flow with injection or suction, and (*c*) steady flow of an electrically conducting fluid in the presence of a magnetic field.

To save space, the nomenclature of [1] is used in the following analysis with occasional introduction of new symbols.

Analysis

Flow With Energy Dissipation. If the energy dissipation is taken into account, the energy equation becomes

$$\frac{\partial G}{\partial t} + u\frac{\partial G}{\partial x} + v\frac{\partial G}{\partial y} = \frac{1}{\sigma}\frac{\partial^2 G}{\partial y^2} + \lambda\left(\frac{\partial u}{\partial y}\right)^2 \tag{1}$$

where $\lambda = g\beta L/c$ and c is the specific heat capacity of the fluid. Introducing f, θ, and η, equation (1) reduces to

$$\frac{1}{\sigma}\theta'' - (a_2\eta - a_5 f)\theta' - (a_6 + a_7 f')\theta + a_{16}\lambda(f'')^2 = 0 \tag{2}$$

where

$$a_{16} = \phi_1^2\phi_2^2/G_w$$

Thus, in order that similarity solutions exist, a_{16} must also be a constant, i.e.,

$$G_w \propto \phi_1^2\phi_2^2 \tag{3}$$

Relation (3) can be combined with equation (16) of reference [1] to yield the condition

$$\phi_2 \propto \phi_1 \tag{4}$$

Therefore only those cases of [1] with $\phi_2 \propto \phi_1$ are valid when energy dissipation is included. They are Case 3, and Case 5 with $a_5 = 0$ (or Case 6 with $p = -2$).

Flow With Injection or Suction. If there is a distribution of injection or suction at the wall with velocity $\bar{v}_w(\bar{x}, \bar{t})$ perpendicular to the wall, the boundary conditions in terms of f and η at the wall must be

$$f'(0) = 0 \tag{5}$$

$$-\left(\frac{\partial\phi_2}{\partial x}\right)f(0) = v_w(x, t) \tag{6}$$

In order that the condition (6) be admissible, the following relation must hold:

$$v_w \propto \frac{\partial\phi_2}{\partial x} \tag{7}$$

Thus all the cases in reference [1] are valid provided that the velocity $\bar{v}_w$ is such that condition (7) holds. This general conclusion would be of value in investigating the effect of injection or suction on free convection. A special case where $G_w \propto x^n$ has been treated recently is by Eichhorn [2].

If energy dissipation is considered, only Case 3 of reference [1] is compatible.

Magnetohydrodynamic Flow. Consider the steady flow of an electrically conducting fluid with a magnetic field of strength $\bar{H}(\bar{x})$ imposed in the $\bar{y}$-direction. In addition to the usual assumptions of constant properties and freedom from excessive charges, the induced magnetic field is regarded as negligible and the electrical field is assumed to be zero [3]. Under these conditions, the momentum and energy equations become

$$u\frac{\partial u}{\partial x} + v\frac{\partial u}{\partial y} = G + \frac{\partial^2 u}{\partial y^2} - \Omega H^2 u \tag{8}$$

$$u\frac{\partial G}{\partial x} + v\frac{\partial G}{\partial y} = \frac{1}{\sigma}\frac{\partial^2 G}{\partial y^2} + \lambda\left(\frac{\partial u}{\partial y}\right)^2 + \lambda\Omega H^2 u^2 \tag{9}$$

where

$$H = \bar{H}/\frac{\nu}{L}\left(\frac{\rho}{\mu_e}\right)^{1/2} \tag{10}$$

$$\Omega = \sigma_e\mu_e\nu \tag{11}$$

μ_e and σ_e are, respectively, the magnetic permeability and electric conductivity. The rationalized MKS system is employed.

In terms of f, θ, and η, equation (8) and (9) can be written as

$$f''' + a_5 ff'' - (a_4 + a_6)(f')^2 + a_7\theta - a_{17}\Omega f' = 0 \tag{12}$$

$$\frac{1}{\sigma}\theta'' + a_5 f\theta' - a_7 f'\theta + a_{16}\lambda(f'')^2 + a_{18}\lambda\Omega(f')^2 = 0 \tag{13}$$

where $a_{17} = H^2/\phi_1^2$ and $a_{18} = a_{16}a_{17}$.

If energy dissipation is neglected, we must have a_{17} as a constant, i.e.,

$$H \propto \phi_1 \tag{14}$$

Thus all the steady cases in reference [1] are applicable provided that the imposed magnetic field satisfies relation (14). A special case where G_w is constant has been obtained by Gupta [3].

If energy dissipation is to be considered, a_{16} must also be a constant. This then limits the possibilities down to Case 3 of reference [1] only.

If injection or suction exists, $\bar{v}_w(\bar{x})$ must again satisfy $v_w \propto d\phi_2/dx$.

---

[1] Graduate Assistant, Department of Mechanical Engineering, Case Institute of Technology, Cleveland, Ohio.

[2] Numbers in brackets designate References at end of Note.

Manuscript received by ASME Applied Mechanics Division, November 30, 1960.

References

1 K.-T. Yang, "Possible Similarity Solutions for Laminar Free Convection on Vertical Plates and Cylinders," JOURNAL OF APPLIED MECHANICS, vol. 27, TRANS. ASME, vol. 82, Series E, 1960, pp. 230–236. See also discussion of this paper in March, 1961, issue of the JOURNAL OF APPLIED MECHANICS, pp. 153–154.

2 R. Eichhorn, "The Effect of Mass Transfer on Free Convection," *Journal of Heat Transfer*—TRANS. ASME, vol. 82, Series C, 1960, pp. 260–263.

3 A. S. Gupta, "Steady and Transient Free Convection of an Electrically Conducting Fluid From a Vertical Plate in the Presence of a Magnetic Field," *Applied Science Research*, Section A, vol. 9, 1960, pp. 319–333.

A Single Formula for the "Law of the Wall"

D. B. SPALDING[1]

Summary

It is shown that experimental velocity distributions may be well fitted, in the laminar sublayer, the transition region, and the turbulent core, by the formula:

$$y^+ = u^+ + 0.1108\{e^{0.4u^+} - 1 - 0.4u^+ - (0.4u^+)^2/2! - (0.4u^+)^3/3! - (0.4u^+)^4/4!\}$$

Omission of the $(0.4u^+)^4$ term gives an equally good fit. The corresponding expressions for the ratio of turbulent shear stress to total shear stress agree with the measurements of Laufer [8][2] quite closely.

Nomenclature

u = time-mean velocity of fluid in x-direction
u^+ = $u\sqrt{\rho/\tau}$
x = distance along the wall in the direction of flow
y = distance from the wall
y^+ = $y\sqrt{\tau\rho}/\mu_{molecular}$
ϵ^+ = $\mu_{total}/\mu_{molecular}$
$\mu_{molecular}$ = absolute viscosity of fluid in laminar motion
μ_{total} = ratio of shear stress to gradient of time-mean velocity
μ_{turb} = $\mu_{total} - \mu_{molecular}$
ρ = density of fluid
ϕ = density of fluid divided by density of fluid adjacent to wall
τ = shear stress in fluid, assumed independent of y

Introduction

Purpose of note. Numerous formulas have been proposed to describe the universal turbulent velocity profile, called by Coles [1] the "law of the wall." The present note discloses a new formula which is valid over the whole range of dimensionless distance y^+.[3] The new formula has a form which, on the one hand, permits analytical determination of several important boundary-layer parameters, and, on the other, may provide the vantage point for a new look at the theory of the turbulent boundary layer. These matters are only touched on briefly in the following.

The universal turbulent velocity profile. Prandtl's [12] postulate, that the velocity in the neighborhood of a wall should obey the relation:

$$u^+ = u^+(y^+) \tag{1}$$

has been confirmed experimentally by Nikuradse [10], and subsequently by many other authors.

The experimental relation has been described analytically in various ways, some of which are listed in Table 1. It will be noted that all the authors mentioned, except Reichardt [15] and van Driest [19], have found it necessary to use at least two expressions, valid for different ranges of y^+, in order to describe the profile adequately.

Table 1 Formulas for the "law of the wall"[a]

Author	Range of validity	Formulas
Prandtl [11][b]	$0 \leqslant y^+ < 11.5$	$u^+ = y^+$
Taylor [18][a]	$11.5 \leqslant y^+$	$u^+ = 2.5 \ln y^+ + 5.5$
von Karman [7]	$0 \leqslant y^+ < 5$	$u^+ = y^+$
	$5 \leqslant y^+ < 30$	$u^+ = 5 \ln y^+ - 3.05$
	$30 \leqslant y^+$	$u^+ = 2.5 \ln y^+ + 5.5$
Reichardt [15]	$0 \leqslant y^+$	$u^+ = 2.5 \ln (1 + 0.4y^+) + 7.8\{1 - e^{-y^+/11} - (y^+/11)e^{-0.33y^+}\}$
Deissler [2]	$0 \leqslant y^+ < 26$	$u^+ = \int_0^{y^+} \frac{dy^+}{1 + n^2u^+y^+(1 - e^{-n^2u^+y^+})}$, $n = 0.124$
	$26 \leqslant y^+$	$u^+ = 2.78 \ln y^+ + 3.8$
van Driest [19]	$0 \leqslant y^+$	$u^+ = \int_0^{y^+} \frac{2dy^+}{1 + \{1 + 0.64y^{+2}[1 - \exp(-y^+/26)]^2\}^{1/2}}$
Rannie [13]	$0 \leqslant y^+ < 27.5$	$u^+ = 14.54 \tan h(0.0688y^+)$
	$27.5 \leqslant y^+$	$u^+ = 2.5 \ln y^+ + 5.5$

[a] See also Hofmann [5], Reichardt [14], Rotta [16], Miles [9], Elrod [3], and Frank-Kamenetsky [21].

[b] These authors did not, at the dates in question, state the formulas attributed to them in the table. However, they did introduce the idea of a sharp division between a laminar sublayer and a fully turbulent core; when compared with experimental data, this idea leads directly to the formulas given.

The problem. A single formula, expressing the $u^+(y^+)$ relation over the whole range of the variables, is both more satisfying aesthetically and more convenient practically than the two-point formulas of Table 1. However, Reichardt's formula is rather complex in form, whereas van Driest's involves a quadrature requiring numerical evaluation. There is need for a simpler, easily evaluated formula.

Such a formula would preferably fit the experimental data closely, contain sufficient adjustable constants to permit modification in the light of new experimental data, and have an analytical form permitting easy integration of the various functions of the velocity distribution which arise in, for example, the theory of heat transfer through a turbulent boundary layer.

Looked at mathematically, our problem is to establish a formula which:

(i) passes through the point: $y^+ = 0$, $u^+ = 0$;
(ii) is tangential at this point to: $u^+ = y^+$;
(iii) is asymptotic at large y^+ to:[4]

$$u^+ = 2.5 \ln y^+ + 5.5 \tag{2}$$

(iv) fits the experimental points at intermediate y^+ values.

[1] Professor of Heat Transfer, Department of Mechanical Engineering, Imperial College of Science and Technology, London, England.

Manuscript received by ASME Applied Mechanics Division, March 8, 1961.

[2] Numbers in brackets indicate References at end of Note.

[3] See Nomenclature at beginning of Note.

[4] Here the most popular constants for the logarithmic velocity profile have been accepted.

The New "Law of the Wall"

The simplest $y^+(u^+)$ relation. The previous efforts to find a single formula fitting the foregoing specification u^+ has been sought explicitly in terms of y^+. There is, however, no need to demand this; a relation giving y^+ explicitly in terms of u^+ is just as good, and indeed may even be better for some purposes.

Once this possibility is recognized, progress can be made swiftly. We now seek a $y^+(u^+)$ relation such that

$$\text{near } u^+ = 0: y^+ = u^+ \tag{3}$$

$$\text{and at large } u^+: y^+ = 0.1108 e^{0.4u^+} \tag{4}$$

the latter equation being derived directly from equation (2).

The equation which immediately suggests itself is:

$$y^+ = u^+ + 0.1108(e^{0.4u^+} - 1 - 0.4u^+) \tag{5}$$

This satisfies requirements (3) and (4). Does it also fit the experimental data? This can be judged by reference to Fig. 1, which contains the experimental data of Laufer [8]. Evidently, equation (5) fits the data fairly well, but gives values of u^+ which are approximately 10 per cent low when y^+ lies between 10 and 50. Fig. 1 also contains, as broken curves, the asymptotic expressions (2) and (3).

Improved $y^+(u^+)$ relations. If we define a dimensionless "total" (i.e., "molecular plus turbulent" viscosity) ϵ^+ by

$$\epsilon^+ = \mu_{\text{total}}/\mu_{\text{molecular}} \tag{6}$$

then the assumption that the shear stress is independent of distance from the wall, when combined with the definitions of u^+ and y^+, leads to the relation:

$$\epsilon^+ = \frac{dy^+}{du^+} \tag{7}$$

Equation (5) therefore implies the $\epsilon^+(u^+)$ relation:

$$\epsilon^+ = 1 + 0.4 \times 0.1108(e^{0.4u^+} - 1)$$

$$= 1 + 0.04432\left\{0.4u^+ + \frac{(0.4u^+)^2}{2!} + \ldots\right\} \tag{8}$$

Now there are theoretical reasons (Reichardt, [15]; Hinze, [4]) against a growth of ϵ^+ in the wall region with a power of y^+ which is less than 3, if the shear stress varies along the wall, and less than 4 if there is no such variation. Equation (8) satisfies neither requirement.[6] However, it is easy to see what must be done to the velocity distribution if either of these requirements is to be satisfied: the distribution formula becomes, respectively:

$$y^+ = u^+ + 0.1108\left\{e^{0.4u^+} - 1 - 0.4u^+ - \frac{(0.4u^+)^2}{2!} - \frac{(0.4u^+)^3}{3!}\right\} \tag{9}$$

or

$$y^+ = u^+ + 0.1108\left\{e^{0.4u^+} - 1 - 0.4u^+ - \frac{(0.4u^+)^2}{2!} - \frac{(0.4u^+)^3}{3!} - \frac{(0.4u^+)^4}{4!}\right\} \tag{10}$$

Curves corresponding to equations (9) and (10) are plotted in Fig. 1. They fit the experimental data rather better than does equation (5), but it is not possible to say which of the two gives the more precise fit. Whether the $(0.4u^+)^4$ term should be included or not will therefore probably have to be decided on other grounds.

[6] Nor, incidentally, do the expressions of Reichardt and van Driest which appear in Table 1.

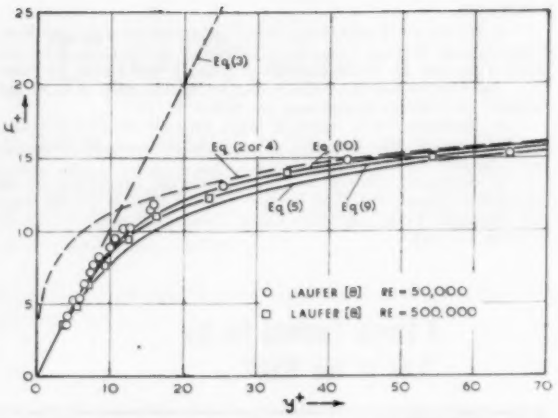

Fig. 1 Experimental data of Laufer [8] for velocity distribution near the wall in turbulent pipe flow, compared with various analytical expressions

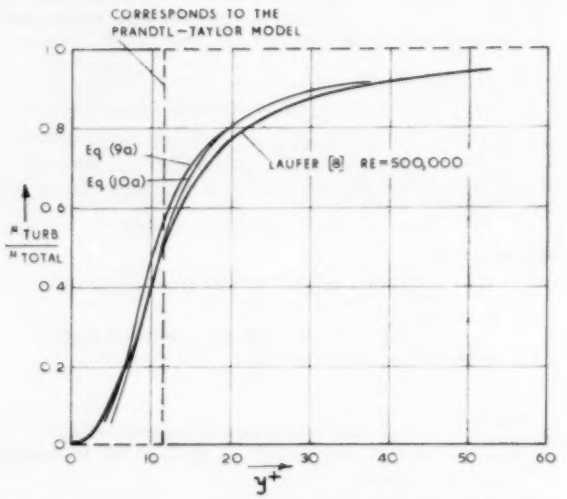

Fig. 2 Experimental data of Laufer on turbulent-stress distribution near the wall in turbulent pipe flow, compared with various analytical expressions

Laufer [8] has also made measurements of the ratio of the turbulent shear stress divided by the total shear stress near the wall. His measurements in a pipe flow, of Reynolds number 500,000, are shown in Fig. 2 as a bold line; y^+ is the abscissa and the viscosity ratio $\mu_{\text{turb}}/\mu_{\text{total}}$ is the ordinate. Also drawn in Fig. 2 are the corresponding relations deduced from equations (9) and (10). These are, respectively:

$$\frac{\mu_{\text{turb}}}{\mu_{\text{total}}} = 1\Big/\left[1 + 1/0.04432\left\{e^{0.4u^+} - 1 - 0.4u^+ - \frac{(0.4u^+)^2}{2!}\right\}\right] \tag{9a}$$

and

$$\frac{\mu_{\text{turb}}}{\mu_{\text{total}}} = 1\Big/\left[1 + 1/0.04432\left\{e^{0.4u^+} - 1 - 0.4u^+ - \frac{(0.4u^+)^2}{2!} - \frac{(0.4u^+)^3}{3!}\right\}\right] \tag{10a}$$

Comparison of these relations with the experimental curves shows that the former equation gives the better fit at low y^+, while the latter gives the better fit at high y^+. However, it is probable that both curves can be regarded as equally satisfactory when experimental scatter is taken into account.

Also plotted in Fig. 2, as a broken steplike curve, is the μ_{turb}/μ_{total} distribution which corresponds to the assumption of a sharp boundary between a laminar sublayer and a fully turbulent outer region. Clearly this gives a very poor representation of the data.

Further possible improvements. Equation (10) fits the requirement that ϵ^+ increases with the fourth power of u^+, and so of y^+, close to the wall. However, even if this is correct, there is no reason why the first nonzero term of the expansion should happen to be that which appears in the expansion of $0.1108e^{0.4u^+}$. In other words, it may be that further terms should appear inside the braces of equations (9) and (10) which have the effect of only partially canceling the corresponding terms in the exponential expansion. Discussion of such further developments will be deferred to a later publication.

Discussion

Practical use of the new formula. Fig. 1 shows that equations (9) or (10) can be used to represent the "law of the wall" within the accuracy of the experimental data. Moreover, as just noted, the general form of these equations is sufficiently flexible to accommodate any further modifications of constants which experiment shows to be necessary. Of course, the constants 0.4 and 0.1108 must not be regarded as sacrosanct.

It should also be noted that the form of the equations is very suitable for analytical work involving such expressions as $\int u^+ dy^+$; for this integral can be written as $\int u^+(dy^+/du^+)du^+$, which can be evaluated in closed form, since dy^+/du^+ is easily obtained by differentiating the $y^+(u^+)$ relation. The way is therefore open to the analytical derivation of drag laws, for example, without the approximations which are usually introduced (e.g., "seventh-power" profiles). These possibilities will be elaborated elsewhere. (See, for example, Spalding [17].)

Theoretical implications. Equations (9) and (10) are presented solely as useful interpolation formulas; they are not based on any postulated mechanism of turbulent transport. Nevertheless, they provoke certain questions which it may be profitable to investigate further. Some of these will now be listed.

(i) Does (10), for example, satisfy a differential equation in which u^+ and y^+ appear *only* as differentials?

The answer is readily seen; it is:

$$\frac{d^3y^+}{du^{+3}} = 0.4\,\frac{d^2y^+}{du^{+2}} \tag{11}$$

Similarly, equation (5) satisfies the differential equation:

$$\frac{d^3y^+}{du^{+3}} = 0.4\,\frac{d^2y^+}{du^{+2}} \tag{12}$$

(ii) Such differential equations are reminiscent of those derived by Prandtl [12] and von Karman [7] as starting points for the logarithmic velocity profile. Can a physical significance be attached to these equations? Could they have been derived by postulation of a physical model followed by dimensional analysis?

(iii) The von Karman differential equation is derived from the consideration that the local "mixing length" must be related to local values of $(\partial u/\partial y)$, $(\partial^2 u/\partial y^2)$, and so forth. Is there any reason why u should have been chosen as dependent and y as independent variable in this analysis, other than the irrelevant one that we happen to perform experiments by fixing the position of the Pitot tube first and then taking the reading? If not, a relation of the mixing length to $(\partial y/\partial u)$, $(\partial^2 y/\partial u^2)$, and so on, is equally valid.

(iv) When the density varies such that density ratio ϕ is a known function of u^+, is it reasonable to calculate the velocity profile from a suitably modified version of (11)? This would run:

$$\frac{d^3y^+}{du^{+3}} = 0.4\phi(u^+)\cdot\frac{d^2u^+}{du^{+2}} \tag{13}$$

which can be evaluated by numerical quadrature without difficulty. This thought might lead to more[6] satisfactory theories of friction and heat transfer in compressible boundary layers. If equation (13) is not as suitable a starting point for analysis as that, for example, of van Driest [20], what is the physical reason for this?

It is not intended to suggest answers to these questions here. They are put forward solely to provoke thought and criticism.

Conclusions

(*a*) Formulas have been presented [equations (9) and (10)] which represent adequately the experimental data for the universal turbulent velocity profile when the viscosity and density of the fluid are uniform.

(*b*) The formulas are flexible enough to permit further adjustment of constants in the light of new experimental data, and simple enough in form to permit analytical integration in important cases of interest.

(*c*) The formulas represent y^+ explicitly in terms of u^+ instead of vice versa. It appears possible that other aspects of turbulent boundary-layer analysis may be profitably re-examined with velocity as the independent variable.

Acknowledgment

The author expresses his gratitude to Prof. J. O. Hinze of Delft, Holland, for his helpful comments on an earlier draft of this Note.

References

1 D. Coles, "The Law of the Wake in the Turbulent Boundary Layer," *Journal of Fluid Mechanics*, vol. 1, 1956, pp. 191–226.

2 R. G. Deissler, "Analysis of Turbulent Heat Transfer, Mass Transfer and Friction in Smooth Tubes at High Prandtl and Schmidt Numbers," NACA Tech. Rep. 1210, 1955 (supersedes NACA Tech. Note 3145, 1954).

3 H. G. Elrod, "Note on the Turbulent Shear Stress Near a Wall," *Journal of the Aeronautical Sciences*, vol. 24, 1957, p. 468.

4 J. O. Hinze, "Turbulence," McGraw-Hill Book Company, New York, N. Y., 1959, p. 472.

5 E. Hofmann, *Forschung a.d. Geb. Ing.*, vol. 11A, 1940, p. 159.

6 T. von Karman, "Mechanische Ähnlichkeit u. Turbulenz," *Nachr. Ges. der Wiss. Göttingen, Math. Phys. Klasse*, vol. 58, 1930.

7 T. von Karman, "The Analogy Between Fluid Friction and Heat Transfer," Trans. ASME, vol. 61, 1939, pp. 705–710.

8 J. Laufer, "The Structure of Turbulence in Fully Developed Pipe Flow," NACA Tech. Rep. 1174, 1954.

9 J. W. Miles, *Journal of the Aeronautical Sciences*, vol. 24, 1957, p. 704.

10 J. Nikuradse, "Gesetzmässigkeiten der turbulenten Strömung in glatten Rohren," *Forschung a.d. Geb. Ing.*, No. 356, 1932.

11 L. Prandtl, "Eine Beziehung zwischen Wärmeaustausch und Strömungswiderstand der Flüssigkeit," *Z. Physik*, vol. 11, 1910, pp. 1072–1078.

12 L. Prandtl, "Über die ausgebildete Turbulenz," *Z. für angew. Math. Mech.*, vol. 5, 1925, p. 136.

13 W. D. Rannie, "Heat Transfer in Turbulent Shear Flow," *Journal of the Aeronautical Sciences*, vol. 23, 1956, p. 485.

14 H. Reichardt, "Die Wärmeübertragung in turbulenten Reibungschichten," *Z. angew. Math. Mech.*, vol. 20, 1940, p. 297.

15 H. Reichardt, "Vollständige Darstellung der turbulenten Geschwindigkeitsverteilung in glatten Leitungen," *Z. angew. Math. Mech.*, vol. 31, 1951, pp. 208–219.

16 J. Rotta, *Ing.-Archiv.*, vol. 18, 1950, p. 277.

17 D. B. Spalding, "Heat Transfer to a Turbulent Stream From a Surface With a Step-Wise Discontinuity in Wall Temperatures," paper to be presented at the joint ASME-I. Mech. E. Heat Transfer Conference, Boulder, Colo., August 28–September 1, 1961.

[6] Or, of course, less.

18 G. I. Taylor, "Conditions at the Surface of a Hot Body Exposed to the Wind," Brit. Aero. Res. Comm. R&M No. 272, 1916, p. 423.
19 E. R. van Driest, "On Turbulent Flow Near a Wall," *Journal of the Aeronautical Sciences*, vol. 23, 1956, p. 1007.
20 E. R. van Driest, "Turbulent Boundary Layer in Compressible Fluids," *Journal of the Aeronautical Sciences*, vol. 18, 1951, p. 145.
21 D. A. Frank-Kamenetsky, "Diffusion and Heat Exchange in Chemical Kinetics," Princeton University Press, 1955, p. 184. First published in the USSR, 1947.

On Classical Normal Modes of a Damped Linear System

MORRIS MORDUCHOW[1]

IT HAS BEEN essentially shown by Rayleigh [1][2] that if the damping matrix of a linear vibrating system is a linear combination of the stiffness and inertia matrices, then the damped system will have principal modes which are exactly the same as those of the undamped system. Caughey [2] has recently developed more general conditions for the existence of classical normal modes with damping, including the above condition as a special case. In both [1] and [2], the analysis is based on the use of normal co-ordinates. The purpose of this Note is to demonstrate Rayleigh's condition (equation (2) below) in a straightforward manner without the use of normal co-ordinates and hence without assuming a knowledge of the theory associated with transformations to such co-ordinates. This procedure, in addition to being instructive, will also lead to explicit results for the damping factor and natural frequency in any principal mode, and will be seen to yield some interesting implications. Finally, the method of analysis given here will be applied to a vibrating beam with simultaneous internal and external damping.

Let a dynamical system be governed by the equations

$$[m]\{\ddot{h}\} + [c]\{\dot{h}\} + [k]\{h\} = 0 \tag{1}$$

where $[m]$, $[c]$, and $[k]$ are square (inertia, damping, and stiffness, respectively) matrices of order n. Moreover, suppose

$$[c] = a[m] + b[k] \tag{2}$$

where a and b are any constants. To solve equations (1), let

$$\{h\} = \{H\}e^{pt} \tag{3}$$

where $\{H\}$ is independent of the time t, and p is a constant. Then, if equation (2) holds, equation (1) reduces to

$$\left([m] + \left(\frac{1 + bp}{p^2 + ap}\right)[k]\right)\{H\} = 0 \tag{4}$$

Equation (4) is seen to be the same as the equation for no damping ($a = b = 0$), but with $(1/p^2)$ replaced by $(1 + bp)/(p^2 + ap)$. Hence the characteristic normalized vectors $\{H\}$ with damping will be the same as those without the damping. Moreover, if in the kth mode without damping $p_k^2 = -\omega_{k_0}^2$ (where ω_{k_0} denotes the undamped natural frequency in the kth mode), then for the kth mode with damping

$$\frac{1 + bp_k}{p_k^2 + ap_k} = -\frac{1}{\omega_{k_0}^2} \tag{5}$$

Thus

$$p_k = -d_k \pm i\omega_k \tag{6a}$$

where

$$d_k = \frac{a + \omega_{k_0}^2 b}{2}, \quad \omega_k = \omega_{k_0}\left[1 - \left(\frac{d_k}{\omega_{k_0}}\right)^2\right]^{1/2} \tag{6b}$$

Equations (6a, b) give the damping factor d_k and the natural frequency ω_k for any principal mode with damping when condition (2) holds. In the latter case, in fact, a necessary and sufficient condition for *dynamic stability* of the system is that

$$a + \omega_{k_0}^2 b \geq 0 \tag{7}$$

for *each* undamped natural frequency ω_{k_0}. [It is interesting to note that (7) can be satisfied even in cases when either a or b (but not both) is negative. Equations (3) through (6b) are valid whether [c] is positive definite or not.]

Consider, finally, a *beam* subjected to an external damping load $f(x)\partial Y/\partial t$ and an internal damping load $(g/\omega)\partial/\partial t(EIY'')''$ (cf., e.g., [3]) per unit length, where $' \equiv \partial/\partial x$. Moreover, suppose $f(x) = c\rho(x)$, where c is a constant,[3] and $\rho(x)$ is the mass per unit length of the beam. Let $Y(x, t) = y(x)e^{pt}$. Then the equation for the free bending vibrations reduces to:

$$(EI(x)y'')'' + \rho(x)\left(\frac{cp + p^2}{1 + \frac{g}{\omega}p}\right)y = 0 \tag{8}$$

Hence the principal mode shapes $y(x)$ will be the same as without any damping, and the value of p in any mode will be such that

$$\frac{cp + p^2}{1 + \frac{g}{\omega_k}p} = -\omega_{k_0}^2 \tag{9}$$

where ω_{k_0} is the undamped natural frequency in the kth mode. Setting $p = -d_k + i\omega_k$, equation (9) implies

$$d_k = \frac{c}{2} + \frac{g}{2}\frac{\omega_{k_0}^2}{\omega_k} \tag{10a}$$

where

$$4\omega_k^4 + (c^2 - 4\omega_{k_0}^2)\omega_k^2 + 2cg\omega_{k_0}^2\omega_k + g^2\omega_{k_0}^4 = 0 \tag{10b}$$

To first powers of g,

$$\omega_k = \omega_{k_0} - \frac{cg}{4}\frac{\omega_{k_0}^2}{\omega_{k_0}^3} \tag{11}$$

where $\omega_{k_0} = [\omega_{k_0}^2 - (c/2)^2]^{1/2}$ = the natural frequency in the kth mode for $g = 0$. In the case of internal damping only ($c = 0$), equations (10a) and (10b) yield:

$$d_k = \frac{g\omega_{k_0}}{\sqrt{2}}\left[1 + (1 - g^2)^{1/2}\right]^{-1/2} = \frac{\omega_{k_0}}{\sqrt{2}}[1 - (1 - g^2)^{1/2}]^{1/2} \tag{12a}$$

$$\omega_k = \frac{\omega_{k_0}}{\sqrt{2}}[1 + (1 - g^2)^{1/2}]^{1/2} \tag{12b}$$

References

1 Lord Rayleigh, "Theory of Sound," vol. 1, Dover Publications, New York, N. Y., pp. 130–131.
2 T. K. Caughey, "Classical Normal Modes in Damped Linear Dynamic Systems," JOURNAL OF APPLIED MECHANICS, vol. 27, Trans. ASME, vol. 82, Series E, June, 1960, pp. 269–271.
3 M. Morduchow, "On Internal Damping of Rotating Beams," NACA Technical Note 1996, December, 1949.
4 M. Morduchow, "On Application of a Quasi-Static Variational Principle to a System With Damping," JOURNAL OF APPLIED MECHANICS, vol. 21, TRANS. ASME, vol. 76, March, 1954, pp. 8–10.

[1] Associate Professor of Applied Mathematics, Polytechnic Institute of Brooklyn, Brooklyn, N. Y.

[2] Numbers in brackets indicate References at end of Note.

Manuscript received by ASME Applied Mechanics Division, March 2, 1961.

[3] In [4] it has been shown that a necessary, as well as sufficient, condition that the mode shapes be entirely unaffected by a damping load of the form $f(x)\partial Y/\partial t$ is that $f(x)$ be proportional to $\rho(x)$.

On Certain Invariants of Symmetric Cartesian Tensors

DAVE PANDRES, JR.[1]

THIS NOTE will define several invariants of a symmetric Cartesian tensor T, which, for certain applications, exhibit advantages over those conventionally used.[2]

We adopt the summation convention and define

$$I_1 = {}^1/_2 T_{ii}$$
$$I_2 = {}^3/_8 (T_{ij}T_{ji} - {}^1/_2 T_{ii}T_{jj})$$
$$I_3 = {}^4/_8 (T_{ij}T_{jk}T_{ki} - T_{ij}T_{ji}T_{kk} + {}^1/_8 T_{ii}T_{jj}T_{kk})$$
$$\theta = {}^1/_2 \arccos I_3/I_2^{3/2}.$$

If, for example, we let T be the stress tensor, then I_1 becomes the mean normal stress, while I_2 and I_3 become essentially the conventional second and third-order invariants of the stress deviation. Since, for an isotropic elastic solid, the stress deviator is proportional to the strain deviator, each invariant of the stress tensor is proportional to the corresponding invariant of the strain tensor—the factor of proportionality depending on the elastic constants of the medium and the order of the particular invariant under consideration (for conventionally defined invariants of the second and third order, no such proportionality exists). In addition, the second invariants of stress and strain (under our definition) become proportional to the density of strain energy of distortion, while the angle θ associated with stress is identical to the strain angle.

The principal values of T are easily seen to be given by

$$\lambda_n = I_1 + I_2^{1/2} \cos (\theta + 2\pi n/3)$$

i.e., by the real parts of

$$Z_n = I_1 + I_2^{1/2} \exp i(\theta + 2\pi n/3)$$

where $n = 1, 2, 3$.

This complex form provides a basis for the graphical construction shown in Fig. 1. The principal values of T may easily be found from this representation as follows:

We locate a point P at a distance I_1 to the right (*left*, if I_1 is negative) of a point O, where both points are on a horizontal straight line. We now draw line segments PQ, PR, and PS of lengths $I_2^{1/2}$ at angles of $2\pi/3$ with one another, and let the angle θ be formed by one of the segments (in this case, PQ) with an extension of the horizontal OP. The principal values of T are now the measured projections along the horizontal line of OQ, OR, and OS—or, as shown in Fig. 1, OQ′, OR′, and OS′.

If T is the stress tensor, this graphical method gives the principal stresses in a form that is especially convenient for the construction of a Mohr diagram.[3]

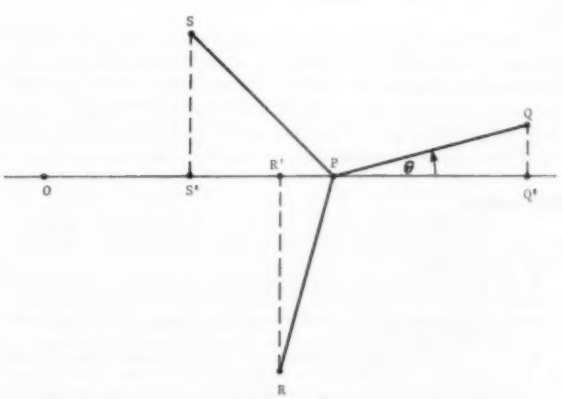

Fig. 1

[1] Associate Research Scientist, The Martin Company, Denver, Colo.

[2] J. B. Hildebrand, "Methods of Applied Mathematics," Prentice-Hall, Inc., New York, N. Y., 1952, p. 53.

Manuscript received by ASME Applied Mechanics Division, September 8, 1960; revised draft, February 24, 1961.

On the Occurrence of Nodal Patterns of Nonparallel Form in Rectangular Orthotropic Plates

N. J. HUFFINGTON, JR.[1]

This note provides a demonstration that an anomalous type of flexural vibration mode, previously discussed only for square isotropic plates, may be expected to occur for rectangular orthotropic plates having a certain ratio of length to width.

Nomenclature

D_1, D_2, D_3 = flexural and twisting rigidities of orthotropic plate
a = length of side of plate parallel to x-axis
b = length of side of plate parallel to y-axis
h = thickness of plate
m = number of nodal lines perpendicular to x-axis, including edge nodes
n = number of nodal lines perpendicular to y-axis, including edge nodes
ρ = mass density of plate material
$\omega_{m,n}$ = circular frequency of m,nth mode

Introduction

Warburton [1][2] has considered the determination of frequencies of free transverse vibrations of isotropic rectangular plates by use of the Rayleigh method and has presented a tabulation of relations for these frequencies for all possible boundary conditions obtained by combining free, simply supported, and fixed edges. He also investigated the occurrence of nonparallel nodal patterns for square and almost square plates. Hearmon [2] extended Warburton's frequency codification to rectangular orthotropic plates with fixed or simply supported edges but omitted any discussion of nonparallel nodal lines. This omission may have resulted from a comment by Warburton [3] that, "unless a plate is isotropic as well as having identical boundary conditions in the x and y-directions, normal modes of nonparallel form cannot exist." In contradiction, this note is intended to show that such normal modes are possible for rectangular orthotropic plates.

Theory

Normal modes with nonparallel nodal lines result from the interaction of a pair of modes each with nodal lines parallel to the sides of the plate, designated m/n and n/m, which have equal or nearly equal frequencies. The interaction modes are designated $m/n \pm n/m$, the relative contribution of the m/n and n/m modes varying with the side ratio a/b.

[2] O. Hoffman and G. Sachs, "Introduction to the Theory of Plasticity for Engineers," McGraw-Hill Book Company, Inc., New York, N. Y., 1953, p. 11.

[1] Chief, Dynamics Research Staff, The Martin Company, Baltimore, Md.

[2] Numbers in brackets indicate References at end of Note.

Manuscript received by ASME Applied Mechanics Division, December 20, 1960.

Since this interaction effect is significant only when the m/n and n/m frequencies are approximately equal, it is important to determine the circumstances under which this occurs. Hearmon [2] has given as his Equation (10) a general expression for the circular frequencies of orthotropic plates[3] which may be restated as

$$\omega_{m,n}^2 = \frac{D_3}{\rho h a^4}\left[\frac{D_1}{D_3} A_{m,n}^4 + \frac{D_2}{D_3}\left(\frac{a}{b}\right)^4 B_{m,n}^4 + 2\left(\frac{a}{b}\right)^2 C_{m,n}\right] \tag{1}$$

where $A_{m,n}$, $B_{m,n}$ and $C_{m,n}$ are given in Hearmon's Table 1 for various boundary conditions. Equating $\omega_{m,n}$ to $\omega_{n,m}$ and noting that, for edge conditions compatible with interaction modes,

$$A_{m,n} = B_{n,m} \qquad A_{n,m} = B_{m,n} \qquad C_{m,n} = C_{n,m},$$

one obtains

$$(A_{m,n}^4 - A_{n,m}^4)\left[\frac{D_1}{D_3} - \frac{D_2}{D_3}\left(\frac{a}{b}\right)^4\right] = 0 \tag{2}$$

Since $A_{m,n} \neq A_{n,m}$ for $m \neq n$, the modes $m/n \pm n/m$ may be expected to occur in the neighborhood of side ratio

$$\frac{a}{b} = \left(\frac{D_1}{D_2}\right)^{1/4} \tag{3}$$

This result is consistent with the occurrence of these modes for square isotropic plates.

The frequencies and mode shapes of normal modes with nonparallel nodal lines may be studied by use of a two-term Ritz approximation using beam eigenfunctions in the manner employed by Warburton [1] for the isotropic case. Such calculations are greatly simplified by use of the tables and formulas of Young and Felger [4, 5]. The results for orthotropic plates are qualitatively similar to those for the isotropic case, the phenomenon of normal modes of nonparallel form occurring for those cases cited by Warburton.

Numerical Example

The two-term Ritz method has been applied to a rectangular plate of orthotropic material, 5-ply maple plywood, for which

$$\frac{D_1}{D_3} = 1.543, \qquad \frac{D_2}{D_3} = 4.810$$

which is clamped on all edges. The first pair of modes of "parallel" type for which the "nonparallel" phenomenon occurs is the 4/2 and 2/4 set. The variations of the frequencies of these modes with side ratio a/b according to Hearmon's analysis, i.e. Equation (1), are depicted in Fig. 1 for a/b in the immediate neighborhood of the value given by Equation (3). Also shown are the frequencies of the real modes $4/2 \pm 2/4$ obtained from the Ritz procedure. It may be seen that there are two distinct frequencies for each value of a/b, and that the interaction effect is localized to the vicinity of the cross-over point of the 4/2 and the 2/4 modes.

The nodal patterns for the $4/2 \pm 2/4$ modes undergo a continuous transition as a/b is varied. For the lower frequency mode, $4/2 - 2/4$, this transition is illustrated in Fig. 2. Beginning with $a/b \ll 0.7526$, only the 2/4 mode is significantly present so that there are two interior nodal lines parallel to the x-axis. As a/b is increased, the contribution of the 2/4 mode decreases and the effect of the 4/2 mode increases until finally, for $a/b \gg 0.7526$, only the 4/2 mode remains and there are two interior nodal lines parallel to the y-axis. The corresponding transition for the higher frequency mode, $4/2 + 2/4$, is depicted in Fig. 3.

[3] The results are restricted to the "specially orthotropic" plate, i.e., one for which the elastic symmetry axes are parallel or normal to the edges of the plate.

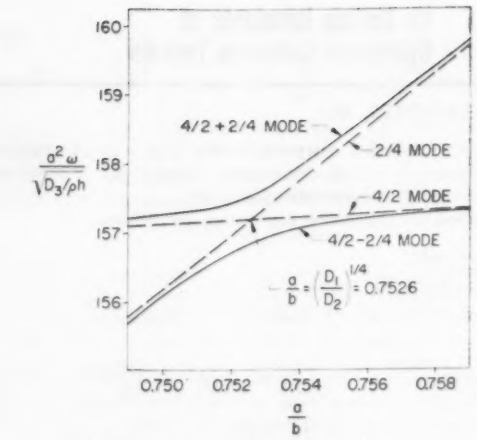

Fig. 1 Variation of frequency with a/b

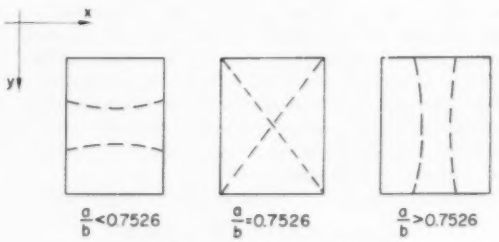

Fig. 2 Nodal patterns for mode 4/2 — 2/4

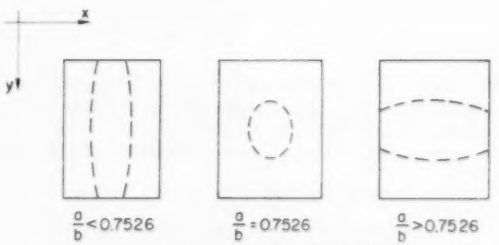

Fig. 3 Nodal patterns for mode 4/2 + 2/4

It should be observed that, for practical purposes, Hearmon's frequency relation is quite adequate. For the numerical example, the greatest discrepancy is only 0.22 per cent. Thus the only criticism of the Rayleigh method is that it is inadequate to predict the phenomenon of normal modes with nonparallel nodal patterns and their associated strain distributions.

References

1 G. B. Warburton, "The Vibration of Rectangular Plates," Proceedings of The Institution of Mechanical Engineers, vol. 168, 1954, pp. 371-384.

2 R. F. S. Hearmon, "The Frequency of Flexural Vibration of Rectangular Orthotropic Plates With Clamped or Supported Edges," Journal of Applied Mechanics, vol. 26, Trans. ASME, vol. 81, Series E, 1959, pp. 537-540.

3 G. B. Warburton, Discussion of: W. H. Hoppmann, II, and L. S. Magness, "Nodal Patterns of the Free Flexural Vibrations of Stiffened Plates," Journal of Applied Mechanics, vol. 25, Trans. ASME, vol. 80, 1958, pp. 313-314.

4 D. Young and R. P. Felgar, Jr., "Tables of Characteristic Functions Representing Normal Modes of Vibration of a Beam," The University of Texas Publication No. 4913, Engineering Research Series No. 44, 1949.

5 R. P. Felgar, Jr., "Formulas for Integrals Containing Characteristic Functions of a Vibrating Beam," The University of Texas, Bureau of Engineering Research, Circular No. 14, 1950.

Three-Dimensional Bending of a Ring on an Elastic Foundation

D. A. RODRIGUEZ[1]

Introduction

THE THREE-DIMENSIONAL bending of a ring (curved beam in the form of a complete circle) of uniform cross-sectional area and supported on a transverse elastic foundation is treated. Distributed transverse forces (normal to the plane of the ring) acting through the shear center of the beam cross section and distributed twisting moments (about the shear center) are the loadings considered. The foundation affords transverse deflectional restraint proportional to the local transverse deflection of the ring and also affords rotational restraint proportional to the local torsional rotation of the ring cross section.

This idealized mechanical model is depicted schematically in Fig. 1. It is a simplified model which may be used for approximate analysis of rings supported by (or supporting) cylindrical, conical, spherical, and other types of shells of revolution. Such problems are of interest in relation to certain types of interconnect structure for rocket vehicles, and solutions are given herein for a loading system arising in connection with this application.

Equations

The equations of equilibrium for a ring on an elastic foundation are the following:[2,3]

$$\frac{dM}{d\phi} - M_T = Va \tag{1}$$

$$\frac{dM_T}{d\phi} + M = -ma + k_1 a\psi \tag{2}$$

$$\frac{dV}{d\phi} = -pa + k_2 aw \tag{3}$$

The equations of deformation[4] express Hooke's law plus kinematic relations and are as follows:

$$M = -\frac{EI}{a}\left(\frac{1}{a}\frac{d^2w}{d\phi^2} + \psi\right) \tag{4}$$

$$M_T = \frac{GJ_T}{a}\left(\frac{d\psi}{d\phi} - \frac{1}{a}\frac{dw}{d\phi}\right) \tag{5}$$

The quantities ϕ, a, w, ψ, p, m, M, M_T, V are indicated in Figs. 1 and 2. The foundation rotational spring constant is denoted by k_1 and the foundation transverse spring constant is k_2. The moments m and M_T are taken with respect to the shear center of the cross-sectional area. The moment M is with respect to the centroid and w is the deflection of the centroid. The moment of inertia about the centroid of the cross-sectional area of the ring is denoted by I, the modulus of elasticity of the material by E, and the torsional rigidity of the cross section by J_T.[5]

After appropriate manipulations the following sixth-order differential equation for the torsional rotation ψ in terms of the applied loads is obtained:

$$\frac{d^6\psi}{d\phi^6} + \left(2 - \frac{k_1a^2}{GJ_T}\right)\frac{d^4\psi}{d\phi^4} + \left(1 + \frac{k_1a^2 + k_2a^4}{EI}\right)\frac{d^2\psi}{d\phi^2} - \frac{k_2a^4}{GJ_T}\left(1 + \frac{k_1a^2}{EI}\right)\psi = \left(1 + \frac{EI}{GJ_T}\right)\frac{a^2}{EI}\frac{d^2p}{d\phi^2} - \frac{a^2}{GJ_T}\left(\frac{d^4m}{d\phi^4} - \frac{GJ_T}{EI}\frac{d^2m}{d\phi^2} + \frac{k_2a^4}{EI}m\right) \tag{6}$$

[1] Senior Engineer, Space Systems Operations, Aeronutronic Division of Ford Motor Company, Newport Beach, Calif.

[2] Aeromechanics TN-002 and TN-003, Aeronutronic Division of Ford Motor Company, December, 1959.

[3] E. Volterra studied a related problem but did not consider a foundation affording *rotational* restraint to the curved beam; he dealt only with loading systems which did not involve distributed applied twisting moments. References: "Bending of a Circular Beam Resting on an Elastic Foundation," JOURNAL OF APPLIED MECHANICS, vol. 19, TRANS. ASME, vol. 74, March, 1952, pp. 1–4; "Deflections of Circular Beams on Elastic Foundations Obtained by Methods of Harmonic Analysis," ibid., vol. 20, TRANS. ASME, vol. 75, June, 1953, pp. 227–232; "Bending of Constrained Circular Beams Resting on Elastic Foundation," *Proceedings ASCE*, vol. 79, Separate No. 205, July, 1953.

[4] Shearing deformations produced by transverse shearing forces V are neglected, as is usually done in engineering beam theory. Stresses associated with restraint of warping deformations also are not included.

Manuscript received by ASME Applied Mechanics Division, July 20, 1960; final draft, April 21, 1961.

[5] See S. Timoshenko and J. N. Goodier, "Theory of Elasticity," McGraw-Hill, 1951, p. 264. (In general, J_T is *not* equal to the polar moment of inertia of the cross-sectional area.)

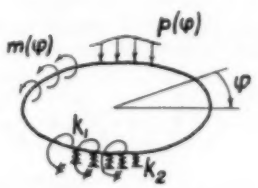

Fig. 1

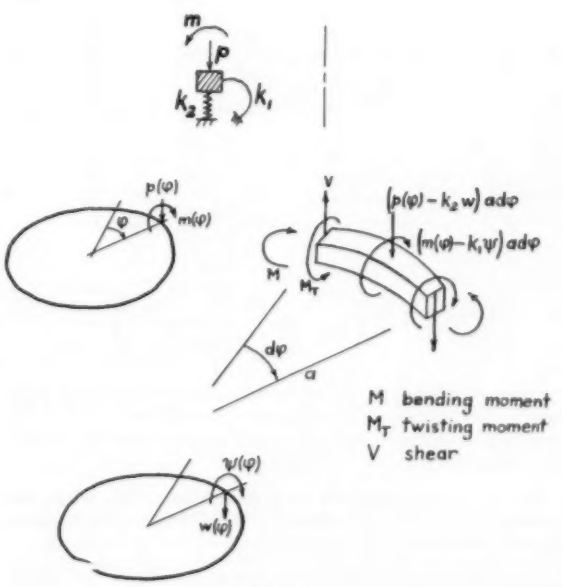

Fig. 2

The transverse deflection w is related to ψ by the following expression:

$$\frac{d^2w}{d\phi^2} = \frac{a}{1 + \dfrac{EI}{GJ_T}} \frac{d^2\psi}{d\phi^2} - \frac{a}{1 + \dfrac{GJ_T}{EI}} \left(1 + \frac{k_1a^2}{EI}\right) \psi + \frac{ma^3}{GJ + EI} \quad (7)$$

Alternatively, one may obtain an *entirely equivalent eighth-order* system of differential equations in which w is given in terms of the applied loads by a sixth-order equation and ψ is then related to w by a second-order expression.

Sinusoidally Distributed Loadings

The following system of loads is of interest in relation to missile interconnect structure:

$$m(\phi) = m_0 \cos \phi$$

$$p(\phi) = -\frac{m_0}{a} \cos \phi \quad (8)$$

Because the ring under consideration is a complete circle, the boundary conditions must express the condition of physical continuity; in other words, the solutions of equations (6) and (7) must be periodic with period 2π. It may be shown that, when the foundation spring constants are *not both* identically zero, there can be no solution of equation (6) involving the solutions of the homogeneous equation (right-hand side set equal to zero) if the periodicity conditions are to be satisfied; that is, the particular solution of the differential equation constitutes the complete solution.[4] The results are

$$\psi = \frac{m_0a^2}{EI + GJ_T} \left(\frac{1}{1 + \dfrac{k_1a^2}{k_2a^4} + \dfrac{k_1a^2}{EI + GJ_T}} \right) \cos \phi \quad (9)$$

$$w = -\frac{m_0a^2}{EI + GJ_T} \left(\frac{k_1a^2/k_2a^4}{1 + \dfrac{k_1a^2}{k_2a^4} + \dfrac{k_1a^2}{EI + GJ_T}} \right) a \cos \phi \quad (10)$$

$$M = -\frac{m_0a \cos \phi}{1 + \dfrac{GJ_T}{EI}} \left(\frac{1 + \dfrac{k_1a^2}{k_2a^4}}{1 + \dfrac{k_1a^2}{k_2a^4} + \dfrac{k_1a^2}{EI + G_T}} \right) \quad (11)$$

$$M_T = -\frac{m_0a \sin \phi}{1 + \dfrac{EI}{GJ_T}} \left(\frac{1 + \dfrac{k_1a^2}{k_2a^4}}{1 + \dfrac{k_1a^2}{k_2a^4} + \dfrac{k_1a^2}{EI + GJ_T}} \right) \quad (12)$$

$$V = m_0 \sin \phi \left(\frac{1 + \dfrac{k_1a^2}{k_2a^4}}{1 + \dfrac{k_1a^2}{k_2a^4} + \dfrac{k_1a^2}{EI + GJ_T}} \right) \quad (13)$$

Interesting limiting cases may be easily obtained from these expressions for various combinations of conditions in which the foundations approach the extremes of complete rigidity or negligible restraint.

(i) For a ring supported on a foundation which offers *only* rotational restraint, $k_2 \to 0$, $k_1 \neq 0$. Taking the limits appropriately, one finds

$$\psi \to 0 \quad (14)$$

$$w \to -\frac{m_0a^2 \cos \phi}{EI + GJ_T} \quad (15)$$

$$M \to -\frac{m_0a \cos \phi}{1 + \dfrac{GJ_T}{EI}} \quad (16)$$

$$M_T \to -\frac{m_0a \sin \phi}{1 + \dfrac{EI}{GJ_T}} \quad (17)$$

$$V \to m_0 \sin \phi \quad (18)$$

It can be shown that these results are entirely identical with those for the case of a ring similarly loaded but *not* supported on an elastic foundation.

(ii) Considering next the converse situation, $k_1 \to 0$, $k_2 \neq 0$, i.e., a ring supported on a foundation which affords restraint against transverse deflection only, one obtains the following limiting values:

$$\psi \to \frac{m_0a^2 \cos \phi}{EI + GJ_T} \quad (19)$$

$$w \to 0 \quad (20)$$

$$M \to -\frac{m_0a \cos \phi}{1 + \dfrac{GJ_T}{EI}} \quad (21)$$

$$M_T \to -\frac{m_0a \sin \phi}{1 + \dfrac{EI}{GJ_T}} \quad (22)$$

$$V \to m_0 \sin \phi \quad (23)$$

It is seen that, in this instance, the bending and twisting moments and the transverse shear are again identical with those for the case of a ring similarly loaded but *unsupported* by an elastic foundation. It may also be demonstrated that the deflections differ only by a "rigid body rotation."

Finally, one may consider the situation in which one or the other of the foundation constants approaches infinity; i.e., the foundation is rigid with respect to the corresponding degree of freedom.

(iii) $k_1 \to \infty$

$$\psi \to 0 \quad (24)$$

$$w \to -\frac{m_0a^3 \cos \phi}{EI + GJ_T + k_2a^4} \quad (25)$$

$$M \to -\frac{m_0a \cos \phi}{1 + \dfrac{GJ_T}{EI} + \dfrac{k_2a^4}{EI}} \quad (26)$$

$$M_T \to -\frac{m_0a \sin \phi}{1 + \dfrac{EI}{GJ_T} + \dfrac{k_2a^4}{GJ_T}} \quad (27)$$

$$V \to \frac{m_0 \sin \phi}{1 + \dfrac{k_2a^4}{EI + GJ_T}} \quad (28)$$

It is seen that, as $k_1 \to 0$, these limits approach the case of a similarly loaded ring with *no* elastic foundation.

[4] Aeromechanics TN-003, Aeronutronic Division of Ford Motor Company, December, 1959, pp. 8–9.

(iv) $k_2 \to \infty$

$$\psi \to \frac{m_0 a^2 \cos\phi}{EI + GJ_T + k_1 a^2} \tag{29}$$

$$w \to 0$$

$$M \to -\frac{m_0 a \cos\phi}{1 + \dfrac{GJ_T}{EI} + \dfrac{k_1 a^2}{EI}} \tag{30}$$

$$M_T \to -\frac{m_0 a \sin\phi}{1 + \dfrac{EI}{GJ_T} + \dfrac{k_1 a^2}{GJ_T}} \tag{31}$$

$$V \to \frac{m_0 \sin\phi}{1 + \dfrac{k_1 a^2}{EI + GJ_T}} \tag{32}$$

As $k_1 \to 0$, these limits approach the case of a similarly loaded ring with no elastic foundation, the deflections differing only by a rigid body rotation.

Pressure-Flow Characteristics of Randomly Oscillating Pipe Flows

C. L. TIEN[1] and J. H. LIENHARD[2]

Introduction

OSCILLATING pipe flows have long presented a special problem in both metering and control. The present Note not only makes a new application of established statistical techniques to a solution of this problem, but gives a simplified spectral transfer function that is numerically tractable as well.

Sexl [1][3] first predicted the flow response of fluid in cylindrical pipes subjected to a cosinsoidal variation in pressure. His mathematical model was a laminar, incompressible, fully developed flow and his results were corroborated by Richardson's experiments [1]. Sexl's hydrodynamic solution was sufficiently complicated, however, that he obtained the mean square of the oscillating velocity only for the two limiting cases of very high and very low frequencies. Since the pressure oscillations of physical systems are not generally of a single frequency as studied by Sexl, but are randomly distributed instead, consideration will now be given to the entire range of frequencies.

Nomenclature

A, B = coefficients defined by comparison of Equation (3) with Equation (4)
a = radius of a pipe
f = normalized spectral density of pressure oscillations
g = normalized spectral density of velocity oscillations
I = a numerical constant equal to Φ evaluated at $n = 0$
K_n = amplitude of the individual pressure oscillations
n = frequency of pressure and velocity oscillations
p = pressure
p_x = axial pressure gradient
R = correlation coefficient
r = radial distance
t = time
u = axial velocity
x = axial distance
η = dimensionless frequency defined in Equation (11)
ν = kinematic viscosity
ξ = variable displacement in time
ρ = fluid density
Φ = spectral transfer function defined in Equation (9)
ω = characteristic frequency of system

General Subscripts

m, relating to the most probable frequency
p, u, relating to pressure and to velocity oscillations
r, t, indicating differentiation with respect to r and t

Analysis

The relation between pressure and velocity oscillations in laminar, incompressible, fully developed, pipe flow are obtained by solving Equation (1):

$$u_t = p_x + \nu\left(u_{rr} + \frac{1}{r}\,u_r\right), \tag{1}$$

where $p_x = -\dfrac{1}{\rho}\dfrac{dp}{dx}$; with boundary conditions $u(a, t) = 0$ and $u_r(0, t) = 0$. If p_x is represented by its Fourier spectrum of cosinsoidal oscillations:

$$p_x = \sum_{n=0}^{\infty} K_n \cos(nt); \tag{2}$$

then the solution to Equation (1) is

$$u(r, t) = \sum_{n=0}^{\infty} \frac{K_n}{n}\left\{\left(1 - \frac{\operatorname{ber}\sqrt{\frac{n}{\nu}}\,a \operatorname{ber}\sqrt{\frac{n}{\nu}}\,r + \operatorname{bei}\sqrt{\frac{n}{\nu}}\,a \operatorname{bei}\sqrt{\frac{n}{\nu}}\,r}{\left(\operatorname{ber}\sqrt{\frac{n}{\nu}}\,a\right)^2 + \left(\operatorname{bei}\sqrt{\frac{n}{\nu}}\,a\right)^2}\right)\sin(nt)\right.$$
$$\left. + \left(\frac{\operatorname{bei}\sqrt{\frac{n}{\nu}}\,a \operatorname{ber}\sqrt{\frac{n}{\nu}}\,r - \operatorname{ber}\sqrt{\frac{n}{\nu}}\,a \operatorname{bei}\sqrt{\frac{n}{\nu}}\,r}{\left(\operatorname{ber}\sqrt{\frac{n}{\nu}}\,a\right)^2 + \left(\operatorname{bei}\sqrt{\frac{n}{\nu}}\,a\right)^2}\right)\cos(nt)\right\} \tag{3}$$

which is of the form:

$$u(r, t) = \sum_{n=0}^{\infty} \frac{K_n}{n}\left[A(r, n)\sin(nt) + B(r, n)\cos(nt)\right], \tag{4}$$

where A and B are defined by comparison with Equation (3).

Application of well-known statistical methods [2] leads to the relationship between the pressure and velocity oscillations as expressed by the following equations in terms of the parameters: $\overline{u^2}$, R_u or g, $\overline{p_x^2}$, and R_p or f:

[1] Assistant Professor of Mechanical Engineering, University of California, Berkeley, Calif.
[2] Associate in Mechanical Engineering, University of California, Berkeley, Calif.
[3] Numbers in brackets indicate References at end of Note.
Manuscript received by ASME Applied Mechanics Division, October 26, 1960.

$$\overline{u^2(r)} = \overline{p_x^2(r)} \int_0^\infty \left[\frac{A^2(r, n) + B^2(r, n)}{n^2}\right] f(r, n)dn; \quad (5)$$

$$f(r, n) = \frac{1}{\pi}\int_{-\infty}^{\infty} R_p(r, \xi)\cos(n\xi)d\xi; \quad (6)$$

$$R_u(r, \xi) = \frac{\overline{p_x^2(r)}}{\overline{u^2(r)}} \int_0^\infty \left[\frac{A^2(r, n) + B^2(r, n)}{n^2}\right] f(r, n)\cos(n\xi)dn; \quad (7)$$

$$g(r, n) = \frac{\overline{p_x^2(r)}}{\overline{u^2(r)}}\left[\frac{A^2(r, n) + B^2(r, n)}{n^2}\right] f(r, n) \quad (8)$$

Central to the evaluation of $\overline{u^2}$ and R_u or g from $\overline{p_x^2}$ and R_p or f, or vice versa, is the evaluation of the "spectral transfer function," Φ, defined as:

$$\Phi \equiv \left[\frac{A^2(r, n) + B^2(r, n)}{n^2}\right]\frac{\nu^2}{a^4}, \quad (9)$$

in which the factor ν^2/a^4 is included to render Φ dimensionless. Equations (5) through (8) are useful only in so far as the complicated function Φ can be put in tractable form. It is possible, however, to construct a very good approximation to Φ for the case of either the center-line or the average velocities. Of these two, the average of velocity across the area of a pipe is of greater physical importance since it is directly proportional to the flow rate. In either case,

$$\Phi = \frac{1 - \exp(-I\eta^2)}{\eta^2}, \quad (10)$$

where I is a numerical constant equal to $^1/_{16}$ in the case of center-line velocities and $^1/_{64}$ in the case of average velocities, and η is a "dimensionless frequency" defined as:

$$\eta \equiv \frac{na^2}{\nu}. \quad (11)$$

The comparison between the exact and approximate expressions for Φ is shown in Fig. 1; the agreement is exact in the two limits: $\eta \to \infty$ and $\eta \to 0$.

The preceding analysis may be repeated for flow in a two-dimensional channel with entirely analogous results. The spectral transfer function is again well represented by Equation (10). In this geometry, I is $^1/_4$ for the center-line velocity and $^1/_9$ for the average velocity, and η is based upon the half-width of the channel instead of a.

An Illustrative Example

The theory developed in the preceding sections will be applied to the specific problem of finding $\overline{u^2}$ and $g(n)$ when $\overline{p_x^2}$ and $f(n)$ have been determined by measurement. The form chosen for $f(n)$ in this illustration will be that of the Maxwell molecular speed distribution:

$$f(n) = \left(\frac{4}{n_m\sqrt{\pi}}\right)\left(\frac{n}{n_m}\right)^2 e^{-(n/n_m)^2}, \quad (12)$$

in which n_m is the most probable frequency. This choice is reasonable from the physical point of view, in that $f(n)$ is finite throughout the range $0 < n < \infty$, and yet vanishes for $n = \infty$ and $n = 0$. A spectral density of imposed pressure oscillations that is very similar in form to Equation (12) has also been observed by Baird and Bechtold [3]. They studied pulsating flow through orifices, however, and the dynamic response of their system was doubtless considerably different from the results obtained here.

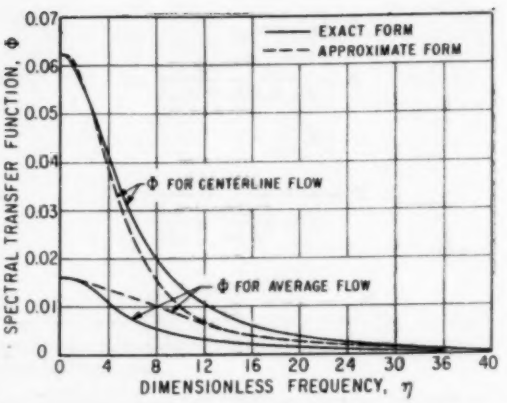

Fig. 1 Exact and approximate forms of Φ for center-line and average pipe flow

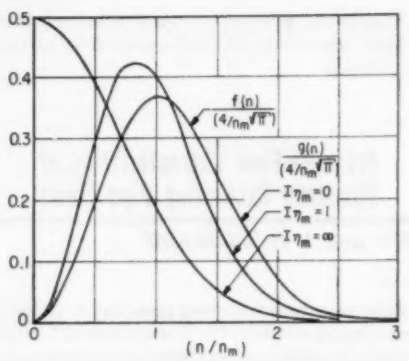

Fig. 2 Velocity response for a Maxwellian spectral density of pressure

Substitution of Equation (12) into Equations (5) through (8) leads to:

$$\overline{u^2} = \overline{p_x^2}\frac{2}{n_m^2}\left[1 - \frac{1}{\sqrt{I\eta_m^2 + 1}}\right], \quad (13)$$

and

$$g(n) = \frac{2}{n_m\sqrt{\pi}}\frac{\sqrt{I\eta_m^2 + 1}}{\sqrt{I\eta_m^2 + 1} - 1}\exp\left(-\left[\frac{n}{n_m}\right]^2\right)\left[1 - \exp\left(-I\eta_m^2\left[\frac{n}{n_m}\right]^4\right)\right]. \quad (14)$$

η_m is a system parameter of some importance, generally defined as:

$$\eta_m \equiv \frac{\omega a^2}{\nu} \quad (15)$$

where ω is the characteristic frequency of the system—in this case, n_m.

The spectral densities of pressure and velocity oscillations as given by Equations (13) and (14) have been nondimensionalized through division by $4/n_m\sqrt{\pi}$ and plotted against n/n_m in Fig. 2. The significance of n_m can now be seen clearly. When the flow is viscous and confined to a small pipe, then η_m becomes very small. In this case, the response tends to duplicate the input as is shown in Fig. 2. When the flow is of low viscosity and contained in a

large pipe, however, the response exhibits an increasing deviation from the input signal, as is shown by the response curves for $I\eta_m = 1$ and ∞. η_m thus appears to play a role in the pulsating flow problem similar to that of the Reynolds number in steady viscous pipe flow.

References

1 H. Schlichting, "Boundary Layer Theory," English translation by J. Kestin, McGraw-Hill Book Company, Inc., New York, N. Y., 1960, pp. 229–231.

2 S. H. Crandall (editor), "Random Vibration," Technology Press of M.I.T., 1958, pp. 77–90.

3 R. C. Baird and I. C. Bechtold, "Dynamics of Pulsative Flow Through Sharp-Edged Restriction," TRANS. ASME, vol. 74, 1952, pp. 1381–1388.

ERRATUM

In the Brief Note by W. R. Schowalter and G. E. Blaker, "On the Behavior of Impact Tubes at Low Reynolds Number," which appeared in the March, 1961, issue of the JOURNAL OF APPLIED MECHANICS, page 136, the three lines beginning with Equation (3) should read:

$$P_{i_{ave}} = p_i - \alpha^2 f(R) \tag{3}$$

where

p_i = impact pressure at the stagnation streamline.

The authors regret this error in the original manuscript.

Journal of APPLIED MECHANICS

Discussion

Information Theory as the Basis for Thermostatics and Thermodynamics[1]

D. E. CHRISTIE.[2] Any program which will make the principles of thermodynamics appear both pertinent and comprehensible to undergraduates surely deserves applause. In this paper the central strategy of theoretical physics, the strategy of exploiting isomorphisms, is used effectively. Exemplifying this strategy in the past, statistical mechanics has provided a motivation for information theory as well as an interpretation for thermodynamics. Now the information theory of Shannon and Jaynes' method of statistical inference by maximum entropy are combined to yield the results of thermostatics and thermodynamics without either the burdensome apparatus of statistical mechanics or the difficult rituals of classical thermodynamics.

With the increasing importance to engineers and scientists of the quantum viewpoint, it is inevitable that the statistical side of thermodynamics should be emphasized in college courses. This does not imply that a full semester of thermodynamics is a prerequisite for the statistical interpretations or even that the statistical part must come last. Many different courses in statistical thermodynamics could meet most of the objections to the traditional pattern. The author's proposal to present statistical thermodynamics as a direct application of information theory raises the questions of whether the subtleties of information theory are less of a pedagogical obstacle than those of introductory statistical physics and of whether the information-theory approach is as instructive as more standard ones. Until the textbook is available, a mild skepticism is probably justified. One should not too readily dismiss the advantages of studying critically macroscopic variables having operational significance.

The interpretation in the paper of reversible heat and work is beguilingly simple, at least until one remembers the complexity of the message i. The generality of this approach to work is somewhat reminiscent of the macroscopic treatment by Brønsted.[3] This brings the writer to the author's remark that thermodynamics is still essentially where Clausius left it. This is possibly true of most textbooks. But many significant modifications have been suggested by, for instance, Carathéodory, Born, and Landsberg.[4] Unfortunately, these reforms have not yet been available in a form to influence significantly the undergraduate curriculum. Also, the recent book of Callen[5] offers a postulational approach which is in tune with modern quantum and statistical physics but preserves the macroscopic emphasis.

R. M. DAVIES.[6] In a thermodynamic system, the particles in the system have a very large number of possible microstates ($10^{10^{20}}$ in a typical size laboratory system). Many of these microstates give rise to macrostates which are measurable by our macroscopic senses or sensing instruments. Some parameters are, for example, pressure, volume, and mol number. Thus, out of the large amount of information contained in the system in any state at any instant, only a small amount is available to us as observers. The question then arises as to how *best* to use this small amount of information to formulate laws which will predict the behavior of the system during or as a result of any process.

Classical thermodynamics does this by accepting as primitive, axioms we call the zeroth, first, second, and third laws of thermodynamics. We may prefer to argue from postulates involving the fundamental particles of the system. These are the author's axioms (a) and (b) (matter is particulate, energy is quantized).

The question now becomes: Given certain macroscopic observations (percepts) and these postulates, how best should we manipulate these data to produce a theory which predicts the behavior of the system; i.e. in our case, which produces first of all the axioms of macroscopic thermodynamics which we are convinced hold, *and* which hopefully will allow further predictions to be made which were not possible without statistical procedures.

The present paper simply and logically accomplishes the first of these and leaves open for further work the second. In addition, the methods outlined in the paper avoid the use of the concepts of phase space and ergodicity which have in the past been found necessary to accomplish this same goal.

---

[1] By Myron Tribus, published in the March, 1961, issue of the JOURNAL OF APPLIED MECHANICS, vol. 28, TRANS. ASME, vol. 83, Series E, pp. 1–8.

[2] Professor of Mathematics, Bowdoin College, Brunswick, Me.

[3] J. N. Brønsted, "Principles and Problems in Energetics," Interscience Publishers, Inc., New York, N. Y., 1955.

[4] For references see P. T. Landsberg, "Foundations of Thermodynamics," *Reviews of Modern Physics*, vol. 28, 1956, pp. 363–392.

[5] H. B. Callen, "Thermodynamics," John Wiley & Sons, Inc., New York, N. Y., 1960.

[6] Formerly, Assistant Professor of Mechanical Engineering, University of Waterloo, Waterloo, Ontario, Canada. Now Lecturer in Mechanical Engineering, University College, London, England.

In the writer's opinion no argument can be made with the author's procedures in this paper once the postulates and the "Jaynes formalism" (the method of manipulating these postulates) are accepted. The writer would like, therefore, to examine this formalism itself.

There are two schools of thought as to the method of handling statistical information in the type of problem which concerns us here. This is the problem in which we argue from a result of an experiment or a measurement of an average to an assignment of probability. The two schools are the objective view of probability in which methods of maximum likelihood are used, and the subjective view of probability used in this paper, in which Jaynes' method of maximizing entropy is used.

The writer would like to show a link between these, which is due to the work of Prof. D. Sprott at the University of Waterloo. This has also been pointed out by Professor Barnard at Imperial College in England.[7]

Essentially, what follows is an indication of the mathematical relationship between the maximum likelihood methods of R. A. Fisher and the maximum entropy methods of E. T. Jaynes.

The following nomenclature will be used:

- n = number of tests or experiments
- x = number of successes or results for which we are looking
- p = probability (treated as a parameter)
- L = likelihood function
- I_s = information of Shannon = S = entropy

Consider an experiment with k possible outcomes with probabilities $p_1 p_2 \ldots\ldots p_k$.

Let

$$L(p_1 \ldots . p_k/x_1 \ldots . x_k) = p_1^{x_1} p_1^{x_2} \ldots p_k^{x_k}$$

The constraints are

$$\begin{cases} \sum_{i=1}^{1} p_i = 1 \\ \sum_{i=1}^{k} x_i = n \end{cases}$$

$$-\log L(p_1 \ldots p_k/x_1 \ldots x_k) = -x_1 \log p_1 - \ldots . - x_k \log p$$

$$= -\sum_{i=1}^{k} x_i \log p_i$$

This is the function which Fisher maximizes to find p_i. Let us take its average value:

$$\langle -\log L(p/x) \rangle = \left\langle -\sum_{i=1}^{k} x_i \log p_i \right\rangle$$

$$= -n \sum_{i=1}^{k} p_i \log p_i$$

$$= nI_s$$

This is the function which Jaynes maximizes to find p_i.

$$\frac{\text{Information}}{\text{Obs}} = -\sum_{i=1}^{k} p_i \log p_i = I_s = S \quad \text{(entropy)}$$

Let us illustrate this relationship by two brief examples.

Jaynes' Method. Maximize S

$$\left.\begin{array}{l} \text{i.e., maximize } \langle -\log L(p/z) \rangle \\ \text{i.e., maximize } -\sum_{i=1}^{k} p_i \log p_i \end{array}\right\} \text{ subject to } \sum_{i=1}^{1} p_i = 1$$

This constraint tells that not all the p_i are independent. Rather than using Lagrange multipliers as the author does, let us in this simple example consider:

$$p_k = 1 - p_1 - p_2 - \ldots\ldots - p_{k-1}$$

$$\text{Maximized: } \frac{\partial \left[-\sum_{i=1}^{k} p_i \log p_i \right]}{\partial p_i}$$

$$= 1 + \log p_i - 1 - \log p_k = 0$$

$$\log p_i = \log p_k$$

$$p_i = p_k$$

$$\sum_{i=1}^{k} p_i = 1 = kp_i$$

$$p_i = \frac{1}{k}$$

Here we have not observed any individual microstate. We have observed the average of a large number of them and the procedure tells us that any one of them is equally probable.

Fisher's Maximum Likelihood Method

$$\text{Maximize } -\log L(p_1 \ldots . p_k/x_1 \ldots . x_k) = \sum_{i=1}^{k} x_i \log p_i$$

$$\frac{\partial(-\log L)}{\partial p_i} = \frac{x_i}{p_i} - \frac{x_k}{p_k} = 0$$

$$\frac{x_i}{p_i} = c \text{ (const)}$$

$$\sum_{i=k}^{k} x_i = c \sum_{i=1}^{k} p_i = c = n$$

$$x_i = np_i$$

$$p_i = \frac{x_i}{n}$$

Here we have observed a unique sample or an individual microstate, and the procedure tells us that probability of seeing that microstate is as observed: x_i/n. Thus, in the author's coin example, the methods of maximum likelihood would give no estimate as to the individual probability of a dime or nickel having a certain outcome since we have observed neither microstate specifically.

Notice that this link can be shown only in the direction from maximum likelihood to maximum entropy. We cannot work in the opposite direction since an averaging procedure is involved which loses information. This indicates, however, that the two theories are not incompatible.

We see that in Fisher's methods we assign probabilities by maximizing the log likelihood based on a specific event having occurred, i.e., from observation of a specific sample or microstate. In Jaynes' method, we assign probabilities by maximizing the average of the log likelihood over a large number of specific events (samples or microstates) on the basis that none of the specific events has been observed, but only the average. If molecular motion were slow enough, and if Heisenberg's uncertainty principle did not hold, then presumably the microstates could be observed and maximum likelihood would be relevant. Here maximizing I_s would lose information.

The objective probability of Fisher is subjective to the extent that one must set up mathematical models mentally, then verify or reject these on the basis of experimentation. In thermody-

[7] *Royal Statistical Society Journal*, sec. B, 12–13, 1950–1951, p. 58.

namics, we cannot perform experiments involving individual microstates. We can only measure averages. Thus our experiments involving microstates must be performed mentally as well. Probability assignments then become quite subjective and the method of Jaynes as used in this paper seems to the writer to be quite reasonable.

Finally, congratulations are due the author on an exceedingly fine piece of work in developing the core of classical thermodynamics on these new foundations. The development is fascinating to pursue since it shows us some familiar relationships in a new light. The author's contribution is unifying in the relations shown among the quantum theory of the physicist, the probability theory of the statistician, and the thermodynamics of the engineer. It is simplifying in the axiomatic and mathematical tools used in comparison with those necessary in previous attempts at the same goal. It is provocative in that it seems probable that these methods might well be useful in future investigations into irreversible thermodynamics, to cite one important example.

Pedagogically, the paper and the author's book, reference [3] of the paper, provide tremendous possibilities in instruction of thermodynamics to engineering students. The writer has found it rewarding indeed to pursue this work in presenting a thermodynamics seminar at the University of Waterloo, where there has been great interest in this new concept. Finally, an undergraduate course has been initiated to follow this approach for Engineering Physics students at Waterloo.

G. M. DUSINBERRE.[8] If one feels somewhat overwhelmed, as the writer often does, by the author's erudition, a convenient antidote is to read a recent comment by Prof. E. E. Drucker of Syracuse University.[9]

In regard to the training of physicists, Drucker says, "Clearly, although quantum mechanics is a fundamental building block in physics, no attempt is made to lay that particular block until the building is at an advanced stage of erection." Of course this does not refute the author's view, it merely states the alternative. But if this alternative is defensible in regard to physicists, how much more so is it in regard to engineers.

Drucker goes on to say, ". . . . pedagogically, it is more desirable in most cases to go from the specific to the general. Certainly our understanding of the physical laws of nature has developed historically in this sense." And further, ". . . . I wish to sound a note of caution to engineering educators to beware that their own level of sophistication does not blind them to the realities of the average student's ability to appreciate the rigorous mathematical niceties."

Besides supporting Drucker's views in general, I would like to register some specific disagreements with the paper.

The author says, "This concept of energy is presumed to be understood from the fields of mechanics, electricity, and magnetism." But electricity itself must wait on the completion of probability theory, matrix algebra, and so on, for an electrical system also "can change its state only in discrete steps." Then is the mechanical engineer to put off thermodynamics until he has completed his electrical studies? And what about the chemical engineer, who needs thermodynamics but usually spends less time on electricity than his mechanical brother?

In his introduction the author asserts, "It is doubtful if more than a small fraction of the students who have studied classical thermodynamics understand it." What do we mean by the word "understand?" If we mean the possession of complete, thorough, infallible knowledge, then *none* of the students and likewise none of us teachers understand it.

Since this is not the meaning, it may be in order to offer an operational and statistical definition. For an engineer to understand a subject means there is only an extremely small "entropy of application"—an extremely small uncertainty as to correct application of the principles of the subject to the work at hand.

Under this definition I will agree that after one semester the average entropy of the students—their probability of making a mistake in practice—is pretty high, maybe 50 per cent. After another semester, by the use of elementary probability principles, we may hope to reduce this to 25 per cent. By the time the man graduates, perhaps 12½ per cent. A little experience in industry reduces this still further.

But perhaps I should not mention industry here. I do not believe the author has industry in mind. I do not see that he has even engineering in mind. He is really meditating on the ideal training for a mathematical physicist.

Undoubtedly we teachers of thermodynamics can improve our performance. But this is not going to be accomplished by making the first thing we teach our undergraduates the latest thing that has been learned by a brilliant Doctor of Philosophy.

FRANK KREITH.[10] Recent advances in engineering, particularly in the fields of rocketry, nuclear power, semiconductors, and direct energy conversion, have brought into focus short comings of conventional thermostatics courses in an up-to-date engineering curriculum. The number of questions posed by inquisitive students which cannot be answered within the framework of thermostatics is becoming embarrassing. Many teachers of engineering thermodynamics have, therefore, become convinced during the past decade that only a treatment which includes the elements of statistical thermodynamics can prepare engineering students for the tasks they will face after graduation in the years ahead.

In view of the pressing need for an approach to thermodynamics which can lay a foundation for engineers to communicate with scientists from various fields in order that they may fully understand advances in science and apply them to the solution of engineering problems, it was inevitable that a new and revolutionary different way of teaching thermodynamics to engineering students had to be found. The method proposed by the author appears to be a step in this direction and seems to meet the needs of a scientifically oriented engineering curriculum.

The reason for this opinion is not merely based on reading this paper which is an abridged version of a textbook by the author (reference [3] of the paper). The textbook has been used in an experimental course in thermodynamics at the University of Colorado during the past semester. Although the experience from a single one-semester course cannot do more than give an indication of the potential of the author's approach, it is worth noting that the students not only seemed to be able to master the material, but actually enjoyed the challenge it offered. Once the instructor (i.e., the writer) was able to overcome his prejudices in favor of conventional thermostatics, the approach suggested by the author made the presentation of the subject material simple because it follows a logical and consistent pattern. The students seemed to learn thermostatics as well as in a conventional course, but also obtained a valuable foundation on which subsequent courses, such as for instance solid-state physics, direct energy conversion, or heat transfer could profitably draw. On the basis of this one experience it seems that the author's method offers new vistas to undergraduate thermodynamics courses in scientifically oriented engineering curriculums.

M. R. EL-SADEN.[11] The author is to be commended on his contribution in this paper to the field of thermodynamics. He has

[8] Department of Mechanical Engineering, The Pennsylvania State University, University Park, Pa. Fellow ASME. (Deceased)

[9] E. E. Drucker, *Journal of Engineering Education*, vol. 51, 1960, p. 133.

[10] Professor of Mechanical Engineering, University of Colorado, Boulder, Colo. Mem. ASME.

[11] Assistant Professor, Department of Mechanical Engineering, The University of Texas, Austin, Texas.

shown in a very simple and direct way that entropy, based on information theory, is a measure of uncertainty, and the mystery surrounding this parameter in classical thermodynamics has been removed. In fact, entropy turns out to be the most primitive among the thermodynamic parameters. Thermal equilibrium is established at a greater depth of meaning. The formulation of the second law and the relation between the entropy change during a process (reversible or irreversible) and the heat exchanged, the optimum work and the actual work in a process are a significant simplification for handling general processes.

This approach in thermodynamics has been used at The University of Texas and has proved to be successful and practical as far as teaching thermodynamics to undergraduate engineering students is concerned. This approach not only accomplishes all the objectives of the classical approach at a better efficiency and greater depth, but it also provides the student with the starting points and the tools that enable him to go on into such fields as rate processes in solid-state physics, plasma dynamics, and thermionic emission. Finally, this approach provides the link between the field of thermodynamics and the more general field of quantum theory.

ALBERT VEINIK.[12] The paper is extremely important in regard to the problem presented and to its solution. The author took upon himself a very difficult task; namely, to put thermostatics and thermodynamics of reversible and irreversible processes on a common methodical basis. The problem was solved in an excellent manner by the author, using the Jaynes' method. On the basis of statistics, the author arrived at the three well-known laws of thermostatics; examined the Carnot theory, open systems and irreversible processes; established the analogy between the equilibrium in thermostatics and the speed of processes in thermodynamics; gave good recommendations for selection of currents and potentials in thermodynamics of irreversible processes.

It is essential to note that the necessity of this work became very clear only recently, when in thermostatics and thermodynamics were accumulated a large number of various applications which were completely unrelated to each other by any theory or method.

In view of such a general (complete) method, permitting us to penetrate deeper into the observed physical phenomena, the author selected the statistical method. In his hands this method became "The Guardian of the Royal Virtue."

The writer highly praises the content of the paper because he himself is involved in the unification of thermostatics and thermodynamics of reversible and irreversible processes, but only on the macroscopic basis. This work is less rewarding, because it requires basic reconstruction and alteration of basic concepts of thermostatics. The results in the paper concerning the statistical method will be very useful in the work mentioned. Evidently the microscopic and macroscopic points of view are destined to aid each other.

It is essential to agree with the author that it would be desirable to conduct a broad discussion on the most important points of the statistical method; also, as claimed by the author to discuss the necessity and the sufficiency of the axioms presented, and desirable to present the result, determined by the correlation (45) (cyclic relation for dQ and dW), because it is difficult to subject to doubt the validity of the statement "not exact" regarding the first law, and so forth. This will better the understanding of the statistical method and will hasten its acceptance into engineering practice.

Undoubtedly, the author's new book, which will be released in the near future, will be beneficial propaganda for the ideas of the statistical method.

[12] Academician, B.S.S.R. Academy of Sciences, Minsk, B.S.S.R. NOTE: Minor changes were made by M. Tribus to conform to the terminology of the paper.

J. N. CANNON,[13] **T. J. CONNOLLY,**[14] **R. H. EUSTIS,**[15] **W. M. KAYS,**[16] **S. J. KLINE,**[17] **and W. C. REYNOLDS.**[18] We have followed with considerable interest Professor Tribus' enthusiastic development of this subject, both in conversations with him and in various drafts of his forthcoming book. As teachers of thermodynamics, we are naturally interested in new ideas on presentation of the subject and particularly in a proposal as broad as that of Professor Tribus.

Professor Tribus proposes that the introduction to thermodynamics for engineering students be made through statistical mechanics. He offers two reasons for this proposal. First, the present approach to the teaching of thermodynamics is unsatisfactory. Second, the recent contributions to the concepts of probability, and the relationship between uncertainty and entropy of Shannon, Jaynes, and others, make possible a development which can be made rigorous, no more demanding of the student, more useful to him, and physically more appealing to him. In the article under discussion, Tribus outlines this development.

Regarding the classical or macroscopic approach to thermodynamics, Tribus objects that it hasn't changed basically since Clausius. We do not see the validity of such an objection. Nor are we inclined to dismiss so lightly the contributions of such workers as J. W. Gibbs, J. H. Keenan, G. N. Lewis, or M. W. Zemansky to the presentation of this subject. We believe that in its present state the subject of thermodynamics is in good order concerning rigor, logical economy, and teachability. A defense of the macroscopic approach is not analogous, for example, to a defense of the caloric theory of heat. The foundations appear to us to be very sound. The analytical tools developed therefrom can be used with rigor in attacking a wide variety of engineering problems. The question is, therefore, a pedagogical one, rather than one of error versus truth.

Questions of appeal to the students and demands on the students are not easily resolved. These are areas of teaching in which suitable measuring devices have yet to be developed. We can offer it only as our opinion, therefore, that the microscopic approach is more demanding of the undergraduate student. In support of this opinion we offer Table 1, which compares the postulates, concepts, and skills required by the two approaches. We do not see that the microscopic approach would be more understandable to beginning students. Most important, however, we cannot see how the necessary groundwork in probability theory, information theory, quantum mechanics, and statistical mechanics can be imparted to the undergraduate student without either being very superficial or drastically increasing the time devoted to thermodynamics.

In following Tribus' treatment through probability theory to the macroscopic statement of the First Law, we are led to question just where any time-saving has been achieved except by concessions to rigor. Surely, in the treatment of quantum mechanics, a treatment essential to the development, the student is asked to accept more without proof than he is in a course in macroscopic thermodynamics. We fail to find the order-of-magnitude simplification of the entire subject that Tribus suggests.

We do not wish to deprecate the contribution represented by Tribus' work. In the particular synthesis which he has effected we find several points on which his treatment is appealing to us. His development of the entropy expression by maximizing uncertainty, and his transition from the microscopic to the macroscopic formulations, both lead to a better insight into the subject. His many physically appealing illustrations are certainly a contribu-

[13] Assistant Professor, Brigham Young University, Provo, Utah.
[14] Associate Professor, Stanford University, Stanford, Calif.
[15] Associate Professor, Stanford University.
[16] Professor, Stanford University.
[17] Professor, Stanford University.
[18] Associate Professor, Stanford University.

Table I

In Both	Macroscopic Only[5]	Tribus Only
I *Starting Concepts and Definitions*		
(a) System, surroundings	(a) Heat, heat engine	(a) Probability, uncertainty
(b) Equilibrium, steady state	(b) Reversible process	(b) Particulate nature of matter
(c) Work[3]	(c) Continuum approx.	(c) Velocity[1], momentum[1]
(d) State, property, process		(d) Virtual work[2]
(e) Efficiency, cycle		(e) Potential[2]
(f) Force, mass		(f) Event, outcome message, microstate, macrostate
		(g) Statistical distribution function, moments of distribution function
		(h) Boltzmann's constant as fundamental unit
		(i) Information = −uncertainty
		(j) Mathematical definition of entropy
II *Postulates*		
(a) State is function of finite number of variables determined by system	(a) First Law	(a) Schrödinger equation gives allowed states
(b) Energy is conservative	(b) Second Law	(b) Allowed states are functions of external co-ordinates only
		(c) Conservation of energy of particles at microscopic level
		(d) Laws of dynamics
		(e) Laws of probability combinatorial rules (Bayes theorem, etc.)
		(f) Minimum bias as given by Jaynes formalism determines equilibrium states
		(g) Associations between statistical averages and macroscopic observables can be made which will give wholly consistent results.
		(h) $E = mc^2$ (3)
III *Tools Needed in Basic Derivations*		
(a) Rudiments of deductive logic	(a) Definitions of common properties: enthalpy specific heats, etc.	(a) Inductive reasoning and statistical inference
(b) Elem. calculus		(b) Analysis of functional equations
		(c) Variational methods (La Grange multipliers)
		(d) Series methods, factorials, Stirling's approximation
		(e) Footnote 4

[1] In classical treatment these concepts are used in application but are not part of the basic derivations.
[2] Items so numbered not essential, but are employed.
[3] Energy is defined somewhat differently, but the essential elements are not altered.
[4] It is only by accepting certain results from Quantum Mechanics as given by solutions to the Schrödinger equation that one avoids introduction of a number of additional tools.
[5] Taken from texts in current wide use in the United States.

tion to the pedagogy of the subject. Although we have not yet studied his approach to irreversible thermodynamics in detail, we expect that his methodology would lend itself to a better treatment of this subject.

There appears much in Tribus' work which has implications for engineering education that goes beyond the subject of thermodynamics. The assignment of least-biased distributions to sets is an example. We expect that we will find ourselves adopting several of his ideas in our own courses. We expect, however, to reserve the microscopic approach to thermodynamics for the senior-graduate level, following courses in the macroscopic approach.

We do not see any disservice to the engineering student in following such a policy. In this manner, the terminal bachelor's student would then receive a useful analytical tool which, in our experience, he can learn to use with confidence and competence. We do see the danger in Tribus' proposal that the undergraduate student will receive a superficial or sugar-coated treatment of the microscopic approach which will leave him without a true understanding or even a base for developing an understanding. We do not believe that the student proceeding to the graduate level will suffer from learning the subject "backwards." There will be nothing to unlearn because, we must insist, the macroscopic approach is every bit as rigorous as the microscopic approach. It is a question of insight and of scope. The very notion of "insight" conveys the idea that something is already known from an instrumental or phenomenological point of view. Such a point of view is provided in the present thermodynamics courses.

Author's Closure

Professor Davies refers to the connection between the maximum likelihood method of Fisher and the maximum entropy estimate by Jaynes. The example chosen does not reveal the real significance of this difference because any function of the probabilities that is not changed by merely changing the subscripts, if maximized subject to the constraint

$$\sum_{i=1}^{k} p_i = 1$$

will give the result p_i = const. Both Fisher's method and Jaynes' method are the result of the application of Bayes' theorem, a matter treated by Jaynes elsewhere.[19]

The comments of Dr. Davies, Dr. El-Saden, and Dr. Veinik in support of the logic of the paper are appreciated.

The comments of the discussers refer mostly to problems of pedagogy. The tone of the comments seems to depend upon whether or not the person commenting has actually taught via the information-theory approach or has speculated on what would happen if he or someone else were to do so.

Questions of pedagogy cannot be resolved by considering the subject of thermodynamics by itself. A systems approach should be used in which the course labeled "Thermodynamics" is regarded as an element of a larger system, depending upon the courses preceding it and supporting the courses which follow. Whether or not the course should use the information-theory approach should depend upon the student's preparation and the material he is expected to know in the following courses. If the decisions concerning what is to be taught are based upon a desire to "preserve" the macroscopic approach (or any other), the "system" will probably suffer, even if the instructor in the course has "optimized" his own position.

The main thesis advanced by those who object to starting with information theory seems to be in two parts:

(*a*) Classical thermodynamics has been successful.

(*b*) The proposed approach will be superficial and will delay the time after which students can work meaningful problems and apply their knowledge in practical cases.

In support of this thesis, Professors Cannon, Connolly, Eustis, Kays, Kline, and Reynolds have prepared Table I. But the author suggests that some items appear in the third column that ought not (for most schools) to be there. The following Table 2 indicates these items:

Table 2

Item	*Comment*
Particulate nature of matter	Already taught in chemistry
Velocity, momentum	Already taught in chemistry and physics
Potential	Already taught in physics
Boltzmann's constant	Gas constant and Avogadro number already taught in physics and chemistry (in high school). Since $k = R/N$, this hardly qualifies as a "new" concept."
Conservation of energy at microscopic level	Already taught in physics
$E = mc^2$	Not required anywhere (though certainly known to students in physics)
Series methods factorials, Stirling's approximation	Already taught in mathematics

In addition to the foregoing eight items, there are six more which pertain to elementary statistics which can be taught in about four weeks (or less). It is the author's experience that more than this amount of time can be saved in "explaining" the zeroeth, first, and second laws. It should be noted in Table 1 that item II(a) in the first column is deduced from item II(b) in the third column, and that item II(c) in the third column is the same as item II(b) of the first column. All in all, it seems that the total of 23 items in the third column of Table 1 might well be reduced by approximately 15 items if a "systems" approach is used in the design of an engineering curriculum. At any rate, it seems to this author that every engineer ought to learn the items in column three somewhere, some time. If, by combining subject matter, the student's time can be saved, it appears to the writer that a gain has been made.

As to the charge of superficiality (and dazzling performances by "bright" young men), those who have had some experience teaching the material do not agree. We are no less sensitive to our students than others. We are, of course, still learning how to teach according to these ideas. But when we see the response of our students to the question, "What is entropy?" and compare with other methods we are gratified. The author would welcome a chance to compare final examinations with anyone who uses another approach. He is confident that the students' problem-solving ability is enhanced, not impaired.

If the judgment of the discussers is that the development in the paper is logically sound and that the only question is one of pedagogy, the author is gratified. Questions of pedagogy are quite subjective. One man's *rigor* is another man's *mortis*.

The author appreciates the efforts put forth by the discussers and thanks them for their comments. He is especially regretful that his friend of fourteen years' standing, Dr. G. M. Dusinberre, is no longer with us to continue the discussion. The force of his personality will be missed.

[19] "Probability Theory in Science and Engineering," McGraw-Hill (in press).

An Improved Integral Procedure for Compressible Laminar Boundary-Layer Analysis[1]

T. R. GOODMAN.[2] The method presented in the paper to improve the accuracy of the Karman-Pohlhausen integral procedure is, as the author points out, an iteration scheme having the usual polynomial profile as its 0th approximation. About 12 years ago, a similar scheme was proposed by Shvets,[3] who also demonstrated his method with many examples. The Yang and Shvets' procedures differ somewhat in detail. In particular, using Shvets' method (with the author's notation) the term $\partial u/\partial \tau$ in equation (15) of the paper is approximated using the profile obtained from the previous iteration, so that the differential equation to be solved for the new profile is even simpler than the author's. In addition, the boundary-layer thickness is left undetermined as a function of λ until after all the iterations are completed, and then it is found by applying the condition $\partial u/\partial \tau = 0$ at $\tau = 1$. Shvets always starts off the procedure using a linear profile and only rarely requires more than one additional iteration to obtain reasonable accuracy. It must be admitted that Shvets never attempts a problem having a profile with humps as does the author, and it is not clear how well his method would operate under these conditions. It would certainly be of interest to compare results using the two approaches. In this connection, Squire[4] has compared the ordinary (unimproved) Karman-Pohlhausen method with the Shvets' procedure with one iteration for the transient heat-conduction problem. There is a certain arbitrariness in the pro-

[1] By Kwang-Tzu Yang, published in the March, 1961, issue of the JOURNAL OF APPLIED MECHANICS, vol. 28, TRANS. ASME, vol. 83, Series E, pp. 9–20.

[2] Manager, Applied Mathematics Department, Allied Research Associates, Inc., a Subsidiary of Boeing Airplane Company, Boston, Mass.

[3] M. E. Shvets, "O Priblizhennom Reshenii Nekotorykh Zadach Gidrodinamiki Pogranichnogo Sloya," *Prikladnaya Matematika i Mekhanika*, vol. 13, 1949. Translated as: "Method of Successive Approximations for the Solution of Certain Problems in Aerodynamics," NACA TM 1286, April, 1951.

[4] W. Squire, comments on "The Heating of Slabs With Arbitrary Heat Inputs," *Journal of the Aero/Space Sciences*, vol. 26, 1959, pp. 756–757.

cedure when the heat flux is given on the boundary instead of the temperature (or the shear instead of the velocity for mass transfer) and this is also discussed by Squire.

The writer believes that we have reached the point in the use of integral methods where some proofs of a purely mathematical nature are needed in order to give the method a rigorous foundation. Does the iteration scheme converge to the exact answer? What is a bound on the error after n-iterations? These are the questions we should be asking, at least for the simpler problems. It is hoped the answers will be forthcoming soon.

E. M. SPARROW.[5] In appraising the new calculation method, there are some points where additional clarification would be useful. It would appear that once the variation of the boundary-layer thickness δ with x has been set from the original (polynomial) approximate solution, there is no way that this can be altered or improved at later stages of the calculation. If this is so, then even if the iterative process were continued until complete convergence is achieved, an exact solution could not be obtained. Instead, there would be found a solution which satisfied the momentum equation exactly in the domain $0 \leq y \leq \delta$. In this connection, it is interesting to inquire whether the accuracy of the results from successive iterations need necessarily approach the exact solution. Even though the successive profiles would come closer to satisfying momentum conservation for the domain $0 \leq y \leq \delta$, the fact that the finite domain is used still remains. It is conceivable that some fortuitous cancellation of errors which might have existed for more approximate profiles is destroyed as the profiles more closely satisfy momentum conservation.

A final remark relates to the connection of the present method with that of Piercy and Preston[6] for similarity boundary layers. The present method is certainly a generalization since it includes the nonsimilarity case. However, it appears not to be able to yield exact solutions as does the Piercy-Preston method.

Author's Closure

The writer wishes to thank Drs. Goodman and Sparrow for their rather constructive comments. The iteration method in laminar-boundary-layer analysis is indeed not new. Other than those quoted by the discussers, there are also articles by Schuh[7] and Klunker and McLean.[8] In all these techniques, the governing partial differential equations, either in their original or transformed forms, are properly linearized such that successive iterations may be performed by solving these linear equations. In the method proposed in the paper, the Karman-Pohlhausen integral solution is specifically chosen as the zeroth-order approximation. As implicitly pointed out in the paper, this choice is based on the belief that the integral solution is capable of taking into account most of the nonlinearities in the problem as those appeared in the coefficients of the profile derivatives, such that one iteration should yield very satisfactory results, and the comparisons shown have certainly well substantiated this belief. Even though the linearization process used by Shvets,[3] as described by Dr. Goodman, is simpler, the corresponding results are not expected to be more accurate, especially in those cases where large profile curvatures are encountered, and also in view of the doubtful general validity of the condition of determining the boundary-layer thickness. The writer strongly believes that keeping the first profile derivatives as unknowns is essential for accurate results.

Although the present method emphasizes obtaining just one iteration based on the original integral solution as the zeroth-order approximation, the question of the possibility of getting exact solution by carrying out the subsequent successive iterations on the basis of the present linearizing approach is nevertheless of basic interest and importance. The writer agrees with Dr. Goodman on the desirability and necessity of a mathematical justification of this iteration procedure concerning its convergence and limit. However, before this difficult problem can be attacked, questions as those raised by Dr. Sparrow indeed have to be cleared away. First, according to this iteration procedure, each iteration should be considered as consisting of a set of solutions to Equations (15) and (16) of the paper and a subsequent integral solution based on these newly obtained profiles. Consequently, the boundary-layer thickness development does not stay fixed in successive iterations. Second, in order to obtain possible exact solutions, boundary conditions at $\tau = 1$ as indicated in Equations (21) and (24) of the paper must be altered to let $\tau \to \infty$. This would necessitate obtaining solutions to Equations (15) and (16) in two separate regions, namely, $0 \leqslant \tau \leqslant 1$ and $1 \leqslant \tau \leqslant \infty$, in view of the assumed profiles, Equations (10), in the integral solution, which are only valid in the region $0 \leqslant \tau \leqslant 1$. The profiles in these two regions may then be matched by a suitable condition, which may possibly be the identity of the first profile derivative evaluated at $\tau = 1$. In conjunction with the mathematical problem mentioned previously, the writer has not been successful in obtaining a general mathematical proof of the convergence of this iterative process because of the extremely complex relationship between profiles from two consecutive iterations. Instead, he is now in the process of developing a general error criterion, which may be readily applied to any iteration to determine its level of error, thus gaining insight to the convergence or even divergence of this iteration process.

Heat Transfer and Sublimation at a Stagnation Point in Potential Flow[1]

B. H. SAGE[2] **and P. A. LONGWELL.**[2] The author's frank and straightforward approach to a difficult problem is commended. The analysis avoids many of the complications normally found in the application of boundary-layer theory to ablative thermal transfer near stagnation. The point of view brought up by the author in his discussion of this simple approach lends credence to the application of the analysis to situations typical of those encountered in the ablation of the forward part of high-velocity missiles. The treatment of the influence of turbulence upon the application of the results does not seem as clear. An increase in the apparent level of turbulence from 0 to 0.15 results in an increase in the macroscopic thermal transfer without material transfer of 30 per cent. This increase is relatively insensitive to the Reynolds number. Near stagnation the influence of level of turbulence is much smaller and perhaps can be neglected as a first-order approximation.

In Fig. 1 of this discussion are shown figure values of the stag-

[5] Professor of Mechanical Engineering, University of Minnesota, Minneapolis, Minn. Assoc. Mem. ASME.

[6] N. A. V. Piercy and G. H. Preston, "A Simple Solution of the Flat Plate Problem of Skin Friction and Heat Transfer," *Philosophical Magazine*, vol. 21, 1936, p. 995.

[7] H. Schuh, "The Solution of the Laminar-Boundary-Layer Equation for the Flat Plate for Velocity and Temperature Fields for Variable Physical Properties and for the Diffusion Field at High Concentration," NACA TM 1275, 1950.

[8] E. B. Klunker and F. E. McLean, "Effect of Thermal Properties of Laminar-Boundary-Layer Characteristics," NACA TN 2916, March, 1953.

[1] By W. W. Short, published in the December, 1960, issue of the JOURNAL OF APPLIED MECHANICS, vol. 27, TRANS. ASME, vol. 82, Series E, pp. 613–616.

[2] California Institute of Technology, Pasadena, Calif.

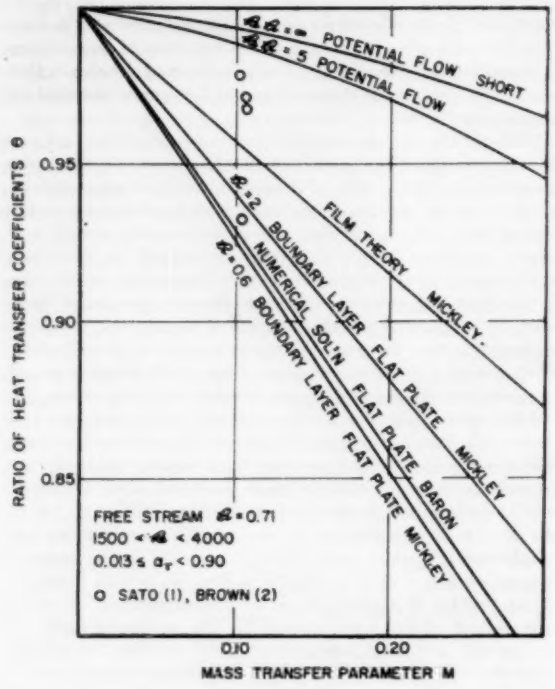

Fig. 1

nation ratio θ of the thermal-transfer coefficient h as a function of the mass-transfer parameter M utilized by the author. Some experimental data under the afore-mentioned conditions from the work of Sato and Sage[3] and Brown, Sato, and Sage[4] have been included and fall between the potential-flow values obtained by the author and the boundary-layer considerations of Mickley. The experimental data show a progressive increase in the ratio of the heat-transfer coefficients with and without material transport with an increase in Reynolds number. However, the experimental data presented are at such a small value of the mass-transfer parameter M that the variations with Reynolds number are not as clearly defined as would be expected at higher rates of ablation. It may be of interest to note that the Nusselt numbers for both local and macroscopic transport from spheres are larger with material transport than they are without it. The reversal of the ratio in the case of the heat-transfer coefficients results from the incorporation of the molecular properties of the fluid in the Nusselt number.

The author should clarify his choice of values of molecular properties of the fluid since there exist, under many of the conditions encountered in ablation cooling, large variations in these properties in passing from the gas phase at the ablating surface to the free stream. The author has used the properties of the ablating material in his presentation and it is expected that this choice will yield more representative values of the behavior at high rates of ablation than at lower values. The same need for clarity exists in relation to the choice of molecular properties in defining the Reynolds number and Prandtl number.

It is difficult to follow the justification that the relations derived for potential flow should apply more satisfactorily to turbulent flow than to viscous flow. It is agreed that the velocity profile for turbulent flow may approach that for potential flow, but the use of molecular thermal conductivity in the associated analysis neglects the large increase in total conductivity encountered under turbulent conditions. The agreement of the simple relations obtained with the limited experimental data indicates that the results may have significant utility in predicting the behavior of ablating surfaces near stagnation. The need for further experimental work to define thoroughly the effects of blowing boundary layers upon heat transfer over a wide range of ablation rates and Reynolds numbers is evident.

G. W. SUTTON.[5] The author's analysis is intriguing and gives some interesting results. However, the steps following equation (12) do not appear to be correct. Equation (12) is

$$(g_0')^{-1} = \int_0^\infty \exp\left\{-y^2(3U + 2v_0)(2aK)^{-1} + v_0 y K^{-1}\right\} dy \qquad (a)$$

In order to integrate the foregoing equation, it is necessary to complete the square; there is then obtained:

$$(g_0')^{-1} = \exp\left\{av_0^2[2K(3U + 2v_0)]^{-1}\right\} \cdot \int_0^\infty \exp\left\{-\frac{3U + 2v_0}{2K}\left[y - \frac{av_0}{3U + 2v_0}\right]^2\right\} dy \qquad (b)$$

At this point, it is convenient to introduce a new variable,

$$\xi = y - av_0/(3U + 2v_0) \qquad (c)$$

and there is a change in limits of integration:

$$y = 0:\ \xi = -av_0/(3U + 2v_0) \qquad (d)$$

$$y = \infty:\ \xi = \infty \qquad (e)$$

Because of the nonzero limit of integration for ξ, the integral becomes the error function plus one[6]; and equation (*b*) becomes

$$g_0' = \frac{[2(3U + 2v_0)/(\pi Ka)]^{1/2} \exp\left\{-av_0^2[2K(3U + 2v_0)]^{-1}\right\}}{1 + \operatorname{erf}\left\{a^{1/2}v_0[2K(3U + 2v_0)]^{-1/2}\right\}} \qquad (f)$$

or in terms of θ, when $P_r R_e \to \infty$:

[3] Kazuhiko Sato and B. H. Sage, "Thermal Transfer in Turbulent Gas Streams. Effect of Turbulence on Macroscopic Transport From Spheres," TRANS. ASME, vol. 80, 1958, pp. 1380–1388.

[4] R. A. S. Brown, Kazuhiko Sato, and B. H. Sage, "Material Transfer in Turbulent Gas Streams. Effect of Turbulence on Macroscopic Transport From Spheres," *Industrial Engineering and Chemistry*, Chemical Engineering Data Series, vol. 3, 1958, pp. 263–272.

[5] Manager, Magnetohydrodynamic Power Generation, Space Sciences Laboratory, General Electric Company, Philadelphia, Pa.

[6] W. Gröbner and N. Hofreiter, "Tables of Definite Integrals," Springer-Verlag, 1959, Integral 314–366.

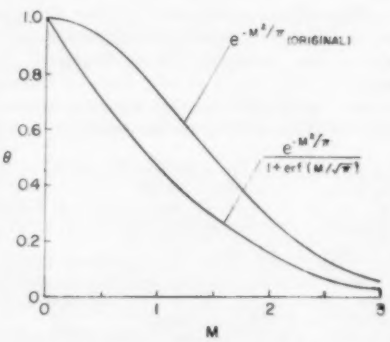

Fig. 2 Original and correct expression for θ

$$\theta = \frac{\exp\{-M^2/\pi\}}{1 + \text{erf}\{M\pi^{-1/2}\}} \qquad (g)$$

The author has omitted the denominator in his analysis.

The expression for θ now bears a better semblance to boundary-layer solutions. For one thing, at $M = 0$, $d\theta/dM = -2/\pi$, in excellent agreement with boundary-layer theory. Also, for $M > 3$, the reduction in heat transfer is twice that previously predicted. A comparison is shown in Fig. 2 of this discussion.

On the Buckling of Circular Cylindrical Shells Under Pure Bending[1]

E. REISSNER.[2] The authors deserve our thanks for re-examining a result of cylinder buckling theory which has always been difficult to understand. Their work is an excellent illustration of the possibilities for definitive answers which now exist through the use of high-speed digital computation.

The deflection pattern as calculated by the authors would seem to be an indication that use of the original Donnell equations for shallow cylindrical shells is justified for the present problem. The writer would like to raise the question as to what extent use of a cylinder theory, which retains its validity for the cos θ, cos 2θ and cos 3θ-components of the radial deflection function, would modify the numerical results obtained by the authors.

E. E. SECHLER.[3] This paper tends to clarify the small-deflection analysis of the instability of circular cylindrical shells under pure bending. From a physical reasoning standpoint, if one assumes a buckle wave length which is small compared to the shell perimeter, it has always been difficult to understand why there should be any difference between the initial buckling stress of a shell under axial compression and one under pure bending. The paper confirms the physical reasoning. The widespread acceptance of a higher buckling stress for bending than compression is undoubtedly the result of experimental evidence which is dependent, not only on the initial buckling point, but also on the nature of the postbuckling behavior. This behavior is quite different for the two loadings considered.

Authors' Closure

The authors wish to thank Professors Reissner and Sechler for their comments. Some new calculations made with a set of equations employing the modification suggested by Morley[4] lowered the buckling coefficients only in the fourth significant figure and had no appreciable effect on the deflection patterns. The authors tend to agree with Professor Sechler's comments on the reason for experimental differences between the buckling stress for bending and compression. We wonder, however, if these differences might also be related to the usual practice in bending tests of orienting longitudinal seams along the neutral axis of the cylinder. Any imperfections due to the seam would thus have little or no effect in bending but might have a significant effect in compression. It would be of interest to investigate this question experimentally.

[1] By Paul Seide and V. I. Weingarten, published in the March, 1961, issue of the JOURNAL OF APPLIED MECHANICS, vol. 28, TRANS. ASME, vol. 83, Series E, pp. 112–116.

[2] Professor, Department of Mathematics, Massachusetts Institute of Technology, Cambridge, Mass. Mem. ASME.

[3] Professor of Aeronautics, California Institute of Technology, Pasadena, Calif.

[4] L. S. D. Morley, "An Improvement on Donnell's Approximation for Thin-Walled Circular Cylinders," *Quarterly Journal of Mechanics and Applied Mathematics*, vol. 12, part 1, February, 1959.

On the Burmester Points of a Plane[1]

O. BOTTEMA.[2] The authors give solution for a problem that is undoubtedly complicated. Making use of complex numbers and following an ingenious procedure they succeed in building up an equation of the fifth degree, four roots of which correspond to the Burmester points belonging to five arbitrary positions of a rigid plane body. Furthermore, the equation is such that a computer program can be developed to solve it numerically in each given case. In the remarks which follow, no criticism or correction on the paper concerned is intended. It mentions only an unsuccessful attempt to attack the problem, and its positive value, if any, is not more than that it gives another formulation of the question, showing that it is identical with a geometrical problem of a kind not unusual in geodesy.

In contrast to the Russian work quoted in their paper, the authors start from a configuration of no more than six poles, by which the five positions of the plane are completely determined. Their choice is, in the well-known notation, the sextuple P_{12}, P_{13}, P_{24}, P_{34}, P_{25}, P_{35}, and this is fully justified by their results. The five positions can also be given by the six poles P_{12}, P_{23}, P_{31}, and P_{14}, P_{45}, P_{51}. They are the vertices of two triangles T_1 and T_2, the angles of which are denoted, respectively, by α_3, α_1, α_2, and β_2, β_1, β_3, Fig. 1, herewith.

It is well known that the motion which leads from position I to position II is the rotation about P_{12} by an angle $2\alpha_3$, and so on. Therefore if A_1, A_2, and A_3 are homologous points of the planes I, II, and III, there is a point Q_1 such that A_1 is the reflection of Q_1 in $P_{12}P_{31}$, A_2 that of Q_1 in $P_{23}P_{12}$, and A_3 that of Q_1 in $P_{31}P_{23}$. Moreover, if M_1 is the circumcenter of $A_1A_2A_3$, it is easily seen that $<Q_1P_{12}P_{31} = <M_1P_{12}P_{23}$, which means that Q_1 and M_1 are isogonally conjugated points with respect to T_1. The analogous property holds for the triangle T_2. Hence, if A_1 is an arbitrary point of position I, Q_1 and Q_2 its reflections in $P_{12}P_{31}$ and $P_{14}P_{51}$, M_1 and M_2 the isogonally conjugated points of Q_1 and Q_2 with respect to T_1 and T_2, then M_1 is the circumcenter of $A_1A_2A_3$ and M_2 that of $A_1A_4A_5$. If M_1 and M_2 are the same point M then it is the center of a circle through A_1, A_2, A_3, A_4, A_5 and, therefore, a Burmester point. In other words, consider the product $S = S_4S_2S_2S_1$ of four transformations, S_1 and S_4 being the isogonal transformations with respect to T_1 and T_2, S_2 and S_2 the reflections in $P_{12}P_{31}$ and in $P_{14}P_{51}$, then the coincidence points of S are the Burmester points. The four transformations are involutorical ($S_i^2 = 1$).

[1] By Ferdinand Freudenstein and George N. Sandor, published in the March, 1961, issue of the JOURNAL OF APPLIED MECHANICS, vol. 28, TRANS. ASME, vol. 83, Series E, pp. 41–49.

[2] Professor, Department of Mathematics, Technological University, Delft, Holland.

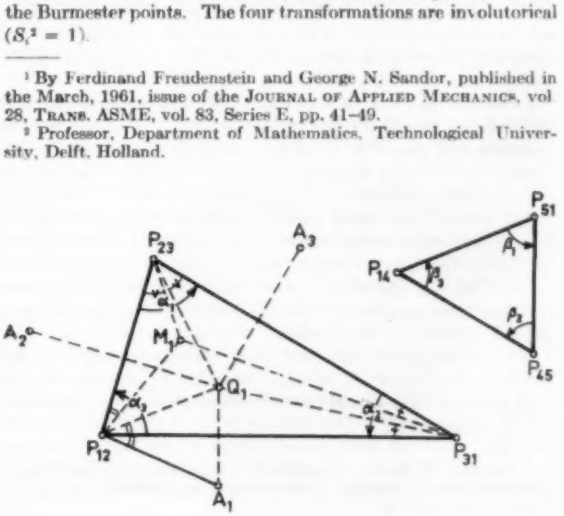

Fig. 1

From Fig. 1 of this discussion, it follows that $<A_1P_{12}M = <P_{31}P_{13}P_{32} = \alpha_3$ and $<A_1P_{21}M = <P_{12}P_{21}P_{23} = -\alpha_2$. Therefore if the four poles P_{12}, P_{13}, P_{14}, P_{15} are given together with the angles of rotation $2\gamma_{12}$, $2\gamma_{13}$, $2\gamma_{14}$, $2\gamma_{15}$ belonging to them, we have the following theorem about the unknown points A_1 and M:

$$<A_1P_{12}M = \gamma_{12}, \quad <A_1P_{13}M = \gamma_{13},$$
$$<A_1P_{14}M = \gamma_{14}, \quad <A_1P_{15}M = \gamma_{15},$$

M being a Burmester point and A_1 the circle point (in plane I) belonging to it. The configuration is given by twelve independent generalized co-ordinates (as in the authors' case); namely, the four poles P_{1i} and the four angles γ_{1i}. The problem therefore comes to this: Four points being given construct the two unknown points A_1 and M such that the angles by which the segment A_1M is seen from the fixed points have given values, Fig. 2 of this discussion.

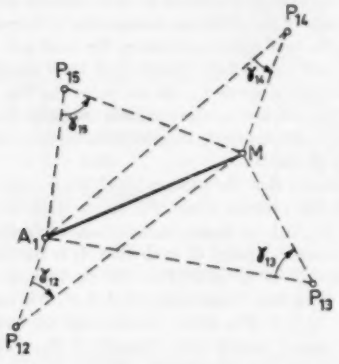

Fig. 2

The situation where unknown points have to be determined by angles measured from given points is not unusual in geodesy. If there are p given points and q unknown points and one knows the angles by which the segments between the unknown points are seen from the known points, then a well-determined problem exists only—as Prof. R. Roelofs informs the writer—in the cases $p = 3, q = 3$ and $p = 4, q = 2$. The first of these is the *Sechseck-problem* studied by Lambert in 1765; the second is identical with our kinematic problem. A solution seems not to be known. An analytical attack leads to the determination of the points of intersection of two cubic curves.

J. DENAVIT[3] and R. S. HARTENBERG.[4] Previously, the two general methods of attack for the synthesis of planar linkages—the algebraic and geometric methods—had proceeded along parallel paths, thus forming separate schools of thought which did not permit cross-fertilization. A problem could often be solved by either method, but rarely could the ease of visualization of the geometric method be combined with the accuracy of the algebraic method. The present paper, which starts from the geometric concept of the Burmester points and proceeds by algebraic methods using complex numbers, provides a very promising connection between the two methods.

The mathematical skill and thoroughness exhibited by the authors in the paper are, as usual, remarkable, and one can only wish that more space would allow greater detail in the explanation of some of the steps.

With the increased availability of computing equipment, the main burden is no longer that of carrying out computations, but rather that of writing computer programs. The fact that the authors have been able to solve the general problem of the location of the Burmester points using their already existing and more specialized program for the synthesis of path-generating mechanisms is in itself a sizable accomplishment.

W. MEYER ZUR CAPELLEN.[5] It is a matter of great merit that the authors have concerned themselves with the Burmester points for five distinct positions. The results are pleasingly simple and indeed suited for practical application. It would be interesting to know whether the results of Reinhold Müller would be reobtained from the limiting process in going to five infinitesimal positions.

T. P. GOODMAN.[6] This paper, which greatly extends the range of applications of the authors' previously published digital-computer program for linkage design, makes a valuable addition to the literature of kinematic synthesis. It is remarkable how many additional applications for their computer program the authors have found by applying Roberts' theorem and the principle of kinematic inversion.

For the seven-bar linkage, the authors' five-precision-point solution does not exploit fully the available design parameters, since theoretically the problem in Fig. 9 of the paper could be solved for eleven precision points if the positions of the tracer point A were not prescribed. Nevertheless, the authors' solution provides a first step—and the only digital-computer program known to the writer—for attacking this formidable kinematic-synthesis problem.

Authors' Closure

The authors are grateful for the stimulating discussions and will offer brief comments on each in turn.

By means of a scholarly analysis, Professor Bottema has discovered the relationship of Burmester theory to a problem in geodesy. Although, as pointed out by Professor Bottema, the problem presented in his Fig. 2 may not be solved directly in closed analytical form, it is amenable to indirect analytical solution by means of the methods of the present paper. One of these is to compute the location of poles P_{24}, P_{34}, P_{23}, and P_{35}, and then, with the aid also of poles P_{12} and P_{13}, to apply the equations in part 1 of the paper to determine the Burmester points. Of these, one will be the "unknown" point M in Fig. 2; point A_1 can thereupon be found as the intersection of two straight lines.

A second indirect, but exact method, which yields simultaneously the co-ordinates both of point M and of point A_1, is based on the approach presented in part 2 of the paper under discussion and utilizes the computer program described in ref. [15]. Table 1a, which follows, lists the procedure and is believed to be self-explanatory.

The authors appreciate learning of the relationship of their studies to a seemingly unrelated field.

Professors Denavit and Hartenberg have called attention to several aspects of mechanisms research with which the authors are in complete agreement. The first refers to the value of a unified treatment of algebraic and geometric theories; the second, a point sometimes overlooked, states that a current limitation on the use of computers frequently involves writing the program, rather than the computer itself. To this, the authors should like to add one more—limitations due to loss of accuracy in extended computations, rather than in the length of the com-

[3] Associate Professor, Department of Mechanical Engineering, Northwestern University, Technological Institute, Evanston, Ill. Assoc. Mem. ASME.

[4] Professor, Department of Mechanical Engineering, Northwestern University, Technological Institute, Evanston, Ill. Mem. ASME.

[5] Professor of Kinematics and Mechanisms Design, Technische Hochschule Aachen, Aachen, Germany.

[6] Kinematics Engineer, General Engineering Laboratory, General Electric Company, Schenectady, N. Y. Mem. ASME.

Table 1a

The Geodetic Problem

Given: $P_{1j}, \gamma_{1j}, j = 2,3,4,5$ (see Fig. 2)

Find: M and A_1 such that $\angle A_1P_{1j}M = \angle \gamma_{1j}$

Method: As shown by Bottema, M and A_1 constitute a Burmester point-pair with P_{1j} as poles, M as centerpoint, and A_1 as circlepoint.

Procedure:

1 Assume an arbitrary point T_1 in position 1 of the moving plane.

2 Using the given poles P_{1j} and semirotations γ_{1j}, construct the corresponding points, T_j, $j = 2,3,4,5$, by vector additions in an arbitrary Cartesian co-ordinate system of axes.

3 Use $r = \mathbf{OT}$ and $\varphi_j = 2\gamma_{1j}$ as input for the computer program #9.5.003 of Ref. [15].

4 Proceed according to Table 1 of the paper to determine the Burmester point-pairs, $M_uK_u^{(1)}$, $u = 1,2$ or $1,2,3,4$, if real.

5 By inspection of an approximate diagram, select the solution $M_u \equiv M$, $K_u^{(1)} \equiv A_1$, where M and A_1 are the points whose locations were to be found.

putations themselves. And finally, as the discussers have observed, the desirability of developing a few, versatile, general-purpose programs in the mechanisms field is becoming increasingly evident.

Concerning the pertinent questions raised by Professor Meyer zur Capellen, the answer seems to us as follows: In proceeding to five infinitesimal positions, the poles all coincide in the limiting position and the results of this paper either reduce to trivial identities or to indeterminate ratios, the evaluation of which would constitute a formidable task. Furthermore, the theory of this paper deals with motion in general, whereas much of R. Müller's pioneering work dealt with the four-bar linkage. An intriguing "inversion" of Professor Meyer zur Capellen's question is the following: Can any of R. Müller's results for infinitesimal displacements be extended to finite displacements? The investigation of this question will, it is hoped, be reported on in joint future work. A unified treatment of both finite and infinitesimal displacements would certainly be advantageous.

The thoughtful comments of Dr. Goodman are in line with, and supporting of, the comments on versatility made by Professors Denavit and Hartenberg. It is true that Roberts' theorem and inversion—techniques which the discusser has applied and explained with success—indeed extend the range of solutions in many problems involving mechanisms and constitute a powerful adjunct to the imagination. The investigation of the seven-bar, two-degree-of-freedom linkage is certainly far from exploiting all available design parameters. It represents, in fact, a mere beginning and was intended to illustrate a possible application of the computer program as well as to encourage further interest in its analysis.

In conclusion, the authors should like to state their conviction that the discussers have added to an unusual degree to the significance of the subject matter reported on in their present study.

Steady-State Behavior of Nonlinear Dynamic Vibration Absorber[1]

F. R. ARNOLD.[2] No doubt the authors have noted that the illustration in Fig. 1 is not appropriate for the particular differential equations (1) and (2) treated in the paper. Fig. 1 should have the damper connected between ground and m_1. Had the equations appropriate to damping between m_1 and m_2 been treated, the device of introducing the phase angle α in the disturbance term could not have been used and the approximating functions for the displacements of m_1 and m_2 would have had the form

$$x_1 \approx z_1 = A_1 \cos \omega t + B_1 \sin \omega t \tag{1}$$

$$x_2 \approx z_2 = A_2 \cos \omega t + B_2 \sin \omega t \tag{2}$$

The authors state that their paper extends previous work by determining an approximate solution for the case where both main and absorber springs are nonlinear. Actually, the extension lies in the inclusion of damping, since various combinations of nonlinear springs in undamped systems have been treated previously as listed in the bibliography of the authors' reference [3].

In describing the solution of the amplitude equations, the authors state that a maximum of nine possible solutions exists for each disturbance frequency. Actually, there are at mostonly three, since equations (15) and (16), or (17) and (18) are only of the third degree in the amplitudes. It is believed that the extraneous solutions have arisen from the computational methods which apparently involved squaring processes and hence yield some roots of the squared equations that will not satisfy the original equations.

In arriving at a solution to the amplitude equations, the following procedure is suggested to avoid graphical methods and to permit any desired accuracy in obtaining data for plotting response diagrams:

1 First, select a value for phase angle α, say α_i, and use the relation

$$\sin \alpha = 2\xi\eta \frac{A_1}{z}$$

to obtain A_1/z as a function of η. A curve of A_1/z versus η^2 may be drawn immediately as the first step in plotting the response diagram corresponding to the selected phase angle.

2 Selecting a value for η^2, say η_i^2, and its corresponding $(A_1/z)_i$ use equation (15) of the paper to find at most three values of $(A/z)_{i(1,2,3)}$.

3 Use equation (16) to find a value for $(A_2/z)_{i(1,2,3)}$ corresponding to each $(A/z)_{i(1,2,3)}$.

4 The complete response diagram corresponding to the selected phase angle may thus be drawn before selecting another phase angle and repeating the process until a set of response diagrams for each of as many phase angles as desired is established.

It is of interest to note the physical significance of the authors' method compared with that of some other methods. The former determines an approximate solution of sinusoidal form with the approximate amplitude of such value that the energy dissipation over the approximate cycle equals the work input of the disturbance. The second Ritz method, a Fourier series approach, or a modified Duffing method applied to the same problem will yield approximate solutions such that the coefficients of the approximating functions will have values that make the resulting approximate solution come as close as possible to satisfying whatever *minimum principle* exists for the dynamical system being considered—even if the principle is unknown.

In conclusion, it is suggested that equation (26) can be misleading without an examination of the response diagram of the system since the equation merely gives conditions for which $\left|A_1/z\right| \equiv 1$. Actually, on each side of the value of η^2, for which $\left|A_1/z\right| = 1$, the amplitude may even be smaller rather than larger. What happens is a matter for determination from the whole response diagram rather than from Fig. 3 alone.

L. F. KREISLE.[3] The authors are to be congratulated for extend-

[1] By W. J. Carter and F. C. Liu, published in the March, 1961, issue of the JOURNAL OF APPLIED MECHANICS, vol. 28, TRANS. ASME, vol. 83, Series E, pp. 67–70.

[2] Associate Professor of Mechanical Engineering, Stanford University, Stanford, Calif. Assoc. Mem. ASME.

[3] Associate Professor of Mechanical Engineering, The University of Texas, Austin, Tex. Mem. ASME.

ing the study of the nonlinear dynamic vibration absorber with a differential equation of the Duffing type previously studied by Arnold [3], Atkinson [4], and Robertson [2].[4]

Apparently there is a discrepancy in Fig. 1 since the entire paper is based upon a physical system different from that indicated in the illustration. If a viscous damper (with viscous damping coefficient B) is inserted between the fixed wall and the mass m_1 in Fig. 1 as printed, and if the damper between masses m_1 and m_2 is deleted, the resulting physical system appears to be that investigated by the authors. It is on this assumption that the following remarks are made:

Evidently, also through a typographical error, a cube has been omitted in the last nonzero term of equation (8). This term should read $\beta^3 A^3 \cos^3 \omega t$ and not $\beta^3 A \cos^3 \omega t$.

In order for equation (15) to be correct as printed and consistent with previous equations, the terms ν, ν_1, and λ^3 must be defined as follows:

$$\nu = \frac{\beta^3 F_m{}^2 k_2}{k_1{}^3}$$

$$\nu_1 = \frac{\gamma^3 F_m{}^4}{k_1{}^3}$$

$$\lambda^3 = \frac{k_2}{\mu k_1}$$

This definition of λ^3 differs from that given in the nomenclature of the paper. If the foregoing three definitions are followed, then η^3/μ should be substituted for the $\mu\eta^3$ term appearing in the equations (18), (21), (22), (23), (24), (25), and the equation for $R(A_2/s)$ appearing before equation (20). In addition, the η^3-term of equation (26) should be revised to η^3/μ.

It is hoped that the data for the curves in Figs. 2 and 3 and the digital-computer results were obtained from correct equations and that the incorrect equations appearing in this paper resulted from typographical errors. Although the writer did not do the calculations necessary to verify it, the curves in Figs. 2 and 3 appear to be correct for $\mu = 10$ rather than $\mu = 0.1$ as stated in the figures. Apparently the authors have employed two different definitions of μ, one being the reciprocal of the other. With $\mu = m_1/m_2$ as defined in the nomenclature, then the suggested revisions in several equations and the indication in Figs. 2 and 3 that $\mu = 10$ appear desirable to make the paper completely consistent. In closure, this paper makes a significant contribution to the analysis of the Duffing-type nonlinear dynamic absorber.

Author's Closure

The authors wish to thank Professors Arnold and Kreisle for their comments. As both of them have noted, Fig. 1 of the paper was in error—the damper should have been between ground and m_1. The authors agree with Professor Arnold that there should be at most only three amplitudes for each disturbance frequency.

Stress Distribution in a Rotating Spherical Shell of Arbitrary Thickness[1]

H. PORITSKY.[2] The problem of stresses in a rotating spherical shell appears to be a popular one nowadays. In addition to the three authors, the writer, too, has had occasion recently to solve the elastic equations for the rotating spherical shell. However, his results have not been published even as an internal company report, since the writer discovered[3] that this problem had been solved over 70 years ago by C. Chree. Chree's paper, entitled "The Equations of an Isotropic Elastic Solid in Polar and Cylindrical Co-ordinates, Their Solution and Application," was presented to the Cambridge Philosophical Society on October 31, 1887.[4] After obtaining general solutions of the elastic equations in spherical co-ordinates and treating several problems of a solid sphere, Mr. Chree solves the problem of a rotating spherical shell.[5]

ROBERT SCHMIDT.[6] This paper is a significant addition to the collection of solutions of the axially symmetric problems in the theory of elasticity. It is also of interest to the investigators in the theory of shells.

The writer believes that there is a simpler and more direct approach to this problem. It can be shown that the problem may be formulated by means of a harmonic function

$$\psi = \sum (A_n r^n + B_n r^{-n-1}) P_n(p) \tag{1}$$

and a biharmonic function

$$\Omega = \chi + \frac{(1+\nu)(11-17\nu)}{360(1-\nu)E}\gamma\omega^2 r^4, \tag{2}$$

where

$$\chi = \sum \left[C_n r^n + D_n r^{-n-1} - \frac{5-4\nu+n}{2(2n+3)(1-\nu)} A_n r^{n+2} + \frac{4-4\nu-n}{2(2n-1)(1-\nu)} B_n r^{-n+1} \right] P_n(p) + \frac{(1+\nu)\gamma\omega^2 r^4}{360E}\left[50p^4 - \frac{3(7-9\nu)}{1-\nu} \right] \tag{3}$$

is a solution of the equation

$$\nabla^2\chi = -\frac{1}{1-\nu}\frac{\partial}{\partial r}(r\psi) - 4\psi + \frac{(1+\nu)\gamma\omega^2 r^2}{3E}\left[\frac{5}{2}(p^2 - p^2) - \frac{1-2\nu}{1-\nu} \right] \tag{4}$$

The stress components are calculated by the formulas

$$\sigma_r = \frac{E}{1+\nu}\frac{\partial}{\partial r}\left(\frac{\partial\chi}{\partial r} + \frac{2-\nu}{1-\nu} r\psi \right) - \gamma\omega^2 r^2 \left[\frac{\nu}{3(1-\nu)} + \frac{1}{2}(p^2 - p^2) \right], \tag{5}$$

$$\tau_{r\theta} = \frac{E}{1+\nu}\frac{\partial}{\partial\theta}\left(\frac{1}{r}\frac{\partial\chi}{\partial r} - \frac{\chi}{r^2} + \psi \right) + \frac{1}{3}\gamma\omega^2 r^2 pp, \tag{6}$$

and so on. These results are similar to those obtained by Hampl.[7]

[4] References in paper.

[1] By M. A. Goldberg, V. L. Salerno, and M. A. Sadowsky, published in the March, 1961, issue of the JOURNAL OF APPLIED MECHANICS, vol. 28, TRANS. ASME, vol. 83, Series E, pp. 127–131.

[2] Consulting Engineer, General Electric Company, Schenectady, N. Y., Mem. ASME.

[3] A. E. H. Lore, "Treatise on Mathematical Memory of Elasticity," McGraw-Hill Book Company, New York, N. Y., 4th ed., p. 255.

[4] Published in *Transactions of the Cambridge Philosophical Society*, vol. 14, 1889, pp. 250–481.

[5] Ibid., section 6, pp. 295–302.

[6] Associate Professor of Civil Engineering, University of Arizona, Tucson, Ariz.

[7] Miloslav Hampl, "The Stress Problem of Axisymmetrically Loaded Thick Spherical Shells," *Der Stahlbau*, 1940, pp. 96–100.

Substituting (1), (3) in (5), (6) and using the boundary conditions

$$\sigma_r = \tau_{r\theta} = 0 \quad \text{on} \quad r = a, b, \tag{7}$$

we obtain a set of algebraic equations for determining the constants A, B, C, D by comparing the coefficients of $P_m(p)$ in (7). At the worst we must solve one 2 by 2 system and two 4 by 4 systems of algebraic equations. The work still could be simplified by certain manipulations of the equations. Thus the use of high-speed computers becomes avoidable.

Authors' Closure

The authors thank Dr. Poritsky for bringing Chree's[4] paper to their attention. However, Dr. Poritsky failed to notice that Chree treated in detail only the solution[5] for the limiting cases of a rotating spherical membrane and thin shell.

Professor Schmidt's statement, regarding a simpler method which would avoid the use of a high-speed computing device, is misleading. We note that Professor Schmidt's analysis would lead to three sets of simultaneous algebraic equations, totaling ten equations in all, for the arbitrary constants. These equations are similar to the system of ten linear algebraic equations obtained by the authors' equation (17).[1] We then obtained explicit representations for the seven nonvanishing coefficients of superposition, equation (18),[1] in terms of the geometric and physical quantities. At this stage, with equations (13)[1] and (18),[1] the problem is completely solved and the solution is amenable for calculations with a slide rule or desk calculator, depending upon the desired accuracy. However, in our opinion, the large volume of numerical results presented could be obtained most efficiently with a high-speed computing device. We are confident that Professor Schmidt would agree with our conclusion if he were to seek similar results using his method.

[4] Chree, Transactions of the Cambridge Philosophical Society, vol. 14, 1889, p. 297, par. 41.

Journal of APPLIED MECHANICS

Book Reviews

Shell Theory

Stresses in Shells. By Wilhelm Flügge. Springer Verlag, Berlin, 1960. Cloth, 6 × 10 in., xi and 499 pp. DM 58.80.

REVIEWED BY L. N. PERSEN[1]

For those who have been working either in practice or in research on elastic shells, the name of W. Flügge has long been known as that of the author of one of the basic books in this field. His first book on the subject was published in 1934 in German, and has since been treasured by many, both as a reference book for the more advanced worker and as an introductory text for those entering the field. In view of the steadily increasing number of new contributions in this particular field in the past decade, the need for another textbook became more and more urgent. The present volume must therefore be greeted as the necessary filling of a gap in the literature in this field.

It should be stressed that the present book is not only a revised version of the earlier book, but that it must rather be regarded as an entirely new contribution even though many of the figures and the layout of the chapters bear a resemblance to the former. The fundamental ideas and the derivations of the basic equations are treated in detail, and the author has taken great pains in trying to convey to the reader a good physical understanding of what forces are acting in a shell, how the shell deforms, and other similar important concepts. Chap. 1 contains the fundamental properties of stress systems in shells; Chaps. 2 to 4 deal with the membrane theory (influence of bending moments neglected); Chaps. 5 and 6 deal with the bending theory of shells of revolution. Since this is one of the most important parts, it may be of interest to quote what the author says about this in his Preface: "In these two chapters an attempt has been made to cover a wide variety of questions and to carry every theory to a definite end, viz., to a set of formulas giving all the stress resultants and the displacements in terms of the constants of integration and the co-ordinates. In many cases it has been possible to present these results in the form of a table. It has, however, mostly been left to the reader to adapt a solution to his particular case of boundary conditions." A short summary of cases of practical importance treated may be of interest: Cylindrical shells with forces applied at the edges; Barrel vaults; Cylindrical tanks with constant and variable thickness; Anisotropic shells; Folded structures; Spherical shells; Shells having a meridian of arbitrary shape; and Conical shells. Chap. 7 deals with the buckling of shells. As our understanding of the nature of buckling of shells and the attempts to develop a mathematical treatment of this phenomenon have been insufficient so far, this chapter is not very rewarding from a designer's point of view—a fact clearly pointed out by the author in the Preface. The present state of knowledge is, nevertheless, summarized very well.

The book contains astonishingly few references in the text. These seem to have been deliberately omitted because of the setup of the bibliography at the end of the book. This bibliography is not merely a listing of papers and books which may be of interest, but more in the nature of a review of some main books and papers to which the reader is referred for further information and study. The bibliography describes in short sentences the main problems treated in the references and also in some cases it gives information on the procedure used to obtain solutions. Even though the author states in his introductory remarks that "it has not been intended to make this bibliography a historical review of shell theory," its composition is such that it bears a great resemblance to such a review. The bibliography lists books and papers in most languages from the Western hemisphere. It is very valuable both for the advanced practical designer and for the research worker as a source of information on what has been or can be done. For the research worker, however, the bibliography may be a trap. Obviously, owing to language difficulties, very few Russian papers have been listed (in fact, the re-

[1] Visiting Professor, Division of Engineering, Brown University, Providence, R. I.

viewer was only able to find *two* Russian contributions from the postwar period). It is known that the Russian standard in this subject is very high, and it may well be that important developments lie hidden in the extensive Russian literature in the field. Furthermore, the reviewer would have liked to see some of the more important tables for the design of cylindrical shells mentioned, and especially a mention of the new tables developed in Eastern Germany several years ago might have added value to the bibliography for the practical designer.

The book was published by Springer Verlag, Berlin, and lives up to this publisher's high standard regarding paper, printing, and figures. It is a pleasure to recommend this book both for its contents and for its appearance.

Multivariable Systems

The Control of Multivariable Systems. By M. D. Mesarovic. John Wiley & Sons, Inc., New York, N. Y., 1960. Cloth, 6 × 9 in., xi and 112 pp. $3.50.

REVIEWED BY RICHARD BELLMAN[3]

THE monograph is divided into two parts. The first part contains some general philosophical discussion culminating in the observation that control of a complex system can be materially improved if more is known of the internal structure. To illustrate this point, the author considers several different types of structures together with their transfer functions and control policies.

The second part is devoted to the synthesis problem. This is first formulated as the problem of minimizing a functional of a collection of state variables, and then is simplified to that of minimizing a quadratic functional. A number of specific calculations are then carried out.

There is no doubt that the author has some interesting ideas in this modern fascinating field of control theory. However, the book is so loosely organized and the results so imprecisely stated that it is exceedingly difficult to discern what they are. This is a book which required a strong editorial hand and did not receive it.

Thermoelectricity

The Dynamic Behavior of Thermoelectric Devices. By Paul E. Gray. John Wiley & Sons, Inc., New York, N. Y., 1960. Cloth, 6 × 9 in., viii and 136 pp. $3.50.

REVIEWED BY W. H. LUCKE[3]

THE title of this book is to be taken literally. It is not for the casual reader; neither will the student seeking to extend his understanding of the phenomena of thermoelectricity benefit. Those who are interested in the performance of thermoelectric devices in detail and in the automatic control of such devices in particular will find it valuable. The present state-of-the-art is such that the major effort to improve performance is being made in the development of better materials rather than the refinement of application of those at hand. From this point of view this book is, perhaps, ahead of its time.

The bulk of the text is in the language of servomechanism and control analysis, and those expert in this field, of which the present writer is not one, should find this an interesting application of older ideas to a new system. Indeed, the author, recognizing that those who speak his language are not apt to be familiar with thermoelectricity, has devoted the first two chapters and an appendix to an exposition of the basic thermoelectric phenomena and their interrelations. This exposition, suffering from a cumbersome notation among other things, is not recommended to those new in the field. It is incorrect in at least one particular in that the second Kelvin relation is called the first. But this is perhaps only nit-picking.

Chapters 3 and 4 are devoted to the "small-signal analysis" of the heat pump and generator, respectively. This is the heart of the book, and appears to be quite sound.

Chapters 5 and 6 give the results of an experimental check of the predictions developed in Chap. 3. The agreement may be described as satisfactory. The differences found and the approximations made are presented with honesty if not with clarity. A great handicap here is the fact that the temperature dependence of the pertinent parameters leads to nonlinear equations so that approximations must be made if an analytic expression is to be written. This problem is fundamental to the analysis of steady-state performance as well; Mr. Gray's analysis is not the only one to suffer from it. His point, that inclusion of a linear approximation to the variation of resistivity with temperature significantly improves the prediction of performance, is well made.

Chapter 7 briefly summarizes the analytic procedure, mentions a couple of design considerations, and closes with recommendations for future work in the area.

An obvious criticism is that the paucity of experimental data presented keeps the book from having the authority one expects of such a work. However, this criticism is forestalled in the foreword by J. A. Stratton in which the work is described as ". . . less ambitious than a finished book."

That the author himself realizes his position is suggested by the following quotation from page 106. "In the opinion of the author, most present-day devices and device applications are 'first generation' in nature. As thermoelectric devices are used more widely for a variety of purposes, the dynamic problems and control problems will quite naturally become more clearly defined." In short, the book is of present interest and value to a very small group but one whose numbers should grow with the use of thermoelectricity. If it is not some day hailed as a landmark, it will at least be considered a sound step forward.

Electrical Conduction

Electronic Processes in Solids. By P. Aigrain, R. J. Coelho, and G. Ascarelli. John Wiley & Sons, Inc., New York, 1960. Cloth, 6 × 9 in., x and 67 pp. $4.

REVIEWED BY CHARLES ELBAUM[4]

THIS short book is based on a series of lectures given by P. Aigrain in 1957, while he was visiting professor at the Massachusetts Institute of Technology. It was prepared by R. J. Coelho and G. Ascarelli from notes taken at these lectures.

After presenting a few basic concepts of crystal lattice dynamics, the author devotes most of the book to the theory of electrical conduction in semiconductors and metals, with special emphasis on semiconductors. Within a limited space a large number of problems is dealt with in a skillfully condensed form. Unfortunately this conciseness is, of necessity, linked with an omission of details and with frequent oversimplifications. The latter are occasionally carried to the point where one may lose sight of the real difficulties that appear in this subject, when an attempt is made to move beyond broad generalities.

This short work will undoubtedly be helpful to the "initiated" as a form of pocket dictionary for quick reference. It is not likely to be of use to those who are not reasonably familiar with the field.

The book includes a general bibliography, but unfortunately original references are not given in connection with specific problems discussed in the text.

[3] The RAND Corporation, Santa Monica, Calif.

[3] Thermoelectric Research Department, U. S. Naval Research Laboratory, Washington, D. C.

[4] Department of Physics, Brown University, Providence, R. I.

Vibrations

Problems of the General Theory of Oscillations and of Chronometry (in French). By J. Haag and R. Chaleat, with preface by J. Peres. Gauthier-Villars, Paris, 1960. Paper, 6¼ × 9½ in., 412 pp. $8.

REVIEWED BY R. M. ROSENBERG[5]

THE form of this attractive and interesting book is uncommon in the recent English-language literature. It consists of 120 carefully stated problems from the field of vibrations, each followed immediately by the detailed solution. None of the problems is of the type usually associated with textbook exercises, and several are of the caliber of papers found in the scientific literature. All problems are concerned with, and stated in the language of, physical applications; while the majority is concerned with problems arising from the theory of the clock (pendulums, balance wheels, escapements, etc.), many of these are directly applicable to other vibrating systems as well.

The first chapter contains the theory and application of astronomic time measurements (gnomon, sun dial, calendar, etc.) Chapters 2–12 and Chap. 14 deal with physical problems whose governing equation is $\theta'' + \omega^2\theta = \lambda f(\theta,\theta',t)$ where f is usually not linear in θ,θ' and is always periodic in t; moreoever, f is not in all problems everywhere continuous in θ' and t. The problems deal with steady-state, and many with transient solutions. It is evident that some are of considerable difficulty. Chapter 13 treats problems of several degrees of freedom, and Chap. 15 contains problems not easily fitted under the well-defined headings of the preceding chapters.

The combination of analytical skill and sound physical understanding makes this book a welcome addition to the growing literature in nonlinear vibrations.

The senior author died several years prior to the publication of this book. Nevertheless, his name appears on the title page because he was the teacher of Chaleat and because he proposed a number of the problems treated in this book.

Mollier Diagrams

Mollier, i, x Diagramme für feuchte Luft. By Dr. Ing. Hans Dieter Baehr. Springer Verlag, Berlin, 1961. Cloth, 8½ × 12 in., 22 pp. DM 12.

REVIEWED BY J. KESTIN[6]

THIS little booklet contains large-scale Mollier, enthalpy-dryness fraction diagrams for humid air.

To some readers of the JOURNAL OF APPLIED MECHANICS, the publication of large working charts of this nature may come as a surprise. We seem to have become accustomed to, or to rely on, digital computers to do most of the design and performance computations for us. The appearance of this booklet is a fresh reminder that graphical methods can still play a useful part in tackling engineering problems. Very often, as is the case with processes in humid air, graphical methods are much easier to apply and are certainly cheaper and lead to results which are just as good as those that might be obtained from an expensive digital computer.

The diagrams are cast in the international MKSA systems, and the reviewer hopes that many more persons will use this exceedingly convenient set of units. The standard of draftsmanship and printing is as high as is normally associated with the publications which come off the presses of Springer Verlag in Germany.

[5] Professor, Engineering Mechanics, University of California, Berkeley, Calif.

[6] Professor, Division of Engineering, Brown University, Providence, R. I.

Structural Mechanics

Structural Mechanics in the USSR 1917–1957. Edited by I. M. Rabinovich; English translation edited by G. Herrmann. Pergamon Press, New York, N. Y., 1960. Cloth, 9 × 5½ in., viii and 431 pp. $8.00.

REVIEWED BY W. PRAGER[7]

THE publication of an English version of this useful survey has been supported financially by the Structural Mechanics Branch of the Office of Naval Research. The nine chapters cover the following fields: Structural mechanics of two and three-dimensional systems of elastic bars (141 pp. incl. a bibliography of 1082 items); Thin-walled members (18 pp., 171 items); Structures on elastic foundations (30 pp., 229 items); Theory of plates (32 pp., 333 items); Analysis of shells and other thin-walled spatial structures (53 pp., 514 items); Dynamic analysis of structures (51 pp., 603 items); Application of plasticity theory to structural analysis (45 pp., 275 items); Extremum and variational principles in the theory of structures (24 pp., 20 items); Pressure and resistance of granular media (31 pp., 175 items). A transliteration table and a list of abbreviations conclude the book; there is no subject index.

Thermodynamics

Engineering Thermodynamics. By James B. Jones and G. A. Hawkins. John Wiley & Sons, Inc., New York, N. Y., 1960. Cloth, 6 × 9 in., xviii and 724 pp. $8.50.

REVIEWED BY P. D. RICHARDSON[8]

TODAY there are many texts available on engineering thermodynamics written in recent times. In most of them the presentation of the subject matter is developed from the pattern pioneered by Professor J. H. Keenan. The sequence and form of presentation of the basic concepts and laws are, indeed, surprisingly uniform throughout these recent texts, variations arising mainly from differences of style and relative emphasis.

The book under review belongs to this family. In its 724 pages there is a comprehensive exposition of material for an undergraduate introductory course. How have the authors sought to distinguish their text from those of similar technical competence and scope? The distinction is in the style: "This book is written directly to students . . . In this manner we hope to free the teacher from the necessity of interpreting the text to his students." This intention is especially followed in the introductory chapters, almost to the extent where the book might be entitled "Teach Yourself Engineering Thermodynamics." The authors emphasize that the order of the material is selected for pedagogical reasons rather than in a quest for logical economy. Within the framework which they have chosen, the authors have given an extensive and readable account.

Science and Scientists

My Life and Times as a Physicist. By I. I. Rabi. The Castle Press, Pasadena, Calif., 1960. Cloth, 6 × 8 in., vi and 55 pp. $2.75.

REVIEWED BY ROHN TRUELL[9]

THIS book contains two thought-provoking lectures by Rabi

[7] L. Herbert Ballou University Professor, Brown University, Providence, R. I.

[8] Assistant Professor, Division of Engineering, Brown University, Providence, R. I. Assoc. Mem. ASME.

[9] Professor, Division of Applied Mathematics, Brown University, Providence, R. I.

given in Los Angeles and at the Associated Colleges of Claremont. The lectures are entitled "The Scientist and the State man" and "Science and the Humanities."

This is an account of Professor Rabi's experiences as an adviser to presidents and heads of national agencies on matters determining national policy. The enormous effects of science and technology on our society demand new directions for public policy, and one of these lectures is concerned with discussion of the importance of scientists and scientific information in all branches of government.

The second lecture is a discussion of the need for the "fusion of science and the humanities" and for "a united effort of science and the humanities" to deal with present-day problems.

These two lectures are very much worth reading by anyone, and they ought to be required reading for everyone in government positions.

FOURTH U. S. NATIONAL CONGRESS OF APPLIED MECHANICS

University of California, Berkeley, Calif.

June 18—21, 1962

The U. S. National Congresses of Applied Mechanics are held every fourth year and are planned to supplement the International Congresses of Applied Mechanics.

Research workers are cordially invited to submit papers constituting original experimental or theoretical contributions to Applied Mechanics, including mechanics of rigid bodies and deformable solids, mechanics of fluids and gases, thermodynamics, and heat transfer.

It is expected that papers accepted will be published in the Proceedings of the Congress. **Complete papers and manuscripts must be submitted to the Chairman of the Editorial Committee before January 1, 1962. The final manuscript must be accepted before May 1, 1962.**

Inquiries regarding the Congress should be addressed to Professor W. Goldsmith, Secretary of Applied Mechanics Congress, University of California, Berkeley 4, Calif.

INTERNATIONAL SYMPOSIUM ON PHOTOELASTICITY

Illinois Institute of Technology

Chicago, Ill.

October 29—31, 1961

The Symposium is sponsored by the Illinois Institute of Technology, Office of Ordnance Research of the U. S. Army, National Science Foundation, Society for Experimental Stress Analysis, Office of Naval Research, Office of Scientific Research, U. S. Air Force, Applied Mechanics Division of The American Society of Mechanical Engineers, and the Chicago Sections of the SESA, ASME, and ASCE.

The tentative technical program consists of four sessions covering the subjects of Birefringent Coatings, Photothermoelasticity and Photoplasticity, and Two and Three-Dimensional Photoelasticity.

All correspondence regarding the Symposium should be addressed to:

Professor M. M. Frocht, Chairman
International Symposium on Photoelasticity
Illinois Institute of Technology
Chicago 16, Ill.

Nonphotoelastic Aspects of Experimental Mechanics will be covered at the International Congress which follows on November 1-3, 1961, at the Hotel New Yorker, New York, N. Y. Inquiries should be addressed to B. E. Rossi, Executive Secretary, SESA, 21 Bridge Square, Westport, Conn.

TRANSACTIONS OF THE ASME
Series E

Journal of
APPLIED MECHANICS
VOLUME 28 . SERIES E . NUMBER 3
September 1961

CONTENTS
CONTINUED

BRIEF NOTES

On Similarity Solutions for Free-Convection Flow Past Flat Plates 454
Pau-Chang Lu

A Single Formula for the "Law of the Wall" 455
D. B. Spalding

On Classical Normal Modes of a Damped Linear System 458
Morris Morduchow

On Certain Invariants of Symmetric Cartesian Tensors 459
Dave Pandres, Jr.

On the Occurrence of Nodal Patterns of Nonparallel Form 459
N. J. Huffington, Jr.

Three-Dimensional Bending of a Ring on an Elastic Foundation 461
D. A. Rodriguez

Pressure-Flow Characteristics of Randomly Oscillating Pipe Flows 463
C. L. Tien and J. H. Lienhard

DISCUSSION

465 Discussion of previously published papers by *Myron Tribus; K.-T. Yang; W. W. Short; Paul Seide and V. I. Weingarten; F. Freudenstein and G. N. Sandor; W. J. Carter and F. C. Liu; M. A. Goldberg, V. L. Salerno, and M. A. Sadowsky*

BOOK REVIEWS

Stresses in Shells 477

Control of Multivariable Systems 478

Dynamic Behavior of Thermoelectric Devices 478

Electronic Processes in Solids 478

479 Problems of the General Theory of Oscillations and of Chronometry

479 Mollier Diagrams

479 Structural Mechanics in the USSR 1917–1957

479 Engineering Thermodynamics

479 My Life and Times as a Physicist

"Proved" Technical Aids for Engineers in the Applied Mechanics Field

Applied Mechanics Reviews

Published monthly
$25 Annually
($12.50 to ASME members)

Engineers who read this magazine regularly are able to keep posted on worldwide developments in applied mechanics, both in its established boundaries and wherever it cuts through other fields of scientific and engineering endeavor.

To provide this service and to give readers potentially useful information which might never have come to their attention, AMR's editorial staff investigates every known information source, scans the 900 engineering periodicals in 40 countries devoted wholly or in part to the field, all new books containing pertinent information, and the reports of industrial specialists everywhere. Each issue contains approximately 600 signed reviews, grouped under the following major classifications.

General: Analytical Methods in Applied Mechanics. Computing Methods and Computers. Analogies. Kinematics, Rigid-body Dynamics, and Oscillations. Instrumentation and Automatic Control. Tables, Charts, Dictionaries, etc. **Mechanics of Solids.** Elasticity. Viscoelasticity. Plasticity. Rods, Beams, Strings. Plates, Shells, Membranes. Buckling. Vibrations of Solids. Wave Motion and Impact in Solids. Soil Mechanics: Fundamental and Applied. Processing of Metals and Other Materials. Fracture (including Fatigue). Experimental Stress Analysis. Material Test Techniques. Properties of Engineering Materials. Structures: Simple and Composite. Machine Elements and Machine Design. Fastening and Joining Methods.
Mechanics of Fluids: Rheology. Hydraulics. Incompressible Flow. Incompressible and Compressible Flow. Boundary Layer. Turbulence. Aerodynamics. Vibration and Wave Motion in Fluids. Fluid Machinery. Flow and Flight Test Techniques and Measurements.
Heat. Thermodynamics. Heat and Mass Transfer. Combustion. Prime Movers and Propulsion Devices.
Combined Fields and Miscellaneous. Magneto Fluid-dynamics. Aeroelasticity. Mechanics of Solids at High and Low Temperatures. Aeronautics. Astronautics. Ballistics, Explosions, Acoustics. Micromeritics. Porous Media. Geophysics, Hydrology, Oceanography, Meterology. Naval Architecture and Marine Engineering. Friction, Lubrication, and Wear.

Each issue of AMR also contains a feature article that focuses attention on progress in a specialized area of applied mechanics.

Section 3 1960 ASME Transactions

$16.00 ($8.00 to ASME members)

This section brings together the 135 technical papers and notes on technical matters in mechanics, design data, discussions, and book reviews published in the four 1960 issues of the Journal of Applied Mechanics. These contributions provide information on analytical and experimental studies in the fields of aerodynamics, elasticity, deformation, flow of fluids, photoelasticity, plasticity, stresses and strains, structures, thermal stresses, vibration, wave mechanics, and other related subjects.

The Theory of Elastic Thin Shells

To be published in October
$15.00 ($12.00 to ASME members)

This monograph by Dr. A. L. Gol'denveizer presents the mathematical foundations of shell theory and discusses in detail the approximate methods of solution. Although originally published in the Russian language in 1953, it is today the only book that formulates as completely as possible the different sets of basic equations and various approximate methods of shell analysis emphasizing asymptotic integration. This English edition has been brought up to date by including a considerable number of additional and recent references, and a supplement which embodies the most recent advances of the method of asymptotic integration. The presentation is arranged in such a manner that each part of the book represents a complete entity.
Partial contents: In Part I the general formulation and equations of the theory of shells are deduced which are based on the well-known hypothesis of the preservation of the normal element, and a brief survey of certain notions of the theory of shells presented. Part II is devoted to the membrane theory. Part III considers methods of analysis of circular, cylindrical shells with the aid of trigonometric series. Part IV is essentially mathematical in character and its purpose is to justify the approximate methods of shell analysis. In Part V approximate methods of analysis of shells are formulated which are based upon the results obtained earlier.

Mechanical Impedance Methods for Mechanical Vibrations

Published 1958 $5.50
($4.40 to ASME members)

Shows how impedance methods apply to lumped and continuous systems of simple and moderate complexity, reviews measurement techniques, demonstrates the power of digital computers by comparing the calculated and measured characteristics of a highly symmetrical system of moderate complexity, gives measured values of typical structures of large size and high complexity, discusses the importance of the impedance in influencing shock and vibration spectra measured in field service, indicates how to apply impedance methods to the calculation of vibration isolator effectiveness, treats impedance of some disordered systems, shows how impedance methods may be used to find the response to random excitation, and describes a dynamic stiffness method that has proved useful in predicting critical speeds of steam turbines.

Shock and Structural Response

Published 1961 $4.50
($3.60 to ASME members)

Presents specific, useful information on shock and structural response and the method of analysis and testing used. The discussion covers the nature and origin of shock loading with examples from several fields; the techniques and instruments used for shock measurement and the manner in which data are presented for engineering applications; the responses of single-degree-of-freedom systems to shock and various ways of presenting information for design application and for indicating requirements for shock-testing machines to simulate conditions occurring in actual service; the modal method of analysis for determining response of complicated systems to shock pulses, and the applications of methods discussed in the book to some of the problems of missile bases designed to withstand ground shock produced by detonations.

Send payment with order and save handling and mailing charges

THE AMERICAN SOCIETY OF MECHANICAL ENGINEERS
United Engineering Center, 345 East 47th Street, New York 17, N. Y.